
The University Of Sheffield.

# Developing approaches and *in vitro* systems for studying and promoting angiogenesis and for regenerative medicine applications

---

**Serkan Dikici**

*A thesis submitted to the University of Sheffield in fulfilment of the requirements for the degree of*

***Doctor of Philosophy***

The University of Sheffield

Faculty of Engineering

Department of Materials Science and Engineering

June 2020

**This page intentionally left blank**

*This dissertation is dedicated to everyone*

*who is not bored to death and still reading enthusiastically*

*even after a couple of hundred pages. You will go to the "good place".*

**This page intentionally left blank**

# Abstract

The main aim of this project was to enhance our knowledge on angiogenesis by developing systems that enable us to study and promote angiogenesis in tissue engineering and regenerative medicine applications.

Over the last 30 years, there have been significant advances in the production of tissue-engineered (TE) materials suitable for use in the clinic. However, one of the key challenges is to ensure rapid neovascularisation into these constructs in order for them to survive post-transplantation. While relatively thin simple TE constructs can survive on well-vascularised wound beds, thicker constructs (>200 μm) usually fail to engraft due to lack of oxygen and nutrients *in vivo*. Both prevascularisation and scaffold functionalisation strategies with the use of angiogenic factors are viewed as promising approaches to accelerate vascular ingrowth into TE constructs to circumvent slow vascularisation after implantation.

Angiogenesis is a tightly regulated process and the majority of the current strategies for promoting rapid neovascularisation focus either on the addition of proangiogenic factors to TE constructs or adding laboratory expanded proangiogenic cells such as endothelial cells, endothelial progenitors or stem cells to tissue engineering scaffold systems prior to implantation.

For functionalisation of the TE constructs with the proangiogenic factors, vascular endothelial growth factor (VEGF) is recognised to be the most well-studied angiogenic factor due to occupying a key role in the angiogenic cascade. VEGF has been proven to have important roles in different steps of the angiogenic process *in vivo*: vasodilation and permeability, destabilisation of vessels and degradation of extracellular matrix (ECM), proliferation and migration of endothelial cells, and lumen formation and vessel stabilisation. However, VEGF acts as part of a well-regulated process, and its actions are highly dose-dependent, and a range of studies show that VEGF addition can lead to excessively leaky, permeable and haemorrhagic vessels such as those that are found in tumorigenesis. Therefore, seeking alternatives to VEGF is inevitable.

Accordingly, I have investigated the angiogenic potential of 2-deoxy-D-Ribose (2dDR) using well-established *in vitro* and *in vivo* models. For the *in vitro* assessments, the

proliferation, migration and tube formation of human aortic endothelial cells (HAECs) in response to different concentrations of *2dDR* were assessed. The angiogenic activity of 2dDR was further assessed *in vivo* using two well-established angiogenesis systems; *ex-ovo* chick chorioallantoic membrane (CAM) assay and diabetic rat wound healing model.

*In vitro* and *in vivo* angiogenesis models are important tools to explore the newly discovered pro-angiogenic or and anti-angiogenic agents. Although *in vivo* assays are the most representative and reliable models for the evaluation of angiogenesis, they are also expensive, technically difficult, time-consuming, and ethically questionable. On the other hand, *in vitro* angiogenesis assays are inexpensive, quick, technically simple, and reproducible, but they are usually based on evaluating only one aspect of angiogenesis (for example, only proliferation, migration or differentiation), and they may produce false results due to the unspecific reaction of cells. Moreover, most of the *in vitro* angiogenesis assays are limited to static, 2D cell culture systems where culturing cells on stiff and flat substrates is a simplified method and does not represent the dynamic and highly complex tissue systems. 2D culture of cells distorts cell-cell and cell-matrix interactions which affects cell proliferation, migration and differentiation, where 3D *in vitro* models better represent the *in vivo* in a cost-effective way and with no ethical concerns. To date, none of the studies demonstrated any *in vitro* models that allow researchers to evaluate angiogenesis assessing both proliferation and migration of ECs in a 3D environment. Thus, in this project, three different systems made of synthetic and natural polymers were developed to be used as *in vitro* platforms to study and promote angiogenesis.

First angiogenesis model was a poly-(3-hydroxybutyrate-co-3-hydroxyvalerate (PHBV) synthetic vascular scaffold developed by combining electrospinning and 3D printing. Nanofibrous PHBV channels were capable of supporting human dermal microvascular endothelial cells (HDMEC) to adhere and create an endothelium monolayer within the channels. The use of the developed system as an *in vitro* platform to study angiogenesis was evaluated using Matrigel. The outgrowth of HDMECs was further analysed using a reconstructed human skin model which was also developed in the scope of this project.

The second model was developed via decellularisation of baby spinach leaves. The natural vascular structure of the leaves was then repopulated with HDMECs in the presence of helper human dermal fibroblasts, and their potential to promote angiogenesis was investigated using *ex-ovo* CAM assay. The decellularised spinach leaves

were further assessed for their potential use as an *in vitro* angiogenesis model where outgrowth of HDMECs was analysed in response to VEGF and 2dDR.

The third synthetic model was developed via a combination of electrospinning and emulsion templating techniques. The developed 3D dynamic model was made of electrospun PHBV tube and polycaprolactone (PCL) polymerised high internal phase emulsion (PolyHIPE). The model was capable of supporting HAECs to form an endothelium-like monolayer within the tubular channel, and the outgrowth of HAECs was investigated in response to 2dDR and VEGF under static and dynamic conditions.

Then, as an alternative to the use of pro-angiogenic agents, I assessed the effectiveness of prevascularisation (use of pro-angiogenic cells) technique for promoting angiogenesis in *ex-ovo* CAM assay. I fabricated basic electrospun PHBV scaffolds and cellularised them with a combination of endothelial cells and fibroblasts to evaluate the potential of these cells to induce angiogenesis *in vivo*.

Finally, in collaboration with my colleague, Betül Aldemir, we investigated an alternative use of the bilayer scaffolds manufactured by combining electrospinning and emulsion templating techniques, which was found very rapid and effective route to produce TE scaffolds that have the potential to be used in various tissue engineering and regenerative medicine applications. To explore the use of these scaffolds as a bilayer barrier membrane for guided tissue regeneration (GTR) applications, we explored the cell-occlusiveness of electrospun layer and the bone promoting properties of the PolyHIPE layer.

**This page intentionally left blank**

# Acknowledgements

I would like to thank my primary supervisor, Prof Sheila MacNeil, for her endless support and guidance throughout my PhD project. She always made me feel at home even from the first second I joined her group in Kroto Research Institute. Her everlasting enthusiasm for science and her years of experience was my driving force to achieve all my research goals. She was always there for me even through the toughest times of my PhD and will always be with me with her countless contribution to my academic development.

I would also like to thank my second supervisor Dr Frederik Claeyssens. Besides having high academic qualifications of supervising a PhD student, he was always a friend to me; who I can reach every time I need. I would not be the same without his guidance and overwhelming support. His continued involvement and interest in my project were an excellent source of motivation for my personal and academic development.

I thank my funding body, the Turkish Ministry of National Education, for providing financial support which allowed me to undertake this great project and create inestimable connections with scientist all over the world.

I owe a huge thank you to many of the scientists in Kroto Research Institute. In particular, Dr Anthony Bullock and Dr Naside Mangir for teaching me the art of cell culture and CAM assay, respectively, Dr Sabiniano Roman Regueros for his guidance on mechanical testing, basic histology and immunohistochemistry, Dr Caroline S. Taylor who taught me the basic principles of electrospinning. I would like to specially thank Dr Muhammad Yar for sharing his pioneering experience on deoxy sugars and for our invaluable collaborative projects.

Many thanks to the Kroto researchers with whom we shared this great research experience together, Dr Hossein Bahmaee, Dr Jose R Aguilar Cosme, Iris Cristina Becerril Rodriguez, Dr Mehri Behbehani, Dr Liam Boyle, Dr Jonathan Field, Dr Samand Pashneh-Tala, Dr George Bullock, Dr Colin Shernborne, Dr Caroline Taylor, Dr Sarina Chand, Dr Thomas Paterson, David H Ramos for their endless support and help throughout my project. Thanks to my lovely friends in England, Enes Durgut, Merve Sasmaz, Yunus Celik,

and Zalike Keskin, for their support and motivation. I am grateful to Suat Sabuncuoglu for his guidance on our way to Sheffield.

I would like to thank everyone in Massachusetts Institute of Technology (MIT), in particular, Prof Elazer R Edelman, Prof Mercedes Balcells-Camps, and Dr Shirin Issa Bhaloo for giving me an amazing opportunity as a visiting PhD student at MIT. Our collaborative research project and joining your lab provided me an invaluable academic perspective. This fruitful collaboration with MIT was a milestone in my academic career. I am truly happy to have the opportunity to be a short-term member of this great lab.

Thanks to Prof Richard Oreffo and Dr Janos Kanczler for giving me a great opportunity to join their lab at the University of Southampton. This great opportunity helped me to improve my skills, especially in CAM assay and the chick bone healing model.

I am very grateful to my family: Gülgün Topcu, Selahittin Dikici, Nurten Aldemir, Metin Aldemir, and Ozan Aldemir. They have always encouraged me to pursue what makes me happy. Thank you for your endless love and support. Even as we have been almost 3800 km away from each other, you have always made me feel like you are by my side. *(Ailem Gülgün Topçu, Selahittin Dikici, Nurten Aldemir, Metin Aldemir ve Ozan Aldemir... Beni mutlu eden şeylerin peşinden gitmem için her zaman teşvik ettikleri için tüm aileme minnettarım. Sonsuz sevginiz ve desteğiniz için teşekkürler. Birbirimizden neredeyse 3800 km uzaktayken bile, bana her zaman yanımda olduğunuzu hissettirdiniz)*.

Finally, the most special thank you goes to my wife, ***Dr Betül Aldemir***, the one who was always there for me when I needed. She has been, is, and she will always be my friend, my teacher, my partner, my colleague and my life. She was always full of love even if it was a very stressful late night in the lab or a very early, cloudy, rainy and depressive Sheffield morning (no offence Sheffield, but for all we know you always were a bit of depressive). Besides her amazing skills being a really good wife, she was also a great colleague who always came up with brilliant ideas when I stuck in my projects. I would not be the same without you. Sharing my private and academic life with you makes me feel truly lucky. Having you by my side is one of the most powerful feelings I have ever felt, and this gives me a driving force to do science, to explore something new every day, and to live. You taught me that the thing that is beautiful is the journey itself; it is not to arrive.

# Outputs

## Publications

2020 **Dikici S.**, Bullock AJ., Yar M., Claeyssens F., MacNeil S., "**2-deoxy-D-ribose (2dDR) upregulates vascular endothelial growth factor (VEGF) and stimulates angiogenesis"**, Microvascular Research, 131, 104035, https://doi.org/10.1016/j.mvr.2020.104035

2020 **Dikici S.**, Claeyssens F., MacNeil S., "**Bioengineering vascular networks to study angiogenesis and vascularisation of physiologically relevant tissue models *in vitro*"**, ACS Biomaterials Science & Engineering 6 (6) : 3513–3528, https://doi.org/10.1021/acsbiomaterials.0c00191

2020 **Dikici S.**, Claeyssens F., MacNeil S., "**Pre-seeding of simple electrospun scaffolds with a combination of endothelial cells and fibroblasts strongly promotes angiogenesis"**, Tissue Engineering and Regenerative Medicine, 17 (4) : 445-458, https://doi.org/10.1007/s13770-020-00263-7

2020 **Dikici S.***, Aldemir Dikici B.* ***(*co-first author)***, Bhaloo IS., Balcells M., Edelman ER., MacNeil S., Reilly GC., Claeyssens F., "**Development of a dynamic 3D model for studying angiogenesis *in vitro*: Evaluating the effect of flow and drugs"**, Frontiers in Bioengineering and Biotechnology, 7:451, https://doi.org/10.3389/fbioe.2019.00451

2019 Aldemir Dikici B.*, **Dikici S.*** ***(*co-first author)***, Reilly GC., MacNeil S., Claeyssens F., "**A Novel Bilayer Polycaprolactone Membrane for Guided Bone Regeneration: Combining Electrospinning and Emulsion Templating"**, Materials 12 (16) : 2643, https://doi.org/10.3390/ma12162643

2019 **Dikici S.**, Claeyssens F., MacNeil S., "**Decellularised baby spinach leaves and their potential use in tissue engineering applications: studying and promoting neovascularisation"**, Journal of Biomaterials Applications 34 (4) : 546-559, https://doi.org/10.1177/0885328219863115

2019 Azam M., **Dikici S.**, Roman S., Mehmood A., Chaudhry Anwar A., Rehman IU., MacNeil S., Yar M., "**Addition of 2-deoxy-D-ribose to clinically used alginate dressings stimulates angiogenesis and accelerates wound healing in diabetic rats"**, Journal of Biomaterials Applications 34 (4) : 463-475, https://doi.org/10.1177/0885328219859991

2019 Mangir N., **Dikici S.**, Claeyssens F., MacNeil S., "**Using *ex-ovo* chick chorioallantoic membrane (CAM) assay to evaluate the biocompatibility and angiogenic response to biomaterials"**, ACS Biomaterials Science & Engineering 5 (7) : 3190-3200, https://doi.org/10.1021/acsbiomaterials.9b00172

2019 **Dikici S.**, Mangir N., Claeyssens F., Yar M., MacNeil S., "**Exploration of 2-deoxy-D-ribose and 17β-Estradiol as alternatives to exogenous VEGF to promote angiogenesis in tissue-engineered constructs"**, Regenerative medicine 14 (3) : 179-197, https://doi.org/10.2217/rme-2018-0068

## Oral Presentations

2020 **2-Deoxy-D-Ribose: A Sweet Alternative to VEGF to Stimulate Angiogenesis and Wound Healing**, Future Leaders Virtual Conference 2020 (UKSB), Jun 24-25, United Kingdom

2020 **2-Deoxy-D-Ribose as an alternative to the use of exogenous VEGF to induce angiogenesis in tissue-engineered constructs**, TCES Virtual Seminar Series 2020, Jun 18, United Kingdom

2019 **Stimulating angiogenesis in tissue-engineered scaffolds using alternative pro-angiogenic agents: 2-deoxy-D-ribose (2dDR) and 17β-Estradiol (E2),** BiTEG 2019, Dec 16, York, United Kingdom, Oral Presentation

2019 **A novel 3D *in vitro* angiogenesis model for investigating endothelial cell migration in response to multiple stimulants.** BioMedEng 19, Sep 5-6, London, United Kingdom, Oral Presentation

2019 **2-Deoxy-D-Ribose (2dDR) and 17β-Estradiol (E2) Releasing Functional Scaffolds for Stimulating Angiogenesis in *ex-ovo* CAM Assay,** Tissue Engineering & Regenerative Medicine International Society (TERMIS) EU 2019, May 27-31, Rhodes, Greece, Oral Presentation

2018 **2-deoxy-D-ribose (2dDR) and 17β-Estradiol (E2) loaded scaffolds for stimulating angiogenesis in *ex-ovo* CAM assay,** International Eurasian Conference on Science, Engineering and Technology, November 22-23, Ankara, Turkey, Oral Presentation

2018 **Use of decellularised spinach leaves as a tissue-engineering scaffold for promoting angiogenesis in *ex-ovo* CAM assay,** International Eurasian Conference on Science, Engineering and Technology, November 22-23, Ankara, Turkey, Oral Presentation

2018 **Approaches to Ensure Rapid Neovascularisation in Tissue-engineered Constructs,** The Engineering Researcher Symposium, June 26, Sheffield, United Kingdom, Oral Presentation

## Posters

2020 **Development of a physiologically relevant model to reduce the use of animals in research: a novel 3D dynamic *in vitro* angiogenesis model,** Sheffield 3Rs Symposium, 2020, Jan 14, Sheffield, United Kingdom, Poster Presentation

2019 **Development of a novel 3D dynamic *in vitro* angiogenesis model for investigating endothelial proliferation and migration in response to multiple stimulants,** BiTEG 2019, Dec 16, York, United Kingdom, Poster Presentation

2019 **Promoting neovascularisation in tissue engineering constructs: 2-deoxy-D-ribose (2dDR) and 17β-Estradiol (E2) as alternatives to VEGF,** BioMedEng 19, Sep 5-6, London, United Kingdom, Poster Presentation

2019 **Development of a Bifunctional PCL-Based Barrier Membrane for Guided Tissue Engineering,** Tissue Engineering & Regenerative Medicine International Society (TERMIS) EU 2019, May 27-31, Rhodes, Greece, Poster Presentation

2018 **Functionalised scaffolds for promoting angiogenesis and bone regeneration: Two potent alternatives to the use of VEGF,** Tissue Engineering & Regenerative Medicine International Society (TERMIS) WC 2018, September 4-7, Kyoto, Japan, Poster Presentation

2018 **A Novel Biphasic Bioresorbable Scaffold for Guided Tissue Regeneration,** Tissue Engineering & Regenerative Medicine International Society (TERMIS) WC 2018, September 4-7, Kyoto, Japan, Poster Presentation

2018 **Development and characterisation of a novel, bilayer PCL-based barrier membrane for guided tissue engineering,** BiTEG 20th Annual White Rose Meeting, December 17, Sheffield, United Kingdom, Poster Presentation

## Collaborative Projects

2019 **Development of a dynamic 3D model for studying angiogenesis *in vitro*: Evaluating the effect of flow and drugs**

Collaborative project with Balcells and Edelman Lab at Institute for Medical Engineering and Science (IMES), Massachusetts Institute of Technology (MIT), Cambridge, MA, USA, February 1 - August 31

2017 - 2018 **Assessment of the performance of PHBV synthetic vascular scaffolds on bone healing and vascularisation**

Collaborative project with Bone and Joint Diseases Group at University of Southampton, Southampton, UK, May 30 – June 2, 2017 **(1st visit)** & June 11-14, 2018 **(2nd visit)**

## Honours & Awards

2019 **Best Oral Presentation**

BITEG 21th Annual White Rose Work in Progress Meeting

2019 **2019 Image Competition Winner in Video Category**

The University of Sheffield, Department of Materials Science and Engineering

2019 **Travel Grant**

Armourers & Brasiers, October 2019

2019 **Travel Grant**

Armourers & Brasiers, April 2019

2019 **Travel Grant**

The University of Sheffield, Learned Society, February 2019

2018 **Highly Commended Poster Award in Biomaterials Category**

The University of Sheffield, 2nd year poster presentations

**This page intentionally left blank**

# Table of Content

# List of Figures

# List of Tables

# Glossary

| | |
|---|---|
| **2dDG** | 2-deoxy-D-Glucose |
| **2dDR** | 2-deoxy-D-Ribose |
| **2dDRP** | 2-deoxy-D-Ribose-1-phosphate |
| **2dLR** | 2-deoxy-L-Ribose |
| **2D** | Two dimensional |
| **3D** | Three dimensional |
| **4PCLMA** | 4-arm PCL methacrylate |
| **AA2P** | L-Ascorbic acid 2-phosphate |
| **AKT** | AKT8 virus oncogene cellular homolog |
| **Ang** | Angiopoietins |
| **ANOVA** | Analysis of variance |
| **AV** | Arteriovenous |
| **BAD** | BCL-2 associated death promoter |
| **BC** | Bacterial cellulose |
| **BCL-2** | B cell leukemia 2 protein |
| **Bio-MEMS** | Bio-microelectromechanical systems |
| **BM** | Barrier membrane |
| **BMP** | Bone morphogenetic protein |
| **BrdU** | Bromodeoxyuridine |
| **BSA** | Bovine serum albumin |
| **CAM** | Chorioallantoic membrane |
| **CD31** | Cluster of differentiation 31 |
| **CM** | Cardiomyocyte |
| **CMEC** | Rat cardiac microvascular endothelial cell |
| **CO2** | Carbon dioxide |
| **CTF** | Cell traction forces |
| **DAB** | 3,3′-Diaminobenzidine |
| **DAPI** | 4'6-diamidino-2-phenylindole |

| | |
|---|---|
| **DCM** | Dichloromethane |
| **DED** | De-epidermised dermis |
| **$dH_2O$** | Distilled water |
| **DMB** | Dimethylmethylene blue |
| **DMEM** | Dulbecco's Modified Eagle Medium |
| **DMSO** | Dimethyl sulfoxide |
| **DNA** | Deoxyribonucleic acid |
| **E2** | Estradiol |
| **EC** | Endothelial cells |
| **EC GM** | Endothelial cell growth medium |
| **ECM** | Extracellular matrix |
| **EDD** | Embryonic development day |
| **EDTA** | Ethylenediaminetetraacetic acid |
| **eNOS** | Endothelial nitric oxide synthase |
| **EPC** | Endothelial progenitor cells |
| **ERK** | Extracellular signal-regulated kinase |
| **ESC** | Embryonic stem cells |
| **FA** | Formaldehyde |
| **FAK** | Focal adhesion kinase |
| **FCS** | Fetal calf serum |
| **FGF** | Fibroblast growth factor |
| **FITC** | Fluorescein isothiocyanate |
| **GAG** | Glycosaminoglycan |
| **GBR** | Guided bone regeneration |
| **GM** | Genetically modified |
| **GRB2** | Growth factor receptor-bound protein |
| **GTR** | Guided tissue regeneration |
| **H&E** | Haematoxylin and Eosin |
| **HA** | Hyaluronic acid |
| **HAEC** | Human aortic endothelial cell |

| | |
|---|---|
| **HDF** | Human dermal fibroblasts |
| **HDMEC** | Human dermal microvascular endothelial cells |
| **HIF-1** | Hypoxia-inducible factor 1 |
| **HMDS** | Hexamethyldisilazane |
| **hPS-CMs** | Embryonic stem cell derived cardiomyocytes |
| **HRP** | Horseradish peroxidase |
| **HSC** | Hematopoietic stem cells |
| **HUVEC** | Human umbilical vein endothelial cells |
| **i3T3** | irradiated mouse 3T3 fibroblasts |
| **ID** | Inner diameter |
| **IgG** | Immunoglobulin G |
| **IHC** | Immunohistochemistry |
| **IMS** | Industrial methylated spirit |
| **LB** | Luria Bertani |
| **LCA** | Lens culinaris agglutinin |
| **$LN_2$** | liquid nitrogen |
| **MAA** | Methacrylic anhydride |
| **MAPK** | Mitogen-activated protein kinase |
| **MEF** | Mouse embryonic fibroblasts |
| **MEMS** | Microelectromechanical systems |
| **MLO-A5** | Murine osteocyte-like cells |
| **MMPs** | Metalloproteinases |
| **MSC** | Mesenchymal stem cell |
| **MV** | Microvascular |
| **NaOH** | Sodium hydroxide |
| **NCK** | Tyrosine kinase adaptor protein |
| **NF-κB** | Nuclear factor kappa B |
| **NO** | Nitric oxide |
| **NOX2** | NADPH oxidase 2 |
| **O2** | Oxygen |

| | |
|---|---|
| **OCT-TFM** | Optimum cutting temperature tissue freezing medium |
| **p38MAPK** | p38 mitogen activated protein kinases |
| **PA** | Peracetic acid |
| **PAK-2** | p21-activated kinase-2 |
| **PBMC** | Peripheral blood mononuclear cells |
| **PBS** | Phosphate buffered saline |
| **PCL** | Polycaprolactone |
| **PDGF** | Platelet derived growth factor |
| **PDMS** | Polydimethylsiloxane |
| **PEG** | Polyethylene glycol |
| **PFA** | Paraformaldehyde |
| **PGA** | Polyglycolic acid |
| **PGS** | Polyglycerol sebacate |
| **PHBV** | Poly 3-hydroxybutyrate-co-3-hydroxyvalerate |
| **PI** | Photoinitiator |
| **PI3K** | Phosphoinositide 3 kinase |
| **$PIP_3$** | Phosphatidylinositol 3,4,5-trisphosphate |
| **PIPAAm** | Poly-(N-isopropylacrylamide) |
| **PKB** | Protein kinase B |
| **PKCs** | Protein kinase C |
| **PKD** | Protein kinase D |
| **PLCγ** | Phospholipase C-γ |
| **PLGA** | Poly(lactic-co-glycolic acid) |
| **PLLA** | Poly-L-lactic-acid |
| **PolyHIPE** | Polymerised high internal phase emulsions |
| **PU** | Polyurethane |
| **PVA** | Polyvinyl alcohol |
| **RAF** | Rapidly accelerated fibrosarcoma |
| **RGB** | Red, green and blue |
| **RGD** | Arginylglycylaspartic acid |

| | |
|---|---|
| **ROCK** | Rho-associated kinase |
| **RPM** | Revolutions per minute |
| **RT** | Room temperature |
| **SD** | Standard deviation |
| **SDS** | Sodium dodecyl sulphate |
| **SEM** | Scanning electron microscopy |
| **SHB** | SH2 Domain Containing Adaptor Protein B |
| **SHH** | Sonic hedgehog homolog |
| **SMC** | Smooth muscle cells |
| **SRC** | Sarcoma virus oncogene |
| **STL** | Standard tessellation language |
| **STSG** | Split thickness skin graft |
| **STZ** | Streptozotocin |
| **SVN** | Synthetic vascular network |
| **TCP** | Tissue culture plastic |
| **TE** | Tissue-engineered |
| **TEA** | Tin (II) 2-ethylhexanoate, triethylamine |
| **TGF-β** | Transforming growth factor beta |
| **Tie-2** | Tyrosine kinase receptor |
| **TP** | Thymidine phosphorylase |
| **TRITC** | Tetramethylrhodamine |
| **TSAd** | T-cell specific adapter |
| **UTS** | Ultimate tensile stress |
| **UV-VIS** | Ultraviolet-visible |
| **VA** | Vascular area |
| **VEGF** | Vascular endothelial growth factor |
| **VEGF-R** | Vascular endothelial growth factor receptor |
| **YS** | Yield strength |
| **α-MEM** | Alpha minimum essential medium |
| **βGP** | β-glycerophosphate |

**This page intentionally left blank**

# CHAPTER I

# Literature Review

## 1.1. Vascular System

### 1.1.1. Structure and function

Beyond the diffusion limit where it is not possible to meet the essential metabolic demands of the cells, a vascular system is responsible for supplying oxygen and nutrients to the tissues and organs via a complex network of interconnected blood vessels. There are three main types of blood vessels; arteries, veins, and capillaries (Figure 1) [1]. All types of blood vessels have a thin layer of endothelial cell (EC) monolayer (endothelium or tunica intima). The capillaries are partially covered by pericytes which promote stabilisation of the vessel and provides a little elasticity. On the other hand, larger arteries and veins have multilayers of smooth muscle cells (SMCs) which stabilise the large vessels and enable contraction. SMCs form a middle layer (tunica media) which is thicker in arteries and highly elastic in order to provide mechanical resistance to pulsatile pressure caused by the blood being pumped from the heart. The outer layer, tunica adventitia, is rich in collagen fibres to provide a mechanical competence for stretching and recoiling [2].

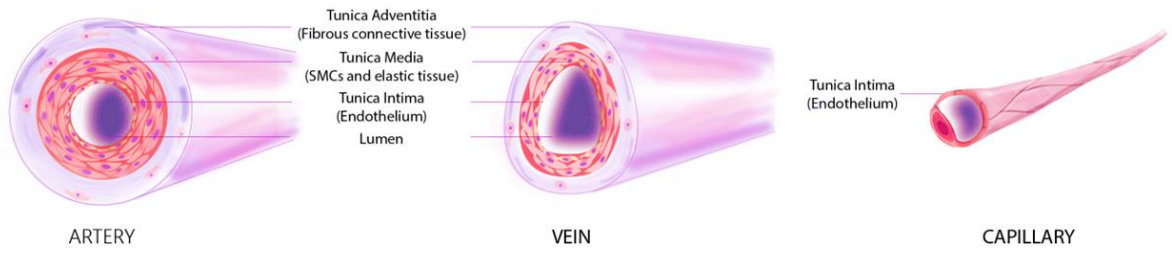


***Figure 1.*** *Three main types of blood vessels in the body; artery, vein and capillary, and their structures*

### 1.1.2. Formation

Blood vessels are crucial for providing oxygen and nutrients to the tissues and organs and start to develop early in embryonic development. Blood vessel formation *in vivo* is mostly based on three strategies: **vasculogenesis**, **angiogenesis,** and **arteriogenesis** (Figure 2) [3].

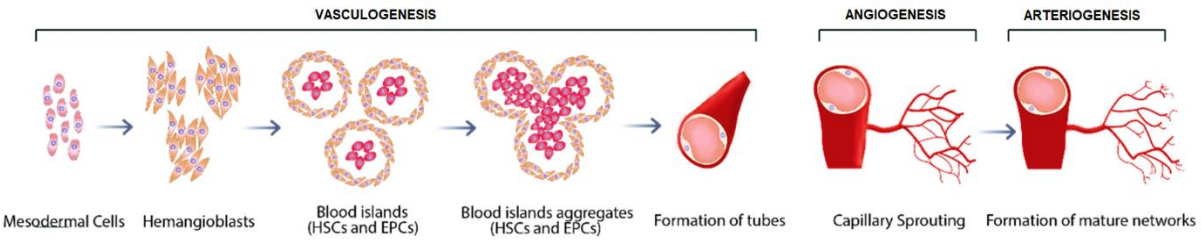


***Figure 2.*** *Vessel formation strategies in vivo: vasculogenesis, angiogenesis, and arteriogenesis*

#### 1.1.2.1. Vasculogenesis

Blood vessel formation is critical for organogenesis and for embryonic and fetal development. Development of very early capillaries occurs by vasculogenesis. Firstly, mesodermal stem cells differentiate to form hemangioblasts which will then differentiate into angioblasts. Clusters of angioblasts form blood islands that are composed of endothelial progenitor cells (EPCs) and hematopoietic stem cells (HSCs). Finally, the blood islands merge, and HSCs differentiate into blood, and EPCs develop into mature ECs, which will then create first primary capillaries [4–7].

#### 1.1.2.2. Angiogenesis

The first capillaries developed by vasculogenesis grow into a primitive network and remodel new blood vessels via angiogenesis which takes place via two mechanisms; sprouting and intussusception [8] (Figure 3).

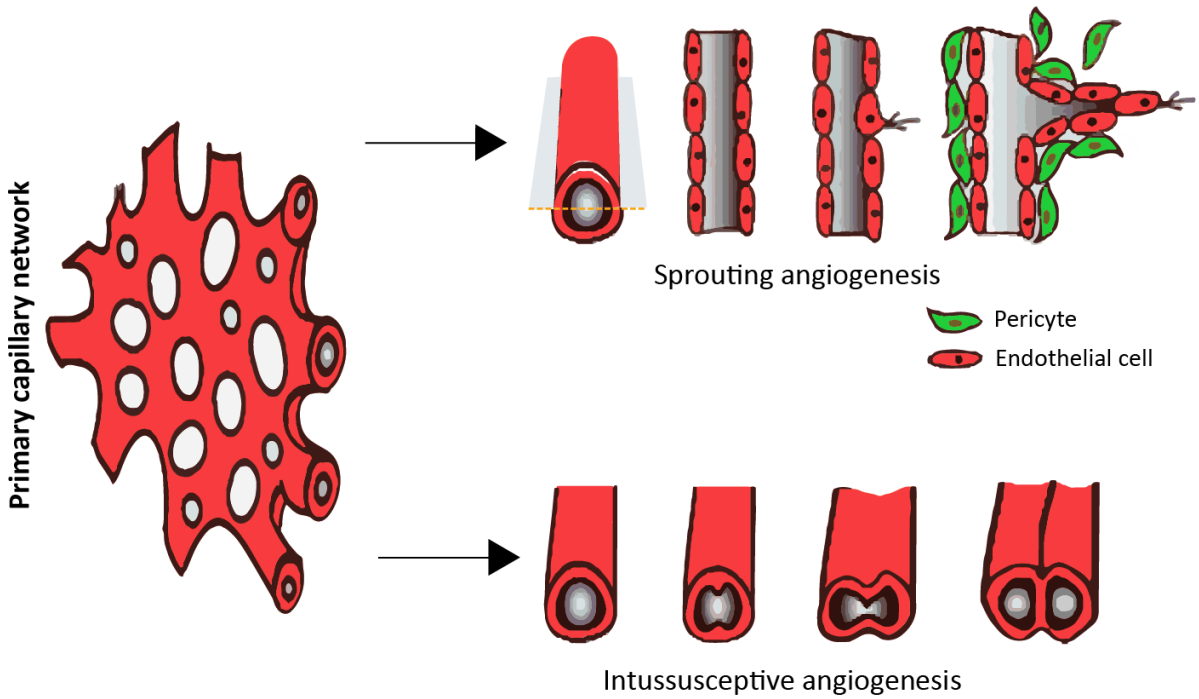


***Figure 3.*** *Process of sprouting and intussusceptive angiogenesis from a primary capillary network formed by vasculogenesis*

Sprouting angiogenesis refers to the process of branching out of new capillaries from an existing vessel via reorganisation of extracellular matrix (ECM) and EC migration, proliferation and stabilisation. The steps of sprouting angiogenesis are outlined below [9,10]:

- **Vasodilation:** increased permeability of the existing vessels, detachment of the pericytes from the capillaries, and degradation of the basement membrane
- **Migration:** migration of the endothelial cells towards the extracellular area and the formation of the endothelial sprouts
- **Proliferation:** proliferation of the endothelial cells from the tip cells
- **Tube formation:** inhibition of the proliferation and migration of the endothelial cells and remodelling into capillary tubes
- **Stabilisation:** Recruitment of periendothelial cells such as pericytes for capillary and smooth muscle cells for large vessels

Intussusceptive (non-sprouting) angiogenesis is an alternative route to sprouting angiogenesis and can be defined as the formation of two new capillaries from a single capillary by the processes given below [8,11]:

- **Intraluminal pillar formation:** creation of a zone of contact between two opposite walls of capillaries.

- **Central perforation formation:** reorganisation of the inter-endothelial cell junctions and the formation of a central perforation
- **Pericyte and myofibroblast invasion:** formation of an interstitial pillar core, invasion of pericytes and myofibroblasts, and consequently deposition of ECM.
- **Enlargement and stabilisation:** Increase in the size of the formed pillars to the size of a normal capillary, split up into new capillaries, and the mechanical stabilisation of the capillary with the formation of ECM.

Angiogenesis is a critical aspect for production of a vascularised tissue during embryonic development, wound healing, cell growth and functions of female reproductive organs such as ovaries and the repair mechanisms in the menstrual cycle [12,13], and it is a highly organised process depending on various factors. These key factors can be identified as molecular mechanisms which are angiogenic regulators used for promoting angiogenesis and biomechanical mechanisms such as role of ECM which does not only support the cells physically, but also regulates cellular functions and other biomechanical forces created by blood flow such as shear stress which has a positive effect on the formation of more sprouts rather than low or no shear stress, or extracellular environment [14–16].

Hypoxia is a key stimulus for growth of blood vessels. It establishes a connection between metabolic oxygen demand and vascular oxygen supply. Normally, cells uptake oxygen by diffusion, but hypoxia triggers the formation of new blood vessels when tissue growth exceeds the diffusion limits for oxygen diffusion [17,18]. At the cellular level, exposure of hypoxia for a long time leads to triggering of molecular pathways to deal with stress due to oxygen deficiency. One of the cellular responses is the formation of new blood vessels to relieve the increased metabolic demands due to hypoxia. Oxygen deficiency stimulates the development and remodelling of the existing vascular structure via upregulating the expression of genes which have important roles in steps of angiogenesis such as vascular endothelial growth factor (VEGF), angiopoietin-1 (Ang-1), angiopoietin-2 (Ang-2), transforming growth factor-beta (TGF-β), platelet-derived growth factor (PDGF) and fibroblast growth factor (FGF) to increase blood flow in an attempt to supply oxygen to hypoxic tissues [13,17].

#### 1.1.2.3. Arteriogenesis

After formation and stabilisation of blood vessels, some vessels are surrounded by muscular layers which provide mechanical strength, elasticity and the capability of vasomotor control and contractile properties to the vessel. This process of increase in the diameter of arterial vessels is referred to arteriogenesis [19].

## 1.2. The Need for Vascularisation in Tissue Engineering Applications

Diffusion of oxygen and nutrients from their higher concentrations to lower concentrations is a frequently used mechanism *in vivo*. However, when the distance is beyond 0.2 mm, it is slow and sometimes impossible to provide the metabolic needs of cells and tissues. At this point, the circulatory system plays a key role to transport the required molecules to tissues and organs. The vascular system consists of three main types of blood vessels: arteries, veins and capillaries, which play a key role in the transportation of blood and nutrients to tissues and organs as well as the removal of metabolic waste products from them. These types of blood vessels are composed of several layers of cells (Figure 4) which dictate their properties and function. All vessels are composed of an inner single EC layer (tunica intima) which is wrapped around by contractile mural cells in order to alter the vessel diameter according to blood flow. This middle layer of smooth muscle cells (or tunica media) stabilises the vascular tube, and its thickness varies in different types of vessels [20,21].

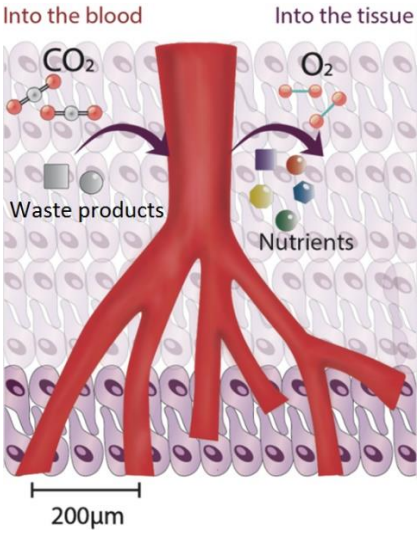


***Figure 4.*** *The greatest distance between capillaries and tissues is approximately 0.2mm (diffusion and transport phenomena in tissues). The figure shows the capillary structures in tissues to provide required oxygen and nutrients to and remove $CO_2$ and waste products from cells*

Tissue and organ failure or losses are major problems that are seen in human health, and tissue engineering offers an opportunity to develop functional substitutes for damaged tissues. Most of the conventional tissue engineering approaches have mainly focused on attachment and proliferation of cells, and their formation of ECM [22]. Over 20 different tissue types such as nerve, cornea, liver, cartilage, heart, bone and skin have been attempted to be engineered, and the most successful ones of these tissue-engineered (TE) constructs are, however, thin (<2mm) or involved cells with low oxygen requirements (avascular). The lack of blood vessels in current TE constructs is one of the most important challenges in the survival of engineered tissue substitutes [23,24]. Although significant progress has been made, the main problem with tissue engineering constructs still remains the same and is based on the slow formation of new blood vessels, known as angiogenesis, after implantation. In the body, blood vessels are subdivided into capillary structures in tissues to provide the required oxygen and nutrients to cells, and the greatest distance between capillaries and tissues is approximately 0.2mm, which is also referred to as the diffusion limit for oxygen [7,25].

When a TE substitute is implanted, nutrients and oxygen must be provided to cells to survive *in vivo*, and formation of vascular structures in TE substitute can take weeks which is a long period for cells to survive without oxygen (hypoxia) and essential nutrients, and this leads to the failure of the constructs [26].

I screened PubMed and Web of Science databases to see how the number of studies on angiogenesis has been increased over the years. All screening results showed that studies on angiogenesis have significantly increased over the last two decades. This data is summarised in Table 1.

***Table 1.*** *Screening of PubMed and Web of Science databases to see how the number of studies on angiogenesis has been increased over the years. The graph on the right shows the distribution of angiogenesis-related studies published on PubMed from 1950 to date*

| Dates | Number of publications studying angiogenesis on: | |
|---|---|---|
| | PubMed | Web of Science |
| *1950 to 1960* | 1 | 1 |
| *1960 to 1970* | 5 | 5 |
| *1970 to 1980* | 169 | 92 |
| *1980 to 1990* | 1038 | 619 |
| *1990 to 2000* | 8657 | 13080 |
| *2000 to 2010* | 43327 | 59312 |
| *2010 to date* | 65229 | 85219 |

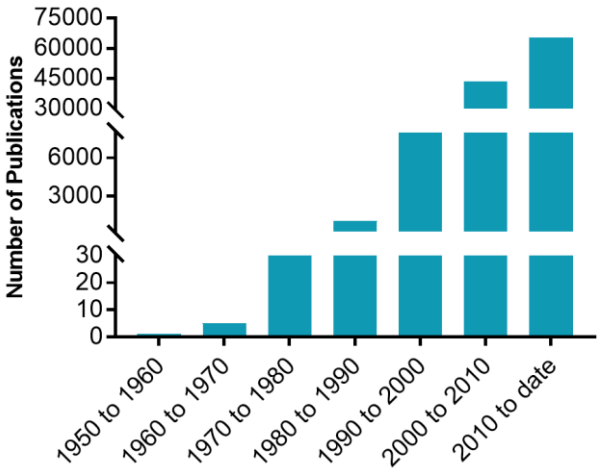


## 1.3. Key Factors in Angiogenesis

### 1.3.1. Molecular factors

Several biochemical factors have been reported as critical for stimulating angiogenesis. These factors are mostly the interaction of cytokines with their receptors and the adhesion of ECM molecules with the integrins [27,28].

#### 1.3.1.1. Cytokines and their receptors

Hypoxia is the reduction in the physiological oxygen level that reaches cells. This is due to the alteration between the requirement and supply of oxygen which is caused by several reasons such as acute and chronic vascular and pulmonary diseases. Hypoxia-inducible factors 1 (HIF-1) is a heterodimeric transcription factor which plays a key role in the cellular responses to hypoxia. HIF-1 is the main regulator of a range of genes which are upregulated in response to oxygen deprivation. The activity of HIF-1α, a subunit of HIF-1 family, is regulated by the prolyl hydroxylase domain (PHD) enzymes. Under physiological oxygen conditions (sufficient oxygen), PHD enzymes hydroxylate HIF-α which initiates binding to the von Hippel–Lindau E3 ubiquitin ligase complex, and thus HIF-α undergoes proteasomal degradation. Under hypoxic conditions, the hydroxylation is suppressed, and as a result, HIF-1α accumulates in the cell and leads to angiogenesis-

related gene activation for the regulation of angiogenic factors such as vascular endothelial growth factor (VEGF), angiopoietin-1 and 2 (Ang-1 and Ang-2), platelet-derived growth factor (PDGF), basic fibroblast growth factor (bFGF), and transforming growth factor-β (TGF-β) [29–31]. These pro-angiogenic factors act via their receptors on the EC surface and promote angiogenesis through EC proliferation, migration, and survival [32].

#### 1.3.1.1.1. Vascular Endothelial Growth Factor (VEGF)

VEGF is a well-established stimulator of angiogenesis. The VEGF family is composed of 7 members: VEGF-A, VEGF-B, VEGF-C, VEGF-D, VEGFE, and VEGF-F. VEGF A (which will be referred as VEGF in the rest of the text) particularly has been reported as an important factor which regulates several angiogenic processes. Although there are several isoforms of VEGF such as $VEGF_{145}$, $VEGF_{165}$, $VEGF_{189}$, and $VEGF_{206}$, $VEGF_{165}$ has been demonstrated to have optimal bioavailability, biological activity and consequently widely-used in studies focusing on promoting angiogenesis [33–35]. VEGF has important roles in the various steps of the angiogenic process: vasodilation and permeability, destabilisation of vessels and degradation of ECM, proliferation and migration of endothelial cells, and lumen formation and vessel stabilisation [13,36–38].
VEGF receptor 2 (VEGFR-2) is generally recognised as the main receptor responsible for regulating the VEGF-dependant angiogenic processes, and it is widely expressed by ECs. Binding of VEGF to VEGFR-2 leads the activation of the multiple intracellular cascades, which triggers angiogenesis [39,40]. The mechanism of action of VEGFR2-dependant angiogenesis is summarised below.

VEGF receptor 1 (VEGFR-1) is expressed on the surface of hematopoietic cells and ECs and has an affinity to VEGF-A. Although VEGFR-1 function is not as clear as VEGFR-2, it has been shown to regulate angiogenesis both in positive and negative manner [41]. Its most important function is the negative regulation of VEGFR-2 by acting as a trap for VEGF-A. Thus, it is recognised as a suppressor of pro-angiogenic signals [42,43].

VEGF receptor 3 (VEGFR-3) is expressed in lymphatic ECs and binds VEGF-C and VEGF-D but not VEGF-A. VEGFR-3 has shown to be involved in the regulation of lymphangiogenesis and lymphatic endothelium maintenance. Furthermore, it also takes a regulatory role in the formation of the blood vessels during embryogenesis [44,45].

*Proliferation:*

VEGF acts as a mitogen for ECs, and it stimulates proliferation via activation of VEGFR-2 which triggers RAS/ Rapidly Accelerated Fibrosarcoma (RAF) /extracellular signal-regulated kinase (ERK)/ Mitogen-activated protein kinase (MAPK) pathway stimulates proliferation of ECs [46,47]. One thing to note is that VEGFR-2 stimulates the ERK via pY1175-dependent phosphorylation of phospholipase C-γ (PLCγ) and subsequent activation of Protein kinase C (PKCs) whereas most of the receptor-type tyrosine kinases (RTK) mainly uses growth factor receptor-bound protein (GRB2)/RAS pathway for this. Alternatively, activation of PKC results in activation of protein kinase D (PKD), which promotes the proliferation of ECs [48].

*Migration:*

Various signal transducers bind to the phosphorylated tyrosines Y951, Y1175, and Y1214 and promote VEGF-dependant migration of endothelial cells. Y951 binds T Cell–Specific Adapter (TSAd) which creates a complex with Rous sarcoma oncogene cellular homolog (SRC) in a VEGF-dependent manner [49]. Y1175 binds SH2 Domain Containing Adaptor Protein B (SHB) which binds focal adhesion kinase (FAK) and regulates cell adhesion dynamics and migration [50]. Y1214 allows the formation of the non-catalytic region of tyrosine kinase adaptor protein (NCK)/FYN complex which promotes phosphorylation of p21-activated kinase-2 (PAK-2) that activates the Cdc42 and p38 mitogen-activated protein kinases (p38MAPK) to induce migration [51].

*Survival:*

VEGFR-2 dependent activation of Phosphoinositide 3 kinase (PI3K)-AKT8 virus oncogene cellular homolog (AKT) signalling with the activation of y951 promotes survival of EC via **the** production of phosphatidylinositol 3,4,5-trisphosphate ($PIP_3$) which mediates phosphorylation of protein kinase B (PKB)/AKT [52]. AKT phosphorylates B cell leukaemia 2 protein (BCL-2) associated death promoter (BAD) and caspase 9 and inhibits apoptotic activity of ECs [53].

*Permeability:*

VEGFR-2 activation regulates the permeability of ECs via endothelial nitric oxide synthase (eNOS)-mediated generation of nitric oxide (NO) [54] which can be activated by either PLCγ or AKT/PKB pathway.

VEGFR-2 signalling and trafficking pathways mediated by VEGF are given in Figure 5.

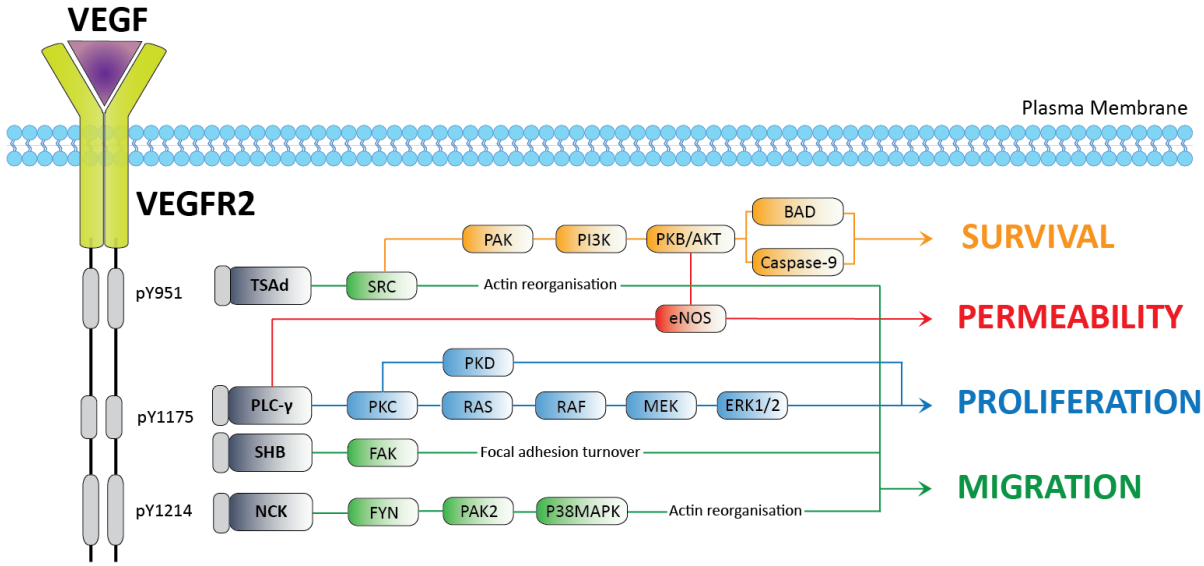


***Figure 5.*** *Molecular mechanism of VEGFR2 dependant angiogenesis*

1.3.1.1.2. Platelet-Derived Growth Factor (PDGF)

PDGF is another stimulator of angiogenesis through its receptors, and it is produced in several cell types, including platelets, macrophages, fibroblasts, and ECs [55]. PDGF signalling stimulates angiogenesis particularly by mediating vessel maturation which causes stabilisation and integrity of the newly formed blood vessels [56].

1.3.1.1.3. Angiopoietins (Ang-1 and Ang-2)

Angiopoietins are paracrine factors, and they are ligands for tyrosine kinase receptor (Tie-2). Ang-2 plays a role in the destabilisation of vessels and degradation of ECM, proliferation and migration of endothelial cells where Ang-1 takes part in vessel stabilisation [17,18].

#### 1.3.1.1.4. Transforming growth factor-beta (TGF-β)

TGF-β is a member of TGF superfamily and has known effects on tissue morphogenesis including apoptosis, cell proliferation, cell adhesion, differentiation, inflammation, cell migration and angiogenesis. Unlike VEGF which protects cells from apoptosis, TGF- β induces EC apoptosis. Although, TGF- β has a positive effect on angiogenesis *in-vivo*, *in-vitro* it inhibits EC growth and proliferation [57]. Thus, the effect of TGF- β on angiogenesis is found to be dependent on its concentration. At low concentrations, it has a positive effect on angiogenesis, whereas the effect is negative at high concentrations. In other words, while low concentrations of TGF- β play a role in proliferation and migration of endothelial cells during sprouting, high doses of TGF- β induce vessel stabilisation [58].

#### 1.3.1.1.5. Fibroblast Growth Factor (FGF)

FGF-1 and FGF-2 are growth factors that have positive effects on angiogenesis and are mitogenic to cell types such as ECs and fibroblasts. Particularly, FGF-2 (also known as bFGF) increases the expression of VEGF, which plays a key role in angiogenesis. Moreover, FGF-2 has a role in the sprouting stage of angiogenesis by stimulating the breakdown of ECM in ECs. This breakdown then allows the migration of ECs to form tubes like capillaries [59,60].

#### 1.3.1.1.6. Estradiol (E2)

As an alternative to VEGF, E2 has been shown to promote endothelial cell migration and proliferation *in vitro* [61,62] and to stimulate new blood vessel formation both *in vitro* and *in vivo* [63]. E2 has an important role in neovascularisation during the menstrual cycle [64,65]. It is used clinically in the treatment of osteoporosis and heart disease [66]. Moreover, blocking the E2 receptor with adjuvants such as tamoxifen for estrogen receptor-positive tumours, in which high estrogen helps the cancer cells grow and spread, is an effective method to reduce tumour vasculature. This therapy has been in clinics for many years, especially for the treatment of breast cancer [67,68]. Recently, our group confirmed that poly-L-lactic-acid (PLLA) scaffolds loaded with E2 were highly angiogenic using the CAM assay [69].

#### 1.3.1.1.7. Thymidine Phosphorylase (TP) & 2-deoxy-D-Ribose (2dDR)

Phosphorylases catalyse the addition of a phosphate group from an inorganic phosphate to an acceptor. In the body, Thymidine phosphorylase (TP) plays an important role to recover nucleosides after DNA degradation. Although the reaction is reversible, TP's function is primarily catabolic [70,71]. TP has an amino acid sequence identical to platelet-derived endothelial cell growth factor (PD-ECGF) [72,73] and is an enzyme that catalyses phosphorylation of thymidine to thymine [74,75] and 2-deoxyribose-1-phosphate (2dDR1P). 2dDR1P will then be dephosphorylated within the cytoplasm to 2-deoxy-D-Ribose (2dDR), which is the form that can pass the cell membrane. It has previously been shown that addition of thymidine to platelets gave rise to thymine and 2dDR but not 2dDR1P in the extracellular medium [70], which clearly shows that the phosphate is removed within the cytoplasm. Dephosphorylation allows the mobility of 2dDR from the cell membrane.

The angiogenic activity of TP is known to be dependent upon its enzymatic activity [76–78] although its molecular mechanism is still unclear. There are two possible reasons for ECs to be attracted (as an indicator of angiogenesis) to an area where there is an enzyme activity; (i) the substrate (thymidine) for the enzymatic reaction or (ii) the products are chemoattractant. Since thymidine has not been found as an chemoattractant for ECs, the latter reason, which is the catalytic release of 2-deoxy-D-ribose (2dDR), has been considered to be the reason for TP's angiogenic activity [71,79]

2dDR is one of the degradation products of thymidine, and it has previously been reported to have a chemotactic and angiogenic activity *in vitro* and *in vivo* [80,81]. However, no other similar molecules, including thymidine, thymine, 2-deoxy-L-ribose (2dLR), 2-deoxy-D-ribose-1-phosphate (2dDR1P) have been reported to be angiogenic when compared to 2dDR [71,81]. To date, several groups explored 2dDR's angiogenic potential using *in vitro* and *in vivo assays*. 2dDR has been shown to enhance proliferation and migration [82], induce tubulogenesis [83,84], inhibit hypoxia-induced apoptosis [85], and increase VEGF and IL-8 production [86] *in vitro*. Recently, our group demonstrated that 2dDR is not only angiogenic but also stimulates wound healing released from a hydrogel in a rat skin wound model [87].

In addition to this very limited literature on 2dDR, during my PhD research, we have demonstrated an effective dose range that can be used to stimulate proliferation, migration and tube formation of ECs *in vitro* [88] and to stimulate angiogenesis and wound healing *in vivo* using the *ex-ovo* CAM assay [89] and diabetic rat wound healing model [90], which will be explained in detail in further chapters of this thesis.

The enzymatic reaction of the degradation of thymidine to thymine catalysed by TP is given in Figure 6.

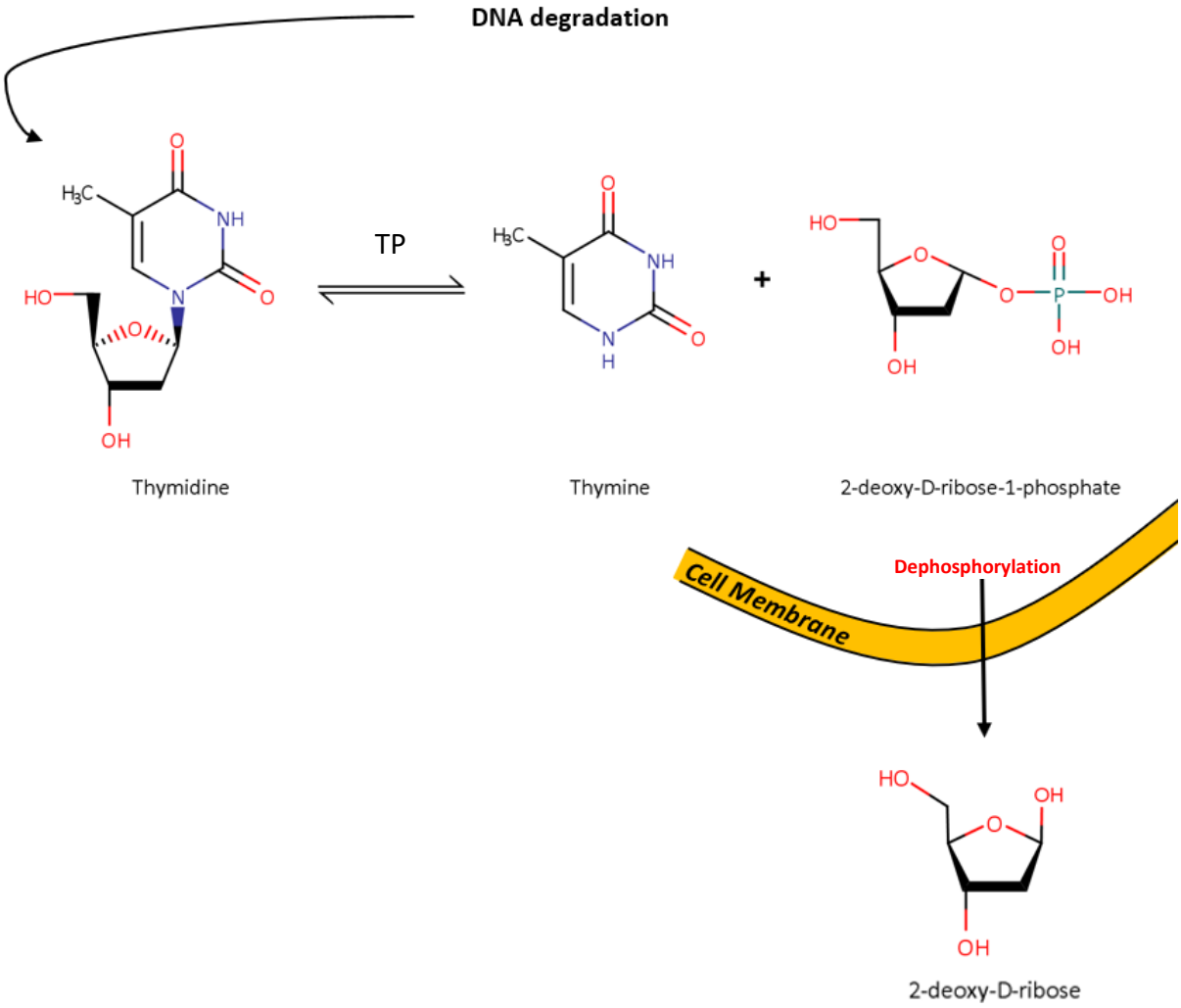


***Figure 6.*** *The enzymatic reaction of the degradation of thymidine to thymine catalysed by TP. Dephosphorylation of 2dDR1P allows the mobility of 2dDR from the cell membrane.*

There are only limited groups working to explore its potential in the field of angiogenesis inducers as explained above. Thus, to date, the literature on the angiogenic activity of 2dDR is not very comprehensive. PubMed was screened for the articles in which 2dDR, TP and VEGF were studied for their angiogenic activity. Only 29 studies (including 3

publications from our group) were found studying the potential angiogenic effect of 2dDR to date whereas there were 447 and 34556 studies on the angiogenic activity of TP and VEGF, respectively. As can be seen from PubMed screening of these three pro-angiogenic agents, the literature on 2dDR still needs to be investigated. Screening of PubMed and Web of Science databases (from 1970 to date) to find the number of publications on several angiogenic factors is given in Table 2.

***Table 2.*** *Screening of PubMed and Web of Science databases to find the number of publications on established pro-angiogenic factors*

| **Pro-angiogenic agent** | **Number of publications on:** | |
|---|---|---|
| | **PubMed** | **Web of Science** |
| *VEGF* | 34556 | 37995 |
| *PDGF* | 2730 | 2801 |
| *TGF-β* | 2584 | 3143 |
| *FGF* | 6595 | 11297 |
| *E2* | 718 | 824 |
| *TP* | 447 | 679 |
| *2dDR* | 29 | 23 |

Distribution of the angiogenesis-related publications about 2dDR and TP (combined) on the PubMed database over the years (from 1970 to date) is given in Figure 7.

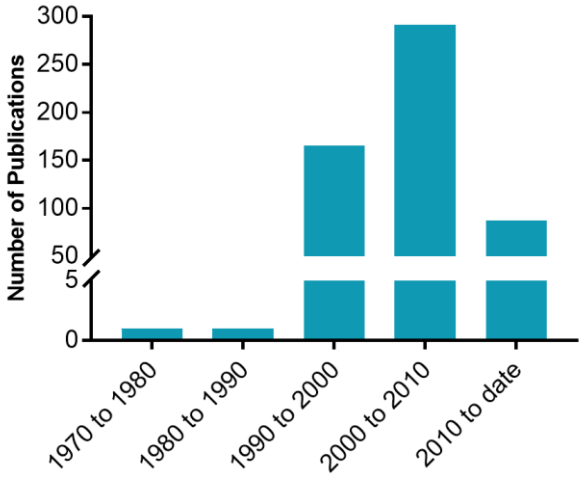


***Figure 7.*** *Distribution of the angiogenesis-related publications about 2dDR and TP (combined) on PubMed database by years (from 1970 to date)*

To clarify the literature on how TP and 2dDR can potentially be an alternative agent as an alternative to VEGF, the milestones of the exploration of them to date are given in Figure 8.

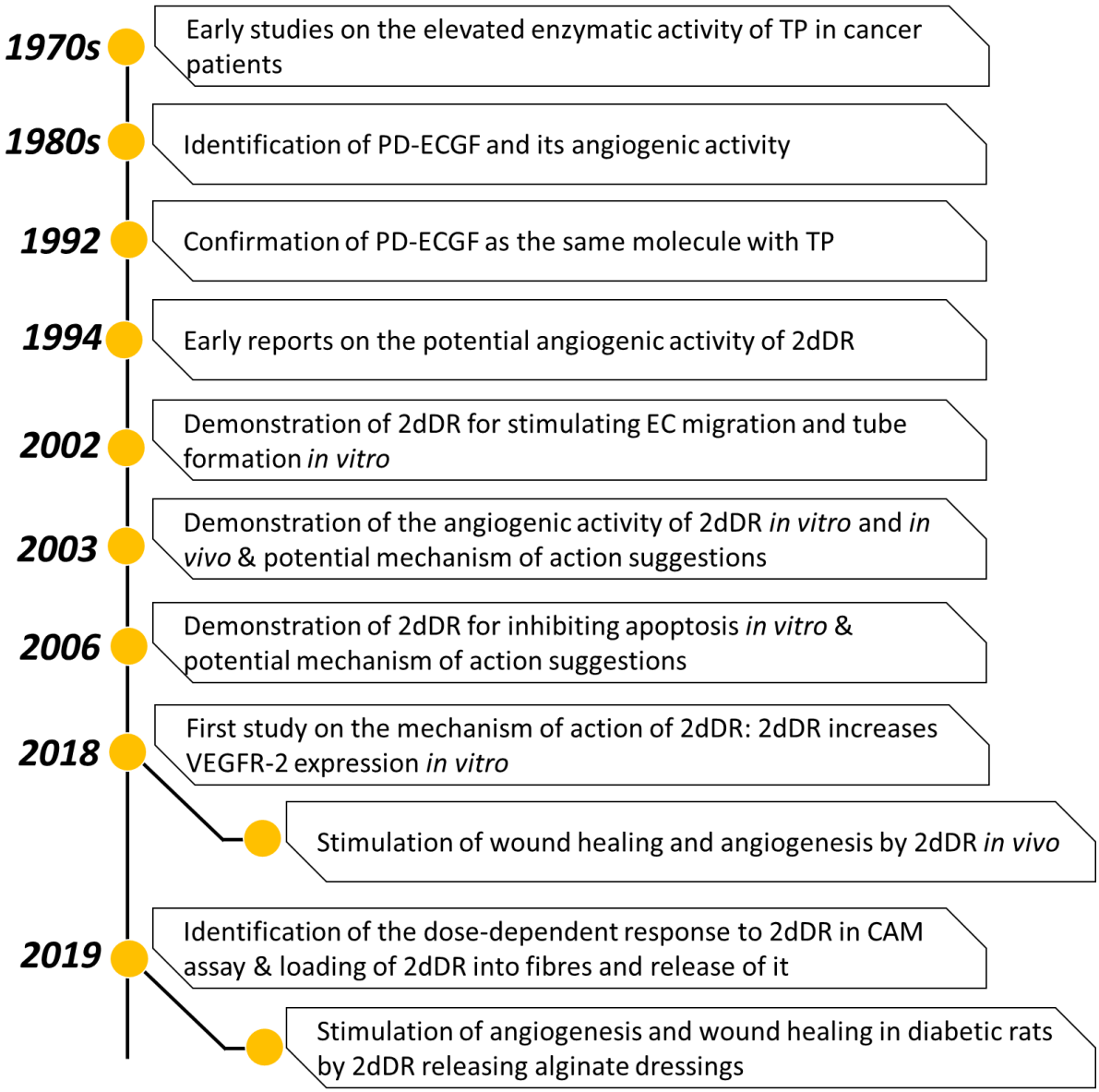


***Figure 8.*** *Timeline showing the key studies on TP and 2dDR for the exploration of the angiogenic activity of 2dDR*

#### 1.3.1.2. ECM integrins and matrix-degrading enzymes

ECM is the non-cellular component and responsible for providing physical support to cells and tissues. However, beside its mechanical support function, it is also involved in many biochemical processes which regulate cellular functions which take part in angiogenesis [91].

The mechanism of action of ECM components is mostly regulated by the cell-surface receptors, integrins. The major integrins found on ECs include but are not limited to $\alpha_1\beta_1$, $\alpha_2\beta_2$, $\alpha_3\beta_1$, $\alpha_5\beta_1$, $\alpha_6\beta_4$, $\alpha_6\beta_1$, and $\alpha_v\beta_3$. Among all these integrins $\alpha_v\beta_3$ has been studied

widely for its importance in the angiogenic processes. In addition to its arginylglycylaspartic acid (RGD) peptide sequence binding properties, the interaction between $\alpha_v\beta_3$ integrin and VEGF-R2 has been investigated [92,93]. The affinities of the integrins to the ECM molecules and the cellular mechanisms that are involved are given in Table 3.

***Table 3.*** *The affinities of the integrins to the ECM molecules and the cellular mechanisms which they involve*

| Integrin | Affinity to | Cellular mechanism |
|---|---|---|
| ***α1β1*** | Collagen | Regulates the responsiveness of VEGFR-2 to VEGF and promotes angiogenesis via VEGF pathway [94] |
| ***α2β1*** | Collagen | Regulates the responsiveness of VEGFR-2 to VEGF, and promotes tube formation [94,95] |
| ***α3β1*** | Laminin | Regulates EC adhesion and promotes migration [96] |
| ***α6β4*** | Laminin | Regulates EC adhesion and promotes migration [97,98] |
| ***α6β1*** | Laminin | Regulates EC adhesion [98,99] |
| ***α5β1*** | RGD sequence: Fibronectin | Regulates / promotes migration [100] |
| ***αvβ3*** | RGD sequence: Vitronectin, Fibronectin | Regulates VEGFR-2 activation: migration, survival, and matrix degradation [93,101] |

Several ECM molecules have been reported for their angiogenic or anti-angiogenic activities. Collagen [102], laminin [103], fibronectin [104], and vitronectin [105] have previously been reported to participate in promoting angiogenesis as summarised in Table 3. Similarly, hyaluronan has been shown to have antiangiogenic effects when it is present in a high molecular weight form under a native environment. However, when it breaks down into smaller segments and has a lower molecular weight, it has been reported to have angiogenic activity [106].

During the angiogenic process in ECM, matrix metalloproteases (MMPs), extracellular endopeptidases which selectively degrades ECM proteins, also plays a critical role in the

degradation of ECM for the release of angiogenic factors that are stored in ECM. However, the enzymatic activity of MMPs is highly regulated by the protease inhibitors in order to prevent over degradation of the ECM which also guides the ECs proliferation and migration and thus, excessive release of angiogenic factors from it. Several types of cells can produce MMPs such as ECs, stromal cells, inflammatory cells, and tumour cells [107,108]. Some of the MMPs produced by ECs and that play a role in angiogenesis are MMP-1 (Collagenase 1), MMP-2 (Gelatinase A), MMP-9 (Gelatinase B), and MMP-14.

### 1.3.2. Mechanical factors

Every single cell in their native environment in body is exposed the several mechanical forces either self-generated, or ECM related [109]. Thus cells continuously receive the mechanical forces and transduce them into biochemical signals which results in alteration of several ECM genes and thus, protein expression levels in order to maintain their structure and shape in their native environment [110]. Apart from the ECM forces they are exposed, cells also generate mechanical forces which will act on ECM. These cellular forces are called as cell traction forces (CTFs). For this reason, adherent cells are under tension created by cell-ECM contacts, and they use these CTFs for remodelling their adhesion and migration profiles, which can be linked with angiogenesis when it comes to ECs and communicating with adjacent cells [110,111].

Blood vessels are also continuously exposed to external forces either due to the flow of blood or the extracellular environment. ECs are highly mechanosensitive, and they are reported to have phenotypic and functional changes based on various flow patterns [112]. Shear stress is the main force acting on ECs, and it has previously been reported to reduce the apoptosis while increasing the VEGF expression [113] and regulates EC proliferation and migration, which are essential for sprouting [114].

The key steps and the biochemical/mechanical regulators of angiogenesis is given in Figure 9.

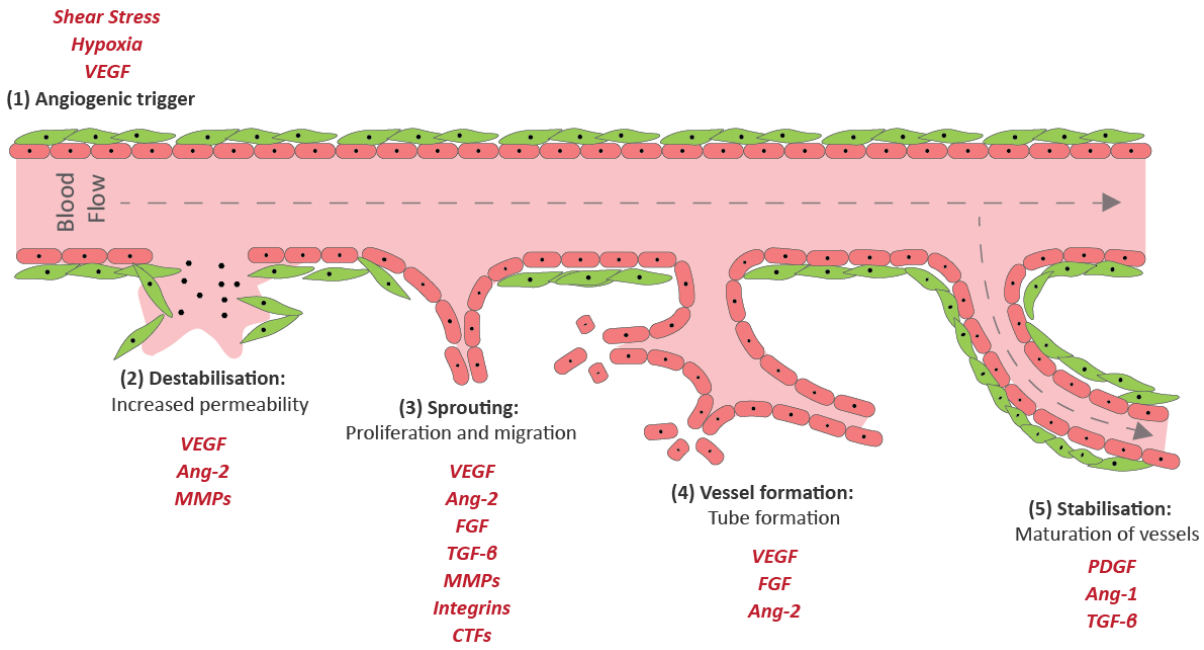


***Figure 9.*** *The key steps and the chemical and mechanical factors that regulate angiogenesis*

The functions of the biochemical and mechanical factors in the steps of angiogenesis are summarised in Table 4.

***Table 4.*** *Summary of biochemical and mechanical factors that regulate the key steps in angiogenesis*

| Angiogenic Step | Factor | Function |
|---|---|---|
| *Angiogenic Trigger* | Hypoxia | Activation of angiogenesis-related genes due to reduction in oxygen [32]. |
| | Shear Stress | Shear stress caused by laminar flow has been reported to reduce the apoptosis while increasing the VEGF expression [113] and demonstrated to regulate EC migration [114]. |
| *Vessel Destabilisation* | VEGF | Increases the vessel permeability [47,115]. |
| | Ang-2 | Mediates EC monolayer destabilisation and loosen EC-pericyte interaction [17,18]. |
| | MMPs | Breaks down ECM to maintain a space for ECs to migrate and proliferate [107,108]. |
| *Vessel sprouting* | VEGF | Stimulates EC proliferation and migration |
| | Ang-2 | Maintains the loosen space for ECs to migrate [17,18]. |
| | FGF | Stimulates to generation of MMPs [59,60]. |
| | MMPs | Degrades ECM not only to maintain a space for ECs to migrate and proliferate but also to regulate the release of angiogenic factors that is naturally stored extracellularly [107,108]. |
| | TGF-β | Induces endothelial proliferation and migration. Regulates MMPs at lower concentrations [58]. |
| | Integrins | Regulates matrix degradation VEGFR-2 activation and subsequently proliferation, migration, and survival of ECs [92,93,101]. |
| | CTFs | Helps ECs to migrate [110,111]. |
| *Vessel Stabilisation* | TGF-β | Inhibits EC proliferation and induces basement membrane reformation [58]. |
| | PDGF | Promotes vessel stabilisation and maintains vascular integrity [56]. |
| | Ang-1 | Induces pericytes recruitment and vascular maturation [116] |

## 1.4. Current Strategies to Overcome Slow Neovascularisation in TE constructs

### 1.4.1. Use of proangiogenic cells (prevascularisation)

Prevascularisation approach aims to generate a preformed microvascular structure within the scaffold prior to implantation. This primitive microvascular network can then anastomose simultaneously with the surrounding host microvasculature rapidly upon implantation and supply nutrients to the construct in a reduced time [26,117].

#### 1.4.1.1. *In vitro* prevascularisation systems

##### 1.4.1.1.1. Seeding vessel-forming (pro-angiogenic) cells

Cell seeding is one of the most widely used *in vitro* prevascularisation technique where cells which have vessel-forming capabilities are seeded on TE or natural (decellularised) scaffolds.

In the early studies, endothelial cells have been used as pro-angiogenic cell sources [118]. Scientists reported successful inosculation of the formed microvasculature with the host tissues within the first ten days of implantation when ECs are seeded on various biomaterials including calcium phosphate cement [119], polymer scaffolds [120,121], collagen [122]. Although they have great potential to be used in prevascularisation studies, use of ECs also bears some disadvantages such as difficulties for harvesting ECs in large quantities, slow proliferation during cultivation, and showing different angiogenic properties in terms of permeability, immune tolerance and angiogenic potential when harvested from different sources [123,124]. Thus, fast proliferating endothelial progenitor cells (EPCs), which can be harvested from bone marrow or peripheral blood, were suggested as alternatives to overcome these drawbacks [125,126]. Apart from EPCs, scientists also reported successful prevascularisation of tissue engineering constructs with the use of mesenchymal stem cells (MSCs) [127,128], which can be harvested from bone marrow or adipose tissue.

Tissue engineering constructs used for *in vitro* prevascularisation approaches can be derived from either synthetic or natural sources, and selection of material is critical as it affects the degradation time *in vivo* and integrity of the TE construct in terms of structure and function [129]. A large number of scaffold materials can be used in this approach.

Synthetic polymers are widely used as scaffold materials because of their controllable properties to mimic the natural environment. Polycaprolactone (PCL) [130–132], Poly-L-lactic acid (PLLA) [133,134], poly(glycolic acid) (PGA) [135], poly(lactic-co-glycolic acid) (PLGA) [136], polyurethane (PU) [137,138], poly(glycerol sebacate) (PGS) [139], and their composites are widely used synthetic biodegradable polymers for prevascularised TE constructs. On the other hand, natural polymers are abundant and contain components that are naturally presented in biological extracellular matrices, which makes these polymers more compatible for implantation and supporting cell function. The most common natural-origin polymers used in tissue engineering applications are Polyhydroxyalkanoates (PHAs) such as Poly (3-hydroxybutyrate) (PHB) [140], Poly (3-hydroxyoctanoate) [141], Poly(3-hydroxybutyrate-co-3-hydroxyvalerate) (PHBV) [142,143], and other natural polymers including collagen [144–146], elastin [147], silk fibroin [148,149], gelatin [59,150], cellulose acetate [151], polyethylene glycol (PEG) [152,153], dextran [154], and hyaluronic acid (HA) [145].

Developing a synthetic vascular architecture is a good approach to promote enough cell attachment as well as storing and releasing angiogenic factors. The channels can be created by combining several methods such as 3D printing and leaching [155], 3D printing and electrospinning [143,156], direct bioprinting of cell-laden hydrogels [157,158] with biomimetic ECM structure [159], photolithography [160] can act as an angiogenic factor releasing bioreactor for appropriate cell types which can be cultured inside the channels to form tubule-like structures prior to implantation.

On the other hand, development of decellularised natural constructs for their use in *in vitro* prevascularisation studies is a well-established and promising way of scaffold fabrication. In this technique, biological tissues or organs with natural vasculature can be obtained by decellularising, and then they can be repopulated with appropriate cells before implantation to create prevascularised TE constructs. These kinds of structures provide a natural environment for cells to attach and form new microvascular structures [161]. Some examples for *in vitro* use of natural structures are acellular cadaveric hearts which were recellularised with cardiac cells and rat aortic ECs [162], decellularised porcine jejunum was seeded with porcine ECs [163], acellular porcine heart was then reseeded with human umbilical vein endothelial cells (HUVEC) [164], and recently our group developed a decellularised rat intestine repopulated with Human Dermal

Fibroblasts (HDFs) and Human Dermal Microvascular Endothelial Cells (HDMECs) [165]. Recently, Gershlak et al., demonstrated that decellularised spinach leaves could be recellularised with human ECs used as prevascularised constructs [166,167].

#### 1.4.1.1.2. Generating spheroids from proangiogenic cells

Spheroids are 3D cell clusters generated by several methods such as the hanging drop, the non-adhesive surface, the micromolding, spinner flask, and rotary system techniques [168], and they are used in various biomedical applications including but not limited to angiogenesis, drug discovery, toxicity analysis, and cancer studies [169–172]. Over the last years, spheroids were also reported for their use in prevascularisation studies. ECs are combined with various cell types to successfully create prevascularised tissue constructs such as prevascularised bone when ECs combined with osteoblasts [173], prevascularised adipose tissue when ECs are combined with adipose-derived stromal cells [174]. Beside the use of ECs, spheroids formed with the use of MSCs were also reported as *in vitro* prevascularised constructs [175].

#### 1.4.1.1.3. Cell sheet technology

Cell sheet technology is a scaffold-free method where a temperature-sensitive smart surface (poly-(N-isopropylacrylamide) (PIPAAm)) is used for generating prevascularised cell sheets [176,177]. Several examples of prevascularised tissues have been reported including but not limited to prevascularised fibroblast cell sheets [178], bone cell sheets [179] cardiac cell sheet with ECs [180,181], and without any other cell types (ECs in isolation) [182] or with periendothelial cells [183].

### 1.4.1.2. *In vivo* prevascularisation systems

*In vivo* prevascularisation is another approach to overcome slow neovascularisation problem. In this approach, natural vasculature of the host (like a natural bioreactor) is used to prevascularised the developed construct. The most basic approach is to implant a scaffold into a well-vascularised part of the host, such as subcutaneous skin [184]. Similarly, prelamination or flap technique, which is defined as the implantation of scaffolds into a muscle flap for prevascularisation to occur [185]. The importance of the flap technique is that this method has been reported as the first successful example of *in*

*vivo* prevascularisation techniques which were clinically used in an adult male patient [186]. The Arteriovenous (AV) loop technique is another method for fabricating prevascularised constructs. It was originally developed in the late 1970s when an arteriovenous fistula was constructed, and its shape is a loop leading to new capillary formation into that loop [187]. The method of prevascularisation via an AV loop technique is that when the AV loop is placed in a protected space (i.e. a chamber) filled with appropriate ECM contents (soft or hard matrices), a prevascularised construct in a defined shaped can be generated [188]. Several matrix materials either enriched with growth factors or not have been reported for their use in an AV loop prevascularisation technique; soft matrices such as Matrigel [189], fibrin [190], and natural dermis [191] and hard matrices such as PLGA [192] and bovine cancellous bone have been used [193,194].

### 1.4.2. Use of pro-angiogenic agents (functionalisation of the scaffolds)

Growth factors are key elements in regulating angiogenesis, and therefore incorporation of these growth factors into TE constructs to ensure rapid neovascularisation upon implantation is a widely studied approach. In the developed scaffolds, growth factors can be directly used either on their own: VEGF [195], PDGF [196] or in combination with other factors such as PDFG and VEGF together [197] to promote vascularisation. Details of the well-established proangiogenic factors were given in Section 1.3.1.1.

In addition to direct use of well-established growth factors, indirect activation of these growth factors have been established with the delivery of other biomolecules such as heparin [198], hypoxia-inducible factor 1 (HIF-1) [199], bone morphogenetic protein (BMP) [200], and sonic hedgehog homolog (SHH) [201].

Functionalised scaffolds with growth factors can be fabricated using either synthetic or natural polymers, and carry single or multiple growth factors in order to deliver these growth factors in a controlled manner [202]. The selection of materials is especially important according to the intended usage area as the growth factor release profile will be influenced by varying degradation rates and the degradation profile of the material, which depends on the chemistry and geometry of the material [26]. One approach to control these factors is material selection. However, a novel approach has been suggested to overcome this problem in an on-demand manner, which is a specific chemical linkage

of the growth factors to a gel matrix which will be degraded by the MMPs that is naturally secreted by the endothelial cells of the host. This degradation will enable cells to release growth factors in response to a need in a local area [203].

## 1.5. Established Angiogenesis Assays

### 1.5.1. *In vitro* angiogenesis assays

#### 1.5.1.1. EC proliferation assays

The proliferation of ECs plays a key role in sprouting angiogenesis. Thus, proliferation assays are commonly used to study angiogenesis *in vitro.* They are quick, reproducible, inexpensive and easy to perform. Proliferation assays can be performed using various tools [204,205].

Determining the net cell number is the simplest method where a defined number of ECs are seeded and treated with proangiogenic or antiangiogenic drugs, and after a certain period of time, the increase in the number of ECs is measured by counting cells using a haemocytometer or automated devices [206,207].

Another widely used method is tracking the metabolic activities of ECs via metabolic activity assays such as the 3-(4,5-dimethylthiazol-2-yl)-2,5-diphenyl-2H-tetrazolium bromide (MTT), which is based on enzymatic conversion of yellow coloured tetrazolium salt to purple/blue coloured water-insoluble formazan crystals by living cells. This enzymatic reaction occurs by the activity of nicotinamide adenine dinucleotide phosphate (NADPH)-dependent cellular oxidoreductase mainly at mitochondria. The water-insoluble formazan crystals then can be dissolved in dimethyl sulfoxide (DMSO), and the solubilised formazan product is quantified using a plate reader. A reference curve can be used to correlate the formed formazan crystals by ECs with the cell number [208,209]. As an alternative to MTT, AlamarBlue® assay (also known as resazurin reduction assay) is a well-established method for the quantification of metabolic activity of cells. The principle of this assay is based on irreversible NADPH-dependant reduction of weakly fluorescent resazurin to purple coloured and highly fluorescent resorufin mainly in the mitochondria of the living cells. The biggest advantage of the AlamarBlue assay is that it is a non-destructive method which means the same samples can be used for the measurement of metabolic activities at different time points [210].

DNA synthesis is another method for the assessment of ECs proliferation, which is based on the determination of bromodeoxyuridine (BrdU), a molecule competing for thymidine for incorporation into DNA during replication, by immunocytochemistry or by ELISA to determine the total number of cells [211,212].

Quantitative methods for the determination of DNA content in different time points is an alternative method to investigate the proliferation of ECs. PicoGreen assay is a well-known method to quantify DNA content which can be used to assess ECs proliferation. The principle of this assay is based on the affinity of PicoGreen fluorescent probe to double-stranded (ds) DNA which creates a highly fluorescent complex. The major interactions of PicoGreen binding to dsDNA are intercalation (the insertion of the dye between the planar bases of dsDNA) and electrostatic attractions [213].

#### 1.5.1.2. EC migration assays

During angiogenesis, ECs migrate into the perivascular area by degrading the basement matrix in response to stimulation. Therefore, assessment of the migratory response of ECs is recognised as an important marker of angiogenesis. A modified version of a Boyden chamber assay, originally developed for studying leukocyte chemotaxis in the 1960s [214], is a frequently used method for the assessment of EC migration *in vitro*. It is a type of transfilter assay which consists of two chambers and is based on the migration of ECs from the upper chamber (upper side of the filter) to the lower chamber (lower side of the filter) in response to a chemoattractant [215]. The migrated cells can be stained with various dyes (such as crystal violet) and quantified by either manual counting of cells by eye, which is difficult and time consuming, or image processing. The Boyden chamber assay is easy to perform, fast, inexpensive, accurate and reproducible [205].

Scratch assays, or *in vitro* wound healing assays, are also widely used assays for the determination of the migratory response of ECs to an external stimulus. Briefly, a scraping tool is used to remove a known area of confluent EC monolayer, which creates a margin for ECs to migrate into and close the scratch [216]. The migration rate and the closure of the scratched area can be calculated by capturing the closure at different time points using several microscopy techniques. The results can be quantified by processing the images using image processing software such as ImageJ. The biggest advantage of this

method is the continuous monitoring of cell migration (at different time points) which can be used to estimate the rate of migratory response [217].

As an alternative method, cell motility can be measured directly by phagokinetic tracking methods. The earliest version of this type of assay was based on using colloidal gold-plated coverslips which were replaced by the preparation of 96-well plates by depositing of 1 μm polystyrene beads onto the bottom of the wells. In both versions of the cell motility assays, ECs generate tracks either on colloidal gold-plated coverslips or polystyrene beads, which can be used to determine the directional properties and total distance of migration [205,218]. Although this method is an accurate way of measuring the motility of ECs, the analysis of the results is time consuming, and it requires complex software to track cell paths.

#### 1.5.1.3. EC differentiation (tube formation) assays

The EC differentiation assays are based on evaluating the formation of tube-like structures that are regarded as mimicking the differentiation stage of angiogenesis in response to proangiogenic or antiangiogenic compounds. The simplest differentiation assays are those where ECs are plated onto/into gel layer (such as Matrigel, collagen or fibrin gel), which act as a basement matrix to promote attachment, migration and tube formation of ECs. The selection of the gel matrix is particularly important for the quality of the assessment. Using collagen I and III can result in enhanced proliferation of ECs but not tube formation while collagen IV and V show an exact opposite reaction [219,220]. Matrigel® is the trade name of a gelatinous protein mixture derived from a hamster fibrosarcoma, which is rich in collagen IV, laminin, proteoglycans and growth factors. This biologically active protein mixture has been shown to be a good candidate for mimicking native basement membrane of ECs *in vitro* and promotes ECs to form tube-like capillary structures [221]. More recently, a company has introduced a growth factor reduced version of Matrigel, which helps to reduce the unspecific reaction of ECs with the cytokines and growth factors naturally presented in the matrix to form tube-like structures [205].

An alternative tube formation assay is that ECs are co-cultured with a stromal type of cells (fibroblasts, SMCs or pericytes) either in the presence or absence of an ECM. The assay is based on the assessment of tube formation within the ECM secreted by stromal cells.

In addition to 2D assays, 3D tube formation assays have previously been developed where ECs are seeded between two layers of gels (such as collagen, fibrin or Matrigel). This method enables the evaluation of the tube formation in two different planes. It has been reported that ECs form tube-like structures in horizontal plane in 7 days, whereas after day 15, the existing tubules branch upwards and create a 3D network [222]. The major drawback of 3D tube formation assays is that the difficulty of analysing the results as the imaging should ideally be performed in more than one plane.

### 1.5.2. *Ex vivo* angiogenesis assays

#### 1.5.2.1. Rat aortic ring assay

The aortic ring assay has been developed following the observation of spontaneous branching from aortas when cultured *in vitro* [223] in order to mimic *in vivo* angiogenesis *in vitro* [204,205]. The aortic ring assay is a commonly used method for studying angiogenic activity in response to a drug. Briefly, the explanted aorta (usually from rats) is cleaned to remove the surrounding fibrous and adipose tissue before cutting into smaller segments (usually 1 mm thick). Aorta segments are then embedded in matrix gels such as collagen, fibrin, or Matrigel [224,225] and the outgrowth of vessels in response to a stimulus or deterrent can be analysed via imaging the rings at different time points. The aortic ring assay is an effective way of evaluating angiogenic or antiangiogenic response. However, the drawbacks of this assay are the ethical concerns, special skill requirement and difficulties of quantification [226].

#### 1.5.2.2. Chick aortic arch assay

A modified version of the rat aortic ring assay is where the chick aortic arch is used to study angiogenesis *ex vivo* [227]. The ECs of chick aortic arch shows the characteristics of microvascular cells. The chick aortic arch assay is rapid and inexpensive and raises less ethical concerns (when compared with rat aortic arch assay). The major disadvantage of this assay is that the aortic rings are explanted from immature embryos, whereas the ECs are very proliferative. Thus, it does not fully represent angiogenic sprouting *in vivo* [205].

### 1.5.3. *In vivo* angiogenesis assays

#### 1.5.3.1. Chick chorioallantoic membrane (CAM) assay

The CAM of the chick embryo is an extraembryonic membrane that functions as an organ for gas exchange between the embryo and the environment. It is home to a lot of blood vessels with a dense capillary network, and because it stays on top of the developing embryo, it is easily accessible for experimental interventions. The chick is relatively immunotolerant, and the CAM assay has traditionally been used to test the pro and anti-angiogenic response to drugs [228], to study many aspects of tumour angiogenesis [229,230], to study mammalian tissue explants [231] since the 1970s when it has been introduced to the world of angiogenesis by Folkman et al. [232]. With recent advances in biomaterials science and engineering, another area where the CAM assay can prove useful is in biomaterials testing.

The CAM assay can be a valuable assay to test biomaterials extensively *in vivo* before they are further investigated in relevant animal models [233]. In the context of biomaterials testing, the CAM can be effectively used as a short term host for grafted materials, organs and tissue samples where the angiogenic response and their safety and biocompatibility can be studied [234]. It is also promising that the CAM assay has recently been demonstrated to produce data that is comparable to mouse assays in testing biodistribution and *in vivo* stability of radiopharmaceuticals [235].

For the purpose of biomaterials testing *in-ovo* [236] and *ex-ovo* [69,237] culture methods have been used. The *ex-ovo* (embryo is cultured outside of the eggshell) modification of the classical *in ovo* CAM assay (embryo is cultured inside of the eggshell) offers several unique advantages for biomaterials testing. The ability to grow *ex-ovo* cultures with comparable survival rates was first reported in 1974 [232]. Although it was reported by several authors that the *ex-ovo* modification is associated with worse survival rates [238], our experience does not confirm this finding. We consistently have survival rates above 80% [69,239,240]. The main advantage of the *ex-ovo* culture method is better visualisation of the growing embryo and access to a larger area of the CAM to study angiogenesis. Additionally, the vascularisation process can be observed at all times during the experiment. Further details of the CAM assay and a step-by-step demonstration of the protocol can be found in our published video protocol paper [241].

Comparison of *in-ovo* and *ex-ovo* CAM assay procedures in terms of survival rate, ease of assay procedure, cost, CAM accessibility, and monitoring of angiogenesis is given in Table 5.

***Table 5.*** *Comparison of in-ovo and ex-ovo CAM assay procedures in terms of survival rate, ease of assay procedure, cost, CAM accessibility, and monitoring of angiogenesis. (+ = very low, ++ = low, +++ = medium, ++++ = high)*

| **Parameters** | ***In-ovo*** | ***Ex-ovo*** |
|---|---|---|
| Survival rate | ++++ | +++ |
| Technical challenge | ++ | ++++ |
| Cost effectivity | ++ | ++ |
| Accessibility of the CAM | ++ | ++++ |
| Monitoring of angiogenesis | + | ++++ |
| Quality of imaging of angiogenesis | ++ | ++++ |

#### 1.5.3.2. Corneal angiogenesis assay

The cornea is an avascular and translucent tissue, which makes it attractive for angiogenesis studies due to the fact that any blood vessel observed on corneal stroma will be newly formed and readily detectable [242,243]. The corneal angiogenesis assay is based on stimulation of ECs from the edge of the cornea to migrate and form new sprouts into space where the corneal epithelium and stromal cells located in response to an angiogenic signal. The corneal assay can be performed in various animal models such as the rabbit, rat, and mouse [244–246]. The major drawbacks of this assay are being expensive and showing different angiogenic responses in response to different types of injuries [247].

#### 1.5.3.3. Zebrafish assay

Zebrafish (Danio rerio), a translucent freshwater fish, is able to produce hundreds of embryos per week, and in recent years, it caught scientist's attention to be used in angiogenesis studies. Zebrafish angiogenesis assay provides some advantages such as being inexpensive, develop rapidly, share many genetic materials with mammals, and the

optical transparency of the embryos [248]. To visualise the newly forming blood vessels, various techniques can be used including such as alkaline phosphatase staining and confocal microangiography [249–251]

#### 1.5.3.4. The dorsal skinfold chamber assay

The principle of the dorsal skinfold chamber assay is based on the implantation of a translucent chamber which enables *in vivo* imaging of the blood vessel development in mammals. The visualisation of the vasculature can be performed via several microscopy techniques such as light transillumination microscopy (where the thickness of the tissue is less than 300 μm), epi-illumination microscopy or intravital microscopy [252]. The earliest example of the transparent chamber models is the rabbit ear chamber that was then adapted to be used in mice models in 1940s [253].

Several animal models have been used for chamber implantation to dorsal skinfold. These include mice, rat and hamster [254–256]. In this assay, a transparent chamber is implanted into dorsal skinfold of the animal, which enables the visualisation and quantification of angiogenesis *in vivo*. The parameters which can be evaluated include blood vessel density and blood flow velocity [248]. The major advantage of this model is that the evaluation of vessel growth in 3D is that it is possible to do when the animal is conscious over four weeks (no need to use multiple animals for different time points). Animals are placed in a restraining chamber for the duration (often several hours) of the assay. However, the assay is technically challenging and requires special skills to perform. Furthermore, the quantification is time consuming, and it requires complex image analysis systems [205].

#### 1.5.3.5. Animal matrix implantation assays

Various materials have been implanted into animals to monitor angiogenesis and/or wound healing. These materials include stainless steel meshes [257], polymer sponge matrices [258], and Matrigel plugs [259]. Such assays are performed by implanting a type of matrix scaffold (frequently Matrigel plug or a polymeric scaffold) subcutaneously into rat, mouse, or rabbit. The implant usually contains a test substance such as pro-angiogenic or anti-angiogenic agents, growth factors, cells, tumour fragments etc..) and angiogenesis in response to the test substance is assessed at the end of the assay which

is typically 7-10 days after implantation. The Matrigel plug or polymer matrix can then be explanted, fixed, sectioned and histologically evaluated for the angiogenesis. Although being relatively easy to set up and less time consuming make this assay versatile and powerful, the main drawbacks of this assay are non-specific host response to the implant, varying results depending on the material properties used (implant size, structure, pore size, porosity, interconnectivity etc..) [204,260]. In addition, Matrigel is an expensive and tumour-derived extract which contains intrinsic growth factors and cytokines, which may cause false-positive results and sectioning of Matrigel can be difficult and time consuming [205].

A summary of established angiogenesis assays is given in Table 6.

***Table 6.*** *A summary of established in vitro, ex vivo, and in vivo angiogenesis assays*

| | | **Advantages** | **Disadvantages** |
|---|---|---|---|
| ***In vitro assays*** | Proliferation assays | • Cost-effective<br>• Highly reproducible<br>• Short duration<br>• Sensitive<br>• Easy to set up<br>• Quantitative results<br>• No ethical concern | • Only one aspect of angiogenesis can be assessed<br>• Static conditions<br>• 2D environment<br>• Low representation of *in vivo* angiogenesis |
| | Migration assays | • Reproducible<br>• Relatively short duration<br>• Sensitive<br>• Can estimate migration rate and cell motility<br>• No ethical concern | • Only one phase of angiogenesis can be assessed<br>• Static conditions<br>• 2D environment<br>• Low representation of *in vivo* angiogenesis<br>• Quantification may lead to false results<br>• Results may vary depending on experimental conditions |
| | Differentiation assays | • Very short duration<br>• Sensitive<br>• Easy to analyse<br>• No ethical concern | • Only one phase of angiogenesis can be assessed<br>• Difficult to perform<br>• Static conditions<br>• 2D environment<br>• Low representation of *in vivo* angiogenesis<br>• Results may vary depending on experimental conditions |

| | | | |
|---|---|---|---|
| ***Ex vivo assays*** | Rat aortic ring assay | • Better mimicking of *in vivo* conditions<br>• Rapid assay procedure<br>• Relatively inexpensive<br>• Less ethical concern | • Technically challenging<br>• Difficult to quantify<br>• Static conditions<br>• Results may vary depending on experimental conditions |
| | Chick aortic arch assay | • More representative of *in vivo* conditions<br>• Rapid assay procedure<br>• Relatively inexpensive<br>• Less ethical concern | • Technically challenging<br>• Difficult to quantify<br>• Static conditions<br>• Results may vary depending on experimental conditions |
| ***In vivo assays*** | CAM assay | • More representative of *in vivo* conditions<br>• Rapid procedure<br>• Reproducible<br>• Relatively inexpensive<br>• Less ethical concern<br>• Allows to test multiple test substances in one experiment | • Technically challenging<br>• Very difficult to quantify<br>• Hard to distinguish between existing and newly formed blood vessels<br>• Non-specific reaction due to experiment conditions such as infection or physical irritation of the membrane |
| | Corneal assay | • Reliable<br>• Easy to quantify | • Expensive assay<br>• Technically challenging<br>• Results may vary depending on experimental procedure such as different wound types<br>• Use of an avascular tissue for studying angiogenesis is disputable<br>• Ethical concern |
| | Zebrafish assay | • Easy to monitor angiogenesis<br>• More representative of *in vivo* conditions<br>• Less ethical concern<br>• Inexpensive<br>• Rapid procedure<br>• Easy to quantify | • Use of fish ECs to study human angiogenesis can be disputable<br>• Requires to establish a zebrafish facility |
| | Dorsal skinfold chamber assay | • More representative of *in vivo* conditions<br>• Reliable results | • High ethical concern<br>• Technically challenging<br>• Invasive procedure<br>• Expensive<br>• Quantification is time consuming<br>• Requires complex image analysis systems |

| | | | |
|---|---|---|---|
| | Matrix implantation assay | • More representative of *in vivo* conditions<br>• Not technically difficult<br>• Easy to set up<br>• Can be used to study more than one aspect such as angiogenesis, wound healing, cell proliferation, invasion etc. | • Time consuming analysis of the explants<br>• Expensive<br>• Ethical concern<br>• Non-specific host tissue response to implant<br>• Variable results depending on the material properties used (implant size, structure, pore size, porosity, interconnectivity etc..) |

## 1.6. The Structure of Human Skin

Skin is the outmost layer of human body and serves as a physical barrier between the body and the external environment. Its function as a barrier is not limited to the prevention against microorganism invasion [261], but also includes prevention from dehydration, mechanical, chemical, and thermal damage, and exposure to ultraviolet (UV) [262,263]. Beside its main barrier function, skin also has a role in sensation and regulation of thermal, chemical, metabolic and immune system functions [264]. Almost 15% of the human body consists of skin which is the largest organ of the body. Its thickness ranges from 40 μm (eyelids) to 1 mm (palm of the hand) [265].

There are three main layers of skin clearly distinguishable: (i) epidermis, (ii) dermis, and (iii) subcutaneous layer [266]. However, basement membrane and skin vasculature also have importance to understand the structural organisation of skin. The schematic illustration showing the layers of skin is given in Figure 9.

### 1.6.1. Epidermis

The epidermis is the outermost layer of skin and consists of mostly keratinocytes (approximately 95%) and other cells including melanocytes (pigment-producing cells), Langerhans cells (cells which form a very early immune defence of skin by presenting antigens), and Merkel cells (cells which acts as transducers of light touch sensation) [265]. The epidermis has distinct layers from the upper layer to the lower layer to down; (i) the stratum corneum consists of cornified keratinocytes and acts as the primary barrier against bacteria entry and water loss, (ii) the stratum granulosum has been named due to the granules (keratohyaline) it contains, which help the aggregation of the

keratin filaments, (iii) the stratum spinosum consists of four to ten layers of polyhedral (spinous) cells, and (iv) the stratum basale which is the lowest layer and plays a key role as the junction between the epidermis and the dermis [267–269].

### 1.6.2. Basement membrane

The basement membrane separates the epidermis from the dermis, acts as a mechanical support and mediates chemical signal passage between these two layers [270,271]. The basement membrane dominantly consists of collagens IV and VII, integrins (predominantly α6β4 that binds to laminin), laminin and elastic fibres which link the epidermis to the dermis [272,273].

### 1.6.3. Dermis

The dermis is localised between the epidermis and the subcutaneous tissues and consists of collagen (responsible for the strength), elastin (responsible for elasticity), glycosaminoglycans (GAGs), dermal fibroblasts (the main type of cells that present in the dermis), macrophages, dendrocytes (dendritic cells which appear to have a role in immune function with their cytochemical characteristics), mast cells (migrant connective tissue cells which mainly take part in allergic reactions and also in wound healing and angiogenesis), blood vessels, and nerves [265].

The dermis has two distinct layers: (i) the papillary dermis which contains thin, loosely arranged elastin and collagen fibres and (ii) the reticular dermis which is mostly composed of disorganised connective tissue (mostly collagen running horizontally to provide mechanical support) [274]. GAGs in dermis supports collagen and elastin fibres and are responsible for holding water (up to a thousand times higher volume than their volume), for aiding the passage of nutrients and other molecules [275].

### 1.6.4. Subcutaneous layer

The subcutaneous layer (also known as the hypodermis) lies below the dermis, and it mainly consists of adipose tissue and connective tissue. It also contains hair roots, blood vessels and nerve endings traversing fat and connective tissues. The subcutaneous layer serves as an insulator to aid regulating body temperature, and it also acts as a cushion that provides mechanical support to protect muscles, bones, organs etc. [265].

### 1.6.5. Vasculature in skin

Blood vessels are present in the dermis have functions in providing oxygen and nutrients to the dermis, removal of waste products and maintaining body temperature by the dilation or contraction of vessels to regulate surface heat loss [264]. Vascular networks in skin consist of two plexuses: (i) superficial plexus and (ii) deep plexus, which lies in the upper and lower parts of reticular dermis, respectively [276].

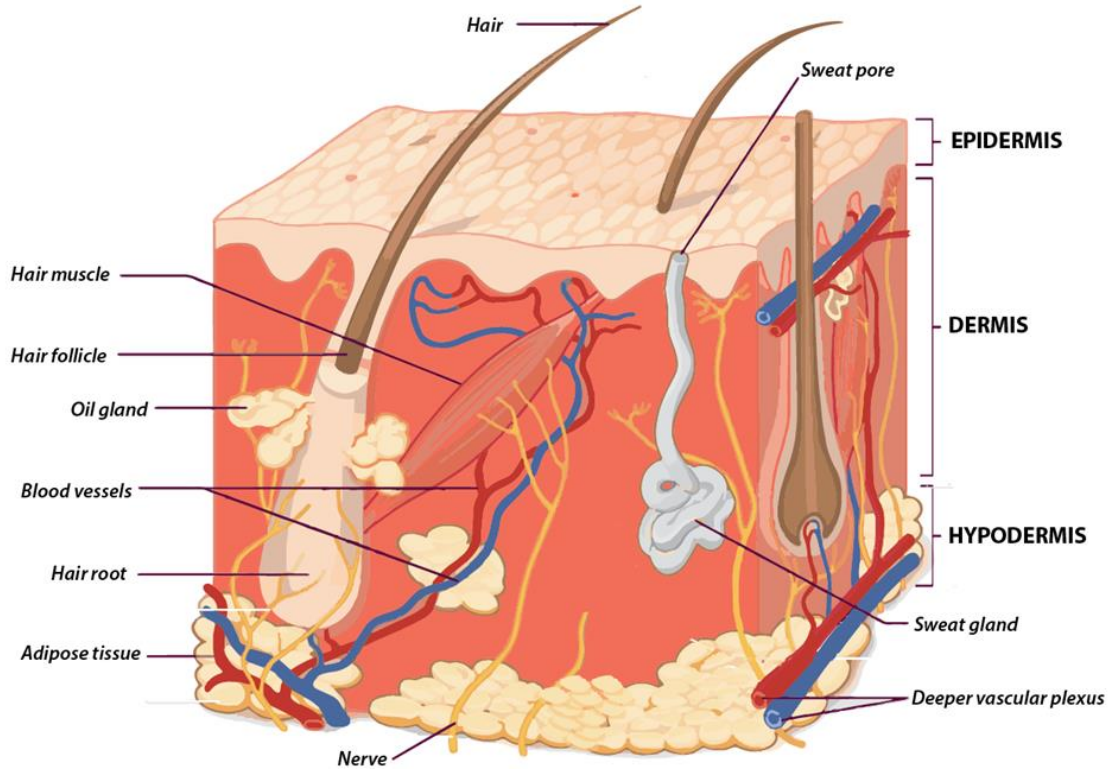


***Figure 10.*** *Schematic illustration of the structure of human skin (figure modified from lumenlearning.com with permission). Skin is composed of three histologically distinguishable layers: (i) epidermis, (ii) dermis, and (iii) hypodermis*

## 1.7. Natural Wound Healing in Cutaneous Wounds

A wound can be defined as an injury that results in disruption or damage to the anatomical structure and function of the native tissue. Wounding can be either as simple as the loss of the epithelial integrity or deeper and more complex, reaching to subcutaneous tissue, including muscles, nerves and blood vessels. Wounds are classified in three main categories: (i) acute wounds which repair themselves anatomically and functionally following the natural order of the wound healing process, (ii) complicated wounds that are mostly a combination of a tissue defect with infection which is a constant threat for wound healing process, and (iii) chronic wounds which do not heal in an

orderly way following the stages of wound healing in a timely manner. Wound healing is a complex series of events involving haemostasis, inflammation, granular tissue formation, proliferation, neovascularisation and remodelling in which many growth factors plays a pivotal role (Figure 10).

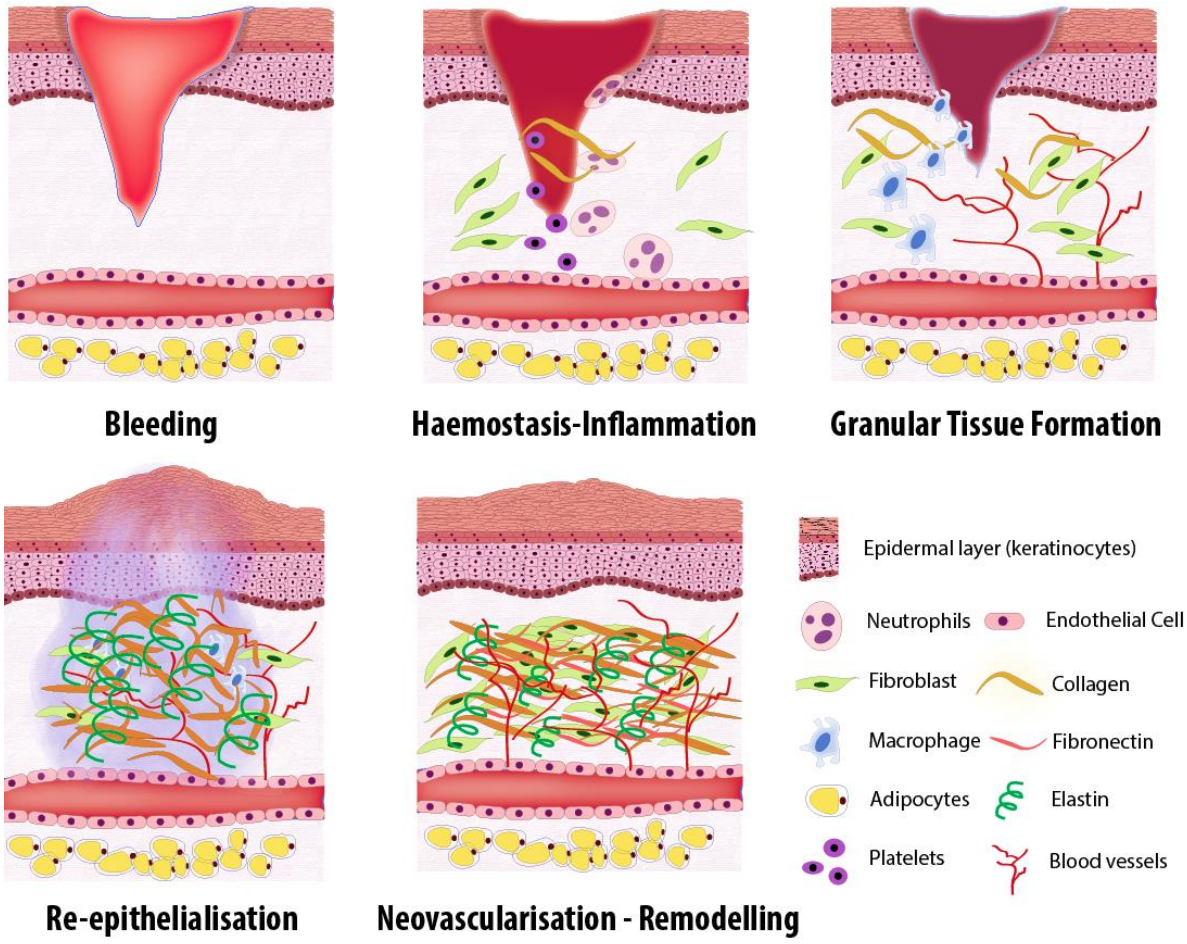


***Figure 11.*** *Schematic illustration showing the wound healing phases: (i) bleeding, (ii) haemostasis, (iii) inflammation, (iv) granular tissue formation, (v) re-epithelialisation, (vi) neovascularisation, and (vii) remodelling*

### 1.7.1. Haemostasis

Haemostasis is defined as the response of body to prevent and stop bleeding by the platelet adhesion and aggregation. Following tissue injury, platelets form a fibrin clot which limits haemorrhage in the wound site [277]. The clot seals the injury and prevents the spread of infection in the area and further bleeding. Although haemostasis is the first stage of wound healing and mainly plays a role in blood clotting, it also provides a matrix for the recruitment of the cells to the injury site [278]. In addition, clotting plays a key role in the activation of the inflammation process [279].

### 1.7.2. Inflammation

The inflammation phase is a result of the host immune response to the wound. Several types of cells, including neutrophils, macrophages, mast cells, T cells and B cells, take part in the inflammatory response to wound healing [280,281]. The inflammatory response begins with the invasion of the site of wound with neutrophils which not only clears out the dead cells, bacteria and other pathogens and debris but also provides a chemotactic stimulus for other inflammatory cells and facilitates their migration by stimulating the release of several ECM molecules [282]. Monocytes (which will become macrophages when migrated to the wound site from the bloodstream) then migrate to the area of inflammation to induce the secretion of cytokines and growth factors which consecutively initiate granular tissue formation. Macrophages have been shown to have a significant role in the transition of the inflammatory response to the wound healing phase. The latest phase of the inflammatory response is the entering of lymphocytes (T cells and B cells) to the wound area in response to interleukin-1 (IL-1) which plays a pivotal role in collagen remodelling and ECM formation [283,284].

### 1.7.3. Granular tissue formation and proliferation

Following the wound creation, haemostasis and inflammatory response phases, the tissue repair phase takes place. About 4-days after injury, granulation tissue which mainly consists of macrophages, fibroblasts, early connective tissue, and blood vessels form [285,286]. The fibrin clot formed during the haemostasis stage provides an ECM to promote granular tissue formation. Macrophages from the inflammatory phase continuously secrete cytokines to promote fibrous tissue formation and angiogenesis in the site of the wound. Particularly TGFβ and PDGF attract fibroblasts, which are the main type of cells that are present in the proliferative phase [287]. Fibroblasts produce fibronectin to replace the fibrin clot and then collagen to gradually replace fibronectin with an ultimate aim of producing a mature ECM, and they begin differentiating into myofibroblasts [288]. In addition, wound contraction begins in the proliferative phase.

### 1.7.4. Re-epithelialisation

Following the granular tissue formation and proliferative phase of fibroblasts, keratinocytes are needed to proliferate and reconstitute the cutaneous barrier [289]. Re-

epithelialisation takes place via cell-cell, cell-basement membrane contact and molecular signalling. Briefly, keratinocytes sense the absence of neighbour cells and begin changing morphologically. Epithelial growth factor (EGF), keratinocyte growth factor (KGF) and TGFβ induces the proliferation and migration of keratinocytes while MMPs generated by damaged keratinocytes facilitate the migration by degrading basal membrane [290]. Once a full closure of the wound is achieved, cell-cell contact of keratinocytes inhibits further proliferation [291,292], and keratinocytes become strongly adhered to the newly formed basement membrane and reconstitute an epithelium [290].

### 1.7.5. Neovascularisation

The neovascularisation of the healing area wound is crucial and involves complex angiogenic phases. After wounding of a tissue, clotting and granulation, capillaries begin invading to the healing site. During the haemostatic and proliferative phase of wound healing, a large number of pro-angiogenic factors including VEGF, TGF-β, PDGF and FGF are released to promote angiogenesis [293–295]. Since the ECs are responsive to these pro-angiogenic factors as well as ECM molecules, capillaries from the surrounding tissues start to invade the formed clot and within a couple of days a microvascular network forms within the area of healing [296]. The details of the angiogenic processes and the signalling pathways were explained in the previous sections.

### 1.7.6. Remodelling

The remodelling phase is the final stage of wound healing which may take up to 1 – 2 years and involves the maturation of the ECM which has been synthesised temporarily during the earlier phases of wound healing [297,298]. The remodelling phase is highly controlled to maintain a balance between degradation and synthesis, where MMPs plays a key role. Collagen fibrils increase in diameter, whereas fibronectin and hyaluronic acid are degraded gradually, and collagen bundles become more oriented from their initial disorganised structures [299,300]. The connective tissue begins shrinking and brings wound margins together. By the time the wound heals, the density of macrophages and fibroblasts reduces [301], and at the end, a fully matured scar is obtained with organised blood vessel network [302,303].

## 1.8. Strategies to Fabricate Vascular Networks for Angiogenesis Studies

### 1.8.1. Natural scaffold systems

Development of natural constructs with an intrinsic 3D architecture of a tissue or organ by decellularisation is an important approach in angiogenesis studies. This technique is mainly based on decellularisation of a tissue or organ to obtain 3D microvascular networks. These networks can be recellularised with cells to study or promote angiogenesis. The major advantage of this method is the retaining of the intrinsic ECM components that improve the attachment and proliferation of ECs.

Use of decellularised biological constructs has become an emerging strategy for producing physiologically relevant scaffolds for use in both pre-clinical and clinical applications [304,305]. The methodology for decellularisation of tissues and organs is well-established, and several studies have reported on the use of this approach for generating patches for tissue regeneration, as *in vitro* models or drug screening platforms. For example, Sarig et al. successfully decellularised a porcine heart and constructed an acellular matrix to be repopulated with progenitor cells and used as an *ex vivo* drug screening platform, as an *in vitro* model for studying human cardiac tissue and transplantable patches. [164] Similarly, our group generated a decellularised rat intestine and repopulated it with human microvascular endothelial and stromal cells successfully as an *in vitro* model to study several aspects of neovascularisation [306]. Melo et al. established an *in vitro* multicellular bronchial model using decellularised porcine luminal trachea membrane [307]. Uygun et al. developed a decellularised liver matrix and recellularised it with adult hepatocytes as a transplantable liver graft [308]. Mertsching et al. developed an acellular porcine small bowel segment and conducted a pilot trial for evaluating the tissue capabilities in terms of vessel patency and tissue viability by clinical transplantation of their bioartificial vascularised scaffold repopulated with patient's peripheral blood cells [309]. Recently, Zhang et al. developed vascularised soft tissue flaps as an alternative to autografting. They generated an acellular skin/adipose tissue and repopulated it with human adipose-derived stem cells and HUVECs [310].

Thus, the use of acellular mammalian scaffolds has great potential in tissue engineering applications, but they are expensive and difficult to obtain. It also requires experience to

harvest tissues or organs from man or animals and prepare these to completely remove cells and cell epitopes to avoid them, causing immune reaction following implantation [311]. On the other hand, decellularised plant tissues and organs are promising possible alternatives to explore as tissue engineering scaffolds. They are readily available, cost-effective and safe to use.

The *in vivo* biocompatibility of plant-derived cellulose has previously been proven by Modulevsky et al. by implanting a decellularised McIntosh Red apple section into mice subcutaneously [312]. Similarly, the results of the subcutaneous implantation of bacterial cellulose (BC) in rats showed full biocompatibility [313]. The use of cellulose in tissue engineering applications has also been reported as a TE scaffold for cartilage tissue engineering [314] and temporary skin substitutes [315]. Interestingly, Gershlak et al. reported that cheap and abundant acellular plant leaves could be used as tissue engineering scaffolds. The study illustrated that embryonic stem cell-derived cardiomyocytes (hPS-CMs) and HUVECs could be grown on decellularised spinach and parsley leaves [166]. The feasibility of using different types of decellularised plant leaves has been further confirmed by a number of studies as tissue engineering scaffolds for different applications. Parsley stems and baby spinach leaves gained attention in vascularisation studies due to the suitability of their intrinsic vascular structure to be recellularised with human ECs [166,167,316]. All the studies above concluded that cellulose is inexpensive, biocompatible and therefore a good candidate for use in tissue engineering applications.

### 1.8.2. Synthetic scaffold systems

Tissue engineering scaffolds are expected to have several properties such as being biocompatible and supporting cell attachment and proliferation, allowing the exchange of gas and media with their porous structure, storing and releasing several agents according to the intended use of the scaffold, being inexpensive, and easy to fabricate. Synthetic scaffolds are important candidates to be used as tissue engineering scaffold systems, and this has led researchers to fabricate synthetic vascular networks for angiogenesis studies.

Use of microfluidic systems is a technique where several methods such as microneedle casting, stamping, sacrificial channel dissolving are used to fabricate 3D microchannels

as networks embedded in PDMS chambers [317]. Yeon et al. manufactured 3D networks using soft lithography and rapid prototyping to study migration and lumen formation *in vitro* [318]. Li et al. demonstrated an alternative technique to create synthetic vascular scaffolds by combining 3D printing, casting and porogen leaching and successfully endothelialised the vascular channels [319]. Similarly, Miller et al. combined 3D printing and porogen leaching to generate carbohydrate glass 3D networks which they repopulated with ECs and perfused with blood [320]. Kim et al. reported the use of rapid prototyping and electrospinning for the fabrication of PCL 3D networks [321]. Similarly, our group has previously combined these two techniques to manufacture PHBV perfusable vascular channels and cellularised these networks with HDMECs [322,323]. Van Duinen et al. used a microchannel platform based on a 384-well plate system to study sprouting and anastomosis *in vitro* [324]. Kim et al. fabricated the microchannels using soft lithography and PDMS replica moulding to be used to study migration and lumen formation *in vitro* [325].

## 1.9. Project Aims and Objectives

The main aims of my PhD project are to:

- Explore the angiogenic potential of 2dDR, a small sugar molecule, as a potent alternative to the well-established pro-angiogenic agent, VEGF, using established *in vitro* and *in vivo* angiogenesis assays.
- Develop *in vitro* systems which have the potential to be used to study aspects of neovascularisation and to promote angiogenesis, and to be used in regenerative medicine applications.

To achieve these aims, the experimental objectives of this project are to:

***(Chapter II)*** Investigate the angiogenic potential and the effective dose range of 2dDR using well-established *in vitro* assays; proliferation, migration and tube formation assays and *in vivo* assays*, ex-ovo* CAM assay and a diabetic rat wound healing model.

***(Chapter III)*** Develop a synthetic vascular scaffold by combining two well-known scaffold fabrication techniques, electrospinning and 3D printing, to study angiogenesis at cellular and tissue levels.

***(Chapter IV)*** Develop a natural vascular scaffold by decellularising plant tissue to retain the intrinsic 3D vascular architecture to study and promote angiogenesis.

***(Chapter V)*** Develop a novel *in vitro* 3D dynamic system as an angiogenesis model to better represent the physiological environment by combining emulsion templating and electrospinning.

***(Chapter VI)*** Investigate the practicability of prevascularisation approach to induce angiogenesis by pre-seeding simple electrospun scaffolds with a combination of endothelial cells and fibroblasts.

***(Chapter VII)*** Develop a bilayer PCL barrier membrane for guided bone/tissue regeneration (GBR/GTR) applications by combining electrospinning and emulsion templating scaffold fabrication techniques.

## 1.10. Statement of Originality

I confirm that the work submitted is my own, apart from the works which have been produced from our collaborative studies. Jointly authored publications have also been included in the chapters with permission from the authors. My and my co-authors' contributions in each chapter have been explicitly indicated below.

**Chapter I:** The literature review presented in this chapter was written solely by me.

**Chapter II:** A part of this chapter includes a collaborative work with Dr Muhammad Yar from the Interdisciplinary Research Centre in Biomedical Materials (IRCBM), COMSATS University Islamabad, Lahore, Pakistan. The preparation of the alginate dressings, stability, sterilisation, 2dDR release tests, and implantation of the dressings were conducted in Pakistan. Permission has been granted from the authors of the published work and from the journal to use these data in my thesis. The rest of the work presented in this chapter are my own.

**Chapter III:** The work presented in this chapter is entirely my own.

**Chapter IV:** The work presented in this chapter is entirely my own.

**Chapter V:** This chapter includes a collaborative work with my colleague Betül Aldemir Dikici from Kroto Research Institute at the University of Sheffield. I was responsible for the experimental design, analysis, acquisition, and interpretation of data, statistical

analysis of the experiments related with the electrospun layer and endothelial cell-related work, while Betül was responsible from the experiments related with the emulsion templated layer. Permission has been granted from the authors and from the journal to use these data in my thesis.

**Chapter VI:** The work presented in this chapter is entirely my own.

**Chapter VII:** The data presented in this chapter is a 6-month collaborative project with Massachusetts Institute of Technology (MIT), and the experiments were conducted jointly with my colleague Betül Aldemir Dikici from the University of Sheffield. I was responsible for the experimental design, analysis, acquisition, and interpretation of data, statistical analysis of the experiments related with the electrospun layer and fibroblast related experiments, while Betül was responsible from the experiments related with the emulsion templated layer. Permission has been granted from the authors and from the journal to use these data in my thesis.

**This page intentionally left blank**

# CHAPTER II

# Exploration of 2-deoxy-D-ribose (2dDR) as an alternative to exogenous VEGF to promote angiogenesis in tissue-engineered constructs

## 2.1. Aims and Objectives

The aim of this chapter is to investigate the angiogenic potential of 2dDR using well-established *in vitro* and *in vivo* angiogenesis assays. In order to satisfy this aim; the objectives of this chapter are to:

- Evaluate the angiogenic dose range of 2dDR by investigating its stimulatory effect on endothelial cell proliferation, migration and tube formation.
- Investigate the angiogenic potential of 2dDR either applied as solutions or released from tissue engineering constructs and explore if it is possible to define certain concentrations of either 2dDR or E2 which are as effective as VEGF in stimulating angiogenesis in the chick chorioallantoic membrane (CAM) bioassay.
- Investigate the stimulatory effect of 2dDR on angiogenesis and wound healing using a diabetic rat model.

## 2.2. Chapter II by Pictures

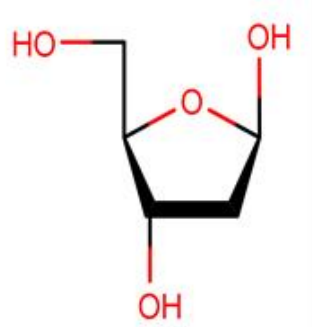


**2-deoxy-D-ribose (2dDR)**

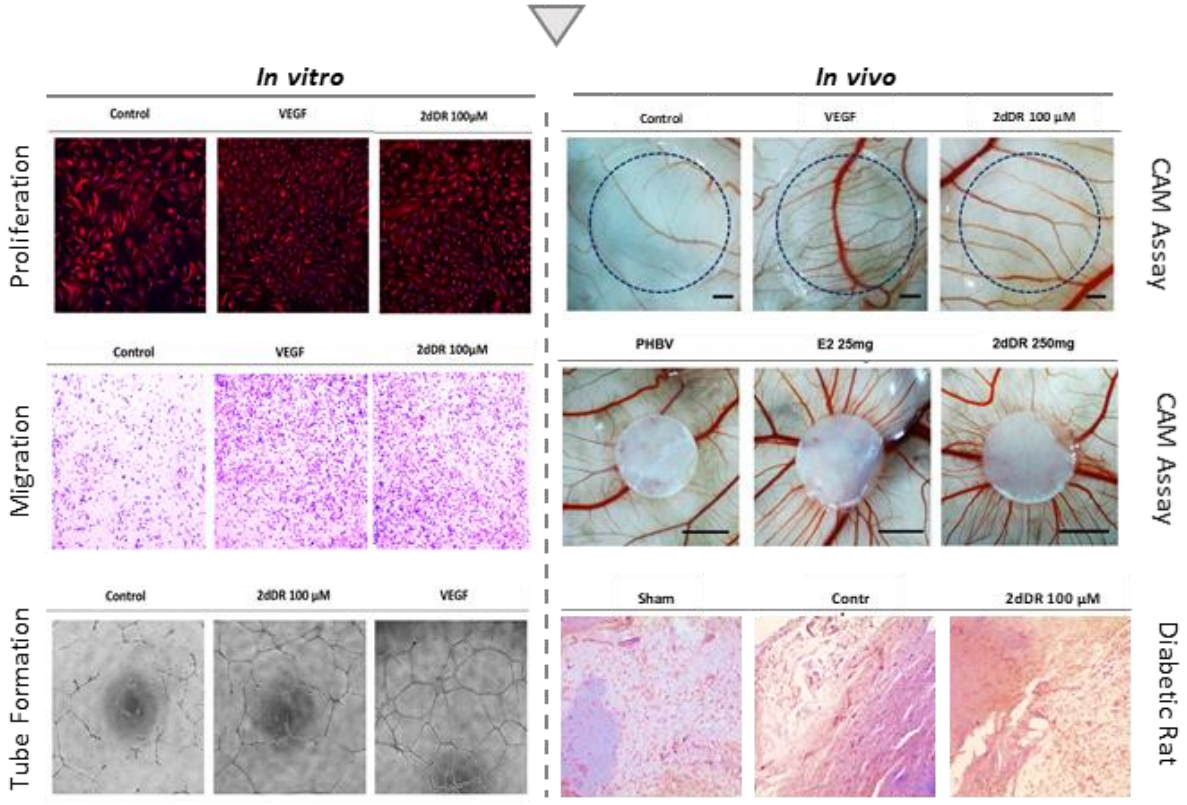

## 2.3. Introduction

Over the last 30 years, there have been significant advances in the production of tissue-engineered materials suitable for use in the clinic. However, one of the key challenges is to ensure rapid neovascularisation into these constructs in order for them to survive post-transplantation [37]. While relatively thin simple tissue-engineered constructs can survive on well-vascularised wound beds, thicker constructs (>200 μm) usually fail to engraft due to lack of oxygen and nutrients *in vivo* [22,24]. Both prevascularisation and scaffold functionalisation strategies with the use of angiogenic factors are viewed as promising approaches to accelerate vascular ingrowth into tissue engineering (TE) constructs to circumvent slow vascularisation after implantation [37,326].

Although there are some well-known growth factors such as transforming growth factor-beta (TGF-β), platelet-derived growth factor (PDGF) and fibroblast growth factor (FGF) which have the potential to promote neovascularisation [327], vascular endothelial growth factor (VEGF) is recognised to be the most well-studied angiogenic factor due to occupying a key role in the angiogenic cascade. The role of VEGF and other pro-angiogenic factors in the angiogenic cascade is described in Section 1.3.1.

VEGF acts as part of a well-regulated process, and its actions are highly dose-dependent. It is largely bound to glycosaminoglycans *in vivo* and released in response to need. Its angiogenic potential has been assessed in many *in vitro* studies such as cell migration assays using Matrigel [328], collagen gels [329] and transwell migration assays [330]. It has also been evaluated in the CAM assay [144,331–333] as well as *in vivo* studies. However, a range of studies shows that VEGF addition can lead to excessively leaky [334], permeable [335] and haemorrhagic [336] vessels such as those that are found in tumorigenesis [337]. Controlled and slow release of VEGF may help to regulate the delivery rate of VEGF and circumvent these problems by creating mature, more durable and stable vessels [338,339]. One promising approach is to use the glycosaminoglycan heparin, which is found on the cell surface and in ECM [340], to bind VEGF. Heparin found in ECM plays a role in the storage and prolonging the release of heparin-binding growth factors such as FGF and VEGF. It also regulates their stability and biological activity as well as long-term stimulation of endothelial cells [341–343]. Our group has previously explored the approach of using heparin bound to biomaterials to deliver VEGF using a layer-by-layer method for coating scaffolds with heparin and then binding VEGF [344],

and we have also reported on chitosan-based hydrogels for binding heparin [345,346]. However, binding VEGF with heparin requires multistep actions to introduce VEGF with the TE scaffolds.

As an alternative to VEGF, 17β-Estradiol (E2) has been shown to promote endothelial cell migration and proliferation *in vitro* [61,62] and to stimulate new blood vessel formation both *in vitro* and *in vivo* [63]. E2 has an important role in neovascularisation during the menstrual cycle [64,65]. It is used clinically in the treatment of osteoporosis and heart disease [66]. Moreover, blocking the E2 receptor with adjuvants such as tamoxifen for estrogen receptor-positive tumours, in which high estrogen helps the cancer cells grow and spread, is an effective method to reduce tumour vasculature. This therapy has been in clinics for many years, especially for the treatment of breast cancer [67,68]. Recently, our group confirmed that poly-L-lactic-acid (PLLA) scaffolds loaded with E2 were highly angiogenic using the CAM assay [69]. In contrast to VEGF, E2 has proven to be safe to be used clinically. To date, the angiogenic response to different doses of E2 has been studied not only by our group but also by several other groups [347–349].

In contrast to VEGF and E2, there is very limited literature on the angiogenic activity of 2dDR as explained in Section 1.3.1.1.7, and none of these studies defined an effective concentration range but only used a single dose of 2dDR to promote angiogenesis. The dosage-dependence to 2dDR remained to be established.

Accordingly, our aim in this chapter was to establish useful proangiogenic concentration ranges of 2dDR *in vitro* and *in vivo* and to compare its angiogenic activities with VEGF to progress our understanding of the potential value of 2dDR to the world of proangiogenic biomaterials and to the problem of improving rapid neovascularisation in TE constructs.

In order to satisfy this aim, our objectives were to:

- explore the angiogenic dose range of 2dDR *in vitro* using well-established angiogenesis assays
- investigate the angiogenic potential of 2dDR either applied as a solution or released from PHBV fibres for stimulating neovascularisation in the CAM assay in which one can demonstrate significant increases in blood vessel formation within seven days, which is a time period very relevant to driving angiogenesis non-

healing chronic wounds *in vivo* and to stimulating the formation of new blood vessels after engraftment of TE constructs.

- demonstrate the stimulatory effect of 2dDR in inducing angiogenesis and wound healing in diabetic rats.

## 2.4. Materials

| Chemical / Reagent | Catalogue Number | Supplier |
|---|---|---|
| Mouse/rabbit specific horseradish peroxidase (HRP)/ 3,3′-Diaminobenzidine (DAB) Detection IHC Kit | ab64264 | **Abcam** |
| Rabbit anti-CD34 | ab81289 | |
| Mouse anti-CD163 | MCA342 | **AbD Serotec** |
| Alginate dressings (10 cm x 10 cm) | 10007431 | **Activeheal** |
| Alexa Fluor® 594 anti-human CD31 Antibody | 303126 | **Biolegend** |
| Matrigel® (Growth Factor Reduced) | 356231 | **Corning** |
| Transwell EC migration assay inserts | 10167000 | |
| Hypermer B246 | - | **Croda** |
| Chloroform | 10784143 | **Fisher Scientific** |
| Dichloromethane (DCM) | 10127611 | |
| DPX mounting medium | D/5319/05 | |
| Industrial methylated spirit (IMS) | M/4450/17 | |
| Methanol | 10626652 | |
| Toluene | 10102740 | |
| Triton X-100 | BP151 | |
| Xylene | X/0100/17 | |
| Poly3-hydroxybutyrate-co-3-hydroxyvalerate (PHBV) (PHV content 12 mol %) | BV326301 | **GoodFellow** |
| Optimum cutting temperature tissue freezing medium (OCT-TFM) | 14020108926 | **Leica Biosystems** |
| Fertilised chicken eggs | - | **MedEggs** |
| Hydrochloric acid fuming 37% | 100317 | **Merck** |

| | | |
|---|---|---|
| RCOM King SURO humidified egg incubator | MX-SURO | **P&T Poultry** |
| EC GM 2 Supplement Pack (for HAECs) | C-39211 | **PromoCell** |
| EC GM MV Supplement Pack (For HDMECs) | C-39220 | |
| Endothelial Cell Growth Medium 2 (EC GM) (for HAECs) | C-22211 | |
| Endothelial Cell Growth Medium MV (EC GM) (for HDMECs) | C-22220 | |
| Human Aortic Endothelial Cells (HAECs) | C-12271 | |
| Human Dermal Microvascular Endothelial Cells (HDMECs) | C-12210 | |
| Mouse anti-CD80 | sc-376012 | **SantaCruz** |
| 17β-Estradiol (E2) | E8875 | **Sigma Aldrich** |
| 2-deoxy-D-glucose (2dDG) | D8375 | |
| 2-deoxy-D-ribose (2dDR) | 121649 | |
| 2-deoxy-L-ribose (2dLR) | 75617 | |
| 37% formaldehyde (FA) solution | F8775 | |
| 4',6-diamidino-2-phenylindole (DAPI) solution | D8417 | |
| AlamarBlue Cell Metabolic Activity Assay | R7017 | |
| Amphotericin B | A2942 | |
| Bovine serum albumin (BSA) | A7030 | |
| Collagenase A | COLLA-RO | |
| Crystal violet | C6158 | |
| D-Glucose (DG) | G8270 | |
| Dimethyl sulphoxide (DMSO) | 472301 | |
| Dulbecco's Modified Eagle's Medium (DMEM) | D6546 | |
| Eosin Y solution | HT110232 | |
| Ethanol | 51976 | |
| Ferric chloride hexahydrate | 236489 | |
| Fetal calf serum (FCS) | F9565 | |
| Formalin solution (10%) | HT501128 | |
| Glutaraldehyde (25%) | G5882 | |

| | | |
|---|---|---|
| Goat serum | G9023 | |
| Hematoxylin solution | HHS16 | |
| Ketamine hydrochloride | BP736 | |
| Luria Bertani (LB) broth | L24040 | |
| Methacrylic anhydride (MAA) | 276685 | |
| Orcinol monohydrate | 447420 | |
| Paraformaldehyde (PFA) | 158127 | |
| Penicillin / Streptomycin | P0781 | |
| Pentaerythritol (98%) | P4755 | |
| Photoinitiator (PI) (2,4,6-Trimethylbenzoyl Phosphine Oxide/2-Hydroxy-2-Methylpropiophenone blend) | 405663 | |
| Polycaprolactone (PCL) (Mn: 80.000 g/mol) | 440744 | |
| Polydimethylsiloxane (PDMS) (SYLGARD®184) | 761036 | |
| Streptozotocin (STZ) | S0130 | |
| Tin (II) 2-ethylhexanoate | S3252 | |
| Triethylamine (TEA) | 471283 | |
| Trypan blue | T6146 | |
| Trypsin EDTA | T3924 | |
| Tween®20 | P1379 | |
| Vascular endothelial growth factor (VEGF) | V7259 | |
| ε-caprolactone | 704067 | |
| Alexa Fluor 594 Phalloidin | A12381 | **ThermoFisher Scientific** |
| Rhodamine labelled lens culinaris agglutinin (LCA) | RL-1042 | **Vector Laboratories** |

## 2.5. Methods

### 2.5.1. General cell culture protocol for Human Aortic Endothelial Cell (HAEC)

HAECs were used between P2 and P6. Cells were taken out from liquid nitrogen ($LN_2$) and immediately thawed at 37°C. Once cell suspensions was completely thawed, it was

transferred into a container with 10 mL of EC GM (PromoCell Endothelial Cell Growth Medium 2 basal medium supplemented with 2% FCS, 5 ng/mL EGF, 10 ng/mL bFGF, 20 ng/mL insulin-like growth factor, 0.5 ng/mL VEGF, 1 µg/mL ascorbic acid, 22.5 µg/mL heparin, 0.2 µg/mL hydrocortisone). HAECs were centrifuged at 1000 rpm for 5 minutes, and the cell pellet was resuspended in EC GM. The cell suspension was split into the desired number of T75 flasks (VWR International, Pennsylvania, USA) and the final volume was then adjusted to 12-15 mL with EC GM. T75 flasks were then incubated at 37°C (Sanyo, Osaka, Japan). The culture media was replaced every 2-3 days until they reached ~80-90% confluency. Once the culture was confluent (around 80-90%) cell culture medium was removed from the flask, and flasks were washed with PBS. Following that, 5 mL of trypsin/EDTA solution was added to each flask, and flasks were incubated at 37°C for 5 minutes. When cells were detached from the surface, trypsin was neutralised with culture medium containing 10% FCS (approximately 15 mL) and the cell suspension was centrifuged at 1000 rpm for 5 minutes. The supernatant was removed, and the cell pellet was broken up by tapping the bottom of the universal container gently. Cells were then resuspended in EC GM to be used in the experiments.

### 2.5.2. Assessment of the angiogenic activity of 2dDR on promoting ECs proliferation with AlamarBlue® metabolic activity assay, fluorescent staining and the assessment of CD31 expression

#### 2.5.2.1. Preparation of the potential angiogenic agent solutions

10 mM 2dDR solution was prepared as the stock solution. To prepare the 10 mM 2dDR stock solution, 0.067 g of 2dDR powder was dissolved in 50 mL of 2% FCS containing low serum EC GM and filter sterilised. Lower concentrations of 2dDR were prepared by serial dilutions of the stock solution EC GM down to 1 mM, 100 µM, 10 µM, and 1 µM concentrations.

10 mM 2-deoxy-L-ribose (2dLR) solution was prepared as the stock solution. To prepare the 10 mM 2dDR stock solution, 0.067 g of 2dLR powder was dissolved in 50 mL of 2% FCS containing low serum EC GM and filter sterilised. Lower concentrations of 2dLR were prepared by serial dilutions of the stock solution EC GM down to 1 mM and 100 µM concentrations.

10 mM 2-deoxy-D-glucose (2dDG) solution was prepared as the stock solution. To prepare the 10 mM 2dDG stock solution, 0.082 g of 2dDG powder was dissolved in 50 mL of 2% FCS containing low serum EC GM and filter sterilised. Lower concentrations of 2dDG were prepared by serial dilutions of the stock solution EC GM down to 1 mM and 100 µM concentrations.

10 mM D-glucose (DG) solution was prepared as the stock solution. To prepare the 10 mM DG stock solution, 0.090 g of DG powder was dissolved in 50 mL of 2% FCS containing low serum EC GM and filter sterilised. Lower concentrations of DG were prepared by serial dilutions of the stock solution EC GM down to 1 mM and 100 µM concentrations.

VEGF solution was used at 80 ng/mL concentration, and the working solution was prepared by the dilution of sterile VEGF stock solution (100 ng/µL) in 2% FCS containing low serum EC GM.

#### 2.5.2.2. AlamarBlue® metabolic activity assay

AlamarBlue® Cell Viability Assay was performed to evaluate the effect of different concentrations of 2dDR (10 mM, 1 mM, 100 µM, 10 µM, and 1 µM) on HAECs growth *in vitro* in comparison with 80 ng/mL VEGF (as positive control). The principle of this assay is the reduction of non-fluorescent resazurin to highly fluorescent resorufin upon entering cells. The viable cells convert resazurin to resorufin continuously.

Once the cells reached confluence, HAECs were trypsinised and seeded into 48-well plates with a seeding density of $1x10^4$ HAECs/$cm^{-1}$. HAECs were cultured with EC GM, either containing different concentrations of 2dDR or VEGF. AlamarBlue Cell Viability Assay was performed at days 1, 4 and 7. Briefly, 0.1 mM AlamarBlue working solution was prepared by 10x dilution of the 1 mM AlamarBlue stock solution with EC GM. Growth medium was removed, and the cells were washed with PBS. 1 mL of AlamarBlue working solution was added to each well and incubated at 37°C for 4 hours. After an incubation period, 200µL of the solution was transferred into a 96-well plate, and the fluorescence readings were done at an excitation wavelength of 540 nm and an emission wavelength of 635 nm.

Following determining the effective concentration range of 2dDR, AlamarBlue Cell Viability Assay was also used to compare the effect of 2dDR with other small sugar

molecules including 2dLR, 2dDG and DG on HAEC's metabolic activities. The metabolic activity assay was conducted following the protocol described above.

#### 2.5.2.3. Fluorescent staining

In order to visualize the cells after 7 days, fluorescent staining was performed by labelling F-actin and cell nuclei of HAECs. Cells were washed with PBS before (once) and after (three times) fixing them in 4% PFA for 15 minutes. 0.1% (v/v) Triton 100x (in PBS) was added on samples, and the samples were incubated for 20-30 minutes at room temperature (RT). After three times washing with PBS, Alexa Fluor 594 Phalloidin (1:40 diluted in PBS from stock solution) solution was added to cells in order to stain F-actin filaments of cells and incubated for 30 minutes at room temperature in the dark. Cells were then washed three times with PBS. In order to stain cell nuclei, DAPI solution (1:1000 diluted in PBS), which strongly binds the adenine-thymine rich regions of DNA, was added and incubated for 10-15 minutes RT in the dark. Cells were washed 3 times with PBS and then examined with a fluorescent microscope (Nikon Eclipse Ti, Tokyo, Japan). The steps of the fluorescent staining protocol are summarised in Table 7.

***Table 7.*** *The steps of the fluorescent staining protocol*

| | Step | Reagent | Time (minutes) |
|---|---|---|---|
| 1 | Washing | PBS | 3 |
| 2 | Permeabilisation | Triton-X 100 | 20 |
| 3 | F-actin staining | Phalloidin solution | 30 |
| 4 | Washing | PBS | 3 |
| 5 | Cell nuclei staining | DAPI solution | 10-15 |
| 6 | Washing | PBS | 3 |

#### 2.5.2.4. CD31 expression

CD31 immunofluorescent staining was performed to evaluate the expression of CD31 of HAECs treated with different concentrations of 2dDR and VEGF. At day 7, cells were fixed with 4% PFA and washed with PBS. To avoid non-specific binding, cells were incubated

with 5% goat serum. Alexa Fluor® 594 anti-human CD31 Antibody staining solution was prepared by the dilution of 1:50 in 5% goat serum. Cells were incubated with the antibody staining solution overnight at 4°C. HAECs were finally counterstained with DAPI (1:1000 diluted in PBS) for 15 minutes after washing three times with PBS. CD31 expression is visualised under a fluorescent microscope after washing the cells with PBS. The steps of the immunofluorescent staining using Alexa Fluor® 594 conjugated antibody are summarised in Table 8.

***Table 8.*** *The steps of the immunofluorescent staining using Alexa Fluor® 594 conjugated antibody*

| | Step | Reagent | Duration | Temperature |
|---|---|---|---|---|
| 1 | Washing | PBS | 1 minute | RT |
| 2 | Blocking unspecific binding | 5% goat serum | 60 minutes | RT |
| 3 | Primary antibody labelling | Alexa Fluor® 594 primary antibody solution | Overnight | 4°C |
| 4 | Washing | PBS | 3 times | RT |
| 5 | Counterstaining with DAPI | DAPI solution | 15 minutes | RT |
| 6 | Washing | PBS | 3 times | RT |

### 2.5.3. Assessment of the angiogenic activity of 2dDR on stimulating ECs migration using a modified Boyden chamber assay

The Boyden chamber assay was developed for analysing the leukocyte chemotaxis in the 1960s [214]. There are two compartments containing two media, and these compartments are separated with a microporous membrane. Cells are seeded into the top compartment (a cell culture insert) and allowed to migrate through the pores, to the other side of the membrane where the chemoattractant is placed in the container below (well plate) (Figure 12). The migration was assessed by investigating the migration of ECs is assessed by quantifying the cells migrated to the bottom surface of the membrane. Here, we used a modified Boyden chamber assay to evaluate the migratory response of HAECs to 2dDR in comparison with VEGF.

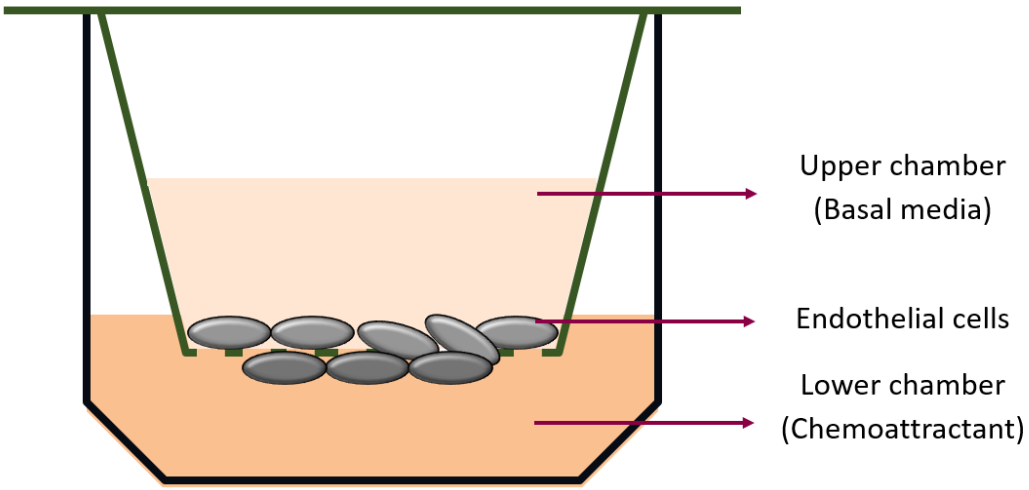


***Figure 12.*** *Schematic illustration of the modified Boyden chamber assay*

Briefly, 800 µL of chemoattractant solutions (80 ng/mL VEGF, 1 mM 2dDR, 100 µM 2dDR, and 10 µM 2dDR) and low serum EC GM (as control) were added to the 24-well plates (lower chamber), and 8 µm pore size cell culture inserts were placed into the chemoattractant solutions carefully to avoid bubble formation. HAECs were trypsinised, centrifuged, and $5x10^4$ HAECs resuspended in 300 µL of low serum EC GM were seeded into the cell culture inserts (upper chamber). After incubation for 4 hours at 37°C, cells which were not migrated were removed from the upper surface of the cell culture insert by scratching with a cotton bud. Cell culture inserts were fixed with 3.7% FA for 10 minutes, and the migrated HAECs were stained with 0.1% crystal violet solution for 10 minutes before washing three times with deionized water.

Bright-field images were taken with the fluorescent microscope, and the migration was quantified with a multi-step image processing of the green channel images exported from microscope software (NIS-Elements, Tokyo, Japan). Briefly, the raw image was split to its three main colour channels (red, green and blue (RGB) channels) using Adobe Photoshop CS6 (ADOBE Systems Inc., San Jose, California, USA). Only the green channel was exported as an image file and then imported to ImageJ (Wayne Rasband, National Institutes of Health, USA) for conversion to binary image. The black pixels in the binary image, which are accounting the cells, were counted using the histograms of each image. Four areas of interest were chosen randomly from each image, and the mean number of migrated cells was taken for each group.

### 2.5.4. Assessment of the angiogenic activity of 2dDR on stimulating tube formation with Matrigel® tube formation assay

*In vivo*, ECs are in direct contact with a basement membrane which is specific and biologically functional for enabling ECs to form tube structures [350]. Matrigel is the trade name of a gelatinous protein mixture which is rich in collagen IV, laminin, proteoglycans and growth factors. This biologically active protein mixture is a wonderful candidate for mimicking native basement membrane of ECs *in vitro* and promotes ECs to form tube-like capillary structures [221]. The tube formation assay is widely used for screening of first biological activity related to neovascularisation. The schematic illustration of the Matrigel tube formation assay and the quantification protocol followed are given in Figure 13.

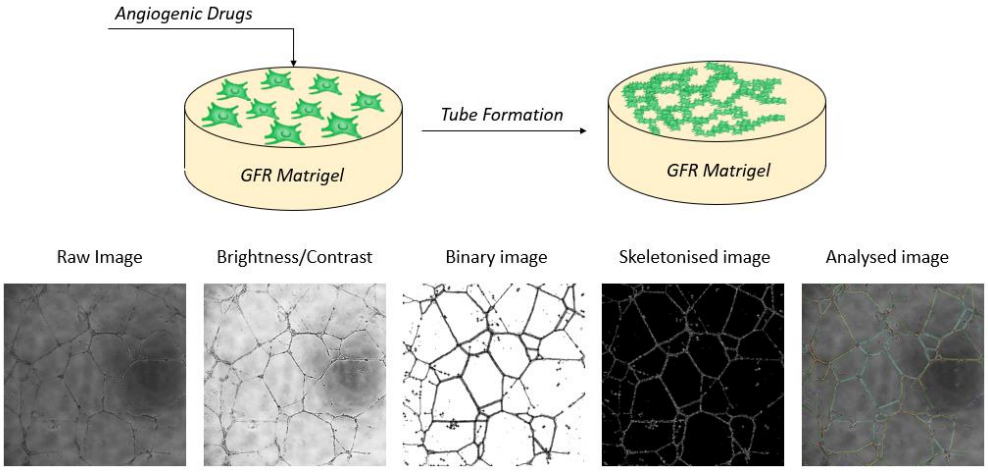


***Figure 13.*** *Schematic illustration of the Matrigel tube formation assay and the quantification protocol followed*

Using Matrigel tube formation assay, we examined whether 2dDR stimulates the tube formation of HAECs using Matrigel tube formation assay. Briefly, working on ice, 48-well plates were thickly coated with growth factor reduced Matrigel by adding 120 µL of Matrigel into each well. Well, plates were placed at 37°C for 60 minutes for solidifying of the Matrigel. HAECs were trypsinised, centrifuged and plated on Matrigel® coated plates at a density of $2.5x10^4$ cells/well and treated with 100 µM of 2dDR in comparison with 80 ng/mL VEGF and non-supplemented control EC GM. HAECs were incubated at 37°C for 18 hours before fixing them in 2% PFA solution containing 0.1% glutaraldehyde for 15 minutes. Tube formation was quantified using Angiogenesis Analyzer plugin of ImageJ [351].

### 2.5.5. Assessment of the VEGF-dependency and the stability of 2dDR-related angiogenic activity

Human VEGF ELISA MAX™ Deluxe Set was used for the quantification of VEGF production of HAECs when treated with either 100 µM or 1 mM of 2dDR. 80 ng/mL VEGF was used as a positive control. The assay was conducted according to the manufacturer instructions. The contents of the Human VEGF ELISA MAX™ Deluxe Set and the preparation of the working solutions of the reagents (dilutions of the stock reagents) are given in Table 9.

***Table 9.*** *The contents of the Human VEGF ELISA MAXTM Deluxe Set and the preparation of the working solutions of the reagents (dilutions of the stock reagents)*

| Material | Dilute with | Dilution |
|---|---|---|
| Coating Buffer A (5x) | Deionised water | 1:5 |
| Capture antibody (200x) | 1x Coating Buffer A | 1:200 |
| Assay Diluent A (5x) | PBS | 1:5 |
| Detection Antibody (200x) | 1x Assay Diluent A | 1:200 |
| Avidin-HRP (1000x) | 1x Assay Diluent A | 1:1000 |
| Assay Diluent D (1x) | - | - |
| Substrate Solution D (1x) | - | - |
| Human VEGF standard (18ng) | 1x Assay Diluent A | 1:2, 1:4, 1:8, 1:16, 1:32, 1:64 |
| Wash buffer (1x) | - | - |
| Stop Solution (1x) | - | - |

To investigate the VEGF production of HAECs in response to 2dDR treatment, cells were incubated in low serum EC GM supplemented with 100 µM of 2dDR, 1 mM of 2dDR, and 80 ng/mL VEGF. Non-supplemented low serum EC GM was used as a control. Growth media of the cells were collected at day 1, 3 and 5, centrifuged at 1000 rpm for 5 minutes, and stored at -20°C.

For quantification of the samples, first, a human 1 mL of VEGF stock solution was prepared as 1500 pg/mL in 1x Assay Diluent A, and then six serial dilutions were done

down to 750, 375, 187.5, 93.8, 46.9, and 23.4 pg/mL in order to draw a reference curve for converting readings to concentrations.

On day 1, 100 µL of 1x Capture antibody was added to each well to coat the well plate with the anti-VEGF antibody. The plate was then sealed using Parafilm® and incubated overnight at 4°C.

On day 2, the plate was washed 4 times with 1x wash buffer, and blocked by adding 200 µL of 1x Assay Diluent A to each well and incubating at RT for 1 hour on a shaker. The plate was then washed 4 times with 1x wash buffer, and 50 µL of 1x Assay Diluent D was added to each well. 50 µL of the samples (growth media from HAECs) and 50 µL of the prepared VEGF concentrations (reference standards) were added to wells, the plate was then sealed and incubated at RT for 2h on a shaker. The plate was washed 4 times with 1x wash buffer, and 100 µL of 1x Detection Antibody was added to each well and incubated at RT for 1 hour on a shaker. The plate was washed 4 times with 1x wash buffer, and 100 µL of 1x Avidin-HRP was added to each well and incubated at RT for 30 minutes on a shaker. The plate was washed 5 times with 1x wash buffer (at least for 30 seconds for each wash), and 100 µL of 1x Substrate Solution D was added to each well and incubated at RT in the dark for 10 minutes. 100 µL of 1x Stop Solution was then added to each well to stop the reaction. The absorbance was read at 450 nm and 570 nm, the reading at 570nm was subtracted from that at 450 nm. The absorbance values were converted to concentrations using the reference curve drawn from the standard VEGF concentrations.

2dDR has many hydroxyl (OH) groups present which are highly reactive and may undergone chemical transformations [352,353]. Thus, the stability of 2dDR in an aqueous environment was assessed using Bial's Orcinol assay as described previously [90]. Briefly, two defined concentrations (100 µM and 1 mM) of 2dDR was prepared in EC GM. The solutions were incubated at 37°C in the presence and absence of HAECs. For this, HAECs were seeded to 24-well plates with a seeding density of $4x10^4$ cells/$cm^2$ and incubated with EC GM supplemented with 2dDR. On days 1, 4, 7, and 14, the growth medium was collected, and Bial's assay was performed [354]. The principle of this test is the formation of furfural (an organic compound: $C_4H_3OCHO$) by the dehydration of pentoses (sugars with five carbon atoms) with Bial's reagent. Furfural will then react with orcinol and generate a substrate with a blue colour. Briefly, Bial's reagent was prepared

by combining 0.4 g of orcinol, 200 mL of 37% concentrated hydrochloric acid, and 0.5 mL of a 10% solution of ferric chloride. 2 mL of media collected from 6-well plate were placed in a test tube, and 2 mL of Bial's reagent was added. The solution was heated to boil using a hot plate, and the sample tubes were then submerged into the boiling Bial's reagent solution for 1 minute. Absorbance was measured using a UV-VIS spectrophotometer at 630 nm.

### 2.5.6. Assessment of the angiogenic activity of 2dDR on stimulating angiogenesis using an *ex-ovo* CAM assay

#### 2.5.6.1. *Ex-ovo* CAM assay

The protocol of *ex-ovo* CAM assay consists of four main steps: (i) incubation of the fertilised eggs in a humidified rotating incubator, (ii) transferring embryos into petri dishes to start the *ex-ovo* culture, (iii) implantation of the agent/scaffold onto CAM, and (iv) analysis of the results. The schematic illustration of the steps is given in Figure 14.

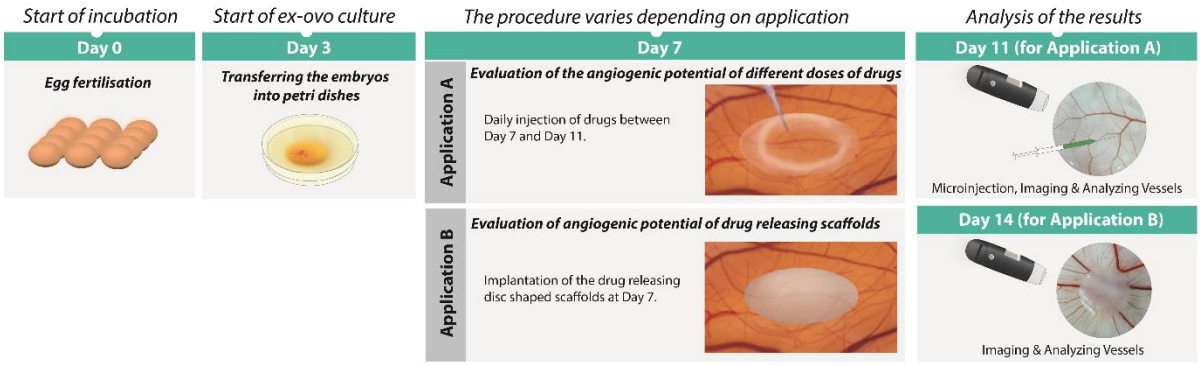


***Figure 14.*** *Schematic illustration of the steps of the direct application of the substances and implantation of the substance releasing scaffolds on chorioallantoic membrane. This figure shows the basic methodology of ex-ovo chorioallantoic membrane assay and quantification of the macro and microimages*

##### 2.5.6.1.1. Incubation of eggs

All CAM experiments were carried out according to the Home Office, UK guidelines. Fertilised chicken eggs (Gallus domesticus) were carefully wiped with 20% industrial methylated spirit solution using hand paper towels to remove dirt and feathers from the shell. The eggs were then incubated at 37.5 °C until embryonic development day (EDD) 3, lying horizontally in a humidified egg incubator.

2.5.6.1.2. Transferring the embryos into petri dishes

On EDD 3, the upper surface of the eggs was marked with a felt pen. The eggs were held horizontally (with the marked surface on top) and cracked on the edge of a 1000 mL glass beaker and kept close to the bottom surface of the petri dishes. The embryos were then transferred gently into sterile petri dishes and kept in a humidified incubator at 38°C. (Figure 15)

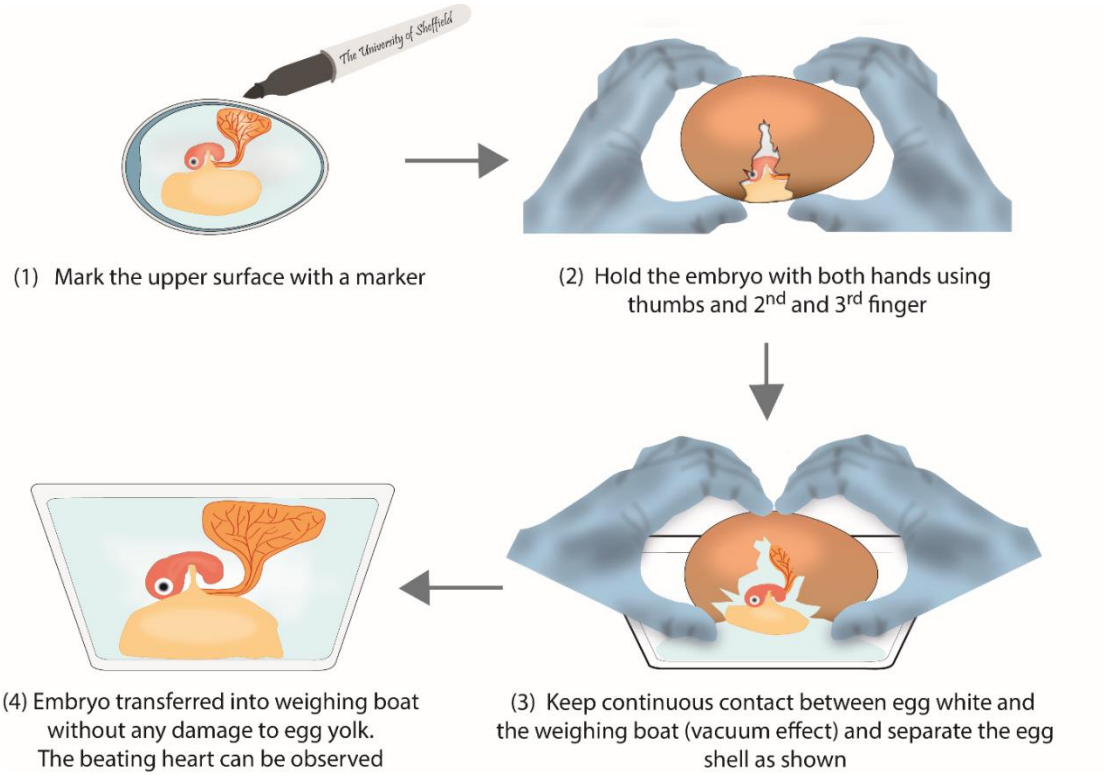


***Figure 15****. Graphical demonstration of egg cracking technique. (1) The egg is kept in a stationary position, and the top surface is marked with a pen. The marked surface stays at the top at all times. (2) The eggshell is cracked at the bottom by hitting it onto a hard surface. The cracked egg is immediately brought into the weighing boat. (3) The eggshell is separated into two halves by pulling it sideways and upward using the thumbs. The eggshell is kept very close to the bottom of the weighing boat during this manoeuvre so that the egg white forms a cushion around the egg yolk. (4) All the egg content is smoothly transferred into the weighing boat.*

Examples of the successful and unsuccessful transferring of embryos into petri dishes are given in Figure 16.


***Figure 16.*** *Observation of a successful embryo transfer with an intact egg yolk and live embryo on embryonic development day 3 (left-hand image). An unsuccessful embryo transfer with a live embryo (middle image) and a successful embryo transfer with an intact egg yolk but a dead embryo (righthand image) can also be observed. Error bars represent 1 cm*

The normal development of the chick embryo from day 3, the start of *ex-ovo* culture, until day 14, the day of euthanisation, is given in Figure 17.

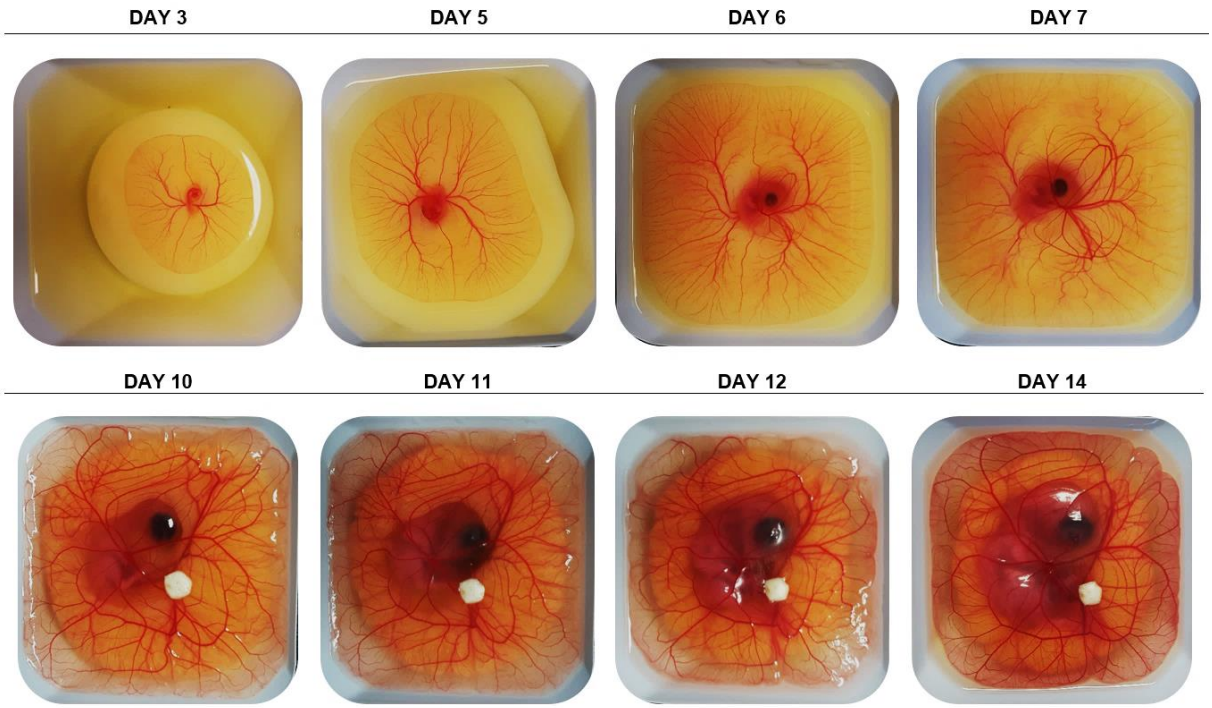


***Figure 17.*** *The development of the chick embryo from day 3, the start of ex-ovo culture, until day 14, the day of euthanising*

#### 2.5.6.2. Determination of the optimum concentration of E2 and 2dDR on angiogenesis using the CAM assay

##### 2.5.6.2.1. Preparation of drug solutions

Three concentrations of E2 and 2dDR were screened in these experiments. E2 was dissolved in methanol then working solutions were prepared with PBS so as to be (a) 100 ng/day (E2-100), (b) 200 ng/day (E2-200), and (b) 600 ng/day (E2-600) concentrations. 2dDR solutions were prepared by dissolving in PBS so as the final concentrations to be (a) 20 µg/day (2dDR-20), (b) 200 µg/day (2dDR-200), and (c) 1000 µg/day (2dDR-1000). VEGF was used as a positive control at a concentration of 80 ng/day (VEGF-80) whereas Sunitinib, an inhibitor of multiple receptor tyrosine kinases, was used as a negative control at a 2 µg/day concentration. Working solutions of all substances were prepared freshly at the beginning of each experiment.

##### 2.5.6.2.2. Application of drugs onto the CAM

Plastic rings (~6.5 mm in diameter), as a reservoir for the drugs and a marker for the implantation area, were placed on the CAM. The substances were applied as 20 µL volume onto the CAM twice a day for 3 days starting from EDD 7. On EDD 11, images of the CAM area circumscribed by the plastic rings were acquired using a digital microscope and embryos were sacrificed immediately after image acquisition.

##### 2.5.6.2.3. Quantification of angiogenesis

Digital images were used for quantification of the results. Multiple image processing steps were applied following previously described protocols [237,355,356]. Firstly, the internal area of the ring was cropped, and the raw image was split to its three main colour channels (red, green and blue (RGB) channels) using Adobe Photoshop CS6 (ADOBE Systems Inc., San Jose, California, USA). Only the green channel was exported as an image file and then imported to ImageJ (Wayne Rasband, National Institutes of Health, USA) for further analysis including unsharp mask filtering, enhancing the local contrast, noise removal, converting the image to binary and segmentation. The green channel was selected because it gave the most accurate and detailed results for blood vessels when converted to binary [357]. Finally, the number of branch points was quantified using

quantification software (AngioTool, National Cancer Institute, USA) and average blood vessel lengths were calculated by using binary image histograms with known pixel/mm ratios in ImageJ (Wayne Rasband, National Institutes of Health, USA). Image processing steps followed for quantification of the results are given in Figure 18.

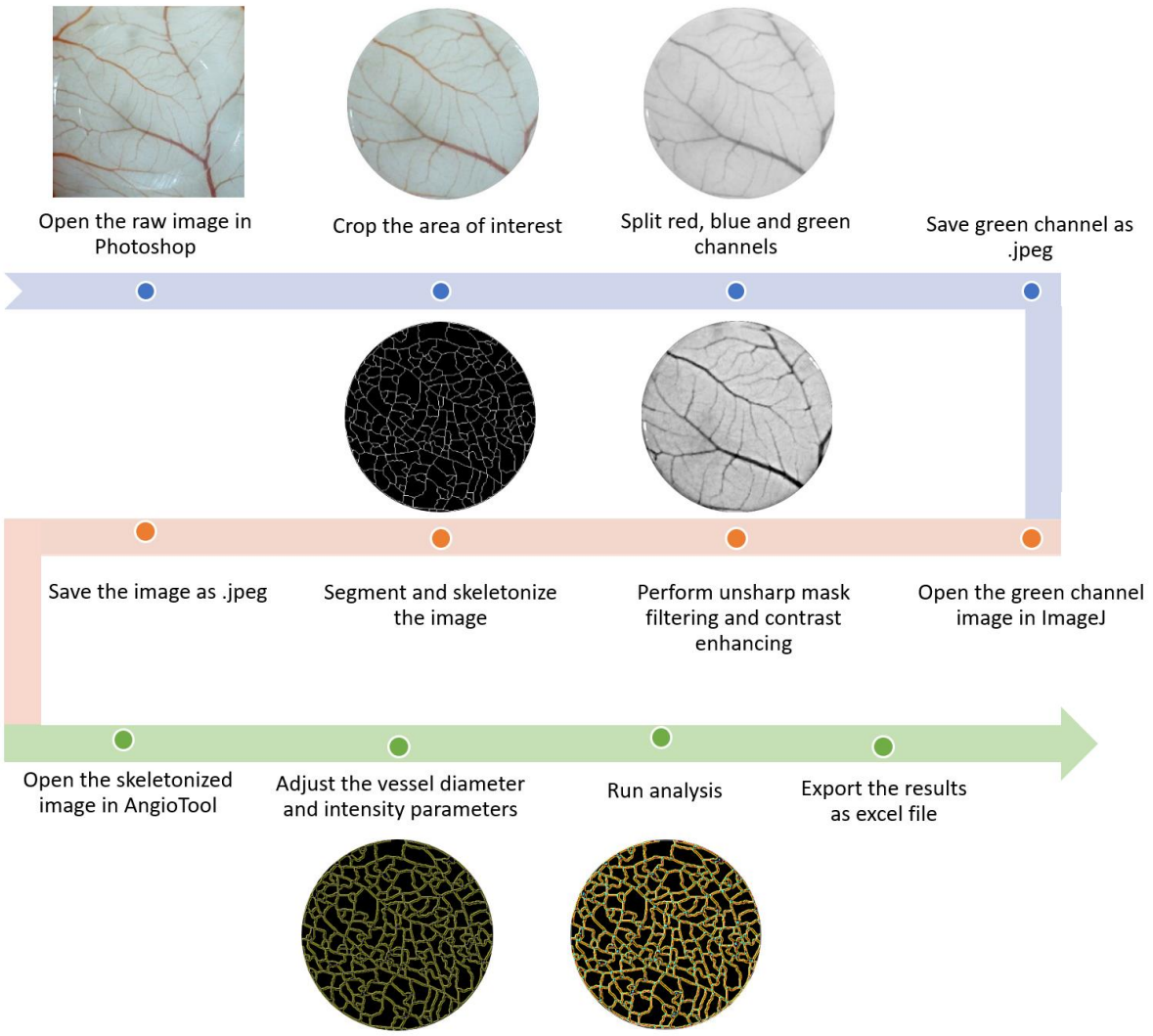


***Figure 18.*** *Flowchart detailing the image analysis technique that can be used to quantify the results of the angiogenesis experiments. The final image that results from each step is demonstrated on the right-hand side*

### 2.5.6.3. Evaluation of the effect of E2 and 2dDR on microvasculature

For these experiments only, one concentration of E2 (E2-200) and 2dDR (2dDR-200) were used as these concentrations were the most effective ones in terms of stimulating angiogenesis in CAM assay. The drugs were applied following the steps described previously.

*Microinjection*

At EDD 11, a 20% solution of rhodamine labelled LCA was injected into the circulation of CAM using 30 G needles under a dissection microscope (Wild Heerbrugg, Heerbrugg, Switzerland) to visualize the microvasculature. After 1 minute of incubation, embryos were sacrificed, and the areas on the CAM under the plastic rings were removed and fixed in 3.7% FA solution. Fixed CAM samples were then imaged under a confocal microscope (Zeiss LSM 510 Meta, Jena, Germany) for investigating the effect of substances on the microvascular structure of the CAMs.

*Quantification of the vascular area*

The percentage vascular areas (VA%) of the microvasculature of CAMs were quantified using confocal images of rhodamine-labelled LCA injected CAM samples, as shown in Figure 3. The images were then imported to ImageJ and converted to binary images after filtering and smoothing processes prior to quantification. VA% was calculated using the histogram list of black and white areas in the image.

2.5.6.4. Construction of E2 and 2dDR releasing PHBV scaffolds

2.5.6.4.1. Electrospinning E2 and 2dDR loaded PHBV scaffolds

*Preparation of the solutions*

10% (w/w) PHBV solution was prepared prior to electrospinning. 1 g of PHBV granules were dissolved in 1 g of methanol and 8 g of DCM in a fume hood. Four 10% of PHBV solutions were prepared prior to the addition of the drugs. Finally, 25 mg E2, 50 mg of E2, 250 mg of 2dDR and 500 mg of 2dDR were then added to each solution per 1 g of PHBV. The solutions were mixed using a magnetic stirrer overnight.

*Electrospinning*

Solutions (~10 mL) were loaded into 10 mL syringes fitted with 0.6 mm inner diameter syringe tips. Syringes were then placed in a syringe pump (GenieTMPlus, KentScientific, Connecticut, USA). Aluminium foil was used as the collector and placed at a distance of 17 cm from the needle tips. The pump was set to 40 μL/minutes, and a 17 kV voltage was applied both to the collector and the tips using a high voltage power supply (Genvolt,

Shropshire, United Kingdom). Electrospinning was done at room temperature until all the polymer solution was used.

2.5.6.4.2. Characterisation of the scaffolds

*Scanning electron microscopy (SEM)*

The surface morphology of E2 and 2dDR releasing scaffolds were observed under SEM (FEI Inspect F, Orlando, USA). The samples were coated with gold using a gold sputter (Edwards sputter coater S150B, Crawley, England) prior to imaging. Fibre diameter and pore sizes were measured using ImageJ. At least 100 measurements were taken from the different areas of each sample, and at least three samples were used for each group.

*E2 and 2dDR release from the scaffolds*

Scaffolds were cut into pieces to fit into a 6-well plate (20 mm x 20 mm), weighed and submerged in 4 mL of PBS. The accumulative E2 and 2dDR concentrations released from each group (25 mg E2, 50 mg E2, 250 mg 2dDR, 500 mg 2dDR) were measured fluorometrically using an ultraviolet-visible (UV-VIS) spectrophotometer (Thermo Fischer Evolution 220, Massachusetts, USA) at 238 nm for 2dDR and 220 nm for E2. Absorbance values were converted into concentrations using a standard curve of known concentrations of E2 and 2dDR.

*Effect of additives on mechanical properties of the scaffolds*

Biomechanical testing samples were prepared by cutting 20 mm x 10 mm pieces from dry scaffolds. The clamps of the device were positioned 10 mm away from each other, and the width and thickness of each scaffold were measured. Test samples were clamped with two grips in a tensiometer (BOSE Electroforce Test Instruments, Minnesota, USA). Tensile tests were performed on each sample at a rate of 0.1 mm/s until the samples failed (n=4). The raw data of these tests were used for drawing stress-strain and load-displacement graphs. Ultimate tensile strength (UTS) and the Young's modulus were calculated from stress (σ) and stress (ε) curves of each sample.

Wettability tests of drug-releasing electrospun scaffolds were also undertaken using a drop shape analyser (Krüss DSA100, Germany) under ambient laboratory conditions in order to see the effect of E2 and 2dDR on wettability of the scaffolds. In brief, a 5 μL water

droplet was dropped onto the scaffold surface, and the retention times of the droplet on scaffolds before complete absorption were calculated from recorded movies of the tests. At least nine measurements (three drops on three different substrates) were taken for measuring the water retention time on each sample.

#### 2.5.6.5. Evaluation of the angiogenic potential of the E2 and 2dDR releasing electrospun PHBV scaffolds

##### 2.5.6.5.1. Implantation of the E2 and 2dDR releasing scaffolds on CAM

Scaffolds were cut into 5.5 mm diameter circles using a laser cutting machine (Epilog Laser Cutter, Clevedon, UK) and sterilised under UV light for 1 hour prior to implantation. Two circular scaffolds were placed on CAM at EDD 7 and embryos were cultured for further 7 days. The correct placement of the test sample on the CAM is demonstrated in Figure 19.

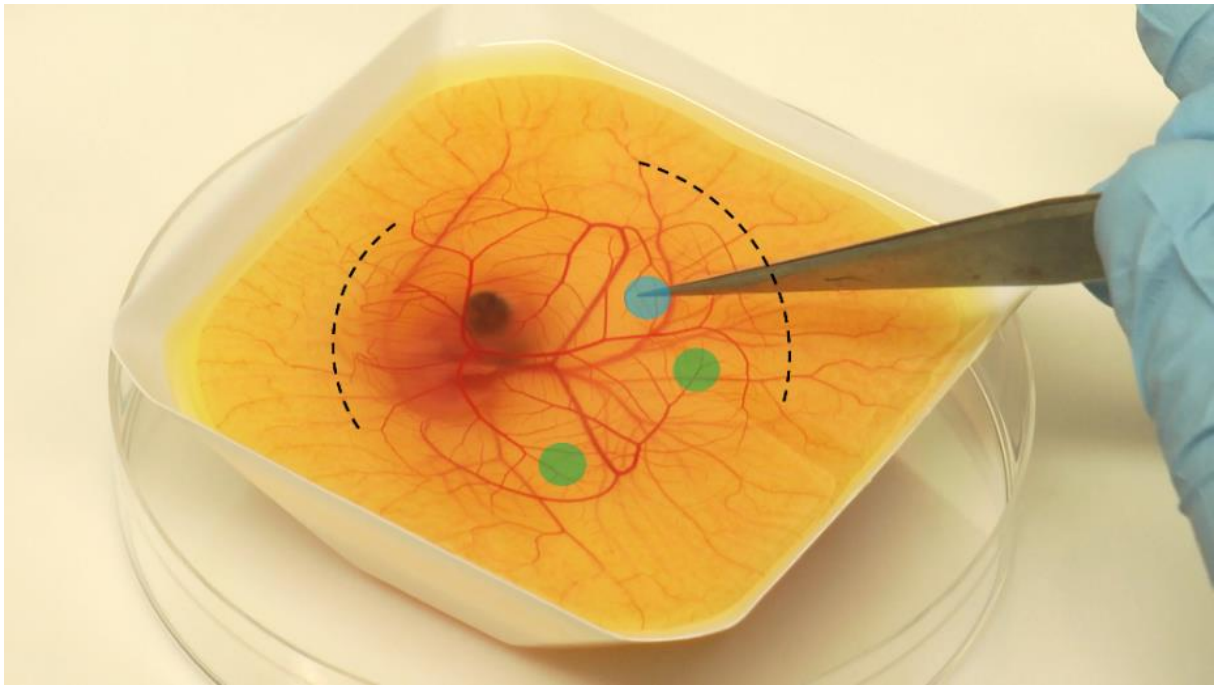

***Figure 19.*** *Correct placement of the test sample on the CAM. The dashed arrows show the borders of the CAM and coloured circles show the possible locations for implantation of the biomaterial*

##### 2.5.6.5.2. Quantification of the angiogenic activity of the drug-releasing scaffolds

Images of the scaffolds implanted on CAM were acquired using a digital microscope at EDD 14. Embryos were then sacrificed, and scaffolds were cut together with a rim of surrounding CAM tissue and fixed in 3.7% FA solution. Angiogenesis was quantified by

counting all blood vessels growing towards the scaffolds in a spoke wheel pattern, as described previously [69].

2.5.6.5.3. Histological evaluation of the E2 and 2dDR releasing scaffolds on CAM

Haematoxylin and Eosin (H&E) staining was performed on cell impregnated scaffolds by modifying a standard protocol [358]. Briefly, fixed samples were embedded in optimal cutting temperature tissue freezing medium (OCT-TFM) and frozen in liquid nitrogen for 3 minutes. Sections were cut 8-10 µm thick using a cryostat (Leica Biosystems, Nussloch, Germany) at -20°C. Sections were then stained with haematoxylin for 90 seconds and eosin for 5 minutes. Finally, H&E images were acquired under a light microscope (Motic DM-B1, Xiamen, China). The total number of blood vessels adjacent to the scaffolds were quantified by counting blood vessels in H&E sections [359]. Briefly, all discernible blood vessels adjacent to the scaffolds were counted by two independent researchers using two independent microscopes at 10× magnification. Three independent CAM experiments were conducted, and in each independent experiment, six embryos were used for each group. For histological analysis of a single group, three embryos were randomly selected out of six embryos from each independent experiment. Six sections were taken on a slide from each of the nine samples, and each slide was investigated under a microscope making a total of 54 counts per group for quantification of the results. The steps of the H&E staining protocol are summarised in Table 10.

***Table 10.*** *The steps of the H&E staining protocol*

| | Step | Reagent | Time |
|---|---|---|---|
| 1 | Removal of OCT | Distilled water | 5 minutes |
| | Removal of wax | Xylene | 3 minutes |
| 2 | Cell nuclei staining | Haematoxylin | 90 seconds |
| 3 | Staining | Tap water (running) | 4 minutes |
| 4 | Intracellular and extracellular staining | Eosin | 5 minutes |
| 5 | Staining | Tap water | 30 seconds |
| 6 | Dehydration | IMS (70%) | 30 seconds |
| 7 | Dehydration | IMS (100%) | 30 seconds |
| 8 | Dehydration | Xylene | 30 seconds |
| 9 | Mounting the sample | DPX | - |

#### 2.5.6.5.4. Statistics

Statistical analysis was carried out using either one-way or two-way analysis of variance (ANOVA) using statistical analysis software (GraphPad Prism, San Diego, CA). Where relevant, n values are given in figure captions. Error bars indicate standard deviations in the graphs unless otherwise stated. The degree of significance was indicated with number of stars, **** $P \leq 0.0001$, *** $P \leq 0.001$, ** $P \leq 0.01$, * $P \leq 0.05$, $^{ns}$ $P \geq 0.05$.

### 2.5.7. Assessment of the angiogenic activity of 2dDR on stimulating angiogenesis and wound healing using a diabetic rat wound healing model

Please note that the *in vivo* assessment of the angiogenic activity of 2dDR on stimulating angiogenesis and promoting wound healing using a diabetic rat wound healing model was conducted in collaboration with Dr Muhammad Yar of the Interdisciplinary Research Centre in Biomedical Materials (IRCBM), COMSATS University Islamabad, Lahore, Pakistan. The preparation of the 2dDR loaded alginate dressings, stability, sterilisation, 2dDR release tests, and implantation were conducted in Pakistan. The histological evaluation of the wounds was performed at the University of Sheffield. The schematic illustration of the diabetic rat wound healing model is given in Figure 20.

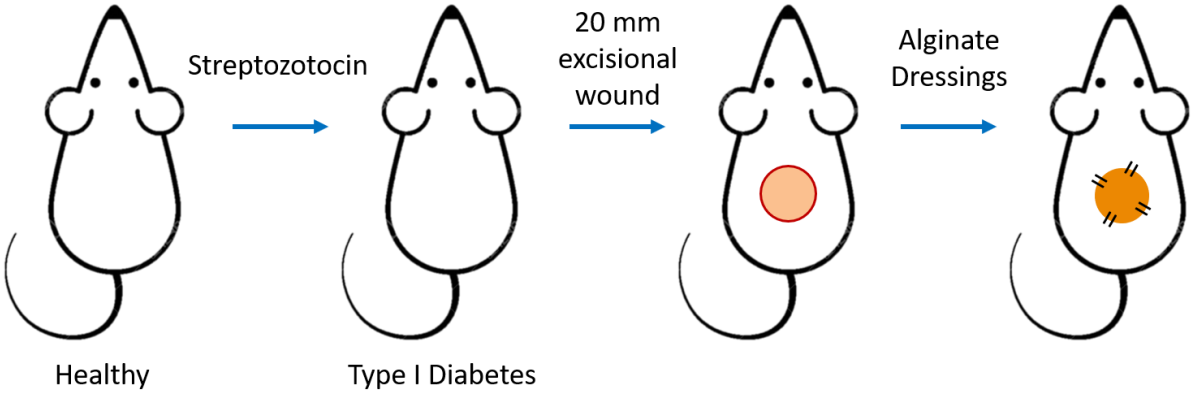


***Figure 20.*** *Schematic illustration of the diabetic rat wound healing model*

#### 2.5.7.1. Loading of 2dDR into alginate dressings

2dDR was loaded into alginate dressings under sterile conditions. For this 20 mm patches of pre-sterilised alginate dressings were cut and syringe filtered solutions of 2dDR (5% and 10%) were loaded onto alginate dressings by submerging dressings into solutions in a sterile environment and then dried at room temperature. In another approach, 5% and

10% 2dDR solutions were prepared and loaded onto 20 mm patches of alginate dressings without filter sterilisation. Once 2dDR loaded dressings were dried at room temperature, gamma sterilisation was conducted with an irradiation dosage of 25 KGy.

#### 2.5.7.2. Sterilisation test

Confirmation of sterilisation of dressings loaded with filter-sterilised 2dDR solutions was performed by culturing these in Luria Bertani (LB) agar broth. For this, sterile alginate dressings (without 2dDR) and alginate dressings loaded with 2dDR (both 5% and10%) were placed in sterilised LB broth and incubated overnight at 37$^{o}$C. LB broth (without dressings) was used as a negative control. After overnight incubation, 250 µL of each sample group was spread on LB agar plates and incubated at 37$^{o}$C for 1 week.

#### 2.5.7.3. Scanning electron microscopy (SEM)

The surface morphology of the 2dDR loaded alginate dressings was examined using SEM. The samples were coated with gold prior to examination at a range of magnifications. Fibre diameter was measured using Image J.

#### 2.5.7.4. Assessment of release of 2dDR

To evaluate 2dDR release from alginate dressings 20 mm patches of 5% and 10% 2dDR loaded alginate dressings were placed in a 6 well plate containing 4 mL PBS solution and maintained at 37$^{o}$C for 8 days. At each time interval (4-hr, 1-day, 2-day, 3-day, 5-day and 8-day) when media was removed to measure absorbance, another 4 mL of fresh PBS was added. Also, the plates had parafilm stretched tightly over the lids to avoid evaporation loss of PBS.

The accumulative concentration of 2dDR released from both groups was measured using Bial's Orcinol assay as described [354]. The principle of this test is the formation of furfural (an organic compound: $C_4H_3OCHO$) by the dehydration of pentoses (sugars with five carbon atoms) with Bial's reagent. Furfural will then react with orcinol and generate a substrate with a blue colour. Briefly, Bial's reagent was prepared by combining 0.4 g of orcinol, 200 mL of 37% concentrated hydrochloric acid, and 0.5 mL of a 10% solution of ferric chloride. 2 mL of media collected from 6-well plate were placed in a test tube, and 2 mL of Bial's reagent was added. The solution was heated to boil using a hot plate, and

the sample tubes were then submerged into the boiling Bial's reagent solution for 1 minute. Absorbance was measured using a UV-VIS spectrophotometer at 630 nm. The release of 2dDR at each time interval (4-hr, 1-day, 2-day, 3-day, 5-day and 8-day) was calculated by converting the absorbance value into a concentration using a standard curve of known concentrations of 2dDR.

#### 2.5.7.5. Stability studies

The stability of 2dDR was assessed as described previously in Section 2.5.5. Briefly, three defined concentrations (1, 2 and 3 mg/mL) of 2dDR was prepared in distilled water and incubated at RT for 14 days. At days 0, 7 and 14, Bial's orcinol assay was performed to measure the amount of 2dDR. A detailed protocol of Bial's orcinol assay was described in Section 2.5.7.4. The absorbance values were measured at 630 nm and converted into concentrations using a standard curve of known concentrations of 2dDR.

#### 2.5.7.6. *In vivo* evaluation of the effect of 2dDR on diabetic wound healing

##### 2.5.7.6.1. Diabetes induction

This *in vivo* study was carried out using male Wistar rats, aged 10-12 weeks of 180-220 g weight. Animals were kept in an animal care facility at CEMB, Lahore, Pakistan according to procedures approved by the Institutional Animal Ethics Committee under maintained pathogen-free controlled climate conditions (humidity 50% to 70% and temperature 25°C) with free access to both filter-sterilised water and food.

Type I DM was induced chemically by using streptozotocin (STZ). Briefly, after a 12-hr fast, rats received a single intraperitoneal injection of STZ (40 mg/kg) freshly prepared in 0.1 M sodium citrate buffer. Normal blood sugar levels of all rats before diabetes induction was in the range of 80-120 mg/dl. Blood glucose was monitored regularly using tail-vein blood using a glucometer (Accu-Chek Aviva Nano, Roche Diagnostics, Penzberg, Germany). At 8 days after STZ injection, rats whose fasting blood glucose levels exceeded 250 mg/dL were considered diabetic and selected for wound creation.

For this, all diabetic rats were randomly divided into four groups. Study groups were (i) Sham-operated (diabetic control with no treatment) (ii) Alginate control (alginate dressing without 2dDR) (iii) Alginate + 5% 2dDR (alginate dressing loaded with 5% 2dDR) and (iv) Alginate + 10% 2dDR (alginate dressing loaded with 10% 2dDR).

2.5.7.6.2. Wound creation and treatment

For wound creation, rats were anaesthetised with ketamine (100 mg/kg body weight) and xylazine (10 mg/kg body weight). The desired surface area on the dorsal surface was shaved using electric hair clippers (Oster heavy duty 97-60, UK). A sterilised circular template (20 mm) was placed on the shaved area of the skin, and a full-thickness excisional wound (1.2 mm thickness) was created carefully using sterilised surgical scissors (Noorani Surgical Medical Supplies, Pakistan). Following the skin excision, alginate dressings (without 2dDR) and 2dDR loaded alginate dressings (5% and 10%) were placed on the wounds and sutured in place for 4 days only (by which time most of the 2dDR will have been released). Dressings were then removed. Sham wounds were dressed with Mepore bandage only while in other groups Mepore was used as a secondary bandage to keep the alginate dressings in place. All animals were kept in separate cages and were allowed free access to both water and food. The wounds were photographed on day 0, 4, 7, 11, 14, 17 and 20 post-wounding to analyse the percent wound closure in each group. The percentage of wound closure was calculated using following formula:

$$\% \text{ of wound closure } = \frac{\text{Wound Area at Day 0} - \text{Open Wound Area}}{\text{Wound Area at Day 0}} \; x\; 100 \qquad (1)$$

On day 20, all experimental rats were euthanised with an anaesthesia overdose to collect skin tissue from the wound bed sites. The samples were preserved in 10% neutral buffer formalin for histological study. Following formalin fixation, tissues were dehydrated by placing in graduated series of increasing ethanol concentration from 70% to 100% and paraffin blocks were prepared.

2.5.7.6.3. Histological evaluation of the angiogenesis, macrophage response and wound healing

The 6 μm thick sections were taken from the paraffin-embedded skin biopsies with a microtome (Leica RM2145, Nussloch, Germany) and the sections were collected on Superfrost®Plus slides (Thermo Fisher, Massachusetts, USA). The H&E staining protocol was adapted from a previously described protocol [358], and DPX mounting medium was used to adhere the coverslip to the slides. For immunohistochemistry (IHC), sections of

the skin biopsies were processed with a mouse/rabbit specific horseradish peroxidase (HRP)/ 3,3′-Diaminobenzidine (DAB) Detection IHC Kit. Briefly, sections were deparaffinised with xylene and re-hydrated with serial alcohol washes. Sections were then incubated with hydrogen peroxide to quench endogenous peroxidase activity and later treated with 0.05% trypsin (v/w) and 0.1% Calcium Chloride (v/w) for antigen retrieval. To avoid non-specific binding, sections were incubated with 1% bovine serum albumin (BSA) before the addition of the primary antibodies. The sections were incubated for 2 hours with 3 different monoclonal antibodies, rabbit anti-CD34 (1:1000 in PBS), mouse anti-CD80 (1:100) and mouse anti-CD163 (1:200) diluted in 1% BSA. This was followed by incubation with biotinylated goat anti-polyvalent antibody (from Abcam Detection IHC Kit) for 10 minutes. Following the incubation of the slides with avidin and biotinylated horseradish peroxidase, the target proteins were visualised by incubation with peroxidase substrate and DAB chromogen (Abcam Detection IHC Kit). Sections were finally counterstained with haematoxylin, dehydrated, and mounted. Samples incubated without primary and secondary antibodies or only without primary antibodies were used as controls.

For quantification of the histological analysis, a semi-quantitative assessment was performed by observers who were blind to the samples presented to them using a qualitative grading scale; 0 = absent, 1 = weak staining, 2 = mild staining, 3 = some staining, 4 = extensive staining. One representative image of the three animals from each group at each time point was assessed by three blinded researchers (n=9). Images describing the grading scales (0, 1, 2, 3, and 4) as references were provided to blind scorers. The M2/M1 ratio was calculated using the values from the blind scoring of the IHC images. The steps of the IHC protocol are summarised Table 11.

***Table 11.*** *The steps of the IHC protocol*

| | Step | Reagent | Time | Temperature |
|---|---|---|---|---|
| 1 | Removal of wax | Xylene | 3 minutes | RT |
| 2 | Removal of wax | Xylene | 3 minutes | RT |
| 3 | Rehydration | 100% ethanol | 3 minutes | RT |
| 4 | Rehydration | 100% ethanol | 3 minutes | RT |
| 5 | Rehydration | 95% ethanol | 10 minutes | RT |
| 6 | Rehydration | Deionised water | 3 minutes | RT |

| | | | | |
|---|---|---|---|---|
| 7 | Washing | PBS/Tween 20 solution | 2 minutes | RT |
| 8 | Washing | PBS/Tween 20 solution | 2 minutes | RT |
| 9 | Blocking endogenous peroxidase | Hydrogen peroxide solution | 10 minutes | RT |
| 10 | Washing | PBS/Tween 20 solution | 2 minutes | RT |
| 11 | Washing | PBS/Tween 20 solution | 2 minutes | RT |
| 12 | Antigen retrieval | 0.05% trypsin + 0.1% $CaCl_2$ solution | 20 minutes | 37°C |
| 13 | Antigen retrieval | 0.05% trypsin + 0.1% $CaCl_2$ solution | 10 minutes | RT |
| 14 | Washing | PBS/Tween 20 solution | 2 minutes | RT |
| 15 | Washing | PBS/Tween 20 solution | 2 minutes | RT |
| 16 | Blocking unspecific binding | 1% BSA | 10 minutes | RT |
| 17 | Primary antibody labelling | Primary antibody solution | 2 hours | RT |
| 18 | Washing | PBS/Tween 20 solution | 2 minutes | RT |
| 19 | Washing | PBS/Tween 20 solution | 2 minutes | RT |
| 20 | Washing | PBS/Tween 20 solution | 2 minutes | RT |
| 21 | Secondary antibody (biotinylated) | Secondary antibody solution | 10 minutes | RT |
| 22 | Washing | PBS/Tween 20 solution | 2 minutes | RT |
| 23 | Washing | PBS/Tween 20 solution | 2 minutes | RT |
| 24 | Washing | PBS/Tween 20 solution | 2 minutes | RT |
| 25 | Avidin-biotin detection | Streptavidin solution | 10 minutes | RT |
| 26 | Washing | PBS/Tween 20 solution | 2 minutes | RT |
| 27 | Washing | PBS/Tween 20 solution | 2 minutes | RT |
| 28 | Washing | PBS/Tween 20 solution | 2 minutes | RT |
| 29 | Visualisation | Chromogen solution | 10 minutes | RT |
| 30 | Washing | PBS/Tween 20 solution | 2 minutes | RT |
| 31 | Washing | PBS/Tween 20 solution | 2 minutes | RT |
| 32 | Counterstaining | Hematoxylin solution | 3-5 seconds | RT |
| 33 | Washing | Distilled water | 4 times | RT |

| | | | | |
|---|---|---|---|---|
| 34 | Dehydration | 95% ethanol | 10 minutes | RT |
| 35 | Dehydration | 100% ethanol | 2 minutes | RT |
| 36 | Dehydration | 100% ethanol | 2 minutes | RT |
| 37 | Dehydration | Xylene | 2 minutes | RT |
| 38 | Dehydration | Xylene | 2 minutes | RT |

2.5.7.6.4. Statistical analysis

The quantitative data were analysed using Graph Pad Prism-5 software (USA). Analysis of variance (ANOVA) followed by Bonferroni post-test was used for multiple comparisons between individual groups. All experiments were performed in triplicate, and data were presented as the mean ± standard deviation of the mean.

For statistical analysis of the qualitative blind scoring of the histological images, the statistical differences between groups at each time point were tested with the multiple comparisons between each group using a non-parametric one-way ANOVA test.

## 2.6. Results

### 2.6.1. 2dDR improves the metabolic activity and proliferation of HAECs in a dose-dependent manner in comparison with other small sugar molecules

The results of metabolic activity assays showed that VEGF at 80 ng/mL concentration increased metabolic activities and the total number of cells as expected. The effect of VEGF was evident even at day 1 (but not statistically significant) but clearly significant by days 4 and 7. By day 7, cell number essentially doubled by the addition of 80 ng/mL of VEGF (Figure 3). At 100 μM, 2dDR was as effective as VEGF in stimulating metabolic activity and cell number without any adverse effect on the appearance of cells. Lower concentrations were found less effective. At higher concentrations, 1 mM 2dDR was slightly less effective when compared with 100 μM, and at 10 mM concentration cells detached from the culture wells by day 4.

The results of the fluorescent staining at day 7 showed that cell proliferation was correlated with the metabolic activities of HAECs. The quantification of the fluorescent images demonstrated that when cells were treated with VEGF for 7 days, the number of cells was increased approximately 2.2-fold in comparison with the controls. Similarly,

100 μM 2dDR almost doubled the cell number at the end of day 7. No statistical difference was observed for other concentrations of 2dDR apart from 10 mM. HAECs detached from the surface of the well plate when which cells were treated with 10 mM of 2dDR for 4 or 7 days.

The treatment of HAECs with VEGF and 2dDR did not affect CD31 expression of HAECs. All groups apart from 10 mM of 2dDR showed similar levels of expression of CD31, which correlated with the number of cells at the end of day 7. No expression of CD31 was observed for 10 mM 2dDR groups, as all cells had detached. Accordingly, for the following migration experiments, 1 μM and 10mM 2dDR concentrations were excluded as 1 μM was too low to be effective and 10mM detached cells after exposure for several days.

The results of the (A) fluorescent staining (DAPI/phalloidin-TRITC), (B) CD31 expression, (C) cell viability and normalised cell count of HAECs over 7 days are given in Figure 21.

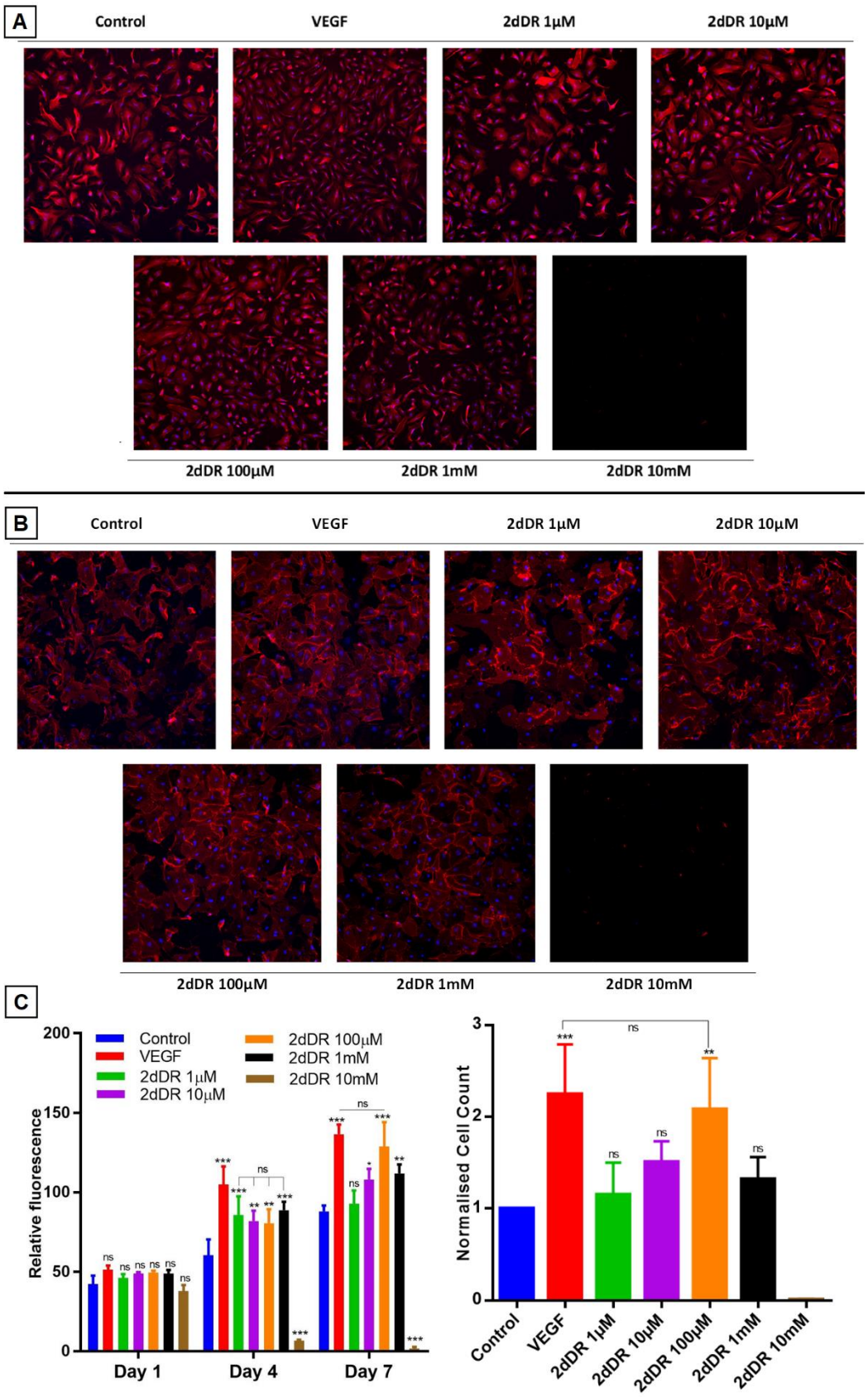


***Figure 21:*** *(A) DAPI/Phalloidin staining and (B) CD31 expressions of HAECs at the end of day 7 when treated with different concentrations of 2dDR compared to VEGF and controls. (C) The metabolic activities of HAECs over 7 days and the normalised number of HAECs at the end of day 7. (***p ≤ 0.001, **p ≤ 0.01, *p ≤ 0.05, not significant (ns) p ≥ 0.05, n = 3)*

Following the determination of the effective concentration range of 2dDR on stimulating HAEC's proliferation, other small sugar molecules were used at the same concentrations to compare their angiogenic potential with 2dDR.

The results of the metabolic activities showed that none of the other small sugar molecules increased the activity of HAECs over 7 days (Figure 22).

At day 1, only the VEGF group showed a significant increase in the metabolic activity of HAECs while 2dDG reduced the activity when given at higher doses (1 mM and 10 mM). No significant difference was found between the other groups.

By day 4, VEGF and lower concentrations of 2dDR (100 μM and 1mM) showed a significant increase in the metabolic activities of HAECs whereas highest concentrations of 2dDR (10 mM), 2dLR (10 mM), and 2dDG (1 mM and 10 mM) dramatically reduced the metabolic activity. DG at any concentration did not show either a positive or negative effect on the growth of cells by day 4.

On day 7, the only two groups increasing the metabolic activities of HAECs were VEGF (80 ng/ mL) and 2dDR (100 μM and 1 mM). All three concentrations of 2dDG were found to reduce the metabolic activity by day 7. None of the concentrations of DG were found to increase or decrease the activity of cells. Lower concentrations of 2dLR (100 μM and 1 mM) were found to slightly increase the activity (but not significantly when compared to controls) while 10 mM of 2dLR significantly decreased the activity similar to 10 mM of 2dDR.

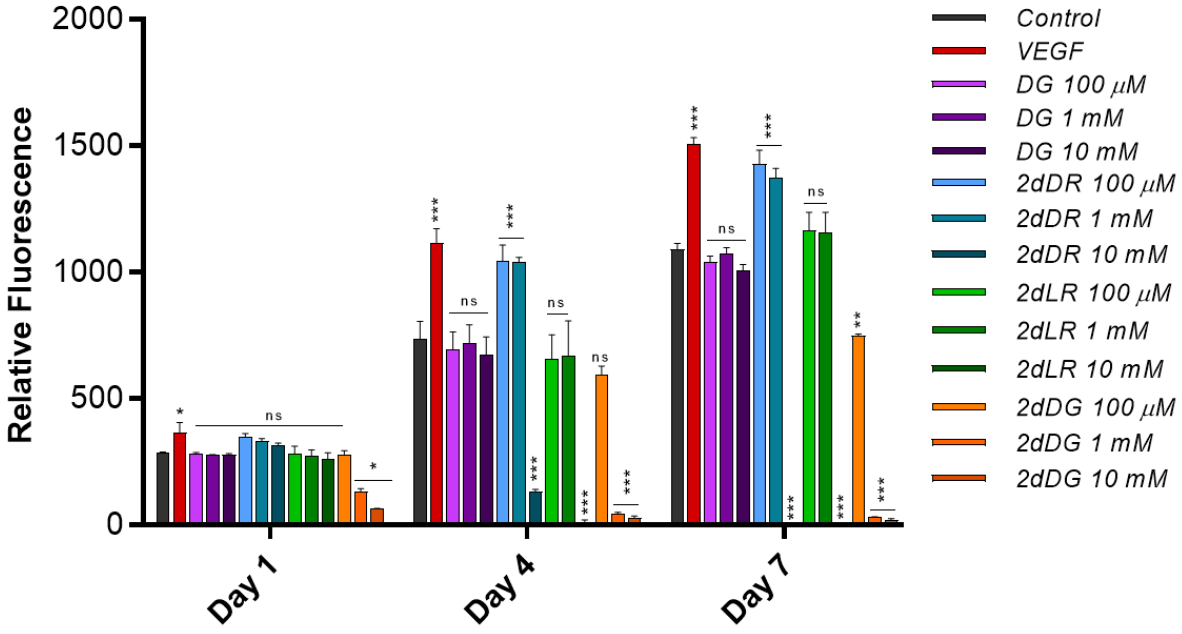


| Group I | Group II | Day 1 | Day 4 | Day 7 |
|---|---|---|---|---|
| Control | *VEGF* | ns | *** | *** |
| | *2dDR 100 μM* | ns | *** | *** |
| | *2dDR 1 mM* | ns | *** | *** |
| | *2dDR 10 mM* | ns | *** | *** |
| | *2dLR 100 μM* | ns | ns | ns |
| | *2dLR 1 mM* | ns | ns | ns |
| | *2dLR 10 mM* | ns | *** | *** |
| | *2dDG 100 μM* | ns | * | *** |
| | *2dDG 1 mM* | ** | *** | *** |
| | *2dDG 10 mM* | *** | *** | *** |
| | *DG 100 μM* | ns | ns | ns |
| | *DG 1 mM* | ** | ns | ns |
| | *DG 10 mM* | ** | ns | ns |
| 2dDR 100 μM | *2dLR 100 μM* | ns | *** | *** |
| | *2dDG 100 μM* | ns | *** | *** |
| | *DG 100 μM* | ns | *** | *** |
| 2dDR 1 mM | *2dLR 1 mM* | ns | *** | *** |
| | *2dDG 1 mM* | *** | *** | *** |
| | *DG 1 mM* | ns | *** | *** |
| 2dDR 10 mM | *2dLR 10 mM* | ns | * | ns |
| | *2dDG 10 mM* | *** | ns | ns |
| | *DG 10 mM* | ns | *** | *** |

***Figure 22***. *Metabolic activities of HAECs over 7 days when treated with other sugar molecules (2dLR, 2dDG, and DG) used at same concentrations (10 mM, 1 mM, and 100 μM) in order to compare their angiogenic potential with 2dDR. The table shows the statistical differences between groups*

### 2.6.2. 2dDR enhances the chemotactic migration of HAECs

All three concentrations of 2dDR and VEGF significantly enhanced the chemotactic migrations compared with the control group. VEGF showed a slightly better performance over 2dDR at all three concentrations (Figure 23). Quantification of the results indicated that the increase in the number of migrated cells was significantly different for 100 µM in comparison with the other two concentrations of 2dDR. The addition of VEGF significantly increased the number of migrated HAECs when compared with 100 µM 2dDR, which was also selected for further tube formation experiments.

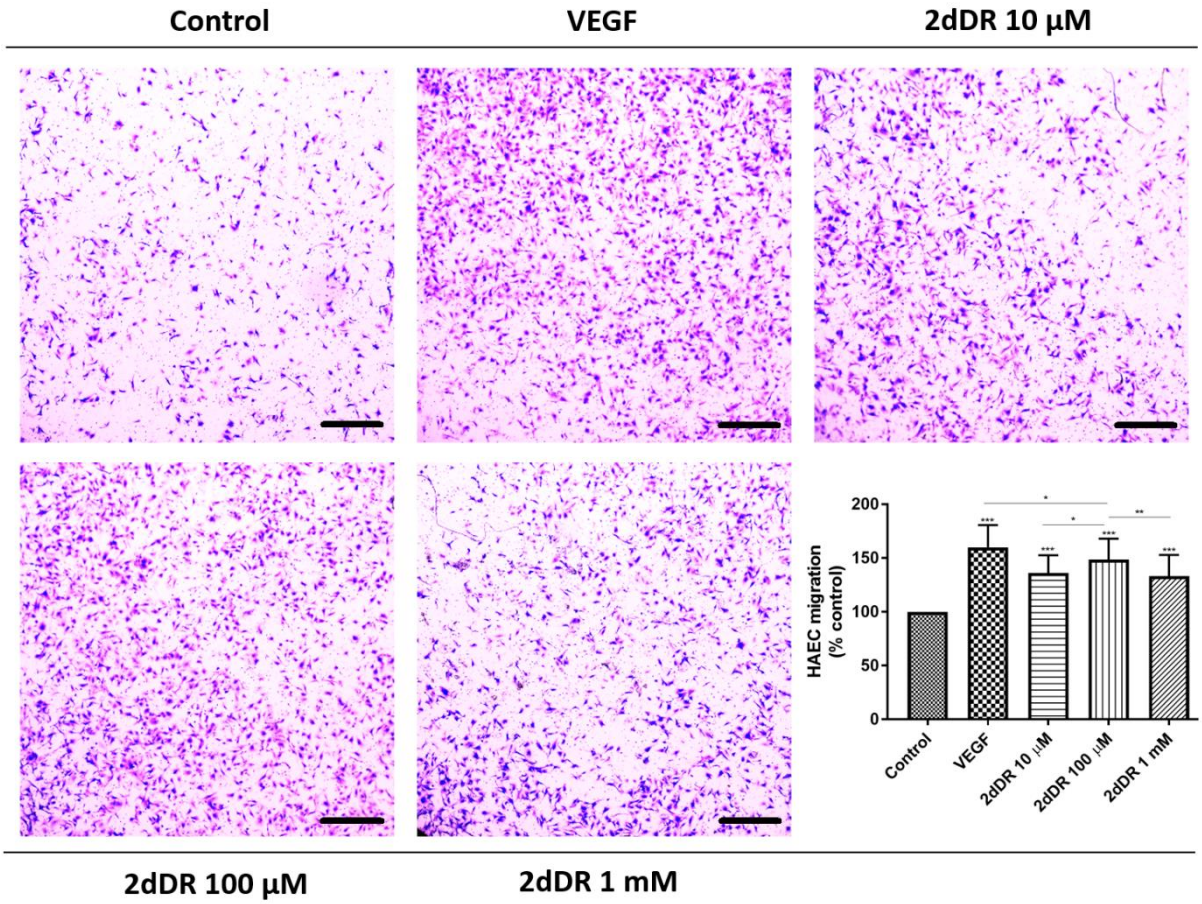


***Figure 23:*** *The migratory effect of different concentrations of 2dDR in comparison with VEGF and controls was evaluated by using a modified Boyden chamber assay. The quantified results were given in the graph bottom-right (***p≤0.001, **p ≤ 0.01, *p ≤ 0.05, not significant (ns) p ≥ 0.05, n = 3). Scale bars represent 250 µm*

### 2.6.3. 2dDR improves the capability of HAECs to form tube-like structures

The administration of 2dDR and VEGF significantly improved the ability of HEACs to form tubes in Matrigel®, whereas cells were partly capable of forming these structures in the

control group (Figure 24). The results indicated that the inclusion of 2dDR and VEGF significantly increased the number of branch points to 86 ± 7 and 100 ± 13, respectively from controls (average number of branch points: 38 ± 10). Similarly, the number of tubes per field was increased 1.8-fold and 2.3-fold with the administration of 2dDR and VEGF, respectively, when compared with control.

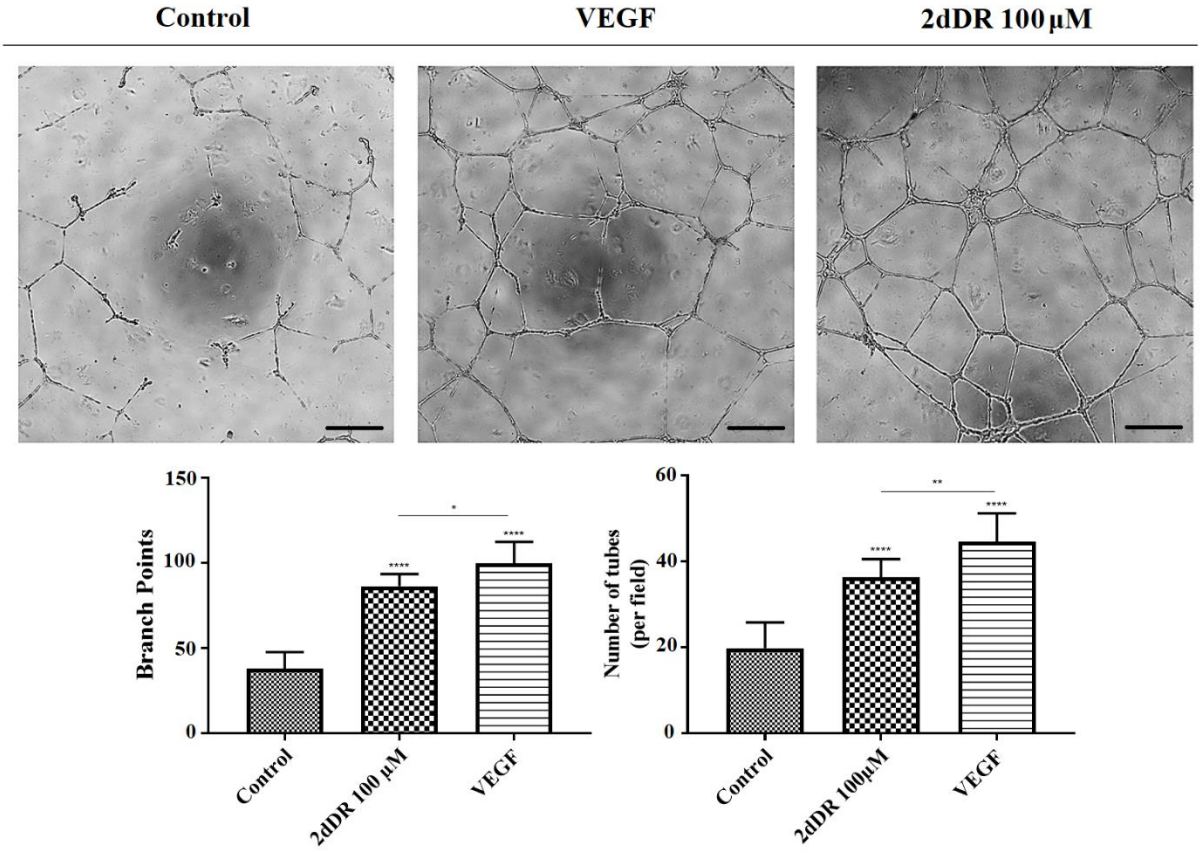


***Figure 24:*** *The effect of 2dDR (100µM) and VEGF (80 ng/ml) on tube formation was assessed with Matrigel tube formation assay. The quantified results of the average number of branch points and the number of tubes per field were given in the graphs given (***p≤0.001, **p ≤ 0.01, *p ≤ 0.05, not significant (ns) p ≥ 0.05, n = 3). Scale bars represent 250 µm*

### 2.6.4. 2dDR increases the VEGF production of HAECs

The results of the VEGF quantification demonstrated that the administration of either 100 µM or 1 mM of 2dDR to HAECs growth media led an increase in the amount of VEGF produced by the cells over 5 days (Figure 25). No VEGF production was observed in control group at any of the time points, where HAECs were incubated with non-supplemented EC GM.

The VEGF production by HAECs in response to 2dDR treatment was statistically significant even at day 1. The amount of VEGF rose up to 871.4 ± 361.7 pg/mL and

1284.5 ± 683.1 pg/mL, respectively for 100 µM and 1 mM of 2dDR treated groups when compared to controls (average VEGF amount: 18.3 ± 1.9 pg/ mL).

By day 5, the amount of VEGF was significantly increased to 1140.6 ± 441.8 pg/mL and 1233.4 ± 384.1 pg/mL, respectively when treated with 100 µM and 1 mM of 2dDR whereas the control group showed almost no change compared to VEGF production on day 1 (15.3 ± 4.4 pg/ mL).

The VEGF added group had significantly higher amount of VEGF than other groups at all time points as expected (3669.2 ± 559.0 pg/mL and 3930.9 ± 850.5 pg/mL of VEGF by days 1 and 5, respectively).

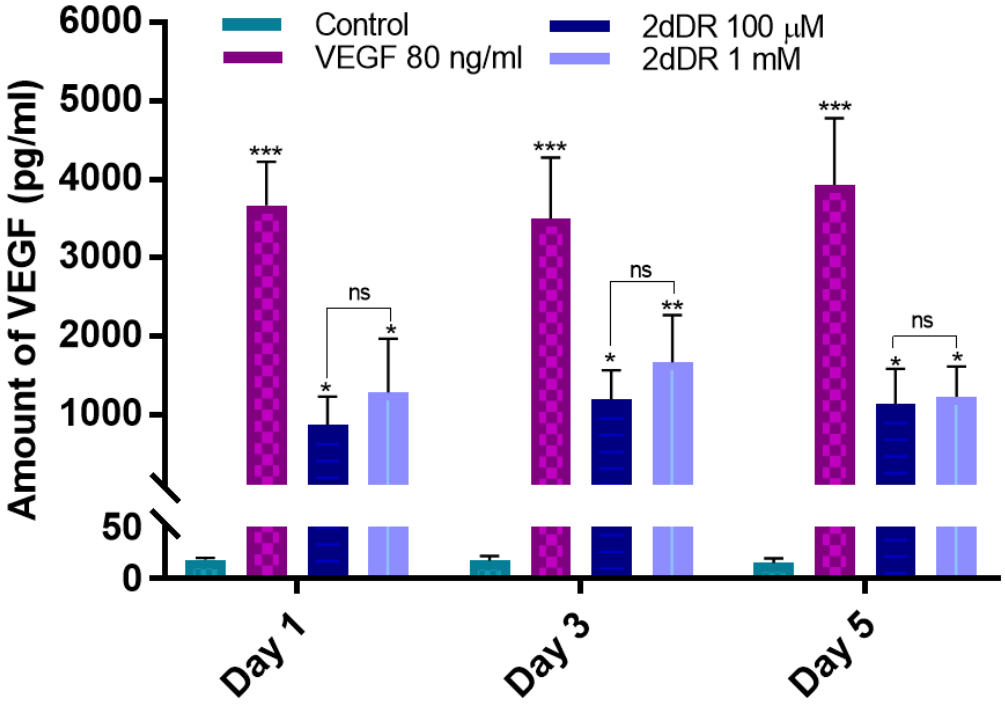


***Figure 25.*** *Quantification of VEGF production by HAECs in response to 2dDR treatment*

The results of the stability studies showed that there was a decrease of 2dDR in the media for over 7 days, either in the presence or absence of HAECs. The percentage reductions of 2dDR on both day 4 and 7 were higher in the presence of HAECs when compared to control groups (no cells).

For 100 µM 2dDR treatment, on day 4, the amount of 2dDR was reduced by 23.6 ± 8.2% and 11.5 ± 2.7% in the presence and absence of HAECs, respectively. On day 7, this further reduced by 37.4 ± 9.5% (with HAECs) and 21.5 ± 6.6% (without HAECs). On day 14, the percentage reductions in the amount of 2dDR were 41.2 ± 9.9% and 37.1 ± 3.5%,

respectively, for cellular ad acellular groups with no statistically significant difference (Figure 26A).

For 1 mM 2dDR treatment, on day 4, the amount of 2dDR was reduced by 28.7 ± 7.7% and 12.8 ± 6.3% in the presence and absence of HAECs, respectively. On day 7, this further reduced by 31.5 ± 4.4% (with HAECs) and 18.5 ± 5.9% (without HAECs). By day 14, the percentage reductions in the amount of 2dDR were 47.1 ± 10.2% and 37.2 ± 10.3%, respectively, when HAECs existed and not existed in the well plates. (Figure 26B).

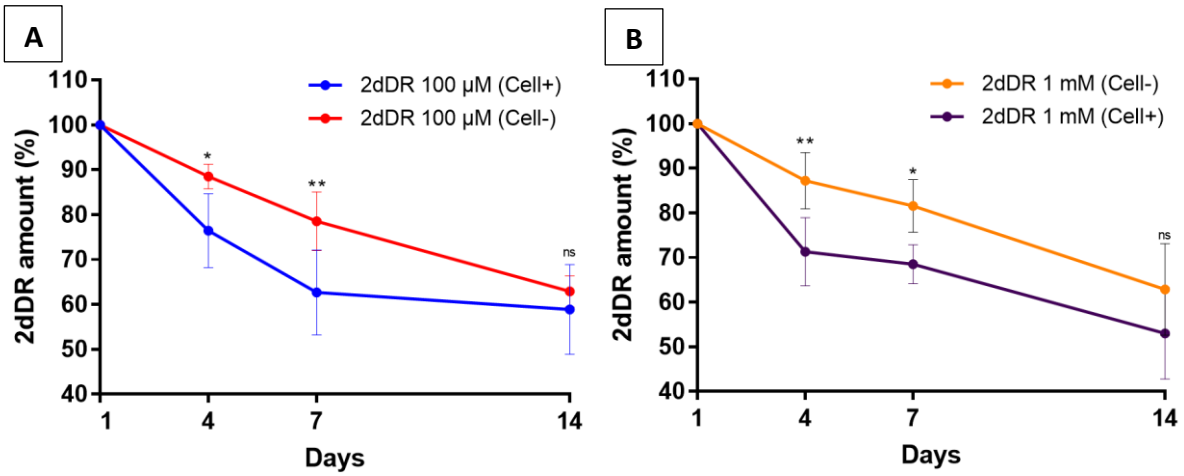


***Figure 26.*** *Bial's Orcinol Assay for the assessment of the stability of 2dDR. (A) 100 µM 2dDR and (B) 1 mM 2dDR in the presence or absence of HAECs over 14 days. (**p ≤ 0.01, *p ≤ 0.05, n = 3)*

### 2.6.5. 2dDR promotes vascularisation in *ex-ovo* CAM assay

#### 2.6.5.1. The results of the angiogenic potential of 2dDR when administered to CAM

##### 2.6.5.1.1. Effect of E2 and 2dDR on the macrostructure of CAM

Quantification of the macroimages of CAMs showed that E2-100, E2-200 and E2-600 groups increased the number of branch points 1.3-fold, 1.5-fold and 1.4-fold respectively and, all concentrations increased the average vessel length approximately 1.2-fold compared to controls over 4 days. In the same way, 2dDR-20 and 2dDR-200 increased the number of branch points by 1.3 times and 1.4 times, respectively. Both concentrations increased the average vessel length approximately 1.2 times while there was no significant difference for the 2dDR-1000 group compared to control scaffolds. VEGF increased the number of branch points by 1.4-fold and the average vessel length by 1.7-fold. Quantification of the branch points and average vessel lengths and the macroimages

of the CAMs with the most effective concentrations of E2 (E2-200) and 2dDR (2dDR-200) are shown in Figure 27.

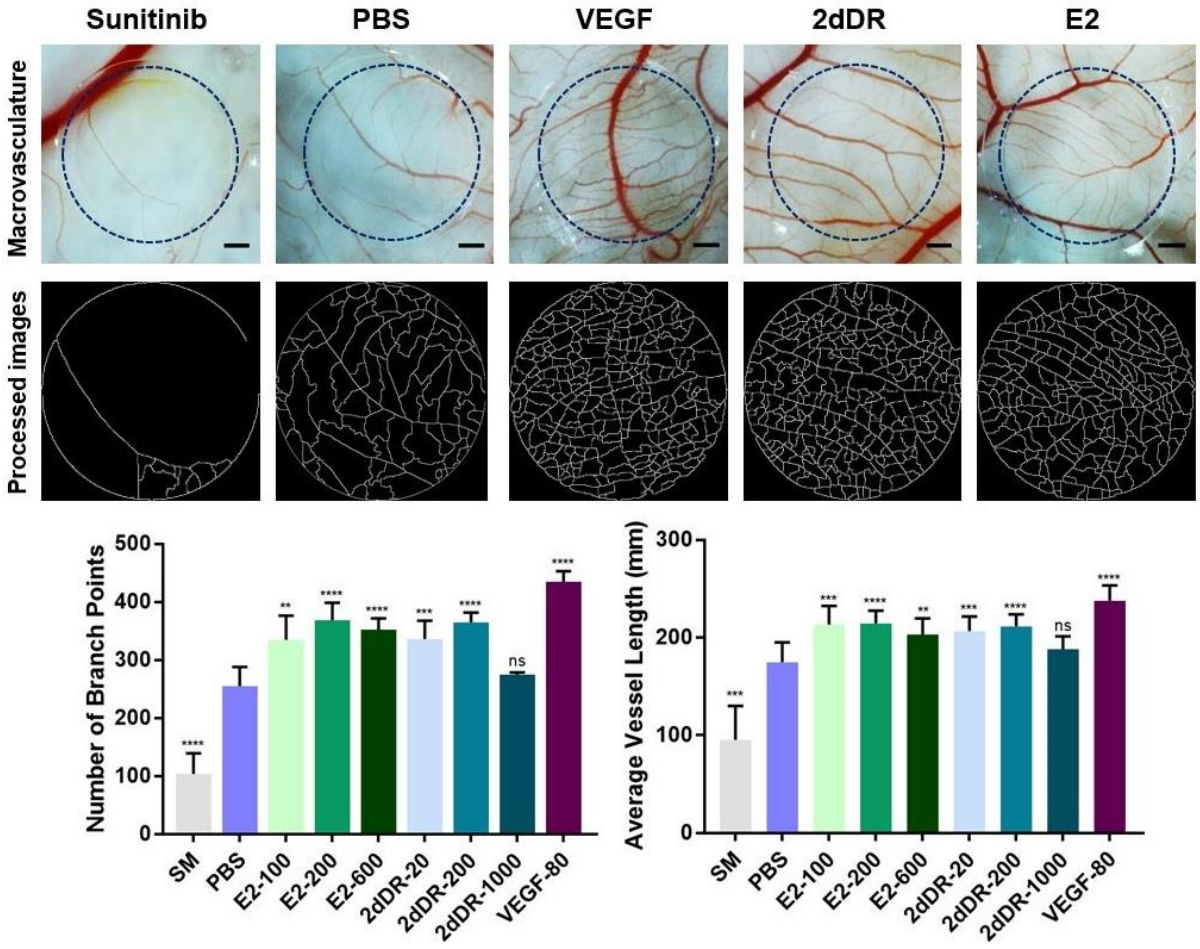


***Figure 27.*** *Evaluation of different concentrations of Estradiol (E2) and 2-deoxy-ribose (2dDR) to stimulate new blood formation in a CAM assay. Three concentrations of both drugs were compared against a negative (SM), PBS and positive (VEGF) control in these experiments. A normal angiogenic response can be seen in the PBS group. A significant increase in the average length of blood vessels and the number of branch points compared to PBS can be observed for both E2 and 2dDR groups (upper row). Representative images are given for E2 (200 ng/day) and 2dDR (200 µg/day). Processed images used for quantification of results are given for each group (middle row). **** P ≤ 0.0001, *** P ≤ 0.001, ** P ≤ 0.01, * P ≤ 0.05, ns P≥0.05, n=9±SD. The number of branch points and average macrovessel lengths seen in response to different concentrations of E2 and 2dDR were calculated and compared to PBS controls over 4 days (lower row). Values represent mean ± SD. Scale bars represent 1 mm*

2.6.5.1.2. Effect of E2 and 2dDR on the microstructure of CAM

Microvascular evaluation of the CAM samples showed that VA% was increased from 55.3% ± 3% to 79.5% ± 5% and 71.7% ± 3% for E2 and 2dDR applied groups respectively compared to controls over 4 days. VEGF and Sunitinib were used as positive and negative controls. Although the vascular area was significantly higher in VEGF groups when

compared with 2dDR and E2 applied CAMs, VEGF also resulted in smaller lacunae formation. Sunitinib, as an inhibitor of angiogenesis, led to much larger lacunae (Figure 28).

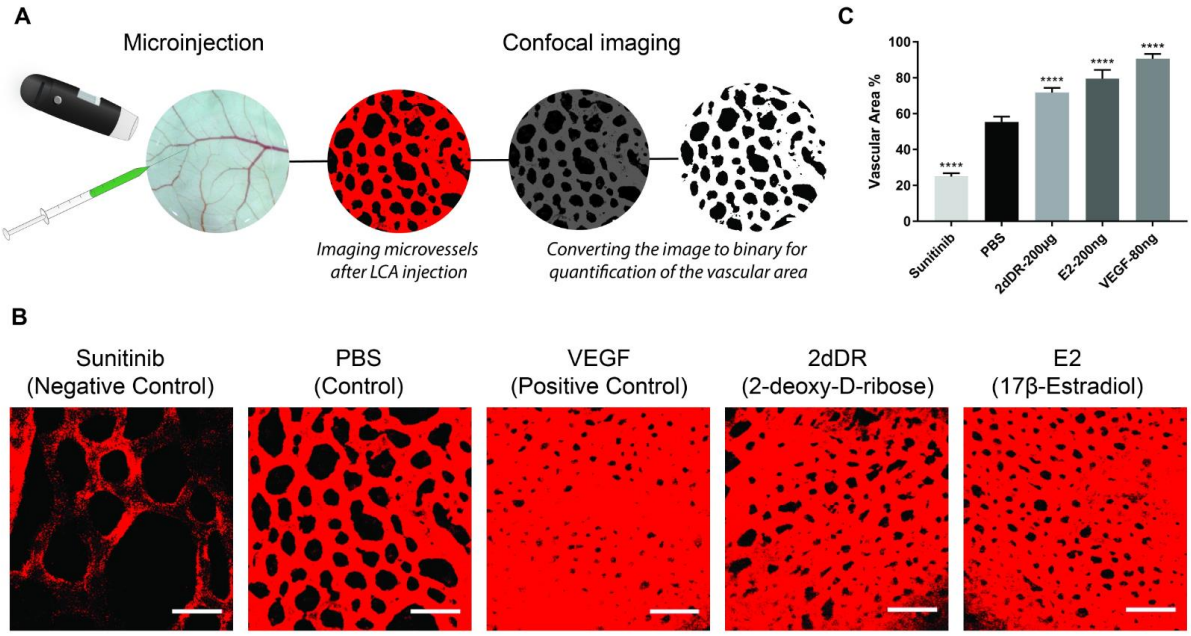


***Figure 28.*** *Demonstration of the effect of Estradiol (E2) and 2-deoxy-D-ribose (2dDR) on microvasculature compared to the application of PBS (Control). Rhodamine-labelled Lens culinaris agglutinin (LCA) was injected into the circulation of the CAM to visualize microvasculature (A). Similar to VEGF group, endothelial cell hypertrophy together with smaller lacunae compared to PBS can be observed for both E2 and 2dDR groups (B). Percentage area covered by endothelial cells was calculated for each group and compared (C). 2dDR was applied as 200 µg/day and E2 as 200 ng/day. **** P ≤ 0.0001, *** P ≤ 0.001 compared to PBS, n=9±SD. Scale bars represent 50 µm*

### 2.6.5.2. The results of the angiogenic potential of 2dDR when released from PHBV fibres

#### 2.6.5.2.1. Characterisation of E2 and 2dDR releasing PHBV scaffolds

*Effect of including E2 and 2dDR on the ultrastructure of the PHBV scaffolds*

SEM images of the E2 and 2dDR releasing PHBV scaffolds can be seen in Figure 4. The diameters of the fibres were significantly increased by the addition of substances in all groups (25 mg E2 (0.83 ± 0.17 µm), 50 mg E2 (0.98 ± 0.35 µm), 250 mg 2dDR (0.89 ± 0.19 µm), 500 mg 2dDR (1.22 ± 0.28 µm)) added PHBV scaffolds when compared with the PHBV control group (0.66 ± 0.16 µm) as shown in the graph on the bottom right corner of Figure 29.

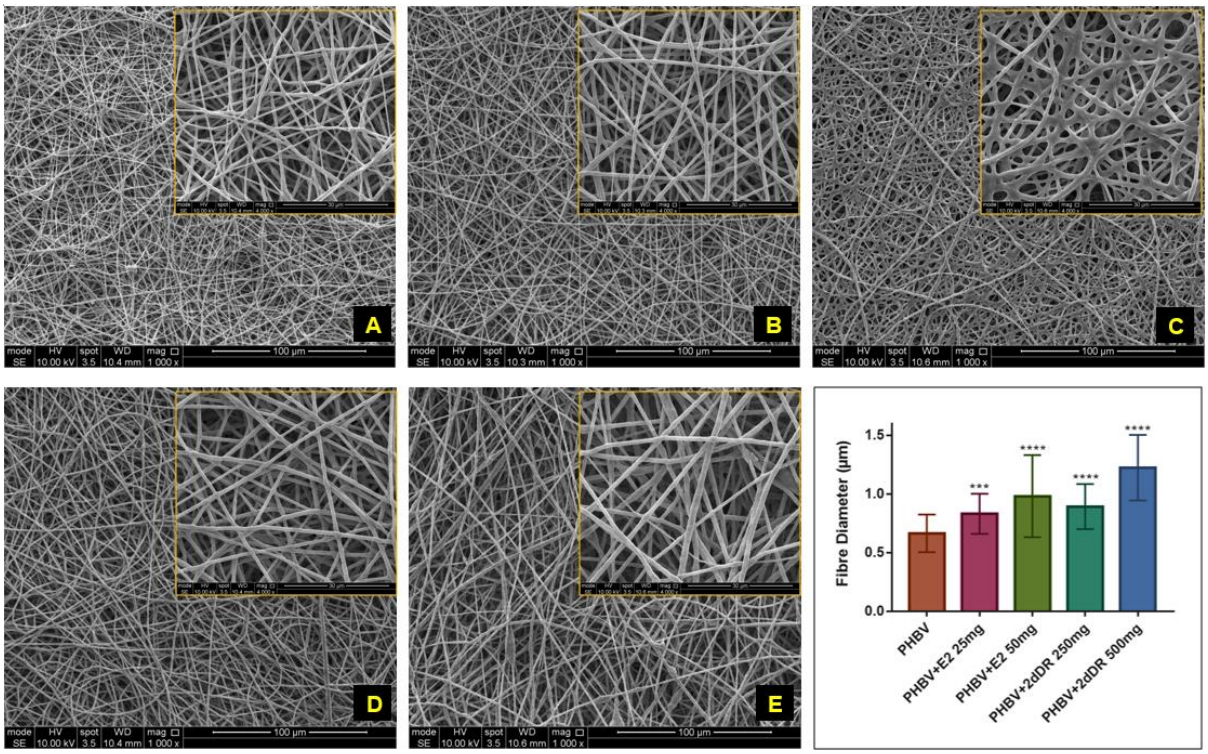


***Figure 29.*** *SEM images of the scaffolds. (A) Plain PHBV, (B) PHBV + 25 mg E2, (C) PHBV + 50 mg E2, (D) PHBV + 250 mg 2dDR, (E) PHBV + 500 mg 2dDR. The graph on the bottom left corner shows the distribution of fibre diameters for each scaffold, **** P ≤ 0.0001, *** P ≤ 0.001. Scale bars represent 100 µm*

*Release of E2 and 2dDR from PHBV scaffolds over 30 days*

The rate of release of E2 and 2dDR from scaffolds was assessed over 30 days as shown in Figure 30A. By 7 days, 2dDR release from the scaffolds was 81.3% and 86.5% of the 2dDR present in the polymer solution for 250 mg and 500 mg 2dDR scaffolds, respectively. In contrast the total E2 release from scaffolds within 7 days represented 1.3% and 1.6% of the initial E2 present in the polymer solution for 25 mg and 50 mg E2 scaffolds respectively.

*Comparison of effects of E2 and 2dDR on the mechanical properties of scaffolds*

The thicknesses of the scaffolds were 105 ± 22 µm, 84 ± 13 µm, 62 ± 10 µm, 136 ± 12 µm, and 124 ± 13 µm for plain, E2 25, E2 50, 2dDR 250, and 2dDR 500 PHBV scaffolds respectively. As can be seen from Figure 30B, the addition of all substances significantly increased the UTS of PHBV scaffolds when compared with plain PHBV scaffolds. Addition of E2 increased the UTS of the scaffolds more when compared with 2dDR added groups. Similarly, the Young's modulus of the scaffolds loaded with 2dDR and E2 was significantly

higher compared to unloaded PHBV scaffolds. 250 mg 2dDR loading increased the Young's modulus of PHBV scaffolds to the greatest extent, as shown in Figure 30B. The wettability of the drug-releasing scaffolds was investigated through a droplet retention time which is calculated using a drop shape analyser. The retention time of the water droplet on drug released scaffolds was given in Figure 30C. This showed that the addition of 2dDR made the scaffolds more wettable while the addition of E2 made the scaffolds less wettable.

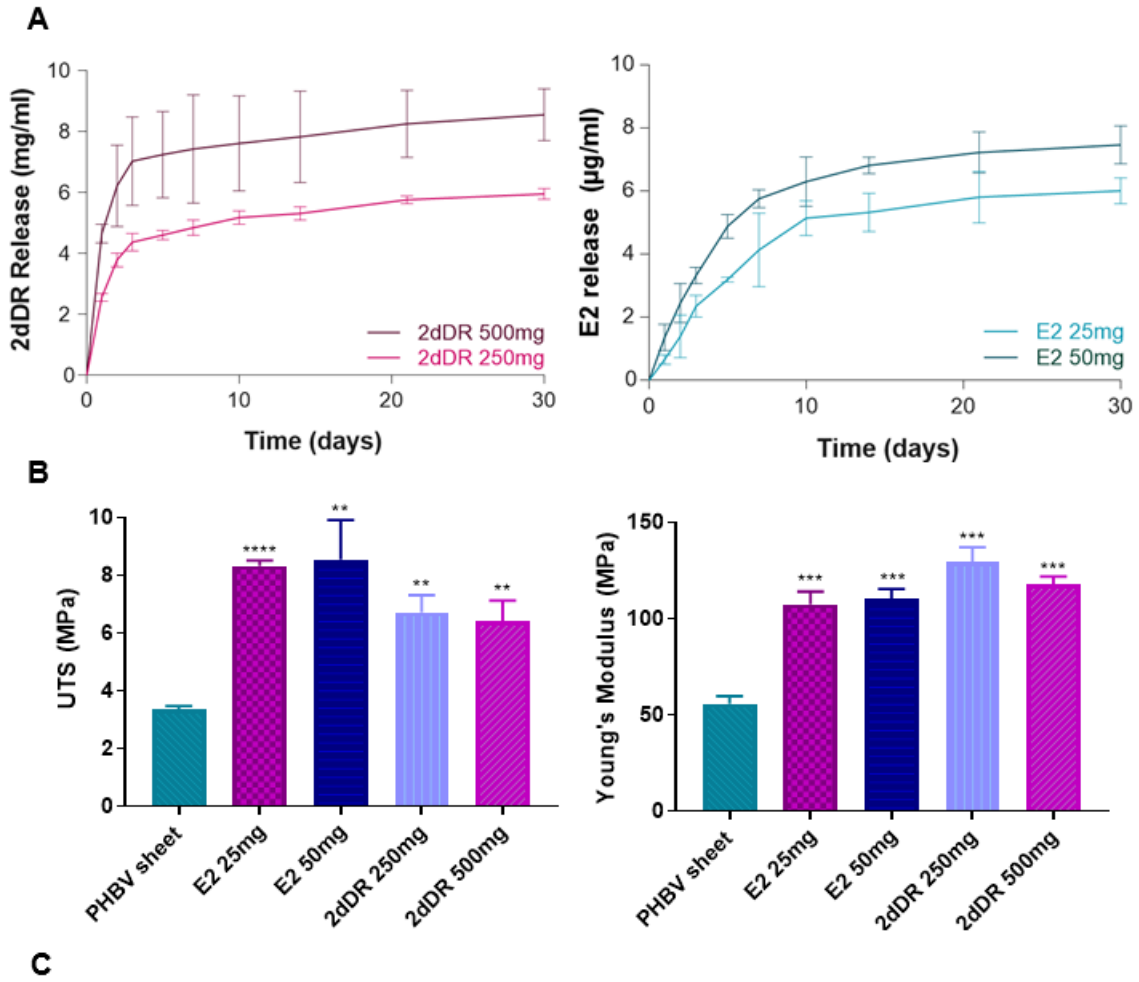


C

| Retention time (sec) | | | | |
|---|---|---|---|---|
| ***PHBV*** | ***2dDR 250*** | ***2dDR 500*** | ***E2 25*** | ***E2 50*** |
| 16.7 ± 1.4 | 2.3 ± 0.3*** | 10.7 ± 0.7* | 28.0 ± 0.3* | 198.3 ± 2.2**** |

***Figure 30.*** *(A) Release of 2dDR and E2 from PHBV scaffolds over 30 days, n=6±SD. (B) comparison of UTS and Young's modulus and (C) droplet retention time on the scaffolds, **** P ≤ 0.0001, *** P ≤ 0.001, ** P ≤ 0.01, * P ≤ 0.05, n=6±SD*

2.6.5.2.2. Assessment of the angiogenic potential of the E2 and 2dDR releasing scaffolds

Assessment of E2 and 2dDR releasing scaffolds on CAM demonstrated that all groups at least doubled the number of discernible blood vessels growing towards the scaffolds in comparison with plain PHBV scaffolds as can be seen in Figure 31. Mean vessel counts for 25 mg E2 loaded scaffolds and 50 mg E2 loaded scaffolds were 49.5 (±0.92) (**** $P \leq 0.0001$) and 37.9 (±1.05) (**** $P \leq 0.0001$) respectively, while it was 48.6 (±1.02) (**** $P \leq 0.0001$) and 37.1 (±1.37) (**** $P \leq 0.0001$) for 250 mg and 500 mg 2dDR loaded scaffolds respectively when compared with control groups (mean vessel count: 23.1 (±1.24)). None of the loaded substances affected the embryo survival rate, which was over 75% for each group.

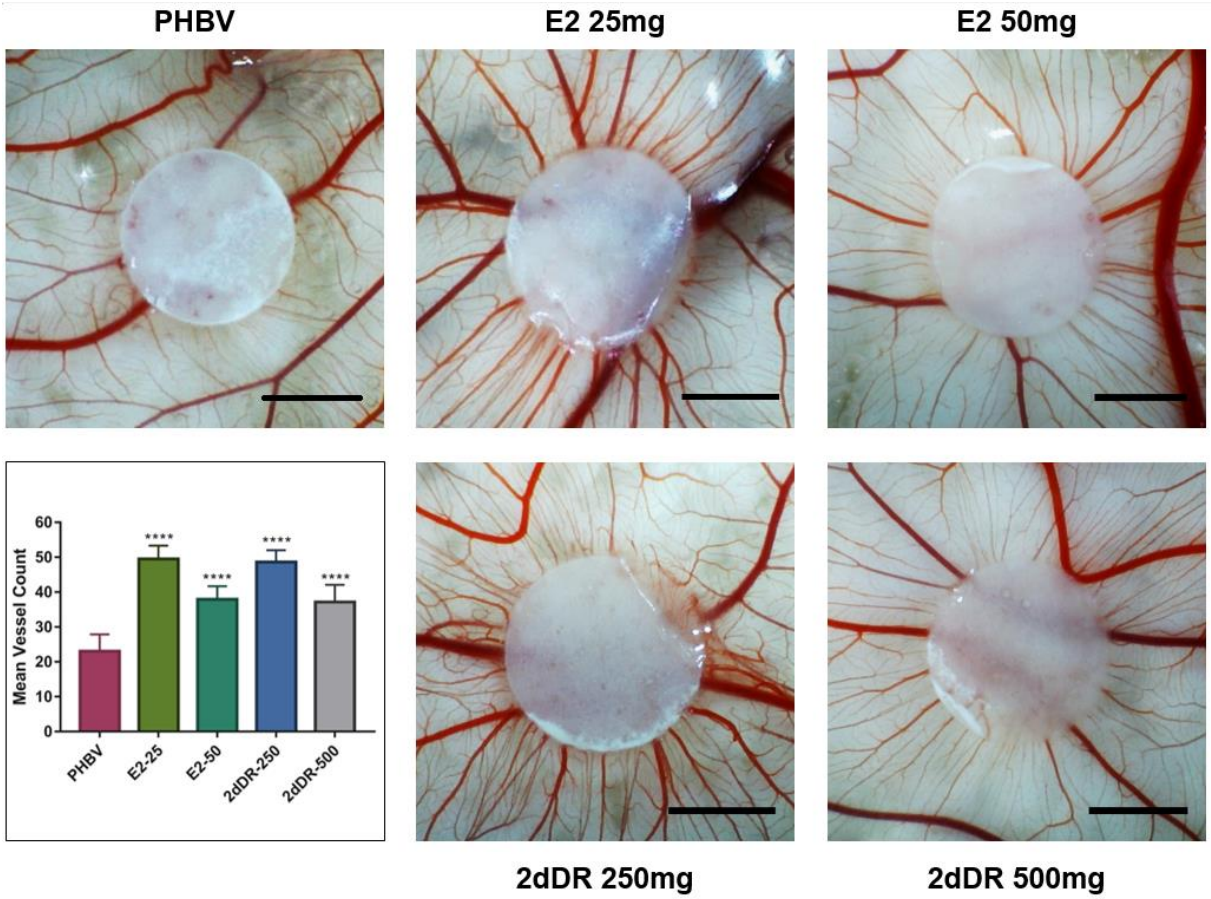


***Figure 31.*** *Representative images demonstrating the angiogenic potential of 2dDR (250 mg and 500 mg) and E2 (25 mg and 50 mg) releasing scaffolds in comparison with PHBV scaffolds. The graph on the bottom left shows the quantitative data from these experiments-mean vessel counts, **** $P \leq 0.0001$. Scale bars represent 3mm, n=6±SD*

#### 2.6.5.2.3. Histological analysis of the E2 and 2dDR releasing scaffolds on CAM

All groups showed good biocompatibility and similar changes in the structure of CAM with a small increase in cell density in the mesoderm layer in all scaffold groups. The mean number of blood vessels adjacent to the scaffolds was significantly increased in response to all concentrations of both E2 and 2dDR releasing scaffolds when compared with controls and CAM only groups (see Figures 32 and 33).

All scaffolds, whether loaded with pro-angiogenic agents or unloaded showed good attachment to the CAM, and all membranes showed similar cellular infiltration. Figure 30 shows representative histology images.

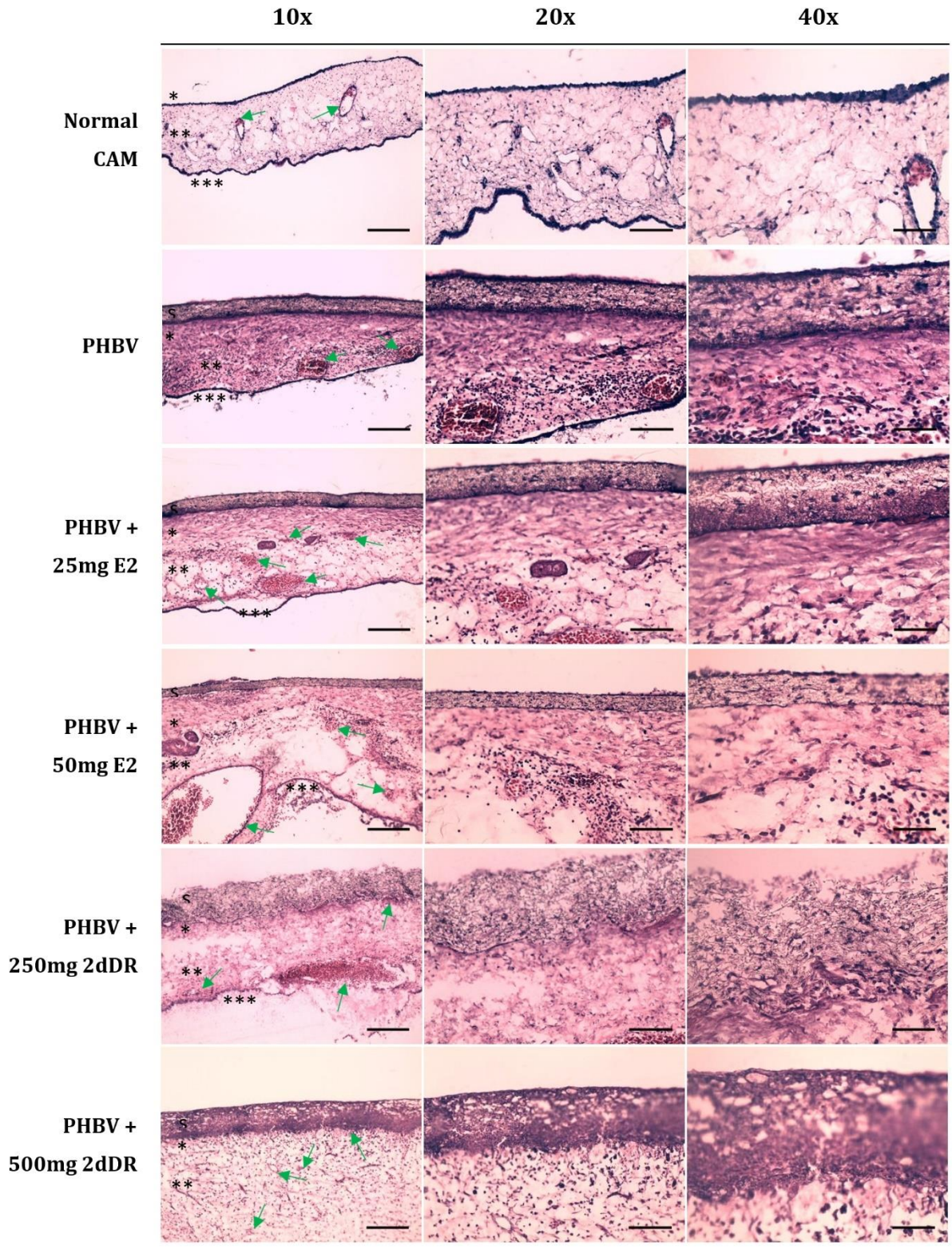


***Figure 32.*** *Histological analysis (H&E staining) of CAMs after 7days of incubation with or without scaffolds in different magnifications. The orientation of the scaffold (s), CAM ectoderm (*), mesoderm (**), and endoderm (***) layers were indicated in the images. Green arrows show the blood vessels. Scale bars = 0.2 mm (10×), 0.1 mm (20×), 0.05 mm (40×)*

| Groups | Mean vessel count |
|---|---|
| CAM only | 6.85 ± 0.31 |
| PHBV | 6.90 ± 0.39 |
| PHBV + E2 25mg | 10.59 ± 0.75 |
| PHBV + E2 50mg | 11.35 ± 0.79 |
| PHBV + 2dDR 250mg | 10.32 ± 0.97 |
| PHBV + 2dDR 500mg | 11.52 ± 0.75 |

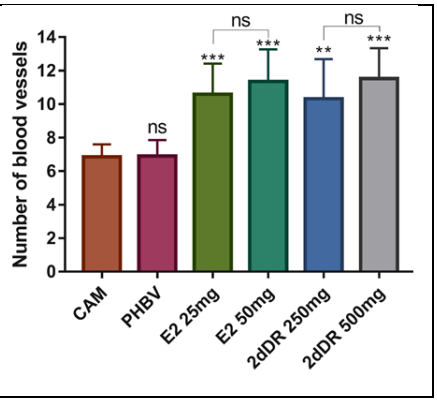


***Figure 33.*** *Quantification of the discernible blood vessels adjacent to the scaffolds at 10× magnification from a total of six different slides for each group and six different areas of interest from each slide. (*** P ≤ 0.001, ** P ≤ 0.01, * P ≤ 0.05, ns P≥0.05)*

### 2.6.6. 2dDR promotes wound healing and angiogenesis in the diabetic rat model

#### 2.6.6.1. Confirmation of diabetes induction of diabetes in rats

Post-wounding diabetes (induced by intraperitoneal administration of streptozotocin) was confirmed by monitoring the blood glucose levels (mg/dl) at day 4, 8, 14 and 20 using *Accu Check Active plus* by a needle prick at the tip of the rat's tail. Blood glucose levels in all rats (n=32) before administration of STZ injection were in the range of 107 – 140 mg/dl. As shown in Figure 34 blood glucose monitoring at day 4, 8, 14 and 20 post diabetes induction (STZ injection) showed blood glucose levels in the range of 350 to 450 mg/dl.

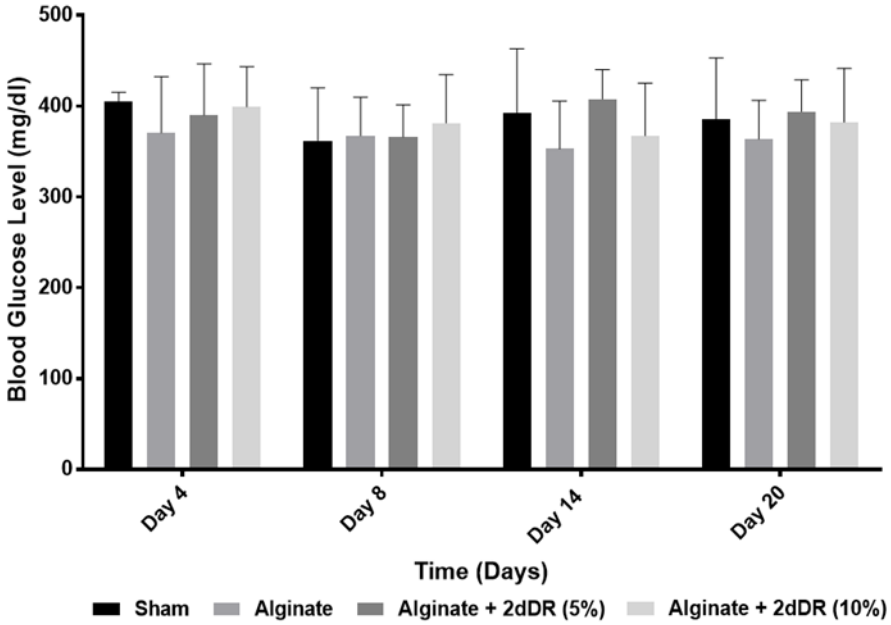


***Figure 34.*** *Blood glucose level (mg/dl) in rats monitored at days 4, 8, 14 and 20 post diabetes induction. Results presented as mean ± SD, n=4*

#### 2.6.6.2. Confirmation of sterilisation of 2dDR loaded dressings

To confirm sterility of 2dDR loaded alginate dressings, these were incubated in LB agar broth for 24 hr. Alginate dressings loaded with filter-sterilised solutions of 2dDR both pre and post gamma irradiation were confirmed to be sterile on the basis that there was no bacterial growth after 7 days culture in bacterial broth.

In this study, the alginate dressings used were those loaded with a filter-sterilised solution of 2dDR.

#### 2.6.6.3. Morphological characterisation of the alginate dressings before and after 2dDR loading

##### 2.6.6.3.1. Scanning Electron Microscopy (SEM)

SEM was performed to examine the morphology of alginate dressings both simple and 5 or 10% 2dDR loaded before and after gamma sterilisation. As can be seen in Figure 35, micrographs showed that more sugar (2dDR) content was present on the surface of alginate fibres in the case of 10% loading than 5%.

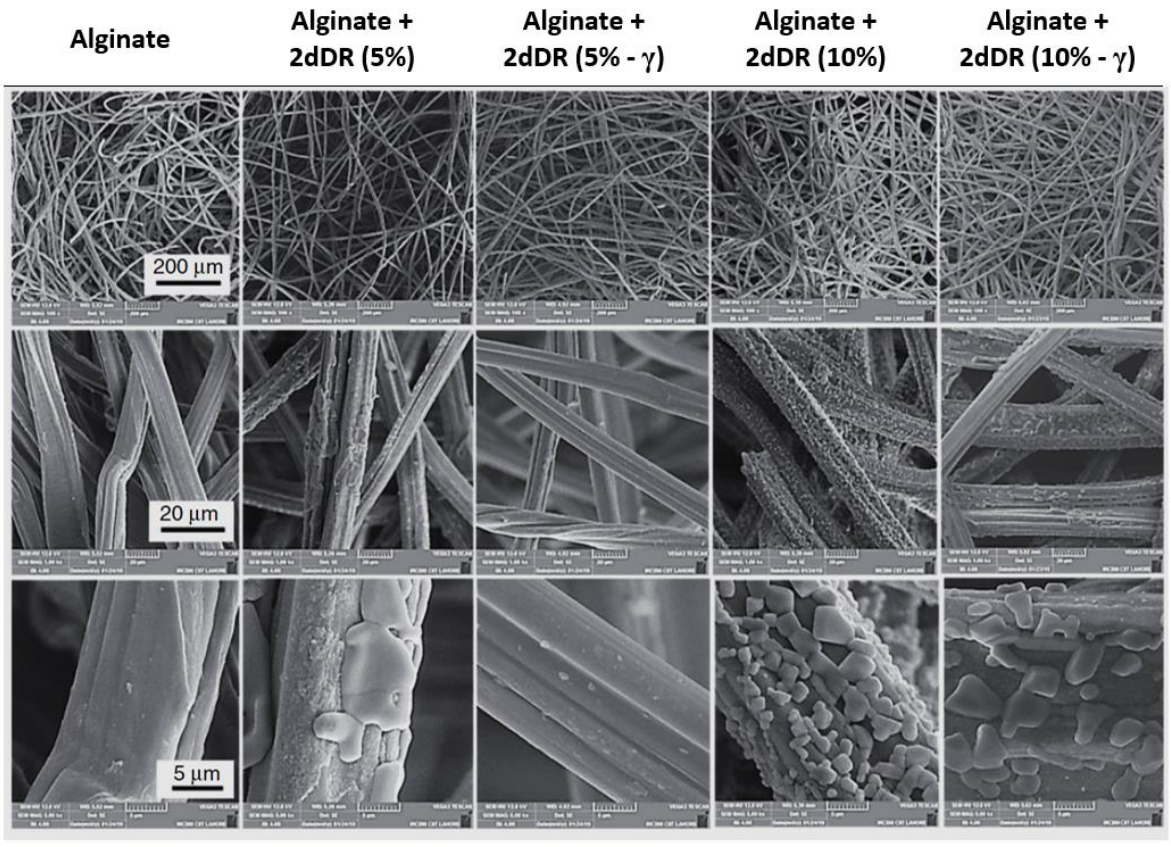


***Figure 35.*** *Scanning electron microscope (SEM) images of alginate dressing loaded with 5 and 10% 2dDR before and after gamma sterilisation at different magnifications.*

2.6.6.3.2. Release of 2dDR from alginate dressing

The release rate of 2dDR from alginate dressings over 8 days was determined following their immersion in PBS at 37° C. Figure 35 shows the cumulative 2dDR release from 5% and 10% loaded alginate dressings before (Figure 36A) and after gamma sterilisation (Figure 36B). Alginate exhibited a steady release of 2dDR over 3 days. Almost all (>90%) loaded 2dDR was released by day 3 with a similar pattern before and after gamma sterilisation.

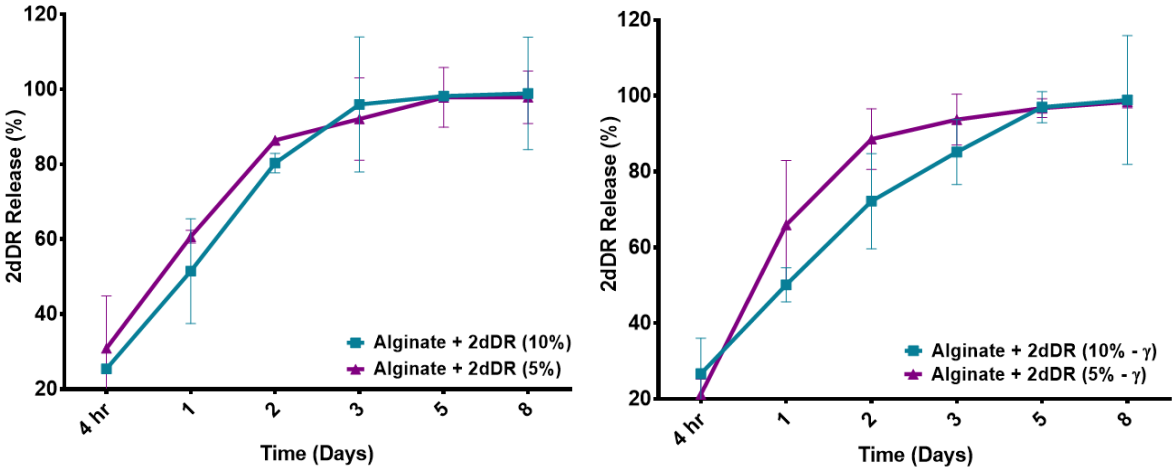


***Figure 36.*** *Drug release study: (a) cumulative release of 2dDR from alginate dressing before and (b) after gamma sterilisation over eight days. Results are presented as mean ± SD, n=3*

2.6.6.4. Assessment of 2dDR stability in water

To evaluate the stability of 2dDR, solutions of 2dDR were kept in distilled water at room temperature over 14 days as shown in Figure 37. As can be seen, there was no significant change in the absorbance measured for all three concentrations of 2dDR (1, 2 and 3 mg/ mL) at different time intervals (0, 7 and 14 days) confirming the sugar stability at room temperature over 2 weeks.

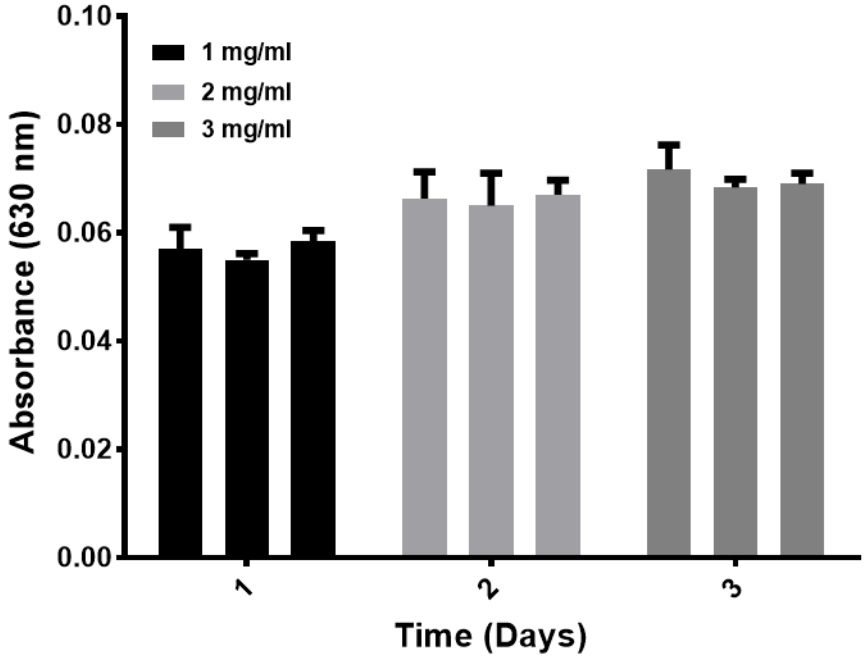


***Figure 37.*** *Stability test of 2dDR over 14 days at room temperature. Results presented as mean ± SD, n=3*

2.6.6.5. Evaluation of wound healing responses to 2dDR loaded alginate dressings on the diabetic rat model

Wound healing in the diabetic rat model was assessed by using a single application of 2dDR loaded alginate dressings kept in place for 4 days. At day 4, when wounds were photographed the dressings were removed as studies had demonstrated over 90% release of 2dDR within three days from our *in vitro* studies.

Figure 39 shows representative macroscopic images of different experimental group wounds at the time of wounding (Day 0) and then at days 4, 7, 11, 14 and 17 until the wound in the first group had healed (Day 20).

Wound areas were assessed by photographing the wounds and then using image J was used to analyse areas. As previously shown, Figure 34 confirms that the rats were diabetic throughout the study as assessed by their elevated blood glucose levels.

The first thing to note is that wounds were slow to heal in these diabetic animals and had failed to heal completely in the control animals by day 20. Alginate treated rats showed slightly better healing than sham operated animals, but wounds were still open at day 20. While the addition of alginate hydrogel did significantly stimulate wound healing compared to the sham operated control the addition of 2dDR at either 5 or 10%

significantly improved the wound healing response in all experimental rats. The rats treated with 2dDR loaded alginate dressings (both 5% and 10%) showed complete wound closure by day 20.

Figure 38 shows the percentage of wound closure in all study groups at 4, 7, 11, 14, 17, and 20 days post-transplantation. Results demonstrated that wound closure was significantly faster overall in both 2dDR treated groups than applying simple alginate and sham operated control except at day 4. Furthermore, no significant difference was observed in the groups treated with either 5% or 10% 2dDR loaded alginate dressing.

Statistical analysis showed the inclusion of 2dDR in alginate dressings improved the rate of wound healing compared to the use of alginate dressings on their own.

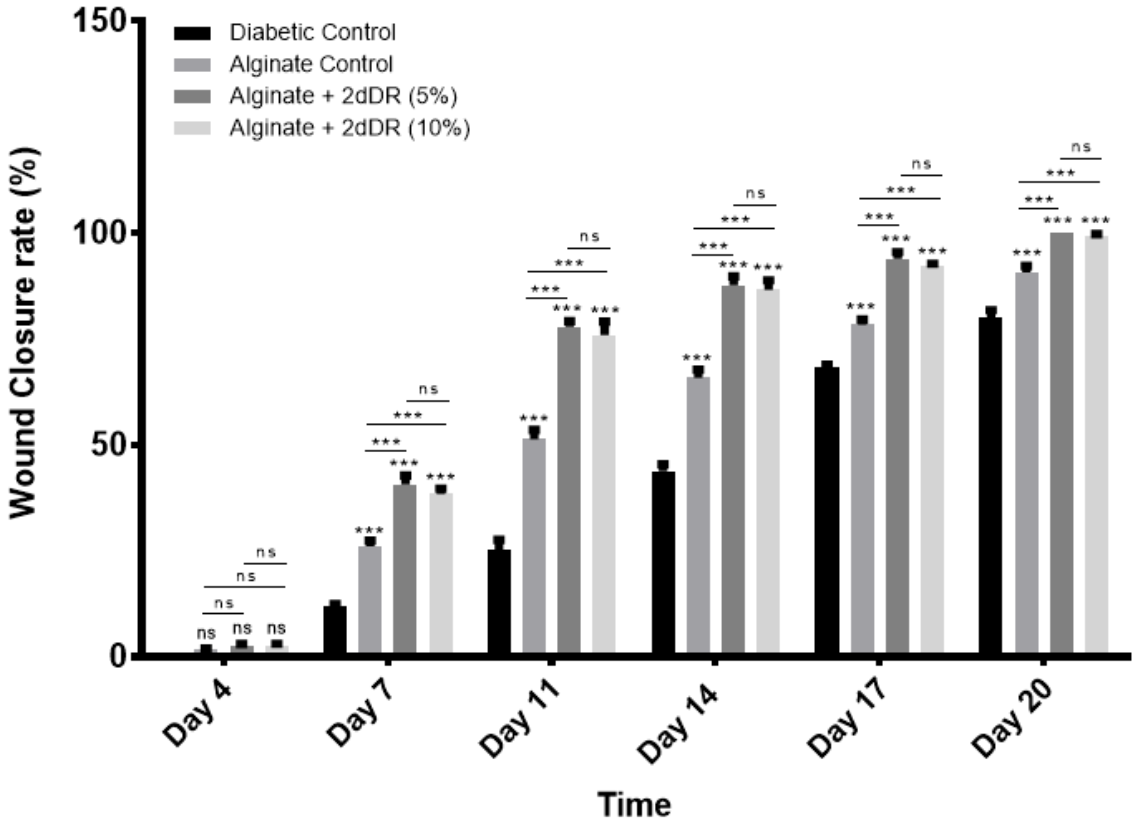


***Figure 38.*** *Graphical representation of wound closure analysis at days 4, 7, 11, 14, 17 and 20 of sham (without any dressing), alginate (without 2-dDR), alginate + 2dDR (5%) and alginate + 2dDR (10%). *** P ≤ 0.001, not significant (ns) P≥0.05, n=4 ± SD*

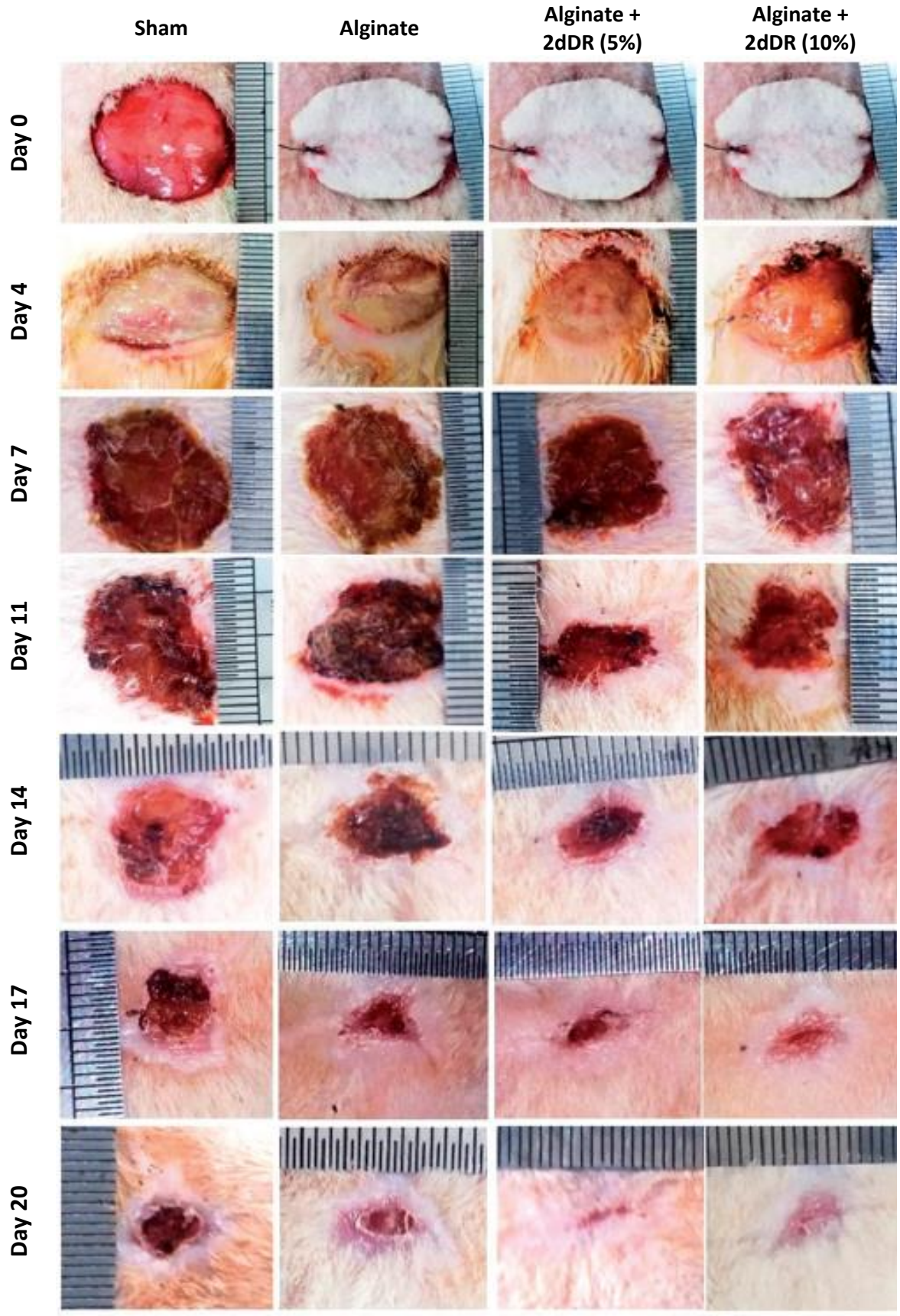


***Figure 39**. Representative macroscopic analysis of wounds; sham (without any dressing), alginate (without 2dDR), alginate + 2dDR (5%) and alginate + 2dDR (10%) are shown at days 0, 4, 7, 11, 14, 17 and 20 post wounding*

#### 2.6.6.6. Histological and Immunohistochemistry analysis of wound beds

Skin wound samples from all groups were harvested on day 7 and 20, for comparison between treated and non-treated diabetic wounds. At day 7 H&E staining demonstrated there was no evident epithelium in any of the wound areas (Figure 40) whereas by day 20 it was possible to see the formation of a new stratified epithelium covering the whole area that was previously wounded for wounds treated with 5% and 10% 2dDR loaded alginate dressings (Figure 41). In contrast, non-treated wounds and wounds treated with the alginate dressing showed disorganised granulation by 20 days (Figure 41).

The samples were then stained for three different antigens (CD34 for progenitor endothelial cells, and CD80 and CD163 for M1 and M2 macrophages, respectively). At both time points, blind scoring of CD34 staining for 5% and 10% 2dDR loaded alginate groups showed a similar significant increase in neovascularisation in the healed areas compared to the non-treated and alginate dressing treated groups (Figure 40 and 41). At both time points, the M1 response did not differ significantly between groups, and similarly, the M2 response was similar between all groups with no significant differences by day 7. By day 20, a significantly higher M2 response was observed for all treated groups compared with the non-treated group (Figure 41).

The ratio of M2 to M1 was above 1 for all groups at both time points as the M2 response was consistently much higher than the M1 response (Figure 40 and 41).

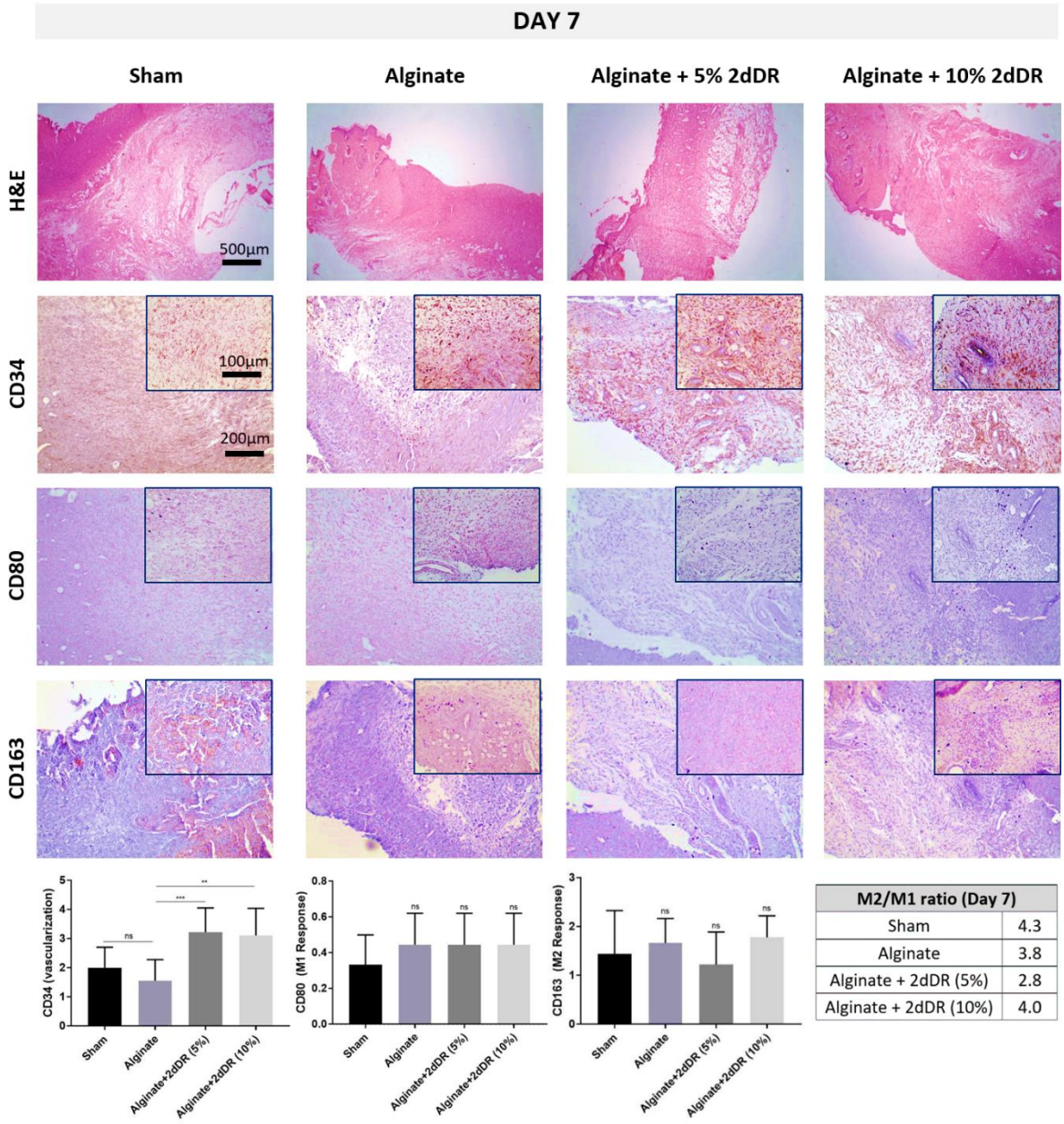


| M2/M1 ratio (Day 7) | |
|---|---|
| Sham | 4.3 |
| Alginate | 3.8 |
| Alginate + 2dDR (5%) | 2.8 |
| Alginate + 2dDR (10%) | 4.0 |

***Figure 40.*** *From top to bottom; images of H&E and immunostaining of CD34, CD80 and CD163 at day 7. Assessment of the immunostainings was done by a blind scoring system. 0 =absence; 1= mild presence; 2 =large presence; 3 =abundance; 4= large abundance. The ratio of M2/M1 is given in the table. *** P ≤ 0.001, ** P ≤ 0.01, ns P≥0.05, n=9±SD. Scale bars represent 500µm for H&E and 200µm and 100µm for lower and higher magnifications of the IHC images*

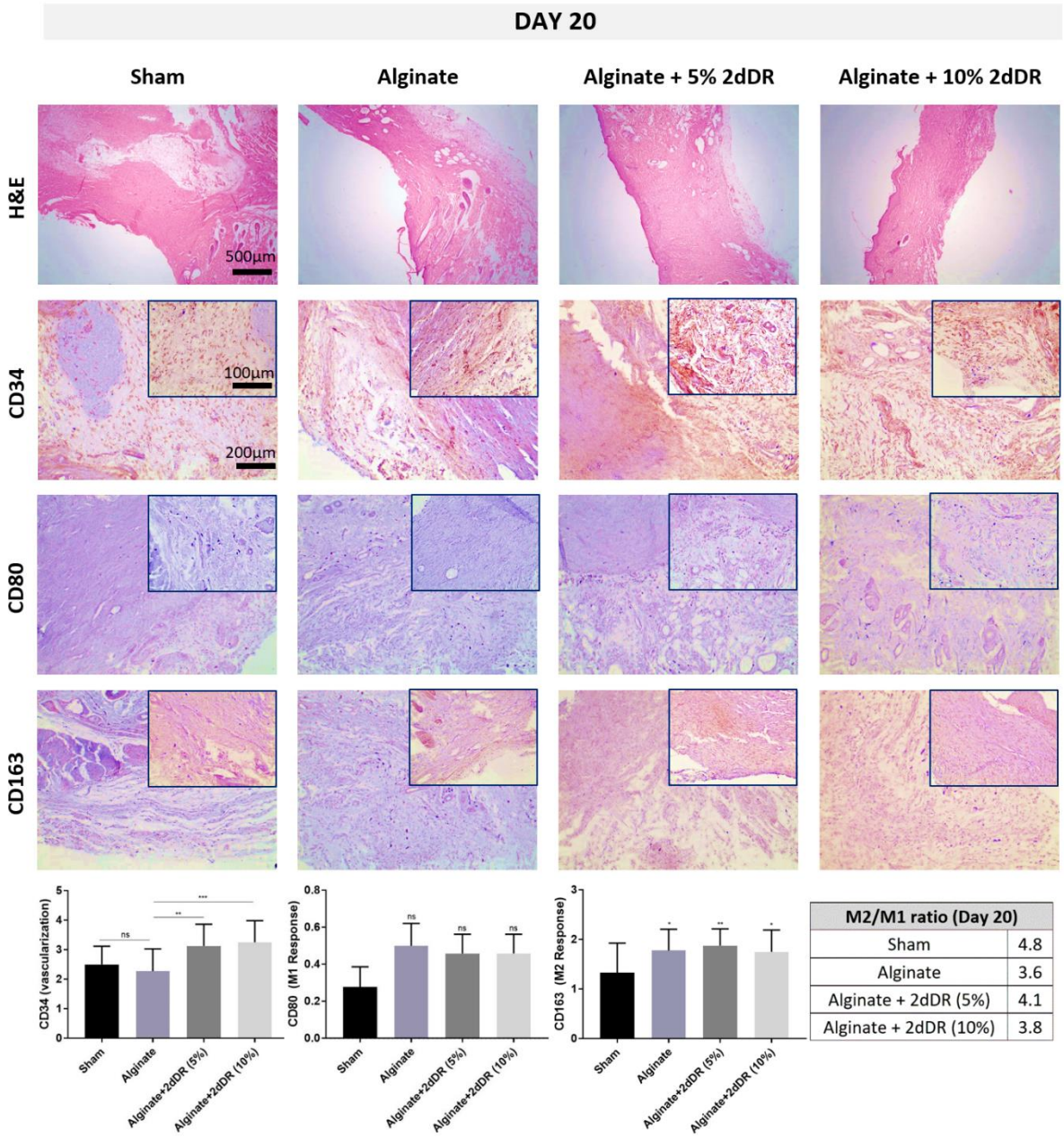


| M2/M1 ratio (Day 20) | |
|---|---|
| Sham | 4.8 |
| Alginate | 3.6 |
| Alginate + 2dDR (5%) | 4.1 |
| Alginate + 2dDR (10%) | 3.8 |

***Figure 41.*** *From top to bottom; images of H&E and immunostaining of CD34, CD80 and CD163 at day 20. Assessment of the immunostainings was done by a blind scoring system. 0 =absence; 1= mild presence; 2 =large presence; 3 =abundance; 4= large abundance. The ratio of M2/M1 is given in the table. *** P ≤ 0.001, ** P ≤ 0.01, ns P≥0.05, n=9±SD. Scale bars represent 500µm for H&E and 200µm and 100µm for lower and higher magnifications of the IHC images*

## 2.7. Discussion

As laboratory production of TE materials has progressed to the clinic, it has become clear that one of the critical barriers to their success is the need to achieve rapid neovascularisation post-implantation. Rapid ingrowth and infiltration of blood vessels are crucial for biomaterials to be able to survive *in vivo* [360]. The need for improved neovascularisation is crucial for tissue engineering, and our laboratory has been seeking to develop biomaterials to promote angiogenesis.

VEGF is a crucial angiogenic factor that plays a key role in promoting angiogenesis [38]. ECs are sensitive to VEGF signalling, which regulates proliferation, migration and their survival [41,361]. Although VEGF is accepted as the gold standard for promoting angiogenesis, the use of exogenous VEGF can promote the formation of leaky [362], permeable [335] and haemorrhagic [336] vessels when administered in an uncontrolled manner. The MacNeil group and many others have sought to deliver materials which bind heparin and are therefore attractive to the binding of VEGF [344,345]. However, introducing VEGF with the TE scaffolds requires multistep actions and a long process. Moreover, the administration of large amounts of exogenous VEGF can lead to the formation of leaky and haemorrhagic vessels [334]. Thus, exploring new alternatives to the use of exogenous VEGF has critical importance. VEGF is a widely studied pro-angiogenic factor, and several reports established the signalling pathway responsible for its angiogenic activity [38,363]. Molecular mechanism of VEGFR-2 dependant angiogenesis is given in Section 1.3.1.1.1.

2dDR is a promising alternative which has been reported to have chemotactic and angiogenic activity by our group and other researchers using current angiogenic assays, Boyden chamber assay [83], tube formation assay [83], CAM assay [81,89] and rat wound healing models [87,90]. However, the dose-dependent response of 2dDR still remained to be investigated *in vitro* to learn what is the effective concentration range to drive angiogenesis at the cellular level.

First, I investigated the effect of 2dDR on proliferation, chemotactic migration and tube formation ability of HAECs. The results of the metabolic activity assay showed a dose-dependent response in the metabolic activity of HAECs. It was not effective when used at low concentrations (1 μM) but significantly improved metabolic activity and proliferation

of HAECs when used at 100 μM and to a lesser extent 1 mM. It inhibited cellular proliferation at higher concentrations (10 mM) by detaching the cells. The 100 μM 2dDR was found approximately 95% as potent as VEGF in terms of enhancing the proliferation of HAECs over 7 days. Following the metabolic activity assay, three concentrations of 2dDR (10 μM, 100 μM and 1mM) were further examined for enhancing the chemotactic migration of HAECs using a modified Boyden chamber assay. All the 2dDR concentrations and VEGF showed a statistical difference when compared with controls in terms of migration of HAECs from the upper chamber to the lower one where the chemoattractant was located. The 100 μM group was then selected for further experiments to evaluate how the addition of 2dDR and VEGF influences the formation of capillary tube-like structures using a well-established method of assessing angiogenesis, Matrigel® tube formation assay [364]. The administration of 100 μM 2dDR and VEGF increased the number of capillary tubes formed and the number of branch points.

The comparison of 2dDR with 2dLR, 2dDG and DG showed that none of the other small sugar molecules increased the activity of HAECs over 7 days. Instead, I demonstrated that 2dDG (when administered at 100 μM, 1 mM and 10 mM) and 2dLR (when used at 10 mM) had an anti-angiogenic effect on HAECs proliferation. The anti-angiogenic impact of 2dDG and 2dLR has been reported by several groups. Uchimiya et al. reported TP-mediated angiogenesis could be suppressed by 2dLR [83]. Similarly, Nakajima et al. showed that 2dLR reduces the vascular area increased by TP-mediated tumour angiogenesis in metastatic nodules [86]. Merchan et al. reported that 2dDG reduces the tube formation *in vitro* and inhibits angiogenesis *in vivo* [365]. Likewise, Chuang et al. reported the inhibition of new tube formation in 2dDG treated rat aortic rings and showed that 2dDG reduced cell viability, tube formation capability, and VEGFR-2 expression of HUVECs *in vitro* [366].

In summary, the *in vitro* assessment of the angiogenic activity of 2dDR showed it to be dose-dependent reproducing all of the actions of VEGF with 2dDR stimulating proliferation, migration and tube formation of HAECs. 100 μM concentration was essentially equivalent to 80 ng/mL of VEGF. None of the other small sugar molecules (2dLR, 2dDG, and DG) were found to be effective for inducing angiogenesis *in vitro.*

Following the *in vitro* assessment of 2dDR, I aimed to investigate the angiogenic potential of 2dDR and E2 either applied as solutions or released from fibrous TE constructs and to

explore if it is possible to define certain concentrations of either 2dDR or E2 which are as effective as VEGF in stimulating angiogenesis in CAM assay. To date, there have been no studies conducted on the effective angiogenic dose range of 2dDR, which is proangiogenic *in vivo*. Therefore, for the first time in this study, I demonstrated the reliable concentration ranges for both 2dDR and E2 for stimulating angiogenesis in CAM assay and compared their proangiogenic activities with the VEGF used as a positive control.

The key findings from this study were that 2dDR and E2 showed dose-dependent angiogenic responses, and our results demonstrate that both were found to be approximately 80% as potent for the production of new blood vessels *in vivo* when compared with VEGF as a positive control. The results of the dose response studies showed that the most effective doses were 200μg/day/embryo and 200ng/day/embryo for 2dDR and E2, respectively. Higher and lower doses of the drugs showed less angiogenic activity in the CAM assay. These results were further confirmed with the investigation of the microvascular structures of CAM when treated with the drugs. In VEGF treated groups, the VA% was far higher than in other groups. However, microvessels upregulated by VEGF showed smaller lacunae formation due to endothelial cell hypertrophy when assessed with confocal microscopy, while a more consistent and stable microvessel structure with a significantly increased VA% was found in 2dDR and E2 treated CAMs. This, we suggest, is important as VEGF has been reported to lead to the formation of leaky and haemorrhagic vessels [334]. Although angiogenic activities of 2dDR and E2 were evaluated with the direct applications of those to CAM, this administration method is only used for determination of the most angiogenic concentrations of the drugs.

The effective concentrations of 2dDR and E2 were then loaded into electrospun PHBV constructs to stimulate angiogenesis with the sustained release of both agents from fibres. PHBV is a natural, biocompatible and biodegradable biopolymer [367]. Although the biodegradability of PHBV is relatively slow when compared to PLA [368], it is still an attractive material for drug release studies because of its excellent biocompatibility, biodegradability, and easy processing properties [369].

Incorporation of 2dDR and E2 into the PHBV scaffolds resulted in some alterations in fibre morphology and hydrophobicity of the scaffolds although no technical problems or adverse effects of introducing E2 and 2dDR into fibres were experienced.

Introduction of both drugs significantly increased fibre diameters in accordance with the increasing concentrations of the drugs, and a change in the fibre structure of electrospun PHBV scaffolds that contain higher concentrations of E2 was observed. Physical crosslinking of electrospun fibres (or fibre fusion) was observed in PHBV scaffolds loaded with a higher dose of E2. The fibre fusion can be explained with the decrease in viscosity of the electrospinning solution with the addition of E2, a highly plasticizing agent [370]. This decrease in viscosity leads to slow evaporation of the solvent during electrospinning [371] which results in fused fibres. Unnithan et al. also reported similar changes in fibrous morphology of E2 loaded electrospun polyurethane (PU) scaffolds due to a change in the viscosity of the electrospinning solution [372]. On the other hand, the incorporation of 2dDR into the electrospun PHBV scaffolds did not affect fibre ultrastructure. However, although the SEM images did not show any change in fibre structure, I did observe reduced structural integrity of the fibres in histologic sections of 2dDR releasing scaffolds. These alterations occurred after the scaffolds were implanted on CAM. Therefore, it is likely that this change was due to rapid deformation of the fibres after the rapid release of 2dDR resulting in an increased surface area for cellular attachment and infiltration.

Addition of E2 significantly increased the hydrophobicity of the scaffolds in a dose-dependent manner. This is not surprising as E2 is known to be highly hydrophobic [373]. In contrast to E2, the addition of 2dDR significantly decreased the hydrophobic character of the PHBV fibres which can be explained by the high solubility of 2dDR in water. The estimated solubility of E2 in water is approximately 30000 times lower than sugars [374,375]. Thus, the addition of these drugs with different solubilities significantly changed the hydrophilicity of the PHBV scaffolds. Furthermore, this influenced the release characteristics. As can be expected, I observed significantly lower and slower release of E2 in comparison with the release of 2dDR from the PHBV fibres. In contrast to the lower and more sustained release of E2 from PHBV fibres, a burst release of 2dDR was observed within 7-days.

Incorporation of both drugs enhanced both the UTS and Young's modulus of the PHBV scaffolds compared with plain PHBV controls. Similarly, Huang et al. reported a similar change in tensile properties of their drug-loaded PCL electrospun scaffolds. They demonstrated that the diameters of the fibres were increased with the addition of higher

concentrations of the resveratrol (a type of antioxidant), and the addition of the drug led to the increased ultimate strength and decreased Young's modulus of their scaffolds [376].

Although both of the factors stimulated angiogenesis when applied directly onto the CAM, a more dramatic increase in the number of discernible blood vessels was seen when 2dDR and E2 releasing PHBV scaffolds were implanted to CAM. E2 was found to be slightly more effective in both application procedures when compared with 2dDR loaded and plain PHBV control groups. This study also established effective concentrations of E2 (25mg/g of PHBV) and of 2dDR (250mg/g of PHBV) to be loaded into scaffolds to achieve a reliable stimulation of neovascularisation. Higher doses of both drugs were found to be less effective in promoting the angiogenesis in CAM assay. The dose dependence of E2 has been studied by many groups. In 2004, Seo et al. reported E2 caused increased angiogenic activity *in vivo* in a dose-dependent manner [347]. Pence et al. studied the endogenous VEGF production of epithelial cells when treated with different doses of E2 *in vitro*. They found that the treatment of cells with 10 nM and 1000 nM E2 stimulated the production of VEGF where addition of 100 nM E2 showed no significant effect on cells [348]. Liu et al. examined the effect of E2 on rat cardiac microvascular endothelial cell (CMEC) proliferation and tube formation *in vitro*. With regards to the proliferation of CMECs, they reported a biphasic response to E2. The lowest and the highest doses of E2 were less effective compared to the optimal dose [349]. In contrast to studies of dosage response of E2, to date, there have not been any such studies exploring the angiogenic response to different doses of 2dDR. In view of the comparatively few studies on this small sugar, not all of which agree, I conducted a dose-dependence study of 2dDR for promoting angiogenesis. While lower doses of promoted angiogenesis, higher doses were found to be less effective. Drug releasing scaffold assays further confirmed these findings. The scaffolds loaded with the higher doses of 2dDR and E2 showed reduced angiogenic activity when compared with the scaffolds loaded with lower doses.

These results were then compared with the histologically stained sections of the scaffolds. In these, more blood vessels were counted adjacent to 2dDR and E2 releasing scaffolds. However, in contrast to the results from the quantified macro images, in histological analysis, the number of blood vessels adjacent to the scaffolds loaded with the higher doses of 2dDR (2dDR 500) and E2 (E2 50) were not significantly but slightly

greater than lower doses. These different results might be caused by our ability to see and count the smaller diameter blood vessels that may not be discernible in the digital CAM analysis used for quantification. Additionally, the histological sections also show blood vessels from different orientations which might not have been detectable on digital CAM images. This might increase the results seen for higher doses of the drugs.

E2 has previously been reported as angiogenic both *in vitro* and *in vivo* by many groups as well as our research group. Albrecht et al. suggested that E2 promotes angiogenesis through up-regulation of VEGF. They reported rapidly increased VEGF expression and cell permeability by E2 administration to ovariectomised baboons [377]. Similarly, elevated VEGF mRNA expression levels were observed in ovariectomised rats after E2 treatment by Hyder et al. [378]. Morales et al. reported that E2 promoted migration of HUVECs and formation of capillary-like networks on Matrigel [63]. Pence et at. indicated that exogenous E2 promoted endogenous production of VEGF by endometrial epithelial cells [348]. More recently, our group has demonstrated the release of E2 from both biodegradable PLA fibres [69] and from nondegradable PU fibres [379] with both electrospun scaffolds showing good proangiogenic activity in the CAM assay.

In contrast to VEGF and E2, there is relatively little literature on the angiogenic activity of 2dDR, and the mechanism of action of 2dDR remains still unclear. Only a few studies have proposed a pathway to explain the angiogenic mechanism behind this small sugar molecule. Briefly, two main mechanisms have been proposed when it comes to the angiogenic activity of 2dDR at the molecular level. In the first proposed mechanism, researchers suggest the endogenous production of 2dDR by enzymatic degradation of thymidine to thymine promotes oxidative stress and consecutively stimulates the secretion of angiogenic factors such as VEGF and interleukin-8 (IL-8) which can be internalised by ECs and promote angiogenesis [82,84,380]. In the second mechanism, which has been recently studied by Vara et al. [381], the 2dDR-1-phosphate (2dDRP) is produced either internally by cells which express TP such as macrophages, platelets and cancer cells and then secrete this extracellularly, or TP may be released from injured cells to act on enzymatic degradation of thymidine and generation of 2dDR extracellularly. 2dDRP then can be taken up by endothelial cells, and this then activates NADPH oxidase 2 (NOX2) which later acts on nuclear factor kappa B (NF-κB). NF-κB then upregulates the

VEGFR2 and thus drives VEGF-dependent angiogenesis. Both mechanisms are summarised in Figure 42.

As must be evident in these early days of studying 2dDR, the clarification of the mechanism of action of 2dDR remains to be definitely established. Herein, I wished to learn more about the biological activity of this sugar using a range of well-established *in vitro* models and in particular to establish the effective concentration range of this small sugar. Throughout, I have used VEGF as a comparator so that I can answer how biologically effective 2dDR is compared to this well documented major pro-angiogenic factor.

Although I have not primarily aimed to establish a mechanism of action for the angiogenic activity of 2dDR, I investigated whether this activity is VEGF-dependent or not. For this, HAECs were incubated in low serum EC GM supplemented with 100 μM of 2dDR, 1 mM of 2dDR, and 80 ng/mL VEGF. Non-supplemented low serum EC GM was used as a control. The analysis of the collected media at day 1, 3 and 5 demonstrated that the VEGF production by HAECs in response to direct treatment of 2dDR was statistically significant even at day 1. The amount of VEGF rose up by approximately 48-fold and 70-fold, respectively by 100 μM and 1 mM 2dDR treatment. At the end of day 5, VEGF production of HAECs was increased by 74-fold and 80-fold, respectively by the addition of 100 μM and 1 mM 2dDR. This data was in support with the current literature, which hypothesises that an increase in the level of VEGF expression of endothelial cells in the presence of 2dDR [82,84].

The stability studies demonstrated that there was a gradual decrease in the amount of 2dDR presented in the growth medium over 14 days either in the presence or absence of HAECs. This decrease has been found to be higher when HAECs were presented in the well plates. This higher decrease is likely to be due to that 2dDR is internalised by HAECs and used to increase the production of VEGF. At the end of day 14, there was approximately 40% to 50% reduction in the amount of 2dDR in the culture medium in the presence of HAECs. The drop of 2dDR amount in culture medium over 7 days is in compliance with the decrease in the amount of VEGF produced by HAECs in response to 2dDR treatment from day 4 to 7. Thus, these data may reveal important information about the safety of 2dDR treatment since both 2dDR and its angiogenic effect is burning out over time.

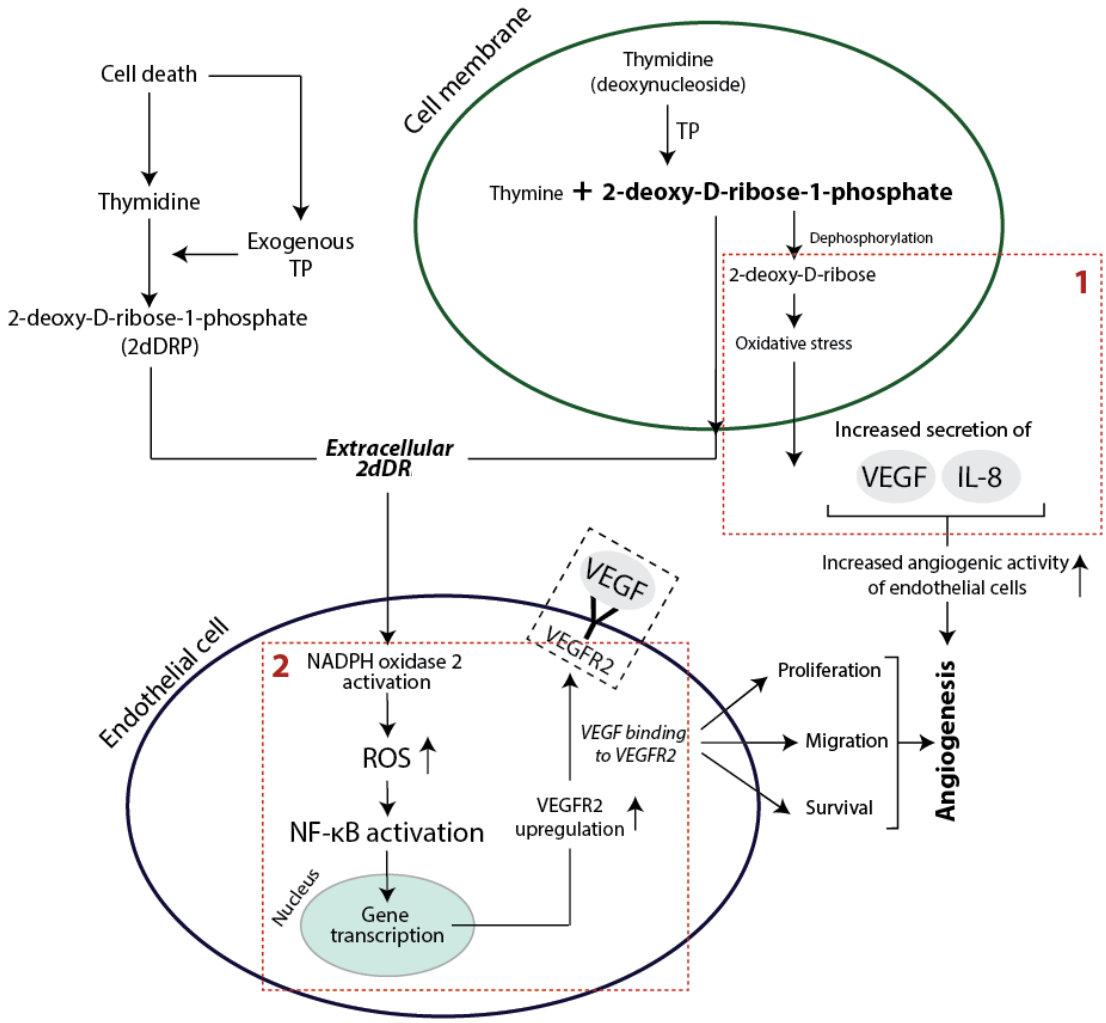


***Figure 42:*** *Proposed pathways for VEGF and 2dDR to promote angiogenesis. (1) endogenous generation of 2dDR stimulates the production of angiogenic factors via stimulation of oxidative stress. (2) 2dDR takes a role in the upregulation of VEGFR2 via generation of ROS and NF-κB*

Alongside with the 2dDR, the literature on small sugars is very limited and conflicting. Uchimiya et al. demonstrated that TP-induced angiogenesis could be reversed by the addition of 2dLR [83]. Nakajima et al. reported that 2dLR inhibits VEGF production and TP-related angiogenesis in metastatic nodules [86] and inhibits Matrigel invasion of tumours [382]. Ikeda et al. showed that 2dLR promotes hypoxia-induced apoptosis of HL-60 cells [383]. Uchimiya et al. demonstrated the inhibition of angiogenesis in a rat corneal assay by 2dLR [83]. Although all these studies reported the anti-angiogenic activity of 2dLR, Yar et al. previously showed the promotion of angiogenesis by the release of 2dLR from hydrogels in CAM assay [87]. Similarly, Sengupta et al. also suggested that 2dLR showed an angiogenic response in sponge granuloma model of angiogenesis [82]. Similar

conflicting literature can be seen for DG, which has previously been reported to induce proliferation, migration and tube formation of ECs by many groups [384–386]. On the contrary, several reports asserted that DG inhibits tube formation *in vitro* [387] and anti-angiogenic *in vivo* [388]. In order to better understand this conflicting literature, I summarised the studies on some of the small sugars that have been found to promote or inhibit angiogenesis in Table 12.

***Table 12.*** *Summary of the studies on some small sugars that have been found to promote or inhibit angiogenesis*

| Sugars | Assay | Result | Effective Doses | Reference |
|---|---|---|---|---|
| *2-deoxy-D-ribose (2dDR)* | *In vitro* | Promotes proliferation, migration and tube formation of ECs | 100 μM to 1 mM | [88] |
| | | Inhibits hypoxia-induced apoptosis | 10 μM | [383] |
| | | Induces Matrigel invasion | 100 μM | [382] |
| | | Stimulates proliferation and migration of ECs | 100 μM to 1 mM | [82] |
| | | Activates NOX2 → NF-κB and upregulates VEGFR2 | 8 μM to 1 mM | [389] |
| | | Increases VEGF production of ECs | 100 μM to 1 mM | [390] |
| | CAM assay | Promotes angiogenesis | 200 μg/day | [89] |
| | | | 1 mg/mL | [87] |
| | *In vivo* | Promotes angiogenesis and wound healing | 1 mg/mL | [87] |
| | | | 5% or 10% (w/v) | [90] |
| | | Promotes angiogenesis | *2* nmol | [82] |
| *2-deoxy-L-ribose (2dLR)* | *In vitro* | Inhibits migration and tube formation and tumour invasion | 100 μM | [83,84,382] |
| | | Inhibits VEGF production | 10 μM to 100 μM | [86] |
| | | Promotes hypoxia-induced apoptosis | 30 μM to 50 μM | [383] |
| | CAM assay | Stimulates angiogenesis | 1 mg/mL | [87] |
| | *In vivo* | Inhibits angiogenesis in a rat corneal assay | 200 ng/pellet | [83] |
| | | Promotes angiogenesis | *2* nmol | [82] |
| *2-deoxy-D-glucose (2dDG)* | *In vitro* | Inhibits the proliferation, migration and tube formation of ECs | 60 μM to 9 mM | [365] |
| | | Inhibits proliferation of cells and reduces ATP levels | 3 mM | [391] |
| | | Inhibits the proliferation, migration and tube formation of ECs | 50 μM to 1 mM | [366] |
| | | Downregulates AKT and ERK pathways and inhibits tube formation | 600 μM | [392] |
| | Rat aortic ring | Inhibits tube formation of ECs | 50 μM to 1 mM | [366] |
| | *In vivo* | Inhibits angiogenesis | 6 mM | [365] |
| *D-Glucose (DG)* | *In vitro* | Induces migration and tube formation of ECs | 25 mM | [384] |
| | | Inhibits proliferation, migration and tube formation of ECs | 5 mM to 30 mM | [385] |
| | | Promotes tube formation of ECs and COX-2 expression | 25 mM to 30.5 mM | [386] |
| | | Inhibits the tube formation of ECs in a dose-dependent manner | 10 mM to 16 mM | [387] |
| | *In vivo* | Reduced angiogenesis | 22 mM | [388] |

In the assessment of these approaches to overcome delayed angiogenesis in TE constructs, I have made extensive use of the *ex-ovo* CAM assay to evaluate angiogenesis. It is an excellent bioassay for assessing the angiogenic response to materials allowing direct imaging and comparison of the newly formed blood vessels. It can also be used as a low cost, rapid and simple tool for testing very early tissue reactions to biomaterials [228]. The CAM assay has been used by our group in recent years to evaluate the biocompatibility and proangiogenic response to a range of different polymers encompassing PLA, PU, PHBV, and CS/collagen.

To place the current results in context, I summarised these preceding studies in a table which summarises the response of the *ex-ovo* CAM assay to these materials in terms of their effect on the structure of the underlying membrane, the infiltration of cells into the material and their effect on angiogenesis in the CAM. Cellular infiltration in the table describes the migration of cells from CAM to biomaterials. In general, highly porous, biocompatible structures, where pore sizes are large enough to allow cellular ingrowth, lead to good cellular/tissue infiltration to a biomaterial [393,394]. Because the diameter of the fibres and the pore size of electrospun PHBV were much smaller, less cellular infiltration was observed in all PHBV scaffold groups than for other polymers studied in the CAM assay (Table 13).

***Table 13.*** *Comparison of the response of CAM to different polymer systems, assessing biocompatibility and proangiogenic activity*

| Polymer | Agent | Average Pore size | Effect on embryo survival | Cell infiltration | Angiogenic activity on CAM |
|---|---|---|---|---|---|
| *PLA* [69] | None | < 5 µm | None | ++++ | - |
| | Vitamin C | | None | ++++ | ++ |
| | E2 | | None | ++++ | ++++ |
| *PU* [379] | None | < 25 µm | None | +++ | - |
| | E2 | | None | +++ | ++++ |
| *CS/PVA/PCL* [345] | Heparin | < 1 µm | None | +++ | ++++ |
| *CS/PVA* [346] | Heparin | < 6 µm | None | +++ | ++++ |
| *CS/Collagen* [87] | 2dDR | < 105 µm | None | +++ | ++++ |
| *PHBV* | None | < 3 µm | None | ++ | - |
| | 2dDR | < 4 µm | None | ++ | +++ |
| | E2 | < 3 µm | None | ++ | ++++ |

As the next step in our investigations, we sought to assess whether 2dDR can stimulate wound healing in a compromised wound model in animals. Healing is a multifaceted process in which the development of new blood vessels plays a major role. This is particularly critical in chronic non-healing wounds. By the time a wound has failed to respond to conventional best practice clinical treatment- often for an arbitrary period of 3 months- they are classified as chronic non-healing wounds. Investigation of the underlying wound beds will often show poor vascularisation, abnormal often exacerbated inflammation and very often some level of bacterial infection.

Impaired wound healing is a major complication endured by patients with diabetes and is the leading cause of non-traumatic lower limb amputation in these patients. Accordingly, the current study aimed to examine to what extent release of this sugar might promote wound healing in a compromised diabetic wound model. To do this, we loaded the sugar into an alginate hydrogel and used it to treat skin wounds in a diabetic rat model.

Alginate dressings are in clinical use for the treatment of heavily exudative, chronic wounds [395] as well as for diabetic wounds. As such, they are a logical choice to use to deliver this sugar. The sugar was loaded on highly absorbent alginate dressings under sterile conditions.

Our findings were that 2dDR was straightforward to load into alginate dressings- these were then air-dried, and when placed in a wet environment, they released approximately 90% of their sugar load within 3 days. The amount released was proportional to the amount loaded. The fibre structure of alginate dressings was retained after deoxy sugar loading. The sugar itself was stable over 3 weeks as assessed at RT.

A well-established diabetic rat model was used in which a full thickness of 20 mm diameter skin wound was made. While the area of these wounds reduced by approximately 70% by 20 days they were still not fully healed. Addition of alginate did significantly accelerate wound healing, but macroscopic wound closure analysis (Figure 37) clearly showed that 2dDR released from alginate further accelerated the wound healing. By day 20, wounds treated with 2dDR were essentially fully healed. Similar results were seen whether alginate was loaded with 5 or 10% sugar. The histological assessment also demonstrated better healing of the skin wounds treated with 2dDR loaded alginate as evidenced by the presence of new epithelium.

We looked for the immune response to the dressings and whether the dressings had any effect on angiogenesis. Overall there was a vigorous M2 macrophage response which is indicative of macrophages promoting new tissue formation [396] -while an M1 response is associated to encapsulation and chronic inflammation with the rejection of the implant [397]. This response was very low for all groups. The addition of the sugar did, however, lead to increased CD34 positive cells in the wound bed indicative of better neovascularisation. This was observed at day 7 for the 2dDR loaded alginate groups and maintained throughout the 20 days of the study. We suggest that the increased vascularisation will have contributed to the accelerated wound healing. Both 5% and 10% loading were effective.

## 2.8. Conclusions and Future Work

In this chapter, the angiogenic potential of 2dDR and its effective concentrations range were revealed using established *in vitro* and *in vivo* angiogenesis assays.

First, it has been shown that the most effective dose range of 2dDR to promote the proliferation, migration and tube formation of HAECs was between 100 μM and 1 mM. When used within this range 2dDR was found approximately 90% as effective as VEGF for promoting angiogenesis *in vitro*. Administration of 2dDR at higher concentration (10 mM) resulted in the detachment of ECs and led to cell death.

Then, an *ex-ovo* CAM assay was used to define a certain concentration range of 2dDR, and it has been found to be 80% as potent as VEGF for inducing angiogenesis in CAM assay when given at the dose of 200 μg/day/embryo. In addition, loading of 250 mg of 2dDR per 1 g of polymer significantly increased the angiogenic activity in the area of implantation when compared to controls.

Finally, the potential of 2dDR for stimulating wound healing and angiogenesis when released from commercially available alginate dressing was demonstrated using a diabetic rat model. The incorporation of 5% and 10% 2dDR to the alginate dressings not only stimulated wound healing and showed a full wound closure (100%) at the end of 20 days when the wound closure was only 70% in the alginate control group but also stimulated angiogenesis in the wound area by day 7 and 20.

In the scope of this chapter, I did not primarily aim to explore the mechanism of action of this small sugar. However, our results clearly showed that 2dDR achieves angiogenesis by upregulating the production of VEGF. It's encouraging performance *in vitro,* in the CAM assay and in a diabetic wound model shows the potential value of this small sugar. In the future, experiments need to be carried out to explore the mechanism of action of this small deoxy sugar molecule to understand what is happening in the molecular level behind the scene. The literature on the mechanism of action of 2dDR still remains unclear, and studies suggest only a few potential pathways mostly focusing on VEGF-R2 dependent signalling.

**This page intentionally left blank**

# CHAPTER III

# Development of the PHBV synthetic vascular networks to study angiogenesis

## 3.1. Aims and Objectives

The aims of this chapter are to design and produce synthetic vascular networks and to investigate its potential to be used as an *in vitro* platform to study angiogenesis. In order to satisfy these aims; the objectives of this chapter are to:

- Compare two widely-used polymers (PHBV and PCL) which are suitable for the manufacturing of vascular networks in terms of their physical, mechanical, and biological performances.
- Design and manufacture the PHBV synthetic vascular networks using a four-step fabrication technique, which combines 3D printing and electrospinning.
- Investigate the biomechanical properties of the scaffolds.
- Evaluate the optimal cell types and co-culture systems for improved survival and growth of the endothelial cells within these channels.
- Investigate the outgrowth of endothelial cells from pre-formed endothelial cell monolayer inside the channels towards Matrigel and reconstructed skin model in the presence and absence of pro-angiogenic agents.

## 3.2. Chapter III by Pictures

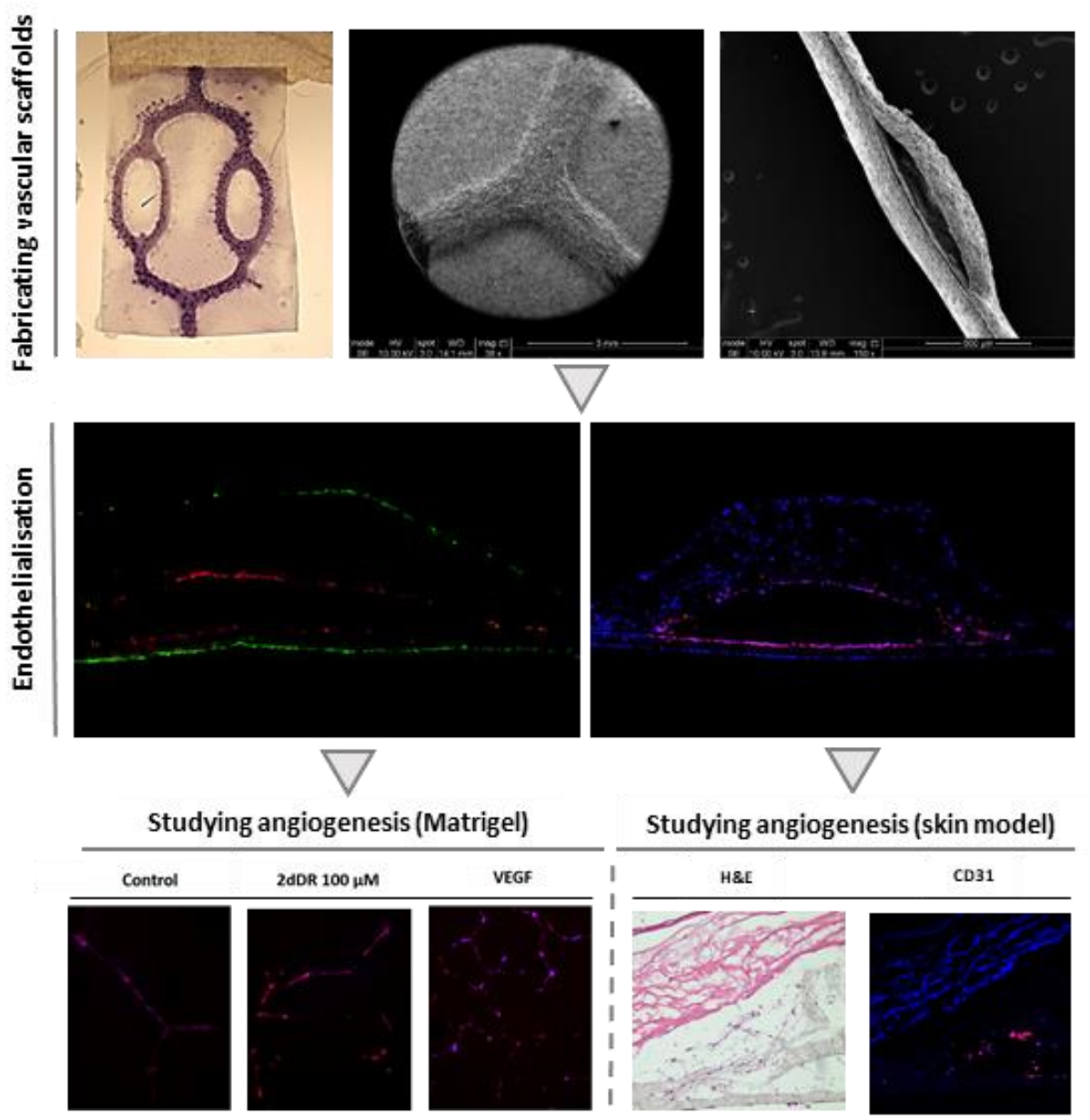

## 3.3. Introduction

Angiogenesis is a sophisticated process regulated by a complex web of interactions of endothelial cells (ECs) with their extracellular matrix (ECM) and with biochemical and mechanical factors as previously explained in Section 1.3. The delayed neovascularisation of tissue-engineered (TE) constructs post-implantation can cause them to fail clinically [398]. Thus, investigating the factors that regulate angiogenesis is particularly important to understand how they are involved in this complex process.

Angiogenesis assays are powerful tools to study aspects of angiogenesis and can be categorised into three main categories: (i) *in vitro*, (ii) *ex vivo,* and (i) *in vivo* [399]. *In vivo* assays are the most representative of native angiogenesis, but since healthy animals are used to perform these assays, they are ethically questionable, require considerable technical skills, and expensive [204]. In contrast, *in vitro* assays are inexpensive and relatively easy to perform. However, the majority of them are based on two-dimensional (2D) cell culture systems which lack the physiological relevance that three-dimensional (3D) structures can provide [400]. Thus, it is important to develop better *in vitro* platforms that enable the study of angiogenesis under more physiologically relevant conditions.

Skin tissue engineering has gained great momentum over the years. However, developing biologically relevant *in vitro* tissue models as alternatives to animal models or as physiologically relevant tissue substitutes for clinical use is always open for improvement. Several *in vitro* skin models have been developed over the last years as alternatives to animal testing, to study wound healing, pigmentation, contraction, tumour invasion, barrier function, and bacterial infection [401,402]. Facy et al. created a reconstructed epidermis model with Langerhans cells and used this model to test the reactivity of these cells to known allergens and UV [403]. Kandarova et al. studied skin irritation using two reconstructed human skin equivalents as an alternative to animal testing [404]. To study pigmentation, Bessous et al. developed an *in vitro* reconstructed epidermis using autologous keratinocytes and melanocytes [405]. Meier et al. developed a human skin equivalent to study melanoma progression, and they reported a close correspondence between the growth of melanoma into engineered skin construct and *in vivo* [406]. Admane et al. reported the direct 3D bioprinting of full-thickness skin constructs that mimics the signalling pathways of skin [407]. Similarly, Kim et al.

developed a 3D printed skin model with perfusable vascular channels to create a vascularised skin model [408]. Kolesky et al. developed a platform using a multi-material 3D bioprinting method, which enables researchers to create thick tissue models with engineered matrix and embedded vasculature [409]. Recently, John et al. demonstrated the regeneration of TE skin substitute on human amniotic membrane [410]. Our laboratory has previously reported a 14-day protocol for the reconstruction of a 3D human skin model that is suitable for clinical use [411], and have previously explored adding Human Dermal Microvascular Endothelial Cells (HDMEC) to TE skin model with very little success-the cells struggled to enter the TE skin and showed no signs of being organised when they did enter [412]. Although TE skin was being studied for a long time to be used as skin substitutes in the clinic or *in vitro* models for research, the main challenge remains the same: studying and improving angiogenesis/vascularisation of a TE skin for translation of it to clinic or for doing research on understanding the basic principles of skin vascularisation. Either for implanting or for *in vitro* laboratory research, developing a vascularised 3D human skin model is highly important for the successful take of TE skin substitute after implantation or studying the effect of chemical, mechanical and environmental factors on neovascularisation of skin. Thus, there is a need to develop new platforms that enable to study vascularisation of complex tissues such as skin.

In this chapter, I initially compared physical, mechanical, and biological performances of two widely-used polymers, Poly-3-hydroxybutyrate-co-3-hydroxyvalerate (PHBV), a biocompatible and biodegradable polyester, belongs to the polyhydroxyalkanoate family. 3-hydroxybutanoic acid, one of its degradation products that are also a natural product produced in the human body [413] which can be linked with its high biocompatibility and polycaprolactone (PCL), another biocompatible and bioresorbable synthetic polymer, which does not produce an overly acidic environment in the degradation process and has been approved by the United States Food and Drug Administration (FDA) as a material for the fabrication of several biomedical devices [414,415]. Then, I selected PHBV as the material for the development of synthetic vascular networks (SVN) by combining two scaffold manufacturing techniques, electrospinning and 3D printing.

The main aim of this study was to create a unique *in vitro* platform that enables researchers to study more than one aspect of angiogenesis both at cellular and tissue

levels. PHBV channels were used as physical support and a structural guide for ECs to create a pre-formed endothelium-like structure. This endothelium-like structure was then used to study the migratory response and tube-forming capability of ECs in response to pro-angiogenic agents *in vitro* and to explore how synthetic channels can be used as a model for the vascularisation studies at tissue level. The CAM assay has been used for the first time as a surrogate for a well-vascularised wound bed to provide the source of blood vessels to grow into the 3D human skin as a positive control to the PHBV SVN vascularisation studies [416].

### 3.4. Materials

| Chemical / Reagent | Catalogue Number | Supplier |
|---|---|---|
| Thrombin (human) | 228-11508 | **Cayman Chemical** |
| Matrigel® (Growth Factor Reduced) | 356231 | **Corning** |
| Chloroform | 10784143 | **Fisher Scientific** |
| Dichloromethane (DCM) | 10127611 | |
| Dimethylformamide (DMF) | 15562393 | |
| DPX mounting medium | D/5319/05 | |
| Industrial methylated spirit (IMS) | M/4450/17 | |
| Methanol | 10626652 | |
| Triton X-100 | BP151 | |
| Xylene | X/0100/17 | |
| Poly3-hydroxybutyrate-co-3-hydroxyvalerate (PHBV) (PHV content 12 mol %) | BV326301 | **GoodFellow** |
| Optimum cutting temperature tissue freezing medium (OCT-TFM) | 14020108926 | **Leica Biosystems** |
| Fertilised chicken eggs | - | **MedEggs** |
| RCOM King SURO humidified egg incubator | MX-SURO | **P&T Poultry** |
| EC GM MV Supplement Pack (For HDMECs) | C-39220 | **PromoCell** |
| Endothelial Cell Growth Medium MV (EC GM) (for HDMECs) | C-22220 | |

| | | |
|---|---|---|
| Human Dermal Microvascular Endothelial Cells (HDMECs) | C-12210 | |
| Epidermal growth factor (EGF) | 236-EG | **R&D Systems** |
| 2-deoxy-D-ribose (2dDR) | 121649 | **Sigma Aldrich** |
| 37% formaldehyde (FA) solution | F8775 | |
| 4',6-diamidino-2-phenylindole (DAPI) solution | D8417 | |
| Adenine | A5665 | |
| AlamarBlue Cell Metabolic Activity Assay | R7017 | |
| Alginic acid sodium salt | 180947 | |
| Amphotericin B | A2942 | |
| Anti-CD31 (PECAM-1) antibody produced in mouse | P8590 | |
| Bovine serum albumin (BSA) | A7030 | |
| Calcium chloride dihydrate | 223506 | |
| Chlorotoxin | C5238 | |
| Collagenase A | COLLA-RO | |
| D-glucose | G7021 | |
| Dimethyl sulphoxide (DMSO) | 472301 | |
| Dulbecco's Modified Eagle's Medium (DMEM) | D6546 | |
| Ethylenediaminetetraacetic acid (EDTA) | E6758 | |
| Eosin Y solution | HT110232 | |
| Ethanol | 51976 | |
| F-12 HAM nutrient mixture | N4888 | |
| Fetal calf serum (FCS) | F9565 | |
| Fibrinogen from human plasma | F3879 | |
| Glutaraldehyde (25%) | G5882 | |
| Glycerol | G5516 | |
| Hematoxylin solution | HHS16 | |
| Hydrocortisone | H0888 | |
| Insulin (human recombinant) | 91077C | |

| | | |
|---|---|---|
| L-glutamine | G3126 | |
| Methylene blue | M9140 | |
| Penicillin / Streptomycin | P0781 | |
| Phalloidin, fluorescein isothiocyanate (FITC) | P5282 | |
| Phalloidin, tetramethylrhodamine isothiocyanate (TRITC) | P1951 | |
| Polycaprolactone (PCL) (Mn: 80.000 g/mol) | 440744 | |
| Sodium hydroxide pellets | 795429 | |
| Trypan blue | T6146 | |
| Trypsin EDTA | T3924 | |
| Tween®20 | P1379 | |
| Vascular endothelial growth factor (VEGF) | V7259 | |
| CellTracker™ Green | C2925 | **ThermoFisher** |
| CellTracker™ Red | C34552 | |
| Goat anti-Human IgG (H+L) Cross-Adsorbed Secondary Antibody, Alexa Fluor 546 | A-21089 | |

## 3.5. Methods

### 3.5.1. Comparison of two polymers that are widely used in tissue engineering applications: PHBV and PCL

#### 3.5.1.1. Comparing the hydrophobicity of the polymers with contact angle measurements

##### 3.5.1.1.1. Preparation of the polymer solutions

The polymer solutions were prepared before contact angle measurements. Firstly, PHBV (10% (w/w)) granules were dissolved in DCM:methanol (90:10 w/w) solvent blend in a fume hood. Then PCL (10% (w/w)) granules were dissolved in and chloroform:DMF (70:30 w/w) solvent blend. The DCM:methanol (90:10 w/w) solvent blend for electrospinning PHBV has previously been found the best composition in our lab [417,418]. The solvent mixture for electrospinning PCL has been optimised in the scope of this thesis and will be explained in Chapter VI. We have recently reported that

chloroform:DMF (70:30 w/w) composition was the best mixture for electrospinning PCL nanofibres [419].

#### 3.5.1.1.2. Contact angle measurements

PHBV and PCL thin films from the polymer solutions were prepared using a spin-coater (Laurell WS-400B, North Wales, Pennsylvania, USA). Contact angle measurements of the PHBV and PCL were performed using a drop shape analyser (Krüss DSA100, Germany) under ambient laboratory conditions. A 5 µL water droplet was dropped onto the polymer films, and the contact angles of the droplet on samples were recorded from the software. The measurements of at least three drops on three different samples were taken for each polymer.

### 3.5.1.2. Electrospinning PHBV and PCL solutions

PHBV and PCL polymer solutions were loaded into two separate 5 mL syringes fitted with 0.6 mm inner diameter syringe tips. Syringes were then placed in a syringe pump (GenieTMPlus, KentScientific, Connecticut, USA). Aluminium foil was used as the collector and placed at a distance of 17 cm from the needle tips. The pump was set to 40 µL/minutes, and 17 kV voltage was applied both to the collector and the tips. Electrospinning was done at room temperature until all the polymer solution was used.

### 3.5.1.3. Biomechanical testing of PHBV and PCL electrospun scaffolds

Biomechanical testing samples were prepared by cutting 20 mm x 10 mm pieces from dry electrospun scaffolds. The clamps of the device were positioned 10 mm away from each other, and the width and thickness of each scaffold were measured. Test samples were clamped with two grips in a tensiometer (BOSE Electroforce Test Instruments, Minnesota, USA). Tensile tests were performed on each sample at a rate of 0.1 mm/s until the samples failed (n=4). UTS and Young's modulus were calculated from stress (σ) and stress (ε) curves of each sample.

### 3.5.1.4. Comparing the microstructures of the electrospun PHBV and PCL using SEM

The surface morphology of PHBV and PCL electrospun nanofibres were observed under SEM (FEI Inspect F, Orlando, USA). The samples were coated with gold using a gold

sputter (Edwards sputter coater S150B, Crawley, England) prior to imaging. Fibre diameter and pore sizes were measured using ImageJ software. At least 100 measurements were taken from the different areas of each sample, and at least three samples were used for each polymer group.

#### 3.5.1.5. Comparing the biocompatibility of the polymers *in vitro* and *in vivo*

##### 3.5.1.5.1. Assessment of the activities of HDFs growing on PHBV and PCL with AlamarBlue® metabolic activity assay

AlamarBlue® Cell Viability Assay (ThermoFisher Scientific, USA was used to compare the biocompatibility of the PHBV and PCL electrospun scaffolds by measuring the metabolic activity of Human Dermal Microvascular Endothelial Cells (HDMECs) cultured on either PHBV or PCL over 11 days.

HDMECs were used between P2 and P4. Cells were thawed and cultured until reaching 80-90% confluency. Following sterilisation of the PHBV and PCL scaffolds with 70% ethanol for 45 minutes, HDMECs were trypsinised and counted. 4 x $10^4$ cells were resuspended in 0.25 mL of EC GM (PromoCell, Heidelberg, Germany) and then seeded onto the scaffolds in 12-well plates. Before adding culture medium, scaffolds were returned to the incubator for an hour to allow HDMECs to attach. Then, 4 mL of HDMECs culture medium was added to each well, and they were incubated at 37°C overnight. Scaffolds were kept in culture for 11 days by changing the culture medium every 2-3 days.

AlamarBlue® Cell Viability Assay was performed at days 1, 4, 7 and 11. Briefly, 0.1 mM AlamarBlue® working solution was prepared by 10x dilution of the 1 mM AlamarBlue® stock solution with growth medium. Growth media were removed, and the scaffolds were washed with PBS. 1 mL of AlamarBlue® working solution was added to each well and incubated at 37°C for 4 hours. After an incubation period, 200 µL of the solution was transferred into 96-well plate, and the fluorescence readings were done at an excitation wavelength of 540 nm and an emission wavelength of 635 nm.

3.5.1.5.2. Assessment of the biocompatibility of the PHBV and PCL using *ex-ovo* CAM assay

To evaluate the initial response of CAM to both polymers, electrospun PHBV and PCL were implanted to CAM. The response of CAM to the polymers was evaluated with macroscopic and histological evaluation of the CAMs after the incubation period. A detailed procedure of the CAM assay, scaffold implantation and histological analysis of electrospun scaffolds is given in Chapter 2.

3.5.2. Manufacturing of SVN from the selected polymer: PHBV

Following the 3D design of SVN using computer-aided design (CAD) software (SolidWorks 2012, Massachusetts, USA), synthetic scaffolds were manufactured via the four-step process as shown in Figure 43. First, a layer of PHBV was electrospun on aluminium foil coated collector using the parameters given in Section 3.5.1.2. Alginate was then used as a sacrificial substrate and 3D printed on to PHBV using a 3D bioprinter (BioBots, Philadelphia, USA). Following that, another layer of PHBV was electrospun on top of the alginate using same parameters. Finally, sacrificial alginate channels were removed via 0.5 M of EDTA solution.

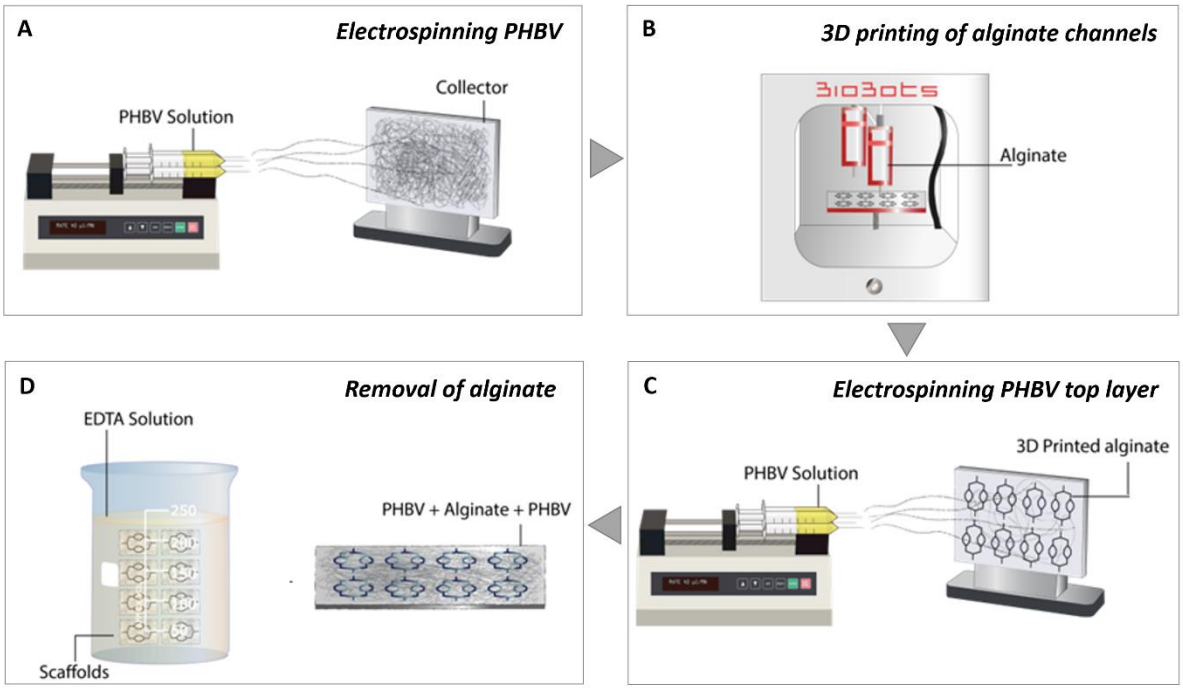


***Figure 43.*** *Schematic illustration showing the four-step manufacturing process of synthetic vascular channels*

### 3.5.3. Computer-aided design (CAD) of the 3D vascular channels

Various designs of synthetic vascular networks (Figure 44) were created using CAD software (SolidWorks 2012, Massachusetts, USA). Once the models were prepared, they were exported as standard tessellation language (STL) format for 3D printing.

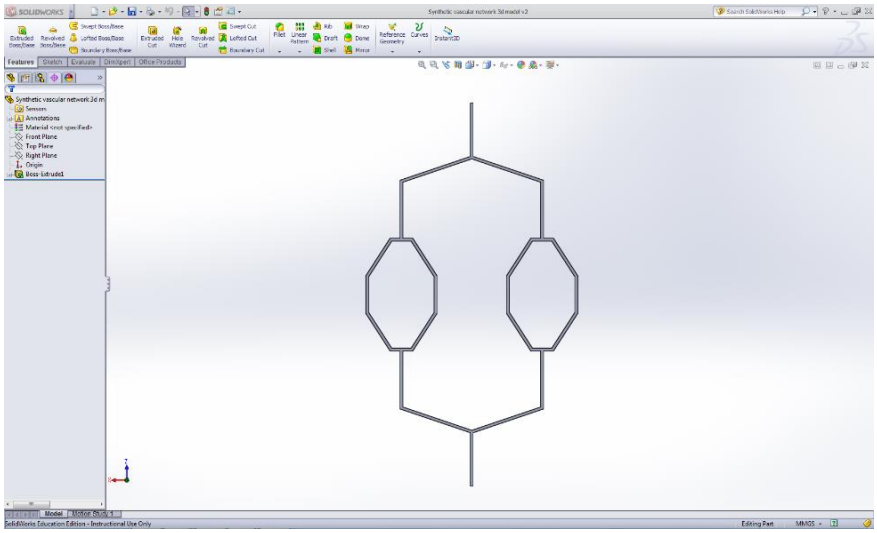

***Figure 44.*** *The CAD of synthetic vascular channels*

### 3.5.4. Electrospinning PHBV

#### 3.5.4.1. Preparation of PHBV solution for electrospinning

10% (w/w) PHBV solution was prepared prior to electrospinning. 6 g of PHBV granules were dissolved in 3 g of methanol and 24 g of DCM in a fume hood, and the mixture was magnetically stirred overnight.

#### 3.5.4.2. Electrospinning PHBV

Approximately 10 mL of PHBV solution was transferred into 4x5 mL syringes with 0.6 mm blunt tips, and the syringes were placed to a syringe pump (Genie™Plus, Kent Scientific, Connecticut, USA). Aluminium foil coated collector was placed at a distance of 17 cm from needle tips, and the pump was set to deliver 40 µL/minute. A voltage of 17 kV was applied to the collector as well as the needle tips. The polymer was electrospun on the collector with the parameters given above for an hour.

### 3.5.5. 3D printing of alginate as a sacrificial material

#### 3.5.5.1. Preparation of alginate paste for 3D printing

1.5 % alginate paste was produced by dissolving 0.2g of calcium chloride dihydrate ($CaCl_2.2H_2O$) into a 72.7 g of distilled water ($dH_2O$) while continuously stirring. The solution was then heated up to 60°C prior to adding 1.5 g of alginic acid sodium salt while continuously stirring on a hot plate magnetic stirrer. Once fully dissolved and dehydrated, 24.25 g (approximately 19.25 mL) of glycerol was added and mixed until a smooth viscous paste was obtained.

#### 3.5.5.2. Alginate printing

Prior to 3D printing, the desired numbers of 3D models were oriented and sliced using g-code generator software (Repetier-Host, Willich, Germany). The model was then exported as g-code using the following parameters: 0.4 mm layer height, 0,40 mm nozzle diameter and 2 mm/s speed. The alginate paste was transferred into a 10mL syringe with 0.40mm blunt tip, and the syringe was inserted to the extruder of 3D bioprinter (BioBots, Philadelphia, USA). The aluminium foil containing electrospun PHBV layer was placed onto the lid of a 6-well plate and fixed using adhesive paper tape. G-code was then uploaded to the 3D printing software (Bioprint, Philadelphia, USA), and the pressure was adjusted between 11-20 psi. Finally, the extruders were calibrated, and the alginate was 3D printed on the PHBV electrospun sheet. Following the 3D printing process, the electrospinning process was repeated using the same parameters to create synthetic vascular channels inside two layers of PHBV.

### 3.5.6. Removal of alginate

#### 3.5.6.1. Preparation of EDTA solution

0.5 M EDTA solution was prepared adding 74.46 g of EDTA (MW: 372.24) to 320 mL of $dH_2O$. The pH was then adjusted to 8.0 using sodium hydroxide (NaOH) beads whilst stirring continuously. Once fully dissolved, the final volume was adjusted to 400 mL.

#### 3.5.6.2. Alginate removal

The synthetic vascular scaffolds were submerged in 0.5 M EDTA solution on a gel-shaker (Fisher Scientific, Massachusetts, USA) set to 70 rpm overnight to create hollow channels between two layers of PHBV sheets by removing alginate. Two ends of the scaffolds were pierced to allow alginate to be removed prior to submerging it into EDTA solution.

### 3.5.7. Biomechanical testing of PHBV SVN

Tensile testing was carried out for the dry (n=4) and wet (n=4) scaffolds using a mechanical testing machine equipped with a 22 N load cell. Scaffolds were submerged in PBS for 1 hour before testing to be wetted. The clamps of the device were positioned 15 mm away from each other, and the width and thickness of each scaffold were measured. Test samples either dry or wet were clamped with two grips in a tensiometer (BOSE Electroforce Test Instruments, Minnesota, USA). Tensile tests were performed on each sample at a rate of 0.1 mm/s until the samples fail (n=4). The raw data of the tests were taken and tabulated before converting them into stress-strain curves. Stress and strain values were calculated using Equation 2 and 3:

$$Stress\ (\sigma) = \frac{Force\ (F)}{Area\ (A)} \qquad (2)$$

$$Strain\ (\varepsilon) = \frac{Length\ of\ stretch\ (\Delta L)}{Original\ length\ (L_0)} \qquad (3)$$

UTS, yield strength (YS) and Young's modulus parameters were calculated using stress (σ) and stress (ε) curves (Figure 45) of each sample.

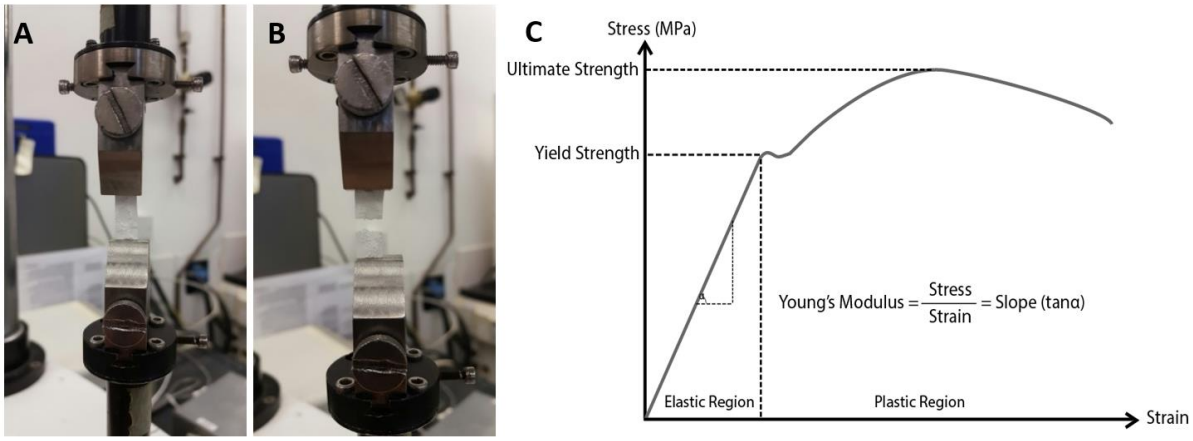


***Figure 45.*** *The mechanical testing of the PHBV SVN scaffolds. Placement of the scaffolds (A) before, (B) after the test to the uniaxial testing machine. (C) A representative stress-strain curve showing relevant parameters and calculations*

Suture retention tests were performed based on the BS EN ISO 7198:2017, which is the standard for testing vascular grafts and patches. Before clamping the samples to a uniaxial testing device, scaffolds were sutured from 2 mm away from the upper end as can be seen in Figure 46 with a suture (Ethicon, New Jersey, USA) which is for use in general soft tissues. To prepare the wet group, the scaffolds were hydrated by submerging in PBS for 1 hour. The distance between clamps was then adjusted, and the tests were conducted at a rate of 0.1 mm/second until the samples fail. Suture retention strength was calculated using Equation 4:

$$Suture\ retention = \frac{Suture\ retention\ force}{Suture\ diameter\ x\ Sample\ thickness} \quad (4)$$

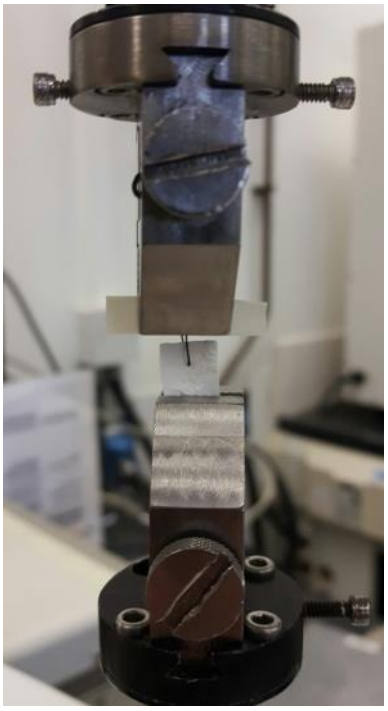

***Figure 46.*** *Placement of the scaffolds for the measurement of their suture retention strength*

### 3.5.8. Cannulation and sterilisation of the synthetic vascular channels

Prior to cell seeding into PHBV SVN, channels were cannulated with a 25 G cannula by perfusing PBS into the channels under a dissection microscope (Wild Heerbrugg, Heerbrugg, Switzerland). Methylene blue was then injected into channels to test the channel structure and patency. Scaffolds were then sterilised using 70% IMS (by submerging in 70% IMS solution for approximately 45 min) and washed 3 times with PBS prior to cell seeding.

### 3.5.9. Cellularisation of synthetic vascular channels

#### 3.5.9.1. General cell culture procedures

Cells at the desired passage were taken from liquid nitrogen ($LN_2$) and immediately thawed at 37°C. Once cell suspension was thawed, it was transferred into a container with 10 mL of appropriate growth medium (the type of culture medium will be revealed in the following sections). Cells were centrifuged at 1000 rpm for 5 minutes, and the cells were resuspended in the growth medium. The suspension of cells was the split into the desired number of T75 flasks (VWR International, Pennsylvania, USA), and the total volume was adjusted to 12 mL with culture medium. T75 flasks were then incubated at 37°C (Sanyo, Osaka, Japan). The culture media was replaced every 2-3 days until they reached ~80-90% confluency. Once the culture was confluent (around 80-90%), the cell culture medium was removed from the flask, and flasks were washed with PBS. Following that, 5 mL of trypsin/EDTA solution was added to each flask, and flasks were incubated at 37°C for 5 minutes. When cells were detached from the surface, trypsin was neutralised with culture medium containing 10% FCS (approximately 15 mL) and the cell suspension was centrifuged at 1000 rpm for 5 minutes. The supernatant was removed, and the cell pellet was homogenised by tapping the bottom of the universal container gently. Cells were then resuspended in growth medium and split into flasks.

To find the cell concentration required for cellularisation of scaffolds, cells were counted under an inverted microscope (Olympus CK40, Tokyo, Japan) using a haemocytometer (Hawksley, London, UK). After resuspending the cells in a certain volume, 50 µL of cell suspension was pipetted into a haemocytometer. The grid lines of the haemocytometer were imaged under a microscope, and cells were counted in a set of 16 squares. To calculate the total cell number, Equation 5 was used.

$$Total\ number\ of\ cells = \frac{No.of\ counted\ cells\ x\ Dilution\ factor\ x\ 10^4\ x\ Total\ volume}{Number\ of\ counted\ squares} \quad (5)$$

#### 3.5.9.2. Cellularisation of the PHBV channels with HDFs in isolation

HDFs were thawed, cultured, passaged and counted as given in Section 3.5.9.1. Following sterilisation, scaffolds were transferred to petri dishes. 0.5 x $10^6$ cells were resuspended

in 0.25 mL of culture medium (DMEM containing 10% (v/v) FBS, 100 IU mL $^{-1}$ penicillin, 100 µg mL $^{-1}$ streptomycin, 2mM L-glutamine and 0.625 µg mL −1 amphotericin B) and then perfused into the SVN using 1mL syringe with 25 G cannula. Before adding culture medium, scaffolds were returned to the incubator (Sanyo, Osaka, Japan) for an hour to allow fibroblasts to attach to the inside of the channels. Then, 10 mL of culture medium was added to each petri dish, and they were incubated at 37°C overnight. Scaffolds were flipped over, and the seeding protocol was repeated to cellularise the other side of the channels on the following day. Scaffolds were kept in culture for 7 days by changing the culture medium every 2-3 days. The cell seeding process is shown in Figure 47.

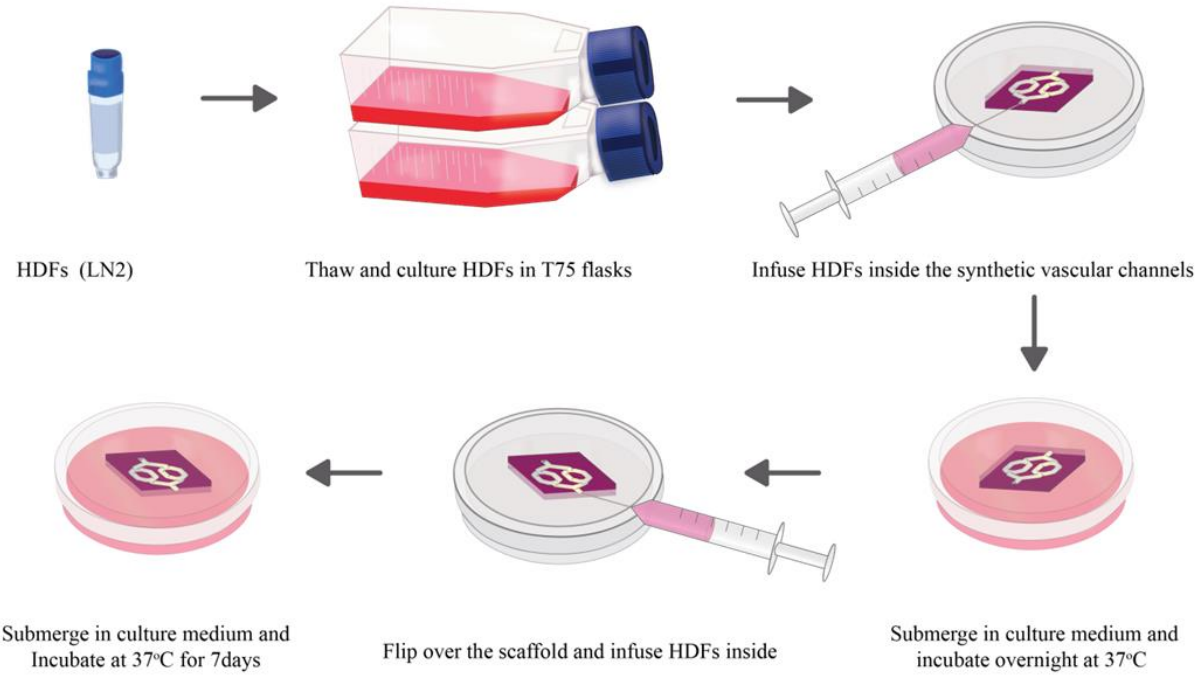


***Figure 47.*** *Illustration showing the steps of cellularisation of synthetic vascular channels with HDFs*

3.5.9.3. Cellularisation of the PHBV channels with HDMECs in isolation

HDMECs were thawed, cultured, passaged and counted as described in Section 3.5.9.1. Following sterilisation, scaffolds were transferred to petri dishes. 0.5 x $10^6$ HDMECs were resuspended in 0.25 mL of EC GM (PromoCell Endothelial Cell Growth Medium MV basal medium supplemented with 2% FCS, 0.4% EC growth supplement, 10 ng/mL EGF, 90 µg/mL heparin, 1 µg/mL hydrocortisone) and then perfused into the SVN using a 1 mL syringe with a 25 G cannula. Before adding culture medium, scaffolds were returned to the incubator for an hour to allow HDMECs to attach to the inside of the channels. Then,

10 mL of HDMECs culture medium was added to each petri dish, and they were incubated at 37°C overnight. Scaffolds were flipped over, and the seeding protocol was repeated to cellularise the other side of the channels on the following day. Scaffolds were kept in culture for 7 days by changing the culture medium every 2-3 days. The cell seeding process was shown in Figure 48.

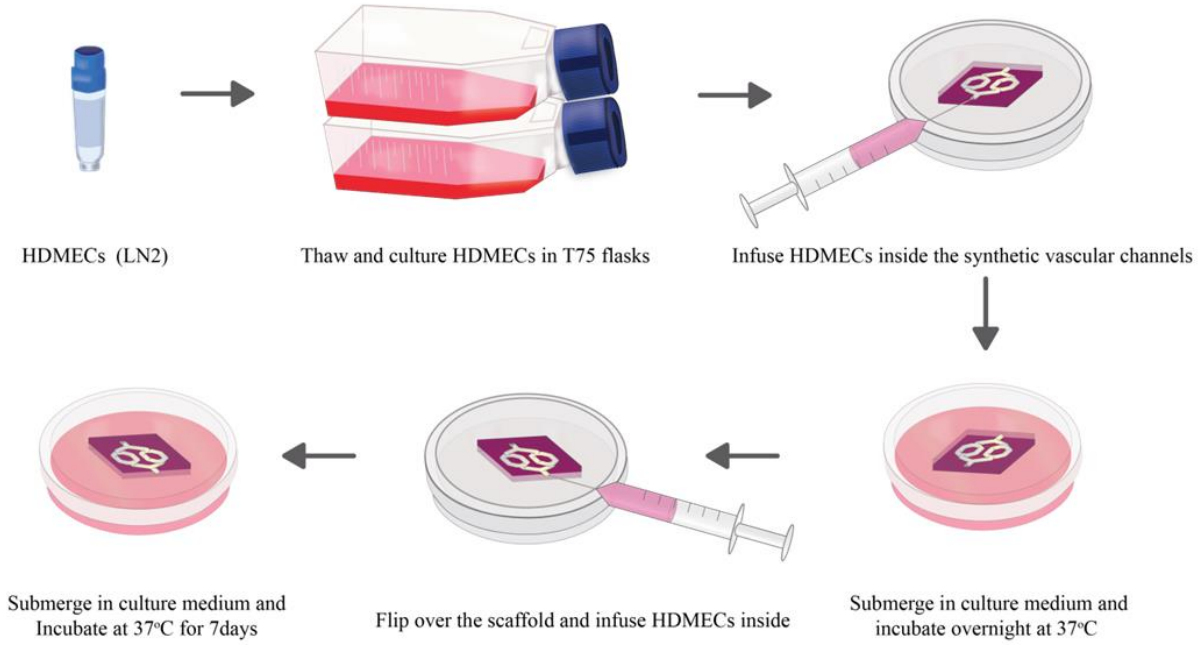


***Figure 48.*** *Illustration showing the steps of cellularisation of synthetic vascular channels with HDMECs*

3.5.9.4. Cellularisation of the PHBV channels with HDMECs (inner surface of the vascular channels) and HDFs (exterior surface of the vascular channels)

HDMECs and HDFs taken from $LN_2$ were thawed, cultured, passaged and counted as given in Section 3.5.9.1. To image them separately under a fluorescent microscope, each cell type was marked using CellTracker™ Fluorescent Probes. To label the HDMECs, 50 µg of CellTracker™ Red dry powder was dissolved in 7.3 µL of dimethyl sulfoxide (DMSO) (Sigma Aldrich, Missouri, USA). Then 3 mL of serum-free HDMECs culture medium was added to prepare a ~25 µM working dye solution. The pre-warmed dye solution was then added gently to T75 flask, and HDMECs were incubated ~1 h under growth conditions. To label the HDFs, 50 µg of CellTracker™ Green dry powder was dissolved in 10.75 µL of DMSO. Then 4.3 mL of serum-free HDFs culture medium was added to prepare ~25 µM working dye solution. The pre-warmed dye solution was then added gently to T75 flask, and HDFs were incubated ~1h under growth conditions. Following the labelling of cells,

sterile scaffolds were transferred to petri dishes. 0.5 x $10^6$ HDMECs were trypsinised, centrifuged and resuspended in 0.25 mL of culture medium and then perfused into the synthetic vascular channels using 1 mL syringe with 25 G cannula. Following that, 0.5 x $10^6$ HDFs were then trypsinised, centrifuged and resuspended in 200 µL of HDMEC growth medium and pipetted on the outer surface of the channels. Before submerging the scaffolds into HDMECs culture medium, scaffolds were incubated at 37°C for 2 hours in order to allow HDFs to be attached on the outer surface. 10 mL of HDMECs culture medium was then added to each petri dish, and they were incubated at 37°C overnight. Scaffolds were flipped over, and the same CellTracker™ labelling and seeding protocol was followed in order to cellularise the other side of the channels on the following day. Scaffolds were kept in culture for 7 days by changing the culture medium every 3 days. The seeding process of HDMECs into the channels and HDFs onto the exterior surface of the channels is shown in Figure 49.

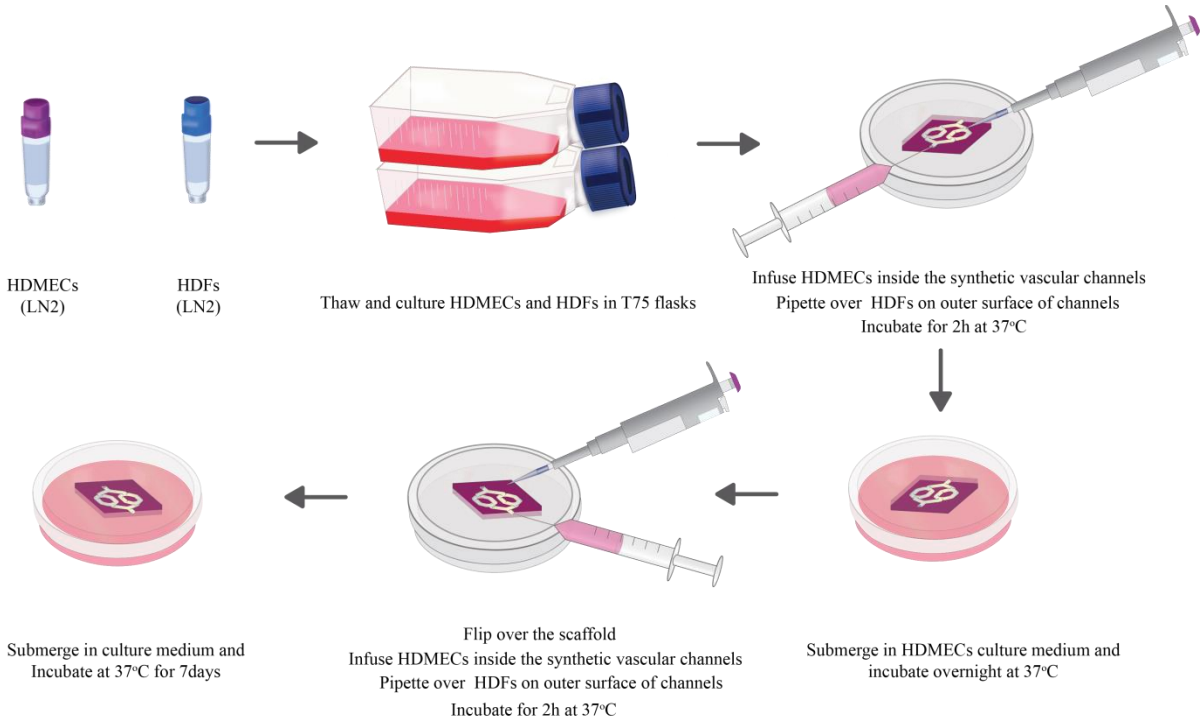


***Figure 49**. Illustration showing the steps of cellularisation of synthetic vascular channels with HDMECs in co-culture with HDFs. The seeding process of HDMECs into the channels and HDFs onto the exterior surface of the channels*

In order to verify the presence and check the distribution of the HDMECs in the PHBV vascular network prior to further experiments, scaffolds were fixed in 3.7% FA. Fixed PHBV scaffolds were embedded in OCT freezing medium and frozen in liquid nitrogen for 3 minutes. Sections were cut 5-10 µm thick using a cryostat (Leica Biosystems Nussloch,

Germany) at -20°C and immunostained for the expression of CD31 and counterstained with DAPI after 7-day culture of HDMECs and HDFs in PHBV synthetic scaffolds. Briefly, a hydrophobic barrier PAP pen was used to create a water repellent barrier as a reservoir on sections for staining reagents. First, cells were incubated in 0.1% Triton-X 100 for 20 minutes at RT for permeabilisation and then in 7.5% BSA at RT for 1 hour to block unspecific binding of the antibodies. The samples were then washed once with 1% BSA and incubated with the primary antibody (1:50 dilution in 1% BSA was used for Anti-CD31 primary antibody) overnight at 4 °C. Next day, samples were washed with 3 x PBS prior to incubating with the diluted secondary antibody (1:500 dilution in 1% BSA is used for AlexaFluor®546 conjugated secondary antibody) for 1 hour at RT. Samples were then washed with 3 x PBS before counterstaining with DAPI (diluted 1:1000 in PBS) for 20 minutes at RT. Slides were washed 3 x PBS and imaged using a fluorescent microscope. The steps of the immunofluorescent staining using unconjugated antibody are summarised Table 14.

***Table 14.*** *The steps of the immunofluorescent staining using unconjugated antibody*

| | Step | Reagent | Time | Temperature |
|---|---|---|---|---|
| 1 | Removal of OCT | Distilled water | 1 minute | RT |
| 2 | Permeabilisation | Triton-X 100 | 20 minutes | RT |
| 3 | Blocking unspecific binding | 7.5% BSA | 60 minutes | RT |
| 4 | Washing | 1% BSA | 1 minute | RT |
| 5 | Primary antibody labelling | Primary antibody solution | Overnight | 4°C |
| 6 | Washing | PBS | 3 times | RT |
| 7 | Secondary antibody labelling | Secondary antibody solution | 60 minutes | RT |
| 8 | Washing | PBS | 3 times | RT |
| 9 | Counterstaining with DAPI | DAPI solution | 20 minutes | RT |
| 10 | Washing | PBS | 3 times | RT |

### 3.5.10. Fluorescent staining

For PHBV SVN cellularised with HDMECs in isolation, the scaffolds were fixed with 3.7% FA for 1 hour and sectioned using a cryostat as described in Section 3.5.9.4. For analysing the distribution of the cells in the PHBV SVN, the sections were stained with Phalloidin tetramethylrhodamine (TRITC) (1:500 diluted in PBS) (or Phalloidin fluorescein isothiocyanate (FITC) (1:500 diluted in PBS) in some of the experiments) to stain cytoskeleton. Sections were then stained with DAPI (1:1000 diluted in PBS) to stain cell nuclei. Briefly, 0.1% (v/v) Triton X 100 (in PBS) was added on samples, and the samples were incubated for 20-30 minutes at room temperature. After three times washing with PBS, either Phalloidin TRITC or FITC (1:500 diluted in PBS from stock solution) solution was added to cells and incubated for 30 minutes at RT at dark. Sections were then washed with 3 x PBS. DAPI solution (1:1000 diluted in PBS) was added and incubated for 10-15 minutes at room temperature in the dark prior to washing with 3 x PBS. Finally, DPX mountant was pipetted on the slides, and samples were covered with a coverslip. Cells were then examined under a fluorescent microscope (Olympus IX3, Tokyo, Japan).

### 3.5.11. Direct imaging of pre-labelled cells

While investigating HDMECS in co-culture with HDFs, cells were pre-labelled using CellTracker™ Fluorescent Probes with the intent of distinguishing them during fluorescent imaging. Use of fluorescent probes prior to cultivating cells in the scaffolds enabled us to image HDMECs and HDFs directly under a fluorescent microscope following the sectioning step.

### 3.5.12. Development of a TE 3D skin model

#### 3.5.12.1. Isolation of human foreskin keratinocytes and HDFs from skin grafts

Skin grafts were obtained from patients who were informed of the use of their skin for research purposes according to a protocol approved by the Sheffield University Hospitals NHS Trust Ethics Committee. Fibroblasts and keratinocytes were isolated from the skin as described by Ghosh et al. [420]. Briefly, skin samples were cut into 0.5 $cm^2$ pieces and incubated overnight in Difco-trypsin (0.1% (w/v) trypsin, 0.1% (w/v) D-glucose in PBS, pH 7.45) before being washed and maintained in PBS.

For isolating keratinocytes, skin samples were taken from the solution and transferred into a petri dish filled with growth media. The epidermis was peeled off, and the surface of the epidermis (papillary surface) was gently scraped, and basal keratinocytes were collected into the growth media. Cells were then harvested by centrifuging at 1000 rpm for 5 minutes, resuspended and seeded into 75 $cm^2$ tissue culture flasks with the presence of a feeder layer (irradiated mouse 3T3 (i3T3) cells) and cultured in Green's media (66% DMEM (v/v), 21.6% F12-HAMS (v/v), 10% FCS (v/v), 0.5% insulin, 0.5% adenine, 0.1% T/T, 0.1% chlorotoxin, 0.016% hydrocortisone, 0.01% EGF, 100 IU $mL^{-1}$ penicillin, 100 µg $mL^{-1}$ streptomycin, 2mM L-glutamine and 0.625 µg mL −1 amphotericin B).

HDFs were isolated by mincing the dermis with into 10 $mm^2$ pieces. The pieces were then incubated overnight at 37 °C in 0.5% (w/v) collagenase A solution. The suspension of fibroblasts was centrifuged at 1000 rpm for 5 minutes and resuspended in DMEM containing 10% (v/v) FBS, 100 IU $mL^{-1}$ penicillin, 100 µg $mL^{-1}$ streptomycin, 2mM L-glutamine and 0.625 µg mL −1 amphotericin B.

#### 3.5.12.2. Preparation of acellular de-epidermised dermis (DED)

DED was prepared from skin grafts according to a modified method described by Chakrabarty et al. [421]. Briefly, the skin graft was treated in 1 M NaCl solution for 24 h at 37ºC and then washed with PBS for 40 minutes. The epidermis was removed by peeling off or scraping gently (if epidermal layer remains, and cells have not been harvested before). DED was kept in media at 37ºC for 2 days to check its sterility.

#### 3.5.12.3. Construction of a 3D TE human skin model

A 3D human skin model was reconstructed *in vitro* to study vascularisation of the skin using a well-established protocol [411]. Briefly, 1 $cm^2$ pieces were cut from DED, and a stainless-steel ring (0.79$cm^2$) was placed onto the papillary side. HDFs were trypsinised and centrifuged at 1000 rpm for 5 minutes before being resuspended in DMEM. 1 x $10^5$ HDFs were seeded into the stainless-steel ring and kept in 37°C while preparing keratinocytes for seeding. The i3T3 feeder layer was removed first using 5 mL of 0.5 M sterile EDTA solution with 3-5 minutes incubation at 37°C. After removal of the feeder layer, keratinocytes were then trypsinised and centrifuged at 1000 rpm for 5 minutes and resuspended in Green's media. 3 x $10^5$ HDFs were seeded into the stainless-steel ring as

a co-culture with HDFs. TE skin models were incubated overnight at 37°C before removing the ring and addition of Green's media. 3D skin models were incubated in Green's media for another day (two days in total) and then raised to air-liquid interface by using a sterile stainless-steel grid and cultured for a total of fourteen days in order to ensure differentiation of the layers of the epidermis. The protocol of the reconstruction of a tissue-engineered skin model is given in Figure 50.

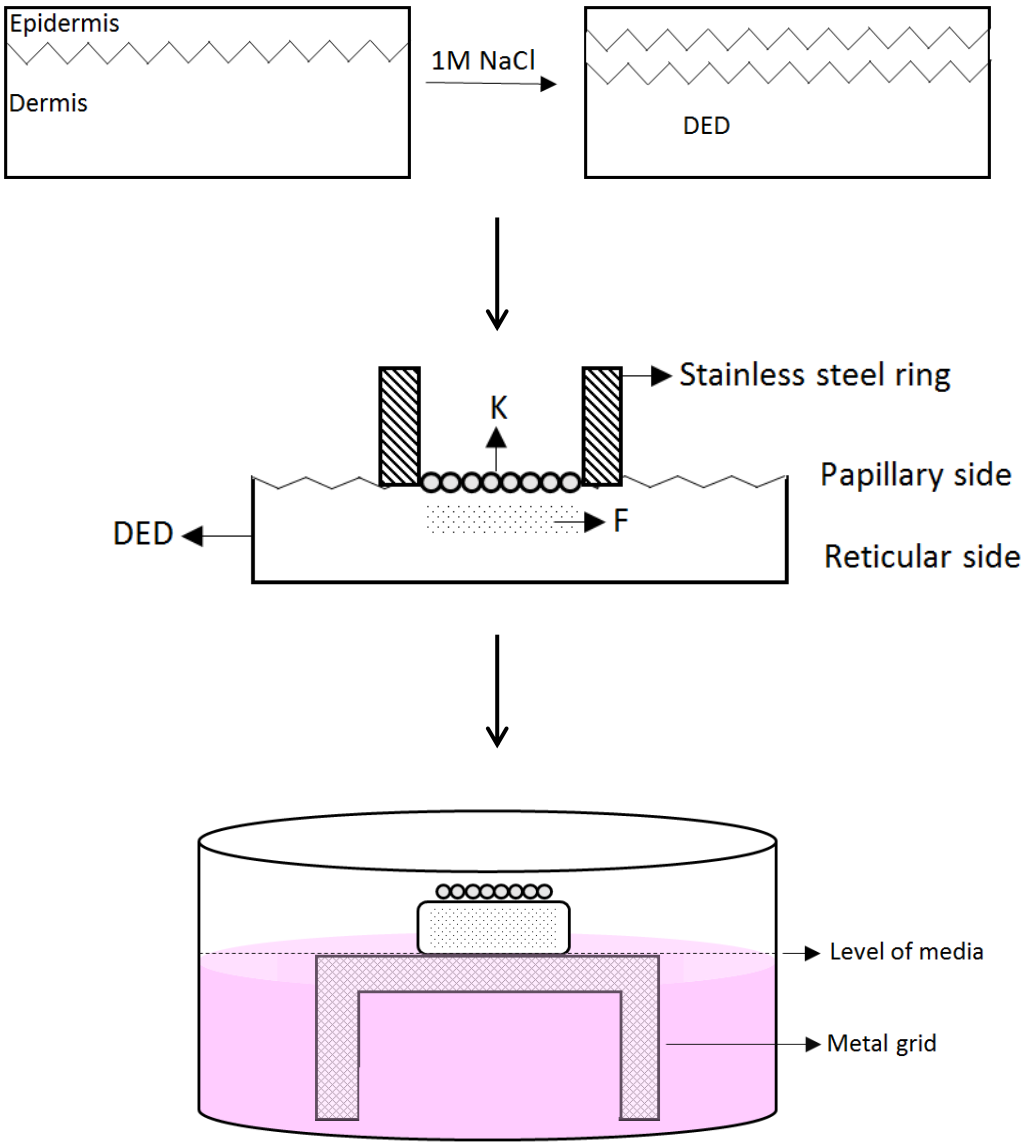


***Figure 50.*** *Schematic illustration of the reconstruction of a 3D tissue-engineered human skin model. K = keratinocytes, F = fibroblasts, DED = de-epidermised dermis*

### 3.5.13. Use of the PHBV SVN to study angiogenesis *in vitro* and to investigate the vascularisation of a reconstructed skin model

Two separate experiments were designed to investigate the potential of the developed PHBV SVN to be used as an *in vitro* platform to study angiogenesis and vascularisation of a TE skin model: (i) Matrigel outgrowth experiments and (ii) TE skin vascularisation studies (Figure 51).

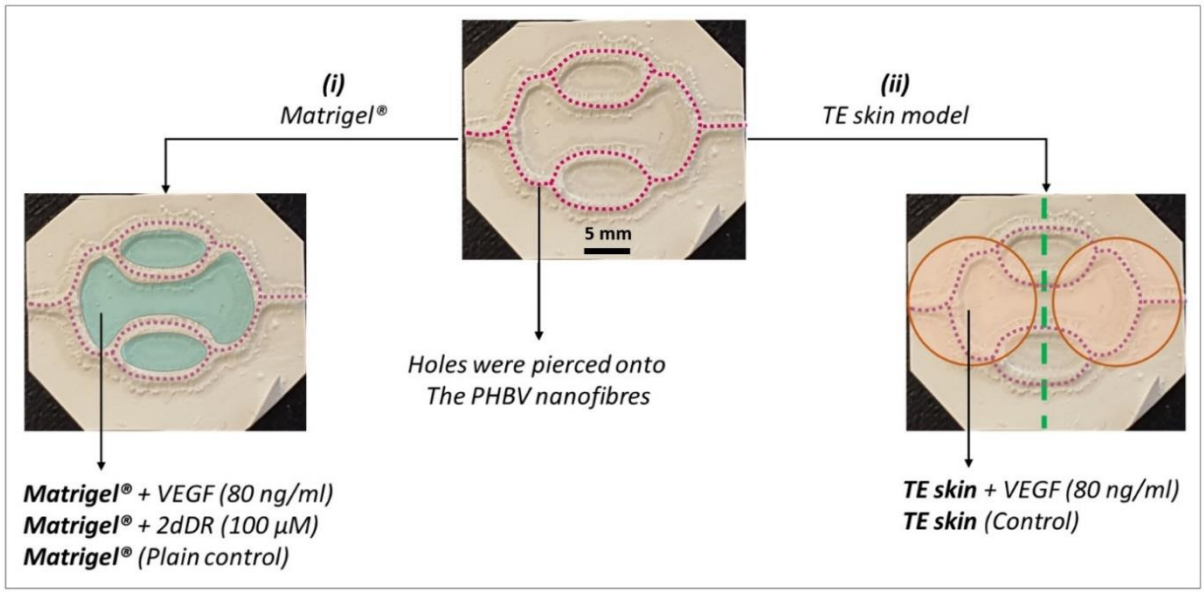


***Figure 51.*** *Designed experiments showing the investigation of the potential of the PHBV SVN to be used as an in vitro platform to study angiogenesis and vascularisation of a TE skin model. Purple dotted lines represent pierced holes. Matrigel and TE skin were indicated with blue and orange color, respectively*

#### 3.5.13.1. Investigating the endothelial outgrowth from PHBV channels to Matrigel and to TE 3D skin equivalent

For Matrigel outgrowth experiments, PHBV SVN repopulated with HDMECs ($1x10^6$ HDMECs per scaffold) were incubated for 7 days as described in Section 3.5.9.3 and then transferred into 6-well plates in a laminar hood. Once an endothelium-like monolayer was obtained, escape holes were pierced on the channels using sterile 30 G syringe needle. Matrigel (protein concentration > 10.8g/ mL) was purchased from Corning. The final concentrations of VEGF and 2dDR within the Matrigel were 80 ng/mL and 1.34 µg/mL respectively. 100 µl of Matrigel was pipetted into hexagonal wells formed by synthetic channels and 200 µl into the well between two hexagonal wells (Figure 52).

Scaffolds were then returned to the incubator for Matrigel to set at 37 °C for 15 minutes. PHBV scaffolds were then cultured in EC GM for 7 days.

For analysing the HDMEC outgrowth through Matrigel after culturing HDMECs in the synthetic PHBV vascular scaffolds, the scaffolds were fixed with 3.7% FA and stained with Phalloidin--TRITC for 30 minutes and DAPI for 15 minutes following permeabilisation of the cells with 0.1% Triton-X100 for 30 minutes. The hydrogels were peeled off from the surface of the PHBV SVN, and fluorescent images were taken within the Matrigel. Tube formation and the number of branch points was quantified as described previously using Angiogenesis Analyzer plugin of ImageJ [351] and AngioTool software, respectively. The results were then statistically analysed using GraphPad Prism software

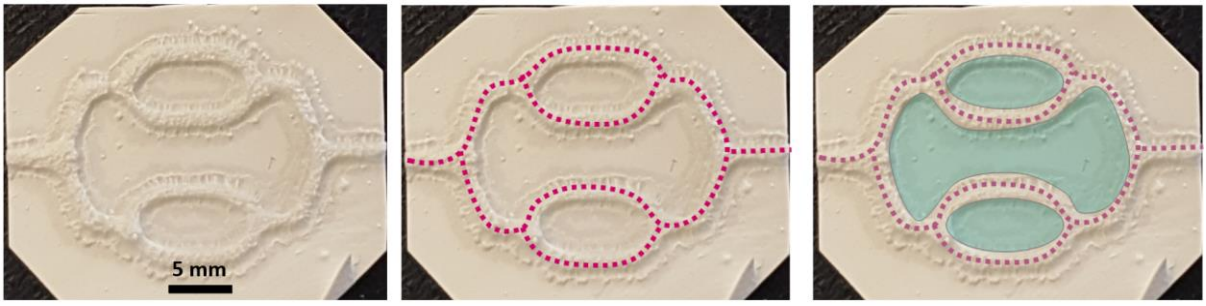


***Figure 52.*** *Schematic illustration of the Matrigel outgrowth experiments showing the pierced holes and loading of Matrigel shown with purple and light blue colour, respectively*

3.5.13.2. Investigating the endothelial outgrow from PHBV channels to reconstructed 3D skin equivalent

For TE skin outgrowth experiments, PHBV synthetic vascular scaffolds repopulated with HDMECs ($1x10^6$ HDMECs per scaffold) and HDFs ($1x10^6$ HDMECs per scaffold) were incubated for 7 days and then transferred into 6-well plates in a laminar hood. Escape holes were pierced on the channels with 30 G syringe needle. TE skin equivalent models were prepared as described in section 3.5.12 and cut circularly at day-7 prior to implantation. A fibrin glue was used to glue TE skin to PHBV SVN. Use of fibrin glue in skin grafts and TE skin replacements has previously been reported [422]. Fibrin glue was prepared by mixing fibrinogen from human plasma (20 mg/mL in 0.9% NaCl solution in dH2O) and human thrombin (25 units/mL in 0.1% BSA). Briefly, 50 µl of fibrinogen was pipetted over the surface of the PHBV SVN channels. Then 50µl of thrombin was pipetted over fibrinogen, and TE skin models were glued immediately on channels (Figure 53). PHBV scaffolds with TE skin models on them were then submerged in EC GM either

supplemented with 80 ng/mL VEGF or non-supplemented (control) and cultured for a further 7 day at the air-liquid interface. Throughout the experiment duration, EC GM either non-supplemented or supplemented with VEGF (80 ng/ mL) was pipetted from the top of the TE skin model twice per day.

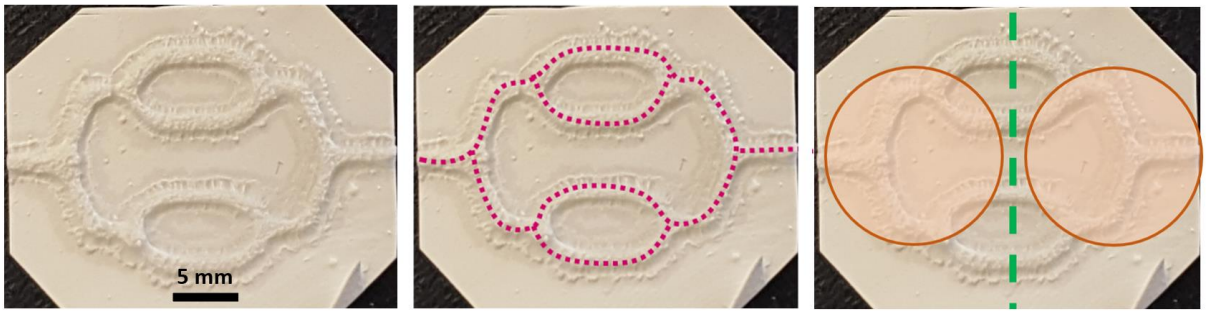


***Figure 53.*** *Schematic illustration of the TE skin outgrowth experiments showing the pierced holes and the placement of the TE skin models shown with purple and orange colour, respectively*

For the investigation of the HDMEC outgrowth through reconstructed TE skin models, scaffolds with TE skin on top of them were fixed in with 3.7% FA. Fixed PHBV scaffolds with TE skin models were then embedded in OCT freezing medium and frozen in liquid nitrogen for 3 minutes. Sections were cut 5-10 µm thick using a cryostat (Leica Biosystems Nussloch, Germany) at -20°C and stained with Phalloidin-TRITC for 30 minutes and DAPI for 15 minutes following permeabilisation of the cells with 0.1% Triton-X100 for 30 minutes in order to see the general appearance of the PHBV SVN and TE skin together. The sections were then immunostained for anti-CD31 and counterstained with DAPI as described at the beginning of this section. The samples were further investigated histologically by staining the sections with haematoxylin for 1.5 minutes and eosin for 5 minutes as described previously. The outgrowth distance of HDMECs was determined using ImageJ software, and the results were then statistically analysed using GraphPad Prism software.

### 3.5.14. Investigating the vascularisation of the reconstructed 3D skin equivalent using *ex-ovo* CAM assay

*Ex-ovo* CAM assay was used to evaluate the vascularisation of the TE skin model as a positive control. The protocol of *ex-ovo* CAM assay was explained in detail in Section 2.5.6. Briefly, fertilised chicken eggs (Gallus domesticus) were purchased from Henry Stewart & Co. MedEggs (Norwich, UK) and cleaned with 20% industrial methylated spirit solution.

Eggs were incubated at 37.5°C for 3 days in a rocking egg incubator (RCOM King SURO, P&T Poultry, Powys, Wales). On day 3, the embryos were transferred gently into sterile petri dishes and incubated at 38°C in a cell culture incubator (Binder, Tuttlingen, Germany). CAM assay was conducted in care of the guidelines of the Home Office, UK. On day 7, reconstructed human skin equivalents (14-day cultured) were cut circular (0.8 mm diameter) using a biopsy punch and implanted to CAMs for a further 7 days. In order to study the effect of proangiogenic drugs, VEGF and 2dDR were added twice a day dropwise throughout the assay duration. The concentrations of the drugs were 80 ng/day/embryo and 200 μg/day/embryo for VEGF and 2dDR, respectively. The preparations of the proangiogenic solutions were described in Section 2.5.4.

Images of the reconstructed skin equivalents implanted on CAM were taken using a digital USB microscope at day 14. Embryos were then sacrificed, and the skins cut with a rim of surrounding CAM tissue and fixed in 3.7% FA solution. Angiogenesis was quantified by counting all blood vessels growing towards the scaffolds in a spoke wheel pattern, as described previously [89]. Histological analysis of the samples was performed with H&E staining as described previously in Section 2.5.4.

#### 3.5.15. Statistical analysis

Statistical analysis was carried out using either student t-test or one-way analysis of variance (ANOVA) using statistical analysis software (GraphPad Prism, CA, USA). Where relevant, n values are given in figure captions. Error bars indicate standard deviations in the graphs unless otherwise stated.

## 3.6. Results

### 3.6.1. Comparison of PHBV vs PCL in terms of their physical, mechanical and biological performances *in vitro* and in CAM assay

The results of the contact angle measurements showed that the contact angle of the water droplet on PCL was lower than the one on PHBV, indicating a less hydrophobic surface. SEM images of the electrospun PHBV and PCL showed that use of both polymers resulted in smooth and beadless nanofibrous fibre formation. Fibre diameters of PHBV and PCL were 0.67 ± 0.13 μm and 0.47 ± 0.1 μm, respectively. No statistically significant difference was found between UTS of the scaffolds (3.62 ± 0.22 MPa and 3.94 ± 0.35 MPa,

respectively for PHBV and PCL). The Young's modulus of the electrospun PHBV scaffolds was found approximately 5-times higher when compared with PCL electrospun scaffolds (67.56 ± 11.36 MPa and 13.14 ± 1.73 MPa, respectively for PHBV and PCL). The results of contact angle measurements, stress-strain curves, and SEM images are given in Figure 54.

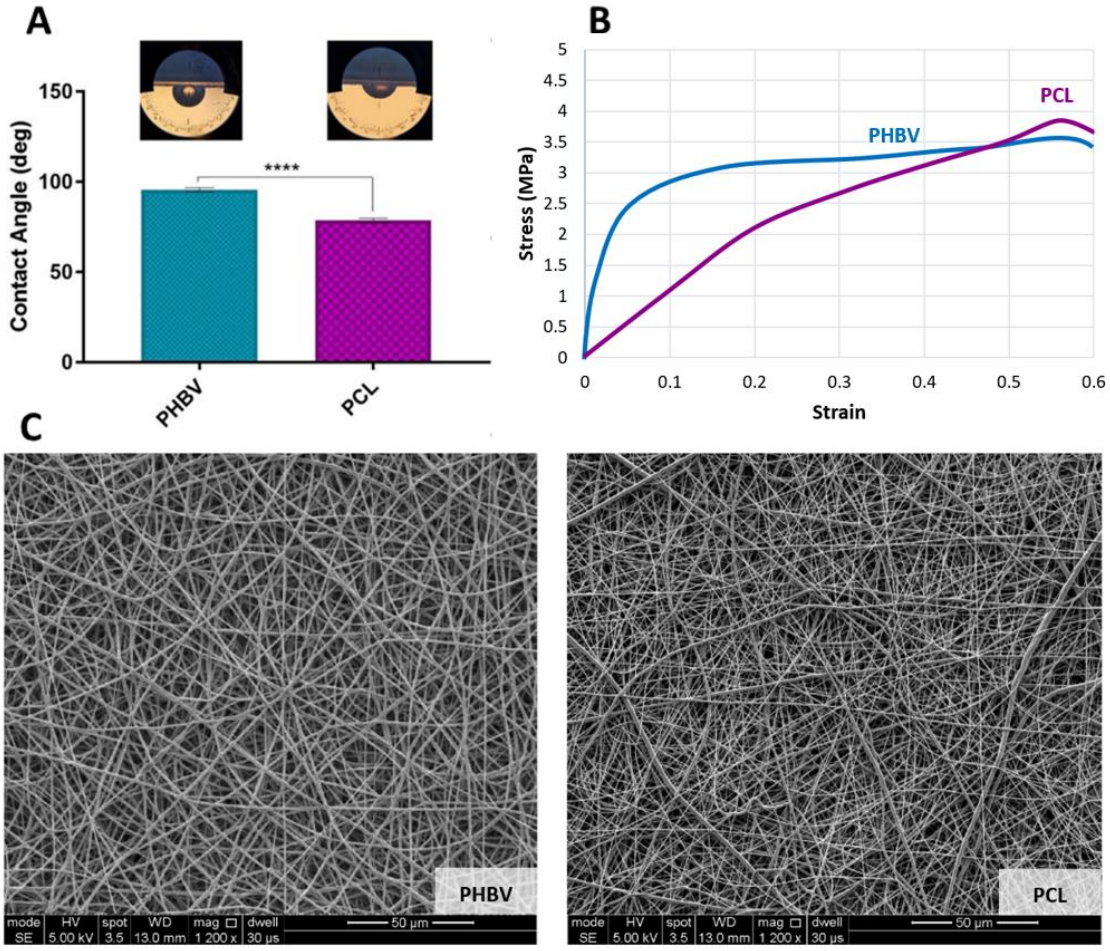


***Figure 54.*** *(A) Contact angle measurements, (B) representative stress-strain curves, (C) Ultrastructure of PHBV and PCL*

The results of the mechanical comparison of PHBV and PCL are summarised in Table 15.

***Table 15.*** *Mechanical properties of PHBV and PCL electrospun fibres. ([a]significantly different ($p<0.05$), [b]significantly different ($p<0.001$), ns= not significant, n=4)*

| Polymer | *Fibre Diameter (µm)* | *UTS (MPa)* | *Young's Modulus (MPa)* |
|---|---|---|---|
| **Electrospun PHBV** | $0.67 \pm 0.13^{a}$ | $3.62 \pm 0.22^{ns}$ | $67.56 \pm 11.36^{b}$ |
| **Electrospun PCL** | $0.47 \pm 0.12^{a}$ | $3.94 \pm 0.35^{ns}$ | $13.14 \pm 1.73^{b}$ |

Metabolic activities of HDMECs on both polymers showed a regular increase over 11 days. By day 1, attachment of HDMECs was approximately 3.4-fold higher on PHBV fibres when compared with PCL fibres. Moreover, no statistically significant difference was found between the metabolic activities of HDMECs on PHBV and TCP by day 1. At each time point, the metabolic activities of HDMECs on PHBV fibres were significantly greater when compared with the activities on PCL fibres. By day 11, the activity of cells on PHBV fibres was 1.1-fold higher than that measured on PCL fibres. Although both PHBV and PCL showed that they are both capable of providing a suitable environment for culturing HDMECs on them, PHBV gave better results in terms of metabolic activity of cells (Figure 55).

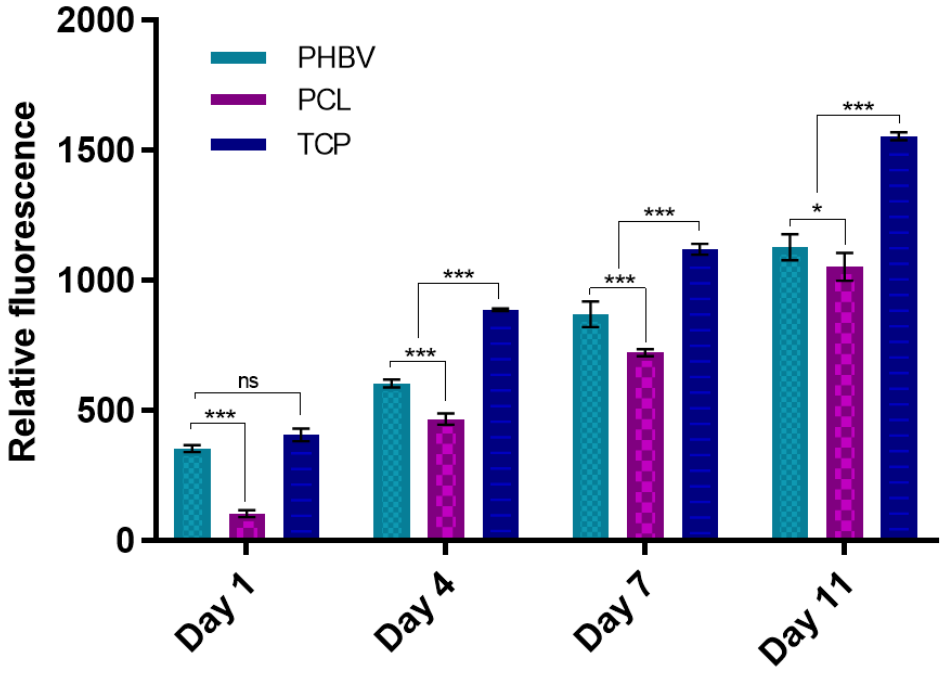


***Figure 55.*** *The metabolic activity of HDMECs cultured on PHBV and PCL over 11 days in comparison with that on TCP. *** $p \leq 0.001$, * $p \leq 0.05$, ns $p \geq 0.05$, error bars indicate SD*

Following the *in vitro* assessment of the PHBV and PCL, both polymers showed good biocompatibility on CAM with no adverse effects on embryo survival rates which were 78.8 % and 76.5 %, respectively for PHBV and PCL implanted groups. The histological evaluation of both implanted scaffolds showed similar changes in the structure of CAM with a small increase in cell density in the mesoderm layer in all scaffold groups. Both electrospun PHBV and PCL scaffolds showed good attachment to the CAM, and they showed similar cellular infiltration from the chick membrane (Figure 56).

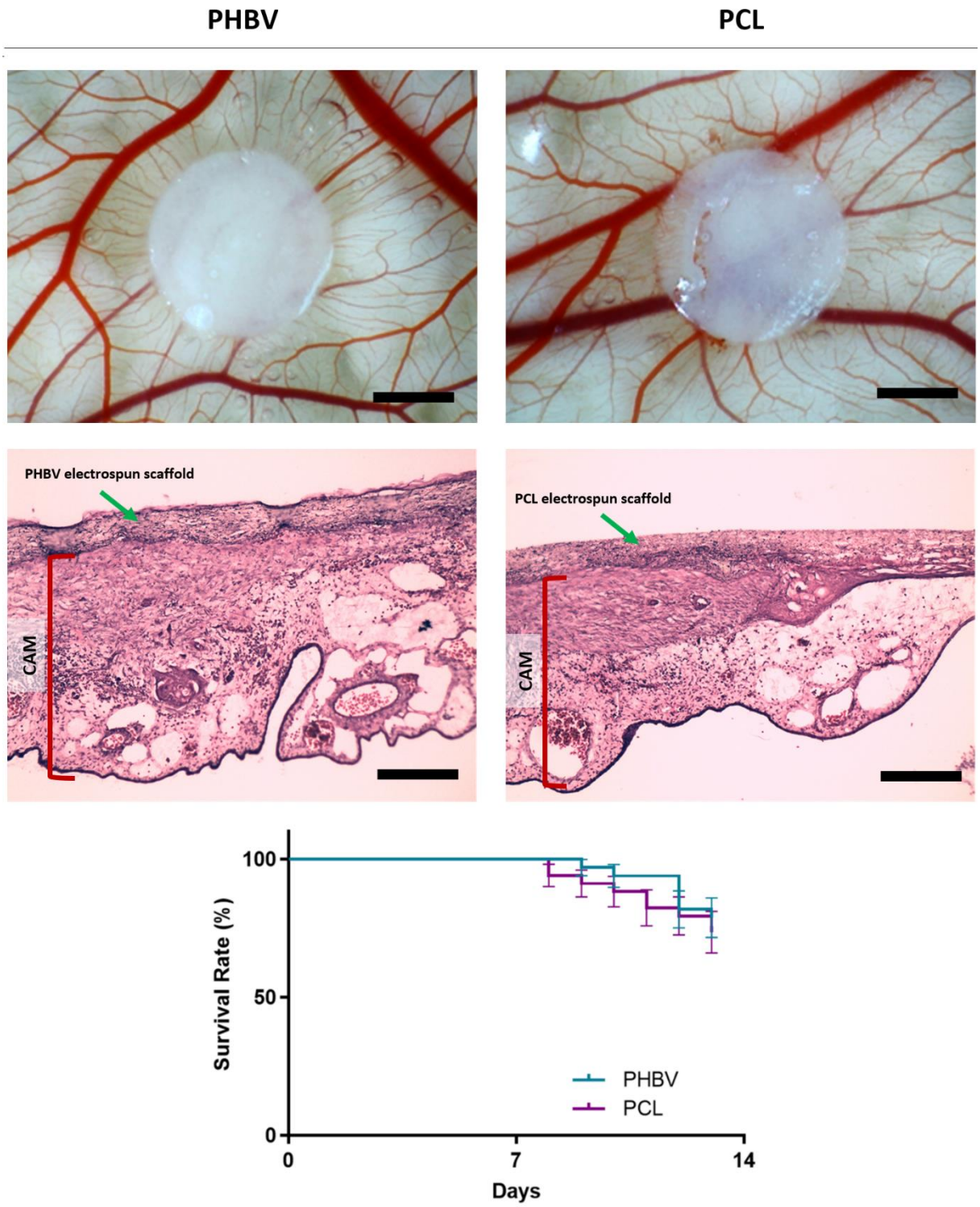


***Figure 56.*** *Macro and the histological images showing the evaluation of biocompatibilities of PHBV and PCL using ex-ovo CAM assay*

### 3.6.2. Results of the characterisation of the PHBV SVN

Following the comparison of PHBV and PCL in terms of their physical, mechanical and biological properties, PHBV was selected as the material for the production of synthetic vascular networks using electrospinning and 3D printing techniques together.

#### 3.6.2.1. Macrostructure and microstructure of the PHBV SVN

Combination of electrospinning and 3D printing allowed the production of a number of replicate scaffolds in a short period of time (in less than 2 hours). The 4-step fabrication route of PHBV SVN is shown in Figure 57.

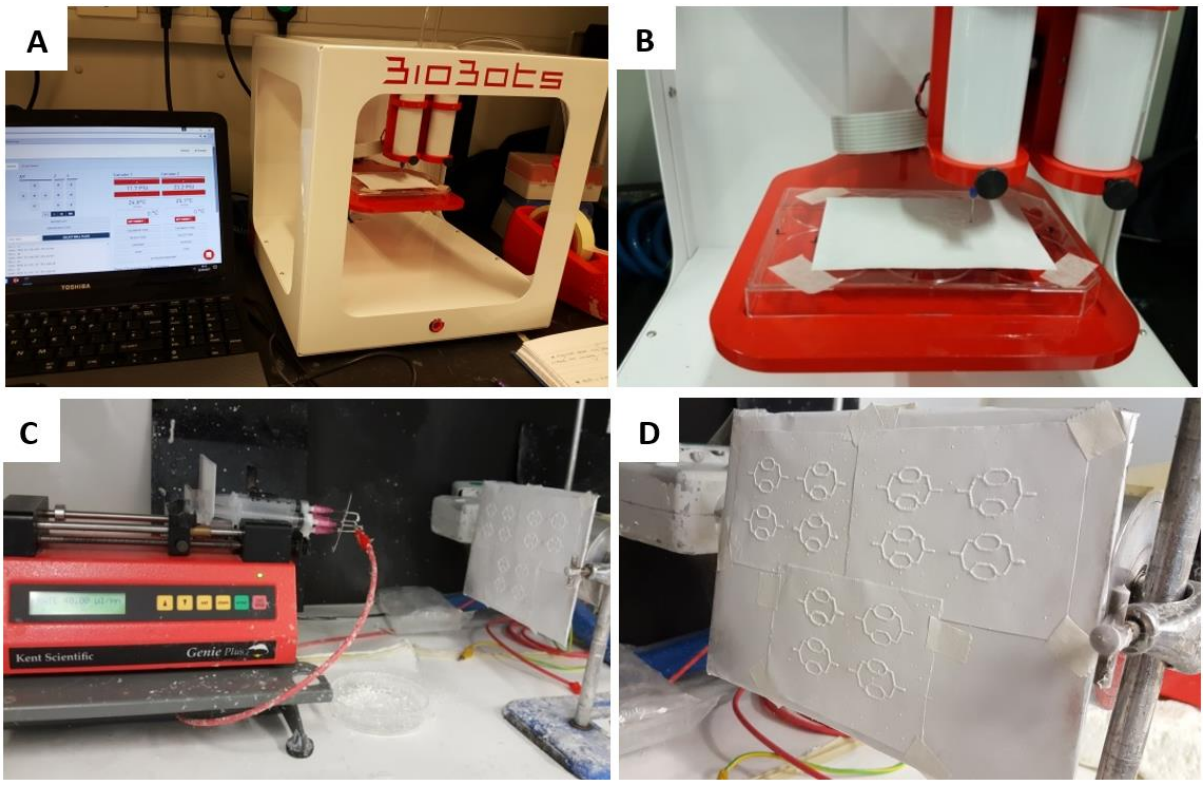


***Figure 57.*** *Production of synthetic scaffolds via electrospinning and 3D printing. 3D printing of alginate to obtain controlled synthetic channel structures can be seen in A and B. Electrospinning of another layer of PHBV on top the alginate channels is given in C and D*

The SEM images of the PHBV SVN showed that it was possible to obtain a connected network of hallow channels after removal of the alginate. The PHBV SVN scaffolds used in this study were approximate ~30 mm in length and ~18 mm wide. For each production batch, approximately 12 scaffolds were produced, and 100% of these was used. The macrostructure and the microstructure of the PHBV SVN scaffolds were given in Figure 58.

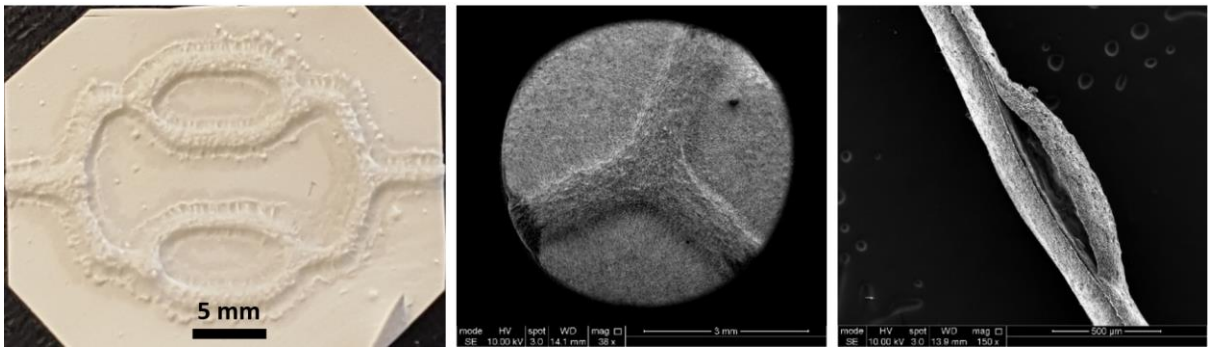


***Figure 58.*** *The macrostructure and the microstructure of the PHBV SVN scaffolds*

### 3.6.2.2. Mechanical Properties of the PHBV SVN

The average diameter of the fibres and the average pore size between the fibres were calculated as 0.76 ± 0.22 μm and 2.73 ± 1.47 μm, respectively. PHBV fibres in these diameters allow transportation of nutrients through fibres while preventing cells from escaping through them for up to 6 weeks [417,423]. In order to determine the mechanical properties of the dry and wet scaffolds such as UTS, YS, Young's modulus, and suture retention, tensile tests were performed using a uniaxial mechanical testing machine. As expected, average UTS was higher under dry conditions (0.87 ± 0.14 MPa) compared to wet scaffolds (0.48 ± 0.12 MPa). The Young's modulus of the PHBV scaffolds dramatically reduced from 80.5 ± 7.71 MPa to 12.80 ± 1.77 MPa when moistened. Similarly, suture retention of the scaffolds in dry state was double of that in wet state (1.70 ± 0.05 MPa and 0.89 ± 0.11 MPa, respectively for dry and wet scaffolds). The results of the mechanical tests are summarised in Table 16.

***Table 16.*** *Morphological and mechanical properties of the PHBV SVN under dry and wet conditions. ([a,d]significantly different (p<0.05), [b,c]significantly different (p<0.005), n/a= not applicable, n=4)*

| Condition | Fibre Diameter (µm) | Pore Size (µm) | UTS (MPa) | Yield Strength (MPa) | Young's Modulus (MPa) | Suture Retention (MPa) |
|---|---|---|---|---|---|---|
| **Dry** | 0.76 ± 0.22 | 2.73 ± 1.47 | 0.87 ± 0.14 [a] | 0.58 ± 0.09 [b] | 80.5 ± 7.71 [c] | 1.70 ± 0.05 [d] |
| **Wet** | n/a | n/a | 0.48 ± 0.12 [a] | 0.12 ± 0.03 [b] | 12.80 ± 1.77 [c] | 0.89 ± 0.11 [d] |

A representative stress-strain graph for dry and wet scaffolds is shown in Figure 59.

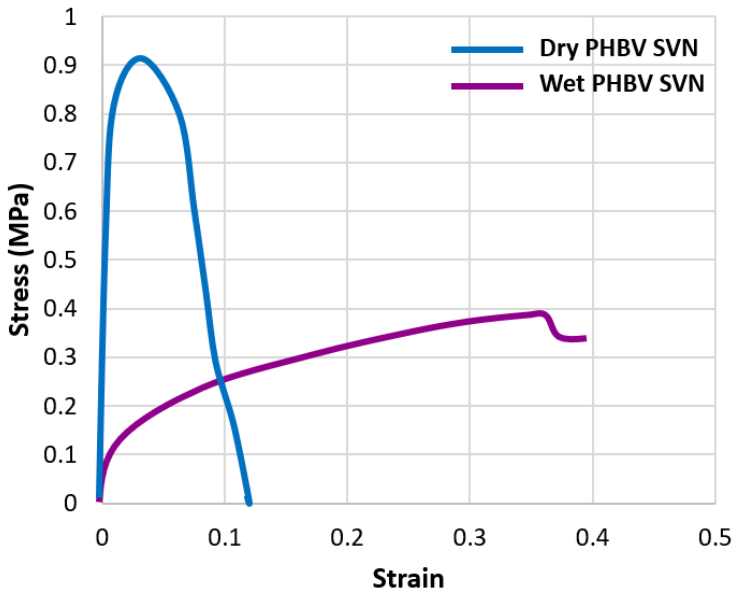


***Figure 59.*** *Representative stress-strain graphs of dry and wet scaffolds*

3.6.2.3. Confirmation of the channel patency of the PHBV SVN

The removal of the sacrificial alginate was confirmed by the cannulation of the PHBV SVN with methylene blue dye. The dye reached all the channels within the network, and the channels, which allowed the perfusion of methylene blue, were found open and interconnected (Figure 60).

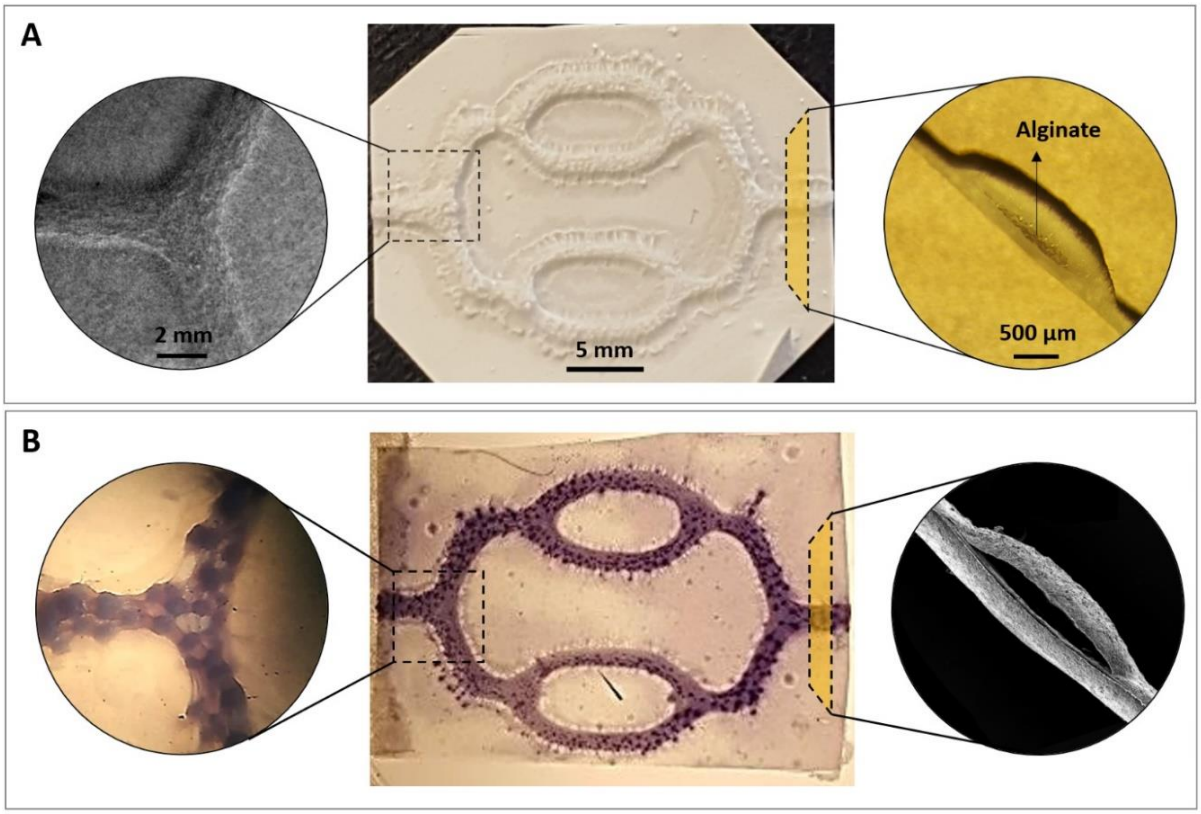


***Figure 60.*** *The macrostructure and the microstructure of the PHBV SVN scaffolds (A) before and (B) after removal of the 3D printed alginate*

### 3.6.3. Results of the cellularisation of the PHBV SVN

#### 3.6.3.1. Cellularisation of the PHBV SVN with HDF in isolation

To investigate the biological characteristics of synthetic vascular scaffolds, synthetic channels were seeded with HDFs in order to determine cellular attachment, proliferation, survival, and formation of tube-like structure. HDFs were cultured inside the channels for 7 days under static conditions (no perfusion). Scaffolds were then analysed for survival and distribution of fibroblasts inside the channels. Different sections of H&E stained scaffolds and cells after 7 days cultivation are shown in Figure 61. To verify the H&E results, phalloidin and DAPI stained sections of scaffolds were given in Figure 62.

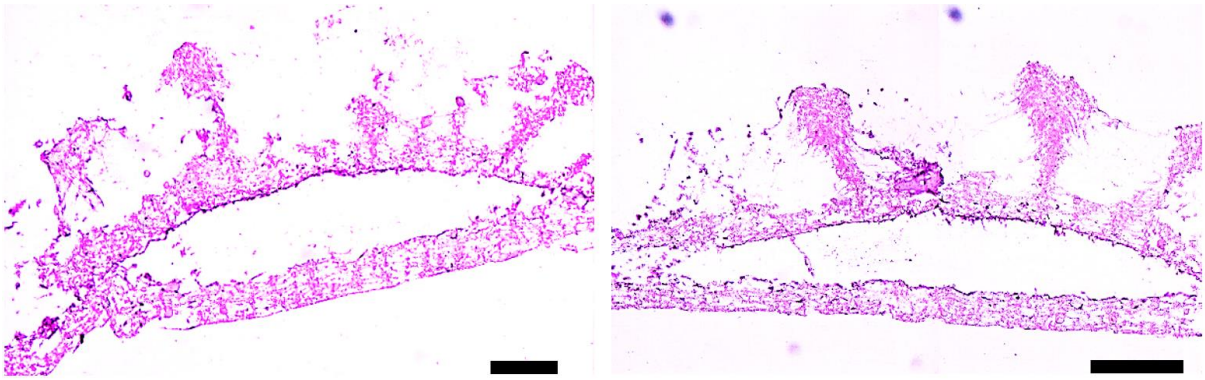

***Figure 61.*** *Histological evaluation of the sections of the synthetic vascular channels cellularised with HDFs. (Scale bars = 100 µm)*

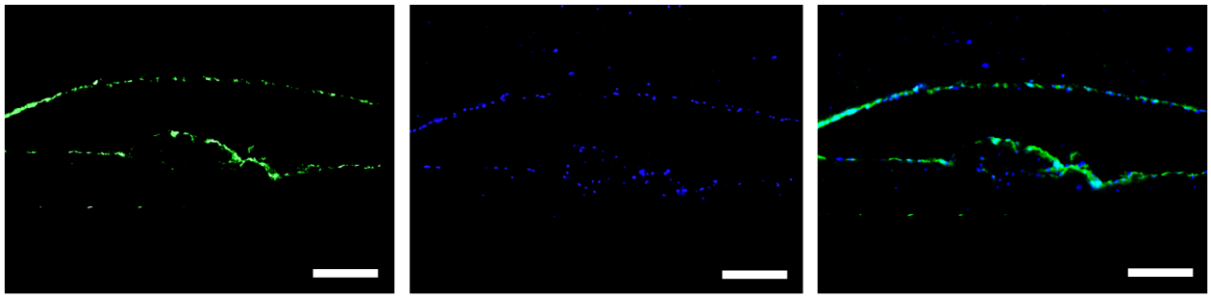

***Figure 62.*** *Phalloidin-FITC and DAPI stained scaffolds cellularised with HDFs only. (A) F-actin staining using phalloidin, (B) cell nuclei staining using DAPI, (C) A merged image showing both green and blue channels. (Scale bars = 100 µm)*

### 3.6.3.2. Cellularisation of the PHBV SVN with HDMECs in isolation

To investigate the survival of HDMECs inside the vascular channels without HDFs as supporter cells, HDMECs were seeded inside the PHBV SVN and cultured for 7 days under static conditions. A complete formation of the HDMEC monolayer within the PHBV SVN has been confirmed with fluorescent and H&E staining. Fluorescent and H&E images of the sections of the PHBV SVN cellularised with HDMECs in isolation showing the complete coverage of the channels are given in Figure 63.

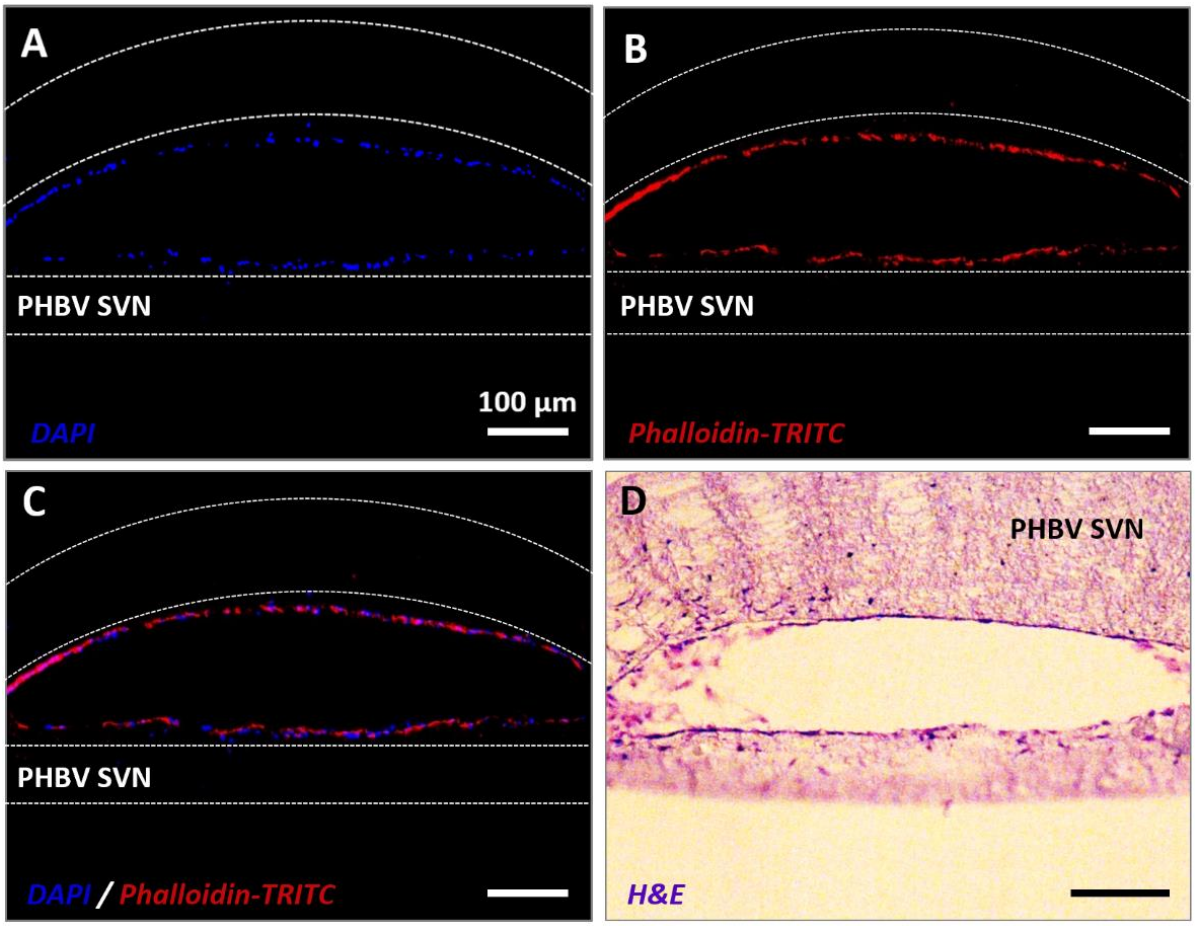


***Figure 63.*** *Fluorescent staining of the sections taken from scaffolds cellularised with HDMECs in isolation. (A) DAPI (blue), (B) phalloidin-TRITC (red) and (C) combined red and blue channels, and (D) H&E staining of the sections from PHBV SVN. (Scale bars = 100 µm)*

### 3.6.3.3. Cellularisation with HDMECs in the presence of helper HDFs

To investigate the formation of a continuous EC monolayer inside the synthetic vascular channels, HDMECs were seeded inside the channels in co-culture with HDFs on the exterior surface. Cells were cultured for 7 days, and then the scaffolds were directly imaged under a fluorescent microscope following the sectioning step for survival and distribution of HDMECs and HDFs. Fluorescent and H&E images of cells are given in Figure 64.

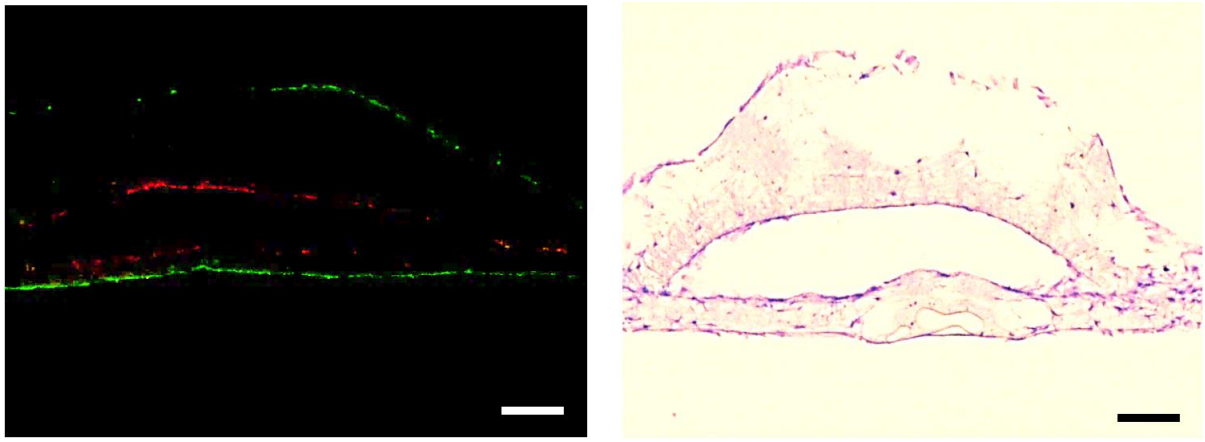

***Figure 64.*** *Sections of scaffolds with HDMECs labelled with CellTracker™Red (inside the channels) and HDFs labelled with CellTracker™Green (seeded onto the outer surface of the channels) on the left. The image on the right shows the histological evaluation (H&E staining) of the scaffolds populated with HDMECs and HDFs. (Scale bars = 100 μm)*

In order to verify the formation of the HDMEC monolayer in the synthetic vascular channels, sections were immunostained for the expression of CD31 and counterstained with DAPI after 7-day culture of HDMECs and HDFs in PHBV synthetic scaffolds.

A merged image of CD31+ (Red) and DAPI (blue) staining of the HDMECs growing on TCP is given in Figure 65. CD31 stained (counterstained with DAPI) sections of the PHBV SVN cellularised with HDMECs and HDFs cultured over 7-days are given in Figure 66. CD31 staining showed an evenly distributed HDMEC monolayer within the channels in both curved and flat surfaces.

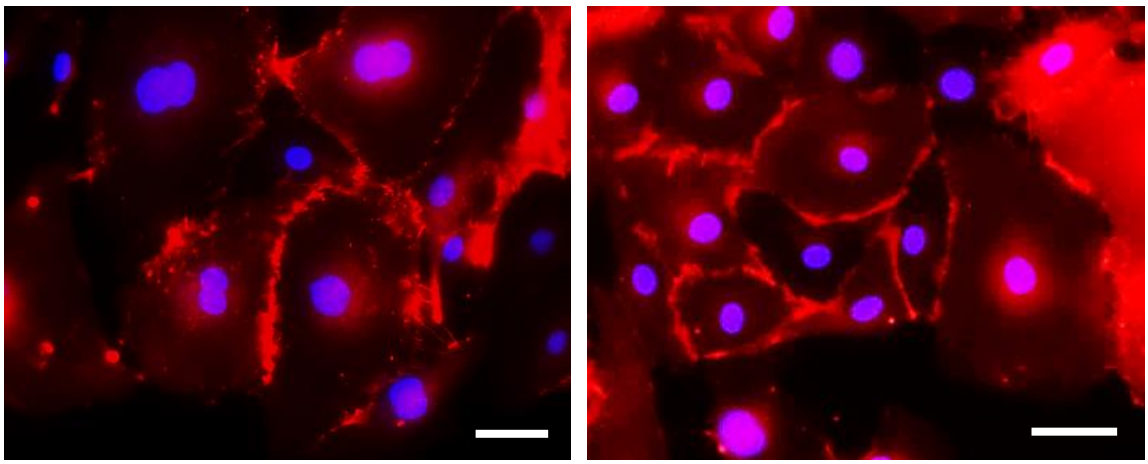

***Figure 65.*** *A merged image of CD31 positive (red) and DAPI-stained (blue) HDMECs growing on TCP. (Scale bars = 20 μm)*

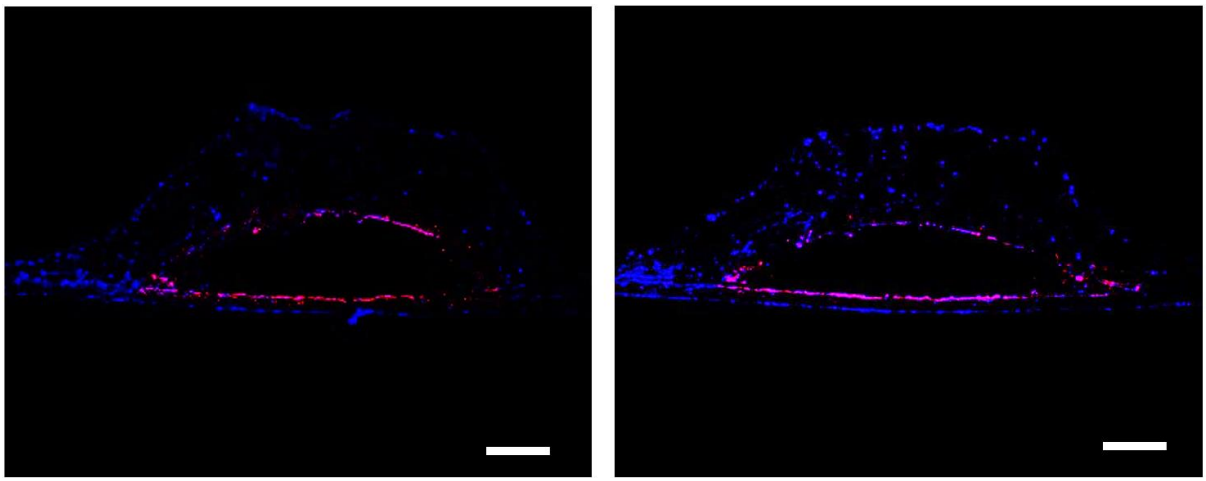

***Figure 66.*** *Immunostained sections of PHBV synthetic vascular scaffolds populated with HDMECs (inner surface of the channels) and HDFs (on the outside of the channels). Stained cell nuclei with DAPI (blue) and CD31+ staining (red) is given in the figure. (Scale bars = 100 μm)*

### 3.6.4. Results of HDMEC outgrow from PHBV SVN to Matrigel

HDMECs were observed as outgrowing and forming interconnected tube-like structures within the Matrigel close to edges of the pierced synthetic PHBV channels by day 7 (Figure 67). Inclusion of both 2dDR and VEGF increased the tube-like formed structures. However, tube-like structures were more obvious and well-organised in VEGF loaded Matrigel groups when compared with 2dDR loaded and control groups. These experiments were repeated 3 times, and 5 replicates were used for each repeat. Please note that the formation of tube-like structures was witnessed only 20% of the experiments for VEGF loaded Matrigel and 13.3% of the 2dDR loaded and control groups.

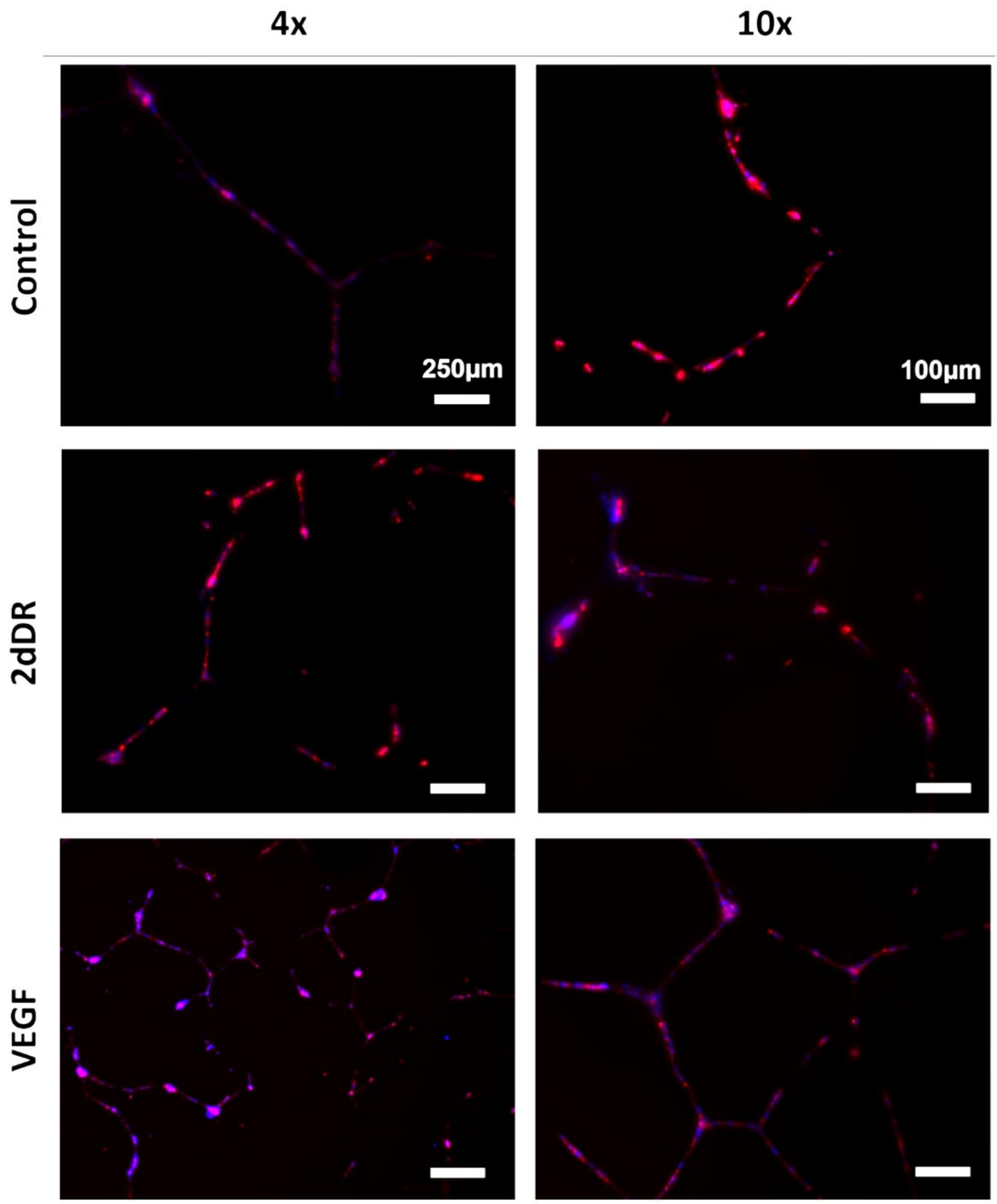


***Figure 67.*** *The figure shows the outgrowing HDMECs from PHBV channels to Matrigel either loaded with VEGF and 2dDR or non-treated groups. tube-like formed structures were obvious and well-organised in VEGF loaded Matrigel groups when compared with 2dDR loaded and control groups*

The quantification of the fluorescent images showed that inclusion of 2dDR and VEGF in Matrigel increased the number of tubes formed within the gel up to 3.5 ± 1.1 and 8.2 ± 4.0, respectively where the number of tubes per field was 1.0 ± 0.9 in control group. Similarly, average branch points were increased from 3.1 ± 1.9 (control) to 12.3 ± 4.4 and

27.6 ± 8.2, respectively, when 2dDR and VEGF loaded to Matrigel. 80 ng/mL VEGF was found significantly more effective for stimulating tube formation and for increasing branch points when compared to 100 µM 2dDR (Figure 68).

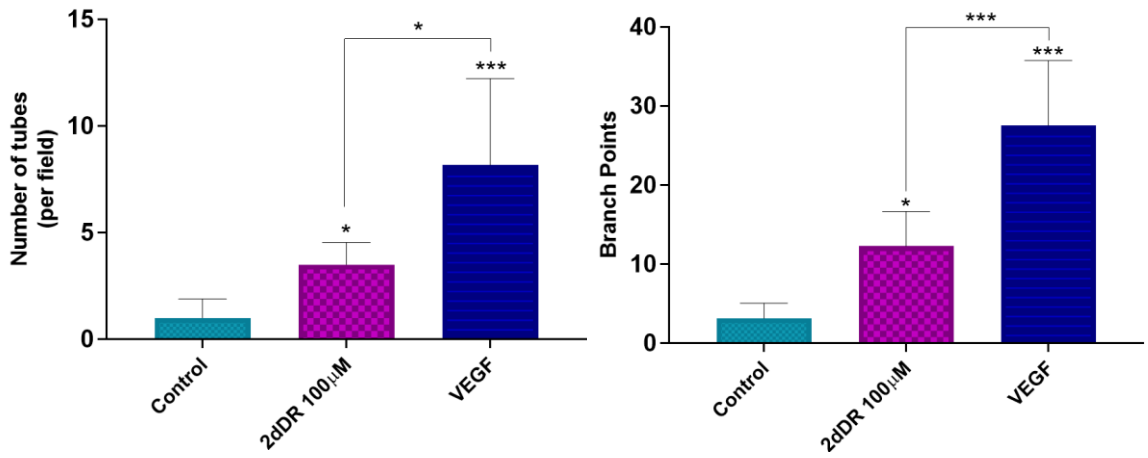


***Figure 68**. Quantified results of the Matrigel outgrowth experiments. The graphs show the increase in the number of tubes formed (on the left) and branch points (on the right) within Matrigel when VEGF and 2dDR were loaded. (***p≤0.001, *p ≤ 0.05, n = 6)*

Tube-like connections between HDMECs witnessed only a minority of the 2dDR and VEGF loaded Matrigel groups. The formation of the tube-like structures was pretty similar to those which can be observed in Matrigel tube formation assays. A representative image of tube-like capillary structures formed by HAECs growing on Matrigel basement membrane is given in Figure 69.

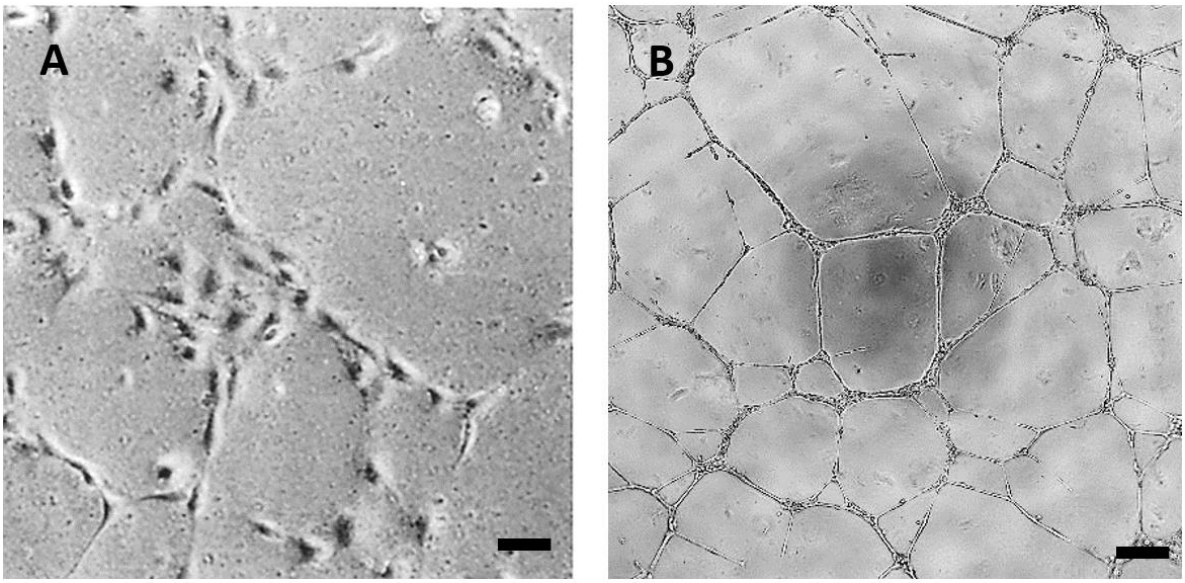


***Figure 69.** HAECs cultured on Matrigel for 1 hour (A) starting to align themselves and after 18 hours (B) forming tube-like capillary structures. Scale bars represent 200 µm*

### 3.6.5. Results of HDMEC outgrowth from PHBV channels to 3D tissue-engineered skin equivalent

#### 3.6.5.1. The appearance of skin-derived cells used in this study under a light microscope

Light microscope images of fibroblasts (Figure 70A) and keratinocytes before and after removal of i3T3 feeder layer are given in Figure 70B and 70C, respectively.

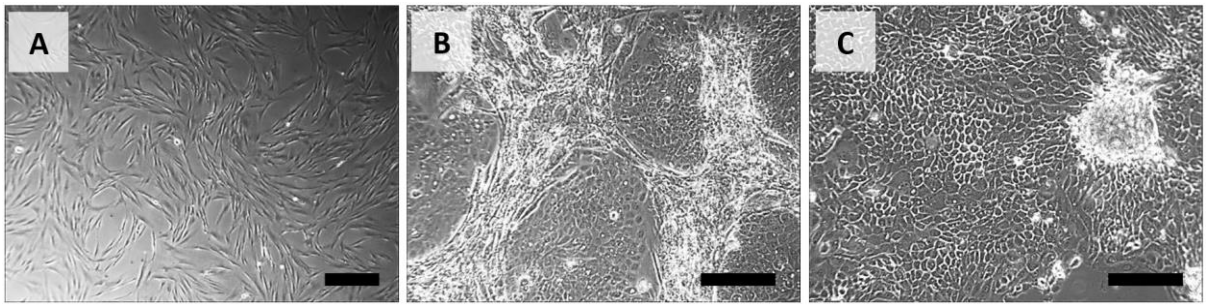


***Figure 70.*** *Light microscope images of the (A) HDFs and (B) keratinocytes (dark cells) growing on i3T3 feeder layer (bright spider web-like cells colonies) and (C) keratinocytes after removal of the feeder layer. Scale bars represent 500 µm for A and 200 µm for B and C.*

#### 3.6.5.2. General appearance and histological evaluation of the 3D tissue-engineered skin models

TE skin model was successfully developed by co-culturing human dermal keratinocytes and HDFs on DED for 14 days (2 days as submerged in media and 12 days at the air-liquid interface). The macro images of the developed skin model showed that the colour of the circular area seeded with HDFs and keratinocytes started to change to a yellowish colour which identifies the formation of a new epithelium on DED (Figure 71). The histological evaluation of the reconstructed TE skin models showed that developed TE skin model achieved a normal-looking gross skin morphology in 14 days. A multi-layered epithelium was formed and found to be well attached to the dermis (Figure 72).

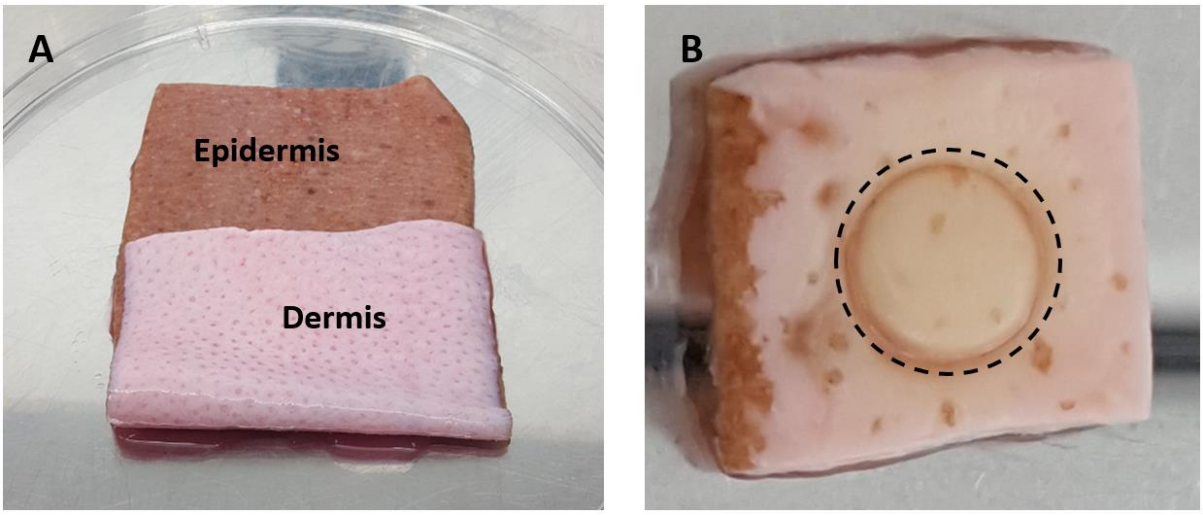


***Figure 71.*** *(A) STSG taken from patients, (B) circular area (on DED) where HDFs and keratinocytes were seeded (papillary surface) is shown with a black dashed circle. Colour change within the circle indicates the formation of a new epithelium on DED*

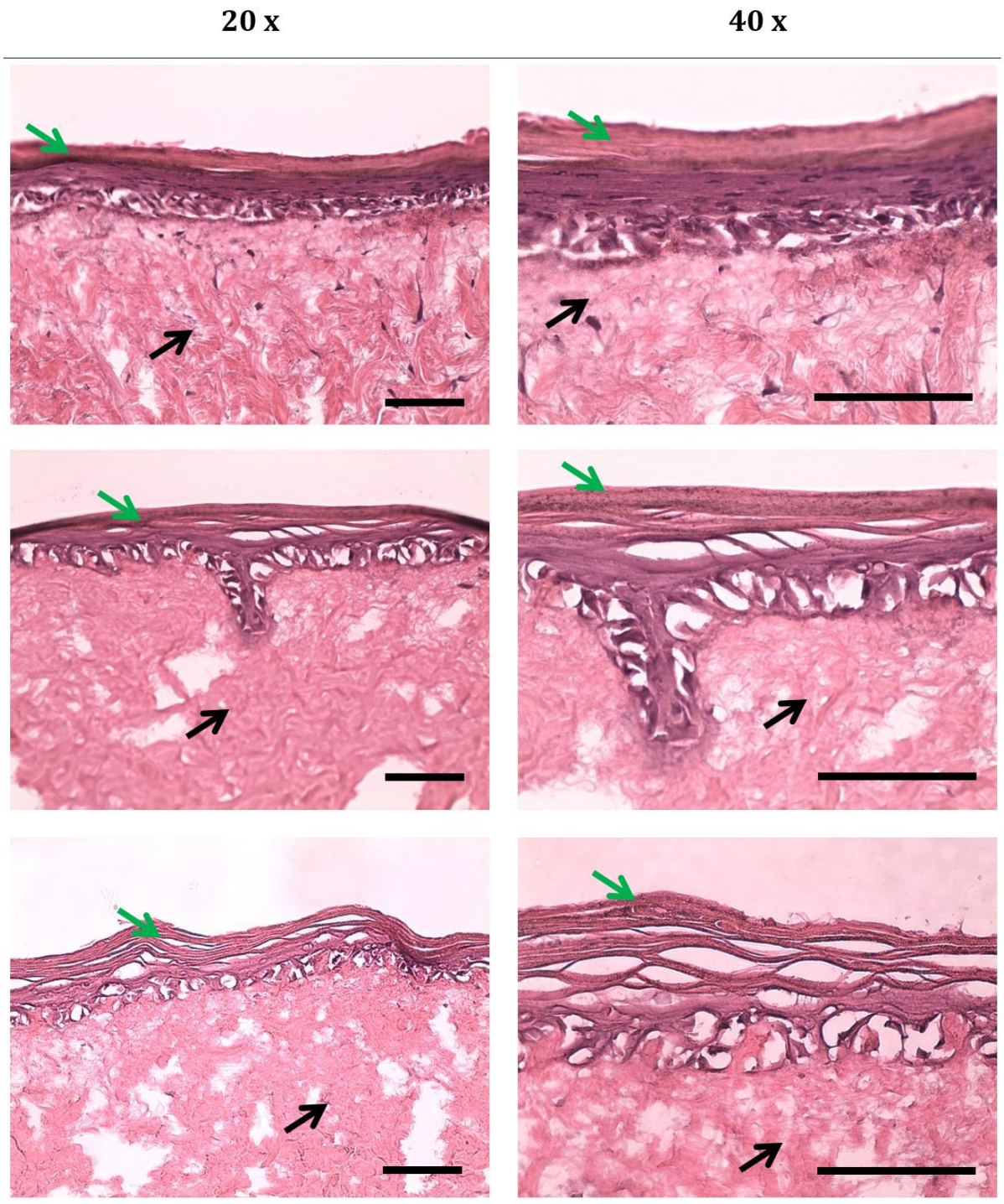


***Figure 72**. Histological evaluation of the TE skin equivalent models incubated 2 days in Green's media and 12 days at the air-liquid interface. Black and green arrows indicate the dermal layer and differentiated epidermal layers, respectively. Scale bars represent 100 µm*

### 3.6.5.3. The results of the endothelial outgrow from PHBV channels to 3D tissue-engineered skin equivalent

Following the encouraging results of HDMEC outgrowth through Matrigel, PHBV scaffolds repopulated with HDMECs and HDFs were investigated for HDMECs outgrowth through reconstructed TE skin equivalent model. After 7-day culture at the air-liquid interface, TE skin equivalent was attached to the top surface of the PHBV SVN (Figure 73) and cultured for a further 7 days at the air-liquid interface.

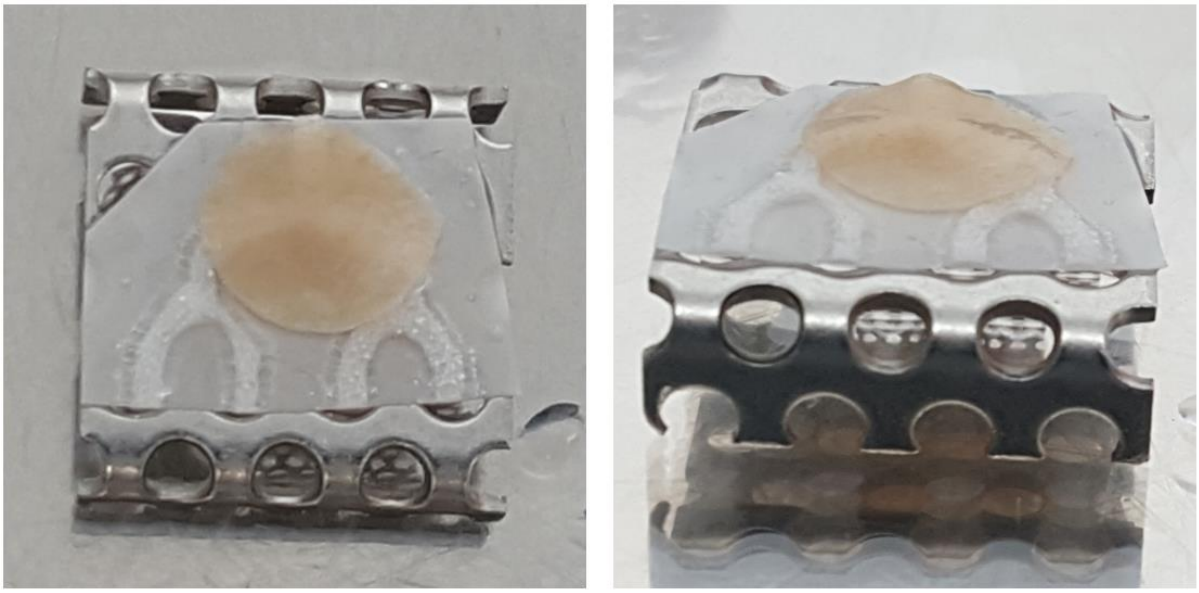

***Figure 73.*** *After 7-day culture at the air-liquid interface, TE skin equivalent was attached to the top surface of the PHBV SVN*

Phalloidin-FITC and DAPI staining of the PHBV SVN repopulated with HDMECs and HDFs and cultured with TE skin on it for 7 days showed that there was a formed monolayer within the scaffold channels and some cells were localised on the outer surface of the scaffolds. There were also some cells outgrowing from PHBV SVN towards reconstructed TE skin. However, it was not possible to identify the type of cells presented in this system (Figure 74). Thus, the sections were immunostained against CD31 to identify HDMECs.

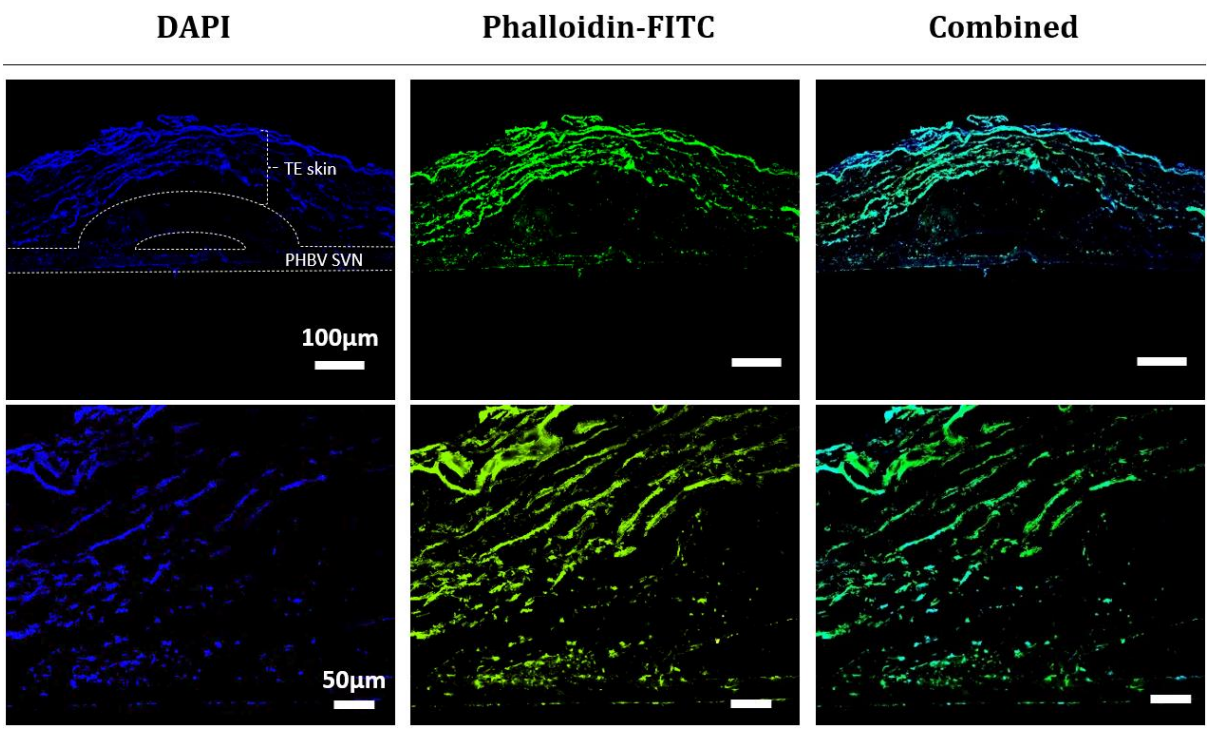


***Figure 74.*** *DAPI (blue) and Phalloidin-FITC (green) staining of the PHBV SVN repopulated with HDMECs and HDFs and cultured with TE skin on it for 7 days. The orientations of the PHBV SVN scaffold and TE skin are highlighted with white dashed lines*

Immunostained (Anti-human CD31+) sections showed that HDMECs were evenly distributed within the channels and formed a monolayer (CD31+ cells are shown with red colour), and the outer surface of the PHBV SVN was covered with HDFs (CD31+ cells shown with blue colour). High magnification images of the immunostained sections revealed that the outgrowing cells from the PHBV channels towards the reconstructed skin models were CD31 positive HDMECs. The outgrowth of HDMECs was mostly observed from the connection edges of two separate electrospun sheets (Figure 75).

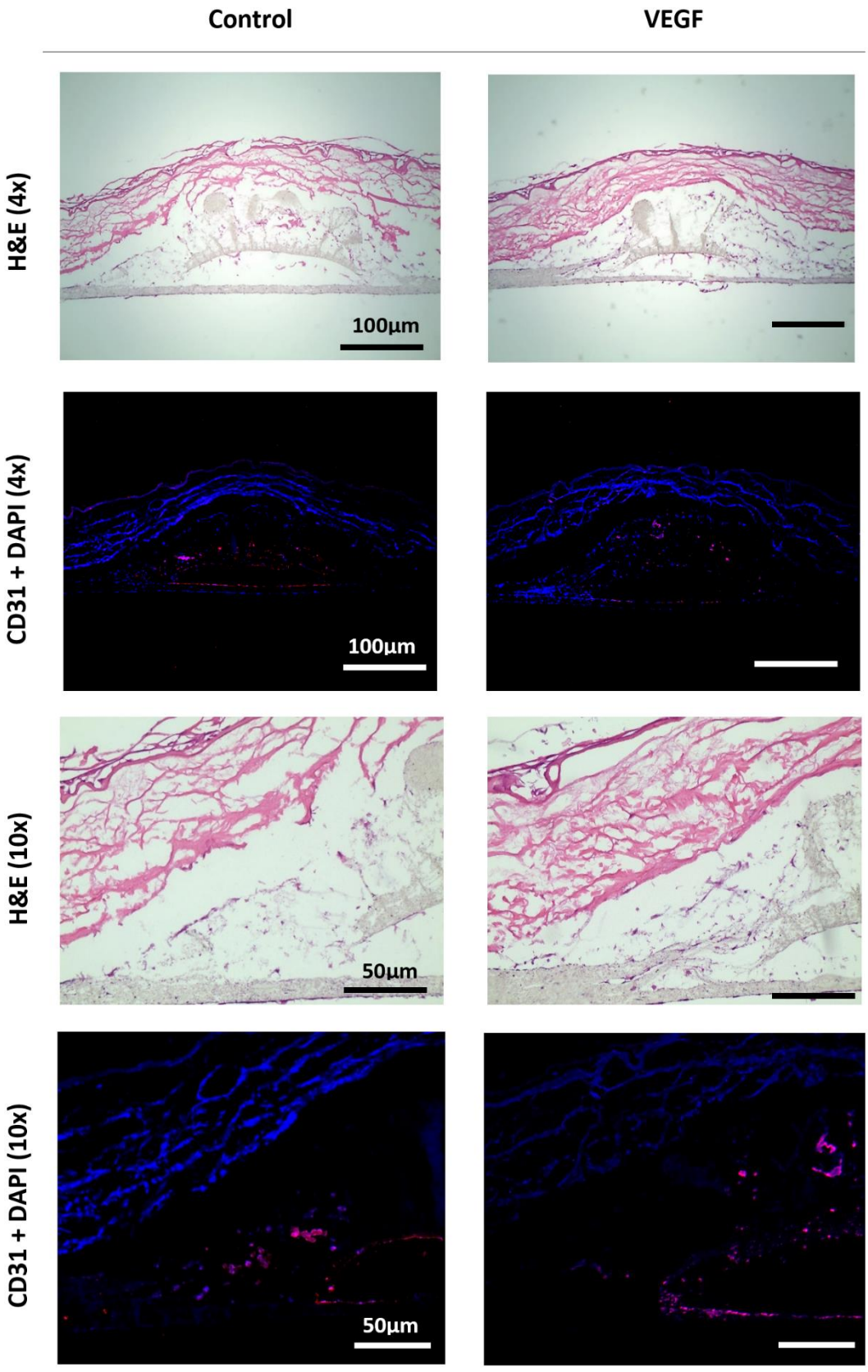


***Figure 75.*** *H&E and immunostained (CD31/DAPI) sections show that HDMECs were outgrowing from the PHBV channels through skin models. The outgrowth was mostly observed from the connection edges of two separate electrospun sheets. Inclusion of VEGF in the growth medium enhanced the outgrowth distance of the HDMECs*

Higher magnification of the H&E and CD31 staining showed that the addition of VEGF to the growth media significantly increased the outgrowth distance of HDMECs towards the reconstructed TE skin model. The distance of migration went up to 121.7 ± 6.3 µm in the VEGF group when compared to non-supplemented controls, where the outgrowth distance was 27.9 ± 11.9 µm (Figure 76).

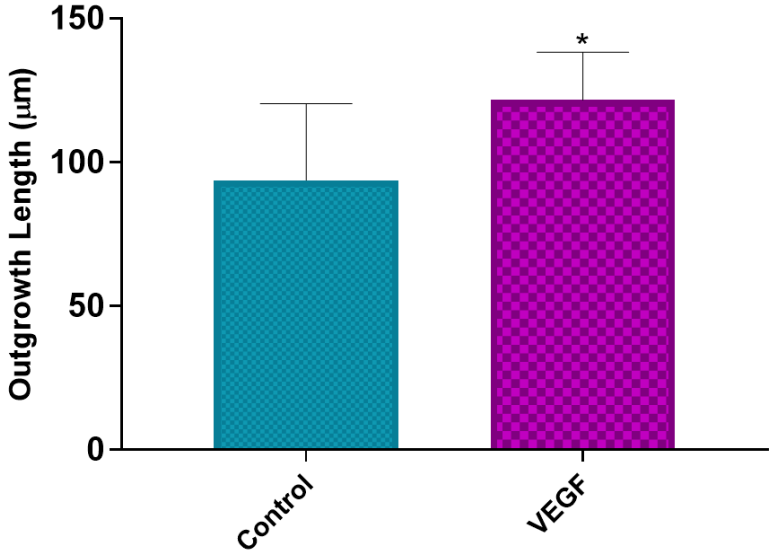


***Figure 76.*** *The graph shows the quantification of the HDMEC outgrowth distance from PHBV SVN to TE skin models when the growth medium was supplemented with VEGF or non-supplemented as control group. (*p ≤ 0.05, n = 6)*

### 3.6.5.4. The results of the vascularisation study of the tissue-engineered skin equivalent on CAM

In order to assess the effect of the presence of cells and pro-angiogenic factors on vascularisation of TE skin equivalents, DEDs and developed skin models were assessed using an *ex-ovo* CAM assay. The results showed that the mean number of blood vessels were the highest in 2dDR added TE skin equivalents, whereas the least blood vessels were observed in DED groups. The presence of cells and the addition of 2dDR significantly increased the mean vessel count growing through the samples (Figure 77). Mean vessel counts for TE skin models (no pro-angiogenic agent added), TE skin models administered with 2dDR added and TE skin models administered with VEGF were 27.0 ± 1.3, 34.4 ± 1.9, and 45.6 ± 2.0, respectively compared to control DED group (Mean vessel count: 19.2 ± 1.5). None of the implanted groups affected the embryo survival rate, which was over 70% for each group.

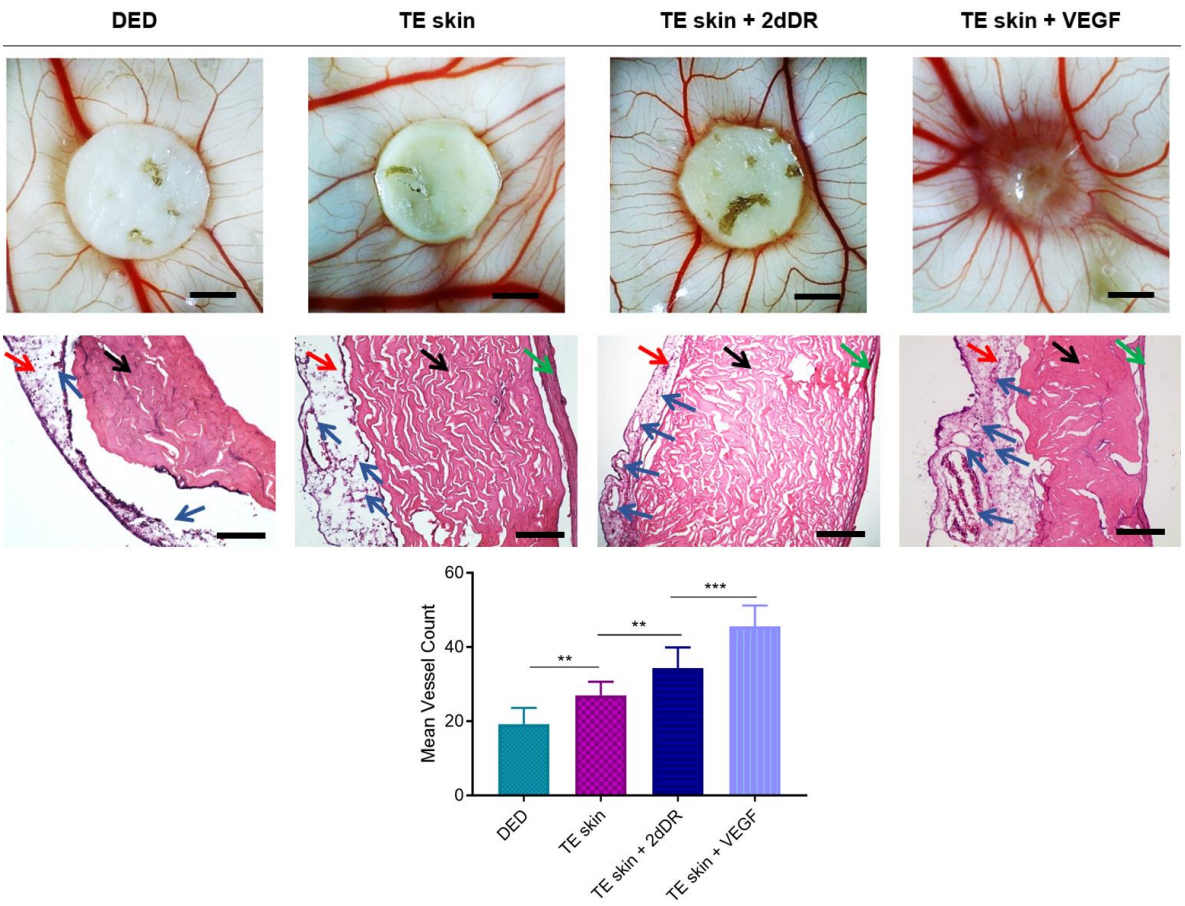


***Figure 77.*** *Representative macroimages given in top row show the angiogenic activity of DED, TE skin only and TE skin with daily addition of 2dDR at the end of EDD14 of chick embryos. Scale bars represent 3mm for macroimages. Histological appearance of the samples can be seen in the middle row. Although no complete integration was shown in any of the groups, DED only group was completely separable from CAM where TE skin samples were partly attached to CAMs. Addition of 2dDR and VEGF increased the number of blood vessels 1.3 and 1.7 fold, respectively when compared with TE skin only group. Black, red, green and blue arrows indicate the CAM, dermal layer, epidermal layer and blood vessels respectively. The graph in the bottom row demonstrates the quantification of blood vessels growing towards the samples. Presence of cells (Keratinocytes and HDFs) increased the mean vessel count by 42% when compared with DED control groups. The total number of blood vessels was 27% higher when 2dDR was added daily to TE skin samples when compared with TE skin only controls. Scale bars for the histological images represents 200 µm. (***p≤0.001, **p ≤ 0.01, n = 4)*

## 3.7. Discussion

PHBV and PCL are widely-used and biocompatible polymers in tissue engineering applications [419,424,425], and both of the polymers are suitable to fabricate tissue engineering scaffolds using electrospinning technique [426,427]. In this chapter, I compared both polymers in terms of their physical, mechanical and biological performances in order to select one of them for the production of synthetic vascular networks.

Our results showed that PCL was slightly less hydrophobic than PHBV, and SEM images of the electrospun PHBV and PCL showed that electrospinning of both polymers resulted in smooth and beadless nanofibre formation. In line with our findings, the high hydrophobicity of PHBV has previously been reported by several groups [425,428]. However, despite the more hydrophobic characteristics of it, the biological evaluation of the polymers showed that the attachment of HDMECs onto PHBV nanofibres was approximately 3.4-fold higher compared to cell attachment to PCL fibres. This might be likely due to that the Young's modulus of the PHBV was approximately five times and the average fibre diameter of PHBV was approximately 1.4-fold higher than those of PCL. Jalali et al. have previously reported that substrate Young's modulus has an effect on the adhesive behaviour of vascular ECs. Their results indicated that the adherence of ECs and their exhibition of dense actin structures were higher when cultured on high Young's modulus surfaces compared to lower ones, although no difference was observed in EC viability [429]. Similarly, Ataollahi et al. showed that the attachment and proliferation of ECs in stiff substrates were higher than those of soft substrates [430]. The average fibre diameter of electrospun fibres has also been shown to have an effect on EC attachment. Rüder et al. reported that EC adhesion was facilitated by increasing fibre diameters [431]. Ko et al. demonstrated that ECs more homogeneously proliferated on the electrospun scaffolds with higher than 600 nm fibre diameter than on the scaffolds with smaller diameters [432].

Although the attachment of HDMECs on PCL was dramatically lower than that on PHBV, on day 11, the metabolic activity of HDMECs on PCL was lower but quite close to that measured on PHBV, but it was still statistically significant. This is likely because the contact inhibition of the growth as the surface area of the scaffolds that cells can attach and grow were almost the same [433,434]. After cells become confluent on the growth area, a reduced metabolic activity, as an indirect measure of proliferation, and cell migration can be observed [435]. Throughout the experiments, the metabolic activities of HDMECs on TCP were significantly higher at all time points. This is an expected outcome since TCP is an optimised material for cell culture, which is positively charged to improve the attachment and consequently, the proliferation of cells on it [436,437].

Further evaluations of PHBV and PCL on CAM indicated that both polymers had similar degrees of biocompatibilities without any adverse effects on embryo survival (78.8 % and

76.5 %, respectively for PHBV and PCL implanted groups) and caused similar changes in the histological structures of CAMs. We have previously reported the average survival rates of the chick embryos when cultured *ex-ovo* (shell-less) as 25%, 68%, and 83% by beginner, intermediate, and experienced users, respectively [241]. In addition, the survival rates of the chicks were between 73-75% when we implanted biphasic PCL barrier membranes [419] and 75% when we implanted drug releasing PHBV scaffolds [89]. *Ex-ovo* CAM assay has many advantages over *in-ovo* CAM assay such as accessibility of the CAM during the implantation period, monitoring of angiogenesis, and quality of imaging of angiogenesis. However, the major drawback of shell-less culture is the comparably lower survival rates than *in-ovo* CAM assay [241].

The favourability of PHBV by HDMECs has previously been demonstrated by our group [143,323], and as can be seen from the results of this chapter, its slightly better biological performance over PCL led us to select this polymer for the fabrication of synthetic vascular networks.

Both electrospinning and 3D printing have various advantages and are frequently used techniques in tissue engineering. In previous studies, our group combined these two methods to benefit from both of the advantages they have [143]. 3D printing technique allows us to control the production of a large number of scaffolds with exactly the same geometries in a short time. On the other hand, electrospinning is a method where we are able to produce tissue-engineered scaffolds with a wide range of properties in terms of material composition, fibre diameter, thickness, porosity, and degradation rates [438–441]. The PHBV polymer was chosen for synthetic vascular scaffolds not only because of the previous experiences of our research group [143,417,423] , but also electrospinning nanofibers which are desirable in this study for creating a barrier for cells which is easier with this material. Furthermore, the comparison of biological performance of the two widely-used polymers, PHBV and PCL, showed us that PHBV was better for supporting ECs to attach and proliferate on it. PHBV SVN was found to be suitable for satisfying the initial requirements of this study, to provide an environment where ECs can attach and form an endothelium-like structure.

Initially, PHBV electrospun fibres with a diameter of ~0.75 μm were successfully manufactured via electrospinning. Each scaffold was designed as ~30 mm in length and ~18 mm wide with two synthetic vascular branches. PHBV nanofibres were successfully

manufactured via electrospinning, and alginate, a natural and biocompatible polysaccharide that is largely preferred for biomaterial applications [442,443], was used as a sacrificial substrate to create temporary support as interconnected networks. PHBV solution was then electrospun on top of the 3D printed alginate channels, and the alginate was removed using an EDTA solution. The perfusion of the channels with methylene blue dye showed that the channels were interconnected, and no leakage was observed neither between the two layers of electrospun PHBV nor through the small pores between fibres. The average fibre diameter and pore size were 0.76 ± 0.22 μm and 2.73 ± 1.47 μm, respectively. PHBV fibres in these diameters have been shown to allow transportation of nutrients through fibres while preventing cells from escaping through them for up to 6 weeks [417,423]. This manufacturing technique is useful because a large number of scaffolds with exactly the same geometries can be produced in a short time. The production errors reported previously by our group caused a 30% reduction in production efficiency [21]. However, using our new bioprinter, four scaffolds were produced successfully in each production batch, which took ~5 minutes, and after three production batches were completed, I was able to use 12 out of 12 scaffolds (100% production efficiency).

For mechanical characterisation of the dry and wet scaffolds, uniaxial tensile tests were performed using a uniaxial mechanical testing unit. The results were found similar with previous PHBV study in our group [143] and showed that dry scaffolds have an average UTS of 0.87 MPa and average UTS of wet scaffolds was 0.48 MPa. The mechanical properties of the synthetic vascular scaffolds were also compared with other polymeric scaffold materials. Steele et al. reported a tensile stress of 0.4 MPa for their bilayer PCL scaffolds [444]. Sant et al. reported a range of UTS between 1.5-2.5 MPa according to the ratio of their PGS-PCL scaffolds [445]. Hong et al., UTS of poly(ester urethane)urea (PEUU)/ECM scaffolds ranged from 0.08 to 0.19 MPa in the longitudinal axis and from 0.04 to 0.09 MPa in the circumferential axis [446]. Tong et al. evaluated the mechanical properties of electrospun PHBV sheets with different diameters and orientations and showed the tensile strengths of the sheets ranged approximately from 0.45 to 3 MPa [447]. The suture retention test results demonstrated that the PHBV SVN was suitable to be used by suturing the tissue models onto the scaffold. The scaffolds were resistant to suture up to 1.70 MPa and 0.89 MPa pull out strength, respectively under dry and wet conditions without any tearing. DuRaine et al. reported the suitability of their TE

constructs with a suture retention strength of 1.45 MPa for *in vivo* implantation by suturing them in place [448]. Selders et al. demonstrated that the suture retention strength of the developed polymer templates was between 0.40 - 1.20 MPa under dry conditions [449]. Similarly, Syedain et al. showed that acellular vascular grafts with a suture retention of approximately 0.15 MPa (reported as 175 g for a 12.1 $mm^2$ graft area) were suitable for suturing *in vivo* as pulmonary artery replacements [450].

A comparison of UTS of the synthetic vascular scaffolds produced with PHBV and other TE scaffold materials studied by other groups is given in Table 17.

***Table 17.*** *Comparison of UTS of synthetic vascular scaffolds produced with PHBV and other scaffold materials studied by several groups*

| Polymeric Scaffold Material | UTS (MPa) | | Reference |
|---|---|---|---|
| PHBV SVN | Dry | 0.87 MPa | This study |
| | Wet | 0.48 MPa | |
| Bilayer-PCL | 0.4 MPa | | Steele et al. [444] |
| PGS-PCL | 1.5-2.5 MPa | | Sant et al. [445] |
| PEUU | Longitudinal axis | 0.08 to 0.19 MPa | Hong et al. [446] |
| | Circumferential axis | 0.04 to 0.09 MPa | |
| PHBV (Sheet) | 0.45 to 3 MPa | | Tong et al. [447] |
| PHBV (Bulk) | 0.60 MPa | | Ortega et al. [322] |

Following the design, production and mechanical characterisation of the scaffolds, HDFs were seeded to both sides of channels and cultivated for 7 days in order to initially investigate biological performances of the scaffolds. The results of the H&E and fluorescent stainings showed the formation of a monolayer of HDFs inside the channels, and that the distribution of cells was continuous on the upper and lower wall of the channels.

Following the cellularisation of the PHBV SVN with HDFs, synthetic channels were then cellularised with HDMECs in isolation, and the cells were kept in culture for 7 days. At the end of the culture period, scaffolds were fixed, stained with phalloidin and DAPI. The results showed that HDMECs adhered and proliferated within the channels and formed a monolayer. However, the seeding density was found as an important factor that affects the survival and growth of HDMECs inside the synthetic channels. High seeding density

(~1 x $10^6$ HDMECs / scaffold) was found essential to be able to obtain a successful formation of the HDMEC monolayer.

In the body, vascular cells are in contact with perivascular cells such as pericytes, smooth muscle cells, fibroblasts or mural cells [451]. Fibroblasts have previously been reported to play a key role in the angiogenic process by producing considerable amounts of ECM molecules (i.e. collagen, fibronectin and other molecules), growth and pro-angiogenic factors which control the shape and density of blood vessels [452,453]. Although fibroblasts secrete some VEGF, the main role of these cells is to create an ECM in which endothelial cells can be embedded to form tubules. This ECM structure is rich in collagen I and fibronectin [454,455]. Based on this knowledge, PHBV synthetic vascular channels were then cellularised with HDMECs, whereas the outer surface of the channels was seeded with HDFs as co-cultures. The introduction of HDFs as supporter cells slightly improved the coverage of the channels with HDMECs. This is more likely due to the secretion of ECM components by fibroblasts, which might provide a more suitable environment for the attachment, survival and growth of HDMECs within the channels. The positive influence of HDFs on the survival and growth of HDMECs has previously been reported by other groups as well as our laboratory [21,143].

Cell culture experiments showed that PHBV SVN could provide a suitable environment for HDMECs to attach, grow and form a monolayer either in the presence or absence of HDFs. However, the use of HDFs was found to be desirable depending on the intended use of the PHBV SVN.

For the use of PHBV SVN as an *in vitro* angiogenesis model, two separate studies were conducted; the outgrowth of HDMECs was investigated; (i) towards the Matrigel loaded with pro-angiogenic agents and (ii) towards a reconstructed TE skin model as a more physiologically relevant tissue model.

The Matrigel experiments, the PHBV SVN was cellularised with HDMECs in isolation, and the outgrowth of HDMECs was investigated towards the Matrigel. 2dDR and VEGF were selected as the pro-angiogenic agents to stimulate HDMECs outgrowth from the pre-formed EC monolayer within the channels.

VEGF is an effective and well-established pro-angiogenic factor [38] which has been proven to be a regulator of EC proliferation, migration and survival [41,361]. 2dDR is a

small sugar that naturally occurs in the body as a result of the enzymatic degradation of thymidine to thymine [71]. As an alternative to the use of exogenous VEGF, we have recently reported the angiogenic potential of 2dDR *in vitro* [88], in *ex-ovo* CAM assay [89], and in diabetic rats [90].

Nanofibres have been shown to provide better surface properties for ECs to adhere and proliferate on them over microfibres [456–458]. This is likely due to the nanofibres being structurally similar to the ECM of natural tissue with their submicron-scale topography and highly packed morphology [456,459]. Furthermore, PHBV nanofibres have previously been shown to be a suitable environment for ECs to form an endothelial monolayer [323]. However, nanofibres also create a physical barrier for cells, which limits the infiltration [460]. Thus, prior to the outgrowth experiments, holes had to be pierced onto the channels of the scaffolds. The results of the Matrigel experiments showed that HDMECs were outgrowing and forming interconnected tube-like structures within the Matrigel (either loaded with VEGF or 2dDR) close to edges of the pierced synthetic PHBV channels. The tube-like formed structures were more obvious and well-organised in 80 ng/mL loaded VEGF loaded Matrigel groups when compared with 100 µM 2dDR loaded and control groups. The formation of the tube-like structures was pretty similar to those which can be observed in Matrigel tube formation assays. *In vivo*, endothelial cells are in direct contact with a basement membrane which is specific and biologically functional for enabling endothelial cells to form tube structures [350]. This biologically active protein mixture is a wonderful candidate for mimicking native basement membrane of endothelial cells *in vitro* and promotes endothelial cells to form tube-like capillary structures [221]. Kubota et al. seeded endothelial cells on a mimicked basement membrane and reported that endothelial cells could attach and form tube-like capillary structures within 2-3 hours [461]. Our observations were validated with the literature, which reports that VEGF regulates the endothelial outgrowth [462–464]. 2dDR also improved the tube formation, which is in correlation with our *in vitro* tube formation results presented in Chapter 2.

Matrigel-HDMEC outgrowth experiments were repeated 3 times, and at least 5 replicates were used for each experiment. It is important to note that the outgrowth of HDMECs was witnessed only 20% of the experiments for VEGF loaded Matrigel and 13.3% of the 2dDR loaded and control groups, respectively. Formation of complete tube-like structures by

HDMECs witnessed only a minority of the VEGF-loaded Matrigel groups. This variability demonstrates that the proposed PHBV SVN model as an *in vitro* platform to study angiogenesis is not reliable enough to investigate angiogenesis by its own. There are several factors that might be the reasons for this variability;

(i) the Matrigel is a protein gel mixture which is rich in ECM proteins such as laminin, collagen heparin sulphate, proteoglycans etc. However, the exact concentrations of the ingredients are not clearly defined, and it shows high batch-to-batch variations [465].

(ii) the thickness of Matrigel was not possible to control very well due to the complex geometry of the PHBV SVN scaffolds even though the same volume was used for each experiment. The effect of gel thickness on EC survival has been studied, and the thickness of gels has been shown to have a negative impact on the survival of ECs and HDFs [205].

(iii) HDMECs are very sensitive to culture conditions and show batch to batch variations [466]. These variations of ECs have been previously shown to be a cause for not being reproducible for *in vitro* angiogenesis models [467]

(iv) the holes pierced on SVN channels were randomly oriented, and their positions and diameters might have an impact on the variations in the outgrowth of HDMECs.

Following the Matrigel® experiments, a more physiologically relevant tissue model, TE skin model, was used with PHBV SVN to study vascularisation of a reconstructed human skin model. TE skin model was successfully developed using a well-established protocol [420]. The air-liquid interface has previously been confirmed to provide a stimulus for the gradual differentiation of keratinocytes [411]. The histological evaluation of the reconstructed TE skin models showed that developed TE skin model achieved a normal-looking gross skin morphology in 14 days. A multi-layered epithelium was formed and found to be well attached to the dermis. Following the reconstruction of TE skin, after 7-day culture at the air-liquid interface, TE skin equivalent was attached to the top surface of the PHBV SVN and cultured for further 7 days at the air-liquid interface.

The outgrowth of HDMECs towards the TE skin model was mostly observed from the connection edges of two separate electrospun sheets, and the inclusion of VEGF to the growth media significantly increased the outgrowth distance of HDMECs approximately 4.4-fold when compared to controls. However, cells were not found to be invading into the dermal layer of the developed skin models either supplemented with VEGF or not.

Santos et al., previously demonstrated that starch-based scaffolds combined with growth factors and fibrin sealant (fibrinogen 75–115 mg/mL, thrombin 4 IU/ mL) were capable of promoting vascular infiltration to newly formed tissue *in vivo* [468]. In addition, the concentration of fibrin glue used in this study is also approximately 3-4 times lower than some commercially available skin graft sealant fibrin glues [469,470]. We have previously demonstrated that fibrin glue with a fibrinogen concentration of 18.75 mg/mL, a similarly high concentration as used in this study, did not hinder cell outgrowth from tissue explants [471]. Thus, the concentration of fibrin glue does not seem to be the major cause of the prevention of cell penetration. The most probable explanations for this are that the outgrowth direction of HDMECs was against gravity; the rate of outgrowth of HDMECs from PHBV channels was low. Furthermore, the orientations, positions and diameters of the manually pierced random holes might also have negatively affected the outgrowth of HDMECs. Our group had previously explored the endothelialisation of a TE skin model and reported that the cells struggled to enter the TE skin and showed no signs of being organised when they did enter [412].

CAM is a well-vascularised membrane, and I hypothesised that CAM might represent a very well-vascularised wound bed. Thus, as a positive control experiment, I implanted the TE skin models to assess the vascularisation of reconstructed skin models from CAM. The results of the *ex-ovo* CAM assay were in compliance with the results obtained from PHBV SVN studies. Although CAM is a highly vascularised and dynamic environment with fast proliferating embryonic cells [472], the results showed that there was no sign of blood vessel or tissue integration into the dermal layer of the reconstructed skin substitutes. However, the presence of dermal cells (fibroblasts and keratinocytes) significantly improved the vascularisation in the area of implantation (towards the implanted TE skin) in comparison with DED (with no cells). In addition, the administration of VEGF and 2dDR showed a further increase in angiogenic activity. Although the major function of fibroblasts is to synthesise and maintain ECM structure, they have been reported to produce collagen, fibronectin, proteoglycans, and connective growth factors, especially in response to wounding [473,474]. They have also been reported as producing soluble angiogenic growth factors such as VEGF [475], transforming growth factor-beta (TGF-β) [476], and Platelet-derived growth factor (PDGF) [477]. Furthermore, keratinocytes have previously been reported to improve the proliferation of endothelial cells and to express VEGF [478]. Recently, the presence of

cells and *in vitro* generated ECM has also been shown to improve angiogenesis in the *ex-ovo* CAM assay [479,480]. The enhanced angiogenic properties of TE skin over DED on CAM might be validated by the studies given above.

While an increased angiogenic activity was observed when cells and drugs were presented to CAMs, the histological evaluation of the implanted TE skin models showed that there was no tissue infiltration and vascularisation through the dermal layer of the reconstructed TE skin models. Although no vascularisation was observed in any of the implants, one important thing to note was that the inclusion of dermal cells (fibroblasts and keratinocytes) and pro-angiogenic agents (VEGF and 2dDR) improved the "take" of TE skin model by CAM when compared to DED with no cells. The attachment of TE skin model to CAM (either supplemented with pro-angiogenic agents or not) was stronger whereas the DED showed no integration with CAM, and it was easily separable from the surface of the membrane after the implantation period.

The developed platform showed encouraging results to be used as an *in vitro* platform to study angiogenesis either at cellular or tissue levels. Future studies need to be conducted to improve the reliability of the proposed *in vitro* platform to and to standardise the methodology for seeding of the cells, loading of Matrigel® to the synthetic vascular scaffolds, piercing holes, and assessing the angiogenesis. In the scope of this study, only one tissue model was developed and assessed on PHBV SVN. However, promising results have shown that through further improvements, the PHBV SVN can offer a great platform for studying *in vitro* vascularisation of tissue models.

## 3.8. Conclusions and Future Work

A synthetic vascular network made of PHBV nanofibres was fabricated successfully via combining electrospinning and 3D printing to be used as an *in vitro* platform to study angiogenesis. Initial characterisation of PHBV SVN showed that a network with hollow channels was produced, and the mechanical properties of the scaffolds were similar to those used in vascular tissue engineering. The results showed that PHBV SVN could be cellularised with evenly distributed HDMECs either in isolation or in the presence of HDFs. The physical appearance of HDFs improved the survival and homogeneous distribution of ECs within the channels. The developed PHBV SVN showed promising results to be used as an *in vitro* model to study angiogenesis. Matrigel experiments

demonstrated that the platform could be used to study sprouting angiogenesis in response to pro-angiogenic agents that were loaded into Matrigel. 80 ng/mL of VEGF and 100 μM of 2dDR promoted HDMECs to migrate towards the Matrigel loaded with chemoattractants. In order to study vascularisation of a more physiologically relevant and complex structure, a tissue-engineered skin model was developed successfully. The outgrowth of HDMECs from the channels towards the skin model was mostly observed from the connection edges of two separate electrospun sheets. 80 ng/mL VEGF significantly increased the outgrowth distance of HDMECs towards the TE skin model. However, no cells reached to the DED and were found to be invading into the dermal layer of the developed skin models.

In the future, studies could focus on the standardisation of the manufacturing method in an attempt to increase the reproducibility of the model by optimising the thickness of Matrigel, orientation and the diameters of the holes. Use of ECs in co-culture with different cell types and investigating their interaction might also bring a new perspective to the use of the developed platform. Further experiments with other pro-angiogenic factors and flow conditions could be performed to study their relation to angiogenesis using the developed model to increase the reliability of the model. Furthermore, the inclusion of flow might increase the reliability of the results obtained from tissue-engineered skin model experiments. The positive influence of shear stress on EC outgrowth has been demonstrated in Chapter V. Finally, the majority of results obtained from these experiments was qualitative results. Future studies could focus on obtaining more quantitative results such as cell viability, expression of angiogenic markers and factors.

**This page intentionally left blank**

# CHAPTER IV

# Development of a 3D natural scaffold by decellularising baby spinach leaves to study and promote angiogenesis

## 4.1. Aims and Objectives

The aim of this chapter is to explore a plant-based natural TE scaffold with an intrinsic 3D vascular architecture by decellularising spinach leaves and to investigate its potential to study and stimulate angiogenesis. In order to satisfy this aim; the objectives of this chapter are to:

- Fabricate natural vascular networks via the retention of the intrinsic 3D vascular architecture of baby spinach leaves by decellularising them.
- Investigate the biocompatibility of the decellularised spinach leaves.
- Recellularise natural vascular networks with endothelial cells to create a prevascularised construct.
- Assess the angiogenic potential of prevascularised spinach leaves using *ex-ovo* CAM assay
- Evaluate the potential of decellularised baby spinach leaves to be used as a model to study angiogenesis *in vitro.*

## 4.2. Chapter IV by Pictures

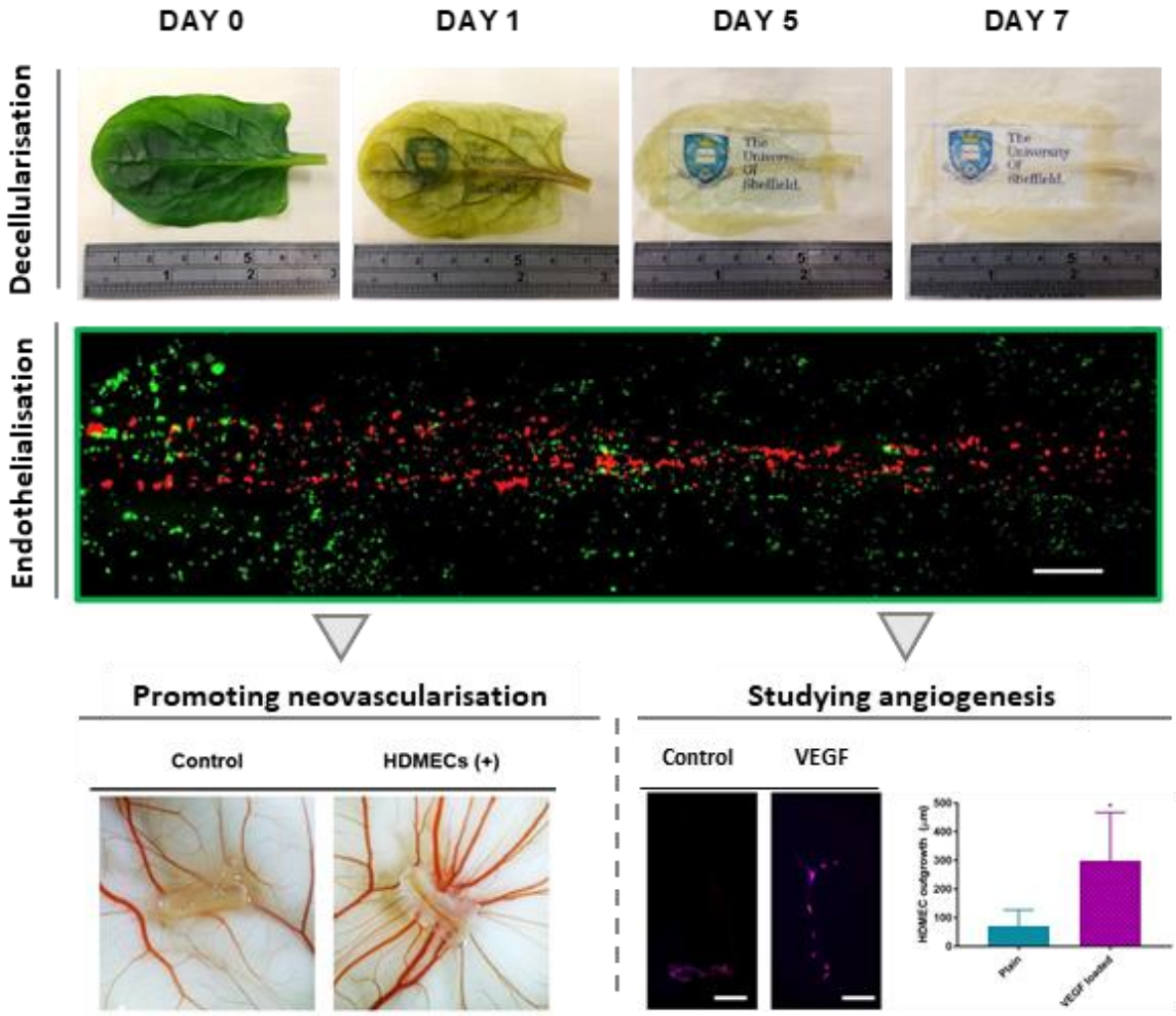

## 4.3. Introduction

Prevascularisation is a promising approach to circumvent slow neovascularisation upon implantation of TE constructs. For prevascularisation of the TE scaffolds, the selection of scaffold material is critical, and several factors need to be considered, such as biocompatibility, degradation time of the material *in vivo* and integrity of the biomaterial in terms of structure and function [129]. A variety of materials can be used as TE scaffolds, and an ideal scaffold biomaterial is expected to be non-toxic and biocompatible, and biodegradable while providing adequate mechanical support and encouraging cellular interactions for tissue development [481]. Synthetic polymers are preferred to be used in TE applications because of their tunability according to the desired mechanical and physical properties without possible immunological concerns [482], whereas natural scaffolds are attractive because of their good biological performance for supporting cell adhesion and function, but care must be taken to remove all bioactive compounds and epitopes to avoid an immune reaction [481,483].

Use of decellularised biological constructs has become an emerging strategy for producing physiologically relevant scaffolds for use in both pre-clinical and clinical applications [304,305]. The main principle of decellularisation is to remove the cellular content of the tissue or organ while preserving the 3D architecture and key ECM elements [164,308]. The methodology for decellularisation of tissues and organs is well-established, and several studies have reported on the use of this approach for generating patches for tissue regeneration, as *in vitro* models or drug screening platforms. For example, Sarig et al. successfully decellularised a porcine heart and constructed an acellular matrix to be repopulated with progenitor cells and used as an *ex vivo* drug screening platform, as an *in vitro* model for studying human cardiac tissue and transplantable patches. [164] Similarly, Dew et al. generated a decellularised rat intestine and repopulated it with human microvascular endothelial and stromal cells successfully as an *in vitro* model to study aspects of neovascularisation [306]. Melo et al. established an *in vitro* multicellular bronchial model using decellularised porcine luminal trachea membrane [307]. Uygun et al. developed a decellularised liver matrix and recellularised it with adult hepatocytes as a transplantable liver graft [308]. Mertsching et al. developed an acellular porcine small bowel segment and conducted a pilot trial for evaluating the tissue capabilities in terms of vessel patency and tissue viability by clinical

transplantation of their bioartificial vascularised scaffold repopulated with patient's peripheral blood cells [309]. Recently, Zhang et al. developed vascularised soft tissue flaps as an alternative to autografting. They generated an acellular skin/adipose tissue and repopulated it with human adipose-derived stem cells and HUVECs [310].

Thus, the use of acellular mammalian scaffolds has great potential in TE applications, but they are expensive and difficult to obtain. It also requires experience to harvest tissues or organs from man or animals and prepare these to completely remove cells and cell epitopes to avoid them causing immune reaction following implantation [311]. On the other hand, decellularised plant tissues and organs are promising possible alternatives to explore as tissue engineering scaffolds. They are readily available, cost-effective and safe to use. Cellulose, the important structural component of plant tissues, is a biocompatible natural polysaccharide which has the potential to be used as tissue engineering scaffolds *in vitro* and *in vivo*.

The *in vivo* biocompatibility of plant-derived cellulose has previously been proven by Modulevsky et al. by implanting a decellularised McIntosh Red apple section into mice subcutaneously [312]. Helenius et al showed the biocompatibility of the BC when implanted subcutaneously in rats [313]. The use of cellulose in tissue engineering applications has also been reported as a TE scaffold for cartilage tissue engineering [314] and temporary skin substitute [315]. Recently, Gershlak et al. successfully developed a prevascularised acellular plant-based scaffold by benefiting from some similarities in the vascular organisation in animal and plant tissues. Although their study proposed the potential of a decellularised spinach leaf to be used in the field of biomaterials and TE as a prevascularised construct, they have not yet assessed the angiogenic potential of the prevascularised acellular spinach leaf scaffolds using any of the well-established angiogenesis assays [166]. Accordingly, in this study, I seek to recapitulate their findings and go beyond this to further explore to what extent plant-based biomaterials may offer significant alternatives to the conventional scaffold materials used in TE applications. Accordingly, I have explored the angiogenic potential of the prevascularised decellularised spinach leaves using an *ex-ovo* CAM assay which is a very useful and reliable platform to study initial responses to biomaterials and to quantitatively study the angiogenic potential of biomaterials. In addition to its use as a prevascularised construct,

I have also assessed the potential use of acellular spinach leaves as a platform which enables us to study angiogenesis *in vitro.*

In addition to spinach, the feasibility of using different types of decellularised plant leaves has been further confirmed by several studies as TE scaffolds for various applications [166,167,316]. All the studies above concluded that cellulose is inexpensive, biocompatible and therefore a good candidate for use in tissue engineering applications.

### 4.4. Materials

| Chemical / Reagent | Catalogue Number | Supplier |
|---|---|---|
| Baby spinach leaves | - | **Co-op Food** |
| Matrigel® (Growth Factor Reduced) | 356231 | **Corning** |
| Industrial methylated spirit (IMS) | M/4450/17 | |
| Methanol | 10626652 | |
| Sodium dodecyl sulphate (SDS) | 15865308 | |
| Sodium hypochlorite | 11448842 | |
| Triton X-100 | BP151 | |
| Fertilised chicken eggs | - | **MedEggs** |
| RCOM King SURO humidified egg incubator | MX-SURO | **P&T Poultry** |
| EC GM MV Supplement Pack (For HDMECs) | C-39220 | |
| Endothelial Cell Growth Medium MV (EC GM) (for HDMECs) | C-22220 | **PromoCell** |
| Human Dermal Microvascular Endothelial Cells (HDMECs) | C-12210 | |
| 37% formaldehyde (FA) solution | F8775 | |
| 4',6-diamidino-2-phenylindole (DAPI) solution | D8417 | |
| Adenine | A5665 | |
| AlamarBlue Cell Metabolic Activity Assay | R7017 | **Sigma Aldrich** |
| Amphotericin B | A2942 | |
| Calcium chloride dihydrate | 223506 | |
| Collagenase A | COLLA-RO | |

| | | |
|---|---|---|
| D-glucose | G7021 | |
| Dulbecco's Modified Eagle's Medium (DMEM) | D6546 | |
| Ethylenediaminetetraacetic acid (EDTA) | E6758 | |
| Ethanol | 51976 | |
| Fetal calf serum (FCS) | F9565 | |
| Gelatin from porcine skin | G1890 | |
| Glutaraldehyde (25%) | G5882 | |
| Glycerol | G5516 | |
| Hexamethyldisilazane (HMDS) | 440191 | |
| L-glutamine | G3126 | |
| Penicillin / Streptomycin | P0781 | |
| Phalloidin, fluorescein isothiocyanate (FITC) | P5282 | |
| Phalloidin, tetramethylrhodamine isothiocyanate (TRITC) | P1951 | |
| Sodium hydroxide pellets | 795429 | |
| Tris-EDTA buffer solution (TrE) | T9285 | |
| Tris hydrochloride (Tris-HCL) | 10812846001 | |
| Trypsin EDTA | T3924 | |
| Vascular endothelial growth factor (VEGF) | V7259 | |
| Zinc chloride ($ZnCl_2$) | 746355 | |
| CellTracker™ Green | C2925 | **ThermoFisher** |
| CellTracker™ Red | C34552 | |
| Quant-iTTM Picogreen® (PG) dsDNA Kit | P7589 | |

## 4.5. Methods

### 4.5.1. Preparation of the acellular spinach leaves for cell culture: Decellularisation, cannulation, sterilisation, and gelatin coating

Baby spinach leaves (Spinacia oleracea) were purchased from a local market. A 7-day immersion decellularisation protocol was adapted and modified from well-established protocols [166,167]. Briefly, the leaves were immersed into a mixture of hexane isomers for 1 hour to remove the cuticles and washed with PBS. The vascular structure was

cannulated and perfused with PBS using a 30G syringe needle (BD Microlance™ Hypodermic Needle, Becton–Dickinson, UK). The leaves were then submerged in 10% sodium dodecyl sulphate (SDS) solution for 5 days, 1% Triton-X100 for 1 day, 0.1% Triton-X100 for 1 day and 10% sodium hypochlorite solution for 4 hours. Leaves were kept on an orbital shaker (PSU-10i, Grant Instruments, Cambridge, UK) at 60 rpm. Solutions were changed daily in order to enhance decellularisation efficiency. After detergent washing steps, decellularised leaves were rinsed using sterile PBS and washed with sterile PBS + antibiotic (1% Penicillin/Streptomycin and 0.25% Fungizone solution prepared in PBS) for 2 days. Intrinsic vascular structures of the decellularised leaves were then cannulated by infusing PBS through the midrib of the leaves, and the leaves were submerged into 0.2% (w/v) porcine gelatin solution and incubated at 37°C for 4 hours. Finally, decellularised leaves were washed with PBS, cannulated, and conditioned with warm Endothelial Cell Growth Medium (EC GM) prior to cell culture. Approximately 30 leaves can be processed as a batch over 9 days including the final detergent removal steps. The decellularisation protocol used in this study is summarised in Table 18.

***Table 18.*** *The summary of the step-by-step protocol of the decellularisation protocol followed in this study*

| Step | Agent | Duration | Temperature |
|---|---|---|---|
| Cuticle Removal | Hexane Isomers | 1 hour on shaker | RT |
| Washing | PBS | 5 minutes | RT |
| Pre-cannulation | PBS | - | RT |
| Anionic Detergent Wash | SDS | 5 days on shaker by refreshing the solution daily | RT |
| Non-ionic Detergent Wash | 1% Triton-X100 | 1 day on shaker | RT |
| | 0.1% Triton-X100 | 1 day on shaker | RT |
| Sterilisation | 10% sodium hypochlorite | 4 hours on shaker | RT |
| Rinsing | PBS | - | RT |
| Washing | PBS + antibiotic | 2 days on shaker by refreshing the solution daily | RT |
| Gelatin coating | 0.2% Gelatin | 4 hours | 37°C |
| Washing | PBS | 5 minutes | RT |
| Conditioning | EC GM | 30 minutes | 37°C |

For the evaluation of the vascular patency of the decellularised spinach leaves, blue food dye was injected through the cannula of the leaves under a dissection microscope (Wild Heerbrugg, Switzerland).

SEM (FEI Inspect F, Orlando, USA) imaging was used to investigate the microstructural alterations between fresh and decellularised spinach leaves. For SEM imaging of the fresh and acellular spinach leaves, the leaves were fixed in 2.5% glutaraldehyde and washed gently with PBS prior to dehydration with serial ethanol (EtOH) washes (35%, 60%, 80%, 90%, and 100%). Hexamethyldisilazane (HMDS) is used as a chemical drying agent, and

the leaves were soaked in HMDS:EtOH (1:1) solution for 1 hour and then transferred into 100% HMDS for 5 minutes. The protocol of biological sample preparation for SEM is summarised in Table 19. The leaves were air-dried overnight in a fume hood and gold-coated at a current of 15 mA for 2.5 minutes with a gold sputter (Edwards sputter coater S150B, Crawley, England) prior to imaging under SEM (FEI Inspect F, Orlando, USA). The SEM images were false coloured using Adobe Photoshop CS6 (Adobe Systems Incorporated, California, USA) in order to emphasize the structural alterations when the leaf is decellularised.

***Table 19.*** *The protocol of biological sample preparation for SEM*

| Step | Solution | Duration |
|---|---|---|
| Washing | PBS x 3 times | 4 minutes |
| Fixation | 2.5% Glutaraldehyde | 60 minutes |
| Washing | PBS x 3 times | 15 minutes |
| Washing | $dH_2O$ | 5 minutes |
| Serial alcohol washes for dehydration | 35% EtOH | 15 minutes |
| | 60% EtOH | 15 minutes |
| | 80% EtOH | 15 minutes |
| | 90% EtOH | 15 minutes |
| | 100% EtOH | 15 minutes |
| Chemical dehydration | HMDS:EtOH (1:1) | 60 minutes |
| | 100% HMDS x 2 times | 5 minutes |
| Drying | Air Drying | 60 minutes |

### 4.5.2. Quantification of DNA content

Quant-iT™ Picogreen® (PG) dsDNA Kit was used to quantify the DNA content and determine the effectiveness of the decellularisation protocol. Fresh and decellularised spinach leaves were washed with PBS three times and equal circular pieces were cut using a 10 mm biopsy puncher (Stiefel Laboratories, Offenbach, Germany) and the leaves were transferred into 24-well plates. 500 µL of cell digestion buffer (10 mM Tris-HCl, 1 mM $ZnCl_2$ and 1% Triton-X100 in distilled water ($dH_2O$)) was added onto the samples and incubated for 30 minutes at RT. Samples were then vortexed for 60 seconds and kept

overnight at 4°C. PG working solution was prepared by diluting 20× Tris-EDTA (TrE) 1:20 in $dH_2O$ (1×TrE) and diluting PG reagent 1:200 in 1× TE. The leaf samples then underwent 3 x freeze-thaw (FT) cycle (10 minutes at - 80°C and 20 minutes at 37°C, 15 seconds vortex between FT the cycles). 100 µL of the lysate was mixed with 100 µL PG working solution in 96-well plates wrapped in foil and incubated at RT for 10 minutes. Fluorescence reading was done at an excitation wavelength of 485 nm and an emission wavelength of 528 nm. The efficiency of decellularisation was determined by comparing %DNA content in fresh and decellularised leaves. The step-by-step summary of the DNA quantification protocol is given in Table 20.

***Table 20.*** *The step-by-step summary of the DNA quantification protocol with Quant-iT™ Picogreen® (PG) dsDNA Kit*

| Step | Agent | Duration | Temperature |
|---|---|---|---|
| Sample preparation | - | - | RT |
| Cell Digestion | Cell Digestion Buffer | 30 minutes | RT |
| Vortex | | 1 minutes | RT |
| Incubation | | Overnight | 4°C |
| Freeze | | 10 minutes | - 80°C |
| Thaw | | 20 minutes | 37°C |
| Vortex | | 15 seconds | RT |
| Freeze | | 10 minutes | - 80°C |
| Thaw | | 20 minutes | 37°C |
| Vortex | | 15 seconds | RT |
| Freeze | | 10 minutes | - 80°C |
| Thaw | | 20 minutes | 37°C |
| Mixing samples with PG working solution 1:1 (vol/vol) | PG working solution | - | RT |
| Incubation | | 10 minutes | RT |
| Fluorescence Reading | | - | RT |

### 4.5.3. Biocompatibility of the decellularised spinach leaves and the effect of gelatin coating

AlamarBlue® Cell Viability Assay (ThermoFisher Scientific, California, USA), fluorescent microscopy and SEM were performed in order to evaluate the performance of the gelatin coated (G+) and non-coated (G-) acellular spinach leaves in terms of cell attachment and proliferation.

Human dermal fibroblasts (HDFs) isolated as described previously [484] were used to evaluate the biological performance of the G+ and G- decellularised leaves. Briefly, HDFs were isolated from human skin taken from patients by mincing the dermis with into 10 $mm^2$ pieces. The pieces were then incubated overnight at 37 °C in 0.5% (w/v) collagenase A solution. The suspension of HDFs was centrifuged at 1000 rpm for 5 minutes and resuspended and cultured in HDF GM. Ethical approval for the use of skin excised in routine surgical operations and not needed for treatment of patients was granted by the local ethical approval committee of National Health Service Trust, Sheffield, UK (Ethics reference: 15/YH/0177). All patients provided written informed consent. For these experiments, HDFs were used between passage 3-6.

G- and G+ acellular spinach leaves were cut circular using a 10 mm biopsy puncher, transferred into 24-well plates and conditioned with warm HDF growth medium (HDF GM) (DMEM with 10% (v/v) FBS, 100 IU $mL^{-1}$ penicillin, 100 µg $mL^{-1}$ streptomycin, 2 mM L-glutamine and 0.625 µg $mL^{-1}$ amphotericin B for 30 minutes at 37°C. 2.5 x $10^4$ HDFs resuspended in 100 µL of HDF GM were seeded onto each leaf and incubated for 2 hours before the addition of HDF GM. The same cell seeding procedure was repeated for G+ and G- TCP. AlamarBlue® Cell Viability Assay was performed at days 1, 4, 7, and 11. Briefly, 0.1 mM AlamarBlue® working solution was prepared by 10x dilution of the 1mM AlamarBlue® stock solution with HDF GM. HDF GM was removed, and the leaves were washed with PBS. 1 mL of AlamarBlue® working solution was added to each well and incubated at 37°C for 4 hours. After an incubation period, 200 µL of the solution was transferred into a 96-well plate, and the fluorescence readings were done at an excitation wavelength of 540 nm and an emission wavelength of 635 nm. Metabolic activity measurement experiments were set up in triplicate in three independent assays.

For visualisation of the HDFs growing on acellular spinach leaves, G+ decellularised leaves were repopulated with HDFs at a density of 2 x $10^5$ cells/$cm^2$.

After 3-day and 7-day culture, the leaves were fixed with 2.5% GA for SEM imaging. The samples were prepared for SEM as summarised in Table 19. Briefly, leaves were washed with PBS and dehydrated with serial EtOH washes, and HMDS was used as a chemical drying agent. The leaves were then air-dried overnight in a fume hood and gold-coated prior to imaging the scaffolds under SEM.

For fluorescent staining, leaves were fixed in 3.7% FA after 7-day culture and washed gently with PBS and submerged into 0.1% (v/v) Triton X 100 (in PBS) solution for 20 minutes. After serial PBS washes, phalloidin-FITC (1:500 diluted in PBS from stock solution) solution was added onto samples to visualize F-actin and incubated for 30 minutes at RT in the dark. The samples were washed three times with PBS. In order to stain cell nuclei, 4',6-diamidino-2-phenylindole (DAPI) solution (1:1000 diluted in PBS) was added onto leaves and incubated for 10-15 minutes at RT in the dark, samples were then washed 3 times with PBS and directly imaged under a fluorescent microscope (Olympus IX3, Tokyo, Japan).

### 4.5.4. Recellularisation of the vascular structure with human ECs

HDMECs derived from juvenile foreskin were cultured and proliferated according to the manufacturer's instructions and used between passage 2 and 4. Briefly, EC GM with 5% FBS and microvascular endothelial cell supplement mix (EC growth supplement (0.004 mL / mL), epidermal growth factor (10 ng/ mL), heparin (90 µg/ mL), hydrocortisone (1 µg/ mL)) were used for culturing HDMECs. HDFs were isolated as described in section 2.3 and used between passage 3-6.

Our group has previously reported that the presence of HDFs while culturing HDMECs is crucial for cell attachment and proliferation [143,306]. Thus, I set up two scenarios for recellularisation of the vascular channels. (i) HDMECs by their own were infused through the cannula and (ii) HDMECs were infused through the channels in the presence of HDFs seeded to the outer layer of the decellularised spinach leaves, as indirect co-culture. Both types of cells were prelabelled using CellTracker™ Fluorescent Probes in order to visualise the cells in channels. For seeding HDMECs only, HDMECs were prelabelled with CellTracker™Red. Briefly, cells were incubated at 37 °C for 45 minutes with 10 µM

CellTracker™ working solution, washed with PBS. Decellularised leaves were transferred into petri dishes, prelabelled HDMECs were trypsinised, and 3 x $10^5$ HDMECs were resuspended in 250 µL of EC GM and infused through the cannula into the leaves and incubated 37°C for 1 hour prior to addition of EC GM. For indirect co-culture of HDMECs and HDFs, HDMECs were labelled with CellTracker™Red and HDFs were labelled with CellTracker™Green as described above. Prelabelled HDMECs were trypsinised, and 3 x $10^5$ HDMECs were resuspended in 250 µL EC GM, and prelabelled HDFs were trypsinised, and 3 x $10^5$ HDFs were resuspended in 200 µL of EC GM. HDMECs were perfused into channels, and HDFs were seeded onto the surface of the decellularised leaves. The leaves seeded with cells were then incubated at 37°C for 2 hours before adding EC GM. Recellularised decellularised leaves were incubated for 4 days, and the images were taken using a fluorescent microscope.

### 4.5.5. Assessment of the angiogenic potential of endothelialised leaves in *ex-ovo* CAM assay

HDMECs were cultured for 7 days in the channels, and HDFs were cultured on the exterior surface of the decellularised spinach leaves prior to implantation to CAM as described in section 2.5.4.

To assess the potential angiogenic effect of decellularised spinach leaves containing HDMECs and HDFs were assessed using an *ex-ovo* CAM assay [89]. In brief, fertilised chicken eggs (Gallus domesticus) were purchased from Henry Stewart & Co. MedEggs (Norwich, UK) and cleaned with 20% industrial methylated spirit solution. Eggs were incubated at 37.5°C for 3 days (until embryonic development day (EDD) 3) in a rocking egg incubator (RCOM King SURO, P&T Poultry, Powys, Wales). On EDD 3, the embryos were transferred gently into sterile petri dishes and incubated at 38°C in a cell culture incubator (Binder, Tuttlingen, Germany). CAM assay was conducted in care of the guidelines of the Home Office, UK.

On EDD 7, the main channel lying through the midrib of the acellular spinach leaves repopulated with HDFs only, HDMECs and HDFs together and with no cells were cut into 1 cm pieces using a sterile scalpel blade, and two pieces were implanted onto a single CAM. Images of the blood vessels growing towards leaf pieces were acquired using a digital USB microscope at EDD 14 before sacrificing the embryos.

The angiogenic activity was quantified by counting the blood vessels that converged towards the leaves [89]. Briefly, all discernible blood vessels that are growing towards the scaffolds in a spoke wheel pattern within a 1-mm imaginary circle drawn around the scaffold were carefully counted. As described by Ribatti et al., the blood vessels branching inside of the imaginary circle are counted as one blood vessel whereas they are counted as two or more if the branching occurs outside the circle [237]. For testing the angiogenic activity of each group, at least 8 embryos were used in each of the three replicates.

### 4.5.6. Assessment of HDMEC outgrowth from decellularised spinach leaves to vascular endothelial growth factor (VEGF) loaded Matrigel

With the aim of assessing the potential of decellularised spinach leaves to be used as an *in vitro* model to study angiogenesis, I studied the potential of endothelial outgrowth from the leaf channels.

Decellularised spinach leaves repopulated with HDMECs ($1.5 \times 10^6$ cells per scaffold) were incubated for 7 days at 37ºC. Using sterile 30G syringe needle approximately 10 - 15 holes were pierced on the main channel (midrib) of each leaf in a class II biological safety cabinet. The aim of piercing the holes was to facilitate the outgrowth of HDMECs from the channels as no outgrowth was observed from unpierced channels.

Reduced growth factor Matrigel (protein concentration > 10.8 g/ mL) was purchased from Corning. The final concentration of VEGF within the Matrigel was adjusted to be 80 ng/mL, and 200 µl of Matrigel either plain (no VEGF) or loaded with VEGF was pipetted onto the midrib of the decellularised spinach leaves (Figure 78). Leaves were then returned to the incubator for gels to set at 37°C for 15 minutes. Decellularised leaves were then submerged in EC GM and cultured statically for further 7 days. The leaves were fixed 3.7% FA as a whole, and, stained with Phalloidin-TRITC and DAPI. Briefly, after fixation and three times PBS washing, phalloidin-TRITC (1:500 diluted in PBS from stock solution) solution was added to cells in order to stain F-actin filaments of cells and incubated for 30 minutes at RT in the dark. Cells were then washed three times with PBS. In order to stain cell nuclei, DAPI solution (1:1000 diluted in PBS) was added and incubated for 15 minutes at RT in the dark, and cells were then washed 3 times with PBS. Matrigel was then carefully peeled from the surface of the spinach leaves, and the outgrowth of the HDMEC was then examined under a fluorescent microscope. The

outgrowth distances of HDMECs through plain and VEGF loaded Matrigel were quantified from fluorescent images of the gels using ImageJ (NIH, Maryland, USA). For the assessment of the HDMEC outgrowth, the experiments were repeated 4 times with at least 7 replicates per experiment.

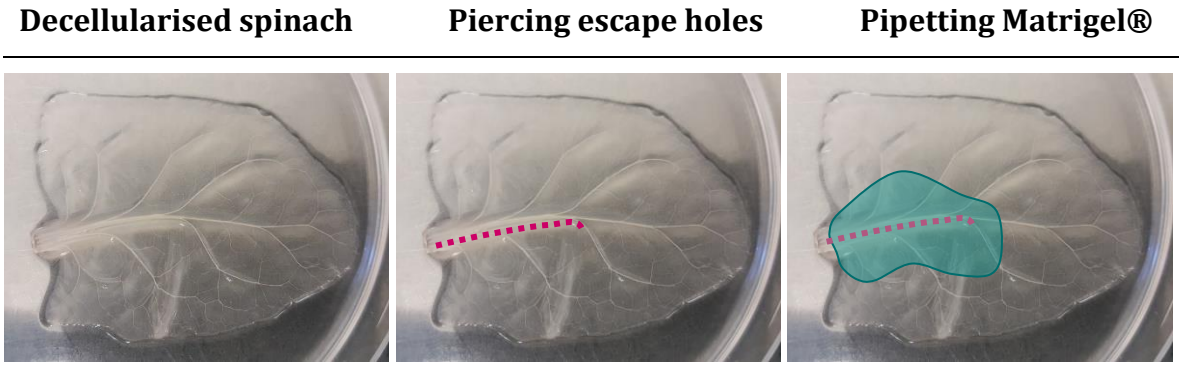


***Figure 78.*** *Schematic illustration of the Matrigel outgrowth experiments. The outgrowth of HDMECs localised within the main channel of the decellularised spinach leaves to Matrigel was assessed. The pierced holes and Matrigel were shown with purple and light blue color*

#### 4.5.7. Statistical analysis

Statistical analysis was carried out using one-way analysis of variance (ANOVA) using statistical analysis software (GraphPad Prism, CA, USA). Where relevant, n values are given in figure captions. Error bars indicate standard deviations in the graphs unless otherwise stated.

## 4.6. Results

#### 4.6.1. Preparation of the acellular spinach leaves for cell culture

After initiation of decellularisation, leaves started to lose their green colour gradually, and by the end of day 7, they were colourless and translucent as can be seen in Figure 79A.

Decellularised leaves maintained their intrinsic 3D vascular architecture seen in native spinach leaves, and SEM images showed that the surface structure of the decellularised leaves was sinuous compared to the surface of the fresh spinach leaves (Figure 79B). PG assay was used to quantitatively confirm the success of the decellularisation protocol by showing an approximately 98% drop in the DNA content (Figure 79C).

The patency of the 3D architecture was evaluated using blue food dye prior to cell seeding into this natural vasculature. Although a minor leakage was observed, the food dye was

able to reach to the smaller branch points showing that the 3D vascular architecture was well-maintained after decellularisation, and the smaller channels were connected and accessible via the main channel (midrib) (Figure 79D).

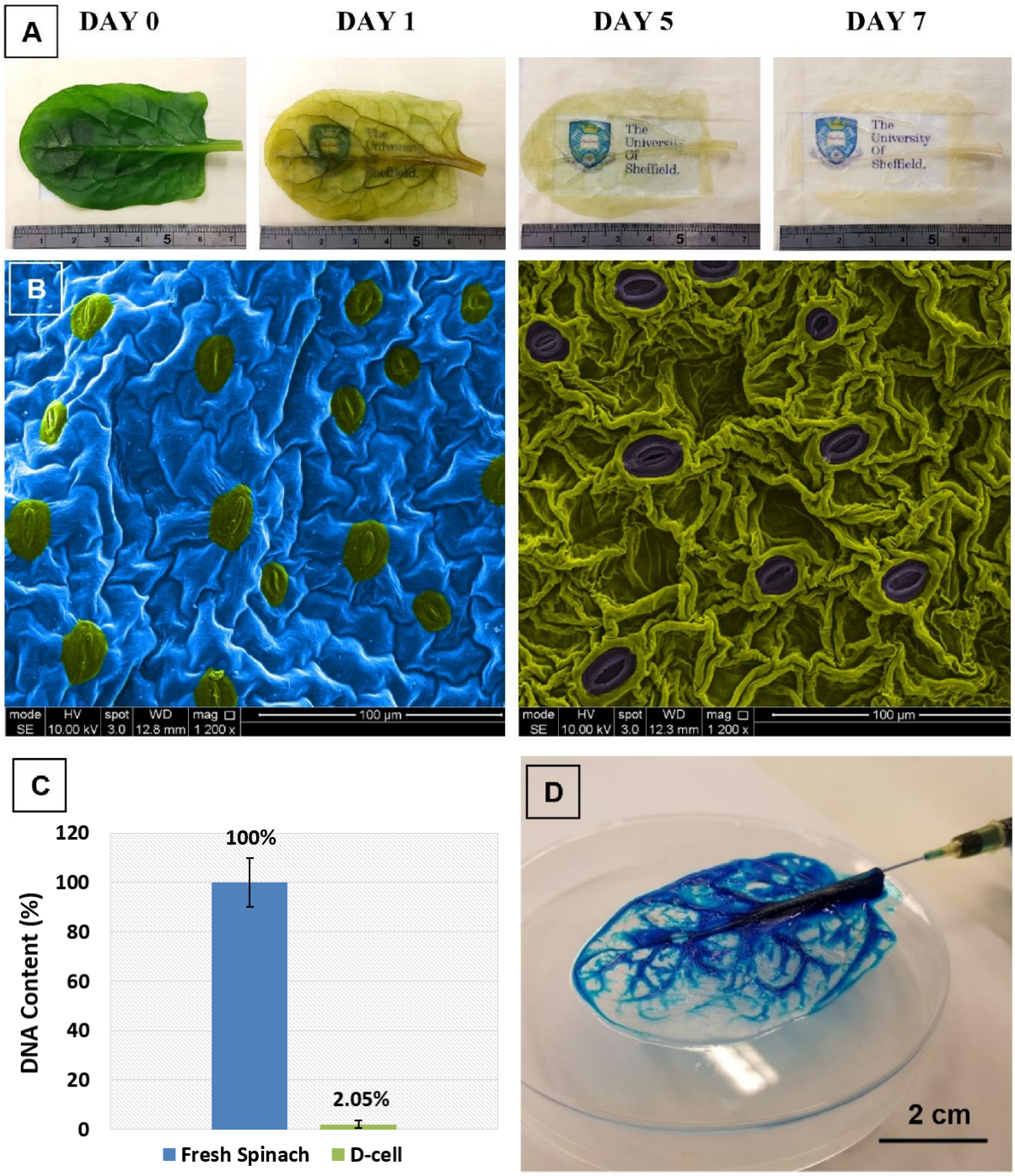


***Figure 79.*** *(a) Colour changes during washing steps for decellularisation can be seen from day 0 to 7. The unit seen on the ruler indicates centimetres. (b) False coloured SEM images showing the microstructure of fresh (on the left) and decellularised (on the right) leaves. (c) DNA content of fresh and decellularised spinach leaves and (d) blue food dye injection through vascular channels is illustrated in the bottom row. Error bars represent SD.*

### 4.6.2. Results of the biocompatibility of the decellularised spinach leaves and the effect of gelatin coating

The results showed a regular increase in the metabolic activities of HDFs from day 1 to day 11 in all groups. Although there was a significant stimulatory effect of gelatin coating on cell attachment and proliferation of the HDFs growing on the decellularised spinach leaves at each time point, gelatin coating did not enhance the metabolic activities of HDFs grown on TCP at any of the time points. The metabolic activity of HDFs on decellularised leaves achieved approximately 60% of that observed in TCP group by 11 days. The results of the AlamarBlue® cell viability assay are shown in Figure 80A.

Phalloidin-FITC and DAPI staining of the HDFs cultured on G+ and G- decellularised leaves for 7 days are given in Figure 80B and 80C, respectively. The morphology of the HDFs showed the usual fibroblast-like spreading structure as observed for cells grown on TCP.

The SEM images of the HDFs growing on G+ and G- decellularised spinach leaves on day 3, 7 and 11 further confirmed the gradual proliferation of HDFs on both surfaces over time. While the surface of the decellularised spinach leaf was partly covered by HDFs on day 3, the HDFs became fully confluent on day 11, as shown in Figure 80D.

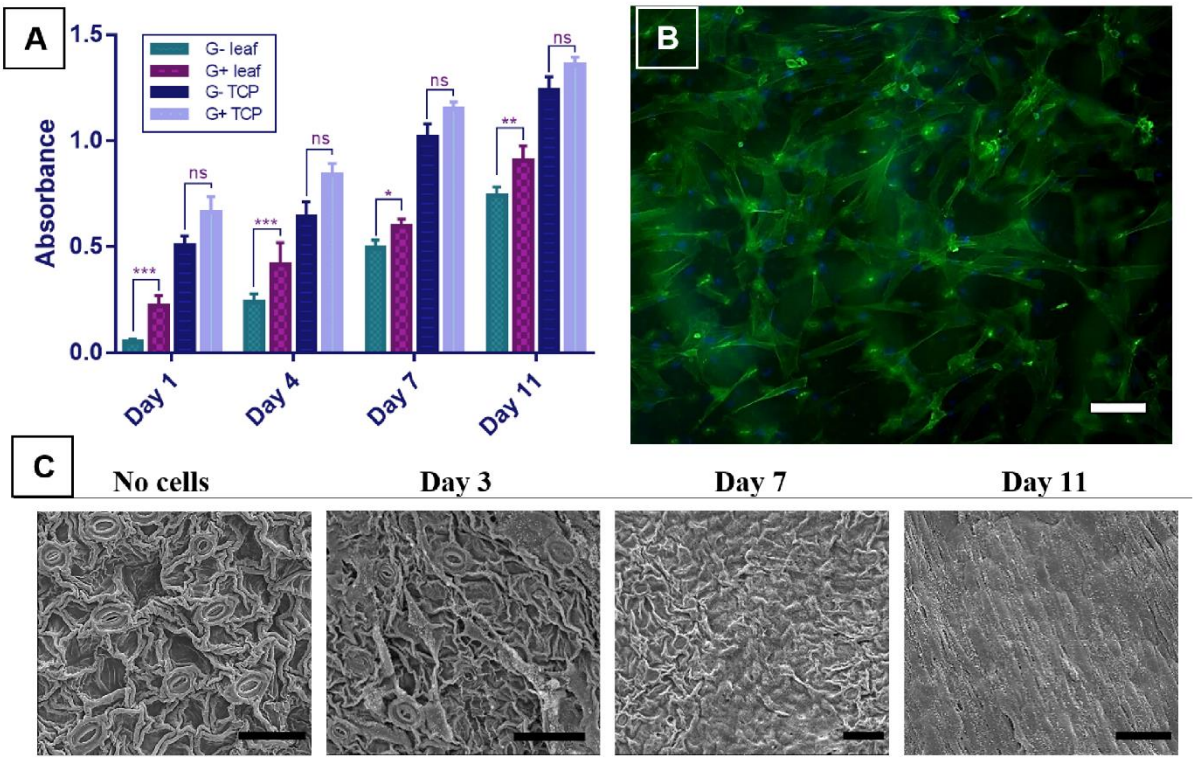


***Figure 80.*** *(A) The metabolic activity of HDFs growing on G+ and G- decellularised scaffolds over 11 days in comparison with HDFs growing on G+ and G- TCP. *** $p \leq 0.001$, ** $p \leq 0.01$, * $p \leq 0.05$, $^{ns}$ $p \geq 0.05$, error bars indicate standard deviation (SD). (B) Phalloidin-FITC and DAPI staining of HDFs cultured on G+ decellularised leaves for 7 days. Scale bar represents 100 µm. (C) SEM images showing the growth of HDFs on G+ decellularised spinach leaf over 11 days are given. Scale bars represent 50 µm*

### 4.6.3. Results of the recellularisation of the vascular structure with HDMECs

The results of the recellularisation showed that the growth of HDMEC was very poor in G- leaf channels, and no cells were observed as proliferating in the channels when HDMECs were seeded in isolation. In contrast, when HDMECs were co-cultured with HDFs, they showed greater attachment and proliferation in the channels in G+ decellularised spinach channels while only several HDMECs and HDFs were found to be attached and proliferating in the G- group.

The distribution of prelabelled HDMECs and HDFs was visualised with fluorescent microscopy in G- (Figure 81A) and G+ (Figure 81B) decellularised spinach leaves at the end of 7 days. HDMECs were found localising mostly along the main vein of the spinach leaf (midrib) only and did not penetrate into the smaller branches although these capillary branches were found to be accessible by the infusion of food dye (Figure 79D).

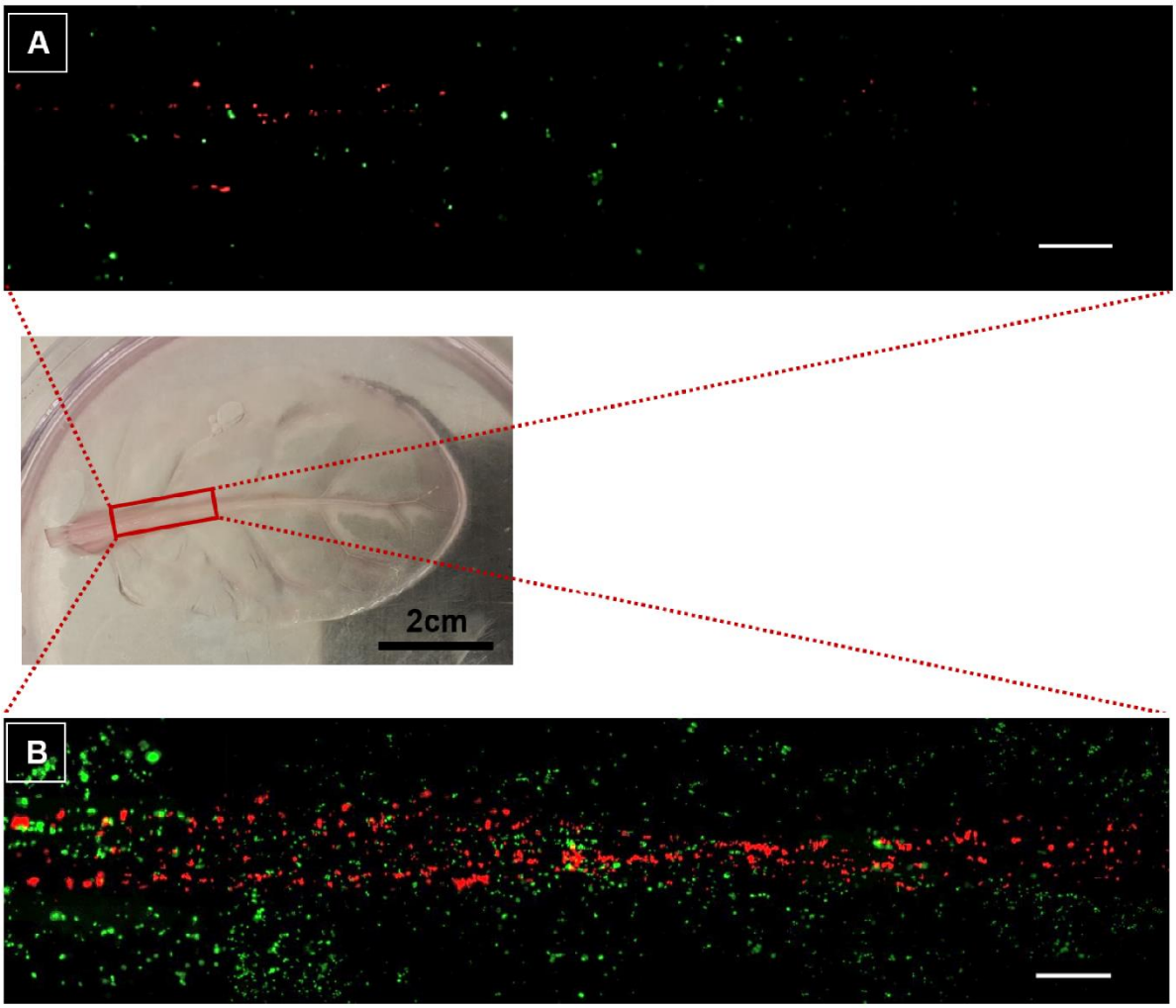


***Figure 81.*** *Distribution of HDMECs (red) growing in the main channel and HDFs (green) growing on the upper surface of the (A) G- and (B) G+ decellularised spinach leaves. Scale bar is 0.5 mm*

### 4.6.4. Results of the assessment of the angiogenic potential of endothelialised leaves in *ex-ovo* CAM assay

A significant increase in the number of blood vessels growing towards the leaves containing HDMECs and HDFs was observed at the end of 7 days. The macro images of the blood vessels in the surrounding area of spinach leaves either without or with cells are given in Figure 82. The mean vessel counts for acellular spinach leaves repopulated with HDFs only, and HDMECs in co-culture with HDFs were 22.1 ± 1.0 and 31.0 ± 1.6, respectively compared with decellularised spinach leaf controls (13.1 ± 4.3). The presence of the HDFs and HDMECs did not affect the embryo survival rate, which was over 77% for this study.

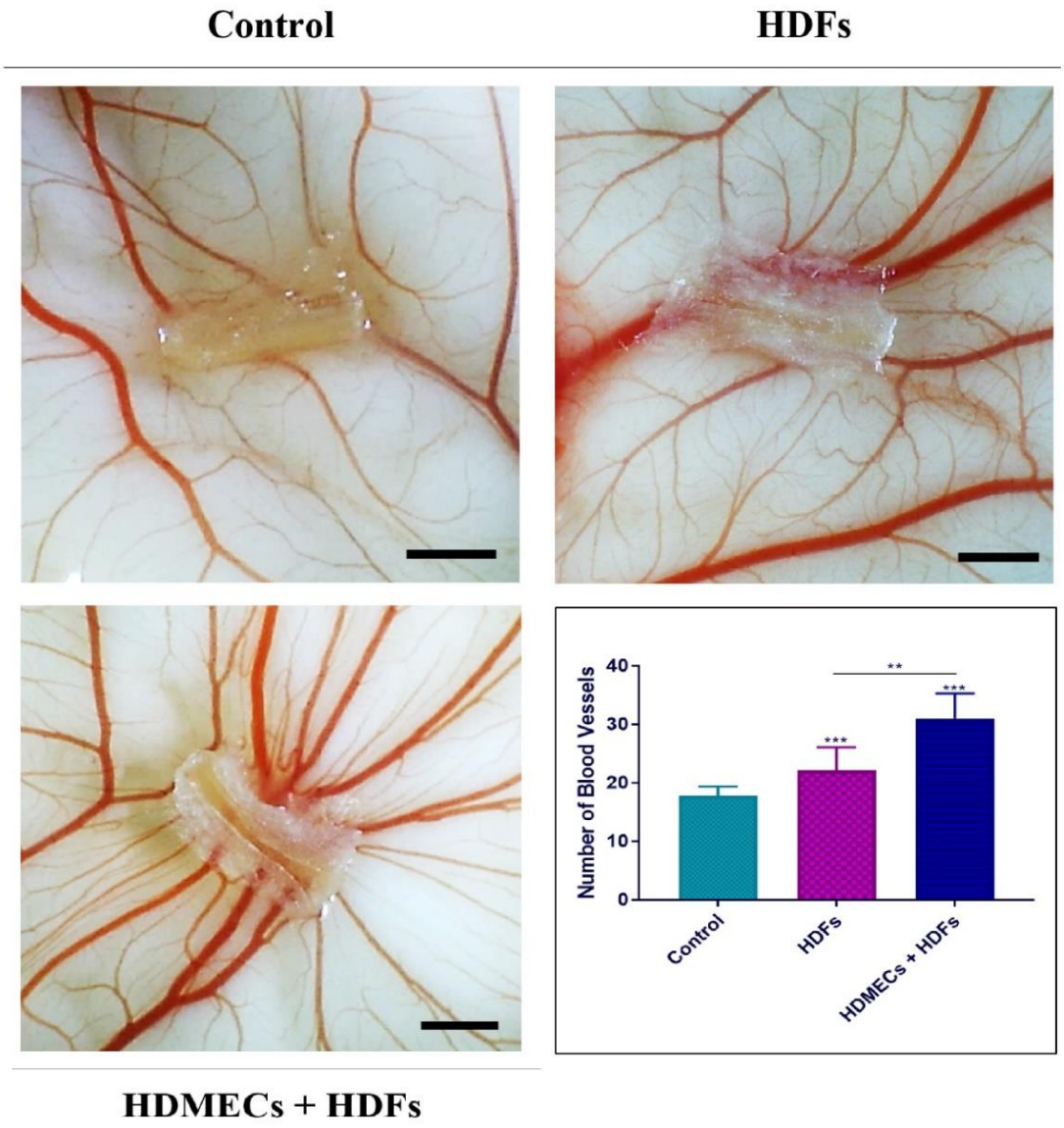


***Figure 82.*** *Representative macroimages demonstrating the angiogenic potential of decellularised spinach leaves repopulated with HDFs only and HDMECs and HDFs in co-culture in comparison with plain decellularised spinach leaves with no cells (control). Quantification of the blood vessels is given with the graph given bottom-right (n=3). Scale bar represents 0.5 cm. *** p ≤ 0.001, ** p ≤ 0.01, error bars indicate SD*

### 4.6.5. Results of the assessment of HDMEC outgrowth from decellularised spinach leaves to VEGF loaded Matrigel

The results of phalloidin-TRITC and DAPI staining showed that HDMECs could, on occasion, grow out from the main channel of the decellularised spinach leaves towards both plain and VEGF loaded Matrigel. However, the outgrowth of HDMECs was rare and witnessed in the range of 15-30% of samples per experiment. The outgrowth distances from the leaves were 81.7 ± 58.6 μm and 339.5 ± 163.3 μm for cells migrating towards plain and VEGF loaded Matrigel, respectively (Figure 83).

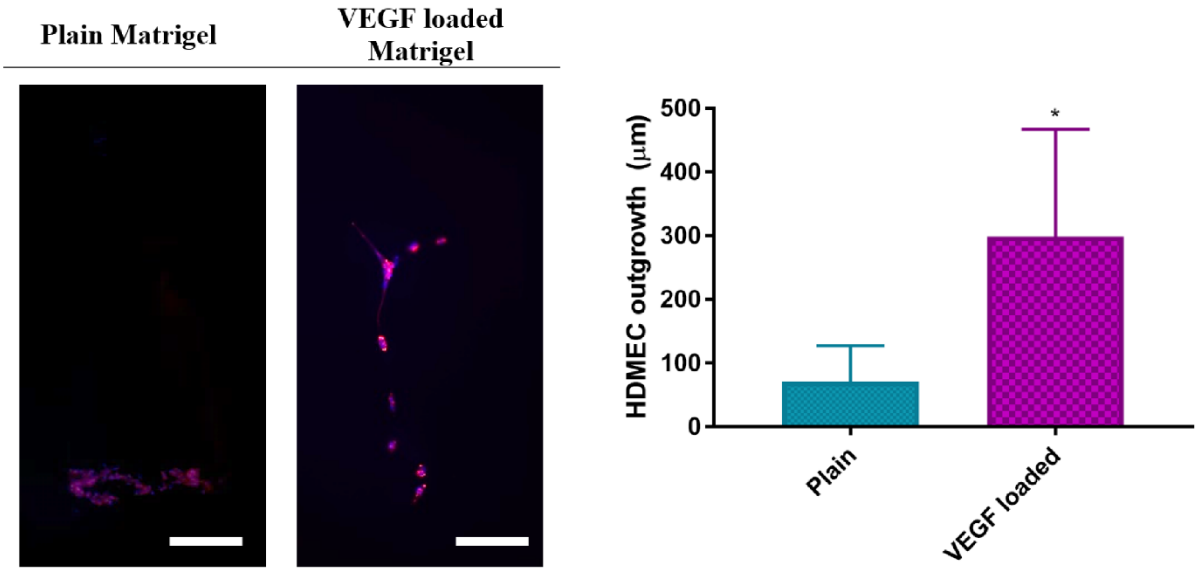


***Figure 83.*** *The images of DAPI (blue) and phalloidin-TRITC (red) fluorescent staining of the outgrowing HDMECs from the decellularised spinach leaves into Matrigel without or with VEGF. Scale bar represents 100µm. The outgrowth distances of HDMECs are given. (n=4, * p ≤ 0.05, error bars indicate SD)*

## 4.7. Discussion

A major barrier to translating TE constructs to the clinic is achieving rapid neovascularisation in the post-implantation period [23,24]. Although significant progress has been made, this problem with TE constructs still remains challenging. Neovascularisation is based on the formation of new blood vessels after implantation, and these must form within a few days to ensure graft survival.

Use of proangiogenic drugs is a well-established technique to overcome slow neovascularisation post-implantation, and VEGF is well-known and recognised as the gold standard in the field of these agents [14]. However, besides being a potent stimulator of angiogenesis, it has also been demonstrated to be possibly unsafe when given in high doses and in a non-regulated manner [334–336]. Thus, it is very timely to explore different strategies for promoting neovascularisation.

*In-vitro* prevascularisation of the TE constructs, which can be derived from synthetic or natural sources prior to implantation is a promising approach to overcome the slow vascularisation problem. The idea of this prevascularisation technique is to shorten the time required for neovascularisation in the post-implantation period by establishing a connection between existing vessels and the cultured ECs [485,486].

Accordingly, in this study, I aimed to explore a recent plant-based naturally-derived TE scaffold with an intrinsic 3D vascular architecture by decellularising spinach leaves and investigating their potential to promote angiogenesis when repopulated with HDMECs.

An immersion decellularisation protocol was adapted and modified from previously published protocols [166,167]. After initiation of decellularisation, leaves began to lose their green colour over time and became translucent by the end of day 7 (Figure 1A). The loss of colour is likely to be due to the removal of chlorophyll [487], which is linked with the chloroplast removal from the leaf tissue during washing steps. Some alterations have been observed in the microstructure of the spinach leaf with the decellularisation procedure. The surface became more sinuous due to burst plant cells and bigger stomatal pores (Figure 1B). The decellularisation protocol used in this study contained high concentrations of detergents which were found to be toxic to mammalian cells [488,489]. Thus, the washing steps after decellularisation are crucial, and no cytotoxic effect was observed in this study. Decellularisation was verified by quantification of the DNA content (Figure 1C). The remnant DNA remaining at the end of decellularisation was low enough to satisfy the suggested criteria for a successful decellularisation [490].

Cellulose is the major component of the plant cell wall [491], and *in vitro* and *in vivo* biocompatibility of the plant-derived cellulose has been previously studied by several groups recently. Modulevsky et al. reported the *in vitro* biocompatibility of decellularised McIntosh Red apple slices by assessing the proliferation of mammalian cells on them [316] They further assessed the biocompatibility of the decellularised apple scaffolds *in vivo* by implanting them into mice subcutaneously, and reported that only low levels of macrophages and foreign body multinucleated cells were visible within the scaffold after 8-weeks of implantation[312]. Recently, Gershlak et al. assessed the feasibility of decellularised spinach and parsley to be used as TE scaffolds. They demonstrated that hPS-CMs were viable and contracting five days after initial seeding [166]. All of these studies concur that cellulose is a readily available, inexpensive, and a biocompatible biomaterial that may prove a good candidate to be used in tissue engineering applications.

In this study, I explored the biocompatibility of decellularised spinach leaves *in vitro* and using an *ex-ovo* CAM assay and demonstrated the usefulness of gelatin coating for enhancing the attachment and proliferation of HDFs. The results demonstrated an

increase in the metabolic activities of HDFs growing on decellularised spinach leaves from day 1 to 11, showing that the material shows no toxicity to cells. This data was further confirmed by a fluorescent image showing the well-spread HDFs in an elongated, flattened morphology (Figure 2B), and with the SEM images showing the proliferation of the HDFs over 11 days (Figure 2C) on decellularised spinach scaffolds. The results of the CAM assay also demonstrated that decellularised spinach leaves showed no toxicity to chick embryos.

*In vivo*, ECs are in contact with an ECM mostly composed of collagen and laminin which is critical for ECs adhesion and formation of a smooth endothelium layer, and fibronectin which plays a major role in adhesion and restoration following vascular injury [492,493]. Beside the adhesion of ECs, the ECM plays an important role in cell migration, morphogenesis, survival, and vessel stabilisation [494]. Many methods have been described to grow ECs *in vitro* using different culture conditions and systems for culturing ECs efficiently. These culture systems are mostly focused on the surface coating with fibronectin, collagen and gelatin and the availability of growth factors and the presence of stromal cells such as HDFs in contact with ECs [37,495,496].

Gelatin, denatured collagen, has been used as an inexpensive alternative for promoting cell attachment and proliferation *in vitro.* In order to assess the efficiency of gelatin coating on cell attachment and proliferation, I compared the metabolic activities of HDFs growing on surfaces coated with gelatin and uncoated. Although gelatin coating showed no significant difference for HDFs growing on TCP, it significantly enhanced the attachment and proliferation of HDFs to decellularised spinach leaf at all time points. The coating procedure used in this study did not include any cross-linking step, and the remarkable effect of gelatin coating was observed at day 1 by which time the non-cross-linked gelatin might be expected to have largely detached from the surface fairly quickly. Non-cross-linked gelatin has previously been reported as dissolvable in aqueous solution at 37°C [497]. Lai et al. showed the degradation of non-cross-linked gelatin membranes within 30 minutes at 37°C in physiological medium containing collagenase [498]. Similarly, Kuijpers et al., reported that although they studied the stability of cross-linked gelatin at 40°C, the stability of non-cross-linked gelatin was not tested as it will dissolve in aqueous solution at that temperature.

The positive influence of gelatin coating on the proliferation of HDFs is most likely to be due to the increased initial cell attachment on acellular spinach leaves. Similar to our results, Vleggeert-Lankamp et al. demonstrated the positive influence of gelatin coating, either cross-linked or non-cross-linked, on attachment and proliferation of human Schwann cells. They demonstrated that the non-cross-linked gelatin coating significantly enhanced the attachment of the cells on day 1, and from day 3 to day 6, the proliferation rate of the cells increased approximately 6 times with the help of non-cross-linked gelatin coating [499].

HDFs were used initially to assess the effect of gelatin coating on cell attachment and proliferation prior to assessing its effect on HDMECs in the recellularisation experiments. Similar to its effect on HDFs, the gelatin coating was found to be crucial for HDMECs. They survived only in 10% of the G- scaffolds (in only 1 out of 10 scaffolds) when seeded by their own. However, the survival of HDMECs in G+ scaffolds (without HDFs) was increased to 50% (in 5 out of 10 scaffolds).

For endothelialisation of the leaf channels, HDMECs were then cultured in indirect contact with HDFs. It was previously reported that fibroblasts have a key role to play in the angiogenic process by producing considerable amounts of ECM molecules (i.e., collagen, fibronectin, and other molecules), growth and pro-angiogenic factors which control the shape and density of blood vessels [452,453]. Although fibroblasts secrete some VEGF, the main role of these cells is to create collagen I and fibronectin rich ECM in which ECs can be embedded to form tubules [454,455]. I confirmed this key feature with that the presence of HDFs enhanced the attachment and survival of HDMECs in the channels of the decellularised leaves even if they were seeded at lower concentrations (less than 1x $10^6$ HDMECs per scaffold) (Figure 3). The survival of HDMECs in the channels increased to approximately 70% (7 out of 10 scaffolds) with the presence of HDFs. The culture of HDMECs in isolation without HDFs was only possible when the initial cell seeding concentration was high enough (more than 1 x $10^6$ cells per scaffold), and the leaves were coated with gelatin. The culture of HDMECs in the acellular spinach channels was found to be the most efficient with the G+ scaffolds and when HDFs were presented in indirect contact.

*In vitro* prevascularisation is a promising technique for the survival of engineered tissue constructs in the early phases of implantation by shortening the time required for

neovascularisation [500]. The effectiveness of the prevascularisation technique has previously been studied by many groups. Tremblay et al. reconstructed an endothelialised skin model repopulated with HUVECs and reported the inosculation of HUVECs with the host mice vasculature during the first 4 days [485]. Similarly, Nor et al. implanted biodegradable poly-L-lactic acid scaffolds prevascularised with HDMECs subcutaneously into immunodeficient mice and demonstrated the differentiation of HDMECs into functional human microvessels which anastomosed with the host vasculature in less than 7 days [501]. Schechner et al. reported the formation of primitive capillary-like structures by HUVECs cultured within a 3D gel and showed successful inosculation of HUVECs with the host vasculature when implanted into mice [118]. Unger et al. investigated the functionality of *in vitro* pre-formed microvasculature *in vivo* and reported that co-culture of HDMECs with osteoblasts stimulated the ingrowth of host's blood vessels into TE construct, and chimeric vessels were also observed at the end of 14-day period [493].

I have shown the stimulatory effect of the prevascularised TE constructs on neovascularisation by implanting the endothelialised acellular spinach leaves into the CAM and investigating angiogenesis over 7 days in the area of implantation. Acellular leaves with no cells and repopulated with HDFs were used as controls. The results showed that there was an increase in the number of newly formed blood vessels towards the leaves containing either only HDFs or HDMECs plus HDFs. The most dramatic increase was observed in the HDMECs plus HDFs group in comparison with decellularised leaves repopulated with HDFs only. The mean number of blood vessels was 31.0 ± 1.6 and 22.1 ± 1.0, respectively. They were both compared with the acellular spinach leaves with no cells as controls (number of blood vessels: 17.9 ± 1.1) (Figure 82). The results demonstrated that the presence of HDMECs enhanced angiogenesis in CAM assay. This data provides evidence on prevascularisation stimulating new blood vessel growth at the site of implantation, further investigation of the inosculation of HDMECs with host vasculature needs to be investigated. Furthermore, even if the leaves were gelatin coated and the HDFs were used as helper cells, HDMECs were not found to penetrate into the smaller branches of the acellular spinach leaves. In considering the potential use of the decellularised spinach leaves as prevascularised constructs, this lack of homogeneity in the distribution of HDMECs might prove a problem for establishing a connection with the endothelial cells of the host tissue. Further developments on

endothelial cell distribution in the scaffolds may lead to a better angiogenic response from a host tissue. In the field of decellularisation of the native tissues and organs, the complete recellularisation of the acellular 3D scaffolds *in vitro* is a long-standing problem, and further investigations are needed to improve the cell distribution in the scaffolds [502].

*In vitro* models are important tools to understand the angiogenic process and assess the activities of anti and pro-angiogenic agents. To date, many migration and differentiation assays have been developed and used to study angiogenesis *in vitro*. Alessandri et al. used a modified Boyden chamber to study endothelial capillary mobilisation in response to a pro-angiogenic agent [215]. Obesso et al. developed a new technique to study endothelial movements by attaching beads to the bottom of a 96-well plate and screening the tracks generated by ECs [503] Liang et al. used an *in vitro* scratch assay based on creating a wound by scraping the ECs in a designated area, to study endothelial migration in 2D [504]. Bach et al. studied the formation of capillary-like structures in the fibrin and collagen gels to address the potential role of the endothelial cadherins [505]. Similarly, Grant et al. studied endothelial tube formation using laminin and Matrigel [506]. Recently, Dew et al. developed a biodegradable synthetic vascular scaffold and assessed its potential use as an *in vitro* model of angiogenesis by investigating the outgrowth of HDMECs into a VEGF loaded collagen gel [507]. In the current study, I combined two *in vitro* approaches (migration and tube formation) and investigated the potential of decellularised spinach leaves to be used as an *in vitro* platform in which I can study angiogenesis in response to exogenous inhibitory or stimulatory agents. Briefly, I explored the outgrowth behaviour of HDMECs from the natural vascular network of decellularised spinach leaves to Matrigel either plain or loaded with VEGF (Figure 83). Unfortunately, our results demonstrated that the outgrowth of the HDMECs from the channels was extremely rare (outgrowing HDMECs were witnessed only in 5% of the experiments). However, the outgrowth distance of the HDMECs through VEGF loaded Matrigel was higher, and a more organised structure was observed when compared with non-loaded Matrigel groups. Obviously, further developments on this assay would be required to increase its reproducibility. It possibly merits more development as it combines both migration and cell differentiation in a 3D environment.

Although the CAM assay is a useful platform to study biocompatibility and angiogenicity of materials *in vivo*, one of its drawbacks is that the chick does not have a fully developed immune system during the period of use for the CAM assay [69,89]. Thus, comparison of plant-derived and animal-derived decellularised constructs using an animal model with a competent immune system will be interesting in the future to compare the relative merits of both.

## 4.8. Conclusions and Future Work

In this chapter, I successfully developed natural vascular networks by decellularising baby spinach leaves. The decellularisation protocol enabled the removal of the 98% of DNA of the baby spinach leaves by serial detergent washes without any damage to the structural integrity of the leaves. The biocompatibility of the acellular spinach leaves was confirmed *in vitro* and *in vivo*. An intrinsic 3D vascular architecture was maintained after decellularisation, and the midrib of the spinach leaf was completely open and suitable for culturing ECs in it. Gelatin coating significantly enhanced the attachment and growth of HDFs on acellular spinach leaves. Gelatin coated acellular spinach leaves repopulated with HDMECs promoted neovascularisation in the CAM assay over 7 days, and the number of blood vessels growing towards the endothelialised leaves was doubled when compared with plain decellularised leaf controls without cells. I also demonstrated that the decellularised baby spinach leaves have some potential to be used as an *in vitro* angiogenesis model to study angiogenesis in response to exogenous inhibitory or stimulatory agents.

In future, further investigation of the inosculation of HDMECs with host vasculature needs to be investigated. Furthermore, even if the leaves were gelatin coated and the HDFs were used as helper cells, HDMECs were not found to penetrate into the smaller branches of the acellular spinach leaves. In considering the potential use of the decellularised spinach leaves as prevascularised constructs, this lack of homogeneity in the distribution of HDMECs might prove a problem for establishing a connection with the endothelial cells of the host tissue. Further developments on endothelial cell distribution in the scaffolds may lead to a better angiogenic response from a host tissue. In the field of decellularisation of the native tissues and organs, the complete recellularisation of the acellular 3D scaffolds *in vitro* is a long-standing problem, and further investigations are

needed to improve the cell distribution in the scaffolds [502]. Although the CAM assay is a useful platform to study biocompatibility and angiogenicity of materials *in vivo*, one of its drawbacks is that the chick does not have a fully developed immune system during the period of use for the CAM assay [69,89]. Thus, comparison of plant-derived and animal-derived decellularised constructs using an animal model with a competent immune system will be interesting in the future to compare the relative merits of both. When it comes to use the developed scaffolds as an *in vitro* platform to study angiogenesis, further developments on this assay would be required to increase its reproducibility. It possibly merits more development as it combines both migration and cell differentiation in a 3D environment.

# CHAPTER V

## Development of a novel *in vitro* 3D dynamic platform to study angiogenesis under physiologically more relevant conditions

### 5.1. Aims and Objectives

The aim of this chapter is to develop a 3D dynamic *in vitro* model by combining emulsion templating and electrospinning techniques to study angiogenesis in a more physiologically relevant environment. In order to satisfy the aim; the objectives of this chapter are to:

- Manufacture the PCL PolyHIPE outer tube by emulsion templating
- Manufacture the PHBV inner tube by electrospinning
- Design and manufacture the flow chamber
- Recellularise the 3D model by rotational seeding
- Study the impact of flow and pro-angiogenic agents on proliferation and migration of ECs

## 5.1. Chapter V by Pictures

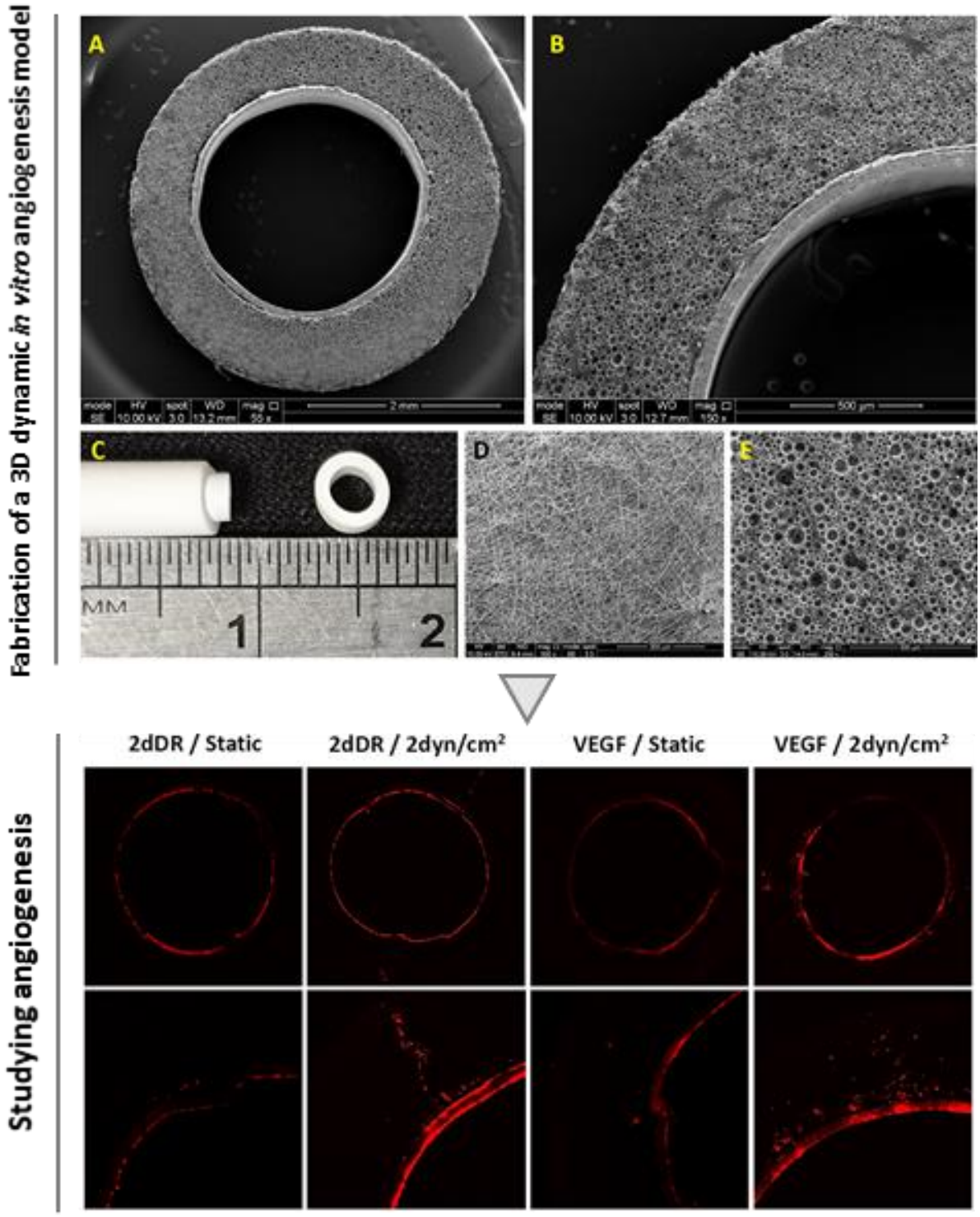

## 5.2. Introduction

Angiogenesis models are important tools to study the angiogenic activity of agents, biomechanical stimulus and cells [205]. Although *in vivo* assays are the most representative and reliable models for the evaluation of angiogenesis, they are also expensive, technically difficult, time-consuming, and ethically questionable [204]. On the other hand, *in vitro* angiogenesis assays are inexpensive, quick, technically simple, and reproducible, but they are usually based on evaluating only one aspect of angiogenesis (for example, proliferation, migration or differentiation), and they may produce false results due to the nonspecific reaction of cells [508]. Moreover, most of the *in vitro* angiogenesis assays are limited to static, two-dimensional (2D) cell culture systems where culturing cells on stiff and flat substrates is a simplified method and does not represent the dynamic and highly complex tissue systems [400,509]. 2D culture of cells distorts cell-cell and cell-matrix interactions which affects cell proliferation, migration and differentiation [510,511], whereas 3D *in vitro* models better represent the *in vivo* situation in a cost-effective way and with no ethical concerns [400]. To date, none of the studies demonstrated an *in vitro* model which allows researchers to evaluate angiogenesis assessing both proliferation and migration of ECs in a 3D dynamic environment.

In this study, we developed a bilayer tubular model as a platform to be used in the evaluation of two phases of angiogenesis together; cell proliferation and migration in a dynamic environment under physiologically more relevant conditions. The nanofibrous structure of the inner tube mimics the basement membrane and provides a suitable environment for EC attachment and formation of an endothelial monolayer whereas the highly porous and interconnected outer polymerised high internal phase emulsion (PolyHIPE) tube enables cell infiltration and migration through the pores.

The experimental procedures in this chapter have been conducted in collaboration with my co-worker Betül Aldemir Dikici during our collaboration with Massachusetts Institute of Technology (MIT). Betül was responsible for the production of PCL PolyHIPE tube including the synthesis of PCL methacrylate, preparation of PCL HIPEs, and polymerisation of the PCL PolyHIPE tubes.

## 5.3. Materials

| Chemical / Reagent | Catalogue Number | Supplier |
|---|---|---|
| Alexa Fluor® 594 anti-human CD31 Antibody | 303126 | **Biolegend** |
| Hypermer B246 | - | **Croda** |
| Chloroform | 10784143 | **Fisher Scientific** |
| Dichloromethane (DCM) | 10127611 | |
| DPX mounting medium | D/5319/05 | |
| Industrial methylated spirit (IMS) | M/4450/17 | |
| Methanol | 10626652 | |
| Toluene | 10102740 | |
| Triton X-100 | BP151 | |
| Xylene | X/0100/17 | |
| Poly3-hydroxybutyrate-co-3-hydroxyvalerate (PHBV) (PHV content 12 mol %) | BV326301 | **GoodFellow** |
| Optimum cutting temperature tissue freezing medium (OCT-TFM) | 14020108926 | **Leica Biosystems** |
| Fertilised chicken eggs | - | **MedEggs** |
| Hydrochloric acid fuming 37% | 100317 | **Merck** |
| RCOM King SURO humidified egg incubator | MX-SURO | **P&T Poultry** |
| EC GM 2 Supplement Pack (for HAECs) | C-39211 | **PromoCell** |
| Endothelial Cell Growth Medium 2 (EC GM) (for HAECs) | C-22211 | |
| Human Aortic Endothelial Cells (HAECs) | C-12271 | |
| 2-deoxy-D-ribose (2dDR) | 121649 | **Sigma Aldrich** |
| 37% formaldehyde (FA) solution | F8775 | |
| 4',6-diamidino-2-phenylindole (DAPI) solution | D8417 | |
| AlamarBlue Cell Metabolic Activity Assay | R7017 | |
| Amphotericin B | A2942 | |
| Bovine serum albumin (BSA) | A7030 | |
| Collagenase A | COLLA-RO | |

| | | |
|---|---|---|
| Dimethyl sulphoxide (DMSO) | 472301 | |
| Eosin Y solution | HT110232 | |
| Ethanol | 51976 | |
| Fetal calf serum (FCS) | F9565 | |
| Glutaraldehyde (25%) | G5882 | |
| Goat serum | G9023 | |
| Hematoxylin solution | HHS16 | |
| Methacrylic anhydride (MAA) | 276685 | |
| Paraformaldehyde (PFA) | 158127 | |
| Penicillin / Streptomycin | P0781 | |
| Pentaerythritol (98%) | P4755 | |
| Photoinitiator (PI) (2,4,6-Trimethylbenzoyl Phosphine Oxide/2-Hydroxy-2-Methylpropiophenone blend) | 405663 | |
| Polydimethylsiloxane (PDMS) (SYLGARD®184) | 761036 | |
| Tin (II) 2-ethylhexanoate | S3252 | |
| Triethylamine (TEA) | 471283 | |
| Trypan blue | T6146 | |
| Trypsin EDTA | T3924 | |
| Vascular endothelial growth factor (VEGF) | V7259 | |
| ε-caprolactone | 704067 | |
| Alexa Fluor 594 Phalloidin | A12381 | **ThermoFisher Scientific** |

## 5.4. Methods

### 5.4.1. Design and manufacturing of the 3D dynamic system

The 3D system was designed to be two-layers; the inner tube of nanofibres to serve as a suitable environment for HAECs to attach, proliferate and form a monolayer to represent an endothelium, and the outer tube of the highly porous and interconnected environment to enable proliferation and migration of HAECs from the formed endothelial monolayer. 3D bilayer tubes used in this study were manufactured combining two manufacturing

methods; emulsion templating and electrospinning, and they were characterised using scanning electron microscopy.

#### 5.4.1.1. Manufacturing of the PCL PolyHIPE outer tube by emulsion templating

The manufacturing of the PCL PolyHIPE outer tube has been carried out in collaboration with my colleague, Betül Aldemir. More information about the details of the following protocols can be found elsewhere for further reading [424].

##### 5.4.1.1.1. Synthesis of PCL methacrylate

The PCL used in this study is 4-arm PCL methacrylate (4PCLMA) which we have previously reported the detailed synthesis [424]. Throughout the paper, the term `PCL polymerised high internal phase emulsion (PolyHIPE)` will be used to describe 4PCLMA PolyHIPE, unless otherwise stated.

Briefly, pentaerythritol (12 g, 0.088 mol) and ε-caprolactone (80.49g, 0.705 mol) were mixed in a round flask at 160°C while stirring continuously at 200 rpm. When pentaerythritol was dissolved, tin (II) 2- ethylhexanoate (as a catalyst) was added, and the system was left for reaction overnight with stirring. Then, stirring was stopped, and the system was removed from the oil bath to cool down in the ambient atmosphere. Hydroxyl-terminated 4-arm PCL was obtained, and to methacrylate functionalise, it was dissolved in 300 mL of DCM, and then TEA (52.65 g, 0.52 mol) was added. The flask was placed in an ice bath. MAAn (80.22 g, 0.52 mol) was dissolved in 100 mL DCM and transferred into a dropping funnel. When the addition of MAAn was completed, the ice bath was removed, and the system was kept at RT overnight with stirring at 375 rpm. To remove the TEA, MAAn and the salts formed, the methacrylated PCL was washed three times with HCl solution (1 M, 1000 mL), separated using a separating funnel, and then washed three times with pure deionised water. Almost all solvent was evaporated using a rotary evaporator. PCL was then dissolved in methanol, then precipitated out of methanol by placing in -80 °C freezer. Three methanol washes were used, and any remaining solvent was removed by using the rotary evaporator. 4PCLMA was stored in an appropriate vessel in the freezer (-20 °C) for further use.

##### 5.4.1.1.2. *Preparation PCL HIPEs*

4PCLMA (0.4 g) and the surfactant Hypermer (10% w/w of polymer) were added into a glass vial and heated to 40°C to dissolve surfactant. The effect of different solvents and solvent blends on the structural parameters of PolyHIPE has recently been demonstrated [424]. In this study, solvent blend (150% w/w of polymer, 80% chloroform, 20% toluene (w/w)) and PI (10% w/w of polymer) were added in the 4PCLMA-surfactant mixture, respectively and mixed at 375 rpm using a magnetic stirrer for 1 minute at RT. Once the homogeneous mixture formed, 2.5 mL of water (internal phase volume 80% v/v) was added dropwise in 3 minutes, and the emulsion was mixed further 30 seconds more. The protocol of HIPE preparation is given in Figure 84.

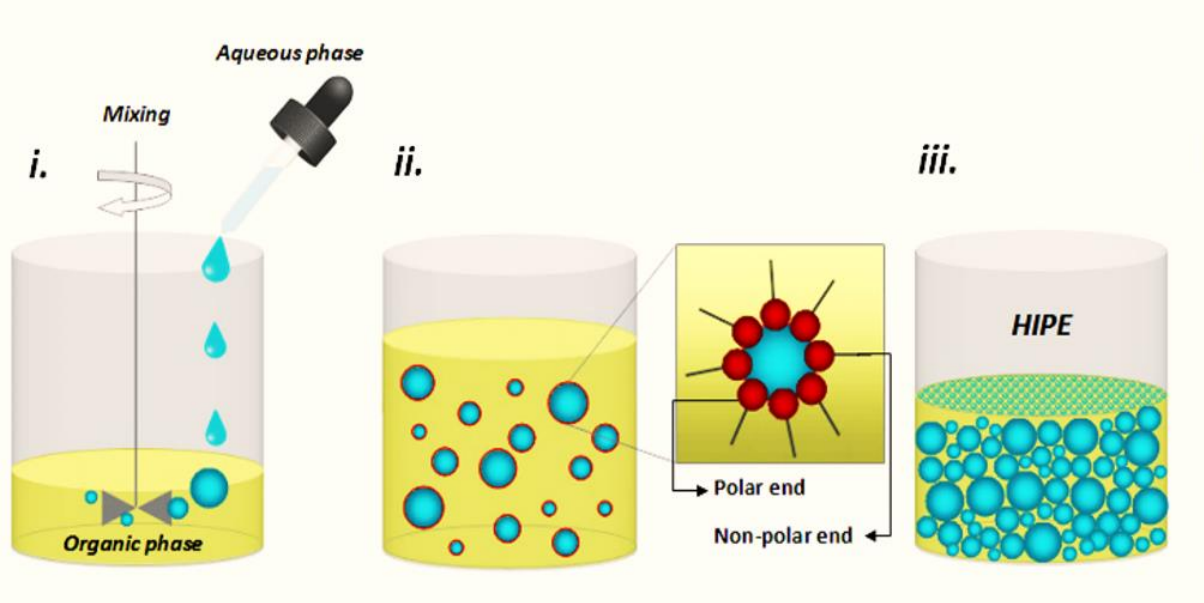


***Figure 84.*** *Preparation of PCL HIPEs. The steps shown are (i) Addition of aqueous phase to organic phase, (ii) creating a stable emulsion suing a surfactant, and (iii) the resultant emulsion that can be defined as HIPE when the aqueous phase content is over 74%*

5.4.1.1.3. The polymerisation of PCL HIPEs

A mould made of silicone tubes, stoppers, and a copper rod was assembled (Figure 85A). PCL HIPE was injected into the mould by using a syringe and polymerised for 3 minutes on both sides using a UV curer with a 100 $W.cm^{-2}$ UV bulb (Omnicure Series 1000, Lumen Dynamics, Canada).

The resulting parts were recovered, soaked in 100% methanol for 24 hours with four changes to remove any remaining contaminants of surfactant, solvent or uncured material. Then the samples were left in methanol (50% (v/v) in water) for 24 hours and

then in water for a further 24 hours. Finally, the samples were taken out from the water and left in the freezer (-80°C) for an hour then transferred into a vacuum oven and left for a day to preserve the porous structure of PCL PolyHIPE without any collapse.

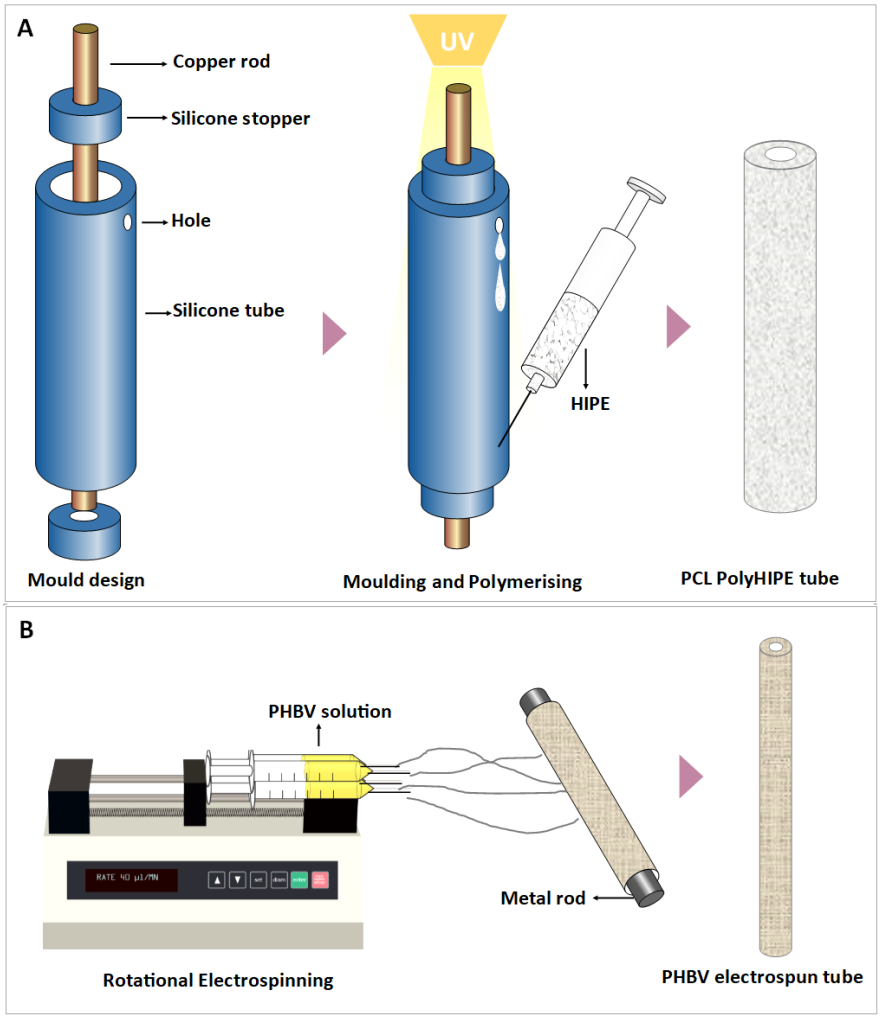


***Figure 85:*** *Manufacturing route of the polymeric bilayer tubes (A) Developed moulding system to manufacture PCL PolyHIPE tubes, (B) Electrospinning setup for manufacturing of PHBV electrospun tubes*

### 5.4.1.2. Manufacturing of the PHBV inner tube by electrospinning

PHBV (10% (w/w)) pellets were dissolved in DCM:methanol (90:10 w/w) solvent blend, and the solution (~5 mL) was loaded into 5 mL syringes fitted with 0.6 mm inner diameter blunt syringe tips. The syringe was then placed in a syringe pump (GenieTMPlus, KentScientific, Connecticut, USA). L-Shape T9 Torx key (~2.5 mm diameter) (purchased from a local supplier) was used as the mandrel and placed at a distance of 17 cm from the needle tip (Figure 83B). The rotator and the pump were set to

250 rpm and 40 µL/minutes, respectively. A 17 kV voltage was applied to both the collector and the tips. The solution was then electrospun at RT for ~10 minutes.

#### 5.4.1.3. Assembling of PCL PolyHIPE and PHBV electrospun tubes

PCL PolyHIPE tube was soaked in ethanol, removed and the excess alcohol was shaken off. Without letting it dry, the PHBV electrospun tube was inserted into PCL PolyHIPE tube, and they were soaked in ethanol and gradually transferred into 70% ethanol for sterilisation and then transferred into PBS for complete integration of two layers which occurred due to the shrinkage of PCL PolyHIPE layer (Figure 86). Then 80 holes per tube were pierced using 23 G syringe needles as escape holes as described previously [507] for enabling the migration of the ECs from the inner PHBV tube to the outer PCL PolyHIPE layer.

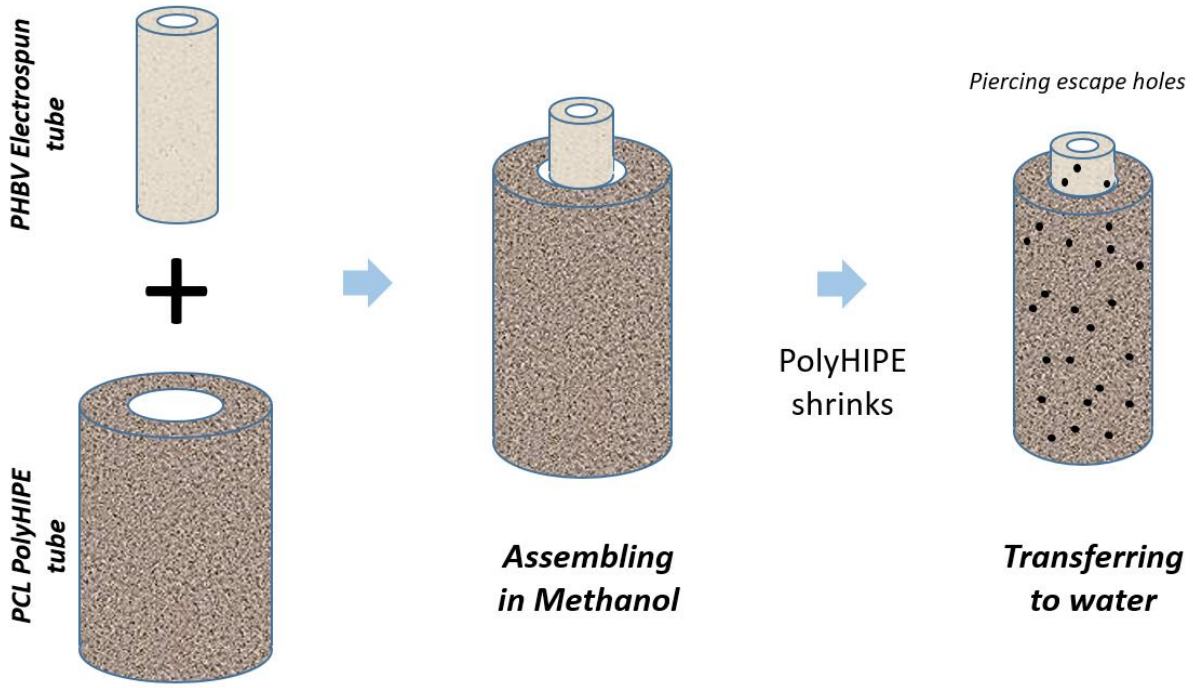


***Figure 86.*** *Assembling of PCL PolyHIPE and PHBV electrospun tubes*

### 5.4.2. Scanning electron microscopy

Micro-architectures of PCL PolyHIPE, PHBV electrospun, and the bilayer tubes were examined using an SEM. All samples were gold-coated with a voltage of 15 kV for 2.5minutes using a gold sputter coater (Edwards sputter coater S150B, Crawley, UK) to increase conductivity. SEM (FEI Inspect F, Orlando, USA) was used with 10 kV power.

### 5.4.3. Design and manufacturing of the chamber

A chamber with a lid was manufactured using 3D printing technique to serve as a reservoir for culture media and to enable the connection of the 3D bilayer tubes to lateral flow.

The 3D models of the chamber and the lid were designed using Autodesk Inventor Professional 2020 (San Rafael, CA, USA). The chamber had inner dimensions of 70x25x25 mm with 2 mm material thickness and with input and output holes which have an inner diameter of 3 mm. The lid had 75x30x5 mm inner dimensions with 2 mm material thickness. The model was then saved as a standard tessellation language (STL) file. The design of the chamber is given in Figure 87.

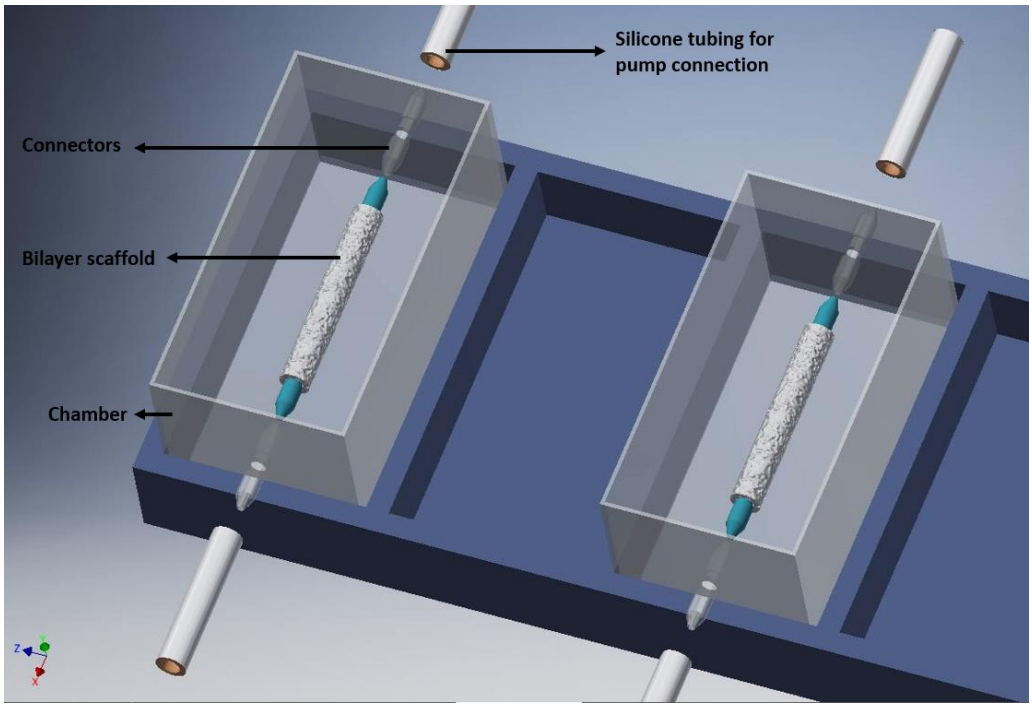


***Figure 87.*** *The design of the chamber. The figure illustrates the connection of the scaffolds to the designed chamber and the chamber to the pump for the introduction of flow to the system*

The STL file was imported into Formlabs Form 2 printer (Somerville, MA, USA) and printed using the resin; Dental LT Clear (Figure 88A). Following this, the chamber and lid were washed with isopropanol, post-cured at 60$^{o}$C for 1 hour and washed with ethanol. Then the chambers were air-dried, and silicone tubes were sealed into the input and output holes of the chambers (Figure 88B). Chamber systems were sterilised using 70% (v/v) ethanol solution (in deionised water). Briefly, they were soaked in the ethanol solution in the laminar hood and left for 2 hours, air-dried in the hood for 1 hour and

washed with PBS three times for 2 hours. The connectors and the silicone tubing were sterilised by using an autoclave, and the whole system was assembled in a laminar hood under sterile conditions using sterile forceps.

### 5.4.4. Testing the diffusion pattern between the tube and the chamber

The bilayer tube was connected to the chamber, and the chamber was filled with 30 mL of DI water. Trypan blue was injected into the silicone tube to be circulated, and 10 dyn/cm$^2$ flow was applied to the system. Macroscopic images of the system were captured at the end of 1, 5 and 10 minutes to observe the diffusion of the trypan blue. At the end of the experiment, deionised water in the chamber was collected, and the volume was measured.

### 5.4.5. Rotational cell seeding into bilayer tubes

One end of the tubes was occluded, as shown in Figure 88C and bilayer tubes were left in 70% ethanol for 2 hours and then washed with PBS three times in sterile conditions. Finally, they were conditioned with media for an hour in the incubator in 24 well plates. HAECs were trypsinised, counted, and centrifuged. The cell pellet was re-suspended in fresh media, and $10^6$ cells/300 µL were injected into tubes using a syringe, as shown in Figure 88D. Once all the cell suspension was injected, the other end was closed using a cap (Figure 88E). Tubes were transferred in a 15 mL centrifuge tube with 10 mL EC GM and placed in a cylindrical rotator turning at 1 rpm in a 37 °C, 5% $CO_2$ humidified incubator for 4 hours for the attachment of HAECs (Figure 88F).

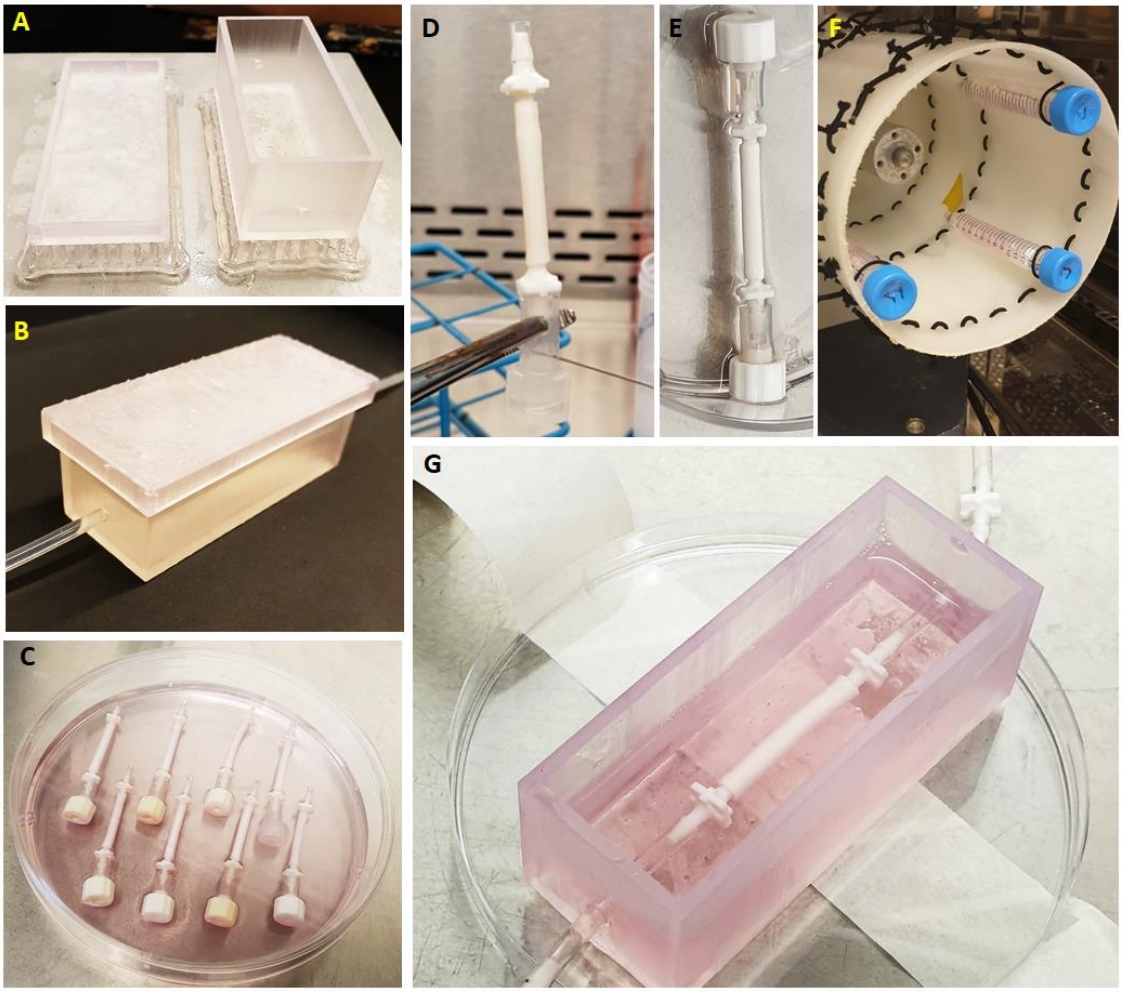


***Figure 88:*** *Protocols we followed starting from the chamber manufacturing to the implementation of the tubes to the fabricated chamber. (A) Manufactured chamber using 3D printing, (B) implementation of the tubing to the chamber, (C) preparation of the tubes for seeding, (D) administration of the cell suspension into tubes using a syringe, (E) closing the other end with a cap to prevent leakage of the cells from the tube upon seeding, (F) rotational incubation of the tubes, and (G) implementation of the cellularised tube to the chamber*

### 5.4.6. 3D culture of HAECs in the newly developed dynamic model for the assessment of angiogenesis

Following cell seeding, caps in both ends of the tubes were removed, and bilayer tubes were connected to silicone tubing in the printed chamber using sterile forceps (Figure 88G). HAECs in bilayer tubes were cultured for a week. In 3D experiments, the individual effect of flow, pro-angiogenic agents and their combined effect on EC infiltration were investigated. Flow experimental groups were static (control), 1 dyn/cm$^2$, 2 dyn/cm$^2$ and 10 dyn/cm$^2$. Then, drug experimental groups; 100 μM 2dDR and VEGF were investigated under static conditions. Finally, 100 μM 2dDR and VEGF were further investigated under 2 dyn/cm$^2$ flow and compared with the static conditions.

### 5.4.7. Hematoxylin and Eosin (H&E) staining

Bilayer tubes cultured with HAECs for a week were stained with H&E using a standard protocol [358]. Briefly, samples were washed with PBS and fixed with 3.7% FA. They washed with PBS, and excess water was removed using filter paper. Meanwhile, cryomoulds were filled with OCT-TFM. Samples were embedded into it, and the rest of the volume was then filled with OCT-TFM to the top. Cryomoulds were placed into -80 °C freezer and incubated for 30 minutes until solidified. Frozen blocks were fixed on mounting platforms, and placed into a cryostat (Leica CM1860 UV, Milton Keynes, UK) before sections were sliced at 5-10 μm and immediately mounted onto Thermo SuperFrost® Plus slides. For H&E staining, slides were stained with hematoxylin for 90 seconds and eosin for 5 minutes and they were dehydrated, cleared and mounted the slide using the permanent mounting medium.

### 5.4.8. Fluorescent staining

Bilayer tubes were fixed with 3.7% FA for 30 minutes and washed gently with PBS prior to submerging into 0.1% (v/v) Triton X 100 (in PBS) solution for 20 minutes and stained in the same way explained in the Section 3.1.4. Then, the stained scaffold was sectioned, as explained in Section 3.2.7 and imaged under a fluorescent microscope (Olympus IX3, Tokyo, Japan).

### 5.4.9. Statistical analysis

Statistical analysis was carried out using one-way and two-way analysis of variance (ANOVA) using statistical analysis software (GraphPad Prism, CA, USA). Where relevant, n values are given in figure captions. Error bars indicate standard deviations in the graphs unless otherwise stated.

## 5.5. Results

### 5.5.1. Design, production and characterisation of the PCL polyHIPE & PHBV electrospun tubes

The 3D bilayer tubes consist of an inner PHBV electrospun tube for ECs to attach and form an endothelial monolayer and an outer PCL PolyHIPE tube which provides a highly

porous and interconnected environment for ECs to infiltrate was developed successfully following the manufacturing route illustrated in Figure 86.

The surface morphology of PHBV electrospun was beadless with random (non-aligned fibres) fibre orientation where the average fibres and pore sizes were 0.70 ± 0.25 µm and 3.64 ± 2.16 µm, respectively (Figure 89D). The outer layer, PCL PolyHIPE, had an average pore size of 30 ± 13 µm (Figure 89E).

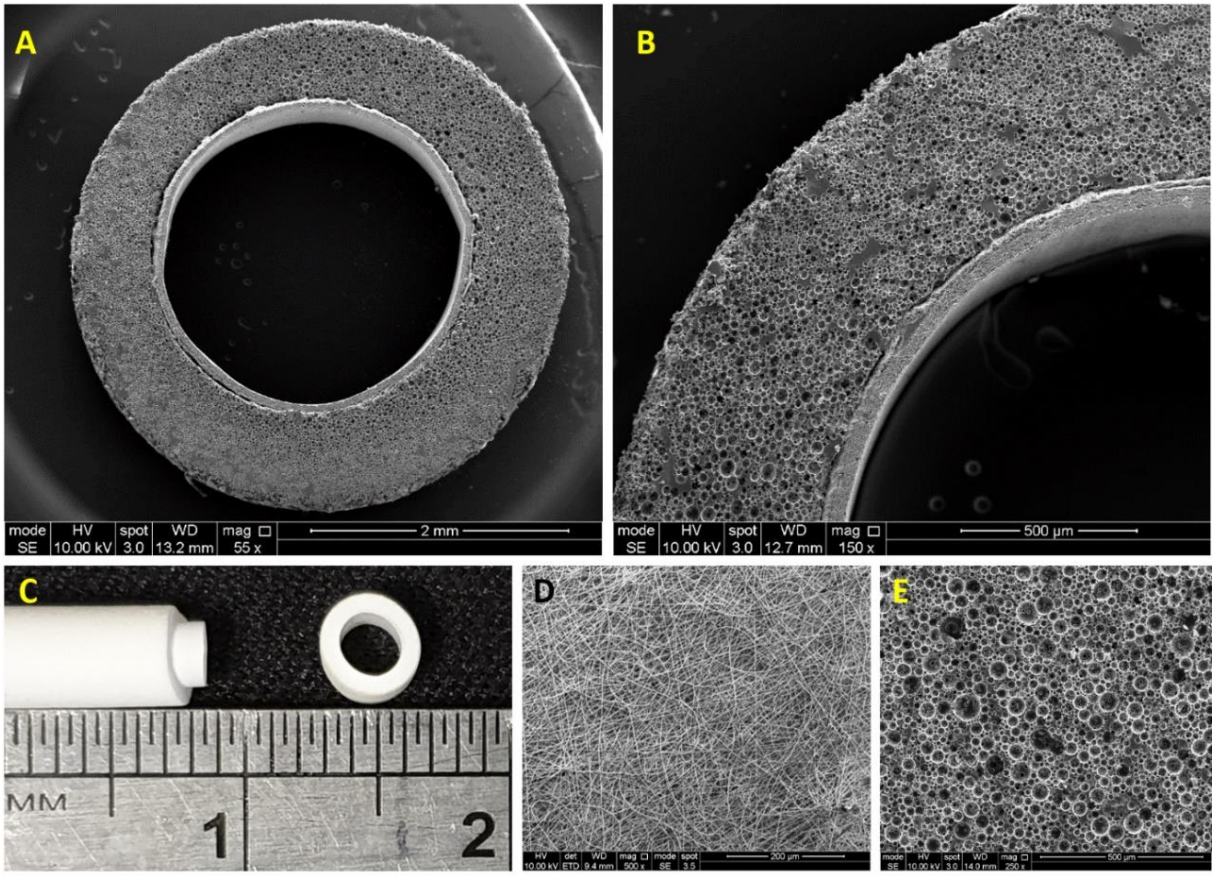


***Figure 89:*** *(A,B) SEM image of the cross-section of the bilayer tube, (C) Macroscopic image of the bilayer tube, (D) SEM images of the surface topology of PHBV electrospun and (E) PCL PolyHIPE*

The 3D culture chamber manufactured using 3D printing was capable of supporting the culture of HAEC in bilayer tube for periods of 7 days. There was no leakage or contamination throughout the experiments. The connection of the scaffolds to the fabricated chamber and the whole system to the flow are given in Figure 90A-C. The resin, Dental LT Clear, used for manufacturing of the chamber was reported to be biocompatible by the manufacturer. It was resilient to 70% ethanol for sterilisation of the chamber. Its transparency was advantageous for bioreactor chambers to be able to allow the visual inspection of the media colour without opening the lid, which reduces the risk of

contamination throughout the culture. This petri-dish inspired design is reproducible, cost-effective ($15/chamber) and allows gas exchange. Its small dimensions enable multiple chambers to be used in the same incubator at the same time.

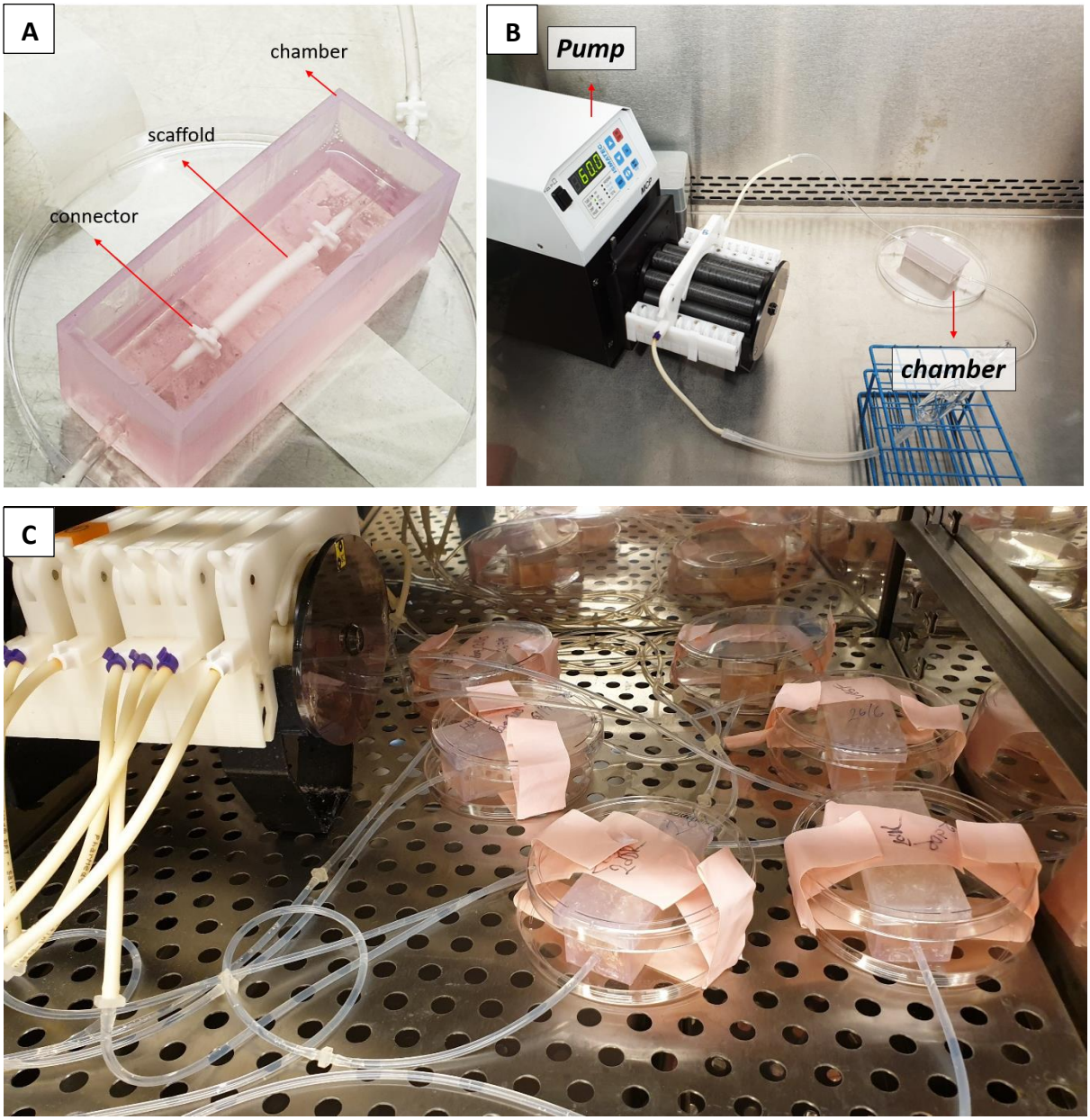


***Figure 90.*** *(A) The connection of the scaffolds to the chamber, (B) the connection of chamber to the pump prior to starting experiments, and (C) the connection of multiple chambers to the pump in a cell culture incubator*

### 5.5.2. Flow mediates proliferation and outgrowth of ECs: Low shear stress promotes proliferation and migration of HAECs

HAECs were seeded in bilayer tubes and cultured under static, 1 dyn/cm$^2$ flow, and 2dyn/cm$^2$ flow formed a continuous endothelial monolayer at the end of a 1-week culture period (Figure 90). The cells cultured in tubes under 10 dyn/cm$^2$ flow showed relatively poor cell distribution, which is likely due to cells were washed out because of the comparably high flow rate which gave the lowest cell density observed amongst all of the groups. However, migration of HAECs through electrospun fibres was higher under 10 dyn/cm$^2$ shear stress (202.6 ± 107.7 μm) compared with the static group where no outgrowth was observed. HAEC outgrowth and cell density in tubes cultured under 2 dyn/cm$^2$ flow were significantly higher and statistically different than other groups. HAECs migrated approximately 533 ± 90.8 μm in 7 days under 2 dyn/cm$^2$ shear stress while the outgrowth was 231.5 ± 70.1 μm when 1 dyn/cm$^2$ shear applied. Moreover, at day 7, the normalised density of cells in the tubes was significantly increased under 2 dyn/cm$^2$, and it was approximately 2-fold, 1.4-fold, and 12-fold higher in comparison with static, 1 dyn/cm$^2$, and 10 dyn/cm$^2$ shear stress conditions, respectively. Fluorescent and H&E staining of the HAECs under static and flow conditions are given in Figure 91.

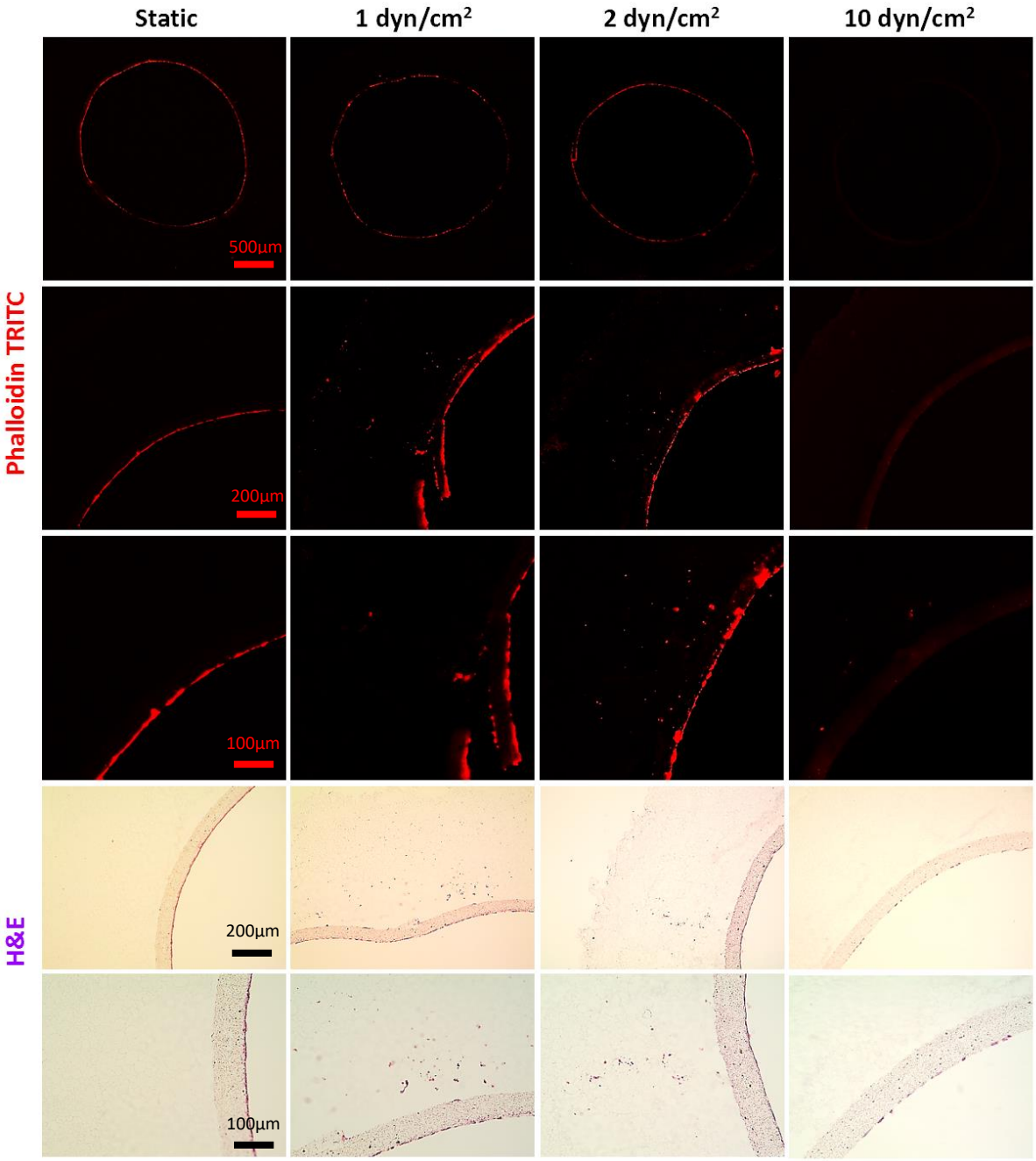


***Figure 91:*** *Effect of flow on the outgrowth distance, cell density and the cell monolayer formation of HAECs. (Top) Phalloidin TRITC, (Bottom) H&E staining of the sections of the bilayer tubes cultured with HAECs for a week under static culture and dynamic culture with 1 dyn/cm², 2 dyn/cm² and 10 dyn/cm² flow from left to right, respectively*

### 5.5.3. Testing the diffusion pattern between the tube and the chamber

To test the diffusion behaviour between the chamber and the tube visually, the trypan blue dye was circulated in the system, and macroscopic images of the chamber were captured at 1, 5 and 10 minutes (Figure 92A). Images showed the gradual release of the dye from the inner tube to the chamber. Also, the volume of the liquid in the chamber was

measured both at the beginning of the experiment and at the end of 10 minutes of circulation, and it was 30 mL at both time points.

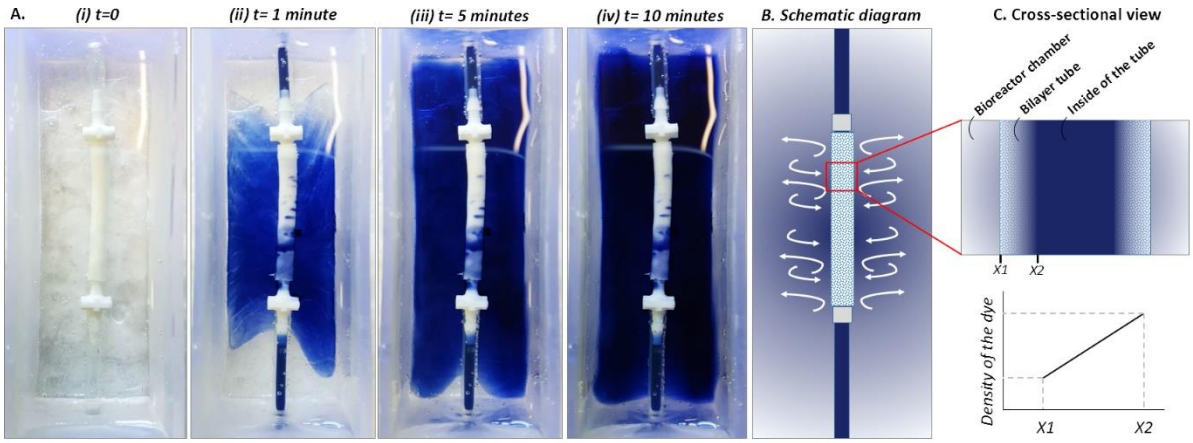


***Figure 92:*** *(A) The diffusion of trypan blue dye from flow system to the outer chamber, (B) Schematic diagram of the system and (C) cross-sectional view of the tube showing the dye gradient between bioreactor chamber and inside of the tube at any point till balance point*

### 5.5.4. 2dDR and VEGF promotes proliferation and outgrowth of HAECs under static conditions

In 2dDR and VEGF supplemented groups, HAECs in the electrospun tube formed a dense-packed endothelial monolayer inside the tube. No HAEC infiltration was observed in the control group which was not supplemented with any drug under static conditions whereas in 2dDR and VEGF supplemented groups, HAECs were able to migrate through PCL PolyHIPE layer approximately 182.2 ± 81.6 μm and 264.9 ± 88.1 μm, respectively. There was no statistically significant difference between VEGF and 2dDR supplemented tubes under static conditions in terms of HAEC outgrowth. The cellular densities in the tubes under static conditions were increased 1.2-fold and 1.5-fold by the addition of 2dDR and VEGF, respectively.

### 5.5.5. Pro-angiogenic agents (2dDR and VEGF) and fluid forces cooperate to improve the outgrowth and proliferation of HAECs

The highest distance of outgrowth and a dramatic increase in the cellular density was observed when HAECs were exposed to the simultaneous application of the angiogenic drugs and the flow. HAECs cultured under 2 dyn/cm$^2$ shear stress with a growth medium supplemented with either 2dDR or VEGF migrated up to 779.8 ± 110.3 μm and 797.3 ± 72.5 μm, respectively. Furthermore, the cellular densities in the tubes were increased 3.8-

fold and 3.2-fold, respectively for 2dDR and VEGF groups under 2 dyn/cm$^2$ shear stress when compared with the drug including static controls. There was no statistically significant difference observed between 2dDR and VEGF groups under 2 dyn/cm$^2$ shear stress in terms of HAEC outgrowth. Fluorescent and H&E staining of the HAECs under static and flow conditions either administered with drugs or non-treated are given in Figure 93. The graph showing the quantified results of flow and drug experiments and the statistical analysis is given in Figure 94.

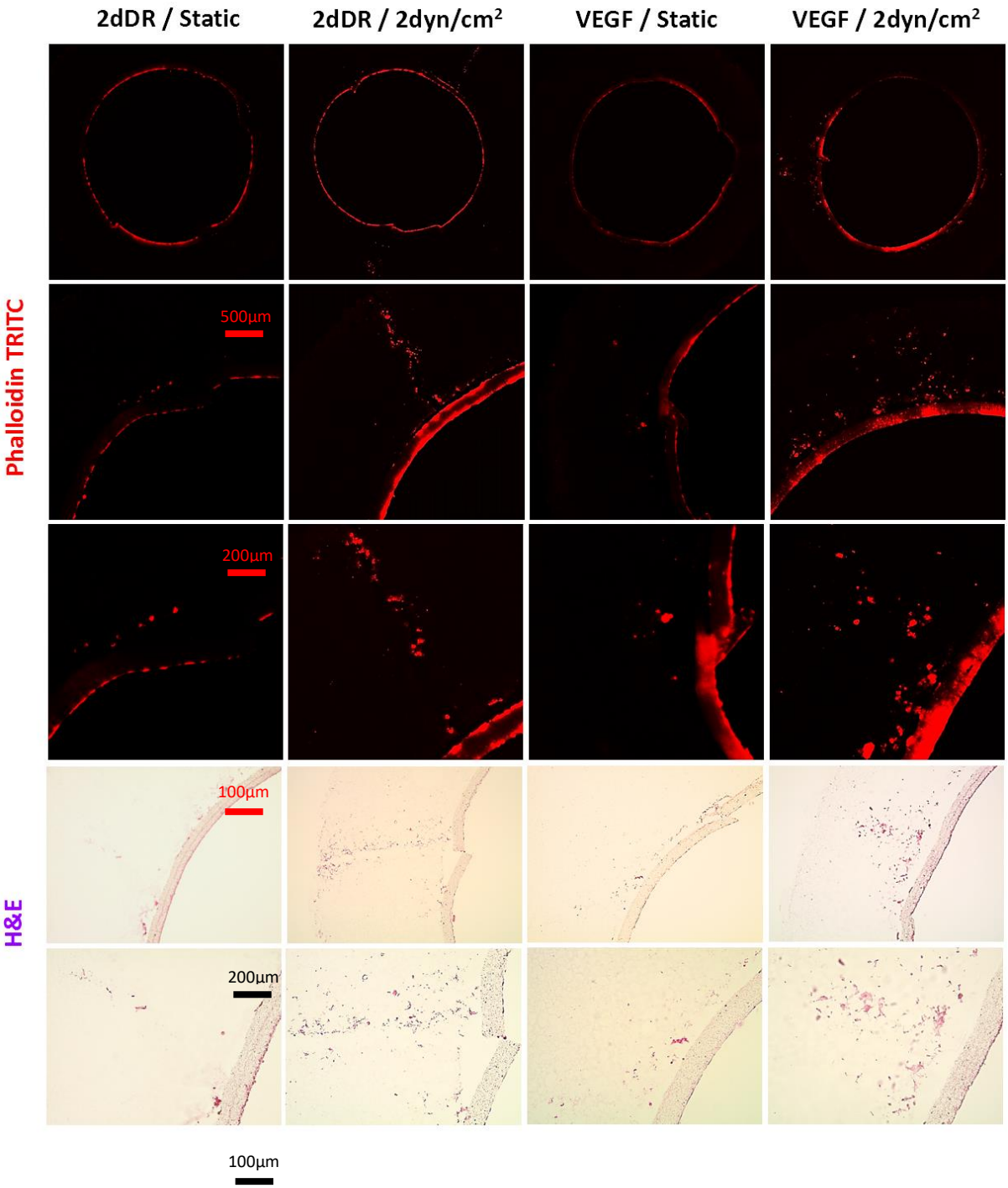


***Figure 93:*** *The combined effect of 2dDR, VEGF, and flow (2dyn/cm²) on the outgrowth distance, cell density and the cell monolayer formation of HAECs. (Top) Phalloidin TRITC, (Bottom) H&E staining of the sections of the bilayer tubes cultured with HAECs under static culture and dynamic culture with 2 dyn/cm² flow and with the implementation of the angiogenic agents (VEGF and 2dDR)*

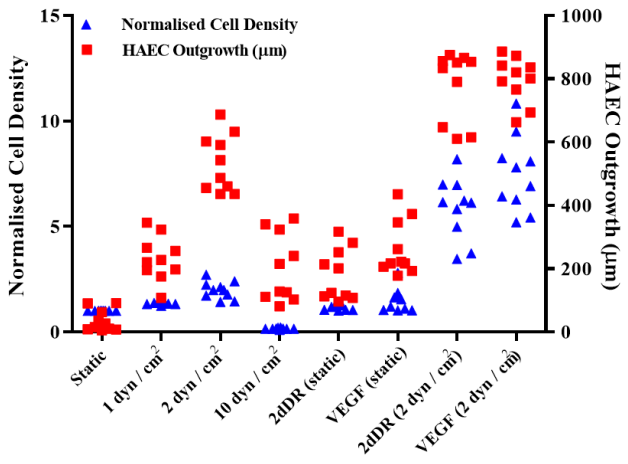


| *Effect of* | *1st parameter* | *2nd parameter* | *Normalised Cell Density* | *HAEC Outgrowth (µm)* |
|---|---|---|---|---|
| *Flow* | Static | 1 dyn/cm$^2$ | **** | **** |
| | Static | 2 dyn/cm$^2$ | **** | **** |
| | Static | 10 dyn/cm$^2$ | **** | **** |
| | 1 dyn/cm$^2$ | 2 dyn/cm$^2$ | ** | **** |
| | 1 dyn/cm$^2$ | 10 dyn/cm$^2$ | **** | *ns* |
| | 2 dyn/cm$^2$ | 10 dyn/cm$^2$ | **** | **** |
| | 2dDR (static) | 2dDR (2 dyn/cm$^2$) | **** | **** |
| | VEGF (static) | VEGF (2 dyn/cm$^2$) | **** | **** |
| *Drug* | Static | 2dDR (static) | ** | ** |
| | Static | VEGF (static) | ** | **** |
| | VEGF (static) | 2dDR (static) | *ns* | * |
| | 2 dyn/cm$^2$ | 2dDR (2 dyn/cm$^2$) | **** | **** |
| | 2 dyn/cm$^2$ | VEGF (2 dyn/cm$^2$) | **** | **** |
| | VEGF (2 dyn/cm$^2$) | 2dDR (2 dyn/cm$^2$) | * | *ns* |

***Figure 94:*** *Quantification of the outgrowth (µm) distance and the cell density (normalised to the static alone group) of HAECs to show the effect of flow and drugs either in isolation or combined (***p ≤ 0.001, **p ≤ 0.01, *p ≤ 0.05, not significant (ns) p ≥ 0.05, n = 3)*

## 5.6. Discussion

To test the angiogenic activity of added pro-angiogenic factors, biomechanical stimulus and cells, angiogenesis models are important tools [205], and the current angiogenesis assays can be divided into three categories: *in vitro* assays which focus on evaluating proliferation, migration, and tube formation capabilities of ECs [512], ex-vivo assays and *in vivo* assays [399]. Although *in vivo*, assays are the most representative and reliable models for the evaluation of angiogenesis, they are also expensive, technically difficult, time-consuming and ethically questionable. On the other hand, *in vitro* angiogenesis assays are inexpensive, quick, technically simple, and reproducible, but they are usually based on evaluating only one aspect of angiogenesis, and as such do not represent the complexity of angiogenesis which occurs *in vivo*. A comparison of current angiogenesis assays in terms of cost-effectivity, ethical concerns, reproducibility, the requirement of special skills, representations of the physiological angiogenesis and the duration of the assay are given in Table 21.

***Table 21.*** *Comparison of current in vitro, ex vivo and in vivo angiogenesis assays with the developed dynamic 3D angiogenesis model. (- = absence, + = very low, ++ = low, +++ = low / medium, ++++ = medium, +++++ = medium / high, ++++++ = high)*

| | Models | Cost | Ethical concerns | Reproducibility | Special skill requirement | Representation of the physiological angiogenesis | Duration of the assay | References |
|---|---|---|---|---|---|---|---|---|
| *In vitro* | Proliferation assays | + | - | ++++++ | + | + | ++ / +++ | [513–516] |
| | Migration assays | ++ | - | ++++++ | + | + | + | [514,515,517] |
| | Tube formation assays | ++ | - | ++++ | ++ | + | + | [518–520] |
| | 3D dynamic angiogenesis model | + | - | ++++++ | + | ++ / +++ | ++ | *this study* |
| *Ex vivo* | Aortic ring/arch assays | ++ | ++ | +++ | +++ | +++ | +++ | [225,521,522] |
| | Retinal assay | ++ | ++ | +++ | +++ | +++ | ++ | [523,524] |
| *In vivo* | *In-ovo* CAM assay | ++ | +++ | +++ | ++++ | ++++ | ++++ | [238,525] |
| | *Ex-ovo* CAM assay | ++ | +++ | +++ | +++++ | ++++ | ++++ | [89,241,419,480] |
| | Dorsal skinfold chamber assay | ++++++ | ++++++ | ++ | ++++++ | ++++++ | +++ | [526,527] |
| | Sponge/Matrigel® plug assay | ++++++ | ++++++ | ++ | ++++++ | ++++++ | ++++ | [528,529] |
| | Corneal assay | +++++ | ++++++ | ++ | +++++ | +++++ | +++ | [516,530] |
| | Zebrafish assay | ++ | +++ | ++ | ++++ | ++++ | ++ | [531,532] |

When all the drawbacks of these methods are considered, there is a need for a 3D dynamic system which enables the study of angiogenesis *in vitro* in a more physiological complex 3D environment which includes the introduction of flow which is a major stimulus for neovascularisation *in vivo*.

Experiments in this study were designed with two key objectives; (i) to develop a 3D dynamic system to be used for testing of angiogenic drugs, (ii) to evaluate the efficiency of 2dDR on encouraging proliferation and infiltration of HAEC using *in vitro* 3D dynamic system we designed for the assessment of the suitability of our model to be used as a 3D *in vitro* angiogenesis model. Throughout these experiments, we have used VEGF as a comparator.

The 3D dynamic system was designed in a tubular form as seen in tissue engineering vascular graft design to enable the application of lateral flow [533–535]. It was designed to be two-layers and manufactured by combining two different manufacturing methods, electrospinning and emulsion templating.

The inner tube was manufactured using electrospinning, and it is made of nanofibres to serve as a suitable environment for HAECs to attach, proliferate and form a monolayer to represent an endothelium. Nanofibres have been shown to provide better surface properties for ECs to adhere to and to proliferate on than microfibres [456–458]. This is likely due to the nanofibres being structurally similar to the ECM of natural tissue with their submicron-scale topography and highly packed morphology [456,459]. Furthermore, nanofibres made of PHBV have previously been shown to be a suitable environment for ECs to form an endothelial monolayer [323]. Although nanofibres are favourable for the formation of the endothelium layer, these close-packed fibres act as a barrier to cell infiltration [419].

In contrast, the outer tube was designed to serve as a suitable environment for cell infiltration. An emulsion templating method was used for the manufacturing of the outer layer as it enables fabrication of the scaffolds with high interconnectivity and up to 99% porosity. We have recently reported the manufacturing route of PCL based PolyHIPEs, and we have also shown the biocompatibility and structural suitability of these scaffolds in terms of cell infiltration [419,424].

Moulding was used for the fabrication of the PolyHIPE tubes. The manufacturing route of PolyHIPE tubes using 3D laser patterning has previously been reported [536]. However, the production of PolyHIPE based 3D structures needs bespoke stereolithography set-ups and careful optimisation of the printing ink, the print speed of the stage and irradiation intensity, to produce good quality prints with PolyHIPEs. Thus, the use of moulds is a practical and convenient method to fabricate PolyHIPEs with uncomplicated designs.

Following the fabrication of the individual layers separately, we combined them by taking advantage of the high swelling degree of PolyHIPEs in organic solvents [537]. The outer diameter of the PHBV electrospun tube and the inner diameter of the PCL PolyHIPE tube were designed to be 2.4 mm when they were soaked in water or culture media. When the PCL PolyHIPE tube was transferred from water to ethanol, the diameter increased by more than 10% and enabled the insertion of the PHBV tube into the PolyHIPE tube. Then, the bilayer tube was transferred into the water, and a shrink-fit connection between the two layers was obtained. After combining PHBV electrospun and PCL PolyHIPE tubes, they maintained their structural integrity, and no delamination was observed at any stage of the experiments over 7 days.

3D experiments were conducted to investigate the effect of (i) flow, (ii) angiogenic agents, and (iii) their combined effect on cellular density and the outgrowth distance of HAEC from the inner tube to PCL PolyHIPE layer. The inner diameter of the 3D tube was 2.4 mm to partially represent the diameter of big blood vessels such as arteries or veins, and accordingly, the shear rates used in this study ranged between 1-10 dyn/cm$^2$ to mimic the physiological shear rates observed in some arteries and veins [538,539].

The results of the 3D flow experiments showed that static culture and lower shear stresses (1 dyn/cm$^2$ and 2 dyn/cm$^2$) enabled the formation of a continuous endothelial monolayer, but the application of higher stress (10 dyn/cm$^2$) resulted in a discrete monolayer of HAECs. This is possibly due to the cells being washed out at the high rate of flow. Similarly, Kitagawa et al. demonstrated a rapid decrease in the number of cells attached to their tubular scaffolds due to the high flow shear stress [540]. Low shear stress promoted the outgrowth of HAECs over 7 days. 2 dyn/cm$^2$ shear stress significantly increased the outgrowth distance of HAECs and normalised cell density when compared with 1 dyn/cm$^2$ and 10 dyn/cm$^2$, whereas no outgrowth was observed

under static culture conditions. Our findings of the effect of flow experiment on ECs are consistent with the literature [541,542]. ECs are mechanosensitive, and they have been reported to show phenotypic and functional changes based on various flow patterns [112]. Shear stress caused by laminar flow has been reported to reduce the apoptosis while increasing the VEGF expression [113] and demonstrated to regulate EC migration [114]. Barron et al. reported a higher EC number and infiltration under flow conditions compared to static culture [543]. Similarly, Sprague et al. demonstrated that the migration of HAECs onto a prosthetic material was positively influenced by shear stress [544]. Urbich et al. showed that the application of shear stress stimulates migration of human umbilical vein ECs in a flow rate dependent manner being at least as effective as VEGF [545]. Mohan et al. reported an increased angiogenesis-related nuclear factor-kB (NF-kB) activity when HAECs were exposed to low shear in comparison with high shear stress conditions [546].

Under static conditions, administration of 2dDR and VEGF stimulated EC outgrowth and cell density when compared with the static control group (no agents administered). However, the most dramatic increase in outgrowth distance and cell density was observed when the pro-angiogenic agents (2dDR and VEGF) were administered under 2 dyn/cm$^2$ shear conditions. The outgrowth distance and cell density of HAECs under flow conditions and when treated with VEGF and 2dDR were significantly higher when compared to that observed when VEGF and 2dDR were administered under static conditions. Similarly, Song et al. reported that VEGF and fluid forces cooperate to improve endothelial invasion into collagen gel matrix [547]. Studying EC outgrowth is particularly important because the formation of new blood vessels involves budding of endothelial cells from established vasculature towards an area of hypoxia and increased the release of pro-angiogenic factors such as VEGF.

Alongside the mechanotactic stimulus, the chemotactic stimulus is the other factor that causes a migratory response of ECs [43]. In our system, an external media reservoir was not used as the media in the chamber was sufficient to keep the cells alive for a 7-day culture period. The bilayer tubes were porous enough to enable the application of flow and the diffusion of the media between the media the inside of the tube and the media in the chamber, as shown in the time-lapse figure (Figure 92A), the trypan blue dye was spread over the chamber by this time and as there was no volume change observed in the

chamber, which indicates the liquid transport both from the tube to the chamber and the chamber to the tube. But as this transportation takes time, even after 10 minutes trypan blue did not cover the top of the tube. During the culture of HAECs in the tubes, there was a continuous nutrient consumption in the inside of the tube by the cells, which probably creates a concentration gradient between the circulating media (in the tube) and the media in the chamber. As the circulating media (represented with trypan blue, Figure 92B,C) was comparably exhausted in terms of supplemented angiogenic agents (2dDR and VEGF) compared to media in the chamber (represented with water, Figure 92B,C), the migration of HAECs from the inner surface of the electrospun tube towards outside PolyHIPE layer can be explained by the chemotactic stimulus for ECs due to the abundance of the drugs in the chamber when compared with the inner tube where perfusion occurs.

The current study makes a novel contribution by demonstrating a novel 3D model which can be used to study angiogenesis *in vitro* in a 3D dynamic environment. Herein, we showed that the 3D *in vitro* model we developed gave results consistent with the established angiogenesis assays for testing of the angiogenic effect of 2dDR in comparison with VEGF. Our model enables users to monitor cell proliferation and migration simultaneously under more physiologically relevant conditions. Our bilayer tubular system will also enable the future co-culture of endothelial cells with another cell line; for example, seeding bone cells into the PolyHIPE tube while ECs are in the electrospun tube to study angiogenesis in bone tissue engineering. This new 3D dynamic model will be suitable for studying several aspects of angiogenesis. For instance, quantitative assessment of angiogenesis markers may give a better insight into the response of ECs to an external stimulus and to flow.

## 5.7. Conclusion and Future Work

In the present study, a 3D bilayer dynamic system which enables one to study angiogenesis *in vitro* was successfully fabricated by combining electrospinning and emulsion templating. The angiogenic activity of 2dDR was evaluated in the 3D dynamic system compared to VEGF under static and flow conditions. Both agents improved endothelial cell density in the tube and the outgrowth of cells under either static or 2 dyn/cm$^2$ shear stress conditions. We conclude that the developed 3D dynamic system

offers the potential to be used as a powerful *in vitro* platform which allows to study more than one aspect of vascularisation in a more physiologically relevant environment.

In the future, studies trying to include quantitative assessment of angiogenesis markers could be trialled in an attempt to give a better insight into the response of ECs to an external stimulus and to flow. This will clearly increase the reliability of the developed model and increase the accuracy of the results obtained. In addition, further studies exploring co-culture of ECs with another cell line could bring a whole new perspective to the use of this model. For example, inclusion of bone cells in the PolyHIPE layer in co-culture with ECs (in the electrospun layer) could enable users to study the aspects of vascularisation in bone tissue engineering. Finally, the assessment of different cell combinations, pro-angiogenic factors, and flow regimes could be studied in relation to angiogenesis in future studies.

**This page intentionally left blank**

# CHAPTER VI

# Seeding of simple electrospun scaffolds with a combination of endothelial cells and fibroblasts to promote angiogenesis

## 6.1. Aims and Objectives

The aim of this chapter is to investigate the practicability of the prevascularisation approach to induce angiogenesis by pre-seeding simple electrospun PHBV scaffolds with a combination of endothelial cells and fibroblasts. In order to satisfy the aim; the objectives of this chapter are to:

- Manufacture simple nanofibrous PHBV scaffolds by electrospinning
- Investigate the effect of gelatin coating and the presence of human dermal fibroblasts (HDFs) as helper cells on human dermal microvascular endothelial cells (HDMECs) growth and survival.
- Evaluate the angiogenic activity of the PHBV scaffolds when cellularised with HDFs in isolation, HDMECs in isolation, and HDMECs in indirect co-culture with HDFs using an *ex-ovo* chick chorioallantoic membrane (CAM) assay.

## 6.2. Chapter VI by Pictures

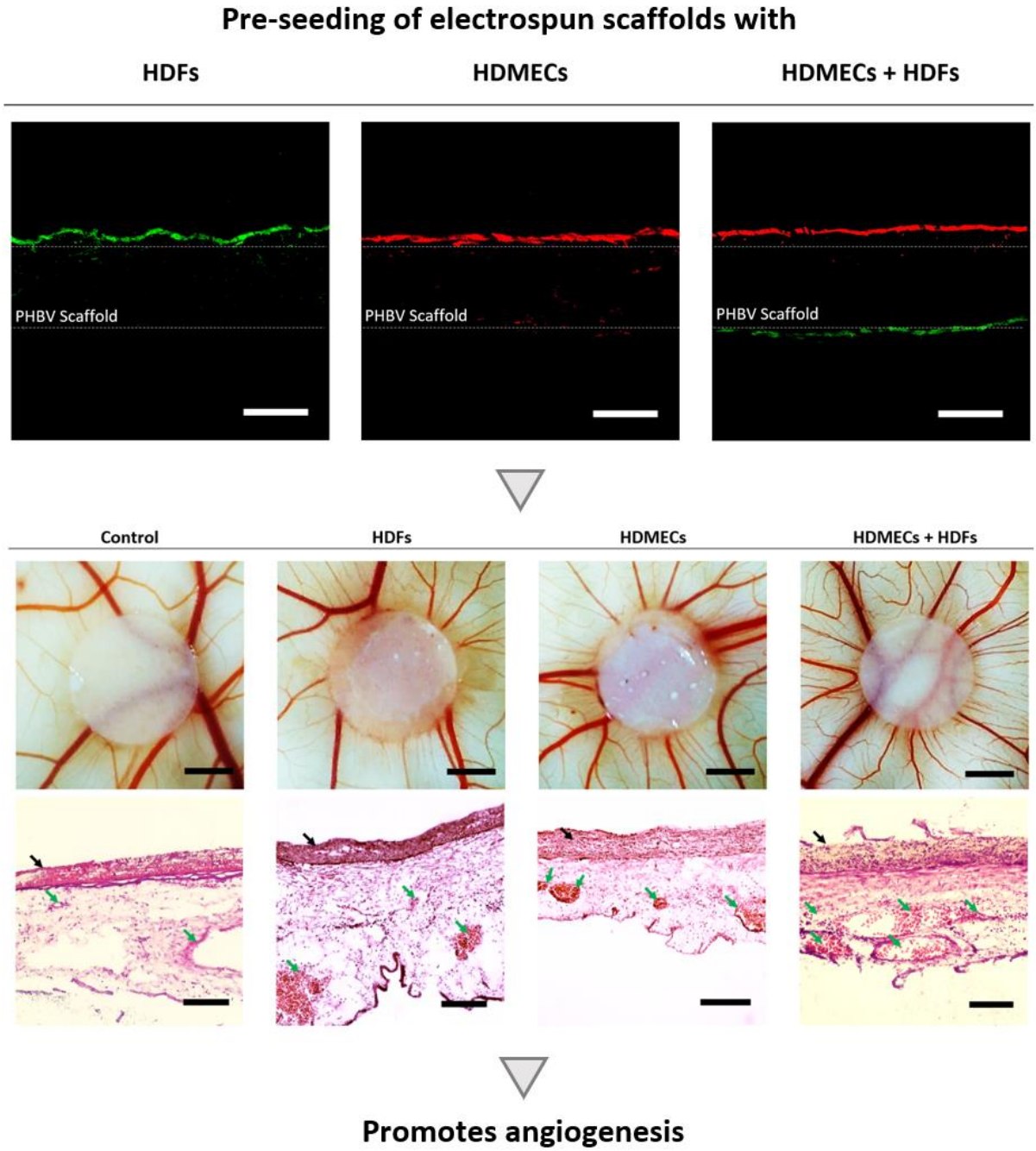

## 6.3. Introduction

Tissue and organ failure or losses are major problems that are seen in human health, and tissue engineering offers an opportunity to develop functional substitutes for damaged tissues. Most of the conventional tissue engineering approaches have mainly focused on attachment and proliferation of cells, and their formation of ECM prior to implantation [22]. However, the lack of blood vessels in tissue-engineered constructs is one of the most critical challenges in the survival of engineered tissue substitutes [23,24]. Although significant progress has been made, the main problem with tissue engineering constructs still remains the same, and it is the slow formation of new blood vessels, also known as neovascularisation, post-implantation. When a TE substitute is implanted, nutrients and oxygen must be provided to enable the cells to survive *in vivo*, and the formation of a vascular network within TE substitutes can take weeks, which leads to the failure of the constructs [26].

The majority of the current strategies to circumvent delayed neovascularisation focus on the addition of pro-angiogenic factors to TE constructs (functionalisation strategy) [22], but the use of laboratory expanded pro-angiogenic cells such as endothelial cells (ECs), endothelial progenitor cells (EPCs), and stem cells to the tissue engineering systems (prevascularisation strategy) prior to implantation is also a well-established approach [125,327]. The successful prevascularisation of a tissue-engineered construct depends on three primary parameters: (i) cell type (single or co-culture of vessel-forming cells), (ii) scaffold material selection (synthetic, natural or composite materials), and (iii) culture conditions [202,548].

Accordingly, in this study, I evaluated the effect of gelatin coating and the presence of human dermal fibroblasts (HDFs) as helper cells on human dermal microvascular endothelial cells (HDMECs) growth and survival. Then, I fabricated simple electrospun scaffolds made of PHBV to study the angiogenic activity of the scaffolds when cellularised with HDFs in isolation, HDMECs in isolation, and HDMECs in indirect co-culture with HDFs using an *ex-ovo* CAM assay [549].

## 6.4. Materials & Methods

### 6.4.1. Materials

37% formaldehyde (FA) solution, 4',6-diamidino-2-phenylindole (DAPI) solution, AlamarBlue Cell Metabolic Activity Assay, Amphotericin B, Dimethyl sulphoxide (DMSO), Dulbecco's Modified Eagle's Medium (DMEM), Fetal calf serum (FCS), Hematoxylin solution, Penicillin / Streptomycin, Phalloidin-fluorescein isothiocyanate (FITC), Phalloidin-tetramethylrhodamine isothiocyanate (TRITC), and Trypsin EDTA were purchased from Sigma Aldrich. Dichloromethane (DCM), DPX mounting medium, Industrial methylated spirit (IMS), Methanol, and Xylene were purchased from Fisher Scientific. Human Dermal Microvascular Endothelial Cells (HDMECs), EC GM MV Supplement Pack (For HDMECs), and Endothelial Cell Growth Medium MV (EC GM) (for HDMECs) were purchased from PromoCell. CellTracker™ Green and CellTracker™ Red were purchased from ThermoFisher. Poly3-hydroxybutyrate-co-3-hydroxyvalerate (12%) (PHBV) was purchased from GoodFellow. Optimum cutting temperature tissue freezing medium (OCT-TFM) was purchased from Leica Biosystems.

### 6.4.2. Methods

#### 6.4.2.1. Assessing the effect of gelatin coating on the attachment of cells to electrospun PHBV nanofibres

##### 6.4.2.1.1. Preparation of the PHBV scaffolds

Electrospun PHBV scaffolds were manufactured as described. Briefly, 10% PHBV was dissolved in DCM:Methanol (90:10) mixture, and then electrospun on an aluminium foil coated collector for random nanofibers from 17cm distance with a rate of 40 µL/minutes at 17kV voltage. PHBV scaffolds were cut into circular pieces and sterilised with 70% ethanol solution for 45 minutes.

#### 6.4.2.1.2. Gelatin coating and cellularisation of the PHBV scaffolds with HDMECs and HDFs

For gelatin coating of the PHBV scaffolds, they were submerged in a sterile 0.2% gelatin solution (w/w in PBS) and incubated at 37°C for 4 hours prior to washing with PBS three times.

For co-culture groups, the PHBV scaffolds were cellularised with HDFs in direct contact with HDMECs. Briefly, HDFs were isolated from human skin grafts taken from patients as described previously [480]. Ethical approval for the use of skin excised in routine surgical operations and not needed for treatment of patients was granted by the local ethical approval committee of National Health Service Trust, Sheffield, UK (Ethics reference: 15/YH/0177). All patients provided written informed consent. HDFs were used between passage 3-6.

HDMECs were purchased from PromoCell and used between passage 2-4. Once both cells reached 80-90% confluency. 2 x $10^4$ HDFs were resuspended in 0.1 mL of EC GM (PromoCell Endothelial Cell Growth Medium MV basal medium supplemented with 2% FCS, 0.4% EC growth supplement, 10 ng/mL EGF, 90 µg/mL heparin, 1 µg/mL hydrocortisone) and then seeded onto the one side of the PHBV scaffolds. Before seeding HDMECs, scaffolds were returned to the incubator for two hours to allow HDFs to attach. Then scaffolds were taken from the incubator and flipped over. 2 x $10^4$ HDMECs were resuspended in 0.1 mL of EC GM and then seeded onto the other surface of the PHBV scaffolds. Before adding culture medium, scaffolds were returned to the incubator for an hour to allow HDMECs to attach. Then, 2 mL of culture medium was added to each well, and they were returned to the incubator.

#### 6.4.2.1.3. AlamarBlue® Cell Viability Assay to evaluate the metabolic activities of HDMECs on PHBV scaffolds

AlamarBlue® Cell Viability Assay was performed to evaluate the effect of gelatin coating and co-culture with HDFs on HDMECs growth. In brief, 0.1 mM AlamarBlue® working solution was prepared by 10x dilution of the 1mM AlamarBlue® stock solution with EC GM. At days 1, 4 and 7, growth media were removed, and the scaffolds were washed with PBS. 1 mL of AlamarBlue® working solution was added to each well and incubated at

37°C for 4 hours. After the incubation period, 200 µL of the solution was transferred into a 96-well plate, and the fluorescence readings were done at an excitation wavelength of 540 nm and an emission wavelength of 635 nm.

#### 6.4.2.2. Preparation of cellularised electrospun PHBV scaffolds for implantation

##### 6.4.2.2.1. Electrospinning PHBV

10% (w/w) PHBV solution was prepared prior to electrospinning. 6 g of PHBV granules were dissolved in 3 g of methanol and 24 g of DCM in a fume hood, and the mixture was magnetically stirred overnight. For gelatin coating of the PHBV scaffolds, they were submerged in a sterile 0.2% gelatin solution (w/w in PBS) and incubated at 37°C for 4 hours prior to washing with PBS three times.

Approximately 10 mL of PHBV solution was transferred into 5 mL syringes with 0.6 mm blunt tips, and the syringes were then placed onto the syringe pump (Genie™Plus, Kent Scientific, Connecticut, USA). An aluminium foil coated collector was placed at a distance of 17 cm from needle tips, and the pump was set to deliver 40 µL/minutes. A voltage of 17 kV was applied to the collector as well as the needle tips. The polymer was electrospun on the collector with the parameters given above for an hour.

##### 6.4.2.2.2. Cellularisation of the electrospun PHBV scaffolds

For cellularisation of the PHBV scaffolds, three cell systems were used: (i) HDFs, (ii) HDMECs, and (Iii) HDMECs seeded on the lower surface of the PHBV fibres followed by HDFs seeded on the upper surfaces of the scaffolds.

*Cellularisation of the scaffolds with HDFs in isolation*

HDFs were used between passage 3-6 when they had reached 80-90% confluency. The PHBV scaffolds were disinfected by submerging them in 70% ethanol for 45 minutes prior to wash with PBS three times. $0.5 \times 10^5$ HDFs were resuspended in 0.1 mL of EC GM (PromoCell Endothelial Cell Growth Medium MV basal medium supplemented with 2% FCS, 0.4% EC growth supplement, 10 ng/mL EGF, 90 µg/mL heparin, 1 µg/mL hydrocortisone) and then seeded onto the PHBV scaffolds. Before adding EC GM, scaffolds were returned to the incubator for an hour to allow HDFs to attach. Then, 2 mL of culture

medium was added to each well, and they were incubated at 37°C overnight prior to implantation.

*Cellularisation of the scaffolds with HDMECs*

HDMECs were used between passage 2-4 and were used at 80-90% confluency. The PHBV scaffolds were sterilised by submerging them in 70% ethanol for 45 minutes prior to washing with PBS three times. Following sterilisation, scaffolds were transferred to 24-well plates. 0.5 x $10^5$ HDMECs were resuspended in 0.1 mL of EC GM and then seeded onto the PHBV scaffolds. Before adding EC GM, scaffolds were returned to the incubator for an hour to allow HDMECs to attach. Then, 2 mL of culture medium was added to each well, and they were incubated at 37°C overnight prior to implantation.

*Cellularisation of the scaffolds with HDMECs in indirect contact with HDFs*

HDMECs and HDFs were cultured as described above and at 80-90% confluency. The PHBV scaffolds were sterilised by submerging them in 70% ethanol for 45 minutes prior to washing with PBS three times. Following sterilisation, scaffolds were transferred to 24-well plates. 0.25 x $10^5$ HDFs were resuspended in 0.1 mL of EC GM and then seeded on one side of the PHBV scaffolds. Before seeding HDMECs, scaffolds were returned to the incubator for two hours to allow HDFs to attach. Then scaffolds were taken out from the incubator and turned over. 0.25 x $10^5$ HDMECs were resuspended in 0.1 mL of EC GM and then seeded onto the other surface of the PHBV scaffolds. Before adding EC GM, scaffolds were returned to the incubator for an hour to allow HDMECs to attach. Then, 2 mL of culture medium was added to each well, and they were incubated at 37°C overnight prior to implantation.

*Pre-labelling of cells for the confirmation of cell seeding*

For imaging cells on the scaffolds prior to implantation, HDFs and HDMECs were pre-labelled with CellTracker™ Green and CellTracker™ Red prior to seeding. In brief, to label HDMECs, 50 μg of CellTracker™ Red dry powder was dissolved in 7.3 μL of dimethyl sulfoxide (DMSO) to prepare 10 mM stock solution. Then, 7 mL of serum-free EC GM was added to prepare a ~10 μM working dye solution. The pre-warmed dye solution was added gently to T75 flask, and HDMECs were incubated ~1 hour under growth

conditions. To label HDFs, 50 µg of CellTracker™ Green dry powder was dissolved in 10.75 µL of DMSO to prepare 10 mM stock solution. Then 10 mL of serum-free EC GM was added to prepare ~10 µM working dye solution. The pre-warmed dye solution was added gently to T75 flask, and HDFs were incubated ~1 hour under growth conditions. Both flasks were washed three times with PBS prior to cell seeding onto PHBV scaffolds as described above.

After incubation of the HDMECs and HDFs on the scaffolds overnight either in isolation or in co-culture, PHBV scaffolds were fixed in 3.7 % formaldehyde for 30 minutes, and the fixed samples were embedded in optimal cutting temperature tissue freezing medium and frozen in liquid nitrogen for 3 minutes. Sections were cut 5-10 µm thick using a cryostat (Leica Biosystems, Nussloch, Germany) at -20°C. Sections were then directly imaged under a fluorescent microscope (Olympus IX3, Tokyo, Japan).

#### 6.4.2.3. Evaluation of the angiogenic activity of the cellularised scaffolds using *ex-ovo* CAM assay

To evaluate the angiogenic activity of cellularised PHBV scaffolds, they were implanted on the CAM for 7 days. Briefly, circles of 7 mm diameter were cut from the scaffold and cellularised with HDMECs, HDFs and HDMECs in indirect culture with HDFs prior to implantation as described above.

Fertilised chicken eggs were incubated at 37.5°C for three days in a rocking egg incubator (RCOM King SURO, P&T Poultry, Powys, Wales). On day 3, the embryos were transferred into sterile petri dishes to start *ex-ovo* culture and incubated at 38°C in a cell culture incubator (Binder, Tuttlingen, Germany) until day 7. On day 7, cellularised PHBV scaffolds were implanted onto the CAM and incubated for a further 7 days. The EC GM was added to the scaffolds twice a day. On day 14, the embryos were euthanised, and the angiogenesis was evaluated macroscopically and histologically.

For histological evaluation, the CAMs were fixed in 3.7% formaldehyde for 30 minutes, and the fixed samples were embedded in optimal cutting temperature tissue freezing medium and frozen in liquid nitrogen for 3 minutes. Sections were cut 5-10 µm thick using a cryostat (Leica Biosystems, Nussloch, Germany) at -20°C. Sections were then stained with haematoxylin for 90 seconds and eosin for 5 minutes, as described previously [89].

#### 6.4.2.4. Quantification of angiogenesis

For the quantification of angiogenesis from macroscopic images, macro images of the scaffolds implanted on CAM were taken using a digital microscope at day 14, and the number of blood vessels was quantified by counting all blood vessels growing towards the scaffolds in a spoke wheel pattern, as described previously [69].

For the quantification of angiogenesis from histological images, the total number of blood vessels adjacent to the scaffolds were quantified by counting blood vessels in H&E sections [345]. Briefly, all discernible blood vessels adjacent to the scaffolds were counted by two independent researchers using two independent microscopes.

#### 6.4.2.5. Statistical analysis

Statistical analysis was carried out using one-way analysis of variance (ANOVA) using statistical analysis software (GraphPad Prism, CA, USA). Where relevant, n values are given in figure captions. Error bars indicate standard deviations in the graphs unless otherwise stated.

## 6.5. Results

### 6.5.1. The effect of gelatin coating and co-culture with HDFs on HDMECs attachment and proliferation

The results of the AlamarBlue assay showed that there was an increase in the activity of HDMECs from day 1 to 7 in all scaffold groups. TCP groups either coated or non-coated with gelatin showed higher activity when compared with the PHBV scaffold groups (Figure 95).

Gelatin coating of TCP did not significantly affect the growth of HDMECs at any of the time points. However, gelatin coating significantly improved the activity on HDMECs seeded on PHBV scaffolds at day 1 and 4. The increases in the metabolic activity with the gelatin coating were 1.9-fold and 1.4-fold at days 1 and 4, respectively. Although the difference was not statistically significant at day 7, gelatin coating improved the activity of HDMECs on PHBV scaffolds 1.2-fold when compared to control PHBV scaffolds.

The presence of HDFs in indirect contact with HDMECs significantly improved the metabolic activity of HDMECs at all time points. The activity of HDMECs was increased 2.7-fold, 2.1-fold, and 1.6-fold at day 1, 4, and 7, respectively.

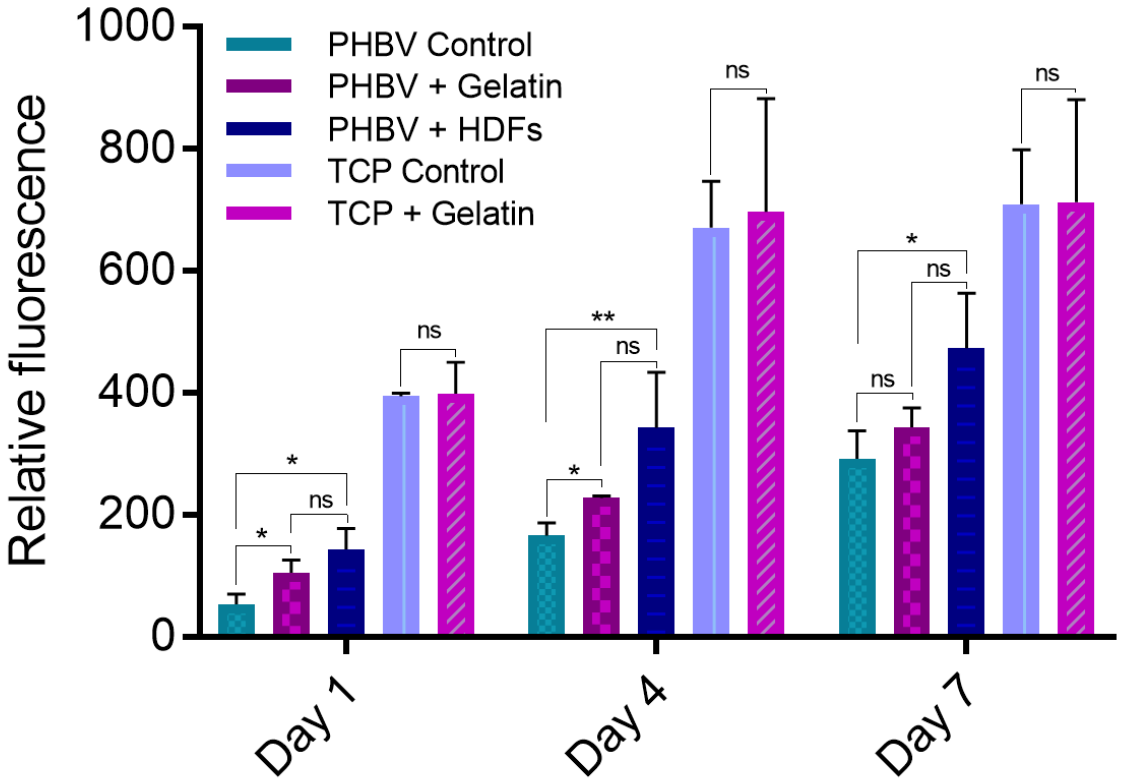


***Figure 95.*** *The results of AlamarBlue® Assay showing the effect of gelatin coating and indirect co-culture with HDFs on HDMECs metabolic activity over 7 days*

Sections of the cellularised scaffolds with CellTracker™ labelled HDFs and HDMECs were directly investigated under a fluorescent microscope prior to implantation to CAMs. The results showed that both types of cells were attached to the surfaces of the scaffolds either when seeded in isolation or in indirect co-culture. Fluorescent images of the scaffold sections are shown in Figure 96.

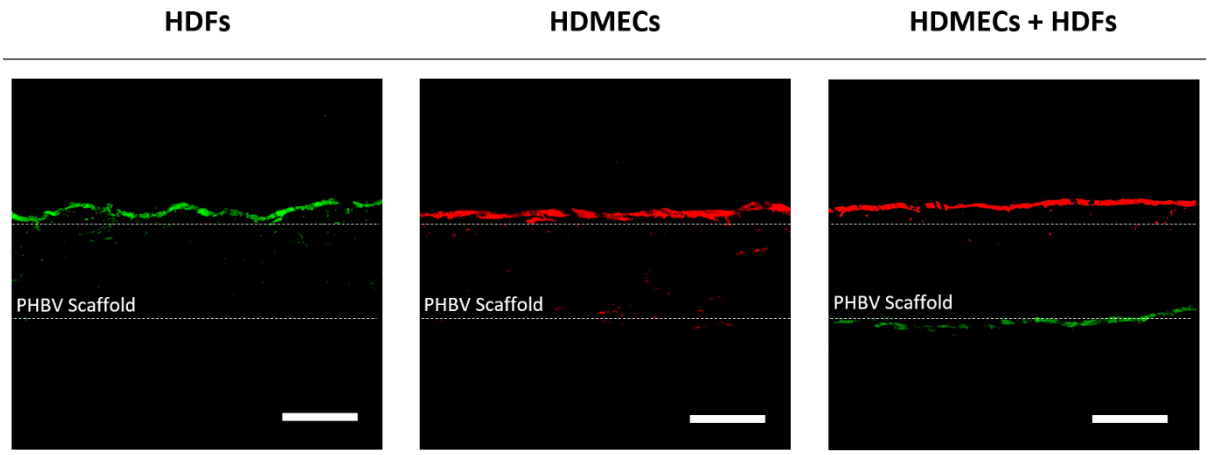


***Figure 96.*** *Cross-sections of the cellularised PHBV scaffolds with HDFs (labelled with CellTracker™ Green) and HDMECs (labelled with CellTracker™ Red) either in isolation or in co-culture prior to implantation to CAM for the evaluation of angiogenic activities. Scale bars represent 100 µm*

### 6.5.2. Evaluation of the angiogenic activity of cellularised PHBV scaffolds in *ex-ovo* CAM assay

The *ex-ovo* CAM assay results showed that the presence of both HDFs and HDMECs either in isolation or when co-cultured together significantly increased the angiogenic activity in the area of implantation. None of the implanted scaffolds affected the embryo survival rate, which was over 77 % for all groups. The presence of HDFs and HDMECs increased the angiogenic activity 1.7-fold and 2.3-fold, respectively. The results showed that when HDMECs were seeded on PHBV scaffolds, they stimulated angiogenesis significantly greater than when HDFs were used on their own. However, the most significant angiogenic response was observed when scaffolds were seeded with both HDMECs and HDFs. PHBV scaffolds cellularised with HDMECs and HDFs increased the number of blood vessels from 17.5 ± 1.9 to 46.0 ± 3.4 compared to PHBV controls. The macroscopic and histologic evaluations of the CAM assay results are summarised in Figure 97.

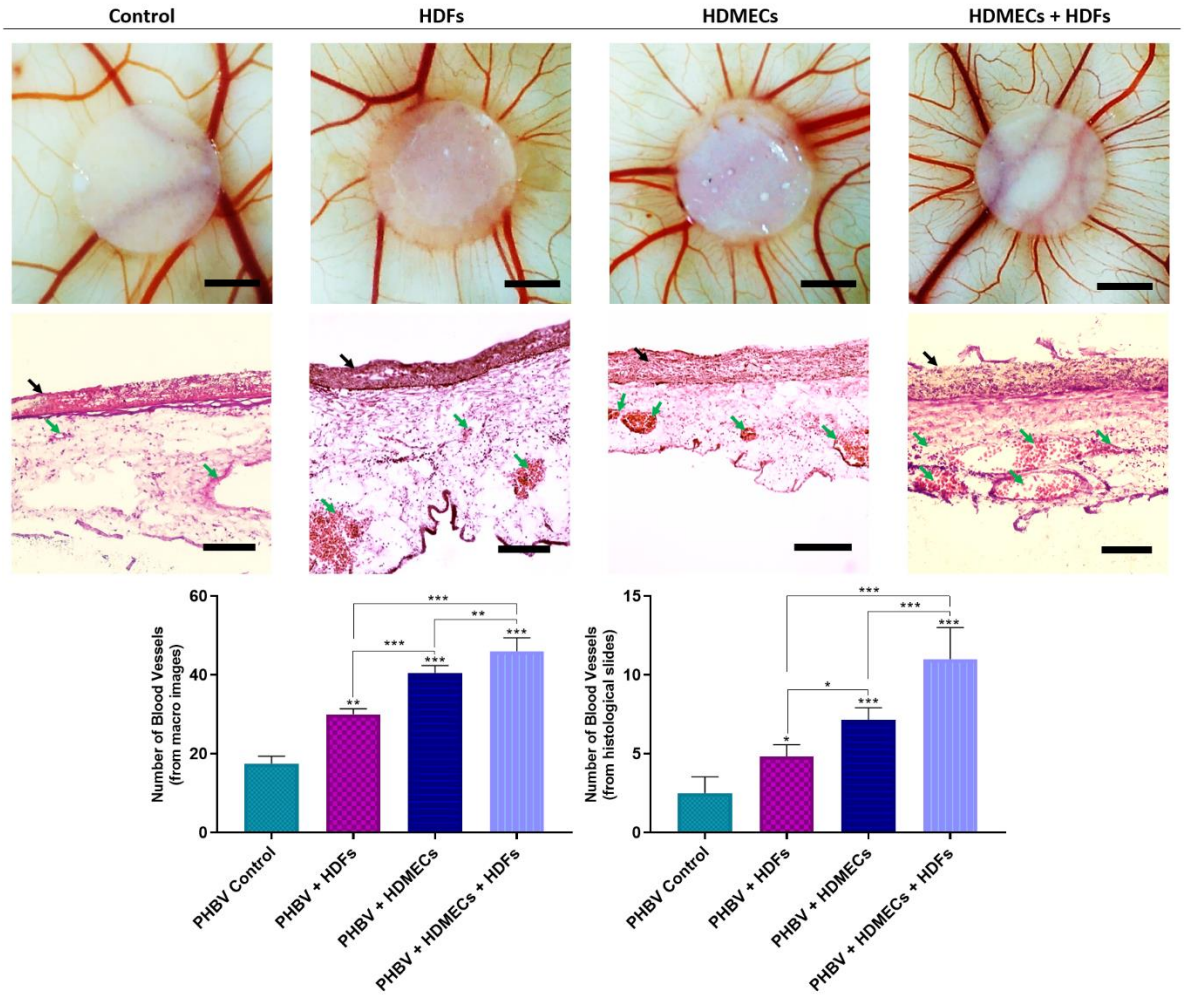


***Figure 97.*** *Representative images demonstrating the angiogenic potential of PHBV scaffolds cellularised with HDMECs or HDFs or HDMECs in indirect culture with HDFs. The graphs below show the quantified results from the macroscopic and histological analysis of the scaffolds. Scale bars represent 3 mm and 250 µm for macroimages and histological images, respectively. Black and green arrows indicate PHBV scaffolds and blood vessels, respectively. *** P ≤ 0.001, ** P ≤ 0.01, * P ≤ 0.05, n=6±SD*

## 6.6. Discussion

I have previously compared PHBV and PCL, two widely used polymers in tissue engineering applications, in terms of their physical, mechanical and biological performances in order to select one of them for further endothelialisation studies in Chapter III. Although biological evaluation of the polymers showed similar degrees of biocompatibility *in vitro* and *in vivo*, the attachment and growth of HDMECs onto PHBV nanofibres was higher compared to cell attachment to PCL fibres. The favourability of PHBV by HDMECs over PCL led us to select this polymer also for further prevascularisation studies.

Electrospinning is a method that enables to produce TE scaffolds with a wide range of properties in terms of material composition, fibre diameter, thickness, porosity, and degradation rates [438–441]. Electrospun nanofibres have been shown to provide better surface properties for ECs to adhere and proliferate on compared to microfibres [456–458]. This is likely due to the nanofibres being structurally similar to the ECM of natural tissue with their submicron-scale topography and highly packed morphology [456,459]. Accordingly, I successfully fabricated PHBV electrospun fibres with a diameter of ~0.67 µm via electrospinning. Our laboratory has previously shown that PHBV nanofibrous scaffolds allow the diffusion of oxygen and nutrients while supporting cell attachment and growth [417,507]. Although PHBV nanofibres provide a relatively favourable environment to ECs, in their natural environment, ECs are in contact with collagen, laminin and fibronectin rich ECM [492,550]. It is known that ECM plays a key role also in EC migration, morphogenesis, survival, vessel stabilisation [494]. Several studies have been reported on how ECs can be grown efficiently *in vitro.* These culture systems are mostly focused on surface coating with fibronectin, collagen and gelatin, and providing essential growth factors and the presence of stromal cells in contact with ECs [495,496]. Communication of ECs with surrounding stromal cells such as SMCs, fibroblasts or pericytes has also been proven to have significant importance for the angiogenic process [551,552].

Our group has previously reported the positive influence of fibroblasts on improving the survival and growth of ECs in polymeric scaffolds when cultured in indirect contact [323]. Recently, I have demonstrated how non-cross-linked gelatin coating can be used to improve the attachment and growth of ECs to biomaterials that have relatively weak biological properties [480]. In line with our results, Ma et al. reported that surface modification of electrospun PCL scaffolds with gelatin coating enhances the EC spreading and proliferation [553]. The positive impact of either non-cross-linked or cross-linked gelatin coating on attachment and proliferation of human Schwann cells has been shown by Vleggeert-Lankamp et al. [499]. Accordingly, in this study, I showed that gelatin coating and co-culture with HDFs are both practical approaches to improve the viability of HDMECs in synthetic nanofibrous channels with an ultimate aim of stimulating angiogenesis as a prevascularisation approach. Our results demonstrated that gelatin coating did not affect the attachment and proliferation of HDMECs on TCP, whereas the metabolic activity of HDMECs grown on gelatin coated PHBV fibres at days 1 and 4 was

significantly higher when compared to controls. Similarly, the presence of HDFs significantly improved the activity of HDMECs at all time points.

The use of pro-angiogenic agents is a well-established approach to promote neovascularisation [37,326], and VEGF is recognised as the most effective stimulator of angiogenesis [41,361] by taking key roles in the angiogenic cascade [38]. However, the exogenous use of VEGF has also been shown to cause leaky [362], permeable [335], and haemorrhagic [336] blood vessels, which is highly observed in tumorigenesis [337]. In addition, the exogenous use of the pro-angiogenic agents is expensive, highly dose-dependent, and the delivery of them requires a very-well controlled system for the administration of the agents at the effective doses [26]. Thus, seeking alternative approaches such as the use of pro-angiogenic cells for the prevascularisation of the tissue engineering scaffolds to promote angiogenesis is crucial to circumvent the delayed neovascularisation of these constructs [117]. Prevascularisation is based on shortening the time required for neovascularisation in the post-implantation period by the inosculation of the pre-formed vasculature with the existing vessels of host tissue [7,122]. To date, the use of several cell types has been reported in prevascularisation studies. Nor et al. prevascularised poly-L-lactic acid (PLLA) scaffolds with HDMECs and showed the anastomosis of them with the natural vasculature of mice [501]. Similarly, Unger et al. reported that co-culture of HDMECs with osteoblasts induced the migration of the host's blood vessels into developed TE construct [493]. Duttenhoefer et al. showed the formation of tubular structures by co-culturing EPCs and mesenchymal stem cells (MSCs) in polyurethane scaffolds for 7 days [125]. Hadjizadeh et al. demonstrated the formation of a network between two neighbouring fibres when PLLA fibres prevascularised with HUVECs were embedded in a fibrin gel and revealed that the presence of fibroblasts was seen on top of the fibrin gel [554].

Following the determination of the optimal culture conditions for HDMECs, three different cell culture systems were investigated in *ex-ovo* CAM assay in terms of improving the angiogenic activity, as a prevascularisation approach. The results of the CAM assay revealed that both HDFs and HDMECs either in isolation or when co-cultured together significantly increased the angiogenic activity in the area of implantation. HDMECs were found to be more effective for stimulating angiogenesis. However, the most significant angiogenic response was observed when HDFs were also present in indirect

contact with HDMECs. This increase in the angiogenic activity is more likely due to the growth factors that are released from cultured ECs in the scaffolds. ECs have previously been shown to secrete VEGF [555,556] and bFGF [557] even under normoxic culture conditions. In addition, co-culture of ECs with the stromal cells has been shown to increase the secretion of more VEGF when compared to mono-cultured cells [558]. Similarly, fibroblasts have previously been reported to play a crucial role in the angiogenic process by generating ECM molecules such as collagen and fibronectin [454,455], growth factors, and pro-angiogenic factors [452,453]. They have previously been shown to secrete VEGF, and fibroblast conditioned media has been reported to enhance the capillary development of ECs [559]. *In vitro* generated ECM has also been demonstrated to increase the neovascularisation of the implanted constructs to a rat animal model, and the researchers hypothesised that this is more likely due to the angiogenic factors that are released to and stored in the generated ECM [560].

The current study reveals essential information about culturing HDMECs in TE constructs and about the angiogenic potential of different types of cell culture systems. The observations made in this study suggest that gelatin coating and co-culture of HDFs both showed a positive impact on HDMECs viability and growth and the physical presence of HDMECs and HDFs either in isolation or in co-culture induced angiogenesis in *ex-ovo* CAM assay.

## 6.7. Conclusion and Future Work

A critical issue in the translation of tissue engineering substitutes into the clinic is the neovascularisation post-implantation. Here, I compared two biocompatible polymers, PHBV and PCL, which are widely used in tissue engineering applications, and selected PHBV for the study of prevascularisation in *ex-ovo* CAM assay. The gelatin coating and co-culture with HDFs were both found to be practicable to increase the favourability of PHBV nanofibres by HDMECs. The results of the CAM assay demonstrated that the presence of HDMECs showed a stronger angiogenic reaction than the introduction of HDFs alone, but the use of HDMECs and HDFs together gave the most significant angiogenic activity.

In future studies, investigating the anastomosis of HDMECs with the host vasculature to confirm the effectivity of prevascularisation technique might be interesting. In addition, the use of patient's stem cells in this prevascularisation system could also provide more

reliable information as the ultimate goal of this technique relies on the use of autologous cells and expansion of them on TE constructs to create a prevascularised construct to shorten the time required for neovascularisation post-implantation [117,561].

# CHAPTER VII

# Development of a bilayer PCL barrier membrane for guided bone/tissue regeneration (GBR/GTR) applications: combining electrospinning and emulsion templating

## 7.1. Aims and Objectives

The aim of this chapter is to develop a bilayer PCL barrier membrane for guided bone/tissue regeneration applications by combining electrospinning and emulsion templating. In order to satisfy the aim; the objectives of this chapter are to:

- Manufacture the PCL PolyHIPE layer by emulsion templating
- Manufacture the PHBV nanofibrous layer by electrospinning
- Investigate the bone promoting properties of PCL PolyHIPE layer
- Evaluate the performance of PCL PolyHIPE for supporting blood vessel ingrowth using *ex-ovo* CAM assay
- Investigate the barrier properties of PHBV electrospun layer

## 7.2. Chapter VI by Pictures

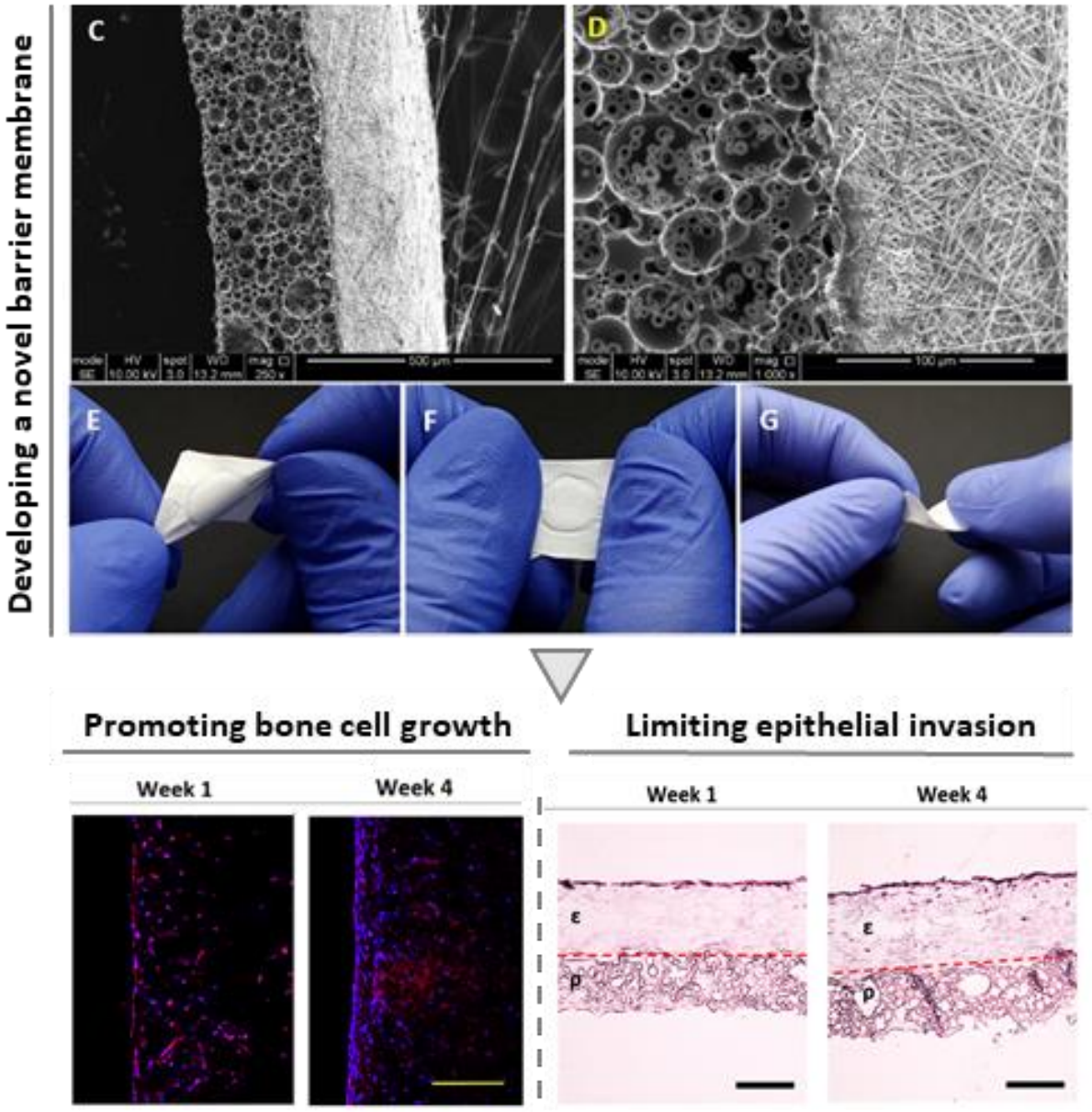

## 7.3. Introduction

Periodontal regenerative procedures require the use of guided tissue regeneration/guided bone regeneration membranes (GTR/GBR) in various conditions such as socket preservation, grafting, maxillary sinus elevation and the treatment of the chronic periodontitis [562]. The main principle of the GTR/GBR procedure is to place a barrier membrane (BM) between epithelial tissue and bone or bone graft to prevent migration of the fast-proliferating epithelial cells into the defect site to be able to preserve a space for infiltration of bone cells into periodontal defect site [563,564].

The earliest developed membranes were made of non-resorbable materials such as cellulose filters, polytetrafluoroethylene (e-PTFE), and titanium meshes but the necessity of a second surgery for removal led to the development of resorbable membranes [565]. The most common natural membranes are made of porcine, bovine, or human collagen. Despite their high biocompatibility, the main disadvantages of collagen membranes are their potential for antigenicity, poor mechanical properties, and rapid degradation [566,567]. Alternatively, synthetic polymers such as PGA and PLLA have been commonly investigated for the fabrication of BMs. Although they are biodegradable and non-cytotoxic, their rapid degradation can generate an acid environment around the implant, which may cause adverse inflammatory tissue reactions [568,569].

PCL is another biocompatible and bioresorbable synthetic polymer, which degrades more slowly and consequently does not produce an overly acidic environment in the degradation process [568]. FDA approved biomedical devices made of PCL are already on the market, which makes PCL a promising material for other biomedical applications. Additionally, due to its ease of fabrication in different forms, PCL is used as a scaffold material for both hard and soft tissue engineering [570]. It has previously been reported for various biomedical applications including drug delivery applications [571,572], periodontal regeneration [573,574], vascular grafts [575], bone tissue engineering applications [576,577], and wound healing [578,579]. One of the main drawbacks of PCL, as with many other synthetic polymers is that it is hydrophobic, which limits the polymer-cell interaction [580,581]. Plasma treatment is one of the most common and effective ways to promote hydrophilicity of the polymer surfaces by adding polar groups to the surface of the material without altering the bulk properties [460,582–585].

A BM is expected to be in contact with both hard and soft tissues, and it has different functions on each side. While being cell occlusive on the side in contact with soft tissue, it should encourage bone regeneration on the other side. There many methods used in barrier membrane fabrication; such as solvent casting [586,587], electrospinning [417,574,588–590], phase inversion, freeze-drying [591,592], and 3D printing [593,594].

Electrospinning is a simple, rapid and versatile technique for fabricating fibres with varying diameters from a few nanometres to several micrometres from a wide variety of materials [595]. PCL is also one of the widely-used polymers that have been electrospun for its use in numerous applications [596]. Several solvents and solvent blends have been reported to be used to dissolve PCL for preparing the electrospinning solution [597]. Although several parameters have been associated with the size of fibres [598], the composition and the ratio of solvents have been demonstrated to have a significant effect on fibre diameters [599]. As electrospun nanofibers are shown to prevent cell infiltration without limiting the diffusion of oxygen and nutrients [22], electrospinning is a promising method to manufacture a physical barrier.

Emulsion templating is another scaffold manufacturing technique where polymer solution and water are mixed in the presence of surfactants to form an emulsion. When the water droplets are encapsulated in a polymer solution, it is called water in oil (w/o) emulsion. If the internal phase volume (water content) is increased over 74% (v/v), the emulsion is called a high internal phase emulsion (HIPE) [536,600–602]. After solidification of the polymer phase (continuous phase) by thermal curing or photo-curing or solvent evaporation, the structure is locked, and water droplets are removed. The resulting porous structure is defined as PolyHIPE. PolyHIPEs are favourable as a tissue engineering scaffolds because of their highly interconnected porous structures which have been previously demonstrated as promoting cell migration and tissue ingrowth [424,603–607].

Manufacturing of scaffolds made of photocurable PCL by using emulsion templating technique is challenging because of the high viscosity of the polymer, which makes it difficult to mix two phases during emulsion formation [53–56]. We have recently developed and reported a production route of PolyHIPEs made of photocurable PCL and showed the biocompatibility of the material by using human dermal fibroblasts [48]. However, this developed composition has not been used for any specific application yet,

and the use of emulsion templated PolyHIPEs in GBR/GTR barrier membrane applications has not previously been reported.

In this study, we combined two methods; emulsion templating and electrospinning to manufacture a bilayer, bioresorbable BM made of polycaprolactone. Emulsion templating is selected for manufacturing of the layer, which will be in contact with bone/bone graft. 250 µm thick PCL PolyHIPE layer was manufactured and treated with air plasma to enhance the cellular infiltration. Following the *in vitro* evaluation of the biological performance, the suitability of PCL PolyHIPE morphology for blood vessel infiltration through the pores was further investigated using an *ex-ovo* CAM assay. Electrospinning was selected to manufacture the nanofibrous barrier layer. Four different solvent compositions were tested in terms of their abilities to enable nanofiber production. The biocompatibility and the barrier properties of the electrospun layer were tested over four weeks *in vitro* by histological staining.

The experimental procedures in this chapter have been conducted in collaboration with my co-worker Betül Aldemir Dikici. Betül was responsible for the production of PCL PolyHIPE layer including the synthesis of PCL methacrylate, preparation of PCL HIPEs, and polymerisation and sectioning of the PCL PolyHIPE layer. She has also conducted the experiments about the biological evaluation of PCL PolyHIPE layer.

## 7.4. Materials

| Chemical / Reagent | Catalogue Number | Supplier |
|---|---|---|
| Alexa Fluor® 594 anti-human CD31 Antibody | 303126 | **Biolegend** |
| Hypermer B246 | - | **Croda** |
| Acetone | 10554634 | **Fisher Scientific** |
| Chloroform | 10784143 | |
| Dichloromethane (DCM) | 10127611 | |
| Dimethylformamide (DMF) | 15562393 | |
| DPX mounting medium | D/5319/05 | |
| Industrial methylated spirit (IMS) | M/4450/17 | |
| Methanol | 10626652 | |

| | | |
|---|---|---|
| Toluene | 10102740 | |
| Triton X-100 | BP151 | |
| Xylene | X/0100/17 | |
| Optimum cutting temperature tissue freezing medium (OCT-TFM) | 14020108926 | **Leica Biosystems** |
| Minimum Essential Alpha Medium (α-MEM) | BE02-002F | **Lonza** |
| Fertilised chicken eggs | - | **MedEggs** |
| Hydrochloric acid fuming 37% | 100317 | **Merck** |
| RCOM King SURO humidified egg incubator | MX-SURO | **P&T Poultry** |
| EC GM 2 Supplement Pack (for HAECs) | C-39211 | **PromoCell** |
| Endothelial Cell Growth Medium 2 (EC GM) (for HAECs) | C-22211 | |
| Human Aortic Endothelial Cells (HAECs) | C-12271 | |
| 2-deoxy-D-ribose (2dDR) | 121649 | **Sigma Aldrich** |
| 37% formaldehyde (FA) solution | F8775 | |
| 4',6-diamidino-2-phenylindole (DAPI) solution | D8417 | |
| AlamarBlue Cell Metabolic Activity Assay | R7017 | |
| Alizarin Red S | A5533 | |
| Amphotericin B | A2942 | |
| Ascorbic acid 2-phosphate (AA2P) | A8960 | |
| Beta-glycerolphosphate (βGP) | 50020 | |
| Bovine serum albumin (BSA) | A7030 | |
| Collagenase A | COLLA-RO | |
| Dimethyl sulphoxide (DMSO) | 472301 | |
| Direct Red 80 (Sirius Red) | 365548 | |
| Eosin Y solution | HT110232 | |
| Ethanol | 51976 | |
| Fetal calf serum (FCS) | F9565 | |
| Gelatin from porcine skin | G1890 | |
| Glutaraldehyde (25%) | G5882 | |
| Goat serum | G9023 | |

| | | |
|---|---|---|
| Hematoxylin solution | HHS16 | |
| L-glutamine | G3126 | |
| Methacrylic anhydride (MAA) | 276685 | |
| Paraformaldehyde (PFA) | 158127 | |
| Penicillin / Streptomycin | P0781 | |
| Pentaerythritol (98%) | P4755 | |
| Perchloric acid | 244252 | |
| Picric acid | 197378 | |
| Photoinitiator (PI) (2,4,6-Trimethylbenzoyl Phosphine Oxide/2-Hydroxy-2-Methylpropiophenone blend) | 405663 | |
| Polycaprolactone (PCL) (Mn: 80.000 g/mol) | 440744 | |
| Polydimethylsiloxane (PDMS) (SYLGARD®184) | 761036 | |
| Tin (II) 2-ethylhexanoate | S3252 | |
| Triethylamine (TEA) | 471283 | |
| Trypan blue | T6146 | |
| Trypsin EDTA | T3924 | |
| Vascular endothelial growth factor (VEGF) | V7259 | |
| ε-caprolactone | 704067 | |
| Alexa Fluor 594 Phalloidin | A12381 | **ThermoFisher Scientific** |

## 7.5. Methods

### 7.5.1. Manufacturing of the PCL PolyHIPE, PCL electrospun, and bilayer membrane

#### 7.5.1.1. Preparation PCL HIPEs

The PCL used in this study is 4-arm PCL methacrylate (4PCLMA), and the detailed synthesis of 4PCLMA (Figure 98A) is described in Section V. 4PCLMA (0.4 g) and the surfactant Hypermer (10% w/w of polymer) were added into a glass vial and heated to 40°C to dissolve surfactant which is crucial for emulsion stability. Solvent blend (150% w/w of polymer, 80% chloroform, 20% toluene (w/w)) and PI (10% w/w of polymer) were added in the 4PCLMA-surfactant mixture, respectively and mixed at 375 rpm using

a magnetic stirrer for 1 minute at RT. Once the homogeneous mixture formed, 2.5 mL of water (internal phase volume 85% v/v) was added dropwise in 2 minutes, and the emulsion was mixed further 2 minutes, as illustrated in Figure 98B.

#### 7.5.1.2. Optimisation of manufacturing of PCL PolyHIPEs

The emulsion templating technique was selected due to its ability to manufacture scaffolds with interconnected architecture. However, during the polymerisation, the material in contact with emulsion has been reported to have a significant effect on PolyHIPE morphology [608].

To find the best manufacturing method in terms of creating interconnected scaffolds, we briefly polymerised PCL HIPEs in PDMS moulds, with the upper surface in contact with air, glass, and PDMS, and we investigated the morphology of the surface and transverse sections with SEM.

#### 7.5.1.3. Manufacturing of PCL PolyHIPE layer

PCL HIPEs were manufactured by either polymerisation in silicone moulding and sectioning of 250 μm samples using a vibratome (Bio-Rad Polaron Division) or syringe moulding and sectioning of 1 mm samples using a scalpel. For the fabrication of a bilayer BM, 250 μm sections of PCL PolyHIPE were used. 1 mm thick PCL PolyHIPE samples were used alone for MLO-A5 cell culture, measurements of their metabolic activity, Alizarin Red and Sirius Red staining, histological evaluation of infiltration of MLO-A5s and CAM experiments.

Briefly, PCL HIPE was pipetted into either silicon templates or 2.5 mL syringes (diameter of 6 mm) and cured 3 minutes to both sides using a UV belt curer with a 100 $W.cm^{-2}$ UV bulb (Figure 98C). The resulting parts were recovered, soaked in 100% methanol for 24 hours with four changes to remove any remaining contaminants of surfactant, solvent or uncured material. Then the samples were left in methanol (50% (v/v) in water) for 24 hours and water for a further 24 hours. Finally, the samples were taken out from the water and left in the freezer (-80°C) for an hour then transferred into a vacuum oven and left for a day to preserve the porous structure of PCL PolyHIPE without any collapse.

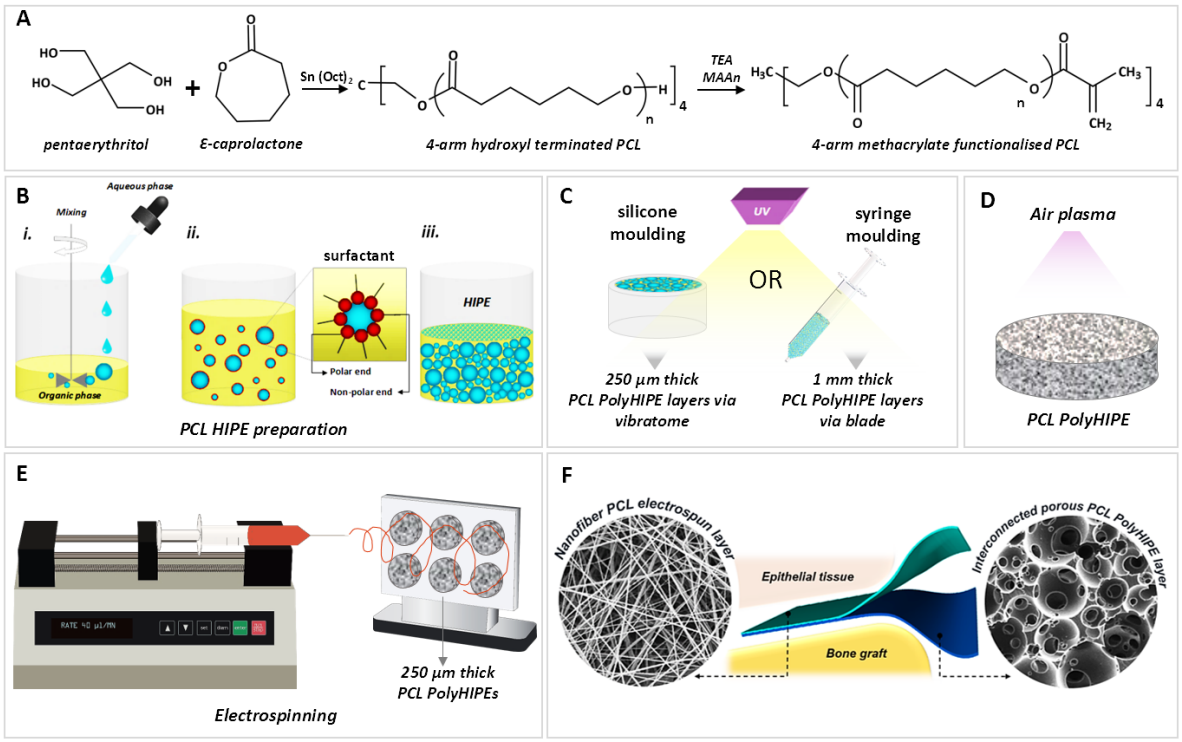


***Figure 98:*** *Summary of the manufacturing process of the bilayer membrane. (A) Synthesis of 4-arm hydroxyl-terminated PCL and methacrylate terminalisation reaction (B) PCL PHIPE preparation process, (C) the polymerisation of PCL HIPEs to obtain PCL PolyHIPE and slicing the samples, (D) air plasma treatment of PCL PolyHIPE, (E) electrospinning of PCL on 250 µm thick PCL PolyHIPE layer, (F) Final representation of the bilayer BM*

For the fabrication of bilayer BM, 250 µm sections of PCL PolyHIPE layer were obtained using a vibratome (Bio-Rad Polaron Division). For metabolic activity, Alizarin red, Sirius red, and CAM experiments, 1 mm sections of dry samples (obtained from syringe moulding) were taken using a scalpel, and these monolayer PCL PolyHIPE samples were used.

Air plasma (Diener Electronic, Ebhausen, Germany) was applied on both surfaces of the PCL PolyHIPE with a power of 50 W and a pressure of 0.8 mbar for 60 seconds to improve cell attachment to the hydrophobic surfaces as demonstrated in our previous work (Figure 98D) [609].

#### 7.5.1.4. Assessment of solvent compositions in terms of their ability to form the nanofibrous structure

Four solvent compositions were investigated in terms of their ability to form the nanofibrous structure. PCL (10% (w/w)) pellets were dissolved in acetone (100%),

acetone:chloroform (30:70 w/w), DCM:methanol (90:10 w/w), and chloroform:DMF (70:30 w/w). The mixtures were magnetically stirred overnight.

Solutions (~5 mL) were loaded into 5 mL syringes fitted with 0.6 mm inner diameter (ID) blunt syringe tips. The syringe was then placed in a syringe pump (GenieTMPlus, KentScientific, Connecticut, USA). Aluminium foil was used as the collector and placed at a distance of 17 cm from the needle tips. The pump was set to 40 µL/minutes, and 17 kV voltage was applied both to the collector and the tips. Solutions of PCL prepared with various solvent blends were then electrospun at RT for 40 minutes.

Single-layer of electrospun PCL (without PolyHIPE layer) manufactured using each polymer solutions were morphologically investigated, as explained in Section 3.1.3. In the rest of the text, the following nomenclatures are used for electrospinning groups. Acetone (100) defines acetone (100%). Acetone:chloroform (30:70) refers to acetone:chloroform (30:70 w/w). DCM:methanol (90:10) denotes DCM:methanol (90:10 w/w), and chloroform:DMF (70:30) refers to chloroform:DMF (70:30 w/w).

#### 7.5.1.5. Manufacturing of bilayer PCL BM

The aluminium foil collector was sprayed with methanol, and 250 µm thick sections of PCL PolyHIPE layer were placed onto it. This step was performed immediately before electrospinning of the PCL barrier layer. Chloroform:DMF (70:30) solvent blend was used for the production of PCL electrospun barrier layer as explained in Section 3.1.3. 10% PCL solution was loaded into 5 mL syringes fitted with 0.6 mm ID blunt syringe tip. PCL was then electrospun onto PCL PolyHIPE layers with a rate of 40 µL/minutes and a voltage of 17 kV for 40 minutes (Figure 98E, F).

### 7.5.2. Morphological, mechanical and surface characterisation

#### 7.5.2.1. Morphological characterisation

Micro-architectures of PCL PolyHIPE, PCL electrospun, and bilayer BM were examined using a SEM. All samples were gold-coated with a voltage of 15 kV for 2.5 minutes using a gold sputter coater (Edwards sputter coater S150B, Crawley, UK) to increase conductivity. SEM (FEI Inspect F, Orlando, USA) was used with 10 kV power.

SEM images of the PCL fibres and PCL PolyHIPE were analysed for the determination of the fibre diameters, pore size distributions, and window size using ImageJ software (Bethesda, MD, USA). Total of 54 different fibre diameters and 54 pore sizes were measured for each group of PCL electrospun layers, 100 pores and 150 windows were measured for PCL PolyHIPE. All measurements were taken from three different areas of three different samples.

#### 7.5.2.2. Mechanical characterisation

The bilayer BM was mechanically tested under dry and wet conditions using a mechanical testing unit (BOSE Electroforce Test Instruments, Minnesota, USA) equipped with a 22.5 N load cell. Briefly, mechanical testing samples were cut into 10 mm x 3 mm pieces and clamped to the device with two tensile grips, and the tensile tests were performed on each sample at a rate of 0.1 mm/s until the samples failed. Elastic modulus (E), UTS and elongation (%) values were calculated from stress (σ) and strain (ε) curves of each sample. The elastic modulus was determined as the slope of the initial linear section of the curve. UTS was obtained from the curve as the maximum stress that the samples could withstand. Ultimate elongation was measured as the percentage elongation of the samples at the break.

#### 7.5.2.3. Contact angle measurements

Contact angle measurements were conducted to evaluate the effect of air plasma treatment on the hydrophilicity of PCL PolyHIPE. In brief, a 5 µL water droplet was dropped onto the surface of the either non-treated or plasma-treated PCL PolyHIPE, and the water contact angles were determined via drop shaper analyser (Krüss DSA100, Germany) under ambient laboratory conditions.

### 7.5.3. Assessment of the biological performance of the developed barrier membrane

#### 7.5.3.1. Cell culture of HDFs

HDFs were isolated from STSGs taken from patients using a well-established protocol [484]. Briefly, the dermis was minced into 10 $mm^2$ pieces, and the pieces were incubated overnight at 37°C in 0.5% (w/v) collagenase A solution. The cell suspension was then centrifuged at 1000 rpm for 5 minutes and resuspended and cultured in DMEM

containing 10% (v/v) FBS, 100 IU mL $^{-1}$ penicillin, 100 µg mL $^{-1}$ streptomycin, 2mM L-glutamine and 0.625 µg mL $^{-1}$ amphotericin B. HDFs were used between passage 4-8. The investigations were carried out following the rules of the Declaration of Helsinki of 1975. Ethical approval for the tissue acquisition was granted by the National Research Ethics Service (NRES) Committee Yorkshire & The Humber–Sheffield (REC ref: 15/YH/0177, REC opinion date: 03/06/2015).

#### 7.5.3.2. Seeding of HDFs onto the PCL electrospun layer to confirm the barrier properties

Bilayer BMs were used as test samples to measure the metabolic activity and for histological assessment of HDFs. BMs were cut into 10 mm circles using a biopsy punch (Stiefel, Slough, UK) and 70% ethanol solution was used as an antiseptic agent for 45 minutes prior to cell seeding. $2\times10^4$ HDFs were trypsinised, centrifuged, and resuspended in 100 µL of DMEM growth medium and pipetted on PCL electrospun (barrier) side of the bilayer BM. Before submerging the BMs into HDFs culture medium, they were incubated at 37°C for 2 hours to allow HDFs to attach. BMs were kept in culture for 4 weeks by changing the culture medium every 2 days.

#### 7.5.3.3. Cell culture of murine long bone osteocytes (MLO-A5)

MLO-A5, murine osteoblast cell line (kindly donated by Dr Lynda Bonewald) was used to evaluate the potential of PCL PolyHIPE as GBR membrane as it was previously used for evaluation of bone tissue engineering applications [604]. The T75 flasks were coated with 0.1% gelatin solution for 2 hours at 37°C and washed gently with PBS prior to cell culture. Cells were expanded on gelatine-coated T75 flasks in basal media containing α-MEM supplemented with 10% fetal bovine serum, 2mM L-glutamine and 100 mg/mL penicillin/streptomycin. MLO-A5s cultured until 90% confluence and media was changed in every 2-3 days. Cells were used between passages 35-36.

#### 7.5.3.4. MLO-A5 cell seeding onto the PCL PolyHIPE layer

To be able to test the full infiltration capacity of MLO-A5s through PCL PolyHIPE, monolayer, 1 mm PCL PolyHIPE samples (without electrospun layer) were used for biological assessment of PCL PolyHIPE.

Prior to cell seeding, PCL PolyHIPEs were left in 70% ethanol for 2 hours and then transferred into PBS in sterile conditions, 4 washes were applied in 24 hours to replace the ethanol with PBS. Finally, they were conditioned with basal media for an hour in the incubator in 24 well plates to remove the PBS completely and not to dilute the media used during the cell seeding stage with PBS. MLO-A5s were trypsinised, counted, and centrifuged. The cell pellet was re-suspended in fresh basal media (2.5 x $10^4$ cells in 20 µm). The cell suspension was placed over the surface of each PCL PolyHIPE homogenously. Before PolyHIPE layers were moved to the fresh wells, and 2 mL basal media was supplied into the wells, they were left for 2 hours in the incubator (37.5°C, 5% $CO_2$) for cell attachment. 2 mL of media was supplied. A day after, basal media was replaced with supplemented media consisting of basal media supplemented with 5 mM β-glycerophosphate (βGP) and 50 µg/mL L-Ascorbic Acid 2-phosphate (AA2P). Media was changed every 2–3 days.

#### 7.5.3.5. Assessment of metabolic activity of the cells seeded on both layers

AlamarBlue® assay was performed in order to track the metabolic activities of HDFs on the PCL electrospun and MLO-A5s on PCL PolyHIPE. 0.1 mM AlamarBlue® working solution was prepared by 10× dilution of the 1 mM AlamarBlue® stock solution with growth medium. At days 1, 7, 14, 21, and 28 growth media were removed, and the samples were washed with PBS. 1 mL of AlamarBlue® working solution was added to each well and incubated at 37°C for 4 hours. After an incubation period, 200 µL of the solution was transferred into 96-well plate, and the fluorescence readings were done at an excitation wavelength of 540 nm and an emission wavelength of 635 nm. Fresh samples were used for the measurements at each time point.

#### 7.5.3.6. Assessment of calcium deposition of MLO-A5s

Alizarin red powder was dissolved in deionized water at 1 w/v% in a water bath and filtered to remove particles to make Alizarin red solution (ARS). PCL PolyHIPEs were submerged in 1 mL of ARS solution and incubated for 1 hour. ARS solution was removed, and the samples were washed every five minutes with deionized water and gentle orbital shaking until the water remains clear. They were submerged with 1 mL of 5% perchloric acid to destain and left for further 30 minutes with gentle orbital shaking. 150 µL of the

destain solution in triplicates were transferred into a clear 96 well plate and read at an absorbance of 405 nm.

#### 7.5.3.7. Assessment of collagen deposition of MLO-A5s

Sirius red (direct 80) powder was dissolved in saturated picric acid (1 w/v%) to form Sirius red solution (SRS) and filtered to ensure no particles remain. PCL PolyHIPE's were submerged with 1 mL of SRS solution and left for 1 hour. SRS solution was removed, and the samples were washed every five minutes with deionized water and gentle orbital shaking until the water remains clear. They were submerged with 1 mL of 0.2 M sodium hydroxide (NaOH):methanol (1:1) to destain and left for 30 minutes with gentle orbital shaking. 150 µL of the destain solution in triplicates were transferred into a clear 96 well plate and read at an absorbance of 405 nm.

#### 7.5.3.8. Haematoxylin & Eosin (H&E) and Alizarin red staining

Bilayer BM and PCL PolyHIPE cultured with HDFs and MLO-A5s, respectively for 1-week and 4-week, and PCL PolyHIPE on CAM were stained with H&E using a standard protocol [358]. Briefly, samples were washed with PBS before (once) and after (three times) fixing them in 3.7% FA for 30 minutes at RT. Meanwhile, cryomoulds were filled with OCT-TFM. Samples were embedded into it, and the rest of the volume was then filled with OCT-TFM to the top. Cryomoulds were placed into liquid nitrogen and incubated for 5-7 minutes until solidified. Frozen blocks were fixed on mounting platforms, and placed into a cryostat (Leica CM1860 UV, Milton Keynes, UK) before sections were sliced at 5-10 µm and immediately mounted onto the surface of Thermo SuperFrost® Plus slides. For H&E staining, slides were stained with hematoxylin for 90 seconds and eosin for 5 minutes. For calcium staining, slides were stained with 2% (w/v, in water) ARS for 5 minutes. Excess dye is shaken off, and the slides were rinsed, dehydrated, cleared and mounted the slide using the permanent mounting medium.

#### 7.5.3.9. Preparation of biological samples for SEM

The protocol for the preparation of biological samples for SEM has previously been summarised in Table 19. On day 28, the PCL PolyHIPE discs seeded with MLO-A5s were washed 3 times with PBS and fixed with 2.5% glutaraldehyde at RT for 1 hour and rinsed

with PBS. Then the discs were soaked in deionised water for 5 minutes prior to dehydration of the samples with serial ethanol washes. Finally, HMDS is used as the chemical drying agent, and the discs were soaked in HMDS:ethanol (1:1) solution for 1 hour and transferred into 100% HMDS for 5 minutes. The samples were then air-dried overnight in a fume hood and gold-coated at a current of 15 mA for 2.5 minutes with a gold sputter (Edwards sputter coater S150B, Crawley, England) prior to imaging under SEM (FEI Inspect F, Orlando, USA).

#### 7.5.3.10. Fluorescent staining

At days 7 and 28, PCL PolyHIPE discs were fixed with 3.7% FA for 30 minutes and washed gently with PBS prior to submerging into 0.1% (v/v) Triton X 100 (in PBS) solution for 20 minutes. After serial PBS washes, phalloidin-TRITC (1:500 diluted in PBS from stock solution) solution was added onto samples to visualize F-actin filaments of the cells and incubated for 30 minutes at RT in the dark. Discs were washed 3 times with PBS. To stain the cell nuclei, DAPI solution (1:1000 diluted in PBS) was added onto the PolyHIPE discs and incubated for 10-15 minutes at RT in the dark; samples were then washed 3 times with PBS and imaged under a fluorescent microscope (Olympus IX3, Tokyo, Japan).

#### 7.5.3.11. *Ex-ovo* CAM assay

An *ex-ovo* CAM assay was used to evaluate the potential of PCL PolyHIPE layer for the suitability of blood vessel ingrowth, as described previously [89,241]. Briefly, fertilised chicken eggs (Gallus Domesticus) were purchased from Henry Stewart & Co. MedEggs (Norwich, UK) and cleaned with 20% IMS solution. Eggs were incubated at 37.5°C for 3 days in an egg incubator (RCOM King SURO, P&T Poultry, Powys, Wales). At the end of day 3, the embryos were transferred gently into sterile Petri dishes and incubated at 38°C in a humidified cell culture incubator (Binder, Tuttlingen, Germany). On day 7, PCL PolyHIPE discs were implanted to CAM, and the chicks were incubated for further 7 days. On day 14, the chicks were euthanised, and the CAMs with the PolyHIPE discs integrated to them were removed and fixed in 3.7% FA solution. Sections of the CAMs were taken and stained with H&E as described previously.

### 7.5.4. Statistical analysis

Statistical analysis was carried out using one-way and two-way analysis of variance (ANOVA) using statistical analysis software (GraphPad Prism, California, USA). Where relevant, n values are given in figure captions. Error bars indicate standard deviations in the graphs unless otherwise stated.

## 7.6. Results and Discussion

### 7.6.1. Manufacturing and characterisation of the PCL PolyHIPE layer

The surface of PCL PolyHIPEs polymerised in contact with air, glass, or PDMS showed different morphologies (Figure 99A-C). When the surface was not covered by any substrate, and UV was directly applied on PCL HIPEs, the surface was porous, but it did not have open interconnected cellular morphology (Figure 99A). When the surface of the HIPE was in contact with glass, the surface showed microscale roughness, rather than pores (Figure 99B). In terms of interconnectivity, the best surface morphology was obtained when the PDMS sheet was used as a cover. PCL PolyHIPE surfaces created this way had a mixture of open and closed porous morphology (Figure 99C).

The significant influence of the mould material on PolyHIPE has been reported previously [608]. This study correlated the surface interconnectivity with the following potential scenarios on the PolyHIPE-mould interface; (i) PolyHIPE can potentially bind to mould surface leading to difficulties in demoulding, (ii) the mould can leach materials leading to contamination of the PolyHIPE surface, and (iii) partial phase separation of the emulsion which leads to closed-pore PolyHIPE surfaces.

Figure 99D shows the transverse section of PCL PolyHIPE. It has a homogenous, open cellular architecture with interconnected porosity. Pore interconnects are pathways for cells, waste and nutrients, the interconnectivity of the scaffold is a crucial feature for cell invasion, tissue integration and vascularisation [610–613]. To be able to benefit from the interconnected inner morphology of the scaffolds, the PCL PolyHIPE layer was decided to be created by sectioning bulk pieces into slices as described in Section 3.1.4.

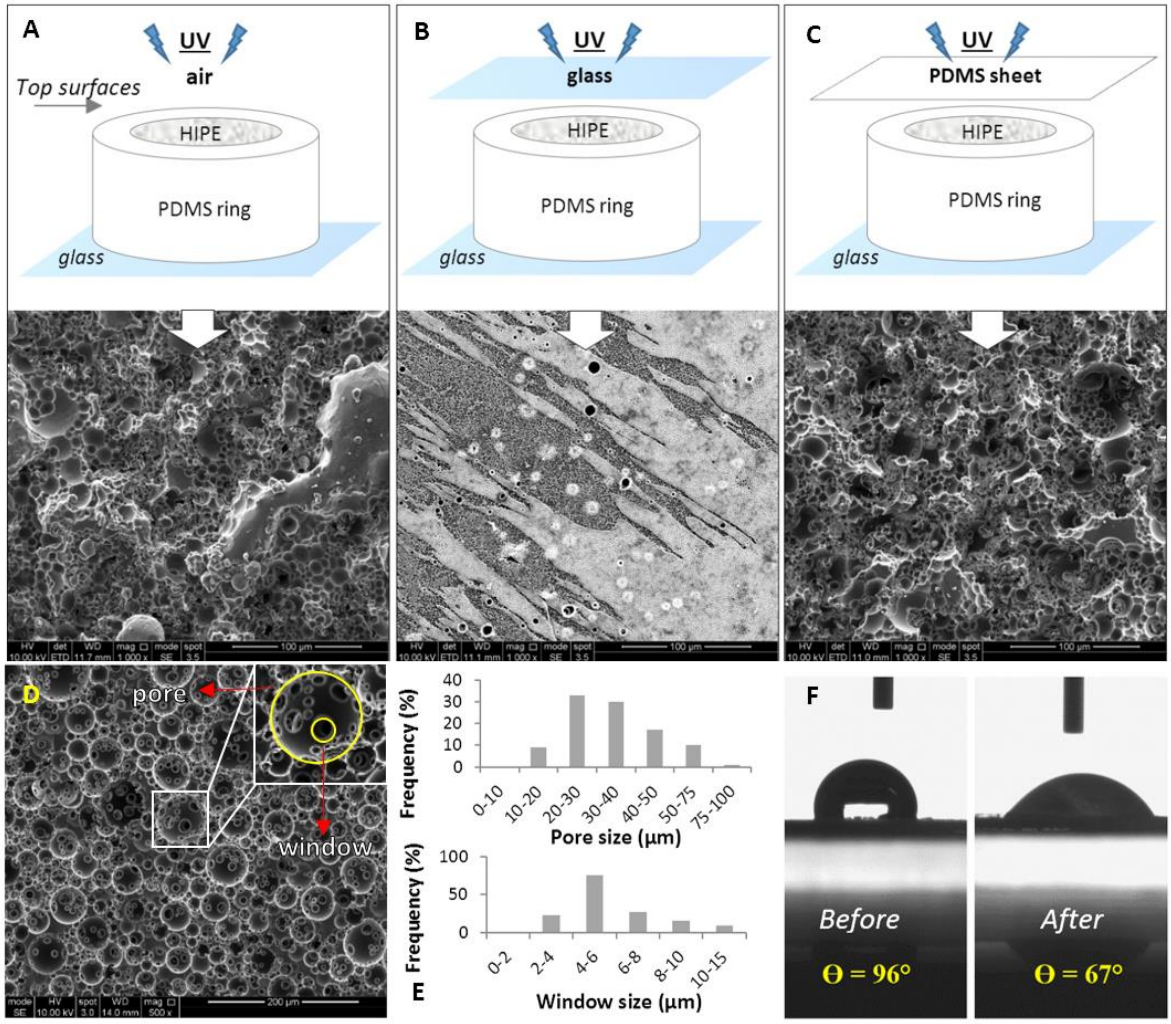


***Figure 99:*** *SEM images of the top surfaces PCL PolyHIPEs cured in contact with; (A) air, (B) glass, and (C) PDMS sheet. (D) SEM image of the transverse section of PCL PolyHIPEs. (E) Pore size and window size distributions of the inner section. (F) Contact angle measurements of a water droplet on PCL PolyHIPE before and after air plasma treatment (n=3)*

The pore sizes of the PCL PolyHIPE layer were distributed between 10-78 µm; the average pore size (D) was found 34±13 µm, 90% of the pores have the pore sizes between 20-75 µm range (Figure 99E). The window sizes were distributed between 2-13 µm range, and the average window size (d) was measured as 6±2 µm (Figure 99E), which gives the degree of connectivity (d/D) as 0.18. In our previous study, when the same solvent composition was used to dilute PCL (80:20 chloroform:toluene (w/w)) the average pore size and the window size was found 20±7 µm and 4±2, respectively [424]. The difference between the pore and window size found in the previous study and the current work can be explained with the two main compositional changes; (i) increasing the internal phase volume from 82% to 85%, and (ii) increasing the total solvent volume from 0.40 mL to 0.46 mL. A higher internal phase volume is expected to reduce the

average pore size while increasing the average window diameter as water droplets will need to be more tightly packed. On the other side, the increasing solvent amount is expected to show a dramatic increase in the average pore diameter [614]. The overall effect of these two compositional changes resulted in approximately 50% increase in average pore size and window diameter.

Oxidising the surface by plasma treatment is one of the most popular methods for enhancing cell attachment [609,615–619]. In this study, our finding also proved that air plasma treatment changes the surfaces from hydrophobic to hydrophilic and this change encourages the cell attachment and cellular infiltration on PCL PolyHIPE layer which will be further discussed following sections. Contact angles of the water droplets on non-treated (P-) and air plasma treated (P+) PCL PolyHIPEs were measured as 67±4° and 96±4°, respectively (Figure 99F).

### 7.6.2. Assessment of the metabolic activity of MLO-A5s on PCL PolyHIPE and the cellular infiltration through PCL PolyHIPE layer

At all-time points, the metabolic activity of MLO-A5s cultured on P+ PCL PolyHIPEs was slightly higher than MLO-A5s cultured on P- PCL PolyHIPEs, but there was no statistical difference observed between these two groups (Figure 100A). Metabolic activities of MLO-A5s on both P+ and P- PCL PolyHIPEs increase from day 1 to day 28 gradually, but the dramatic decrease was observed in the metabolic activity of the MLO-A5s on TCP after day 7 which is also discussed in Section 4.4.

Figure 99B and 99C clearly show the positive impact of air plasma treatment of PCL PolyHIPE on the attachment of MLO-A5s to the surface at day 28. While the layer of MLO-A5s is peeled off from the surface of P- PCL PolyHIPE, cells on P+ PCL PolyHIPE are still integrated with the PolyHIPE layer. The preparation steps of the biological samples for SEM includes multiple washing steps and drying (Section 3.3.9). The loosely attached cell layer detached from P- PCL PolyHIPE at the end of all these steps, probably due to limited cell penetration into the pores.

Although air plasma treatment seems as it has not had a significant effect on the metabolic activity of MLO-A5s, H&E and fluorescent images support the finding from SEM images, and they show that air plasma treatment has a huge impact on cell infiltration (Figure 100D, E). At week 1, while MLO-A5s only accumulated on the surface of the P- PCL

PolyHIPE with nearly no infiltration, they were observed as migrating through the pores the P+ PCL PolyHIPE.

Even during the seeding of the MLO-A5s on the PCL PolyHIPE layer, the positive effect of plasma treatment was observed. Once the cell suspension was placed on the top of the PCL PolyHIPE, it immediately absorbed by P+ PolyHIPE but stayed as a droplet on the P- layer. This indicates that even from the cell-seeding stage onwards, plasma treatment encourages cells to migrate into the pores of the PCL PolyHIPE layer. Although MLO-A5s tend to densely accumulate on the top of both PCL PolyHIPEs at week 4, cell migration up to 400 μm was observed on P+ PolyHIPEs. This positive influence of air plasma treatment on polymer scaffold has also been demonstrated *in vivo*. Valence et al. had reported improvement of cell attachment and infiltration within a vascular graft upon plasma treatment when materials were implanted subcutaneously [585].

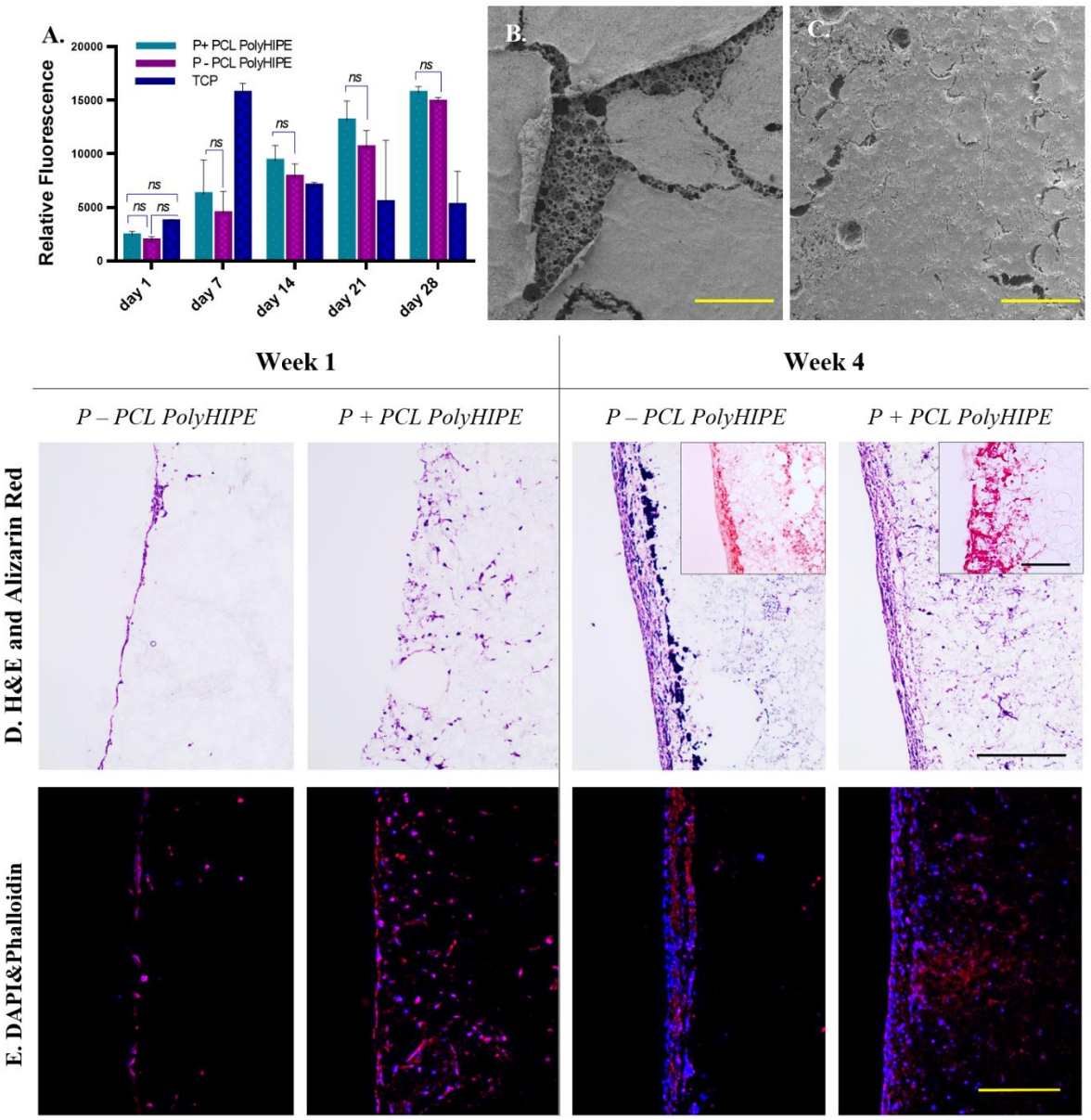


***Figure 100:*** *(A) Metabolic activity of MLO-A5s cultured on P-, P+ PCL PolyHIPEs, and TCP for 4 weeks. SEM images of the top surfaces of (B) P+ and (C) P- PCL PolyHIPEs cultured MLO-A5s on for 4 weeks (Scale bar represents 500 µm). (D) H&E and Alizarin Red, and (E) Fluorescent staining of MLO-A5s cultured on P+ and P- PCL PolyHIPEs for 1 week and 4 weeks (Scale bar represents 250 µm, blue: DAPI, red: Phalloidin TRITC)*

Interestingly, on H&E slides, very small-sized haematoxylin-stained particles (different than haematoxylin stained cells) were observed only at week 4 at both P+ and P- PCL PolyHIPEs (Figure 100D). Fluorescent staining shows that they are not cells. It has been previously reported that haematoxylin selectivity stains calcium-containing particles [620]. Alizarin red staining images shows densely accumulated calcium on the top of P-PCL PolyHIPE and comparably less dense stains in deeper pores, while there is dense calcium deposition P+ PCL PolyHIPE up to 400 µm deep (Figure 100D).

### 7.6.3. Assessment of the extracellular matrix (ECM) deposition of MLO-A5s on PCL PolyHIPE layer

As MLO-A5s cultured in supplemented media, they were expected to deposit calcified ECM [604,621,622]. Prideaux et al. previously reported that supplementation of MLO-A5 cell cultures with AA2P and βGP showed a significant increase in ECM mineralisation compared to the non-supplemented group [14].

Calcium and collagen deposition on P+ PCL PolyHIPE gradually increased from day 7 to day 28 (All subsequent studies were conducted on P+ PCL PolyHIPE only). ECM deposition, mineral nodules, and collagen fibres of MLO-A5s cultured on PCL PolyHIPE layer for 4 weeks are shown in Figure 101B. An SEM image of the cross-section of the PCL PolyHIPE shows the pores densely filled with cells and extracellular material (Figure 101C). Additionally, sub-micrometric crystalline debris was observed in regions beyond the maximum cell ingrowth (Figure 101D, E), these indicate the existence of calcium deposits deep within the PolyHIPE layer, as also observed in on H&E and Alizarin red images.

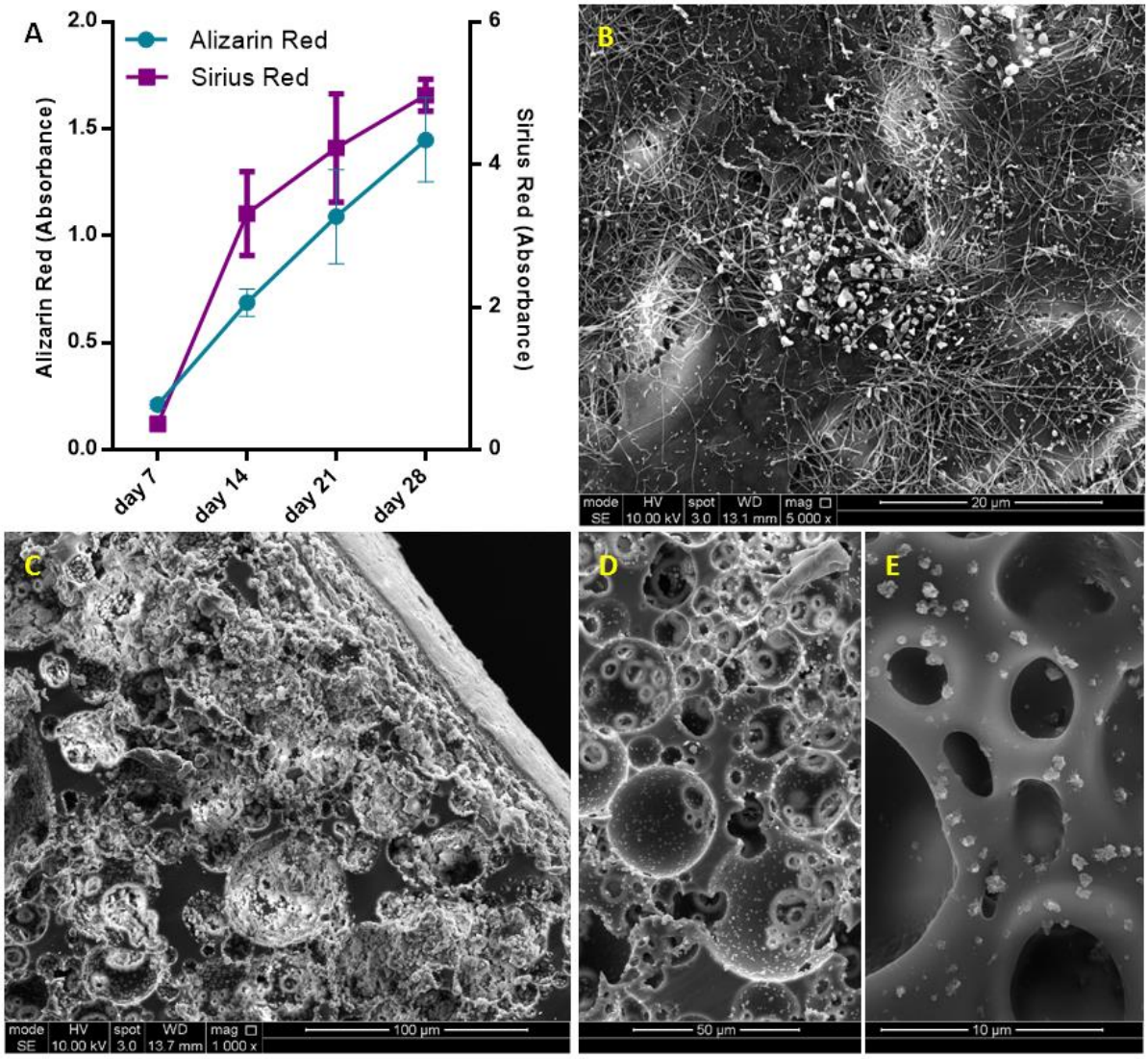


***Figure 101:*** *(A) Assessment of calcium and collagen deposition of MLO-A5s after 7, 14, 21 and 28-day culture on PCL PolyHIPE by using Alizarin Red and Sirius Red, respectively. (B) Surface (C, D, E) cross-section of PCL PolyHIPE cultured with MLO-A5s for 28 days in supplemented media*

These calcium deposits look similar to surfaces of PolyHIPE layer incubated in simulated body fluid, which is commonly used to test the ability of the formation of bone-like apatite or mineral deposition on scaffolds [623–625]. The source and mechanism of the formation of the deposited calcium-containing crystals will be investigated in future studies.

### 7.6.4. Assessment of the performance of PCL PolyHIPE for supporting blood vessel ingrowth using *ex-ovo* CAM assay

The CAM assay is a well-established assay for the assessment of angiogenesis and initial response to biomaterials [89,241,480]. In an *ex-ovo* CAM assay, the embryos are

transferred into petri dish on day 3 (Figure 102A) and incubated until day 7 (Figure 102B) which is the day of material implantation. At day 14, the following features can be assessed macroscopically (Figure 102C) and histologically (Figure 102D): (i) biocompatibility, (ii) cellular infiltration capacity and (iii) the performance of the PCL PolyHIPE layer for supporting vascularisation.

Our laboratory has reported the average survival rate for the *ex-ovo* CAM assay as 68% for intermediate and 83% for experienced users [241]. The survival rate of the chicks was approximately 75% and 73% for non-implanted, and PCL PolyHIPE implanted groups, respectively, in line with previous investigations. Thus, the PCL PolyHIPE showed good biocompatibility, and the implantation of the material did not affect the survival rate of the chicks.

The integration of the CAM tissue into PCL PolyHIPE was examined. Extensive cell infiltration was observed from the CAM tissue to PCL PolyHIPE, showing complete integration of the material with the membrane. During the isolation of the PCL PolyHIPE from the CAM, it was not possible to separate it from the CAM, which is also an indication of strong integration. This is in line with studies reported by other groups on the good-integration of PCL porous scaffolds with CAM [626–628]. The infiltration capacity of the cells into PCL PolyHIPE was better in the *ex-ovo* CAM assay (Figure 102D) when compared with the *in vitro* histology data (Figure 100D). This is potentially due to the continuous contact of the PCL PolyHIPE with a dense and dynamic cell population in the CAM.

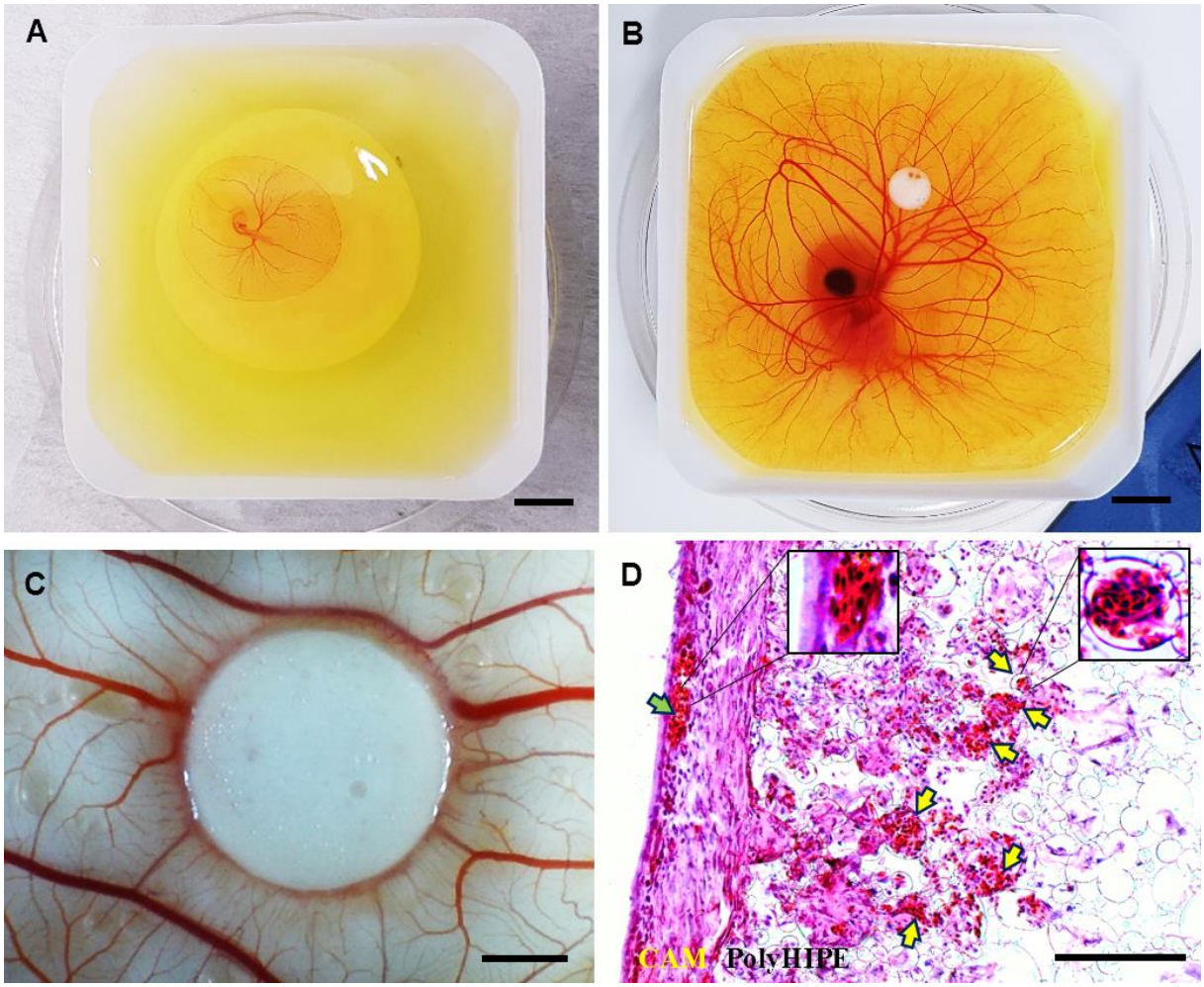


***Figure 102:*** *Chick embryos in a petri dish on (A) embryonic development day 3 and (B) embryonic development day 7 (Scale bar represents 10 mm). (C) PCL PolyHIPE on CAM at day 14 (Scale bar represents 2 mm). (D) H&E images of PCL PolyHIPE on CAM at day 14. (Green arrow indicates the blood vessel on CAM itself; yellow arrows indicate the blood vessels in PCL PolyHIPE. Scale bar represents 100 µm)*

Assessment of the PolyHIPE material on the CAM demonstrated that the structure and the pore size of the PolyHIPE were suitable for supporting blood vessel ingrowth through the PolyHIPE. H&E staining shows that alongside the high level of integration of the host CAM tissue with the PolyHIPE layer, many blood vessels were found growing into the pores of PCL PolyHIPE and through the interconnections (Figure 102D) in only 7 days.

Current understanding of vascularisation of porous scaffolds indicates that the pore size should be at least 250 µm for vascularisation to occur [24,26], but some studies suggest smaller pore sizes can also allow for the ingrowth of blood vessels. Madden et al. have shown that 30-40 µm pore size with 15 µm interconnects are suitable for vascularisation in rats [629]. Similarly, Baker et al. reported that particulate-leached PCL scaffolds with 5-200 µm pore range allowed extensive vascularisation in the scaffold when implanted

subcutaneously into rats [630]. Klenke et al. observed vascularisation in ceramic particles with macropores ranged from 40 to 280 μm [631]. Finally, our group has demonstrated the vascularisation of polylactic acid electrospun scaffolds with a mean pore size of 4.25 μm in the CAM assay [69].

By using the CAM assay, we have shown the performance of the developed BM for supporting tissue integration and vascularisation. Both are critical factors in avoiding delay in osteogenesis and tissue regeneration and overcoming the rejection of an implant [632,633].

### 7.6.5. Assessment of solvent compositions in terms of their ability to form the nanofibrous structure

The mean diameters of the PCL fibres where polymer solutions were prepared with different solvents were 0.35 ± 0.10 μm, 0.74 ± 0.32 μm, 1.69 ± 0.75 μm, and 0.47 ± 0.22 μm, and the average pore sizes were 6.28 ± 2.30 μm, 8.34 ± 4.96 μm, 9.84 ± 5.25 μm, and 3.57 ± 2.08 μm for acetone (100), acetone:chloroform (30:70), DCM:methanol (90:10), and chloroform:DMF (70:30) groups, respectively (Figure 103).

Except for the acetone (100) group, a decrease in the pore sizes was observed when the diameter of the PCL fibres gets smaller. Although the acetone (100) led to the formation of the smallest diameter PCL fibres, the smallest pore size was calculated for the electrospun layer prepared with chloroform:DMF (70:30).

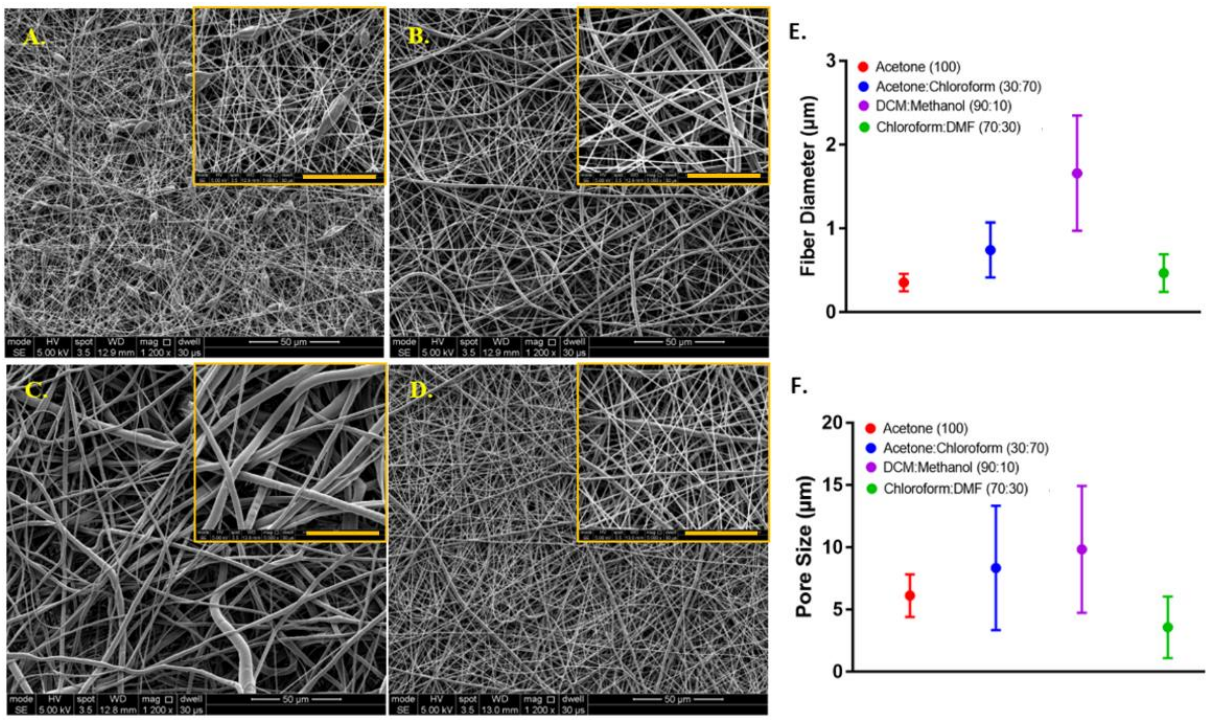


***Figure 103:*** *Morphological characterisation of the electrospun PCL fibres, where polymer solutions were prepared with different solvents. SEM image of PCL electrospun prepared by dissolving PCL in (A) acetone (100), (B) acetone:chloroform (30:70), (C) DCM:methanol (90:10), (D) chloroform:DMF (70:30). The graphs show (E) the fibre diameter and (F) the pore size distributions, respectively. Yellow scale bars represent 20 µm*

When acetone was used as the sole solvent, it was difficult to electrospin the solution, and bead formation occurred. The undesirable bead formation during electrospinning is likely to increase pore size between the fibres [634]. One of the main reason for the formation of thinner fibres and beads has been reported as the lower viscosity of the electrospinning solution [635]. It has previously been shown that among the five solvents used in this study, acetone has the lowest viscosity [636]. Zverev et al. reported that the viscosity of the polymer solution changes with the solubility, and low viscosity is linked with poor solubility when other parameters kept constant [637].

The electrospinnability of the PCL solutions from high to low was: chloroform:DMF (70:30) > acetone:chloroform (30:70) > acetone (100) > DCM:methanol (90:10). The quality of the PCL electrospinning was assessed based on smooth fibre formation, bead or particle formation and continuous electrospinning of the solution, which depend on parameters such as solubility, viscosity, dielectric constant, and conductivity [638].

The solubility of the polymer in a solvent has a major effect on electrospinning nanofibres. DCM, methanol, chloroform, DMF and acetone (as single solvents or solvent

blends) are common solvents for dissolving PCL and widely used for the production of PCL fibres with electrospinning [597,639]. Among these solvents, PCL has a higher solubility in chloroform and DCM, whereas the solubility of PCL is poor in DMF, acetone, and methanol [640].

When acetone was used as the single solvent to dissolve PCL, the solution resulted in poor electrospinnability and the formation of undesired beads during the electrospinning process. Using the acetone:chloroform (30:70) solvent blend significantly increased the electrospinnability of PCL, which can be explained by the addition of chloroform to the solvent mixture, in which PCL has higher solubility [641]. The ability to electrospin PCL dissolved in DCM:methanol (90:10) was very poor, and we did not manage to obtain nanofibers when this solvent used for electrospinning. This can be explained by the low dielectric constant and conductivity of the main solvent, DCM, in the solvent blend [642]. The best solvent blend for electrospinning PCL nanofibers was chloroform:DMF (70:30) solvent composition used. Although DMF is not classified as a good solvent for PCL, it has a high dielectric constant and, it is a polyelectrolyte [643]. Due et al. previously reported that the addition of DMF to the solvent blend improves the electrospinnability of PCL and leads to smaller diameter fibre formation. [644]. Kanani et al. had shown that when DMF was added to methylene chloride, and the solvent mixture used for electrospinning PCL, the spinning process was improved, and uniform nanofibers were obtained [599]. Hsu et al. demonstrated a reduction in the diameter of electrospun PCL fibres with the addition of DMF to chloroform [645]. Bolgen et al. observed a dramatic decrease in diameter (from 1300 nm to 300 nm) when DMF was included in the solvent mixture up to 40% [646].

In this study, the chloroform:DMF (70:30) solvent blend was selected for the manufacturing of nanofibrous barrier layer due to multiple factors including the improved electrospinnability, the decreased fibre diameter, and the smaller pore size.

### 7.6.6. Manufacturing and characterisation of the PCL bilayer barrier membrane

Following the optimisations of manufacturing of PCL electrospun and PCL PolyHIPE layers, two layers were combined to fabricate the bilayer BM (Figure 104A-D). The complete integration of both layers can be seen from SEM images. This is more likely due to the fact that both polymers are PCL, and the solvent composition used for electrospinning PCL can partially dissolve the surface of the PCL PolyHIPE layer. No

delamination of the two layers was observed, and the BM preserved its integrity during the experiments.

Figure 104E-J shows the handling ability of the PCL bilayer BM. The resulting BM was very flexible and allowed manual handling, including bending and twisting without losing its structural integrity. Figure 104I shows the space making ability of the BM, which is defined as the ability to maintain a space for cells without any collapse.

For this study, the thicknesses of the PCL electrospun and PCL PolyHIPE layers were determined as 200 μm and 250 μm, respectively. The thicknesses of the PCL electrospun and PCL PolyHIPE layers can be controlled easily by changing the electrospinning time and slicing thickness, respectively. To show the controllability of the thickness of the PCL electrospun layer, Figure 104B shows a bilayer membrane with a low thickness where PCL was electrospun on PolyHIPE for 20 minutes instead of 40 minutes. Thicker membranes are assumed to have better barrier performances in addition to higher mechanical strength [647] and a longer degradation time and which results in the GTR membrane being present during a longer time period [648]. The question of the optimum barrier membrane thickness can be answered to some extent, experimentally *in vitro*, but ideally, it needs to be investigated *in vivo* in future studies. Here, the tunability of the thickness of individual layers is an advantage in our manufacturing method as we can provide BMs of varying thicknesses for comparative evaluation of performance and rate of breakdown *in vivo*.

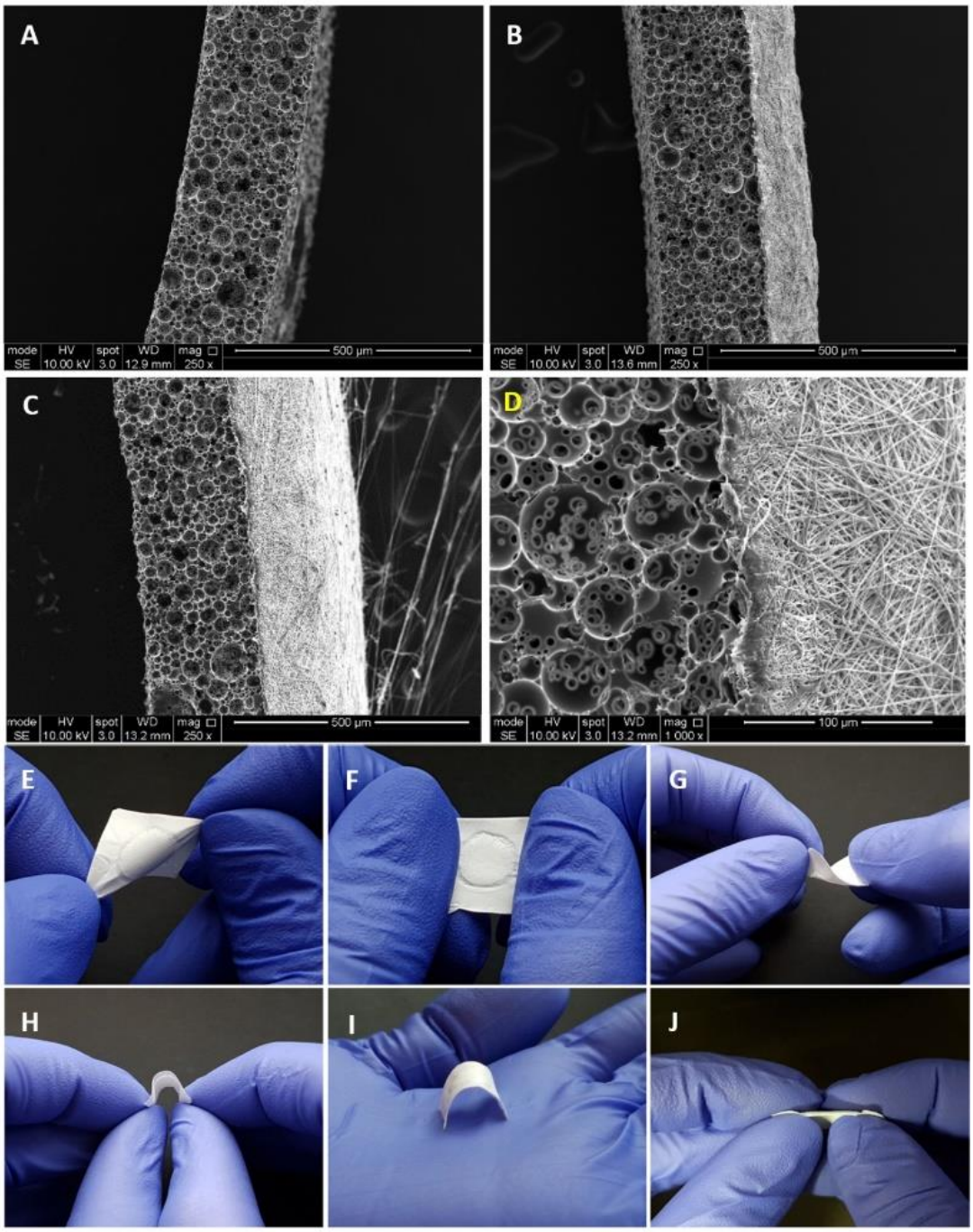


***Figure 104****: SEM images of (A) 250 µm sectioned PCL PolyHIPE layer, (B) 20 minutes PCL electrospun on PCL PolyHIPE, (C) 40 minutes PCL electrospun on PCL PolyHIPE, (D) Higher magnification SEM image showing the border of two layers. Macro images of the bilayer PCL BM to show the suitability of the design for (E-F) stretching in different axes, (G-H) bending, (I) space making, and (J) side view of the BM to show the integration of the two layers*

Tensile tests of the BMs were conducted on both dry and wet conditions. Biomedical implants are usually in contact with body fluids, which significantly influences their performance in comparison with their dry state. The mechanical behaviour of an implant under wet conditions is important for better representing the *in vivo* conditions [649].

Both the E and UTS values of dry BMs were significantly higher compared with the wet BM samples. But there was not any statistically significant difference between the elongation of the BMs in dry and wet state (Figure 105).

The UTS of the BM s were measured as 137.3±6.7 KPa and 75.0±4.2 KPa for dry and wet samples, respectively. The elastic modulus and elongation of dry and wet BMs are 452.1±24.5 KPa and 304.2±12.9 KPa; and 79.3 ± 3.5% and 83.2 ± 2.1%, respectively.

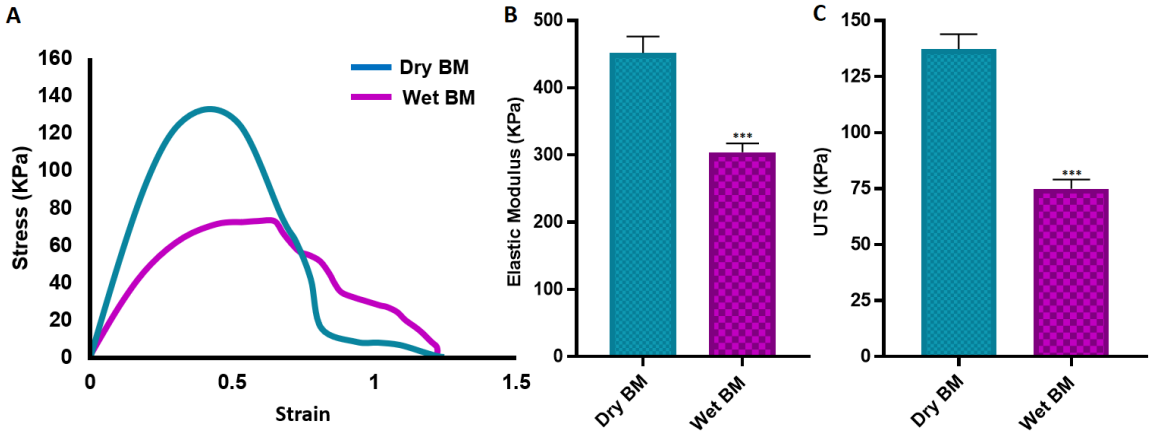


***Figure 105:*** *Mechanical properties of the BM under dry and wet conditions. (A) Representative stress-strain curves, (B) Elastic modulus, (C) UTS of the BMs under dry and wet conditions (*** $p \leq 0.001$, ns $p \geq 0.05$, $n = 3$)*

The mechanical properties of the developed membrane show similarities with other developed membranes in literature. Lee et al. reported tensile strength of commercial collagen membrane (Ossix plus) around 110 KPa and 20 KPa for the dry and wet state, respectively [647]. Poly(lactic-co-glycolic acid) (PLGA) membrane fabricated with freezing and lyophilisation has been reported to have similar UTS with our BM where the elongation of the PLGA membrane was approximately eight times lower [650]. Similarly, the tensile strength of the freeze gelated chitosan membrane has been demonstrated approximately four times and ten times lower, respectively under dry and wet conditions when compared with the developed BM in this study [592]. Electrospun chitosan membrane with random fibre orientation has been shown to have slightly higher UTS in wet state, but at the same time, it was approximately ten times less elastic than our BM, and the elongation was almost six times lower [651]. Another study has revealed that the polysaccharide/bioactive glass membrane produced using the layer by layer deposition technique has very similar mechanical properties in terms of UTS and E values with our BM [652].

### 7.6.7. Assessment of the metabolic activity of HDFs on PCL electrospun layer and the ability of the PCL electrospun layer to act as a cell barrier

The metabolic activities of HDFs growing on the PCL electrospun layer gradually increased from day 1 to 28 (Figure 106) showing the biocompatibility of the bilayer PCL membrane. Although the metabolic activities of the HDFs growing on TCP were higher at each time point, they started to drop after day 14. This decrease is more likely to be due to contact inhibition of proliferation. Two dimensional structure of TCP may restrict the capacity of cells to expand further [653].

Histological analysis of the PCL electrospun layer showed that HDFs were not able to penetrate due to the small pore sizes of nanofibrous random PCL fibres. Instead, they were observed as growing on the surface of the electrospun barrier layer and not migrating towards the PolyHIPE layer (Figure 106) confirming the cell-occlusiveness properties of the electrospun PCL layer. Randomly orientated nanofibrous scaffolds have been demonstrated as a physical barrier to cell penetration while allowing the diffusion of nutrients. Previous work from our laboratory has shown that keratinocytes and fibroblasts were successfully segregated when separated by a nanofibrous Poly(3-hydroxybutyrate-co-3-hydroxyvalerate) (PHBV) layer [417]. Similarly, Vaquette et al. showed that fibroblasts seeded on a random fibre mat did not penetrate the scaffold and colonized on the surface and formed a 30 μm thick cell sheet [654].

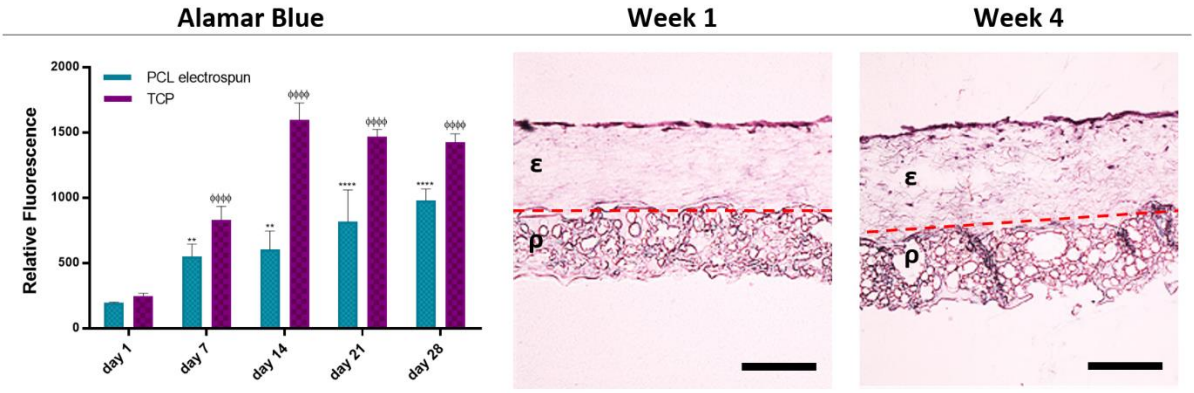


***Figure 106:*** *Evaluation of the biocompatibility and the barrier properties of the bilayer BM. The metabolic activity of the HDFs growing on PCL electrospun layer from day 1 to day 28 is given in the graph (*** and ΦΦΦ $p \leq 0.001$, ** and ΦΦ $p \leq 0.01$, * and Φ $p \leq 0.05$, $n = 3$). Histological images demonstrate the barrier properties of the PCL electrospun layer over 4 weeks. ε and ρ indicate the electrospun layer and PCL PolyHIPE layer, respectively. Dotted line indicates the boundary of the two layers (Scale bar represents 200 μm)*

As the crucial time for epithelial invasion has been reported as the first 14 days of implantation, then the barrier function limiting the epithelial invasion up to 14 days is considered sufficient for GBR applications [655,656].

## 7.7. Conclusions and Future Work

In the present study, a bilayer BM made of a biodegradable synthetic polymer, PCL was successfully fabricated by combining electrospinning and with emulsion templating. The resulting BM showed no delamination, and its structure was qualitatively resilient to torsion and stretching, and it was straightforward to handle. The electrospun layer of the BM has been confirmed for its barrier features for the prevention of soft tissue invasion whereas the interconnected PCL PolyHIPE layer has shown potential for use as the bone promoting layer providing the key requirements such as cell compatibility, supporting cellular infiltration, and promoting collagen and mineral deposition. Furthermore, the pore structure of the PCL PolyHIPE layer has been found to be suitable for blood vessel ingrowth. In conclusion, by combining two methods of fabricating an FDA approved polymer, PCL, a bilayer BM that is a good candidate for a diverse range of GTR applications can be fabricated.

In future, studies could focus on culture of both cell types together to see the effect of cell-cell interaction on the behaviour of both cells. The *in vitro* results were very encouraging for further assessments of the BM. Thus the assessment of the *in vivo* performance of the BM could be really interesting and might potentially reveal the potential of the developed BM to be used in the clinic.

# CHAPTER VIII

## Overall Discussion and Future Perspectives

As laboratory production of TE materials has progressed to the clinic, it has become clear that one of the critical barriers to their success is the need to achieve rapid neovascularisation post-implantation. While relatively thin simple TE constructs can survive on well-vascularised wound beds, thicker constructs (>200 μm) usually fail to engraft due to lack of oxygen and nutrients *in vivo* [22,24]. Thus, rapid ingrowth and infiltration of blood vessels are crucial for biomaterials to be able to survive *in vivo* [360].

Prevascularisation, the use of pro-angiogenic cells, and scaffold functionalisation, the use of pro-angiogenic agents, are viewed as promising approaches to accelerate vascular ingrowth into tissue engineering (TE) constructs to circumvent slow vascularisation after implantation [37,326].

When it comes to scaffold functionalisation, VEGF is a crucial pro-angiogenic factor that plays a key role in promoting angiogenesis [38]. ECs are known to be sensitive to VEGF signalling, which regulates proliferation, migration and their survival [41,361]. Although VEGF is accepted as the gold standard for promoting angiogenesis, the exogenous use of VEGF can promote the formation of leaky [362], permeable [335] and haemorrhagic [336] vessels when administered in an uncontrolled manner. Thus, the need for alternative pro-angiogenic drugs to promote neovascularisation is clear.

2dDR is a promising alternative which has been reported to have chemotactic and angiogenic activity by our group and other researchers using current angiogenic assays; Boyden chamber assay [83], tube formation assay [83], CAM assay [81,89] and rat wound healing models [87,90]. However, the dose-dependent response of 2dDR still remained to be investigated *in vitro* to learn what is the effective concentration range to drive angiogenesis at the cellular level.

In **Chapter II**, I demonstrated the angiogenic potential of 2dDR and defined its effective concentration ranges *in vitro* and *in vivo.* The *in vitro* assessment of the angiogenic activity of 2dDR showed it to be dose-dependent reproducing all of the actions of VEGF with 2dDR stimulating proliferation, migration and tube formation of HAECs when used at 100 μM and 1 mM concentrations. Lower concentrations (1 μM) were not found effective and higher concentrations (10 mM) led the death of HAECs by day 4. The comparison of 2dDR with 2dLR, 2dDG and DG evidenced that none of the other small sugar molecules increased the activity of HAECs *in vitro*. Instead, 2dDG (when administered at 100 μM, 1 mM and 10 mM) and 2dLR (when used at 10 mM) showed an anti-angiogenic effect on HAECs proliferation. Our results were in concordance with the literature. The anti-angiogenic impact of 2dDG [365,366] and 2dLR [83,86] have previously been reported by several groups, mostly focusing their potential applications on the inhibition of tumour angiogenesis. Following the *in vitro* assessment of 2dDR, I explored that if it is possible to define certain concentrations of 2dDR which are as effective as VEGF in stimulating angiogenesis in *ex-ovo* CAM assay. To date, there have been no studies conducted on the effective angiogenic dose range of 2dDR, which is proangiogenic *in vivo*. Therefore, for the first time in this study, I demonstrated the reliable concentration ranges for 2dDR for stimulating angiogenesis in CAM assay and compared their proangiogenic activities with the E2 and VEGF as positive controls. The results of the CAM assay confirmed the dose-dependent angiogenic response of 2dDR, and 200μg/day/embryo was at least 80% as effective as VEGF when given as solution for inducing angiogenesis *in vivo*. Higher and lower doses of the drugs showed less angiogenic activity in the CAM assay. Following the determination of the effective dose range, 2dDR was loaded into electrospun PHBV fibres to stimulate angiogenesis with the release of it in CAM assay over 7 days. PHBV is a natural, biocompatible and biodegradable biopolymer [367]. Although the biodegradability of PHBV is relatively slow when compared to PLA [368], it is still an attractive material for drug release studies because of its excellent biocompatibility, biodegradability, easy processing properties [369].

Incorporation of 2dDR into the PHBV scaffolds resulted in increased activity on CAM by the release of the agent from fibres. This study established an effective concentration range of 2dDR (250mg/g of PHBV) to be loaded into scaffolds to achieve a reliable stimulation of neovascularisation over 7 days. Higher doses of 2dDR were found to be

less effective in promoting the angiogenesis in *ex-ovo* CAM assay. These results were further confirmed with the histologically stained sections of the scaffolds. In these, more blood vessels were counted adjacent to 2dDR releasing scaffolds. However, in contrast to the results from the quantified macro images, in histological analysis, the number of blood vessels adjacent to the scaffolds loaded with the higher dose of 2dDR (2dDR 500) were not significantly but slightly greater than the lower dose. This differential result might be caused by our ability to see and count the smaller diameter blood vessels that may not be discernible in the digital CAM analysis used for quantification. Additionally, the histological sections also show blood vessels from different orientations which might not have been detectable on digital CAM images. This might increase the results seen for higher doses of the drugs.

Finally, I evaluated the activity of 2dDR on enhancing angiogenesis and wound healing upon implantation using a diabetic rat wound healing model. The current study follows on from recent work from our group showing that a small sugar, 2dDR, is proangiogenic as demonstrated in a chick bioassay and that it stimulated wound healing in a full-thickness skin wound in a rat model [87]. Alginate dressings are in clinical use for the treatment of heavily exudative, chronic wounds [395] as well as for diabetic wounds. As such, they are a logical choice to use to deliver this sugar. The sugar was loaded on highly absorbent alginate dressings under sterile conditions. Our findings were that 2dDR was straightforward to load into alginate dressings. These were then air-dried, and when placed in a wet environment, they released approximately 90% of their sugar load within 3 days. A well-established diabetic rat model was used in which a full-thickness 20 mm diameter skin wound was made. While the area of these wounds reduced by approximately 70% by 20 days they were still not fully healed. Addition of alginate did significantly accelerate wound healing but macroscopic wound closure analysis clearly showed that 2dDR released from alginate further improved the wound healing in the area of implantation. By day 20, wounds treated with 5 or 10% 2dDR loaded alginate dressing were essentially fully healed. The histological assessment also demonstrated a better healing of the skin wounds and an increased angiogenic activity in the implantation are when treated with 2dDR loaded alginate as evidenced by the presence of a new epithelium and blood vessels, respectively.

Although I did not primarily aim to establish a complete mechanism of action for the angiogenic activity of 2dDR, I investigated whether this activity is VEGF-dependent or not. For this, HAECs were incubated in low serum EC GM supplemented with 100 μM of 2dDR, 1 mM of 2dDR, and 80 ng/mL VEGF. Non-supplemented low serum EC GM was used as a control. The analysis of the collected media at day 1, 3 and 5 demonstrated that the VEGF production by HAECs in response to direct treatment of 2dDR was statistically significant even at day 1. The amount of VEGF went up by approximately 48-fold and 70-fold, respectively by 100 μM and 1 mM 2dDR treatment. At the end of day 5, VEGF production of HAECs was increased by 74-fold and 80-fold, respectively by the addition of 100 μM and 1 mM 2dDR. This data was in support with the current literature, which hypothesises that an increase in the level of VEGF expression of endothelial cells in the presence of 2dDR [82,84].

In the future, experiments need to be carried out to explore the complete mechanism of action of this small deoxy sugar molecule to understand what is happening in the molecular level.

To test the angiogenic activity of alternative drugs, biomechanical stimulus and cells, angiogenesis models are important tools [22], and the current angiogenesis assays can be divided into three categories: *in vitro* assays which focus on evaluating proliferation, migration, and tube formation capabilities of ECs [512], ex-vivo assays and *in vivo* assays [23]. Although *in vivo*, assays are the most representative and reliable models for the evaluation of angiogenesis, they are also expensive, technically difficult, time-consuming and ethically questionable. On the other hand, *in vitro* angiogenesis assays are inexpensive, quick, technically simple, and reproducible, but they are usually based on evaluating only one aspect of angiogenesis, and as such do not represent the complexity of angiogenesis which occurs *in vivo*.

When all the drawbacks of these methods are considered, there is a need for a 3D dynamic system which enables the study of angiogenesis *in vitro* in a more physiological complex 3D environment which includes the introduction of flow which is a major stimulus for neovascularisation *in vivo*.

In **Chapter III, IV and V**, I demonstrated the development of three different platforms which enable researchers to study several aspects of sprouting angiogenesis under either static or dynamic conditions.

First, I developed a synthetic vascular network made of PHBV combining electrospinning and 3D printing in **Chapter III**. 3D printing technique allows the control of the production of a large number of scaffolds with exactly the same geometries in a short time while electrospinning enables the production of TE scaffolds with a wide range of properties in terms of material composition, fibre diameter, thickness, porosity, and degradation rates [438–441]. The PHBV polymer was chosen for synthetic vascular scaffolds not only because of the previous experiences of our research group [143,417,423], but also because electrospinning of PHBV nanofibers can be used to create a barrier for cells which is easier to do with this material. Furthermore, the comparison of the biological performance of the two widely-used polymers, PHBV and PCL, showed us that PHBV was better for supporting the attachment and proliferation of ECs. For the production of the synthetic vascular channels, alginate, which is a natural, and biocompatible polysaccharide was largely preferred for biomaterial applications [442,443] and was used as a sacrificial substrate to create a temporary support material as synthetic channels. Our initial experiments aimed to mechanically characterise the scaffolds. The results of the mechanical testing showed us the scaffolds had similar properties with those used in vascular tissue engineering.

Following the production and mechanical characterisation of the scaffolds, synthetic channels were repopulated with HDFs to gain experience and to confirm the bio-suitability of the scaffolds for cells to adhere and form a uniform layer. HDMECs were then seeded to channels either in isolation or in the presence of HDFs on the outer surface to support. Results showed that the physical appearance of HDFs improved the survival and homogeneous distribution of ECs within the channels. However, I found that PHBV SVN could be cellularised with evenly distributed ECs either in isolation or in the presence of HDFs depending on the intended purpose of use. Once a uniform endothelium monolayer was obtained, the developed SVN was tested for its potential use in studying angiogenesis with two sets of experiments. In the first experiment, the outgrowth of HDMECs to VEGF and 2dDR loaded Matrigel was investigated. The results of the Matrigel experiments showed that HDMECs were outgrowing and forming interconnected tube-

like structures within the Matrigel close to edges of the pierced synthetic PHBV channels. The tube-like formed structures were obvious and well-organised in 80 ng/mL loaded VEGF loaded Matrigel groups when compared with 100 μM 2dDR loaded and control groups. The formation of the tube-like structures was pretty similar to those which can be observed in Matrigel tube formation assays [350]. Our observations were in support of the literature where VEGF has been reported to regulate outgrowth of ECs [462–464]. I have also demonstrated that 2dDR improved the tube formation of ECs at 100 μM concentration (the data presented in Chapter 2). Although the results showed some promising steps for this model to be used as an alternative *in vitro* system to study the aspects of neovascularisation, the reproducibility and the reliability of the model were found to be fairly low. The outgrowth of ECs was witnessed in only 20% of the experiments for VEGF loaded Matrigel and 13.3% of the 2dDR loaded and control groups, respectively. Formation of complete tube-like structures by ECs was seen in only a minority of the VEGF-loaded Matrigel groups.

This lack of reproducibility demonstrates that the proposed PHBV SVN model as an *in vitro* platform to study angiogenesis is not fully reliable to investigate angiogenesis by its own. The causes behind this variation in these results were not studied further due to the complex structure of the developed model. I hypothesised that the most probable reasons could be: (a) Matrigel is rich in ECM proteins, but the exact concentrations of the ingredients are not clearly defined, and it shows high batch-to-batch variations, (b) the thickness of Matrigel was not possible to control very well due to the complex geometry of the PHBV SVN scaffolds even though the same volume was used for each experiment. The gel thickness might cause a variation in EC survival and migration, (c) Microvascular ECs are very sensitive to culture conditions and show batch to batch variations which might be a cause for these variations, (d) the holes were pierced on SVN channels manually, and they were randomly oriented, and their positions and diameters might have an impact on the variations in the outgrowth of ECs.

Following the Matrigel experiments, a more physiologically relevant tissue model, TE skin model, was next explored for assessing the vascularisation potential. The TE skin model was successfully developed by co-culturing human dermal keratinocytes and HDFs on DED for 14 days (2 days as submerged in media and 12 days at the air-liquid interface) using a well-established protocol [420]. The air-liquid interface has previously been

confirmed to provide a strong stimulus for the gradual differentiation of keratinocytes [411]. The histological evaluation of the reconstructed TE skin models showed that the TE skin model achieved a normal-looking gross skin morphology in 14 days. A multi-layered epithelium was formed and found to be well attached to the dermis. Once a skin model was successfully developed, the performance of the PHBV SVN to be used for vascularisation of a reconstructed TE skin model (with or without VEGF added to growth medium) were then investigated in comparison with the vascularisation studies of TE skin models on CAM. Phalloidin-FITC and DAPI staining showed that there was a monolayer which had formed within the channels and some cells were localised on the outer surface of the scaffolds.

In order to identify the type of cells present in the system, immunostained (Anti-human CD31+) sections showed that HDMECs were evenly distributed within the channels and formed a monolayer, and the HDFs were localised evenly on the outer surface of the PHBV SVN either in VEGF-added or non-supplemented control groups. High magnification images of the immunostained sections revealed that the outgrowing cells from the PHBV channels towards the reconstructed skin models were CD31 positive HDMECs. The outgrowth of HDMECs was mostly observed from the connection edges of two separate electrospun sheets, and the inclusion of VEGF to the growth media significantly increased the outgrowth distance of HDMECs approximately 4.4-fold (when compared to controls) towards the reconstructed TE skin model.

Unfortunately, no cells were able to reach to the DED layer, and they were not found to be invading into the dermal layer of the developed skin models in any of the groups. The most probable explanations for this are those (i) the outgrowth direction of HDMECs was against the gravity, (ii) the rate of outgrowth of HDMECs from PHBV channels was very low. Furthermore, (iii) the orientations, positions and diameters of the manually pierced random holes might also negatively affected the outgrowth of HDMECs.

These results were consistent with the CAM assay studies. Even though CAM is a highly vascularised and dynamic environment, the results showed that there were no blood vessels growing into the dermal layer of the reconstructed skin substitutes. However, the presence of dermal cells significantly improved the vascularisation in the area of implantation. In addition, the administration of 80 ng/day/embryo VEGF and

200 µg/day/embryo 2dDR showed increased angiogenic activity in the implantation area.

In the future, studies could focus on the standardisation of the manufacturing method to increase the reproducibility of this *in vitro* platform by optimising the thickness of Matrigel, orientation and the diameters of the holes. Use of ECs in co culture with different cell types and investigating their interaction might also bring a new perspective to the use of developed platform. Further experiments with other pro-angiogenic factors and flow conditions could be performed to study their relation to angiogenesis using the developed model to increase the reliability of the model. Furthermore, inclusion of flow might increase the reliability of the results that can be obtained from the TE skin model experiments. The positive influence of shear stress on EC outgrowth was demonstrated in Chapter V. Finally, the majority of results obtained from these experiments were qualitative results. Future studies could focus on obtaining more quantitative results such as cell viability, expression of angiogenic markers and factors.

Then, I developed a natural synthetic vascular network by decellularising baby spinach leaves and explored their potential for studying and inducing angiogenesis in **Chapter IV**. An immersion decellularisation protocol was adapted and modified from previously published protocols [166,167]. After initiation of decellularisation, leaves began to lose their green colour over time and became translucent by the end of day 7. The surface became more wavy due to burst plant cells and bigger stomatal pores, and the success of the decellularisation protocol followed was verified by quantification of the DNA content which showed that 98% of the DNA content of spinach leaves was successfully removed.

The biocompatibility of decellularised spinach leaves was investigated *in vitro* and using an *ex-ovo* CAM assay. The results demonstrated an increase in the metabolic activities of HDFs growing on decellularised spinach leaves from day 1 to 11, and the results of the CAM assay confirmed that decellularised spinach leaves showed no toxicity to chick embryos. Furthermore, gelatin coating significantly enhanced the attachment and proliferation of HDFs to decellularised spinach leaf at all time points. Cellulose is the major component of the plant cell wall [491], and *in vitro* and *in vivo* biocompatibility of the plant-derived cellulose has been previously studied by several groups recently. Modulevsky et al. reported the *in vitro* biocompatibility of decellularised McIntosh Red apple slices by assessing the proliferation of mammalian cells on them [316] Recently,

Gershlak et al. assessed the feasibility of decellularised spinach and parsley to be used as TE scaffolds. They demonstrated that hPS-CMs were viable and contracting five days after initial seeding [166]. Our experiments showed results which were in agreement with the literature. Cellulose is a readily available, inexpensive, and a biocompatible biomaterial that may prove a good candidate to be used in tissue engineering applications.

Decellularised baby spinach leaves have been developed for two purposes: (a) to promote angiogenesis (when repopulated with pro-angiogenic cells) and (b) to be used as an *in vitro* platform for the study of angiogenesis.

*In-vitro* prevascularisation of TE constructs, which can be derived from synthetic or natural sources prior to implantation is a promising approach to overcome the slow vascularisation problem. The idea of this prevascularisation technique is to shorten the time required for neovascularisation in the post-implantation period by establishing a connection between existing vessels and the cultured ECs [485,486]. The effectiveness of the prevascularisation technique has previously been studied by many groups. Tremblay et al. reconstructed an endothelialised skin model repopulated with HUVECs and reported the inosculation of HUVECs with the host mice vasculature during the first 4 days [485]. Similarly, Nor et al. implanted biodegradable poly-L-lactic acid scaffolds prevascularised with HDMECs subcutaneously into immunodeficient mice and demonstrated the differentiation of HDMECs into functional human microvessels which anastomosed with the host vasculature in less than 7 days [501]. Schechner et al. reported the formation of primitive capillary-like structures by HUVECs cultured within a 3D gel and showed successful inosculation of HUVECs with the host vasculature when implanted into mice [118]. Unger et al. investigated the functionality of *in vitro* pre-formed microvasculature *in vivo* and reported that co-culture of HDMECs with osteoblasts stimulated the ingrowth of host's blood vessels into TE construct, and chimeric vessels were also observed at the end of 14-day period [493].

Accordingly, in this study, I repopulated the acellular spinach leaves with HDMECs (in the presence of helper HDFs which have been found to help to increase the survival of ECs in the channels). The angiogenesis was evaluated using *ex-ovo* CAM assay. The results showed that endothelialised spinach leaves increased the angiogenic activity when compared to HDFs only and leaf only controls in the area of implantation. This data

provided evidence on prevascularisation stimulating new blood vessel growth at the site of implantation.

Finally, I tested the potential of decellularised spinach leaves to be used as an *in vitro* platform to study angiogenesis. For this aim, I investigated the outgrowth of HDMECs from the channels towards a chemical attractant. Briefly, I explored the outgrowth of HDMECs from the channels of decellularised spinach leaves to Matrigel either plain or loaded with VEGF. Unfortunately, our results demonstrated that the outgrowth of the HDMECs from the channels was extremely rare (outgrowing HDMECs were witnessed only in 5% of the experiments). However, the outgrowth distance of the HDMECs through VEGF loaded Matrigel was higher, and a more organised structure was observed when compared with non-loaded Matrigel groups.

In future, further investigation of the inosculation of HDMECs with host vasculature needs to be investigated. Furthermore, even if the leaves were gelatin coated and the HDFs were used as helper cells, HDMECs were not found to penetrate into the smaller branches of the acellular spinach leaves. In considering the potential use of the decellularised spinach leaves as prevascularised constructs, this lack of homogeneity in the distribution of HDMECs might prove a problem for establishing a connection with the endothelial cells of the host tissue. Further developments on endothelial cell distribution in the scaffolds may lead to a better angiogenic response from host tissue.

In the field of decellularisation of the native tissues and organs, the complete recellularisation of the acellular 3D scaffolds *in vitro* is a long-standing problem, and further investigations are needed to improve the cell distribution in the scaffolds [502]. Although the CAM assay is a useful platform to study biocompatibility and angiogenicity of materials *in vivo*, one of its drawbacks is that the chick does not have a fully developed immune system during the period of use for the CAM assay [69,89]. Thus, comparison of plant-derived and animal-derived decellularised constructs using an animal model with a competent immune system will be interesting in the future to compare the relative merits of both. When it comes to using the developed scaffolds as an *in vitro* platform to study angiogenesis, further developments on this assay would be required to increase its reproducibility. It possibly merits more development as it combines both migration and cell differentiation in a 3D environment.

In **Chapter V,** we developed a 3D dynamic system through the combination of electrospinning and emulsion templating to be used for testing of angiogenic drugs and flow in a more physiologically relevant environment to stimulate angiogenesis. Experiments in this study were designed with two key objectives; (i) to develop a 3D dynamic system to be used for testing of angiogenic drugs, (ii) to evaluate the efficiency of 2dDR to encourage proliferation and infiltration of HAEC using *in vitro* 3D dynamic system. We investigated the suitability of our model to be used as a 3D *in vitro* angiogenesis model. The 3D dynamic system was designed as a tubular form as seen in tissue engineering vascular graft (TEVG) design to enable the application of lateral flow [533–535]. It was designed to be two-layers; the inner tube of PHBV electrospun nanofibres to serve as a suitable environment, mimicking the basement membrane, for ECs to adhere, proliferate and form a monolayer to represent an endothelium, and the emulsion templated PCL PolyHIPE outer tube was expected to be highly porous to enable proliferation and migration of ECs from the formed endothelial monolayer to the outer tube. Nanofibres have been shown to provide better surface properties for ECs to adhere and proliferate on them over microfibres [456–458]. The manufacturing route of PCL based PolyHIPEs was recently reported by our group, and biocompatibility and structural suitability of the PCL PolyHIPE for cell infiltration were also shown [419,424].

The results of the 3D flow experiments showed that static culture and lower shear stresses (1 dyn/cm$^2$ and 2 dyn/cm$^2$) enabled the formation of a continuous endothelial monolayer, but the application of higher stress (10 dyn/cm$^2$) resulted in a discrete layer of HAECs (no monolayer formation was observed in any of the experiments when high shear stress was applied). This is possibly due to the cells being washed out at the high rate of flow [540]. Low shear stress promoted the outgrowth of HAECs for over 7 days. 2 dyn/cm$^2$ shear stress significantly increased the outgrowth distance of HAECs and normalised cell density when compared with 1 dyn/cm$^2$ and 10 dyn/cm$^2$, whereas no outgrowth was observed under static culture conditions. Our findings of the effect of flow experiments on ECs are consistent with the literature [541,542]. Under static conditions, administration of 2dDR and VEGF stimulated EC outgrowth and cell density when compared with the static control group (no agents administered). However, the most dramatic increase in outgrowth distance and cell density was observed when the pro-angiogenic agents (2dDR and VEGF) were administered under 2 dyn/cm$^2$ shear

conditions. Similar to our results, Song et al. have previously reported that VEGF and fluid forces cooperate to improve endothelial invasion [547].

This chapter makes a novel contribution by demonstrating a novel 3D model which can be used to study angiogenesis *in vitro* in a 3D dynamic environment. Our model enables users to monitor cell proliferation and migration simultaneously under more physiologically relevant conditions.

In the future, studies trying to include a quantitative assessment of angiogenesis markers could be trialled in an attempt to give a better insight into the response of ECs to an external stimulus and to flow. This will clearly increase the reliability of the developed model and increase the accuracy of the results obtained. In addition, further studies exploring co-culture of ECs with another cell line could bring a whole new perspective to the use of this model. For example, the inclusion of bone cells in the PolyHIPE layer in co-culture with ECs (in the electrospun layer) could enable users to study aspects of vascularisation in bone tissue engineering. Finally, the assessment of different cell combinations, pro-angiogenic factors, and flow regimes could be studied in relation to angiogenesis in future studies.

Overall, I aimed to circumvent the drawbacks of the current angiogenesis systems by developing three angiogenesis models in the scope of this thesis. All of them offer some novel and promising alternatives to the established *in vitro* angiogenesis models and have pros and cons. The comparison of the pros and cons of the developed *in vitro* angiogenesis models are summarised in Table 22.

***Table 22.*** *A comparison of the pros and cons of the in vitro angiogenesis models developed. The levels of each parameter have been indicated as "+++" = high, "++" = medium, and "+" = low*

| **Parameters** | **Angiogenesis Model** | | |
|---|---|---|---|
| | ***PHBV Synthetic Vascular Network*** | ***Decellularised Baby Spinach Leaves*** | ***Bilayer 3D dynamic tubular model*** |
| *Ease of Fabrication* | ++ | +++ | + |
| *Duration of Fabrication* | ~ 2 days | ~ 9 days | ~ 5 days |
| *Cost* | ++ | + | ++ |
| *Reproducibility* | +++ | +++ | +++ |
| *Ease of Cellularisation* | + | ++ | +++ |
| *Multiple channel structure* | Yes | No | No |
| *Batch to Batch Variation* | No | Yes | No |
| *Suitable for the Introduction of Flow* | Yes | No | Yes |
| *Suitable for the Investigation of* | Migration, Tube Formation | Migration | Proliferation, Migration |
| *Suitable for the Histological Analysis* | Yes | No | Yes |
| *Ease of Visualisation* | ++ | +++ | ++ |

Alongside working with the development of several angiogenesis models, I also investigated the practicability of the prevascularisation approach to promote angiogenesis in an *ex-ovo* CAM assay by pre-seeding simple electrospun PHBV scaffolds with a combination of endothelial cells and fibroblasts **(Chapter VI)**. The investigation of the effect of gelatin coating and the presence of HDFs, as helper cells, showed that gelatin coating and co-culture of HDFs both showed a positive impact on HDMECs viability and growth.

Communication of ECs with surrounding stromal cells such as SMCs, fibroblasts or pericytes has also been proven to have significant importance for the angiogenic process

[551,552]. Our group has previously reported the positive effect of HDFs on improving the survival and growth of HDMECs [323]. Recently, I revealed that non-cross-linked gelatin coating is a simple and effective method to improve the attachment and growth of HDMECs to biomaterials that have relatively weak biological properties [480]. In line with our results, Ma et al. reported that surface modification of electrospun PCL scaffolds with gelatin coating enhances the EC spreading and proliferation [553]. The positive impact of either non-cross-linked or cross-linked gelatin coating on attachment and proliferation of human Schwann cells has been shown by Vleggeert-Lankamp et al. [499].

Following the determination of the optimal culture conditions for HDMECs, three different cell culture systems were investigated in the *ex-ovo* CAM assay in terms of improving the angiogenic activity, as a prevascularisation approach. The results of the CAM assay revealed that both HDFs and HDMECs either in isolation or when co-cultured together significantly increased the angiogenic activity in the area of implantation. HDMECs were found to be more effective for stimulating angiogenesis. However, the most significant angiogenic response was observed when HDFs were also present in indirect contact with HDMECs.

In the future, studies could focus on investigating the anastomosis of HDMECs with the host vasculature to confirm the effectivity of the prevascularisation technique. In addition, the use of stem cells in this prevascularisation system could be interesting to provide more reliable information as the ultimate goal of this technique is the translation of it to the clinic. This is more applicable when patient's own cells are harvested and expanded on TE constructs to create a prevascularised construct to shorten the time required for neovascularisation post-implantation.

Alongside the work I have done in an attempt to contribute to the world of angiogenesis, we also aimed to develop systems to be used in tissue engineering and regenerative medicine. For this, we developed a bilayer PCL barrier membrane (BM) in **Chapter VII** to be used in guided bone/tissue regeneration (GBR/GTR) applications by combining electrospinning and emulsion templating. Periodontal regenerative procedures require the use of GTR/GBR in various conditions such as socket preservation, grafting, maxillary sinus elevation and the treatment of the chronic periodontitis [562]. The main principle of the GTR/GBR procedure is to place a BM between epithelial tissue and bone or bone graft to prevent migration of the fast-proliferating epithelial cells into the defect site to

be able to preserve a space for infiltration of bone cells into periodontal defect site [563,564].

A BM is expected to be in contact with both hard and soft tissues, and it has different functions on each side. While being cell occlusive on the side in contact with soft tissue, it should encourage bone regeneration on the other side. Accordingly, our BM has been designed to have two layers: (a) PCL electrospun layer to limit epithelial invasion, (b) PCL PolyHIPE layer to support bone growth. Initially, several solvent compositions were tried to find the best blend for manufacturing PCL electrospun nanofibres. The chloroform:DMF (70:30) composition was found to be the best and selected for the manufacturing of nanofibrous barrier layer due to multiple factors including the improved electrospinnability, the decreased fibre diameter, and the smaller pore size. First, the PolyHIPE layer was fabricated via emulsion templating, and PCL was then electrospun on top of the PolyHIPE layer using the selected solvent blend. The resulting BM showed no delamination, and its structure was qualitatively resilient to torsion and stretching, and it was straightforward to handle. Following the fabrication of the BM, both layers were tested for their intended purpose of use. The nanofibrous electrospun PCL has been shown to have barrier properties by limiting the ingrowth of HDFs up to 4 weeks *in vitro* while the metabolic activity of the cells increased. Then the highly porous and interconnected structure of PCL PolyHIPE layer was proven to provide a favourable environment for murine osteocyte-like cells to attach, migrate, and proliferate. PolyHIPE layer also stimulated the deposition of collagen and minerals on this layer, and the *ex-ovo* CAM assay was used to reveal that the pore structure and size of PolyHIPE was suitable for allowing the ingrowth of blood vessels from the chick membrane.

In future, studies could focus on the culture of both cell types together to see the effect of cell-cell interaction on the behaviour of both cells. The *in vitro* results were very encouraging for further assessments of the BM. Thus the assessment of the *in vivo* performance of the BM could be really interesting and might potentially reveal the potential of the developed BM to be used in the clinic.

**This page intentionally left blank**

# CHAPTER IX

## Overall Conclusion

The overall aim of this project is to enhance our knowledge in the world of angiogenesis and regenerative medicine by designing systems that have the capability of being used to induce and study angiogenesis particularly for regenerative medicine applications.

**Initially,** the dose-dependent angiogenic activity of 2dDR was revealed using well-established *in vitro* and *in vivo* systems. Results showed us 2dDR was a promising pro-angiogenic agent to stimulate angiogenesis and wound healing as an alternative to the use of exogenous VEGF. The loading of 2dDR into polymer-based and hydrogel-based tissue-engineered constructs has been found to be a very effective way of delivering it to the implantation area and stimulating angiogenesis post-implantation. To conclude, 2dDR was a great alternative for the upregulation of VEGF rather than the exogenous use of it. 2dDR was found not only to be highly angiogenic but also a potential agent to accelerate wound healing in non-healing diabetic wounds. This work involved a collaboration with Associate Professor Muhammad Yar in Pakistan

**Secondly,** I developed several systems that enable the study of angiogenesis under physiologically more relevant conditions.

In the first system, I demonstrated the development of synthetic vascular networks made of PHBV nanofibres to be used as an *in vitro* platform to study angiogenesis and to investigate the vascularisation of complex tissue models. The nanofibrous PHBV channels were found to provide a suitable environment for HDMECs to form a monolayer either in the presence or absence of HDFs. The indirect co-culture with HDFs was shown to be a desirable approach depending on the intended use of the PHBV SVN. This *in vitro* platform enabled the study of more than one aspect of angiogenesis (migration and tube formation) when combined with Matrigel. In addition, PHBV SVN provided a convenient

platform to study vascularisation of a reconstructed human skin model as a physiologically more relevant and complex structure.

The second model was a natural vascular network fabricated via decellularisation of a baby spinach leaves to retain the natural vasculature of it. The results demonstrated that 98% of the native DNA of the baby spinach leaves was removed successfully by serial detergent washes without any damage to the structural integrity of the leave. The intrinsic 3D vascular architecture was maintained after decellularisation, and these channels were then successfully recellularised with HDMECs and the potential use of the developed system to stimulate neovascularisation and to study angiogenesis was revealed.

In the third model, we developed a 3D dynamic system that can be used to study the angiogenic activity of agents under flow conditions. This project was conducted in collaboration with my colleague, Betül Aldemir, and carried out at the Institute for Medical Engineering and Science, Massachusetts Institute of Technology. This research focused on the development of the bilayer tubular scaffolds composed of an emulsion templated PCL PolyHIPE outer tube and an electrospun PHBV inner tube. The dynamic system was then successfully cellularised with HAECs, and the potential use of the system in the study of angiogenesis was demonstrated by evaluating the proliferation and migration of HAECs in response to flow and the pro-angiogenic agents, 2dDR and VEGF.

**Thirdly,** I showed the effectiveness of a prevascularisation technique to induce angiogenesis by pre-seeding simple electrospun scaffolds with combinations of HDMECs and HDFs. I used an *ex-ovo* CAM assay to reveal that the presence of HDMECs showed a stronger angiogenic response than the introduction of HDFs alone, but the use of HDMECs and HDFs together gave the most significant angiogenic activity.

**Finally,** as a side project, I developed a bilayer barrier (BM) membrane to be used in GTR/GBR applications. The experiments in this project were carried out in collaboration with my colleague, Betül Aldemir. In this study, a bilayer BM made of PCL was successfully fabricated by combining electrospinning and emulsion templating. The electrospun nanofibrous PCL layer has been confirmed for its barrier features for the prevention of soft tissue invasion whereas the interconnected PCL PolyHIPE layer has shown potential for use as a bone promoting layer providing the key requirements of cell compatibility,

supporting cellular infiltration, and promoting collagen and mineral deposition. The biocompatibility of the membrane and the suitability of the pore size of the developed BM were further examined with an *ex-ovo* CAM assay. The results showed that the pore size, interconnectivity and the pore structure of the PCL PolyHIPE layer were suitable for blood vessel ingrowth.

Overall, the developed approaches offer novel ways to increase our knowledge on how external factors affect the angiogenic process. The pros and cons of all these systems with future perspectives are discussed in Chapter VIII. All models have shown promising results to overcome the drawbacks of the current systems and to be very useful in studying neovascularisation.

**This page intentionally left blank**

# BIBLIOGRAPHY


1. Pugsley, M.K.; Tabrizchi, R. The vascular system: An overview of structure and function. *J. Pharmacol. Toxicol. Methods* **2000**, *44*, 333–340.

2. Rushmer, R.F. Structure and Function of the Cardiovascular System. In *Handbook of Research Methods in Cardiovascular Behavioral Medicine*; Schneiderman, N., Weiss, S.M., Kaufmann, P.G., Eds.; Springer US: Boston, MA, 1989; pp. 5–22 ISBN 978-1-4899-0906-0.

3. Carmeliet, P. Mechanisms of angiogenesis and arteriogenesis. *Nat. Med.* **2000**, *6*, 389–395.

4. Patan, S. Vasculogenesis and angiogenesis as mechanisms of vascular network formation, growth and remodeling. *J. Neurooncol.* **2000**, *50*, 1–15.

5. Drake, C.J. Embryonic and adult vasculogenesis. *Birth Defects Res. Part C - Embryo Today Rev.* **2003**, *69*, 73–82.

6. Risau, W.; Flamme, I. Vasculogenesis. *Annu. Rev. Cell Dev. Biol.* **1995**, *11*, 73–91.

7. Novosel, E.C.; Kleinhans, C.; Kluger, P.J. Vascularization is the key challenge in tissue engineering. *Adv. Drug Deliv. Rev.* **2011**, *63*, 300–311.

8. Burri, P.H.; Djonov, V. Intussusceptive angiogenesis - The alternative to capillary sprouting. *Mol. Aspects Med.* **2002**, *23*, 1–27.

9. Ribatti, D.; Crivellato, E. “Sprouting angiogenesis”, a reappraisal. *Dev. Biol.* **2012**, *372*, 157–165.

10. Carmeliet, P. Mechanisms of angiogenesis and arteriogenesis. *Nat. Med.* **2000**, *6*, 389–395.

11. Djonov, V.; Baum, O.; Burri, P.H. Vascular remodeling by intussusceptive angiogenesis. *Cell Tissue Res.* **2003**, *314*, 107–117.

12. Reynolds, L.P.; Grazul-Bilska, A.T.; Redmer, D.A. Angiogenesis in the female reproductive organs: Pathological implications. *Int. J. Exp. Pathol.* **2002**, *83*, 151–163.

13. Tahergorabi, Z.; Khazaei, M. A review on angiogenesis and its assays. *Iran. J. Basic Med. Sci.* **2012**, *15*, 1110–1126.

14. Bramfeld, H.; Sabra, G.; Centis, V.; Vermette, P. Scaffold Vascularization: A Challenge for Three-Dimensional Tissue Engineering. *Curr. Med. Chem.* **2010**, *17*, 3944–3967.

15. Krishnan, L.; Hoying, J. Interaction of angiogenic microvessels with the extracellular matrix. *Am. J. …* **2007**, *293*, H3650–H3658.

16. Galie, P.A.; Nguyen, D.-H.T.; Choi, C.K.; Cohen, D.M.; Janmey, P.A.; Chen, C.S. Fluid shear stress threshold regulates angiogenic sprouting. *Proc. Natl. Acad. Sci.* **2014**, *111*, 7968–7973.

17. Pugh, C.W.; Ratcliffe, P.J. Regulation of angiogenesis by hypoxia: role of the HIF system. *Nat. Med.* **2003**, *9*, 677–684.

18. Hickey, M.M.; Simon, M.C. Regulation of Angiogenesis by Hypoxia and Hypoxia-Inducible Factors. *Curr. Top. Dev. Biol.* **2006**, *76*, 217–257.

19. Heil, M.; Eitenmüller, I.; Schmitz-Rixen, T.; Schaper, W. Arteriogenesis versus angiogenesis: Similarities and differences. *J. Cell. Mol. Med.* **2006**, *10*, 45–55.

20. Pugsley, M.K.; Tabrizchi, R. The vascular system: An overview of structure and function. *J. Pharmacol. Toxicol. Methods* **2000**, *44*, 333–340.

21. Dew, L. Development of angiogenic models to investigate neovascularisation for tissue engineering applications, PhD Thesis, The University of Sheffield, 2015.

22. Langer, R.; Vacanti, J.P. Tissue Engineering. *Science (80-. ).* **1993**, *260*, 920–926.

23. Langer, R. Tissue Engineering. *Mol. Ther.* **2000**, *1*, 12–15.

24. Rivron, N.C.; Liu, J.; Rouwkema, J.; De Boer, J.; Van Blitterswijk, C.A. Engineering vascularised tissues in vitro. *Eur. Cells Mater.* **2008**, *15*, 27–40.

25. Lovett, M.; Lee, K.; Edwards, A.; Kaplan, D.L. Vascularization strategies for tissue engineering. *Tissue Eng. - Part B Rev.* **2009**, *15*, 353–370.

26. Rouwkema, J.; Rivron, N.C.; van Blitterswijk, C.A. Vascularization in tissue engineering. *Trends Biotechnol.* **2008**, *26*, 434–441.

27. Conway, E.M.; Collen, D.; Carmeliet, P. Molecular mechanisms of blood vessel growth. *Cardiovasc. Res.* **2001**, *49*, 507–521.

28. Potente, M.; Gerhardt, H.; Carmeliet, P. Basic and therapeutic aspects of angiogenesis. *Cell* **2011**, *146*, 873–887.

29. Chen, L.; Endler, A.; Shibasaki, F. Hypoxia and angiogenesis: Regulation of hypoxia-inducible factors via novel binding factors. *Exp. Mol. Med.* **2009**, *41*, 849–857.

30. Krock, B.L.; Skuli, N.; Simon, M.C. Hypoxia-Induced Angiogenesis: Good and Evil. *Genes and Cancer* **2011**, *2*, 1117–1133.

31. Ziello, J.E.; Jovin, I.S.; Huang, Y. Hypoxia-Inducible Factor (HIF)-1 regulatory pathway and its potential for therapeutic intervention in malignancy and ischemia. *Yale J. Biol. Med.* **2007**, *80*, 51–60.

32. Duda, D.G.; Fukumura, D.; Jain, R.K. Role of eNOS in neovascularization: NO for endothelial progenitor cells. *Trends Mol. Med.* **2004**, *10*, 143–145.

33. Ferrara, N. Role of vascular endothelial growth factor in regulation of physiological angiogenesis. *Am. J. Physiol. - Cell Physiol.* **2001**, *280*, C1358–1366.

34. Ferrara, N. VEGF-A: A critical regulator of blood vessel growth. *Eur. Cytokine Netw.* **2009**, *20*, 158–163.

35. Soker, S.; Takashima, S.; Miao, H.Q.; Neufeld, G.; Klagsbrun, M. Neuropilin-1 is expressed by endothelial and tumor cells as an isoform- specific receptor for vascular endothelial growth factor. *Cell* **1998**, *92*, 735–745.

36. Distler, J.H.W.; Hirth, A.; Kurowska-Stolarska, M.; Gay, R.E.; Gay, S.; Distler, O. Angiogenic and angiostatic factors in the molecular control of angiogenesis. *Q. J. Nucl. Med.* **2003**, *47*, 149–61.

37. Dew, L.; MacNeil, S.; Chong, C.K. Vascularization strategies for tissue engineers. *Regen. Med.* **2015**, *10*, 211–224.

38. Hoeben, A.N.N.; Landuyt, B.; Highley, M.S.M.; Wildiers, H.; Oosterom, A.T.V.A.N.;

Bruijn, E.A.D.E.; Van Oosterom, A.T.; De Bruijn, E.A. Vascular endothelial growth factor and angiogenesis. *Pharmacol. Rev.* **2004**, *56*, 549–580.

39. Peach, C.J.; Mignone, V.W.; Arruda, M.A.; Alcobia, D.C.; Hill, S.J.; Kilpatrick, L.E.; Woolard, J. Molecular pharmacology of VEGF-A isoforms: Binding and signalling at VEGFR2. *Int. J. Mol. Sci.* **2018**, *19*.

40. Zhu, X.; Zhou, W. The emerging regulation of VEGFR-2 in triple-negative breast cancer. *Front. Endocrinol. (Lausanne).* **2015**, *6*.

41. Olsson, A.K.; Dimberg, A.; Kreuger, J.; Claesson-Welsh, L. VEGF receptor signalling - In control of vascular function. *Nat. Rev. Mol. Cell Biol.* **2006**, *7*, 359–371.

42. Kendall, R.L.; Thomas, K.A. Inhibition of vascular endothelial cell growth factor activity by an endogenously encoded soluble receptor. *Proc. Natl. Acad. Sci. U. S. A.* **1993**, *90*, 10705–10709.

43. Shibuya, M. Vascular endothelial growth factor receptor-1 (VEGFR-1/Flt-1): a dual regulator for angiogenesis. *Angiogenesis* **2006**, *9*, 225–230.

44. Dumont, D.J.; Jussila, L.; Taipale, J.; Lymboussaki, A.; Mustonen, T.; Pajusola, K.; Breitman, M.; Alitalo, K. Cardiovascular failure in mouse embryos deficient in VEGF receptor-3. *Science (80-. ).* **1998**, *282*, 946–949.

45. Deng, Y.; Zhang, X.; Simons, M. Molecular controls of lymphatic VEGFR3 signaling. *Arterioscler. Thromb. Vasc. Biol.* **2015**, *35*, 421–429.

46. Meadows, K.N.; Bryant, P.; Pumiglia, K. Vascular Endothelial Growth Factor Induction of the Angiogenic Phenotype Requires Ras Activation. *J. Biol. Chem.* **2001**, *276*, 49289–49298.

47. Zachary, I.; Gliki, G. Signaling transduction mechanisms mediating biological actions of the vascular endothelial growth factor family. *Cardiovasc. Res.* **2001**, *49*, 568–581.

48. Wong, C.; Jin, Z.G. Protein kinase C-dependent protein kinase D activation modulates ERK signal pathway and endothelial cell proliferation by vascular endothelial growth factor. *J. Biol. Chem.* **2005**, *280*, 33262–33269.

49. Holmqvist, K.; Cross, M.; Riley, D.; Welsh, M. The Shb adaptor protein causes Src-

dependent cell spreading and activation of focal adhesion kinase in murine brain endothelial cells. *Cell. Signal.* **2003**, *15*, 171–179.

50. Parsons, J.T. Focal adhesion kinase: The first ten years. *J. Cell Sci.* **2003**, *116*, 1409–1416.

51. Lamalice, L.; Houle, F.; Huot, J. Phosphorylation of Tyr 1214 within VEGFR-2 triggers the recruitment of Nck and activation of Fyn leading to SAPK2/p38 activation and endothelial cell migration in response to VEGF. *J. Biol. Chem.* **2006**, *281*, 34009–34020.

52. Cantley, L.C. The phosphoinositide 3-kinase pathway. *Science (80-. ).* **2002**, *296*, 1655–1657.

53. Cardone, M.H.; Roy, N.; Stennicke, H.R.; Salvesen, G.S.; Franke, T.F.; Stanbridge, E.; Frisch, S.; Reed, J.C. Regulation of cell death protease caspase-9 by phosphorylation. *Science (80-. ).* **1998**, *282*, 1318–1321.

54. Fukumura, D.; Gohongi, T.; Kadambi, A.; Izumi, Y.; Ang, J.; Yun, C.O.; Buerk, D.G.; Huang, P.L.; Jain, R.K. Predominant role of endothelial nitric oxide synthase in vascular endothelial growth factor-induced angiogenesis and vascular permeability. *Proc. Natl. Acad. Sci. U. S. A.* **2001**, *98*, 2604–2609.

55. Ross, R.; Raines, E.W.; Bowen-Pope, D.F. The biology of platelet-derived growth factor. *Cell* **1986**, *46*, 155–169.

56. Laschke, M.W.; Elitzsch, A.; Vollmar, B.; Vajkoczy, P.; Menger, M.D. Combined inhibition of vascular endothelial growth factor (VEGF), fibroblast growth factor and platelet-derived growth factor, but not inhibition of VEGF alone, effectively suppresses angiogenesis and vessel maturation in endometriotic lesions. *Hum. Reprod.* **2006**, *21*, 262–268.

57. Ferrari, G.; Cook, B.D.; Terushkin, V.; Pintucci, G.; Mignatti, P. Transforming Growth Factor-Beta 1 (Tgf-B1) Induces Angiogenesis Through Vascular Endothelial Growth Factor (VEGF)-Mediated Apoptosis. *J. Cell. Physiol.* **2009**, *219*, 449–458.

58. Maragoudakis, M.E. Angiogenesis in health and disease. *Gen. Pharmacol. Vasc. Syst.* **2000**, *35*, 225–226.

59. Doi, K.; Ikeda, T.; Marui, A.; Kushibiki, T.; Arai, Y.; Hirose, K.; Soga, Y.; Iwakura, A.; Ueyama, K.; Yamahara, K.; et al. Enhanced angiogenesis by gelatin hydrogels incorporating basic fibroblast growth factor in rabbit model of hind limb ischemia. *Heart Vessels* **2007**, *22*, 104–108.

60. Cross, M.J.; Claesson-Welsh, L. FGF and VEGF function in angiogenesis: Signalling pathways, biological responses and therapeutic inhibition. *Trends Pharmacol. Sci.* **2001**, *22*, 201–207.

61. Nikhil, K.; Sharan, S.; Wishard, R.; Palla, S.R.; Krishna Peddinti, R.; Roy, P. Pterostilbene carboxaldehyde thiosemicarbazone, a resveratrol derivative inhibits 17β-Estradiol induced cell migration and proliferation in HUVECs. *Steroids* **2016**, *108*, 17–30.

62. Rubanyi, G.M.; Johns, A.; Kauser, K. Effect of estrogen on endothelial function and angiogenesis. *Vascul. Pharmacol.* **2002**, *38*, 89–98.

63. Morales, D.E.; McGowan, K.A.; Grant, D.S.; Maheshwari, S.; Bhartiya, D.; Cid, M.C.; Kleinman, H.K.; H. William Schnaper Estrogen Promotes Angiogenic Activity in Human Umbilical Vein Endothelial Cells In Vitro and in a Murine Model. *Circulation* **1995**, *91*, 755–63.

64. Losordo, D.W.; Isner, J.M. Estrogen and Angiogenesis : A Review. *Arterioscler. Thromb. Vasc. Biol.* **2001**, *21*, 6–12.

65. Matsubara, Y.; Matsubara, K. Estrogen and progesterone play pivotal roles in endothelial progenitor cell proliferation. *Reprod. Biol. Endocrinol.* **2012**, *10*, 2.

66. Stefanick, M.L. Estrogens and progestins: Background and history, trends in use, and guidelines and regimens approved by the US Food and Drug Administration. In Proceedings of the American Journal of Medicine; 2005; Vol. 118.

67. Fisher, B.; Costantino, J.; Redmond, C.; Poisson, R.; Bowman, D.; Couture, J.; Dimitrov, N. V; Wolmark, N.; Wickerham, D.L.; Fisher, E.R. A randomized clinical trial evaluating tamoxifen in the treatment of patients with node-negative breast cancer who have estrogen-receptor-positive tumors. *N. Engl. J. Med.* **1989**, *320*, 479–84.

68. Early Breast Cancer Trialists Collaborative Group Tamoxifen for early breast cancer: an overview of the randomised trials. *Lancet* **1998**, *351*, 1451–1467.

69. Mangır, N.; Hillary, C.J.; Chapple, C.R.; MacNeil, S. Oestradiol-releasing Biodegradable Mesh Stimulates Collagen Production and Angiogenesis: An Approach to Improving Biomaterial Integration in Pelvic Floor Repair. *Eur. Urol. Focus* **2019**, *5*, 280–289.

70. Desgranges, C.; Razaka, G.; Rabaud, M.; Bricaud, H. Catabolism of thymidine in human blood platelets purification and properties of thymidine phosphorylase. *BBA Sect. Nucleic Acids Protein Synth.* **1981**, *654*, 211–218.

71. Brown, N.S.; Bicknell, R. Thymidine phosphorylase, 2-deoxy-D-ribose and angiogenesis. *Biochem. J.* **1998**, *334*, 1–8.

72. Barton, G.J.; Ponting, C.P.; Spraggon, G.; Finnis, C.; Sleep, D. Human platelet-derived endothelial cell growth factor is homologous to Escherichia coli thymidine phosphorylase. *Protein Sci.* **1992**, *1*, 688–690.

73. Usuki, K.; Saras, J.; Waltenberger, J.; Miyazono, K.; Pierce, G.; Thomason, A.; Heldin, C.H. Platelet-derived endothelial cell growth factor has thymidine phosphorylase activity. *Biochem. Biophys. Res. Commun.* **1992**, *184*, 1311–1316.

74. Friedkin, M.; Roberts, D. The enzymatic synthesis of nucleosides. I. Thymidine phosphorylase in mammalian tissue. *J. Biol. Chem.* **1954**, *207*, 245–256.

75. Furukawa, T.; Yoshimura, A.; Sumizawa, T.; Haraguchi, M.; Akiyama, S.I.; Fukui, K.; Ishizawa, M.; Yamada, Y. Angiogenic factor [12]. *Nature* **1992**, *356*, 668.

76. Moghaddam, A.; Zhang, H.T.; Fan, T.P.; Hu, D.E.; Lees, V.C.; Turley, H.; Fox, S.B.; Gatter, K.C.; Harris, A.L.; Bicknell, R. Thymidine phosphorylase is angiogenic and promotes tumor growth. *Proc. Natl. Acad. Sci. U. S. A.* **1995**, *92*, 998–1002.

77. Ishikawa, F.; Miyazono, K.; Hellman, U.; Drexler, H.; Wernstedt, C.; Hagiwara, K.; Usuki, K.; Takaku, F.; Risau, W.; Heldin, C.H. Identification of angiogenic activity and the cloning and expression of platelet-derived endothelial cell growth factor. *Nature* **1989**, *338*, 557–562.

78. Miyadera, K.; Sumizawa, T.; Haraguchi, M.; Yoshida, H.; Konstanty, W.; Yamada, Y.;

Akiyama, S. Role of thymidine phosphorylase activity in the angiogenic effect of platelet derived endothelial cell growth factor/thymidine phosphorylase. *Cancer Res.* **1995**, *55*, 1687–1690.

79. Moghaddam, A.; Choudhuri, R.; Bicknell, R. Thymidine phosphorylase/platelet-derived endothelial cell growth factor: an angiogenic enzyme Tumour Angiogenesis. In *Tumour Angiogenesis*; 1997; pp. 251–260.

80. Matsushita, S.; Nitanda, T.; Furukawa, T.; Sumizawa, T.; Tani, A.; Nishimoto, K.; Akiba, S.; Miyadera, K.; Fukushima, M.; Yamada, Y.; et al. The effect of a thymidine phosphorylase inhibitor on angiogenesis and apoptosis in tumors. *Cancer Res.* **1999**, *59*, 1911–1916.

81. Haraguchi, M.; Miyadera, K.; Uemura, K.; Sumizawa, T.; Furukawa, T.; Yamada, K.; Akiyama, S.; Yamada, Y. Angiogenic activity of enzymes. *Nature* **1994**, *368*, 198.

82. Sengupta, S.; Sellers, L.A.; Matheson, H.B.; Fan, T.P.D. Thymidine phosphorylase induces angiogenesis in vivo and in vitro: An evaluation of possible mechanisms. *Br. J. Pharmacol.* **2003**, *139*, 219–231.

83. Uchimiya, H.; Furukawa, T.; Okamoto, M.; Nakajima, Y.; Matsushita, S.; Ikeda, R.; Gotanda, T.; Haraguchi, M.; Sumizawa, T.; Ono, M.; et al. Suppression of thymidine phosphorylase-mediated angiogenesis and tumor growth by 2-deoxy-L-ribose. *Cancer Res.* **2002**, *62*, 2834–2839.

84. Nakajima, Y.; Madhyastha, R.; Maruyama, M. 2-Deoxy-D-Ribose, a Downstream Mediator of Thymidine Phosphorylase, Regulates Tumor Angiogenesis and Progression. *Anticancer. Agents Med. Chem.* **2009**, *9*, 239–245.

85. Ikeda, R.; Che, X.F.; Ushiyama, M.; Yamaguchi, T.; Okumura, H.; Nakajima, Y.; Takeda, Y.; Shibayama, Y.; Furukawa, T.; Yamamoto, M.; et al. 2-Deoxy-D-ribose inhibits hypoxia-induced apoptosis by suppressing the phosphorylation of p38 MAPK. *Biochem. Biophys. Res. Commun.* **2006**, *342*, 280–285.

86. Nakajima, Y.; Gotanda, T.; Uchimiya, H.; Furukawa, T.; Haraguchi, M.; Ikeda, R.; Sumizawa, T.; Yoshida, H.; Akiyama, S.I. Inhibition of Metastasis of Tumor Cells Overexpressing Thymidine Phosphorylase by 2-Deoxy-L-Ribose. *Cancer Res.* **2004**, *64*, 1794–1801.

87. Yar, M.; Shahzadi, L.; Mehmood, A.; Raheem, M.I.; Román, S.; Chaudhry, A.A.; ur Rehman, I.; Ian Douglas, C.W.; MacNeil, S. Deoxy-sugar releasing biodegradable hydrogels promote angiogenesis and stimulate wound healing. *Mater. Today Commun.* **2017**, *13*, 295–305.

88. Dikici, S.; Aldemir Dikici, B.; Bhaloo, S.I.; Balcells, M.; Edelman, E.R.; MacNeil, S.; Reilly, G.C.; Sherborne, C.; Claeyssens, F. Assessment of the angiogenic potential of 2-deoxy-D-ribose using a novel in vitro 3D dynamic model in comparison with established in vitro assays. *Front. Bioeng. Biotechnol.* **2019**, *7*, 451.

89. Dikici, S.; Mangir, N.; Claeyssens, F.; Yar, M.; MacNeil, S. Exploration of 2-deoxy-D-ribose and 17β-Estradiol as alternatives to exogenous VEGF to promote angiogenesis in tissue-engineered constructs. *Regen. Med.* **2019**, *14*, 179–197.

90. Azam, M.; Dikici, S.; Roman, S.; Mehmood, A.; Chaudhry, A.A.; U Rehman, I.; MacNeil, S.; Yar, M. Addition of 2-deoxy-d-ribose to clinically used alginate dressings stimulates angiogenesis and accelerates wound healing in diabetic rats. *J. Biomater. Appl.* **2019**, *34*, 463–475.

91. Neve, A.; Cantatore, F.P.; Maruotti, N.; Corrado, A.; Ribatti, D. Extracellular matrix modulates angiogenesis in physiological and pathological conditions. *Biomed Res. Int.* **2014**, *2014*, 756078.

92. Soldi, R.; Mitola, S.; Strasly, M.; Defilippi, P.; Tarone, G.; Bussolino, F. Role of α(v)β3 integrin in the activation of vascular endothelial growth factor receptor-2. *EMBO J.* **1999**, *18*, 882–892.

93. Somanath, P.R.; Malinin, N.L.; Byzova, T. V. Cooperation between integrin αvβ3 and VEGFR2 in angiogenesis. *Angiogenesis* **2009**, *12*, 177–185.

94. Serini, G.; Napione, L.; Arese, M.; Bussolino, F. Besides adhesion: New perspectives of integrin functions in angiogenesis. *Cardiovasc. Res.* **2008**, *78*, 213–222.

95. Davis, G.E.; Camarillo, C.W. An α2β1 integrin-dependent pinocytic mechanism involving intracellular vacuole formation and coalescence regulates capillary lumen and tube formation in three-dimensional collagen matrix. *Exp. Cell Res.* **1996**, *224*, 39–51.

96. Lafoya, B.; Munroe, J.A.; Miyamoto, A.; Detweiler, M.A.; Crow, J.J.; Gazdik, T.; Albig, A.R. Beyond the matrix: The many non-ECM ligands for integrins. *Int. J. Mol. Sci.* **2018**, *19*.

97. Grose, R.; Hutter, C.; Bloch, W.; Thorey, I.; Watt, F.M.; Fässler, R.; Brakebusch, C.; Werner, S. A crucial role of β1 integrins for keratinocyte migration in vitro and during cutaneous wound repair. *Development* **2002**, *129*, 2303–2315.

98. Schnittert, J.; Bansal, R.; Storm, G.; Prakash, J. Integrins in wound healing, fibrosis and tumor stroma: High potential targets for therapeutics and drug delivery. *Adv. Drug Deliv. Rev.* **2018**, *129*, 37–53.

99. Koivisto, L.; Heino, J.; Häkkinen, L.; Larjava, H. Integrins in Wound Healing. *Adv. Wound Care* **2014**, *3*, 762–783.

100. Hakkinen, L.; Heino, J.; Koivisto, L.; Larjava, H. Altered interaction of human granulation-tissue fibroblasts with fibronectin is regulated by alpha 5 beta 1 integrin. *Biochim Biophys Acta* **1994**, *1224*, 33–42.

101. Erb, L.; Liao, Z.; Seye, C.I.; Weisman, G.A. P2 receptors: Intracellular signaling. *Pflugers Arch. Eur. J. Physiol.* **2006**, *452*, 552–562.

102. Twardowski, T.; Fertala, A.; Orgel, J.; San Antonio, J. Type I Collagen and Collagen Mimetics as Angiogenesis Promoting Superpolymers. *Curr. Pharm. Des.* **2007**, *13*, 3608–3621.

103. Simon-Assmann, P.; Orend, G.; Mammadova-Bach, E.; Spenlé, C.; Lefebvre, O. Role of laminins in physiological and pathological angiogenesis. *Int. J. Dev. Biol.* **2011**, *55*, 455–465.

104. Nicosia, R.F.; Bonanno, E.; Smith, M. Fibronectin promotes the elongation of microvessels during angiogenesis in vitro. *J. Cell. Physiol.* **1993**, *154*, 654–661.

105. Li, R.; Luo, M.; Ren, M.; Chen, N.; Xia, J.; Deng, X.; Zeng, M.; Yan, K.; Luo, T.; Wu, J. Vitronectin regulation of vascular endothelial growth factor-mediated angiogenesis. *J. Vasc. Res.* **2014**, *51*, 110–117.

106. West, D.C.; Kumar, S. Hyaluronan and angiogenesis. In *Ciba Foundation symposium*; 1989; Vol. 143, pp. 187–207.

107. Marmé, D.; Fusenig, N. *Tumor angiogenesis: Basic mechanisms and cancer therapy*; 2008; ISBN 9783540331766.

108. Egeblad, M.; Werb, Z. New functions for the matrix metalloproteinases in cancer progression. *Nat. Rev. Cancer* **2002**, *2*, 161–174.

109. Benjamin, M.; Hillen, B. Mechanical Influences on Cells, Tissues and Organs - "Mechanical Morphogenesis." *Eur. J. Morphol.* **2003**, *41*, 3–7.

110. Wang, J.H.C. Cell traction forces (CTFs) and CTF microscopy applications in musculoskeletal research. *Oper. Tech. Orthop.* **2010**, *20*, 106–109.

111. Shiu, Y.T.; Weiss, J.A.; Hoying, J.B.; Iwamoto, M.N.; Joung, I.S.; Quam, C.T. The role of mechanical stresses in angiogenesis. *Crit. Rev. Biomed. Eng.* **2005**, *33*, 431–510.

112. Chistiakov, D.A.; Orekhov, A.N.; Bobryshev, Y. V. Effects of shear stress on endothelial cells: go with the flow. *Acta Physiol.* **2017**, *219*, 382–408.

113. dela Paz, N.G.; Walshe, T.E.; Leach, L.L.; Saint-Geniez, M.; D'Amore, P.A. Role of shear-stress-induced VEGF expression in endothelial cell survival. *J. Cell Sci.* **2012**, *125*, 831–843.

114. Simmers, M.B.; Pryor, A.W.; Blackman, B.R. Arterial shear stress regulates endothelial cell-directed migration, polarity, and morphology in confluent monolayers. *Am. J. Physiol. - Hear. Circ. Physiol.* **2007**, *293*, H1937–H1946.

115. Byrne, A.M.; Bouchier-Hayes, D.J.; Harmey, J.H. Angiogenic and cell survival functions of Vascular Endothelial Growth Factor (VEGF). *J. Cell. Mol. Med.* **2005**, *9*, 777–794.

116. Carmeliet, P. Angiogenesis in health and disease. *Nat. Med.* **2003**, *9*, 653–660.

117. Laschke, M.W.; Menger, M.D. Prevascularization in tissue engineering: Current concepts and future directions. *Biotechnol. Adv.* **2016**, *34*, 112–121.

118. Schechner, J.S.; Nath, K.; Zheng, L.; Kluger, M.S.; Hughes, C.C.; Sierra-Honigmann, M.R.; Lorber, M.I.; Tellides, G.; Kashgarian, M.; Bothwell, L.; et al. In vivo formation of complex microvessels lined by human endothelial cells in an immunodeficient mouse. *Proc. Natl. Acad. Sci. U. S. A.* **2000**, *97*, 9191–6.

119. Chen, W.; Thein-Han, W.; Weir, M.D.; Chen, Q.; Xu, H.H.K. Prevascularization of biofunctional calcium phosphate cement for dental and craniofacial repairs. *Dent. Mater.* **2014**, *30*, 535–544.

120. Peters, M.C.; Polverini, P.J.; Mooney, D.J. Engineering vascular networks in porous polymer matrices. *J. Biomed. Mater. Res.* **2002**, *60*, 668–678.

121. Nör, J.E.; Peters, M.C.; Christensen, J.B.; Sutorik, M.M.; Linn, S.; Khan, M.K.; Addison, C.L.; Mooney, D.J.; Polverini, P.J. Engineering and characterization of functional human microvessels in immunodeficient mice. *Lab. Investig.* **2001**, *81*, 453–463.

122. Tremblay, P.L.; Hudon, V.; Berthod, F.; Germain, L.; Auger, F.A. Inosculation of tissue-engineered capillaries with the host's vasculature in a reconstructed skin transplanted on mice. *Am. J. Transplant.* **2005**, *5*, 1002–1010.

123. Baiguera, S.; Ribatti, D. Endothelialization approaches for viable engineered tissues. *Angiogenesis* **2013**, *16*, 1–14.

124. Baldwin, J.; Antille, M.; Bonda, U.; De-Juan-Pardo, E.M.; Khosrotehrani, K.; Ivanovski, S.; Petcu, E.B.; Hutmacher, D.W. In vitro pre-vascularisation of tissue-engineered constructs A co-culture perspective. *Vasc. Cell* **2014**, *6*, 1–13.

125. Duttenhoefer, F.; Lara De Freitas, R.; Meury, T.; Loibl, M.; Benneker, L.M.; Richards, R.G.; Alini, M.; Verrier, S. 3D scaffolds co-seeded with human endothelial progenitor and mesenchymal stem cells: Evidence of prevascularisation within 7 days. *Eur. Cells Mater.* **2013**, *26*, 49–65.

126. Wu, X.; Rabkin-Aikawa, E.; Guleserian, K.J.; Perry, T.E.; Masuda, Y.; Sutherland, F.W.H.; Schoen, F.J.; Mayer, J.E.; Bischoff, J. Tissue-engineered microvessels on three-dimensional biodegradable scaffolds using human endothelial progenitor cells. *Am. J. Physiol. - Hear. Circ. Physiol.* **2004**, *287*, H480–H487.

127. Liu, J.; Liu, C.; Sun, B.; Shi, C.; Qiao, C.; Ke, X.; Liu, S.; Liu, X.; Sun, H. Differentiation of Rabbit Bone Mesenchymal Stem Cells into Endothelial Cells In Vitro and Promotion of Defective Bone Regeneration In Vivo. *Cell Biochem. Biophys.* **2014**, *68*, 479–487.

128. Miranville, A.; Heeschen, C.; Sengenès, C.; Curat, C.A.; Busse, R.; Bouloumié, A. Improvement of postnatal neovascularization by human adipose tissue-derived

stem cells. *Circulation* **2004**, *110*, 349–355.

129. Abruzzo, A.; Fiorica, C.; Palumbo, V.D.; Altomare, R.; Damiano, G.; Gioviale, M.C.; Tomasello, G.; Licciardi, M.; Palumbo, F.S.; Giammona, G.; et al. Using Polymeric Scaffolds for Vascular Tissue Engineering. *Int. J. Polym. Sci.* **2014**, *2014*, 1–9.

130. Zhang, W.J.; Liu, W.; Cui, L.; Cao, Y. Tissue engineering of blood vessel. *J. Cell. Mol. Med.* **2007**, *11*, 945–57.

131. Singh, S.; Wu, B.M.; Dunn, J.C.Y. Accelerating vascularization in polycaprolactone scaffolds by endothelial progenitor cells. *Tissue Eng. Part A* **2011**, *17*, 1819–30.

132. Pektok, E.; Nottelet, B.; Tille, J.C.; Gurny, R.; Kalangos, A.; Moeller, M.; Walpoth, B.H. Degradation and healing characteristics of small-diameter poly(??-caprolactone) vascular grafts in the rat systemic arterial circulation. *Circulation* **2008**, *118*, 2563–2570.

133. Hegen, A.; Blois, A.; Tiron, C.E.; Hellesøy, M.; Micklem, D.R.; Nör, J.E.; Akslen, L.A.; Lorens, J.B. Efficient in vivo vascularization of tissue-engineering scaffolds. *J. Tissue Eng. Regen. Med.* **2011**, *5*, 1–19.

134. Jia, L.; Prabhakaran, M.P.; Qin, X.; Ramakrishna, S. Stem cell differentiation on electrospun nanofibrous substrates for vascular tissue engineering. *Mater. Sci. Eng. C* **2013**, *33*, 4640–4650.

135. Hoerstrup, S.P.; Cummings, I.; Lachat, M.; Schoen, F.J.; Jenni, R.; Leschka, S.; Neuenschwander, S.; Schmidt, D.; Mol, A.; Günter, C.; et al. Functional growth in tissue-engineered living, vascular grafts: Follow-up at 100 weeks in a large animal model. *Circulation* **2006**, *114*, 159–167.

136. Iwai, S.; Sawa, Y.; Ichikawa, H.; Taketani, S.; Uchimura, E.; Chen, G.; Hara, M.; Miyake, J.; Matsuda, H. Biodegradable polymer with collagen microsponge serves as a new bioengineered cardiovascular prosthesis. *J. Thorac. Cardiovasc. Surg.* **2004**, *128*, 472–479.

137. Grasl, C.; Bergmeister, H.; Stoiber, M.; Schima, H.; Weigel, G. Electrospun polyurethane vascular grafts: In vitro mechanical behavior and endothelial adhesion molecule expression. *J. Biomed. Mater. Res. - Part A* **2010**, *93*, 716–723.

138. Huang, C.; Chen, R.; Ke, Q.; Morsi, Y.; Zhang, K.; Mo, X. Electrospun collagen-chitosan-TPU nanofibrous scaffolds for tissue engineered tubular grafts. *Colloids Surfaces B Biointerfaces* **2011**, *82*, 307–315.

139. Motlagh, D.; Yang, J.; Lui, K.Y.; Webb, A.R.; Ameer, G.A. Hemocompatibility evaluation of poly(glycerol-sebacate) in vitro for vascular tissue engineering. *Biomaterials* **2006**, *27*, 4315–4324.

140. Akaraonye, E.; Filip, J.; Safarikova, M.; Salih, V.; Keshavarz, T.; Knowles, J.C.; Roy, I. Composite scaffolds for cartilage tissue engineering based on natural polymers of bacterial origin, thermoplastic poly(3-hydroxybutyrate) and micro-fibrillated bacterial cellulose. *Polym. Int.* **2016**, *65*, 780–791.

141. Bagdadi, A. V.; Safari, M.; Dubey, P.; Basnett, P.; Sofokleous, P.; Humphrey, E.; Locke, I.; Edirisinghe, M.; Terracciano, C.; Boccaccini, A.R.; et al. Poly(3-hydroxyoctanoate), a promising new material for cardiac tissue engineering. *J. Tissue Eng. Regen. Med.* **2018**, *12*, e495–e512.

142. Sultana, N.; Khan, T.H. In vitro degradation of PHBV scaffolds and nHA/PHBV composite scaffolds containing hydroxyapatite nanoparticles for bone tissue engineering. *J. Nanomater.* **2012**, *2012*.

143. Ortega, I.; Dew, L.; Kelly, A.G.; Chong, C.K.; MacNeil, S.; Claeyssens, F. Fabrication of biodegradable synthetic perfusable vascular networks via a combination of electrospinning and robocasting. *Biomater. Sci.* **2015**, *3*, 592–596.

144. Zhu, C.; Fan, D.; Duan, Z.; Xue, W.; Shang, L.; Chen, F.; Luo, Y. Initial investigation of novel human-like collagen/chitosan scaffold for vascular tissue engineering. *J. Biomed. Mater. Res. - Part A* **2009**, *89*, 829–840.

145. Zhu, C.; Fan, D.; Wang, Y. Human-like collagen/hyaluronic acid 3D scaffolds for vascular tissue engineering. *Mater. Sci. Eng. C* **2014**, *34*, 393–401.

146. Berglund, J.D.; Nerem, R.M.; Sambanis, A. Incorporation of Intact Elastin Scaffolds in Tissue-Engineered Collagen-Based Vascular Grafts. *Tissue Eng.* **2004**, *1010*, 1526–35.

147. Engbers-Buijtenhuijs, P.; Buttafoco, L.; Poot, A.A.; Dijkstra, P.J.; De Vos, R.A.I.; Sterk,

L.M.T.; Geelkerken, R.H.; Vermes, I.; Feijen, J. Biological characterisation of vascular grafts cultured in a bioreactor. *Biomaterials* **2006**, *27*, 2390–2397.

148. Marelli, B.; Achilli, M.; Alessandrino, A.; Freddi, G.; Tanzi, M.C.; Farè, S.; Mantovani, D. Collagen-Reinforced Electrospun Silk Fibroin Tubular Construct as Small Calibre Vascular Graft. *Macromol. Biosci.* **2012**, *12*, 1566–1574.

149. Lovett, M.; Eng, G.; Kluge, J. a; Cannizzaro, C.; Vunjak-novakovic, G.; Kaplan, D.L. Tubular silk sca olds for small diameter vascular grafts. *Organogenesis* **2010**, *6*, 217–224.

150. Panzavolta, S.; Gioffrè, M.; Focarete, M.L.; Gualandi, C.; Foroni, L.; Bigi, A. Electrospun gelatin nanofibers: Optimization of genipin cross-linking to preserve fiber morphology after exposure to water. *Acta Biomater.* **2011**, *7*, 1702–1709.

151. Tengood, J.E.; Ridenour, R.; Brodsky, R.; Russell, A.J.; Little, S.R. Sequential delivery of basic fibroblast growth factor and platelet-derived growth factor for angiogenesis. *Tissue Eng Part A* **2011**, *17*, 1181–1189.

152. Mason, M.N.; Mahoney, M.J. A novel composite construct increases the vascularization potential of PEG hydrogels through the incorporation of large fibrin ribbons. *J. Biomed. Mater. Res. - Part A* **2010**, *95*, 283–293.

153. Jiang, B.; Waller, T.M.; Larson, J.C.; Appel, A. a.; Brey, E.M. Fibrin-Loaded Porous Poly(Ethylene Glycol) Hydrogels as Scaffold Materials for Vascularized Tissue Formation. *Tissue Eng. Part A* **2013**, *19*, 224–234.

154. Sun, G.; Shen, Y.I.; Kusuma, S.; Fox-Talbot, K.; Steenbergen, C.J.; Gerecht, S. Functional neovascularization of biodegradable dextran hydrogels with multiple angiogenic growth factors. *Biomaterials* **2011**, *32*, 95–106.

155. Li, S.; Liu, Y.Y.; Liu, L.J.; Hu, Q.X. A Versatile Method for Fabricating Tissue Engineering Scaffolds with a Three-Dimensional Channel for Prevasculature Networks. *ACS Appl. Mater. Interfaces* **2016**, *8*, 25096–25103.

156. Kim, G.; Son, J.; Park, S.; Kim, W. Hybrid process for fabricating 3D hierarchical scaffolds combining rapid prototyping and electrospinning. *Macromol. Rapid Commun.* **2008**, *29*, 1577–1581.

157. Skardal, A.; Zhang, J.; Prestwich, G.D. Bioprinting vessel-like constructs using hyaluronan hydrogels crosslinked with tetrahedral polyethylene glycol tetracrylates. *Biomaterials* **2010**, *31*, 6173–6181.

158. Lee, V.K.; Kim, D.Y.; Ngo, H.; Lee, Y.; Seo, L.; Yoo, S.S.; Vincent, P.A.; Dai, G. Creating perfused functional vascular channels using 3D bio-printing technology. *Biomaterials* **2014**, *35*, 8092–8102.

159. Vanderburgh, J.; Sterling, J.A.; Guelcher, S.A. 3D Printing of Tissue Engineered Constructs for In Vitro Modeling of Disease Progression and Drug Screening. *Ann. Biomed. Eng.* **2017**, *45*, 164–179.

160. Rujing, Z.; Mikkel, J.; Niels, L. Stereolithography-based 3D printing of micro-channels for vascularized hydrogels. *Front. Bioeng. Biotechnol.* **2016**, *4*, 01303.

161. Vunjak-Novakovic, G.; Lui, K.O.; Tandon, N.; Chien, K.R. Bioengineering heart muscle: a paradigm for regenerative medicine. *Annu Rev Biomed Eng.* **2011**, *13*, 245–267.

162. Ott, H.C.; Matthiesen, T.S.; Goh, S.-K.; Black, L.D.; Kren, S.M.; Netoff, T.I.; Taylor, D. a Perfusion-decellularized matrix: using nature's platform to engineer a bioartificial heart. *Nat. Med.* **2008**, *14*, 213–221.

163. Linke, K.; Schanz, J.; Hansmann, J.; Walles, T.; Brunner, H.; Mertsching, H. Engineered liver-like tissue on a capillarized matrix for applied research. *Tissue Eng.* **2007**, *13*, 2699–707.

164. Sarig, U.; Au-Yeung, G.C.T.; Wang, Y.; Bronshtein, T.; Dahan, N.; Boey, F.Y.C.; Venkatraman, S.S.; Machluf, M. Thick acellular heart extracellular matrix with inherent vasculature: a potential platform for myocardial tissue regeneration. *Tissue Eng. Part A* **2012**, *18*, 2125–37.

165. Dew, L.; English, W.R.; Chong, C.K.; MacNeil, S. Investigating neovascularization in rat decellularized intestine - an in vitro platform for studying angiogenesis. *Tissue Eng. Part A* **2016**, *22*, ten.TEA.2016.0131.

166. Gershlak, J.R.; Hernandez, S.; Fontana, G.; Perreault, L.R.; Hansen, K.J.; Larson, S.A.; Binder, B.Y.K.; Dolivo, D.M.; Yang, T.; Dominko, T.; et al. Crossing kingdoms: Using

decellularized plants as perfusable tissue engineering scaffolds. *Biomaterials* **2017**, *125*, 13–22.

167. Fontana, G.; Gershlak, J.; Adamski, M.; Lee, J.S.; Matsumoto, S.; Le, H.D.; Binder, B.; Wirth, J.; Gaudette, G.; Murphy, W.L. Biofunctionalized Plants as Diverse Biomaterials for Human Cell Culture. *Adv. Healthc. Mater.* **2017**, *6*, 1–16.

168. Lin, R.Z.; Chang, H.Y. Recent advances in three-dimensional multicellular spheroid culture for biomedical research. *Biotechnol. J.* **2008**, *3*, 1172–1184.

169. Ivascu, A.; Kubbies, M. Rapid generation of single-tumor spheroids for high-throughput cell function and toxicity analysis. *J. Biomol. Screen.* **2006**, *11*, 922–932.

170. Korff, T.; Kimmina, S.; Martiny-Baron, G.; Augustin, H.G. Blood vessel maturation in a 3-dimensional spheroidal coculture model: Direct contact with smooth muscle cells regulates endothelial cell quiescence and abrogates VEGF responsiveness. *FASEB J.* **2001**, *15*, 447–457.

171. Ware, M.J.; Colbert, K.; Keshishian, V.; Ho, J.; Corr, S.J.; Curley, S.A.; Godin, B. Generation of homogenous three-dimensional pancreatic cancer cell spheroids using an improved hanging drop technique. *Tissue Eng. - Part C Methods* **2016**, *22*, 312–321.

172. Mehta, G.; Hsiao, A.Y.; Ingram, M.; Luker, G.D.; Takayama, S. Opportunities and challenges for use of tumor spheroids as models to test drug delivery and efficacy. *J. Control. Release* **2012**, *164*, 192–204.

173. Rouwkema, J.; De Boer, J.; Van Blitterswijk, C.A. Endothelial cells assemble into a 3-dimensional prevascular network in a bone tissue engineering construct. *Tissue Eng.* **2006**, *12*, 2685–2693.

174. Verseijden, F.; Posthumus-van Sluijs, S.J.; Farrell, E.; Van Neck, J.W.; Hovius, S.E.R.; Hofer, S.O.P.; Van Osch, G.J.V.M. Prevascular structures promote vascularization in engineered human adipose tissue constructs upon implantation. *Cell Transplant.* **2010**, *19*, 1007–1020.

175. Bhang, S.H.; Lee, S.; Shin, J.Y.; Lee, T.J.; Kim, B.S. Transplantation of cord blood mesenchymal stem cells as spheroids enhances vascularization. *Tissue Eng. - Part*

*A* **2012**, *18*, 2138–2147.

176. Sekiya, S.; Shimizu, T.; Okano, T. Vascularization in 3D tissue using cell sheet technology. *Regen. Med.* **2013**, *8*, 371–377.

177. Haraguchi, Y.; Shimizu, T.; Sasagawa, T.; Sekine, H.; Sakaguchi, K.; Kikuchi, T.; Sekine, W.; Sekiya, S.; Yamato, M.; Umezu, M.; et al. Fabrication of functional three-dimensional tissues by stacking cell sheets in vitro. *Nat. Protoc.* **2012**, *7*, 850–858.

178. Tsuda, Y.; Shimizu, T.; Yamato, M.; Kikuchi, A.; Sasagawa, T.; Sekiya, S.; Kobayashi, J.; Chen, G.; Okano, T. Cellular control of tissue architectures using a three-dimensional tissue fabrication technique. *Biomaterials* **2007**, *28*, 4939–4946.

179. Pirraco, R.P.; Obokata, H.; Iwata, T.; Marques, A.P.; Tsuneda, S.; Yamato, M.; Reis, R.L.; Okano, T. Development of osteogenic cell sheets for bone tissue engineering applications. *Tissue Eng. - Part A* **2011**, *17*, 1507–1515.

180. Sekiya, S.; Shimizu, T.; Yamato, M.; Kikuchi, A.; Okano, T. Bioengineered cardiac cell sheet grafts have intrinsic angiogenic potential. *Biochem. Biophys. Res. Commun.* **2006**, *341*, 573–582.

181. Sekine, H.; Shimizu, T.; Hobo, K.; Sekiya, S.; Yang, J.; Yamato, M.; Kurosawa, H.; Kobayashi, E.; Okano, T. Endothelial cell coculture within tissue-engineered cardiomyocyte sheets enhances neovascularization and improves cardiac function of ischemic hearts. *Circulation* **2008**, *118*.

182. Cerqueira, M.T.; Pirraco, R.P.; Martins, A.R.; Santos, T.C.; Reis, R.L.; Marques, A.P. Cell sheet technology-driven re-epithelialization and neovascularization of skin wounds. *Acta Biomater.* **2014**, *10*, 3145–3155.

183. Mendes, L.F.; Pirraco, R.P.; Szymczyk, W.; Frias, A.M.; Santos, T.C.; Reis, R.L.; Marques, A.P. Perivascular-like cells contribute to the stability of the vascular network of osteogenic tissue formed from cell sheet-based constructs. *PLoS One* **2012**, *7*, e41051.

184. Laschke, M.W.; Rücker, M.; Jensen, G.; Carvalho, C.; Mülhaupt, R.; Gellrich, N.C.; Menger, M.D. Improvement of vascularization of PLGA scaffolds by inosculation of in situ-preformed functional blood vessels with the host microvasculature. *Ann.*

*Surg.* **2008**, *248*, 939–947.

185. Erol, O. The transformation of a free skin graft into a vascularized pedicled flap. *Plast. Reconstr. Surg.* **1976**, *58*, 470–477.

186. Warnke, P.; Springer, I.; Wiltfang, P.J.; Acil, P.Y.; Eufinger, P.H.; Wehmöller, M.; Russo, P.; Bolte, H.; Sherry, E.; Behrens, E.; et al. Growth and transplantation of a custom vascularised bone graft in a man. *Lancet* **2004**, *364*, 766–770.

187. Erol, O.; Spira, M. New capillary bed formation with a surgically constructed arteriovenous fistula. *Plast. Reconstr. Surg.* **1979**, *66*, 109–115.

188. Lokmic, Z.; Stillaert, F.; Morrison, W.A.; Thompson, E.W.; Mitchell, G.M. An arteriovenous loop in a protected space generates a permanent, highly vascular, tissue-engineered construct. *FASEB J.* **2007**, *21*, 511–522.

189. CASSELL, O.C.S.; MORRISON, W.A.; MESSINA, A.; PENINGTON, A.J.; THOMPSON, E.W.; STEVENS, G.W.; PERERA, J.M.; KLEINMAN, H.K.; HURLEY, J. V.; ROMEO, R.; et al. The Influence of Extracellular Matrix on the Generation of Vascularized, Engineered, Transplantable Tissue. *Ann. N. Y. Acad. Sci.* **2006**, *944*, 429–442.

190. Arkudas, A.; Tjiawi, J.; Bleiziffer, O.; Grabinger, L.; Polykandriotis, E.; Beier, J.P.; Stürzl, M.; Horch, R.E.; Kneser, U. Fibrin gel-immobilized VEGF and bFGF efficiently stimulate angiogenesis in the AV loop model. *Mol. Med.* **2007**, *13*, 480–487.

191. Tanaka, Y.; Tsutsumi, A.; Crowe, D.M.; Tajima, S.; Morrison, W.A. Generation of an autologous tissue (matrix) flap by combining an arteriovenous shunt loop with artificial skin in rats: Preliminary report. *Br. J. Plast. Surg.* **2000**, *53*, 51–57.

192. Cao, Y.; Mitchell, G.; Messina, A.; Price, L.; Thompson, E.; Penington, A.; Morrison, W.; O'Connor, A.; Stevens, G.; Cooper-White, J. The influence of architecture on degradation and tissue ingrowth into three-dimensional poly(lactic-co-glycolic acid) scaffolds in vitro and in vivo. *Biomaterials* **2006**, *27*, 2854–2864.

193. Kneser, U.; Polykandriotis, E.; Ohnolz, J.; Heidner, K.; Grabinger, L.; Euler, S.; Amann, K.U.; Hess, A.; Brune, K.; Greil, P.; et al. Engineering of vascularized transplantable bone tissues: Induction of axial vascularization in an osteoconductive matrix using an arteriovenous loop. *Tissue Eng.* **2006**, *12*, 1721–1731.

194. Arkudas, A.; Beier, J.P.; Heidner, K.; Tjiawi, J.; Polykandriotis, E.; Srour, S.; Sturzl, M.; Horch, R.E.; Kneser, U. Axial prevascularization of porous matrices using an arteriovenous loop promotes survival and differentiation of transplanted autologous osteoblasts. *Tissue Eng.* **2007**, *13*, 1549–1560.

195. Cheng, H.L.M.; Wallis, C.; Shou, Z.; Farhat, W.A. Quantifying angiogenesis in VEGF-enhanced tissue-engineered bladder constructs by dynamic contrast-enhanced MRI using contrast agents of different molecular weights. *J. Magn. Reson. Imaging* **2007**, *25*, 137–145.

196. Chen, W.; Shi, C.; Yi, S.; Chen, B.; Zhang, W.; Fang, Z.; Wei, Z.; Jiang, S.; Sun, X.; Hou, X.; et al. Bladder Regeneration by Collagen Scaffolds With Collagen Binding Human Basic Fibroblast Growth Factor. *J. Urol.* **2010**, *183*, 2432–2439.

197. Zhou, L.; Yang, B.; Sun, C.; Qiu, X.; Sun, Z.; Chen, Y.; Zhang, Y.; Dai, Y. Coadministration of Platelet-Derived Growth Factor-BB and Vascular Endothelial Growth Factor with Bladder Acellular Matrix Enhances Smooth Muscle Regeneration and Vascularization for Bladder Augmentation in a Rabbit Model. *Tissue Eng. Part A* **2013**, *19*, 264–276.

198. Jeon, O.; Powell, C.; Solorio, L.D.; Krebs, M.D.; Alsberg, E. Affinity-based growth factor delivery using biodegradable, photocrosslinked heparin-alginate hydrogels. *J. Control. Release* **2011**, *154*, 258–266.

199. Déry, M.A.C.; Michaud, M.D.; Richard, D.E. Hypoxia-inducible factor 1: Regulation by hypoxic and non-hypoxic activators. *Int. J. Biochem. Cell Biol.* **2005**, *37*, 535–540.

200. Deckers, M.M.L.; Van Bezooijen, R.L.; Van Geertje Horst, D.E.R.; Hoogendam, J.; Van Chris Bent, D.E.R.; Papapoulos, S.E.; Löwik, C.W.G.M. Bone morphogenetic proteins stimulate angiogenesis through osteoblast-derived vascular endothelial growth factor A. *Endocrinology* **2002**, *143*, 1545–1553.

201. Pola, R.; Ling, L.E.; Silver, M.; Corbley, M.J.; Kearney, M.; Blake Pepinsky, R.; Shapiro, R.; Taylor, F.R.; Baker, D.P.; Asahara, T.; et al. The morphogen Sonic hedgehog is an indirect angiogenic agent upregulating two families of angiogenic growth factors. *Nat. Med.* **2001**, *7*, 706–711.

202. Kaully, T.; Kaufman-Francis, K.; Lesman, A.; Levenberg, S. Vascularization--the

conduit to viable engineered tissues. *Tissue Eng. Part B. Rev.* **2009**, *15*, 159–169.

203. Ehrbar, M.; Metters, A.; Zammaretti, P.; Hubbell, J.A.; Zisch, A.H. Endothelial cell proliferation and progenitor maturation by fibrin-bound VEGF variants with differential susceptibilities to local cellular activity. *J. Control. Release* **2005**, *101*, 93–109.

204. Staton, C.A.; Stribbling, S.M.; Tazzyman, S.; Hughes, R.; Brown, N.J.; Lewis, C.E. Current methods for assaying angiogenesis in vitro and in vivo. *Int. J. Exp. Pathol.* **2004**, *85*, 233–248.

205. Staton, C.A.; Reed, M.W.R.; Brown, N.J. A critical analysis of current in vitro and in vivo angiogenesis assays. *Int. J. Exp. Pathol.* **2009**, *90*, 195–221.

206. Irvin, M.W.; Zijlstra, A.; Wikswo, J.P.; Pozzi, A. Techniques and assays for the study of angiogenesis. *Exp. Biol. Med.* **2014**, *239*, 1476–1488.

207. Veeramani, V.P.; Veni, G. An essential review on current techniques used in angiogenesis assays. *Int. J. PharmTech Res.* **2010**, *2*, 2379–2387.

208. Denizot, F.; Lang, R. Rapid colorimetric assay for cell growth and survival. Modifications to the tetrazolium dye procedure giving improved sensitivity and reliability. *J. Immunol. Methods* **1986**, *89*, 271–277.

209. Wemme, H.; Pfeifer, S.; Heck, R.; Müller-Quernheim, J. Measurement of Lymphocyte Proliferation: Critical Analysis of Radioactive and Photometric Methods. *Immunobiology* **1992**, *185*, 78–89.

210. Voytik-Harbin, S.L.; Brightman, A.O.; Waisner, B.; Lamar, C.H.; Badylak, S.F. Application and evaluation of the alamarblue assay for cell growth and survival of fibroblasts. *Vitr. Cell. Dev. Biol. - Anim.* **1998**, *34*, 239–246.

211. Stoddart, M.J. Cell viability assays: introduction. *Methods Mol. Biol.* 2011, *740*, 1–6.

212. Niles, A.L.; Riss, T.L. "Multiplexed viability, cytotoxicity, and caspase activity assays." *Methods Mol. Biol.* **2015**, *1219*, 21–33.

213. Ng, K.W.; Leong, D.T.W.; Hutmacher, D.W. The challenge to measure cell proliferation in two and three dimensions. *Tissue Eng.* **2005**, *11*, 182–191.

214. Boyden, S. The chemotactic effect of mixtures of antibody and antigen on polymorphonuclear leucocytes. *J. Exp. Med.* **1962**, *115*, 453–466.

215. Alessandri, G.; Raju, K.; Gullino, P.M. Mobilization of capillary endothelium in vitro induced by effectors of angiogenesis in vivo. *Cancer Res.* **1983**, *43*, 1790–1797.

216. Wong, M.K.K.; Gotlieb, A.I. In vitro reendothelialization of a single-cell wound: Role of microfilament bundles in rapid lamellipodia-mediated wound closure. *Lab. Investig.* **1984**, *51*, 75–81.

217. Pepper, M.S.; Belin, D.; Montesano, R.; Orci, L.; Vassalli, J.D. Transforming growth factor-beta 1 modulates basic fibroblast growth factor-induced proteolytic and angiogenic properties of endothelial cells in vitro. *J. Cell Biol.* **1990**, *111*, 743–755.

218. Zetter, B.R. Assay of Capillary Endothelial Cell Migration. *Methods Enzymol.* **1987**, *147*, 135–144.

219. Lawley, T.J.; Kubota, Y. Induction of morphologic differentiation of endothelial cells in culture. *J. Invest. Dermatol.* **1989**, *93*, 59–61.

220. Kanzawa, S.; Endo, H.; Shioya, N. Improved in vitro angiogenesis model by collagen density reduction and the use of type III collagen. *Ann. Plast. Surg.* **1993**, *30*, 244–251.

221. Kleinman, H.K.; Martin, G.R. Matrigel: Basement membrane matrix with biological activity. *Semin. Cancer Biol.* **2005**, *15*, 378–386.

222. Gagnon, E.; Cattaruzzi, P.; Griffith, M.; Muzakare, L.; LeFlaol, K.; Faure, R.; Béliveau, R.; Hussain, S.N.; Koutsilieris, M.; Doillon, C.J. Human vascular endothelial cells with extended life spans: In vitro cell response, protein expression, and angiogenesis. *Angiogenesis* **2002**, *5*, 21–33.

223. Nicosia, R.F.; Tchao, R.; Leighton, J. Histotypic angiogenesis in vitro: Light microscopic, ultrastructural, and radioautographic studies. *In Vitro* **1982**, *18*, 538–549.

224. Nicosia, R.F. The aortic ring model of angiogenesis: A quarter century of search and discovery. *J. Cell. Mol. Med.* **2009**, *13*, 4113–4136.

225. Baker, M.; Robinson, S.D.; Lechertier, T.; Barber, P.R.; Tavora, B.; D'Amico, G.; Jones,

D.T.; Vojnovic, B.; Hodivala-Dilke, K. Use of the mouse aortic ring assay to study angiogenesis. *Nat. Protoc.* **2012**, *7*, 89–104.

226. Tahergorabi, Z.; Khazaei, M. A review on angiogenesis and its assays. *Iran. J. Basic Med. Sci.* **2012**, *15*, 1110–1126.

227. Auerbach, R.; Muthukkaruppan, V. The Chick Embryo Aortic Arch Assay. In *The Textbook of Angiogenesis and Lymphangiogenesis: Methods and Applications*; 2012; pp. 149–157.

228. Valdes, T.I.; Kreutzer, D.; Moussy, F. The chick chorioallantoic membrane as a novel in vivo model for the testing of biomaterials. *J. Biomed. Mater. Res.* **2002**, *62*, 273–282.

229. Vogel, H.B.; Berry, R.G. Chorioallantoic membrane heterotransplantation of human brain tumors. *Int. J. Cancer* **1975**, *15*, 401–408.

230. Auerbach, R.; Arensman, R.; Kubai, L.; Folkman, J. Tumor-induced angiogenesis: Lack of inhibition by irradiation. *Int. J. Cancer* **1975**, *15*, 241–245.

231. Ausprunk, D.H.; Folkman, J. Vascular injury in transplanted tissues - Fine structural changes in tumor, adult, and embryonic blood vessels. *Virchows Arch. B Cell Pathol.* **1976**, *21*, 31–44.

232. Auerbach, R.; Kubai, L.; Knighton, D.; Folkman, J. A simple procedure for the long-term cultivation of chicken embryos. *Dev. Biol.* **1974**, *41*, 391–4.

233. Valdes, T.I.; Kreutzer, D.; Moussy, F. The chick chorioallantoic membrane as a novelin vivo model for the testing of biomaterials. *J. Biomed. Mater. Res.* **2002**, *62*, 273–282.

234. Moreno-Jiménez, I.; Kanczler, J.M.; Hulsart-Billstrom, G.; Inglis, S.; Oreffo, R.O.C. * The Chorioallantoic Membrane Assay for Biomaterial Testing in Tissue Engineering: A Short-Term In Vivo Preclinical Model. *Tissue Eng. Part C. Methods* **2017**, *23*, 938–952.

235. Haller, S.; Ametamey, S.M.; Schibli, R.; Müller, C. Investigation of the chick embryo as a potential alternative to the mouse for evaluation of radiopharmaceuticals. *Nucl. Med. Biol.* **2015**, *42*, 226–233.

236. Moreno-Jiménez, I.; Hulsart-Billstrom, G.; Lanham, S.A.; Janeczek, A.A.; Kontouli, N.; Kanczler, J.M.; Evans, N.D.; Oreffo, R.O. The chorioallantoic membrane (CAM) assay for the study of human bone regeneration: a refinement animal model for tissue engineering. *Sci. Rep.* **2016**, *6*, 32168.

237. Ribatti, D.; Nico, B.; Vacca, A.; Presta, M. The gelatin sponge-chorioallantoic membrane assay. *Nat. Protoc.* **2006**, *1*, 85–91.

238. Lokman, N.A.; Elder, A.S.F.; Ricciardelli, C.; Oehler, M.K. Chick chorioallantoic membrane (CAM) assay as an in vivo model to study the effect of newly identified molecules on ovarian cancer invasion and metastasis. *Int. J. Mol. Sci.* **2012**, *13*, 9959–70.

239. Eke, G.; Mangir, N.; Hasirci, N.; MacNeil, S.; Hasirci, V. Development of a UV crosslinked biodegradable hydrogel containing adipose derived stem cells to promote vascularization for skin wounds and tissue engineering. *Biomaterials* **2017**, *129*, 188–198.

240. Mangir, N.; Raza, A.; Haycock, J.W.; Chapple, C.; Macneil, S. An improved in vivo methodology to visualise tumour induced changes in vasculature using the chick chorionic allantoic membrane assay. *In Vivo (Brooklyn).* **2018**, *32*.

241. Mangir, N.; Dikici, S.; Claeyssens, F.; MacNeil, S. Using ex Ovo Chick Chorioallantoic Membrane (CAM) Assay to Evaluate the Biocompatibility and Angiogenic Response to Biomaterials. *ACS Biomater. Sci. Eng.* **2019**, *5*, 3190–3200.

242. Gimbrone, M.A.; Cotran, R.S.; Leapman, S.B.; Folkman, J. Tumor growth and neovascularization: an experimental model using the rabbit cornea. *J. Natl. Cancer Inst.* **1974**, *52*, 413–427.

243. Henkind, P. Ocular neovascularization. The Krill memorial lecture. *Am. J. Ophthalmol.* **1978**.

244. Ziche, M.; Morbidelli, L. The corneal pocket assay. In *Vascular Morphogenesis: Methods and Protocols*; 2014; pp. 15–28 ISBN 9781493914623.

245. Fournier, G.A.; Lutty, G.A.; Watt, S.; Fenselau, A.; Patz, A. A corneal micropocket assay for angiogenesis in the rat eye. *Investig. Ophthalmol. Vis. Sci.* **1981**, *21*, 351–

354.

246. Muthukkaruppan, V.; Auerbach, R. Angiogenesis in the mouse cornea. *Science (80-. ).* **1979**, *205*, 1416–1418.

247. Norrby, K. In vivo models of angiogenesis. *J. Cell. Mol. Med.* **2006**, *10*, 588–612.

248. Chávez, M.N.; Aedo, G.; Fierro, F.A.; Allende, M.L.; Egaña, J.T. Zebrafish as an emerging model organism to study angiogenesis in development and regeneration. *Front. Physiol.* **2016**, *7*, 56.

249. Chico, T.J.A.; Ingham, P.W.; Crossman, D.C. Modeling Cardiovascular Disease in the Zebrafish. *Trends Cardiovasc. Med.* **2008**, *18*, 150–155.

250. Weinstein, B.M.; Stemple, D.L.; Driever, W.; Fishman, M.C. Gridlock, a localized heritable vascular patterning defect in the zebrafish. *Nat. Med.* **1995**, *1*, 1143–1147.

251. Childs, S.; Chen, J.N.; Garrity, D.M.; Fishman, M.C. Patterning of angiogenesis in the zebrafish embryo. *Development* **2002**, *129*, 973–982.

252. Vajkoczy, P.; Menger, M.D.; Vollmar, B.; Schilling, L.; Schmiedek, P.; Hirth, K.P.; Ullrich, A.; Fong, T.A. Inhibition of tumor growth, angiogenesis, and microcirculation by the novel Flk-1 inhibitor SU5416 as assessed by intravital multi-fluorescence videomicroscopy. *Neoplasia* **1999**, *1*, 31–41.

253. Algire, G.H. An adaptation of the transparent-chamber technique to the mouse. *J. Natl. Cancer Inst.* **1943**, *4*, 1–11.

254. Papenfuss, H.D.; Gross, J.F.; Intaglietta, M.; Treese, F.A. A transparent access chamber for the rat dorsal skin fold. *Microvasc. Res.* **1979**, *18*, 311–318.

255. Endrich, B.; Asaishi, K.; Götz, A.; Meßmer, K. Technical report-a new chamber technique for microvascular studies in unanesthetized hamsters. *Res. Exp. Med.* **1980**, *177*, 125–134.

256. Lehr, H.A.; Leunig, M.; Menger, M.D.; Nolte, D.; Messmer, K. Dorsal skinfold chamber technique for intravital microscopy in nude mice. *Am. J. Pathol.* **1993**, *143*, 1055–1062.

257. Schilling, J.A.; Joel, W.; Shurley, H.M. Wound healing: A comparative study of the

histochemical changes in granulation tissue contained in stainless steel wire mesh and polyvinyl sponge cylinders. *Surgery* **1959**, *46*, 702–710.

258. Andrade, S.P.; Fan, T.P.D.; Lewis, G.P. Quantitative in-vivo studies on angiogenesis in a rat sponge model. *Br. J. Exp. Pathol.* **1987**, *68*, 755–766.

259. KLEINMAN, H.K.; GRAF, J.; IWAMOTO, Y.; KITTEN, G.T.; OGLE, R.C.; SASAKI, M.; YAMADA, Y.; MARTIN, G.R.; LUCKENBILL-EDDS, L. Role of Basement Membranes in Cell Differentiation. *Ann. N. Y. Acad. Sci.* **1987**, *513*, 134–145.

260. Jain, R.K.; Schlenger, K.; Höckel, M.; Yuan, F. Quantitative angiogenesis assays: Progress and problems. *Nat. Med.* **1997**, *3*, 1203–1208.

261. Lee, S.H.; Jeong, S.K.; Ahn, S.K. An update of the defensive barrier function of skin. *Yonsei Med. J.* **2006**, *47*, 293–306.

262. Forslind, B.; Engström, S.; Engblom, J.; Norlén, L. A novel approach to the understanding of human skin barrier function. *J. Dermatol. Sci.* **1997**, *14*, 115–125.

263. Rees, J. Understanding barrier function of the skin. *Lancet* **1999**, *354*, 1491–1492.

264. Wysocki, A.B. Skin anatomy, physiology, and pathophysiology. *Nurs. Clin. North Am.* **1999**, *34*, 777–797.

265. Zaidi, Z. Skin: Structure and Function. In *Dermatology in Clinical Practice*; Springer London: London, 2010; pp. 1–15 ISBN 978-1-84882-862-9.

266. Honari, G. Skin structure and function. In *Sensitive Skin Syndrome, Second Edition*; 2017 ISBN 9781498737357.

267. Elias, P.M. Stratum corneum defensive functions: An integrated view. *J. Invest. Dermatol.* **2005**, *125*, 183–200.

268. Hardman, M.J.; Moore, L.; Ferguson, M.W.J.; Byrne, C. Barrier formation in the human fetus is patterned. *J. Invest. Dermatol.* **1999**, *113*, 1106–1113.

269. Madison, K.C. Barrier function of the skin: "La Raison d'Être" of the epidermis. *J. Invest. Dermatol.* **2003**, *121*, 231–241.

270. Clark, R.A.F. Overview and General Considerations of Wound Repair. In *The Molecular and Cellular Biology of Wound Repair*; 1998; pp. 3–33.

271. Liotta, L.A.; Tryggvason, K.; Garbisa, S.; Hart, I.; Foltz, C.M.; Shafie, S. Metastatic potential correlates with enzymatic degradation of basement membrane collagen. *Nature* **1980**, *284*, 67–68.

272. Leigh, I.M.; Eady, R.A.J.; Heagerty, A.H.M.; Purkis, P.E.; Whitehead, P.A.; Burgeson, R.E. Type VII collagen is a normal component of epidermal basement membrane, which shows altered expression in recessive dystrophic epidermolysis bullosa. *J. Invest. Dermatol.* **1988**, *90*, 639–642.

273. WEBER, L.; KRIEG, T.; K.MÜLLER, P.; KIRSCH, E.; TIMPL, R. Immunofluorescent localization of type IV collagen and laminin in human skin and its application in junctional zone pathology. *Br. J. Dermatol.* **1982**, *106*, 267–273.

274. James, W.; Berger, T.; Elston, D. *Andrews' Diseases of the Skin: Clinical Dermatology*; 10th editi.; Saunders, 2005;

275. Waller, J.M.; Maibach, H.I. Age and skin structure and function, a quantitative approach (I): Blood flow, pH, thickness, and ultrasound echogenicity. *Ski. Res. Technol.* **2005**, *11*, 221–235.

276. Chao, C.Y.L.; Cheing, G.L.Y. Microvascular dysfunction in diabetic foot disease and ulceration. *Diabetes. Metab. Res. Rev.* **2009**, *25*, 604–614.

277. Feedar, J.A.; McCulloch, J.M.; Kloth, L.C. *Wound healing: alternatives in management.*; 2nd editio.; F. A. Davies Company, 1995;

278. Tonnesen, M.G.; Feng, X.; Clark, R.A.F. Angiogenesis in wound healing. *J. Investig. Dermatology Symp. Proc.* **2000**, *5*, 40–46.

279. Clark, R. Fibrin and Wound Healing. *Ann. N. Y. Acad. Sci.* **2006**, *936*, 355–367.

280. Noble, P.W.; Jiang, D. Matrix regulation of lung injury, inflammation, and repair: The role of innate immunity. In Proceedings of the Proceedings of the American Thoracic Society; 2006; Vol. 3, pp. 401–404.

281. Jameson, J.; Ugarte, K.; Chen, N.; Yachi, P.; Fuchs, E.; Boismenu, R.; Havran, W.L. A role for skin γδ T cells in wound repair. *Science (80-. ).* **2002**, *296*, 747–749.

282. Lee, W.L.; Harrison, R.E.; Grinstein, S. Phagocytosis by neutrophils. *Microbes Infect.* **2003**, *5*, 1299–1306.

283. Badiu, D.; Vasile, M.; Teren, O. Regulation of wound healing by growth factors and cytokines. *Wound Heal. Process. Phases Promot.* **2011**, 73–93.

284. Chen, G.; Li, J.; Ochani, M.; Rendon-Mitchell, B.; Qiang, X.; Susarla, S.; Ulloa, L.; Yang, H.; Fan, S.; Goyert, S.M.; et al. Bacterial endotoxin stimulates macrophages to release HMGB1 partly through CD14- and TNF-dependent mechanisms. *J. Leukoc. Biol.* **2004**, *76*, 994–1001.

285. Werner, S.; Krieg, T.; Smola, H. Keratinocyte-fibroblast interactions in wound healing. *J. Invest. Dermatol.* **2007**, *127*, 998–1008.

286. Halloran, C.M.; Slavin, J.P. Pathophysiology of Wound Healing. *Surg.* **2002**, *20*, i–v.

287. Hsieh, P.; Chen, L.B. Behavior of cells seeded in isolated fibronectin matrices. *J. Cell Biol.* **1983**, *96*, 1208–1217.

288. Gabbiani, G.; Ryan, G.B.; Majno, G. Presence of modified fibroblasts in granulation tissue and their possible role in wound contraction. *Experientia* **1971**, *27*, 549–550.

289. Kirfel, G.; Herzog, V. Migration of epidermal keratinocytes: Mechanisms, regulation, and biological significance. *Protoplasma* **2004**, *223*, 67–78.

290. Matsuzaki, K.; Inoue, H.; Kumagai, N. Reepithelialisation and the possible involvement of the transcription factor, basonuclin. *Int. Wound J.* **2004**, *1*, 135–140.

291. Martin, P. Wound healing - Aiming for perfect skin regeneration. *Science (80-. ).* **1997**, *276*, 75–81.

292. Freyman, T.M.; Yannas, I. V.; Gibson, L.J. Cellular materials as porous scaffolds for tissue engineering. *Prog. Mater. Sci.* **2001**, *46*, 273–282.

293. Servold, S.A. Growth factor impact on wound healing. *Clin. Podiatr. Med. Surg.* **1991**, *8*, 937–953.

294. Pierce, G.F.; Vande Berg, J.; Rudolph, R.; Tarpley, J.; Mustoe, T.A. Platelet-derived growth factor-BB and transforming growth factor beta1 selectively modulate glycosaminoglycans, collagen, and myofibroblasts in excisional wounds. *Am. J. Pathol.* **1991**, *138*, 629–646.

295. Takeshita, S.; Zheng, L.P.; Brogi, E.; Kearney, M.; Pu, L.Q.; Bunting, S.; Ferrara, N.;

Symes, J.F.; Isner, J.M. Therapeutic angiogenesis. A single intraarterial bolus of vascular endothelial growth factor augments revascularization in a rabbit ischemic hind limb model. *J. Clin. Invest.* **1994**, *93*, 662–670.

296. Velnar, T.; Bailey, T.; Smrkolj, V. The wound healing process: An overview of the cellular and molecular mechanisms. *J. Int. Med. Res.* **2009**, *37*, 1528–1542.

297. Witte, M.B.; Barbul, A. General principles of wound healing. *Surg. Clin. North Am.* **1997**, *77*, 509–528.

298. Samuels, P.; Andre, K.W. Fetal scarless wound healing. *J. Can. d ' Otolaryngol.* **1999**, *28*, 296–302.

299. Hunt, T.K.; Hopf, H.; Hussain, Z. Physiology of wound healing. *Adv. Skin Wound Care* **2000**, *13*, 6–11.

300. Baum, C.L.; Arpey, C.J. Normal cutaneous wound healing: Clinical correlation with cellular and molecular events. *Dermatologic Surg.* **2005**, *31*, 674–686.

301. Greenhalgh, D.G. The role of apoptosis in wound healing. *Int. J. Biochem. Cell Biol.* **1998**, *30*, 1019–1030.

302. Falanga, V. Wound healing and chronic wounds. *J. Cutan. Med. Surg.* **1998**, *3*, 1S-5S.

303. O'Kane, S. Wound remodelling and scarring. *J. Wound Care* **2002**, *11*, 296–299.

304. Yu, Y.; Alkhawaji, A.; Ding, Y.; Mei, J. Decellularized scaffolds in regenerative medicine. *Oncotarget* **2016**, *7*, 58671–58683.

305. Badylak, S.F. Xenogeneic extracellular matrix as a scaffold for tissue reconstruction. *Transpl. Immunol.* **2004**, *12*, 367–377.

306. Dew, L.; English, W.R.; Chong, C.K.; MacNeil, S. Investigating Neovascularization in Rat Decellularized Intestine: An in Vitro Platform for Studying Angiogenesis. *Tissue Eng. - Part A* **2016**, *22*, 1317–1326.

307. Melo, E.; Kasper, J.Y.; Unger, R.E.; Farre, R.; Kirkpatrick, C.J. Development of a Bronchial Wall Model: Triple Culture on a Decellularized Porcine Trachea. *Tissue Eng. Part C. Methods* **2015**, *21*, 909–921.

308. Uygun, B.E.; Soto-Gutierrez, A.; Yagi, H.; Izamis, M.L.; Guzzardi, M.A.; Shulman, C.;

Milwid, J.; Kobayashi, N.; Tilles, A.; Berthiaume, F.; et al. Organ reengineering through development of a transplantable recellularized liver graft using decellularized liver matrix. *Nat. Med.* **2010**, *16*, 814–820.

309. Mertsching, H.; Schanz, J.; Steger, V.; Schandar, M.; Schenk, M.; Hansmann, J.; Dally, I.; Friedel, G.; Walles, T. Generation and transplantation of an autologous vascularized bioartificial human tissue. *Transplantation* **2009**, *88*, 203–210.

310. Zhang, Q.; Johnson, J.A.; Dunne, L.W.; Chen, Y.; Iyyanki, T.; Wu, Y.; Chang, E.I.; Branch-Brooks, C.D.; Robb, G.L.; Butler, C.E. Decellularized skin/adipose tissue flap matrix for engineering vascularized composite soft tissue flaps. *Acta Biomater.* **2016**, *35*, 166–184.

311. Sabetkish, S.; Kajbafzadeh, A.M.; Sabetkish, N.; Khorramirouz, R.; Akbarzadeh, A.; Seyedian, S.L.; Pasalar, P.; Orangian, S.; Hossein Beigi, R.S.; Aryan, Z.; et al. Whole-organ tissue engineering: Decellularization and recellularization of three-dimensional matrix liver scaffolds. *J. Biomed. Mater. Res. - Part A* **2015**, *103*, 1498–1508.

312. Modulevsky, D.J.; Cuerrier, C.M.; Pelling, A.E. Biocompatibility of Subcutaneously Implanted Plant-Derived Cellulose Biomaterials. *PLoS One* **2016**, *11*, e0157894.

313. Helenius, G.; Bäckdahl, H.; Bodin, A.; Nannmark, U.; Gatenholm, P.; Risberg, B. In vivo biocompatibility of bacterial cellulose. *J. Biomed. Mater. Res. - Part A* **2006**, *76*, 431–438.

314. Svensson, A.; Nicklasson, E.; Harrah, T.; Panilaitis, B.; Kaplan, D.L.; Brittberg, M.; Gatenholm, P. Bacterial cellulose as a potential scaffold for tissue engineering of cartilage. *Biomaterials* **2005**, *26*, 419–431.

315. Fontana, J.D.; De Souza, A.M.; Fontana, C.K.; Torriani, I.L.; Moreschi, J.C.; Gallotti, B.J.; De Souza, S.J.; Narcisco, G.P.; Bichara, J.A.; Farah, L.F.X. Acetobacter cellulose pellicle as a temporary skin substitute. *Appl. Biochem. Biotechnol.* **1990**, *24–25*, 253–264.

316. Modulevsky, D.J.; Lefebvre, C.; Haase, K.; Al-Rekabi, Z.; Pelling, A.E. Apple derived cellulose scaffolds for 3D mammalian cell culture. *PLoS One* **2014**, *9*, e97835.

317. Wang, X.Y.; Jin, Z.H.; Gan, B.W.; Lv, S.W.; Xie, M.; Huang, W.H. Engineering

interconnected 3D vascular networks in hydrogels using molded sodium alginate lattice as the sacrificial template. *Lab Chip* **2014**, *14*, 2709–2716.

318. Yeon, J.H.; Ryu, H.R.; Chung, M.; Hu, Q.P.; Jeon, N.L. In vitro formation and characterization of a perfusable three-dimensional tubular capillary network in microfluidic devices. *Lab Chip* **2012**, *12*, 2815–2822.

319. Li, S.; Liu, Y.Y.; Liu, L.J.; Hu, Q.X. A Versatile Method for Fabricating Tissue Engineering Scaffolds with a Three-Dimensional Channel for Prevasculature Networks. *ACS Appl. Mater. Interfaces* **2016**, *8*, 25096–25103.

320. Miller, J.S.; Stevens, K.R.; Yang, M.T.; Baker, B.M.; Nguyen, D.H.T.; Cohen, D.M.; Toro, E.; Chen, A.A.; Galie, P.A.; Yu, X.; et al. Rapid casting of patterned vascular networks for perfusable engineered three-dimensional tissues. *Nat. Mater.* **2012**, *11*, 768–774.

321. Kim, G.H.; Son, J.G.; Park, S.; Kim, W.D. Hybrid process for fabricating 3D hierarchical scaffolds combining rapid prototyping and electrospinning. *Macromol. Rapid Commun.* **2008**, *29*, 1577–1581.

322. Ortega, I.; Dew, L.; Kelly, A.G.; Chong, C.K.; MacNeil, S.; Claeyssens, F. Fabrication of biodegradable synthetic perfusable vascular networks via a combination of electrospinning and robocasting. *Biomater. Sci.* **2015**, *3*, 592–596.

323. Dew, L.; English, W.R.; Ortega, I.; Claeyssens, F.; Macneil, S. Fabrication of biodegradable synthetic vascular networks and their use as a model of angiogenesis. *Cells Tissues Organs* **2016**, *202*, 319–328.

324. van Duinen, V.; Zhu, D.; Ramakers, C.; van Zonneveld, A.J.; Vulto, P.; Hankemeier, T. Perfused 3D angiogenic sprouting in a high-throughput in vitro platform. *Angiogenesis* **2019**, *22*, 157–165.

325. Kim, C.; Kasuya, J.; Jeon, J.; Chung, S.; Kamm, R.D. A quantitative microfluidic angiogenesis screen for studying anti-angiogenic therapeutic drugs. *Lab Chip* **2015**, *15*, 301–310.

326. Richardson, T.P.; Peters, M.C.; Ennett-Shepard, A.B.; Mooney, D.J. Polymeric system for dual growth factor delivery. *Nat. Biotechnol.* **2001**, *19*, 1029–1034.

327. Novosel, E.C.; Kleinhans, C.; Kluger, P.J. Vascularization is the key challenge in tissue engineering. *Adv. Drug Deliv. Rev.* **2011**, *63*, 300–311.

328. Obi, N.; Toda, H. Human Umbilical Vein Endothelial Cells Migration in Matrigel by the Concentration Gradient of Vascular Endothelial Growth Factor. *J. Biotechnol. Biomater.* **2015**, *5*, 210.

329. Vernon, R.B.; Sage, E.H. A novel, quantitative model for study of endothelial cell migration and sprout formation within three-dimensional collagen matrices. *Microvasc. Res.* **1999**, *57*, 118–133.

330. Poldervaart, M.T.; Gremmels, H.; Van Deventer, K.; Fledderus, J.O.; Öner, F.C.; Verhaar, M.C.; Dhert, W.J.A.; Alblas, J. Prolonged presence of VEGF promotes vascularization in 3D bioprinted scaffolds with defined architecture. *J. Control. Release* **2014**, *184*, 58–66.

331. Gupta, P.; Arumugam, M.; Azad, R.V.; Saxena, R.; Ghose, S.; Biswas, N.R.; Velpandian, T. Screening of antiangiogenic potential of twenty two marine invertebrate extracts of phylum Mollusca from South East Coast of India. *Asian Pac. J. Trop. Biomed.* **2014**, *4*, *Supplem*, S129--S138.

332. Parsons-Wingerter, P.; Chandrasekharan, U.M.; McKay, T.L.; Radhakrishnan, K.; DiCorleto, P.E.; Albarran, B.; Farr, A.G. A VEGF165-induced phenotypic switch from increased vessel density to increased vessel diameter and increased endothelial NOS activity. *Microvasc. Res.* **2006**, *72*, 91–100.

333. Chen, H.; Treweeke, A.T.; West, D.C.; Till, K.J.; Cawley, J.C.; Zuzel, M.; Toh, C.H. In vitro and in vivo production of vascular endothelial growth factor by chronic lymphocytic leukemia cells. *Blood* **2000**, *96*, 3181–3187.

334. Yancopoulos, G.D.; Davis, S.; Gale, N.W.; Rudge, J.S.; Wiegand, S.J.; Holash, J. Vascular-specific growth factors and blood vessel formation. *Nature* **2000**, *407*, 242–248.

335. Cao, R.; Eriksson, A.; Kubo, H.; Alitalo, K.; Cao, Y.; Thyberg, J. Comparative Evaluation of FGF-2-, VEGF-A-, and VEGF-C-Induced Angiogenesis Lymphangiogenesis, Vascular Fenestrations, and Permeability. *Circ. Res.* **2004**, *94*, 664–670.

336. Cheng, S.Y.; Nagane, M.; Huang, H.S.; Cavenee, W.K. Intracerebral tumor-associated hemorrhage caused by overexpression of the vascular endothelial growth factor isoforms VEGF121 and VEGF165 but not VEGF189. *Proc. Natl. Acad. Sci. U. S. A.* **1997**, *94*, 12081–7.

337. Oka, N.; Soeda, A.; Inagaki, A.; Onodera, M.; Maruyama, H.; Hara, A.; Kunisada, T.; Mori, H.; Iwama, T. VEGF promotes tumorigenesis and angiogenesis of human glioblastoma stem cells. *Biochem. Biophys. Res. Commun.* **2007**, *360*, 553–559.

338. Ehrbar, M.; Zeisberger, S.M.; Raeber, G.P.; Hubbell, J.A.; Schnell, C.; Zisch, A.H. The role of actively released fibrin-conjugated VEGF for VEGF receptor 2 gene activation and the enhancement of angiogenesis. *Biomaterials* **2008**, *29*, 1720–1729.

339. Formiga, F.R.; Pelacho, B.; Garbayo, E.; Abizanda, G.; Gavira, J.J.; Simon-Yarza, T.; Mazo, M.; Tamayo, E.; Jauquicoa, C.; Ortiz-de-Solorzano, C.; et al. Sustained release of VEGF through PLGA microparticles improves vasculogenesis and tissue remodeling in an acute myocardial ischemia-reperfusion model. *J. Control. Release* **2010**, *147*, 30–37.

340. Berry, D.; Shriver, Z.; Natke, B.; Kwan, C.-P.; Venkataraman, G.; Sasisekharan, R. Heparan sulphate glycosaminoglycans derived from endothelial cells and smooth muscle cells differentially modulate fibroblast growth factor-2 biological activity through fibroblast growth factor receptor-1. *Biochem. J.* **2003**, *373*, 241–9.

341. Folkman, J.; Shing, Y. Control of angiogenesis by heparin and other sulfated polysaccharides. *Adv Exp Med Biol* **1992**, *313*, 355–364.

342. Rema, R.B.; Rajendran, K.; Ragunathan, M. Angiogenic efficacy of Heparin on chick chorioallantoic membrane. *Vasc Cell* **2012**, *4*, 8.

343. Salbach, P.B.; Bruckmann, M.; Turovets, O.; Kreuzer, J.; Kubler, W.; Walter-Sack, I. Heparin-mediated selective release of hepatocyte growth factor in humans. *Br J Clin Pharmacol* **2000**, *50*, 221–226.

344. Gigliobianco, G.; Chong, C.K.; MacNeil, S. Simple surface coating of electrospun poly-L-lactic acid scaffolds to induce angiogenesis. *J. Biomater. Appl.* **2015**, *0*, 1–11.

345. Yar, M.; Gigliobianco, G.; Shahzadi, L.; Dew, L.; Siddiqi, S.A.; Khan, A.F.; Chaudhry, A.A.; Rehman, I.U.; MacNeil, S. Production of chitosan PVA PCL hydrogels to bind heparin and induce angiogenesis. *Int. J. Polym. Mater. Polym. Biomater.* **2016**, *65*, 466–476.

346. Shahzadi, L.; Yar, M.; Jamal, A.; Siddiqi, S.A.; Chaudhry, A.A.; Zahid, S.; Tariq, M.; Rehman, I.U.; MacNeil, S. Triethyl orthoformate covalently cross-linked chitosan-(poly vinyl) alcohol based biodegradable scaffolds with heparin-binding ability for promoting neovascularisation. *J. Biomater. Appl.* **2016**, *31*, 582–593.

347. Seo, K.H.; Lee, H.S.; Jung, B.; Ko, H.M.; Choi, J.H.; Park, S.J.; Choi, I.H.; Lee, H.K.; Im, S.Y. Estrogen enhances angiogenesis through a pathway involving platelet-activating factor-mediated nuclear factor-κB activation. *Cancer Res.* **2004**, *64*, 6482–6488.

348. Pence, J.C.; Clancy, K.B.H.; Harley, B.A.C. The induction of pro-angiogenic processes within a collagen scaffold via exogenous estradiol and endometrial epithelial cells. *Biotechnol. Bioeng.* **2015**, *112*, 2185–2194.

349. Liu, H.; Tao, Y.; Chen, M.; Yu, J.; Li, W.-J.; Tao, L.; Li, Y.; Li, F. 17β-Estradiol Promotes Angiogenesis of Rat Cardiac Microvascular Endothelial Cells In Vitro. *Med. Sci. Monit.* **2018**, *24*, 2489–2496.

350. Kalluri, R. Basement membranes: Structure, assembly and role in tumour angiogenesis. *Nat. Rev. Cancer* **2003**, *3*, 422–433.

351. Brown, R.M.; Meah, C.J.; Heath, V.L.; Styles, I.B.; Bicknell, R. Tube-forming assays. In *Methods in Molecular Biology*; 2016; Vol. 1430, pp. 149–157.

352. Baldwin, A.D.; Kiick, K.L. Polysaccharide-modified synthetic polymeric biomaterials. *Biopolymers* **2010**, *94*, 128–140.

353. Hwang, M.R.; Kim, J.O.; Lee, J.H.; Kim, Y. Il; Kim, J.H.; Chang, S.W.; Jin, S.G.; Kim, J.A.; Lyoo, W.S.; Han, S.S.; et al. Gentamicin-loaded wound dressing with polyvinyl alcohol/dextran hydrogel: Gel characterization and in vivo healing evaluation. *AAPS PharmSciTech* **2010**, *11*, 1092–1103.

354. Patterson, J.; Mura, C. Rapid colorimetric assays to qualitatively distinguish RNA

and DNA in biomolecular samples. *J. Vis. Exp.* **2013**, *72*, e50225.

355. Roma-Rodrigues, C.; Heuer-Jungemann, A.; Fernandes, A.R.; Kanaras, A.G.; Baptista, P. V. Peptide-coated gold nanoparticles for modulation of angiogenesis in vivo. *Int. J. Nanomedicine* **2016**, *11*, 2633–2639.

356. Brooks, P.; Montgomery, A.P.; Cheresh, D. Use of the 10-Day-Old Chick Embryo Model for Studying Angiogenesis. *Integrin Protoc.* **1999**, *129*, 257–269.

357. El Abbadi, N.; Al Saadi, E. Automatic Early Diagnosis of Diabetic Retinopathy Using Retina Fundus Images. *Eur. Acad. Res.* **2014**, *II*, 11397–11418.

358. Fischer, A.H.; Jacobson, K.A.; Rose, J.; Zeller, R. Hematoxylin and eosin staining of tissue and cell sections. *Cold Spring Harb. Protoc.* **2008**, *3*, 1–2.

359. Minajeva, A.; Kase, M.; Saretok, M.; Adamson-Raieste, A.; Kase, S.; Niinepuu, K.; Vardja, M.; Asser, T.; Jaal, J. Impact of Blood Vessel Quantity and Vascular Expression of CD133 and ICAM-1 on Survival of Glioblastoma Patients. *Neurosci. J.* **2017**, *2017*, 8 pages.

360. Griffith, C.K.; Miller, C.; Sainson, R.C.A.; Calvert, J.W.; Jeon, N.L.; Hughes, C.C.W.; George, S.C. Diffusion Limits of an in Vitro Thick Prevascularized Tissue. *Tissue Eng.* **2005**, *11*, 257–266.

361. Wang, S.; Li, X.; Parra, M.; Verdin, E.; Bassel-Duby, R.; Olson, E.N. Control of endothelial cell proliferation and migration by VEGF signaling to histone deacetylase 7. *Proc. Natl. Acad. Sci. U. S. A.* **2008**, *105*, 7738–7743.

362. Yancopoulos, G.D.; Davis, S.; Gale, N.W.; Rudge, J.S.; Wiegand, S.J.; Holash, J. Vascular-specific growth factors and blood vessel formation. *Nature* **2000**, *407*, 242–248.

363. Koch, S.; Tugues, S.; Li, X.; Gualandi, L.; Claesson-Welsh, L. Signal transduction by vascular endothelial growth factor receptors. *Biochem. J.* **2011**, *437*, 169–183.

364. Ponce, M.L. Tube formation: an in vitro matrigel angiogenesis assay. *Methods Mol. Biol.* **2009**, *467*, 183–188.

365. Merchan, J.R.; Kovács, K.; Railsback, J.W.; Kurtoglu, M.; Jing, Y.; Piña, Y.; Gao, N.; Murray, T.G.; Lehrman, M.A.; Lampidis, T.J. Antiangiogenic activity of 2-deoxy-D-

glucose. *PLoS One* **2010**, *5*, e13699.

366. Chuang, I.C.; Yang, C.M.; Song, T.Y.; Yang, N.C.; Hu, M.L. The anti-angiogenic action of 2-deoxyglucose involves attenuation of VEGFR2 signaling and MMP-2 expression in HUVECs. *Life Sci.* **2015**, *139*, 52–61.

367. Yang, D.; Zhang, J.; Xue, J.; Nie, J.; Zhang, Z. Electrospinning of Poly(3-hydroxybutyrate-co-3-hydroxyvalerate) nanofibers with feature surface microstructure. *J. Appl. Polym. Sci.* **2013**, *127*, 2867–2874.

368. Nasonova, M. V.; Glushkova, T. V.; Borisov, V. V.; Velikanova, E.A.; Burago, A.Y.; Kudryavtseva, Y.A. Biocompatibility and Structural Features of Biodegradable Polymer Scaffolds. *Bull. Exp. Biol. Med.* **2015**, *160*, 134–140.

369. Shrivastav, A.; Kim, H.Y.; Kim, Y.R. Advances in the applications of polyhydroxyalkanoate nanoparticles for novel drug delivery system. *Biomed Res. Int.* **2013**, *2013*, 581684.

370. Zamani, M.; Morshed, M.; Varshosaz, J.; Jannesari, M. Controlled release of metronidazole benzoate from poly ε-caprolactone electrospun nanofibers for periodontal diseases. *Eur. J. Pharm. Biopharm.* **2010**, *75*, 179–185.

371. Wei, X.; Xia, Z.; Wong, S.C.; Baji, A. Modelling of mechanical properties of electrospun nanofibre network. *Int. J. Exp. Comput. Biomech.* **2009**, *1*, 45.

372. Unnithan, A.R.; Sasikala, A.R.K.; Murugesan, P.; Gurusamy, M.; Wu, D.; Park, C.H.; Kim, C.S. Electrospun polyurethane-dextran nanofiber mats loaded with Estradiol for post-menopausal wound dressing. *Int. J. Biol. Macromol.* **2015**, *77*, 1–8.

373. Adeel, M.; Song, X.; Wang, Y.; Francis, D.; Yang, Y. Environmental impact of estrogens on human, animal and plant life: A critical review. *Environ. Int.* **2017**, *99*, 107–119.

374. Shareef, A.; Angove, M.J.; Wells, J.D.; Johnson, B.B. Aqueous solubilities of estrone, 17β-estradiol, 17α- ethynylestradiol, and bisphenol A. *J. Chem. Eng. Data* **2006**, *51*, 879–881.

375. Jamehbozorg, B.; Sadeghi, R. Evaluation of the effect of ionic-liquids as soluting-out agents on the solubility of carbohydrates in aqueous solutions. *Fluid Phase Equilib.*

**2018**, *459*, 73–84.

376. Huang, Z.M.; He, C.L.; Yang, A.; Zhang, Y.; Han, X.J.; Yin, J.; Wu, Q. Encapsulating drugs in biodegradable ultrafine fibers through co-axial electrospinning. *J. Biomed. Mater. Res. - Part A* **2006**, *77*, 169–179.

377. Albrecht, E.D.; Babischkin, J.S.; Lidor, Y.; Anderson, L.D.; Udoff, L.C.; Pepe, G.J. Effect of estrogen on angiogenesis in co-cultures of human endometrial cells and microvascular endothelial cells. *Hum. Reprod.* **2003**, *18*, 2039–2047.

378. Hyder, S.M.; Stancel, G.M.; Chiappetta, C.; Murthy, L.; Boettger-Tong, H.L.; Makela, S. Uterine expression of vascular endothelial growth factor is increased by estradiol and tamoxifen. *Cancer Res.* **1996**, *56*, 3954–3960.

379. Shafaat, S.; Mangir, N.; Regureos, S.R.; Chapple, C.R.; MacNeil, S. Demonstration of improved tissue integration and angiogenesis with an elastic, estradiol releasing polyurethane material designed for use in pelvic floor repair. *Neurourol. Urodyn.* **2018**, *37*, 716–725.

380. Brown, N.S.; Jones, A.; Fujiyama, C.; Harris, A.L.; Bicknell, R. Thymidine phosphorylase induces carcinoma cell oxidative stress and promotes secretion of angiogenic factors. *Cancer Res.* **2000**, *60*, 6298–6302.

381. Vara, D.; Watt, J.M.; Fortunato, T.M.; Mellor, H.; Burgess, M.; Wicks, K.; Mace, K.; Reeksting, S.; Lubben, A.; Wheeler-Jones, C.P.D.; et al. Direct Activation of NADPH Oxidase 2 by 2-Deoxyribose-1-Phosphate Triggers Nuclear Factor Kappa B-Dependent Angiogenesis. *Antioxidants Redox Signal.* **2018**, *28*, 110–130.

382. Nakajima, Y.; Haraguchi, M.; Furukawa, T.; Yamamoto, M.; Nakanishi, H.; Tatematsu, M.; Akiyama, S.I. 2-Deoxy-L-ribose inhibits the invasion of thymidine phosphorylase- overexpressing tumors by suppressing matrix metalloproteinase-9. *Int. J. Cancer* **2006**, *119*, 1710–1716.

383. Ikeda, R.; Furukawa, T.; Kitazono, M.; Ishitsuka, K.; Okumura, H.; Tani, A.; Sumizawa, T.; Haraguchi, M.; Komatsu, M.; Uchimiya, H.; et al. Molecular basis for the inhibition of hypoxia-induced apoptosis by 2-deoxy-D-ribose. *Biochem. Biophys. Res. Commun.* **2002**, *291*, 806–812.

384. Shigematsu, S.; Yamauchi, K.; Nakajima, K.; Iijima, S.; Aizawa, T.; Hashizume, K. IGF-1 regulates migration and angiogenesis of human endothelial cells. *Endocr. J.* **1999**, *46*, 59–62.

385. Yu, P.; Yu, D.M.; Qi, J.C.; Wang, J.; Zhang, Q.M.; Zhang, J.Y.; Tang, Y.Z.; Xing, Q.L.; Li, M.Z. High D-glucose alters PI3K and Akt signaling and leads to endothelial cell migration, proliferation and angiogenesis dysfunction. *Natl. Med. J. China* **2006**, *86*, 3425–3430.

386. Madonna, R.; Giovannelli, G.; Confalone, P.; Renna, F.V.; Geng, Y.J.; De Caterina, R. High glucose-induced hyperosmolarity contributes to COX-2 expression and angiogenesis: Implications for diabetic retinopathy. *Cardiovasc. Diabetol.* **2016**, *15*, 18.

387. Jiraritthamrong, C.; Kheolamai, P.; U-Pratya, Y.; Chayosumrit, M.; Supokawej, A.; Manochantr, S.; Tantrawatpan, C.; Sritanaudomchai, H.; Issaragrisil, S. In vitro vessel-forming capacity of endothelial progenitor cells in high glucose conditions. *Ann. Hematol.* **2012**, *91*, 311–320.

388. Teixeira, A.S.; Andrade, S.P. Glucose-induced inhibition of angiogenesis in the rat sponge granuloma is prevented by aminoguanidine. *Life Sci.* **1999**, *64*, 655–662.

389. Vara, D.; Watt, J.M.; Fortunato, T.M.; Mellor, H.; Burgess, M.; Wicks, K.; Mace, K.; Reeksting, S.; Lubben, A.; Wheeler-Jones, C.P.D.; et al. Direct Activation of NADPH Oxidase 2 by 2-Deoxyribose-1-Phosphate Triggers Nuclear Factor Kappa B-Dependent Angiogenesis. *Antioxid. Redox Signal.* **2018**, *28*, 110–130.

390. Dikici, S.; Bullock, A.J.; Yar, M.; Claeyssens, F.; MacNeil, S. 2-deoxy-D-ribose (2dDR) upregulates vascular endothelial growth factor (VEGF) and stimulates angiogenesis. *Microvasc. Res.* **2020**, *131*, 104035.

391. Tagg, S.L.C.; Foster, P.A.; Leese, M.P.; Potter, B.V.L.; Reed, M.J.; Purohit, A.; Newman, S.P. 2-Methoxyoestradiol-3,17-O,O-bis-sulphamate and 2-deoxy-D-glucose in combination: A potential treatment for breast and prostate cancer. *Br. J. Cancer* **2008**, *99*, 1842–1848.

392. Kovacs, K.; Decatur, C.; Toro, M.; Pham, D.G.; Liu, H.; Jing, Y.; Murray, T.G.; Lampidis, T.J.; Merchan, J.R. 2-deoxy-glucose downregulates endothelial AKT and ERK via

interference with N-linked glycosylation, induction of endoplasmic reticulum stress, and GSK3β activation. *Mol. Cancer Ther.* **2016**, *15*, 264–275.

393. Ng, K.W.; Khor, H.L.; Hutmacher, D.W. In vitro characterization of natural and synthetic dermal matrices cultured with human dermal fibroblasts. In Proceedings of the Biomaterials; 2004; Vol. 25, pp. 2807–2818.

394. Feng, C.; Xu, Y.M.; Fu, Q.; Zhu, W.D.; Cui, L.; Chen, J. Evaluation of the biocompatibility and mechanical properties of naturally derived and synthetic scaffolds for urethral reconstruction. *J. Biomed. Mater. Res. - Part A* **2010**, *94*, 317–325.

395. Collins, F. *A-Z Dictionary of Wound Care [Book Review]*; Quay Books, 2002; Vol. 10;.

396. Badylak, S.F.; Valentin, J.E.; Ravindra, A.K.; McCabe, G.P.; Stewart-Akers, A.M. Macrophage phenotype as a determinant of biologic scaffold remodeling. *Tissue Eng. - Part A.* **2008**, *14*, 1835–1842.

397. Pradhan Nabzdyk, L.; Kuchibhotla, S.; Guthrie, P.; Chun, M.; Auster, M.E.; Nabzdyk, C.; Deso, S.; Andersen, N.; Gnardellis, C.; Logerfo, F.W.; et al. Expression of neuropeptides and cytokines in a rabbit model of diabetic neuroischemic wound healing. *J. Vasc. Surg.* **2013**, *58*, 766–775.

398. Novosel, E.C.; Kleinhans, C.; Kluger, P.J. Vascularization is the key challenge in tissue engineering. *Adv. Drug Deliv. Rev.* **2011**, *63*, 300–311.

399. Stryker, Z.I.; Rajabi, M.; Davis, P.J.; Mousa, S.A. Evaluation of angiogenesis assays. *Biomedicines* **2019**, *7*, 37.

400. Ravi, M.; Paramesh, V.; Kaviya, S.R.; Anuradha, E.; Paul Solomon, F.D. 3D cell culture systems: Advantages and applications. *J. Cell. Physiol.* **2015**, *230*, 16–26.

401. MacNeil, S. Progress and opportunities for tissue-engineered skin. *Nature* **2007**, *445*, 874–880.

402. Groeber, F.; Holeiter, M.; Hampel, M.; Hinderer, S.; Schenke-Layland, K. Skin tissue engineering - In vivo and in vitro applications. *Adv. Drug Deliv. Rev.* **2011**, *63*, 352–366.

403. Facy, V.; Flouret, V.; Régnier, M.; Schmidt, R. Reactivity of Langerhans cells in

human reconstructed epidermis to known allergens and UV radiation. *Toxicol. Vitr.* **2005**, *19*, 787–795.

404. Kandárová, H.; Liebsch, M.; Schmidt, E.; Genschow, E.; Traue, D.; Spielmann, H.; Meyer, K.; Steinhoff, C.; Tornier, C.; De Wever, B.; et al. Assessment of the skin irritation potential of chemicals by using the SkinEthic reconstructed human epidermal model and the common skin irritation protocol evaluated in the ECVAM skin irritation validation study. *ATLA Altern. to Lab. Anim.* **2006**, *34*, 393–406.

405. Bessou, S.; Surlève-Bazeille, J.E.; Pain, C.; Donatien, P.; Taïeb, A. Ex vivo study of skin phototypes. *J. Invest. Dermatol.* **1996**, *107*, 684–688.

406. Meier, F.; Nesbit, M.; Hsu, M.-Y.; Martin, B.; Van Belle, P.; Elder, D.E.; Schaumburg-Lever, G.; Garbe, C.; Walz, T.M.; Donatien, P.; et al. Human Melanoma Progression in Skin Reconstructs. *Am. J. Pathol.* **2000**, *156*, 193–200.

407. Admane, P.; Gupta, A.C.; Jois, P.; Roy, S.; Chandrasekharan Lakshmanan, C.; Kalsi, G.; Bandyopadhyay, B.; Ghosh, S. Direct 3D bioprinted full-thickness skin constructs recapitulate regulatory signaling pathways and physiology of human skin. *Bioprinting* **2019**, *15*, e00051.

408. Kim, B.S.; Gao, G.; Kim, J.Y.; Cho, D.W. 3D Cell Printing of Perfusable Vascularized Human Skin Equivalent Composed of Epidermis, Dermis, and Hypodermis for Better Structural Recapitulation of Native Skin. *Adv. Healthc. Mater.* **2019**, *8*, 1801019.

409. Kolesky, D.B.; Homan, K.A.; Skylar-Scott, M.A.; Lewis, J.A. Three-dimensional bioprinting of thick vascularized tissues. *Proc. Natl. Acad. Sci. U. S. A.* **2016**, *113*, 3179–3184.

410. John, S.; Kesting, M.R.; Paulitschke, P.; Stöckelhuber, M.; von Bomhard, A. Development of a tissue-engineered skin substitute on a base of human amniotic membrane. *J. Tissue Eng.* **2019**, *10*, 1–14.

411. MacNeil, S.; Shepherd, J.; Smith, L. Production of tissue-engineered skin and oral mucosa for clinical and experimental use. *Methods Mol. Biol.* **2011**, *695*, 129–153.

412. Sahota, P.S.; Burn, J.L.; Heaton, M.; Freedlander, E.; Suvarna, S.K.; Brown, N.J.; Mac

Neil, S. Development of a reconstructed human skin model for angiogenesis. *Wound Repair Regen.* **2003**, *11*, 275–284.

413. Quillaguamán, J.; Guzmán, H.; Van-Thuoc, D.; Hatti-Kaul, R. Synthesis and production of polyhydroxyalkanoates by halophiles: Current potential and future prospects. *Appl. Microbiol. Biotechnol.* **2010**, *85*, 1687–1696.

414. Tay, F.R.; Pashley, D.H.; Williams, M.C.; Raina, R.; Loushine, R.J.; Weller, R.N.; Kimbrough, W.F.; King, N.M. Susceptibility of a polycaprolactone-based root canal filling material to degradation. I. Alkaline hydrolysis. *J. Endod.* **2005**, *31*, 593–598.

415. Woodward, S.C.; Brewer, P.S.; Moatamed, F.; Schindler, A.; Pitt, C.G. The intracellular degradation of poly(ε-caprolactone). *J. Biomed. Mater. Res.* **1985**, *19*, 437–444.

416. Dikici, S.; Claeyssens, F.; MacNeil, S. Bioengineering Vascular Networks to Study Angiogenesis and Vascularization of Physiologically Relevant Tissue Models in Vitro. *ACS Biomater. Sci. Eng.* **2020**, *6*, 3513–3528.

417. Bye, F.J.; Bissoli, J.; Black, L.; Bullock, A.J.; Puwanun, S.; Moharamzadeh, K.; Reilly, G.C.; Ryan, A.J.; MacNeil, S. Development of bilayer and trilayer nanofibrous/microfibrous scaffolds for regenerative medicine. *Biomater. Sci.* **2013**, *1*, 942–951.

418. Bye, F.J.; Wang, L.; Bullock, A.J.; Blackwood, K.A.; Ryan, A.J.; Macneil, S. Postproduction processing of electrospun fibres for tissue engineering. *J. Vis. Exp.* **2012**, *66*, e4172.

419. Aldemir Dikici, B.; Dikici, S.; Reilly, G.C.; MacNeil, S.; Claeyssens, F. A Novel Bilayer Polycaprolactone Membrane for Guided Bone Regeneration: Combining Electrospinning and Emulsion Templating. *Materials (Basel).* **2019**, *12*, 2643.

420. Ghosh, M.M.; Boyce, S.; Layton, C.; Freedlander, E.; Mac Neil, S. A comparison of methodologies for the preparation of human epidermal-dermal composites. *Ann. Plast. Surg.* **1997**, *39*, 390–404.

421. Chakrabarty, K.H.; Dawson, R.A.; Harris, P.; Layton, C.; Babu, M.; Gould, L.; Phillips, J.; Leigh, I.; Green, C.; Freedlander, E.; et al. Development of autologous human

dermal-epidermal composites based on sterilized human allodermis for clinical use. *Br. J. Dermatol.* **1999**, *141*, 811–823.

422. Currie, L.J.; Sharpe, J.R.; Martin, R. The use of fibrin glue in skin grafts and tissue-engineered skin replacements: A review. *Plast. Reconstr. Surg.* **2001**, *108*, 1713–1726.

423. Bye, F.J.; Bullock, A.J.; Singh, R.; Sefat, F.; Roman, S.; MacNeil, S. Development of a Basement Membrane Substitute Incorporated Into an Electrospun Scaffold for 3D Skin Tissue Engineering. *J. Biomater. Tissue Eng.* **2014**, *4*, 686–692.

424. Aldemir Dikici, B.; Sherborne, C.; Reilly, G.C.; Claeyssens, F. Emulsion templated scaffolds manufactured from photocurable polycaprolactone. *Polymer (Guildf).* **2019**, *175*, 243–254.

425. Wang, L.; Du, J.; Cao, D.; Wang, Y. Recent Advances and the Application of Poly(3-hydroxybutyrate- co -3-hydroxyvalerate) as Tissue Engineering Materials. *J. Macromol. Sci. Part A Pure Appl. Chem.* **2013**, *50*, 885–893.

426. Sangsanoh, P.; Waleetomcheepsawat, S.; Suwantong, O.; Wutticharoenmongkol, P.; Weeranantanapan, O.; Chuenjitbuntaworn, B.; Cheepsunthom, P.; Pavasant, P.; Supaphol, P. In vitro biocompatability of Schwann cells on surfaces of biocompatible polymeric electrospun fibrous and solution-cast film scaffolds. *Biomacromolecules* **2007**, *8*, 1587–1594.

427. Alagoz, A.S.; Rodriguez-Cabello, J.C.; Hasirci, V. PHBV wet-spun scaffold coated with ELR-REDV improves vascularization for bone tissue engineering. *Biomed. Mater.* **2018**, *13*, 055010.

428. Lei, C.; Zhu, H.; Li, J.; Li, J.; Feng, X.; Chen, J. Preparation and characterization of polyhydroxybutyrate-co-hydroxyvalerate/silk fibroin nanofibrous scaffolds for skin tissue engineering. *Polym. Eng. Sci.* **2015**, *55*, 907–916.

429. Jalali, S.; Tafazzoli-Shadpour, M.; Haghighipour, N.; Omidvar, R.; Safshekan, F. Regulation of Endothelial Cell Adherence and Elastic Modulus by Substrate Stiffness. *Cell Commun. Adhes.* **2015**, *22*, 79–89.

430. Ataollahi, F.; Pramanik, S.; Moradi, A.; Dalilottojari, A.; Pingguan-Murphy, B.; Wan

Abas, W.A.B.; Abu Osman, N.A. Endothelial cell responses in terms of adhesion, proliferation, and morphology to stiffness of polydimethylsiloxane elastomer substrates. *J. Biomed. Mater. Res. - Part A* **2015**, *103*, 2203–2213.

431. Rüder, C.; Sauter, T.; Kratz, K.; Haase, T.; Peter, J.; Jung, F.; Lendlein, A.; Zohlnhöfer, D. Influence of fibre diameter and orientation of electrospun copolyetheresterurethanes on smooth muscle and endothelial cell behaviour. *Clin. Hemorheol. Microcirc.* **2013**, *55*, 513–522.

432. Ko, Y.G.; Park, J.H.; Lee, J.B.; Oh, H.H.; Park, W.H.; Cho, D.; Kwon, O.H. Growth behavior of endothelial cells according to electrospun poly(D,L-lactic-co-glycolic acid) fiber diameter as a tissue engineering scaffold. *Tissue Eng. Regen. Med.* **2016**, *13*, 343–351.

433. Stoker, M.G.P.; Rubin, H. Density dependent inhibition of cell growth in culture. *Nature* **1967**, *215*, 171–172.

434. Frame, K.K.; Hu, W. -S A model for density-dependent growth of anchorage-dependent mammalian cells. *Biotechnol. Bioeng.* **1988**, *32*, 1061–1066.

435. Tremel, A.; Cai, A.; Tirtaatmadja, N.; Hughes, B.D.; Stevens, G.W.; Landman, K.A.; O'Connor, A.J. Cell migration and proliferation during monolayer formation and wound healing. *Chem. Eng. Sci.* **2009**, *64*, 247–253.

436. De Silva Thompson, D.; Peticone, C.; Burova, I.; Shipley, R.J.; Knowles, J.C.; Kim, H.W.; Micheletti, M.; Wall, I.B. Assessing behaviour of osteoblastic cells in dynamic culture conditions using titanium-doped phosphate glass microcarriers. *J. Tissue Eng.* **2019**, *10*, 1–13.

437. Lerman, M.J.; Lembong, J.; Muramoto, S.; Gillen, G.; Fisher, J.P. The Evolution of Polystyrene as a Cell Culture Material. *Tissue Eng. - Part B Rev.* **2018**, *24*, 359–372.

438. Lannutti, J.; Reneker, D.; Ma, T.; Tomasko, D.; Farson, D. Electrospinning for tissue engineering scaffolds. *Mater. Sci. Eng. C* **2007**, *27*, 504–509.

439. Blackwood, K.A.; McKean, R.; Canton, I.; Freeman, C.O.; Franklin, K.L.; Cole, D.; Brook, I.; Farthing, P.; Rimmer, S.; Haycock, J.W.; et al. Development of biodegradable electrospun scaffolds for dermal replacement. *Biomaterials* **2008**,

*29*, 3091–3104.

440. Szentivanyi, A.; Chakradeo, T.; Zernetsch, H.; Glasmacher, B. Electrospun cellular microenvironments: Understanding controlled release and scaffold structure. *Adv. Drug Deliv. Rev.* **2011**, *63*, 209–220.

441. Pham, Q.P.; Sharma, U.; Mikos, A.G. Electrospinning of polymeric nanofibers for tissue engineering applications: a review. *Tissue Eng.* **2006**, *12*, 1197–211.

442. Augst, A.D.; Kong, H.J.; Mooney, D.J. Alginate hydrogels as biomaterials. *Macromol. Biosci.* **2006**, *6*, 623–633.

443. Rowley, J.A.; Madlambayan, G.; Mooney, D.J. Alginate hydrogels as synthetic extracellular matrix materials. *Biomaterials* **1999**, *20*, 45–53.

444. Steele, J.A.M.; McCullen, S.D.; Callanan, A.; Autefage, H.; Accardi, M.A.; Dini, D.; Stevens, M.M. Combinatorial scaffold morphologies for zonal articular cartilage engineering. *Acta Biomater.* **2014**, *10*, 2065–2075.

445. Sant, S.; Hwang, C.M.; Lee, S.H.; Khademhosseini, A. Hybrid PGS-PCL microfibrous scaffolds with improved mechanical and biological properties. *J. Tissue Eng. Regen. Med.* **2011**, *5*, 283–291.

446. Hong, Y.; Huber, A.; Takanari, K.; Amoroso, N.J.; Hashizume, R.; Badylak, S.F.; Wagner, W.R. Mechanical properties and in vivo behavior of a biodegradable synthetic polymer microfiber-extracellular matrix hydrogel biohybrid scaffold. *Biomaterials* **2011**, *32*, 3387–3394.

447. Tong, H.W.; Wang, M. Electrospinning of fibrous PHBV tissue engineering scaffolds: Fiber diameter control, fiber alignment and mechanical properties. In Proceedings of the 5th Int. Conference on Information Technology and Applications in Biomedicine; 2008; pp. 535–538.

448. DuRaine, G.D.; Arzi, B.; Lee, J.K.; Lee, C.A.; Responte, D.J.; Hu, J.C.; Athanasiou, K.A. Biomechanical evaluation of suture-holding properties of native and tissue-engineered articular cartilage. *Biomech. Model. Mechanobiol.* **2015**, *14*, 73–81.

449. Selders, G.S.; Fetz, A.E.; Speer, S.L.; Bowlin, G.L. Fabrication and characterization of air-impedance electrospun polydioxanone templates. *Electrospinning* **2016**, *1*, 20–

30.

450. Syedain, Z.; Reimer, J.; Lahti, M.; Berry, J.; Johnson, S.; Tranquillo, R.T. Tissue engineering of acellular vascular grafts capable of somatic growth in young lambs. *Nat. Commun.* **2016**, *7*, 12951.

451. Bergers, G.; Song, S. The role of pericytes in blood-vessel formation and maintenance. *Neuro. Oncol.* **2005**, *7*, 452–464.

452. Black, a F.; Berthod, F.; L'heureux, N.; Germain, L.; Auger, F. a In vitro reconstruction of a human capillary-like network in a tissue-engineered skin equivalent. *FASEB J.* **1998**, *12*, 1331–1340.

453. Hudon, V.; Berthod, F.; Black, A.F.; Damour, O.; Germain, L.; Auger, F.A. A tissue-engineered endothelialized dermis to study the modulation of angiogenic and angiostatic molecules on capillary-like tube formation in vitro. *Br. J. Dermatol.* **2003**, *148*, 1094–1104.

454. Sorrell, J.M.; Baber, M.A.; Caplan, A.I. A self-assembled fibroblast-endothelial cell co-culture system that supports in vitro vasculogenesis by both human umbilical vein endothelial cells and human dermal microvascular endothelial cells. *Cells Tissues Organs* **2007**, *186*, 157–168.

455. Bishop, E.T.; Bell, G.T.; Bloor, S.; Broom, I.J.; Hendry, N.F.; Wheatley, D.N. An in vitro model of angiogenesis: basic features. *Angiogenesis* **1999**, *3*, 335–344.

456. Keun Kwon, I.; Kidoaki, S.; Matsuda, T. Electrospun nano- to microfiber fabrics made of biodegradable copolyesters: Structural characteristics, mechanical properties and cell adhesion potential. *Biomaterials* **2005**, *26*, 3929–3939.

457. Beachley, V.; Wen, X. Polymer nanofibrous structures: Fabrication, biofunctionalization, and cell interactions. *Prog. Polym. Sci.* **2010**, *35*, 868–892.

458. Venugopal, J.; Low, S.; Choon, A.T.; Ramakrishna, S. Interaction of cells and nanofiber scaffolds in tissue engineering. *J. Biomed. Mater. Res. - Part B Appl. Biomater.* **2008**, *84*, 34–48.

459. Gunn, J.; Zhang, M. Polyblend nanofibers for biomedical applications: Perspectives and challenges. *Trends Biotechnol.* **2010**, *28*, 189–197.

460. Shafei, S.; Foroughi, J.; Chen, Z.; Wong, C.S.; Naebe, M. Short oxygen plasma treatment leading to long-term hydrophilicity of conductive PCL-PPy nanofiber scaffolds. *Polymers (Basel).* **2017**, *9*, 614.

461. Kubota, Y.; Kleinman, H.K.; Martin, G.R.; Lawley, T.J. Role of laminin and basement membrane in the morphological differentiation of human endothelial cells into capillary-like structures. *J. Cell Biol.* **1988**, *107*, 1589–1598.

462. Blanco, R.; Gerhardt, H. VEGF and Notch in tip and stalk cell selection. *Cold Spring Harb. Perspect. Med.* **2013**, *3*, 657–659.

463. Gerhardt, H.; Golding, M.; Fruttiger, M.; Ruhrberg, C.; Lundkvist, A.; Abramsson, A.; Jeltsch, M.; Mitchell, C.; Alitalo, K.; Shima, D.; et al. VEGF guides angiogenic sprouting utilizing endothelial tip cell filopodia. *J. Cell Biol.* **2003**, *161*, 1163–1177.

464. Jakobsson, L.; Franco, C.A.; Bentley, K.; Collins, R.T.; Ponsioen, B.; Aspalter, I.M.; Rosewell, I.; Busse, M.; Thurston, G.; Medvinsky, A.; et al. Endothelial cells dynamically compete for the tip cell position during angiogenic sprouting. *Nat. Cell Biol.* **2010**, *12*, 943–953.

465. Reis, L.; Chiu, L.L.Y.; Feric, N.; Fu, L.; Radisic, M. Injectable biomaterials for cardiac regeneration and repair. In *Cardiac Regeneration and Repair: Biomaterials and Tissue Engineering*; 2014; pp. 49–81 ISBN 9780857096593.

466. Richard, L.; Velasco, P.; Detmar, M. Isolation and culture of microvascular endothelial cells. *Methods Mol Med* **1999**, *18*, 261–269.

467. Bahramsoltani, M.; Harms, T.; Drewes, B.; Plendl, J. Searching for markers to identify angiogenic endothelial cells: A proteomic approach. *Clin. Hemorheol. Microcirc.* **2013**, *55*, 255–269.

468. Santos, T.C.; Morton, T.J.; Moritz, M.; Pfeifer, S.; Reise, K.; Marques, A.P.; Castro, A.G.; Reis, R.L.; Van Griensven, M. Vascular endothelial growth factor and fibroblast growth factor-2 incorporation in starch-based bone tissue-engineered constructs promote the in vivo expression of neovascularization mediators. *Tissue Eng. - Part A* **2013**, *19*, 834–848.

469. Reddy, K.S.; Chittoria, R.K.; Babu, P.; Marimuthu, S.K.; Kumar, S.H.; Subbarayan, E.K.;

Chavan, V.; Mohapatra, D.P.; Sivakumar, D.K.; Friji, M.T. Effectiveness of fibrin glue in adherence of skin graft. *J. Cutan. Aesthet. Surg.* **2017**, *10*, 72–75.

470. Park, W.; Kim, W.H.; Lee, C.H.; Kim, D.Y.; Choi, J.H.; Huh, J.W.; Sung, H.M.; Kim, I.S.; Kweon, O.K. Comparison of two fibrin glues in anastomoses and skin closure. *J. Vet. Med. Ser. A Physiol. Pathol. Clin. Med.* **2002**, *49*, 385–389.

471. Deshpande, P.; Ramachandran, C.; Sefat, F.; Mariappan, I.; Johnson, C.; McKean, R.; Hannah, M.; Sangwan, V.S.; Claeyssens, F.; Ryan, A.J.; et al. Simplifying corneal surface regeneration using a biodegradable synthetic membrane and limbal tissue explants. *Biomaterials* **2013**, *34*, 5088–5106.

472. Gabrielli, M.G.; Accili, D. The chick chorioallantoic membrane: A model of molecular, structural, and functional adaptation to transepithelial ion transport and barrier function during embryonic development. *J. Biomed. Biotechnol.* **2010**, *2010*, 940741.

473. Sato, N.; Maehara, N.; Goggins, M. Gene expression profiling of tumor-stromal interactions between pancreatic cancer cells and stromal fibroblasts. *Cancer Res.* **2004**, *64*, 6950–6956.

474. Chang, H.Y.; Sneddon, J.B.; Alizadeh, A.A.; Sood, R.; West, R.B.; Montgomery, K.; Chi, J.T.; Van De Rijn, M.; Botstein, D.; Brown, P.O. Gene expression signature of fibroblast serum response predicts human cancer progression: Similarities between tumors and wounds. *PLoS Biol.* **2004**, *2*, e39.

475. Kellouche, S.; Mourah, S.; Bonnefoy, A.; Schoëvaert, D.; Podgorniak, M.P.; Calvo, F.; Hoylaerts, M.F.; Legrand, C.; Dosquet, C. Platelets, thrombospondin-1 and human dermal fibroblasts cooperate for stimulation of endothelial cell tubulogenesis through VEGF and PAI-1 regulation. *Exp. Cell Res.* **2007**, *313*, 486–499.

476. Paunescu, V.; Bojin, F.M.; Tatu, C.A.; Gavriliuc, O.I.; Rosca, A.; Gruia, A.T.; Tanasie, G.; Bunu, C.; Crisnic, D.; Gherghiceanu, M.; et al. Tumour-associated fibroblasts and mesenchymal stem cells: More similarities than differences. *J. Cell. Mol. Med.* **2011**, *15*, 635–646.

477. Antoniades, H.N.; Galanopoulos, T.; Neville-Golden, J.; Kiritsy, C.P.; Lynch, S.E. Injury induces in vivo expression of platelet-derived growth factor (PDGF) and PDGF

receptor mRNAs in skin epithelial cells and PDGF mRNA in connective tissue fibroblasts. *Proc. Natl. Acad. Sci. U. S. A.* **1991**, *88*, 565–569.

478. Ballaun, C.; Weninger, W.; Uthman, A.; Weich, H.; Tschachler, E. Human keratinocytes express the three major splice forms of vascular endothelial growth factor. *J. Invest. Dermatol.* **1995**, *104*, 7–10.

479. Aldemir Dikici, B.; Reilly, G.C.; Claeyssens, F. Boosting the Osteogenic and Angiogenic Performance of Multiscale Porous Polycaprolactone Scaffolds by in Vitro Generated Extracellular Matrix Decoration. *ACS Appl. Mater. Interfaces* **2020**, *12*, 12510–12524.

480. Dikici, S.; Claeyssens, F.; MacNeil, S. Decellularised baby spinach leaves and their potential use in tissue engineering applications: Studying and promoting neovascularisation. *J. Biomater. Appl.* **2019**, *34*, 546–559.

481. Mano, J.F.; Silva, G.A.; Azevedo, H.S.; Malafaya, P.B.; Sousa, R.A.; Silva, S.S.; Boesel, L.F.; Oliveira, J.M.; Santos, T.C.; Marques, A.P.; et al. Natural origin biodegradable systems in tissue engineering and regenerative medicine: Present status and some moving trends. *J. R. Soc. Interface* **2007**, *4*, 999–1030.

482. Magnusson, J.P.; Saeed, A.O.; Fernández-Trillo, F.; Alexander, C. Synthetic polymers for biopharmaceutical delivery. *Polym. Chem.* **2011**, *2*, 48–59.

483. Guo, B.; Ma, P.X. Synthetic biodegradable functional polymers for tissue engineering: A brief review. *Sci. China Chem.* **2014**, *57*, 490–500.

484. Bullock, A.J.; Higham, M.C.; MacNeil, S. Use of human fibroblasts in the development of a xenobiotic-free culture and delivery system for human keratinocytes. *Tissue Eng.* **2006**, *12*, 245–255.

485. Tremblay, P.L.; Hudon, V.; Berthod, F.; Germain, L.; Auger, F.A. Inosculation of tissue-engineered capillaries with the host's vasculature in a reconstructed skin transplanted on mice. *Am. J. Transplant.* **2005**, *5*, 1002–1010.

486. Laschke, M.W.; Vollmar, B.; Menger, M.D. Inosculation: Connecting the Life-Sustaining Pipelines. *Tissue Eng. Part B Rev.* **2009**, *15*, 455–465.

487. SCHWARTZ, S.J.; VON ELBE, J.H. Kinetics of Chlorophyll Degradation to

Pyropheophytin in Vegetables. *J. Food Sci.* **1983**, *48*, 1303–1306.

488. Nishi, C.; Nakajima, N.; Ikada, Y. In vitro evaluation of cytotoxicity of diepoxy compounds used for biomaterial modification. *J. Biomed. Mater. Res.* **1995**, *29*, 829–834.

489. Dayeh, V.R.; Chow, S.L.; Schirmer, K.; Lynn, D.H.; Bols, N.C. Evaluating the toxicity of Triton X-100 to protozoan, fish, and mammalian cells using fluorescent dyes as indicators of cell viability. *Ecotoxicol. Environ. Saf.* **2004**, *57*, 375–382.

490. Syed, O.; Walters, N.J.; Day, R.M.; Kim, H.W.; Knowles, J.C. Evaluation of decellularization protocols for production of tubular small intestine submucosa scaffolds for use in oesophageal tissue engineering. *Acta Biomater.* **2014**, *10*, 5043–5054.

491. Chen, H. Chemical Composition and Structure of Natural Lignocellulose. In *Biotechnology of Lignocellulose*; 2014; pp. 25–71 ISBN 9789400768987.

492. Dejana, E.; Colella, S.; Languino, L.R.; Balconi, G.; Corbascio, G.C.; Marchisio, P.C. Fibrinogen induces adhesion, spreading, and microfilament organization of human endothelial cells in vitro. *J. Cell Biol.* **1987**, *104*, 1403–1411.

493. Unger, R.E.; Ghanaati, S.; Orth, C.; Sartoris, A.; Barbeck, M.; Halstenberg, S.; Motta, A.; Migliaresi, C.; Kirkpatrick, C.J. The rapid anastomosis between prevascularized networks on silk fibroin scaffolds generated in vitro with cocultures of human microvascular endothelial and osteoblast cells and the host vasculature. *Biomaterials* **2010**, *31*, 6959–6967.

494. Davis, G.E.; Senger, D.R. Endothelial extracellular matrix: Biosynthesis, remodeling, and functions during vascular morphogenesis and neovessel stabilization. *Circ. Res.* **2005**, *97*, 1093–1107.

495. Schor, A.M.; Schor, S.L.; Allen, T.D. Effects of culture conditions on the proliferation, morphology and migration of bovine aortic endothelial cells. *J Cell Sci* **1983**, *62*, 267–285.

496. Anderson, D.E.J.; Hinds, M.T. Extracellular matrix production and regulation in micropatterned endothelial cells. *Biochem. Biophys. Res. Commun.* **2012**, *427*, 159–

164.

497. Kuijpers, A.J.; Engbers, G.H.M.; Krijgsveld, J.; Zaat, S.A.J.; Dankert, J.; Feijen, J. Cross-linking and characterisation of gelatin matrices for biomedical applications. *J. Biomater. Sci. Polym. Ed.* **2000**, *11*, 225–243.

498. Lai, J.Y.; Li, Y.T. Evaluation of cross-linked gelatin membranes as delivery carriers for retinal sheets. *Mater. Sci. Eng. C* **2010**, *30*, 677–685.

499. Vleggeert-Lankamp, C.L.A.M.; Pêgo, A.P.; Lakke, E.A.J.F.; Deenen, M.; Marani, E.; Thomeer, R.T.W.M. Adhesion and proliferation of human Schwann cells on adhesive coatings. *Biomaterials* **2004**, *25*, 2741–2751.

500. Laschke, M.W.; Menger, M.D. Prevascularization in tissue engineering: Current concepts and future directions. *Biotechnol. Adv.* **2016**, *34*, 112–121.

501. Nör, J.E.; Peters, M.C.; Christensen, J.B.; Sutorik, M.M.; Linn, S.; Khan, M.K.; Addison, C.L.; Mooney, D.J.; Polverini, P.J. Engineering and characterization of functional human microvessels in immunodeficient mice. *Lab. Investig.* **2001**, *81*, 453–463.

502. Badylak, S.F.; Weiss, D.J.; Caplan, A.; MacChiarini, P. Engineered whole organs and complex tissues. *Lancet* **2012**, *379*, 943–952.

503. Obeso, J.L.; Auerbach, R. A new microtechnique for quantitating cell movement in vitro using polystyrene bead monolayers. *J. Immunol. Methods* **1984**, *70*, 141–152.

504. Liang, C.C.; Park, A.Y.; Guan, J.L. In vitro scratch assay: A convenient and inexpensive method for analysis of cell migration in vitro. *Nat. Protoc.* **2007**, *2*, 329–333.

505. Bach, T.L.; Barsigian, C.; Chalupowicz, D.G.; Busler, D.; Yaen, C.H.; Grant, D.S.; Martinez, J. VE-cadherin mediates endothelial cell capillary tube formation in fibrin and collagen gels. *Exp. Cell Res.* **1998**, *238*, 324–334.

506. Grant, D.S.; Kibbey, M.C.; Kinsella, J.L.; Cid, M.C.; Kleinman, H.K. The Role of Basement Membrane in Angiogenesis and Tumor Growth. *Pathol. Res. Pract.* **1994**, *190*, 854–863.

507. Dew, L.; English, W.R.; Ortega, I.; Claeyssens, F.; MacNeil, S. Fabrication of biodegradable synthetic vascular networks and their use as a model of

angiogenesis. *Cells Tissues Organs* **2016**, *202*, 319–328.

508. Bahramsoltani, M.; Plendl, J.; Janczyk, P.; Custodis, P.; Kaessmeyer, S. Quantitation of angiogenesis and antiangiogenesis in vivo, ex vivo and in vitro - An overview. *ALTEX* **2009**, *26*, 95–107.

509. Hutmacher, D.W. Biomaterials offer cancer research the third dimension. *Nat. Mater.* **2010**, *9*, 90–93.

510. Cukierman, E.; Pankov, R.; Stevens, D.R.; Yamada, K.M. Taking cell-matrix adhesions to the third dimension. *Science (80-. ).* **2001**, *294*, 1708–1712.

511. Pampaloni, F.; Reynaud, E.G.; Stelzer, E.H.K. The third dimension bridges the gap between cell culture and live tissue. *Nat. Rev. Mol. Cell Biol.* **2007**, *8*, 839–845.

512. Hayakawa, K.; Liang, A.C.L.; Xing, C.; Lo, E.H.; Arai, K. In vitro angiogenesis assay: Endothelialmigration, proliferation, and tube formation. In *Handbook of Vascular Biology Techniques*; Slevin, M., McDowell, G., Eds.; Springer Netherlands: Dordrecht, 2015; pp. 3–12 ISBN 9789401797160.

513. Goodwin, A.M. In vitro assays of angiogenesis for assessment of angiogenic and anti-angiogenic agents. *Microvasc. Res.* **2007**, *74*, 172–183.

514. Chiu, W.C.; Chiou, T.J.; Chiang, A.N. β 2 -Glycoprotein I inhibits endothelial cell migration through the nuclear factor κB signalling pathway and endothelial nitric oxide synthase activation. *Biochem. J.* **2012**, *445*, 125–133.

515. Logie, J.J.; Ali, S.; Marshall, K.M.; Heck, M.M.S.; Walker, B.R.; Hadoke, P.W.F. Glucocorticoid-mediated inhibition of angiogenic changes in human endothelial cells is not caused by reductions in cell proliferation or migration. *PLoS One* **2010**, *5*, 1–10.

516. Arbiser, J.L.; Klauber, N.; Rohan, R.; Van Leeuwen, R.; Huang, M.T.; Fisher, C.; Flynn, E.; Byers, H.R. Curcumin is an in vivo inhibitor of angiogenesis. *Mol. Med.* **1998**, *4*, 376–383.

517. Kye, W.P.; Grouse, D.; Lee, M.; Karnik, S.K.; Sorensen, L.K.; Murphy, K.J.; Kuo, C.J.; Li, D.Y. The axonal attractant Netrin-1 is an angiogenic factor. *Proc. Natl. Acad. Sci. U. S. A.* **2004**, *101*, 16210–16215.

518. Langenfeld, E.M.; Langenfeld, J. Bone Morphogenetic Protein-2 stimulates angiogenesis in developing tumors. *Mol. Cancer Res.* **2004**, *2*, 141–149.

519. DeCicco-Skinner, K.L.; Henry, G.H.; Cataisson, C.; Tabib, T.; Curtis Gwilliam, J.; Watson, N.J.; Bullwinkle, E.M.; Falkenburg, L.; O'Neill, R.C.; Morin, A.; et al. Endothelial cell tube formation assay for the in vitro study of angiogenesis. *J. Vis. Exp.* **2014**, e51312.

520. Hung, S.-C.; Pochampally, R.R.; Chen, S.-C.; Hsu, S.-C.; Prockop, D.J. Angiogenic Effects of Human Multipotent Stromal Cell Conditioned Medium Activate the PI3K-Akt Pathway in Hypoxic Endothelial Cells to Inhibit Apoptosis, Increase Survival, and Stimulate Angiogenesis. *Stem Cells* **2007**, *25*, 2363–2370.

521. Masson, V.; Devy, L.; Grignet-Debrus, C.; Bernt, S.; Bajou, K.; Blacher, S.; Roland, G.; Chang, Y.; Fong, T.; Carmeliet, P.; et al. Mouse aortic ring assay: A new approach of the molecular genetics of angiogenesis. *Biol. Proced. Online* **2002**, *4*, 24–31.

522. Auerbach, R.; Muthukkaruppan, V. The Chick Embryo Aortic Arch Assay. In *The Textbook of Angiogenesis and Lymphangiogenesis: Methods and Applications*; Zudaire, E., Cuttitta, F., Eds.; Springer Netherlands: Dordrecht, 2012; pp. 149–157 ISBN 978-94-007-4581-0.

523. Sawamiphak, S.; Ritter, M.; Acker-Palmer, A. Preparation of retinal explant cultures to study ex vivo tip endothelial cell responses. *Nat. Protoc.* **2010**, *5*, 1659–1665.

524. Rezzola, S.; Belleri, M.; Ribatti, D.; Costagliola, C.; Presta, M.; Semeraro, F. A novel ex vivo murine retina angiogenesis (EMRA) assay. *Exp. Eye Res.* **2013**, *112*, 51–56.

525. Vargas, A.; Zeisser-Labouèbe, M.; Lange, N.; Gurny, R.; Delie, F. The chick embryo and its chorioallantoic membrane (CAM) for the in vivo evaluation of drug delivery systems. *Adv. Drug Deliv. Rev.* **2007**, *59*, 1162–1176.

526. Laschke, M.W.; Vollmar, B.; Menger, M.D. The dorsal skinfold chamber: Window into the dynamic interaction of biomaterials with their surrounding host tissue. *Eur. Cells Mater.* **2011**, *22*, 147–167.

527. Rücker, M.; Laschke, M.W.; Junker, D.; Carvalho, C.; Schramm, A.; Mülhaupt, R.; Gellrich, N.C.; Menger, M.D. Angiogenic and inflammatory response to

biodegradable scaffolds in dorsal skinfold chambers of mice. *Biomaterials* **2006**, *27*, 5027–5038.

528. Akhtar, N.; Dickerson, E.B.; Auerbach, R. The sponge/Matrigel angiogenesis assay. *Angiogenesis* **2002**, *5*, 75–80.

529. Malinda, K.M. In vivo matrigel migration and angiogenesis assay. *Methods Mol. Biol.* **2009**, *467*, 287–294.

530. Ziche, M.; Morbidelli, L.; Masini, E.; Amerini, S.; Granger, H.J.; Maggi, C.A.; Geppetti, P.; Ledda, F. Nitric oxide mediates angiogenesis in vivo and endothelial cell growth and migration in vitro promoted by substance P. *J. Clin. Invest.* **1994**, *94*, 2036–2044.

531. Serbedzija, G.N.; Flynn, E.; Willett, C.E. Zebrafish angiogenesis: A new model for drug screening. *Angiogenesis* **1999**, *3*, 353–359.

532. Nicoli, S.; Presta, M. The zebrafish/tumor xenograft angiogenesis assay. *Nat. Protoc.* **2007**, *2*, 2918–2923.

533. Kurobe, H.; Maxfield, M.W.; Tara, S.; Rocco, K.A.; Bagi, P.S.; Yi, T.; Udelsman, B.; Zhuang, Z.W.; Cleary, M.; Iwakiri, Y.; et al. Development of small diameter nanofiber tissue engineered arterial grafts. *PLoS One* **2015**, *10*, e0120328.

534. Nieponice, A.; Soletti, L.; Guan, J.; Deasy, B.M.; Huard, J.; Wagner, W.R.; Vorp, D.A. Development of a tissue-engineered vascular graft combining a biodegradable scaffold, muscle-derived stem cells and a rotational vacuum seeding technique. *Biomaterials* **2008**, *29*, 825–833.

535. Ye, L.; Cao, J.; Chen, L.; Geng, X.; Zhang, A.Y.; Guo, L.R.; Gu, Y.Q.; Feng, Z.G. The fabrication of double layer tubular vascular tissue engineering scaffold via coaxial electrospinning and its 3D cell coculture. *J. Biomed. Mater. Res. - Part A* **2015**, *103*, 3863–3871.

536. Johnson, D.W.; Sherborne, C.; Didsbury, M.P.; Pateman, C.; Cameron, N.R.; Claeyssens, F. Macrostructuring of emulsion-templated porous polymers by 3D laser patterning. *Adv. Mater.* **2013**, *25*, 3178–3181.

537. Busby, W.; Cameron, N.R.; Jahoda, C.A.B. Emulsion-derived foams (PolyHIPEs)

containing poly(Sε-caprolactone) as matrixes for tissue engineering. *Biomacromolecules* **2001**, *2*, 154–164.

538. Wasserman, S.M.; Topper, J.N. Adaptation of the endothelium to fluid flow: In vitro analyses of gene expression and in vivo implications. *Vasc. Med.* **2004**, *9*, 35–45.

539. Chatterjee, S. Endothelial mechanotransduction, redox signaling and the regulation of vascular inflammatory pathways. *Front. Physiol.* **2018**, *9*, 1–16.

540. Kitagawa, T.; Yamaoka, T.; Iwase, R.; Murakami, A. Three-dimensional cell seeding and growth in radial-flow perfusion bioreactor for in vitro tissue reconstruction. *Biotechnol. Bioeng.* **2006**, *93*, 947–954.

541. Mohan, S.; Mohan, N.; Sprague, E.A. Differential activation of NF-κB in human aortic endothelial cells conditioned to specific flow environments. *Am. J. Physiol. - Cell Physiol.* **1997**, *273*, C572–C578.

542. Mohan, S.; Mohan, N.; Valente, A.J.; Sprague, E.A. Regulation of low shear flow-induced HAEC VCAM-1 expression and monocyte adhesion. *Am. J. Physiol. - Cell Physiol.* **1999**, *276*, C1100–C1107.

543. Barron, M.J.; Goldman, J.; Tsai, C.J.; Donahue, S.W. Perfusion flow enhances osteogenic gene expression and the infiltration of osteoblasts and endothelial cells into three-dimensional calcium phosphate scaffolds. *Int. J. Biomater.* **2012**, *2012*, 915620.

544. Sprague, E.A.; Luo, J.; Palmaz, J.C. Human aortic endothelial cell migration onto stent surfaces under static and flow conditions. *J. Vasc. Interv. Radiol.* **1997**, *8*, 83–92.

545. Urbich, C.; Dernbach, E.; Reissner, A.; Vasa, M.; Zeiher, A.M.; Dimmeler, S. Shear stress-induced endothelial cell migration involves integrin signaling via the fibronectin receptor subunits α5 and β1. *Arterioscler. Thromb. Vasc. Biol.* **2002**, *22*, 69–75.

546. Mohan, S.; Mohan, N.; Sprague, E.A. Differential activation of NF-kappa B in human aortic endothelial cells conditioned to specific flow environments. *Am. J. Physiol. Physiol.* **2017**, *273*, C572–C578.

547. Song, J.W.; Munn, L.L. Fluid forces control endothelial sprouting. *Proc. Natl. Acad. Sci.* **2011**, *108*, 15342–15347.

548. Yow, K.H.; Ingram, J.; Korossis, S.A.; Ingham, E.; Homer-Vanniasinkam, S. Tissue engineering of vascular conduits. *Br. J. Surg.* **2006**, *93*, 652–661.

549. Dikici, S.; Claeyssens, F.; MacNeil, S. Pre-seeding of simple electrospun scaffolds with a combination of endothelial cells and fibroblasts strongly promotes angiogenesis. *Tissue Eng. Regen. Med.* **2020**, *17*, in press.

550. Young, W.C.; Herman, I.M. Extracellular matrix modulation of endothelial cell shape and motility following injury in vitro. *J. Cell Sci.* **1985**, *73*, 19–32.

551. Hughes, C.C.W. Endothelial-stromal interactions in angiogenesis. *Curr. Opin. Hematol.* **2008**, *15*, 204–209.

552. Ribatti, D.; Nico, B.; Crivellato, E. The role of pericytes in angiogenesis. *Int. J. Dev. Biol.* **2011**, *55*, 261–268.

553. Ma, Z.; He, W.; Yong, T.; Ramakrishna, S. Grafting of gelatin on electrospun poly(caprolactone) nanofibers to improve endothelial cell spreading and proliferation and to control cell orientation. *Tissue Eng.* **2005**, *11*, 1149–1158.

554. Hadjizadeh, A.; Doillon, C.J. Directional migration of endothelial cells towards angiogenesis using polymer fibres in a 3D co-culture system. *J. Tissue Eng. Regen. Med.* **2010**, *4*, 524–531.

555. Lloyd-Griffith, C.; McFadden, T.M.; Duffy, G.P.; Unger, R.E.; Kirkpatrick, C.J.; O'Brien, F.J. The pre-vascularisation of a collagen-chondroitin sulphate scaffold using human amniotic fluid-derived stem cells to enhance and stabilise endothelial cell-mediated vessel formation. *Acta Biomater.* **2015**, *26*, 263–273.

556. Young, S.K.; Jae, C.K. Inhibition of corneal neovascularization by rapamycin. *Exp. Mol. Med.* **2006**, *38*, 173–179.

557. Shima, D.T.; Adamis, A.P.; Ferrara, N.; Yeo, K.T.; Yeo, T.K.; Allende, R.; Folkman, J.; D'Amore, P.A. Hypoxic induction of endothelial cell growth factors in retinal cells: identification and characterization of vascular endothelial growth factor (VEGF) as the mitogen. *Mol. Med.* **1995**, *1*, 182–193.

558. Wu, J.; Wu, Z.; Xue, Z.; Li, H.; Liu, J. PHBV/bioglass composite scaffolds with co-cultures of endothelial cells and bone marrow stromal cells improve vascularization and osteogenesis for bone tissue engineering. *RSC Adv.* **2017**, *7*, 22197–22207.

559. Griffith, C.K.; George, S.C. The effect of hypoxia on in vitro prevascularization of a thick soft tissue. *Tissue Eng. Part A* **2009**, *15*, 2423–2434.

560. Pham, Q.P.; Kasper, F.K.; Mistry, A.S.; Sharma, U.; Yasko, A.W.; Jansen, J.A.; Mikos, A.G. Analysis of the osteoinductive capacity and angiogenicity of an in vitro generated extracellular matrix. *J. Biomed. Mater. Res. - Part A* **2009**, *88*, 295–303.

561. Post, M.J.; Rahimi, N.; Caolo, V. Update on vascularization in tissue engineering. *Regen. Med.* **2013**, *8*, 759–770.

562. Dimova, C.; Evrosimovska, B.; Zlatanovska, K.; Zarkova, J. Alveolar augmentation using different bone substitutes. In *Handbook of Bioceramics and Biocomposites*; 2016; pp. 1159–1199 ISBN 9783319124605.

563. Saghiri, M.A.; Asatourian, A.; Garcia-Godoy, F.; Sheibani, N. The role of angiogenesis in implant dentistry part II: The effect of bone-grafting and barrier membrane materials on angiogenesis. *Med. Oral Patol. Oral Cir. Bucal* **2016**, *21*, e526–e537.

564. Buser, D.; Hoffmann, B.; Bernard, J.P.; Lussi, A.; Mettler, D.; Schenk, R.K. Evaluation of filling materials in membrane-protected bone defects - A comparative histomorphometric study in the mandible of miniature pigs. *Clin. Oral Implants Res.* **1998**, *9*, 137–150.

565. Rowe, M.J.; Kamocki, K.; Pankajakshan, D.; Li, D.; Bruzzaniti, A.; Thomas, V.; Blanchard, S.B.; Bottino, M.C. Dimensionally stable and bioactive membrane for guided bone regeneration: An in vitro study. *J. Biomed. Mater. Res. - Part B Appl. Biomater.* **2016**, *104*, 594–605.

566. Lee, S.-W.; Kim, S.-G. Membranes for the Guided Bone Regeneration. *Maxillofac. Plast. Reconstr. Surg.* **2017**, *36*, 239–246.

567. Bottino, M.C.; Thomas, V.; Schmidt, G.; Vohra, Y.K.; Chu, T.M.G.; Kowolik, M.J.; Janowski, G.M. Recent advances in the development of GTR/GBR membranes for

periodontal regeneration - A materials perspective. *Dent. Mater.* **2012**, *28*, 703–721.

568. Wang, J.; Wang, L.; Zhou, Z.; Lai, H.; Xu, P.; Liao, L.; Wei, J. Biodegradable polymer membranes applied in guided bone/tissue regeneration: A review. *Polymers (Basel).* **2016**, *8*, 1–20.

569. Liu, J.; Kerns, D.G. Mechanisms of Guided Bone Regeneration: A Review. *Open Dent. J.* **2014**, *8*, 56–65.

570. Woodruff, M.A.; Hutmacher, D.W. The return of a forgotten polymer - Polycaprolactone in the 21st century. *Prog. Polym. Sci.* **2010**, *35*, 1217–1256.

571. Cheng, G.; Yin, C.; Tu, H.; Jiang, S.; Wang, Q.; Zhou, X.; Xing, X.; Xie, C.; Shi, X.; Du, Y.; et al. Controlled Co-delivery of Growth Factors through Layer-by-Layer Assembly of Core-Shell Nanofibers for Improving Bone Regeneration. *ACS Nano* **2019**, *13*, 6372–6382.

572. Rai, B.; Teoh, S.H.; Hutmacher, D.W.; Cao, T.; Ho, K.H. Novel PCL-based honeycomb scaffolds as drug delivery systems for rhBMP-2. *Biomaterials* **2005**, *26*, 3739–3748.

573. Inanç, B.; Arslan, Y.E.; Seker, S.; Elçin, A.E.; Elçin, Y.M. Periodontal ligament cellular structures engineered with electrospun poly(DL-lactide-co-glycolide) nanofibrous membrane scaffolds. *J. Biomed. Mater. Res. - Part A* **2009**, *90*, 186–195.

574. Bottino, M.C.; Thomas, V.; Janowski, G.M. A novel spatially designed and functionally graded electrospun membrane for periodontal regeneration. *Acta Biomater.* **2011**, *7*, 216–224.

575. Wise, S.G.; Byrom, M.J.; Waterhouse, A.; Bannon, P.G.; Ng, M.K.C.; Weiss, A.S. A multilayered synthetic human elastin/polycaprolactone hybrid vascular graft with tailored mechanical properties. *Acta Biomater.* **2011**, *7*, 295–303.

576. Cheng, G.; Ma, X.; Li, J.; Cheng, Y.; Cao, Y.; Wang, Z.; Shi, X.; Du, Y.; Deng, H.; Li, Z. Incorporating platelet-rich plasma into coaxial electrospun nanofibers for bone tissue engineering. *Int. J. Pharm.* **2018**, *547*, 656–666.

577. Cheng, G.; Chen, J.; Wang, Q.; Yang, X.; Cheng, Y.; Li, Z.; Tu, H.; Deng, H.; Li, Z. Promoting osteogenic differentiation in pre-osteoblasts and reducing tibial

fracture healing time using functional nanofibers. *Nano Res.* **2018**, *11*, 3658–3677.

578. Chong, E.J.; Phan, T.T.; Lim, I.J.; Zhang, Y.Z.; Bay, B.H.; Ramakrishna, S.; Lim, C.T. Evaluation of electrospun PCL/gelatin nanofibrous scaffold for wound healing and layered dermal reconstitution. *Acta Biomater.* **2007**, *3*, 321–330.

579. Choi, J.S.; Leong, K.W.; Yoo, H.S. In vivo wound healing of diabetic ulcers using electrospun nanofibers immobilized with human epidermal growth factor (EGF). *Biomaterials* **2008**, *29*, 587–596.

580. Cheng, Z.; Teoh, S.H. Surface modification of ultra thin poly (ε-caprolactone) films using acrylic acid and collagen. *Biomaterials* **2004**, *25*, 1991–2001.

581. Miroshnichenko, S.; Timofeeva, V.; Permyakova, E.; Ershov, S.; Kiryukhantsev-Korneev, P.; Dvořaková, E.; Shtansky, D.; Zajíčková, L.; Solovieva, A.; Manakhov, A. Plasma-Coated Polycaprolactone Nanofibers with Covalently Bonded Platelet-Rich Plasma Enhance Adhesion and Growth of Human Fibroblasts. *Nanomaterials* **2019**, *9*, 637.

582. Jokinen, V.; Suvanto, P.; Franssila, S. Oxygen and nitrogen plasma hydrophilization and hydrophobic recovery of polymers. *Biomicrofluidics* **2012**, *6*, 16501–1650110.

583. Abedalwafa, M.; Wang, F.; Wang, L.; Li, C. Biodegradable poly-epsilon-caprolactone (PCL) for tissue engineering applications: A review. *Rev. Adv. Mater. Sci.* **2013**, *34*, 123–140.

584. Ivanova, A.A.; Syromotina, D.S.; Shkarina, S.N.; Shkarin, R.; Cecilia, A.; Weinhardt, V.; Baumbach, T.; Saveleva, M.S.; Gorin, D.A.; Douglas, T.E.L.; et al. Effect of low-temperature plasma treatment of electrospun polycaprolactone fibrous scaffolds on calcium carbonate mineralisation. *RSC Adv.* **2018**, *8*, 39106–39114.

585. Valence, S. De; Tille, J.C.; Chaabane, C.; Gurny, R.; Bochaton-Piallat, M.L.; Walpoth, B.H.; Möller, M. Plasma treatment for improving cell biocompatibility of a biodegradable polymer scaffold for vascular graft applications. *Eur. J. Pharm. Biopharm.* **2013**, *85*, 78–86.

586. Hurt, A.P.; Getti, G.; Coleman, N.J. Bioactivity and biocompatibility of a chitosan-tobermorite composite membrane for guided tissue regeneration. *Int. J. Biol.*

*Macromol.* **2014**, *64*, 11–16.

587. Mota, J.; Yu, N.; Caridade, S.G.; Luz, G.M.; Gomes, M.E.; Reis, R.L.; Jansen, J.A.; Frank Walboomers, X.; Mano, J.F. Chitosan/bioactive glass nanoparticle composite membranes for periodontal regeneration. *Acta Biomater.* **2012**, *8*, 4173–4180.

588. Xue, J.; He, M.; Liang, Y.; Crawford, A.; Coates, P.; Chen, D.; Shi, R.; Zhang, L. Fabrication and evaluation of electrospun PCL-gelatin micro-/nanofiber membranes for anti-infective GTR implants. *J. Mater. Chem. B* **2014**, *2*, 6867–6877.

589. Kharaziha, M.; Fathi, M.H.; Edris, H. Development of novel aligned nanofibrous composite membranes for guided bone regeneration. *J. Mech. Behav. Biomed. Mater.* **2013**, *24*, 9–20.

590. Fu, L.; Wang, Z.; Dong, S.; Cai, Y.; Ni, Y.; Zhang, T.; Wang, L.; Zhou, Y. Bilayer poly(Lactic-co-glycolic acid)/nano- hydroxyapatite membrane with barrier function and Osteogenesis promotion for guided bone regeneration. *Materials (Basel).* **2017**, *10*, 257.

591. Lee, E.J.; Shin, D.S.; Kim, H.E.; Kim, H.W.; Koh, Y.H.; Jang, J.H. Membrane of hybrid chitosan-silica xerogel for guided bone regeneration. *Biomaterials* **2009**, *30*, 743–750.

592. Qasim, S.B.; Delaine-Smith, R.M.; Fey, T.; Rawlinson, A.; Rehman, I.U. Freeze gelated porous membranes for periodontal tissue regeneration. *Acta Biomater.* **2015**, *23*, 317–328.

593. Tayebi, L.; Rasoulianboroujeni, M.; Moharamzadeh, K.; Almela, T.K.D.; Cui, Z.; Ye, H. 3D-printed membrane for guided tissue regeneration. *Mater. Sci. Eng. C* **2017**, *84*, 148–158.

594. Zhang, H.Y.; Jiang, H.B.; Ryu, J.-H.; Kang, H.; Kim, K.-M.; Kwon, J.-S. Comparing Properties of Variable Pore-Sized 3D-Printed PLA Membrane with Conventional PLA Membrane for Guided Bone/Tissue Regeneration. *Materials (Basel).* **2019**, *12*, 1718.

595. Li, D.; Xia, Y. Electrospinning of nanofibers: Reinventing the wheel? *Adv. Mater.* **2004**, *16*, 1151–1170.

596. Pham, Q.P.; Sharma, U.; Mikos, A.G. Electrospinning of polymeric nanofibers for tissue engineering applications: a review. *Tissue Eng.* **2006**, *12*, 1197–211.

597. Qin, X.; Wu, D. Effect of different solvents on poly(caprolactone)(PCL) electrospun nonwoven membranes. *J. Therm. Anal. Calorim.* **2012**, *107*, 1007–1013.

598. Beachley, V.; Wen, X. Effect of electrospinning parameters on the nanofiber diameter and length. *Mater. Sci. Eng. C* **2009**, *29*, 663–668.

599. Bahrami, S.H.; Gholipour Kanani, A. Effect of changing solvents on poly(ε-Caprolactone) nanofibrous webs morphology. *J. Nanomater.* **2011**, *2011*, 1–10.

600. Langford, C.; Cameron, N. Materials for Tissue Engineering and 3D Cell Culture. *Bio-Inspired Polym.* **2016**, 460–480.

601. Zhang, H.; Cooper, A.I. Synthesis and applications of emulsion-templated porous materials. *Soft Matter* **2005**, *1*, 107–113.

602. Cameron, N.R.; Sherrington, D.C. High internal phase emulsions (HIPEs) — Structure, properties and use in polymer preparation. In *Biopolymers Liquid Crystalline Polymers Phase Emulsion*; Springer Berlin Heidelberg: Berlin, Heidelberg, 1996; pp. 163–214.

603. Hollister, S.J. Porous scaffold design for tissue engineering. *Nat. Mater.* **2005**, *4*, 518–24.

604. Sherborne, C.; Owen, R.; Reilly, G.C.; Claeyssens, F. Light-based additive manufacturing of PolyHIPEs: Controlling the surface porosity for 3D cell culture applications. *Mater. Des.* **2018**, *156*, 494–503.

605. Christenson, E.M.; Soofi, W.; Holm, J.L.; Cameron, N.R.; Mikos, A.G. Biodegradable fumarate-based polyHIPEs as tissue engineering scaffolds. *Biomacromolecules* **2007**, *8*, 3806–3814.

606. Johnson, D.W.; Langford, C.R.; Didsbury, M.P.; Lipp, B.; Przyborski, S. a.; Cameron, N.R. Fully biodegradable and biocompatible emulsion templated polymer scaffolds by thiol-acrylate polymerization of polycaprolactone macromonomers. *Polym. Chem.* **2015**, *6*, 7256–7263.

607. Akay, G.; Birch, M.A.; Bokhari, M.A. Microcellular polyHIPE polymer supports

osteoblast growth and bone formation in vitro. *Biomaterials* **2004**, *25*, 3991–4000.

608. Cameron, N.R. High internal phase emulsion templating as a route to well-defined porous polymers. *Polymer (Guildf).* **2005**, *46*, 1439–1449.

609. Owen, R.; Sherborne, C.; Paterson, T.; Green, N.H.; Reilly, G.C.; Claeyssens, F. Emulsion templated scaffolds with tunable mechanical properties for bone tissue engineering. *J. Mech. Behav. Biomed. Mater.* **2016**, *54*, 159–172.

610. Gao, C. Polymeric biomaterials for tissue regeneration: From surface/interface design to 3D constructs. In *Polymeric Biomaterials for Tissue Regeneration: From Surface/Interface Design to 3D Constructs*; Springer Singapore: Singapore, 2016; pp. 1–386 ISBN 9789811022937.

611. Mastrogiacomo, M.; Scaglione, S.; Martinetti, R.; Dolcini, L.; Beltrame, F.; Cancedda, R.; Quarto, R. Role of scaffold internal structure on in vivo bone formation in macroporous calcium phosphate bioceramics. *Biomaterials* **2006**, *27*, 3230–3237.

612. Marcacci, M.; Kon, E.; Moukhachev, V.; Lavroukov, A.; Kutepov, S.; Quarto, R.; Mastrogiacomo, M.; Cancedda, R. Stem Cells Associated with Macroporous Bioceramics for Long Bone Repair: 6- to 7-Year Outcome of a Pilot Clinical Study. *Tissue Eng.* **2007**, *13*, 947–955.

613. Somo, S.I.; Akar, B.; Bayrak, E.S.; Larson, J.C.; Appel, A.A.; Mehdizadeh, H.; Cinar, A.; Brey, E.M. Pore Interconnectivity Influences Growth Factor-Mediated Vascularization in Sphere-Templated Hydrogels. *Tissue Eng. Part C Methods* **2015**, *21*, 773–785.

614. Wright, A.J.; Main, M.J.; Cooper, N.J.; Blight, B.A.; Holder, S.J. Poly High Internal Phase Emulsion for the Immobilization of Chemical Warfare Agents. *ACS Appl. Mater. Interfaces* **2017**, *9*, 31335–31339.

615. Ma, Z.; He, W.; Yong, T.; Ramakrishna, S. Grafting of Gelatin on Electrospun Poly(caprolactone) Nanofibers to Improve Endothelial Cell Spreading and Proliferation and to Control Cell Orientation. *Tissue Eng.* **2005**, *11*, 1149–1158.

616. Prabhakaran, M.P.; Venugopal, J.; Chan, C.K.; Ramakrishna, S. Surface modified electrospun nanofibrous scaffolds for nerve tissue engineering. *Nanotechnology*

**2008**, *19*, 455102.

617. Fujihara, K.; Kotaki, M.; Ramakrishna, S. Guided bone regeneration membrane made of polycaprolactone/calcium carbonate composite nano-fibers. *Biomaterials* **2005**, *26*, 4139–4147.

618. Zander, N.E.; Orlicki, J.A.; Rawlett, A.M.; Beebe, T.P. Quantification of protein incorporated into electrospun polycaprolactone tissue engineering scaffolds. *ACS Appl. Mater. Interfaces* **2012**, *4*, 2074–2081.

619. Can-Herrera, L.A.; Ávila-Ortega, A.; de la Rosa-García, S.; Oliva, A.I.; Cauich-Rodríguez, J. V.; Cervantes-Uc, J.M. Surface modification of electrospun polycaprolactone microfibers by air plasma treatment: Effect of plasma power and treatment time. *Eur. Polym. J.* **2016**, *84*, 502–513.

620. McGEE-RUSSELL, S.M. Histochemical methods for calcium. *J. Histochem. Cytochem.* **1958**, *6*, 22–42.

621. Bhaskar, B.; Owen, R.; Bahmaee, H.; Wally, Z.; Sreenivasa Rao, P.; Reilly, G.C. Composite porous scaffold of PEG/PLA support improved bone matrix deposition in vitro compared to PLA-only scaffolds. *J. Biomed. Mater. Res. - Part A* **2018**, *106*, 1334–1340.

622. Wally, Z.J.; Haque, A.M.; Feteira, A.; Claeyssens, F.; Goodall, R.; Reilly, G.C. Selective laser melting processed Ti6Al4V lattices with graded porosities for dental applications. *J. Mech. Behav. Biomed. Mater.* **2019**, *90*, 20–29.

623. Mazón, P.; De Aza, P.N. Porous scaffold prepared from α′L-Dicalcium silicate doped with phosphorus for bone grafts. *Ceram. Int.* **2018**, *44*, 537–545.

624. Tang, L.; Wei, W.; Wang, X.; Qian, J.; Li, J.; He, A.; Yang, L.; Jiang, X.; Li, X.; Wei, J. LAPONITE® nanorods regulating degradability, acidic-alkaline microenvironment, apatite mineralization and MC3T3-E1 cells responses to poly(butylene succinate) based bio-nanocomposite scaffolds. *RSC Adv.* **2018**, *8*, 10794–10805.

625. Rajzer, I.; Kurowska, A.; Jabłoński, A.; Jatteau, S.; Śliwka, M.; Ziąbka, M.; Menaszek, E. Layered gelatin/PLLA scaffolds fabricated by electrospinning and 3D printing-

for nasal cartilages and subchondral bone reconstruction. *Mater. Des.* **2018**, *155*, 297–306.

626. Augustine, R.; Dominic, E.A.; Reju, I.; Kaimal, B.; Kalarikkal, N.; Thomas, S. Investigation of angiogenesis and its mechanism using zinc oxide nanoparticle-loaded electrospun tissue engineering scaffolds. *RSC Adv.* **2014**, *4*, 51528–51536.

627. Singh, S.; Wu, B.M.; Dunn, J.C.Y. Delivery of VEGF using collagen-coated polycaprolactone scaffolds stimulates angiogenesis. *J. Biomed. Mater. Res. - Part A* **2012**, *100 A*, 720–727.

628. New, S.E.P.; Ibrahim, A.; Guasti, L.; Zucchelli, E.; Birchall, M.; Bulstrode, N.W.; Seifalian, A.M.; Ferretti, P. Towards reconstruction of epithelialized cartilages from autologous adipose tissue-derived stem cells. *J. Tissue Eng. Regen. Med.* **2017**, *11*, 3078–3089.

629. Madden, L.R.; Mortisen, D.J.; Sussman, E.M.; Dupras, S.K.; Fugate, J.A.; Cuy, J.L.; Hauch, K.D.; Laflamme, M.A.; Murry, C.E.; Ratner, B.D. Proangiogenic scaffolds as functional templates for cardiac tissue engineering. *Proc. Natl. Acad. Sci.* **2010**, *107*, 15211–15216.

630. Baker, S.C.; Rohman, G.; Hinley, J.; Stahlschmidt, J.; Cameron, N.R.; Southgate, J. Cellular Integration and Vascularisation Promoted by a Resorbable, Particulate-Leached, Cross-Linked Poly(ε-caprolactone) Scaffold. *Macromol. Biosci.* **2011**, *11*, 618–627.

631. Klenke, F.M.; Liu, Y.; Yuan, H.; Hunziker, E.B.; Siebenrock, K.A.; Hofstetter, W. Impact of pore size on the vascularization and osseointegration of ceramic bone substitutes in vivo. *J. Biomed. Mater. Res. - Part A* **2008**, *85*, 777–786.

632. Barbeck, M.; Lorenz, J.; Kubesch, A.; Böhm, N.; Booms, P.; Choukroun, J.; Sader, R.; Kirkpatrick, C.J.; Ghanaati, S. Porcine Dermis-Derived Collagen Membranes Induce Implantation Bed Vascularization Via Multinucleated Giant Cells: A Physiological Reaction? *J. Oral Implantol.* **2014**, *41*, e238–e251.

633. De Santana, R.B.; de Mattos, C.M.L.; Francischone, C.E.; Van Dyke, T. Superficial Topography and Porosity of an Absorbable Barrier Membrane Impacts Soft Tissue Response in Guided Bone Regeneration. *J. Periodontol.* **2010**, *81*, 926–933.

634. Moroni, L.; Licht, R.; de Boer, J.; de Wijn, J.R.; van Blitterswijk, C.A. Fiber diameter and texture of electrospun PEOT/PBT scaffolds influence human mesenchymal stem cell proliferation and morphology, and the release of incorporated compounds. *Biomaterials* **2006**, *27*, 4911–4922.

635. Fong, H.; Chun, I.; Reneker, D.H. Beaded nanofibers formed during electrospinning. *Polymer (Guildf).* **1999**, *40*, 4585–4592.

636. van der Wal, S. Low viscosity organic modifiers in reversed-phase HPLC. *Chromatographia* **1985**, *20*, 274–278.

637. Zverev, M.P.; Zubov, P.I.; Barash, A.N.; Nikonorova, L.P.; Ivanova, L. V. The properties of solutions of polymers in good and poor solvents and of articles prepared from these solutions. *Polym. Sci. U.S.S.R.* **1974**, *16*, 589–598.

638. Haider, A.; Haider, S.; Kang, I.K. A comprehensive review summarizing the effect of electrospinning parameters and potential applications of nanofibers in biomedical and biotechnology. *Arab. J. Chem.* **2018**, *11*, 1165–1188.

639. Katsogiannis, K.A.G.; Vladisavljević, G.T.; Georgiadou, S. Porous electrospun polycaprolactone (PCL) fibres by phase separation. *Eur. Polym. J.* **2015**, *69*, 284–295.

640. Bordes, C.; Fréville, V.; Ruffin, E.; Marote, P.; Gauvrit, J.Y.; Briançon, S.; Lantéri, P. Determination of poly(ε-caprolactone) solubility parameters: Application to solvent substitution in a microencapsulation process. *Int. J. Pharm.* **2010**, *383*, 236–243.

641. Luo, C.J.; Stride, E.; Edirisinghe, M. Mapping the influence of solubility and dielectric constant on electrospinning polycaprolactone solutions. *Macromolecules* **2012**, *45*, 4669–4680.

642. Jahangir, M.A.; Rumi, T.M.; Wahab, A.; Rahman, M.A.; Sayed, Z. Bin Poly Lactic Acid (PLA) Fibres: Different Solvent Systems and Their Effect on Fibre Morphology and Diameter. *Am. J. Chem.* **2017**, *2017*, 177–186.

643. Zhu, Y.; Cao, Y.; Pan, J.; Liu, Y. Macro-alignment of electrospun fibers for vascular tissue engineering. *J. Biomed. Mater. Res. - Part B Appl. Biomater.* **2010**, *92*, 508–

516.

644. Du, L.; Xu, H.; Zhang, Y.; Zou, F. Electrospinning of polycaprolatone nanofibers with DMF additive: The effect of solution proprieties on jet perturbation and fiber morphologies. *Fibers Polym.* **2016**, *17*, 751–759.

645. Hsu, C.M.; Shivkumar, S. N,N-dimethylformamide additions to the solution for the electrospinning of poly(ε-caprolactone) nanofibers. *Macromol. Mater. Eng.* **2004**, *289*, 334–340.

646. Bölgen, N.; Menceloğlu, Y.Z.; Acatay, K.; Vargel, I.; Pişkin, E. In vitro and in vivo degradation of non-woven materials made of poly(ε-caprolactone) nanofibers prepared by electrospinning under different conditions. *J. Biomater. Sci. Polym. Ed.* **2005**, *16*, 1537–1555.

647. Lee, Y.J.; An, S.J.; Bae, E. Bin; Gwon, H.J.; Park, J.S.; Jeong, S.I.; Jeon, Y.C.; Lee, S.H.; Lim, Y.M.; Huh, J.B. The effect of thickness of resorbable bacterial cellulose membrane on guided bone regeneration. *Materials (Basel).* **2017**, *10*, 320.

648. Bubalo, M.; Lazic, Z.; Matic, S.; Tatic, Z.; Milovic, R.; Petkovic-Curcin, A.; Djurdjevic, D.; Loncarevic, S. The impact of thickness of resorbable membrane of human origin on the ossification of bone defects: A pathohistologic study. *Vojnosanit. Pregl. Med. Pharm. J. Serbia* **2012**, *69*, 1076–1083.

649. Liao, S.; Wang, W.; Uo, M.; Ohkawa, S.; Akasaka, T.; Tamura, K.; Cui, F.; Watari, F. A three-layered nano-carbonated hydroxyapatite/collagen/PLGA composite membrane for guided tissue regeneration. *Biomaterials* **2005**, *26*, 7564–7571.

650. Yoshimoto, I.; Sasaki, J.I.; Tsuboi, R.; Yamaguchi, S.; Kitagawa, H.; Imazato, S. Development of layered PLGA membranes for periodontal tissue regeneration. *Dent. Mater.* **2018**, *34*, 538–550.

651. Qasim, S.B.; Najeeb, S.; Delaine-Smith, R.M.; Rawlinson, A.; Ur Rehman, I. Potential of electrospun chitosan fibers as a surface layer in functionally graded GTR membrane for periodontal regeneration. *Dent. Mater.* **2017**, *33*, 71–83.

652. Rodrigues, J.R.; Alves, N.M.; Mano, J.F. Biomimetic polysaccharide/bioactive glass nanoparticles multilayer membranes for guided tissue regeneration. *RSC Adv.*

**2016**, *6*, 75988–75999.

653. Anton, D.; Burckel, H.; Josset, E.; Noel, G. Three-dimensional cell culture: A breakthrough in vivo. *Int. J. Mol. Sci.* 2015, *16*, 5517–5527.

654. Vaquette, C.; Cooper-White, J.J. Increasing electrospun scaffold pore size with tailored collectors for improved cell penetration. *Acta Biomater.* **2011**, *7*, 2544–2557.

655. Kodama, T.; Minabe, M.; Hori, T.; Watanabe, Y. The Effect of Various Concentrations of Collagen Barrier on Periodontal Wound Healing. *J. Periodontol.* **2012**, *60*, 205–210.

656. Bunyaratavej, P.; Wang, H.-L. Collagen Membranes: A Review. *J. Periodontol.* **2005**, *72*, 215–229.